frontiers | Research Topics

Emerging insights into immunological mechanisms driving neurological and psychiatric diseases

Edited by
Juehua Yu, Mingyao Ying, Xiaobo Mao, Lei Sun and Joseph Scafidi

Published in
Frontiers in Immunology
Frontiers in Neurology

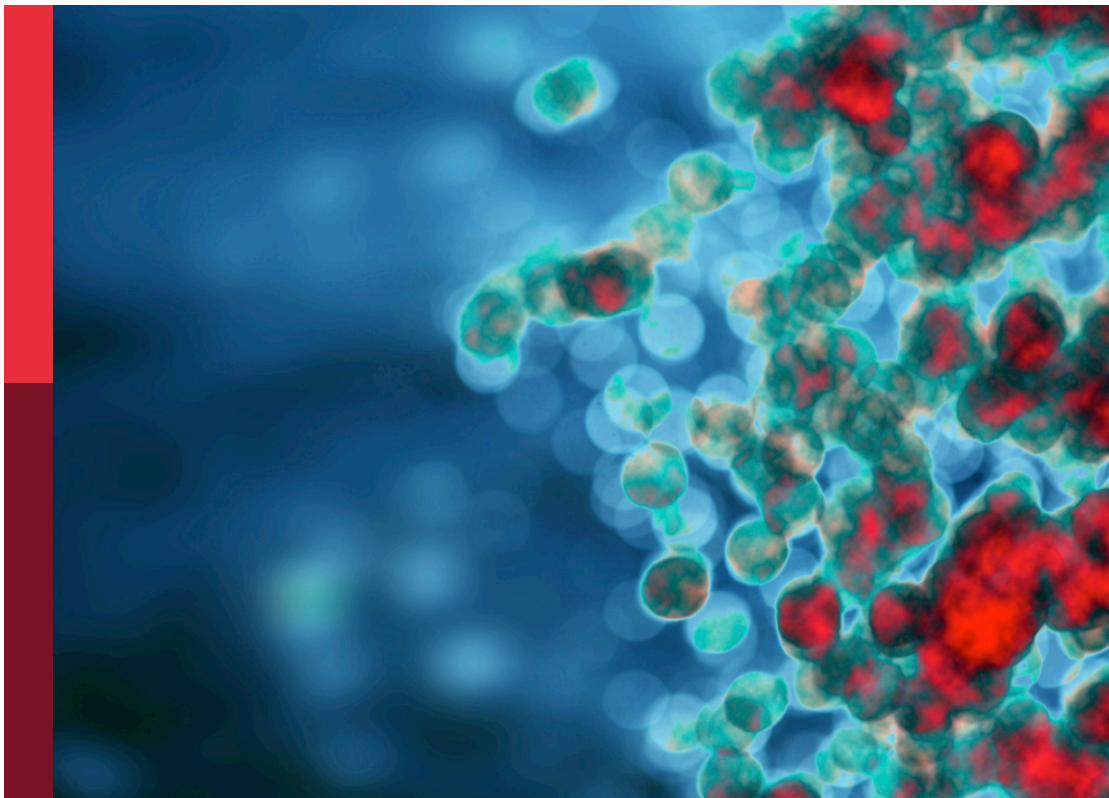

ISSN 1664-8714
ISBN 978-2-83251-859-5
DOI 10.3389/978-2-83251-859-5

About Frontiers

Frontiers is more than just an open access publisher of scholarly articles: it is a pioneering approach to the world of academia, radically improving the way scholarly research is managed. The grand vision of Frontiers is a world where all people have an equal opportunity to seek, share and generate knowledge. Frontiers provides immediate and permanent online open access to all its publications, but this alone is not enough to realize our grand goals.

Frontiers journal series

The Frontiers journal series is a multi-tier and interdisciplinary set of open-access, online journals, promising a paradigm shift from the current review, selection and dissemination processes in academic publishing. All Frontiers journals are driven by researchers for researchers; therefore, they constitute a service to the scholarly community. At the same time, the *Frontiers journal series* operates on a revolutionary invention, the tiered publishing system, initially addressing specific communities of scholars, and gradually climbing up to broader public understanding, thus serving the interests of the lay society, too.

Dedication to quality

Each Frontiers article is a landmark of the highest quality, thanks to genuinely collaborative interactions between authors and review editors, who include some of the world's best academicians. Research must be certified by peers before entering a stream of knowledge that may eventually reach the public - and shape society; therefore, Frontiers only applies the most rigorous and unbiased reviews. Frontiers revolutionizes research publishing by freely delivering the most outstanding research, evaluated with no bias from both the academic and social point of view. By applying the most advanced information technologies, Frontiers is catapulting scholarly publishing into a new generation.

What are Frontiers Research Topics?

Frontiers Research Topics are very popular trademarks of the *Frontiers journals series*: they are collections of at least ten articles, all centered on a particular subject. With their unique mix of varied contributions from Original Research to Review Articles, Frontiers Research Topics unify the most influential researchers, the latest key findings and historical advances in a hot research area.

Find out more on how to host your own Frontiers Research Topic or contribute to one as an author by contacting the Frontiers editorial office: frontiersin.org/about/contact

Emerging insights into immunological mechanisms driving neurological and psychiatric diseases

Topic editors

Juehua Yu — The First Affiliated Hospital of Kunming Medical University, China
Mingyao Ying — The Johns Hopkins Hospital, Johns Hopkins Medicine, United States
Xiaobo Mao — Johns Hopkins University, United States
Lei Sun — Fudan University, China
Joseph Scafidi — Johns Hopkins University, United States

Citation

Yu, J., Ying, M., Mao, X., Sun, L., Scafidi, J., eds. (2023). *Emerging insights into immunological mechanisms driving neurological and psychiatric diseases*. Lausanne: Frontiers Media SA. doi: 10.3389/978-2-83251-859-5

Table of contents

frontiers in Immunology

ORIGINAL RESEARCH
published: 04 January 2022
doi: 10.3389/fimmu.2021.815840

Dysregulated TP53 Among PTSD Patients Leads to Downregulation of miRNA let-7a and Promotes an Inflammatory Th17 Phenotype

*Philip B. Busbee[1], Marpe Bam[1], Xiaoming Yang[1], Osama A. Abdulla[1], Juhua Zhou[1], Jay Paul (Jack) Ginsberg[1,2], Allison E. Aiello[3], Monica Uddin[4], Mitzi Nagarkatti[1] and Prakash S. Nagarkatti[1]**

[1] Department of Pathology, Microbiology, and Immunology, School of Medicine, University of South Carolina, Columbia, SC, United States, [2] Departments of Psychophysiology, Clinical Psychology, and Research Office, Saybrook University, Pasadena, CA, United States, [3] Department of Epidemiology, University of North Carolina (UNC) Gillings School of Global Public Health, University of North Carolina, Mcgavran-Greenberg Hall, Chapel Hill, NC, United States, [4] Genomics Program, University of South Florida College of Public Health, Tampa, FL, United States

OPEN ACCESS

Edited by:
Juehua Yu,
The First Affiliated Hospital of Kunming Medical University, China

Reviewed by:
Murugaiyan Gopal,
Harvard Medical School, United States
Hong Zan,
The University of Texas Health Science Center at San Antonio, United States

***Correspondence:**
Prakash S. Nagarkatti
prakash@mailbox.sc.edu

Specialty section:
This article was submitted to Multiple Sclerosis and Neuroimmunology, a section of the journal Frontiers in Immunology

Received: 15 November 2021
Accepted: 15 December 2021
Published: 04 January 2022

Citation:
Busbee PB, Bam M, Yang X, Abdulla OA, Zhou J, Ginsberg JP (J), Aiello AE, Uddin M, Nagarkatti M and Nagarkatti PS (2022) Dysregulated TP53 Among PTSD Patients Leads to Downregulation of miRNA let-7a and Promotes an Inflammatory Th17 Phenotype. Front. Immunol. 12:815840. doi: 10.3389/fimmu.2021.815840

Post-traumatic stress disorder (PTSD) is a psychiatric disorder and patients diagnosed with PTSD often express other comorbid health issues, particularly autoimmune and inflammatory disorders. Our previous reports investigating peripheral blood mononuclear cells (PBMCs) from PTSD patients showed that these patients exhibit an increased inflammatory T helper (Th) cell phenotype and widespread downregulation of microRNAs (miRNAs), key molecules involved in post-transcriptional gene regulation. A combination of analyzing prior datasets on gene and miRNA expression of PBMCs from PTSD and Control samples, as well as experiments using primary PBMCs collected from human PTSD and Controls blood, was used to evaluate TP53 expression, DNA methylation, and miRNA modulation on Th17 development. In the current report, we note several downregulated miRNAs were linked to tumor protein 53 (TP53), also known as p53. Expression data from PBMCs revealed that compared to Controls, PTSD patients exhibited decreased TP53 which correlated with an increased inflammatory Th17 phenotype. Decreased expression of TP53 in the PTSD population was shown to be associated with an increase in DNA methylation in the *TP53* promotor region. Lastly, the most significantly downregulated TP53-associated miRNA, let-7a, was shown to negatively regulate Th17 T cells. Let-7a modulation in activated CD4+ T cells was shown to influence Th17 development and function, *via* alterations in IL-6 and IL-17 production, respectively. Collectively, these studies reveal that PTSD patients could be susceptible to inflammation by epigenetic dysregulation of TP53, which alters the miRNA profile to favor a proinflammatory Th17 phenotype.

Keywords: post-traumatic stress disorder, tumor protein 53, microRNA, inflammation, T helper 17 cells

INTRODUCTION

Post-traumatic stress disorder (PTSD) is a psychiatric disorder caused by exposure to a severe traumatic event, such as combat, domestic violence, sexual assault, and natural disasters (1–3). In addition to classic psychiatric and psychologic symptoms of this disorder, such as emotional numbing, repetitive recollections of the traumatic event, and states of hyperarousal (4), other medical disorders have been linked to PTSD, including arthritis, diabetes, cardiovascular-associated conditions, and various inflammatory disorders (5–8). Increased risk of these comorbid medical disorders and medical complications in PTSD patients reduces the effective treatment of these patients, and studies have shown that PTSD patients have increased annual healthcare costs (4.2-9.3%) when compared to patients with other mental disorders (9). While the prevalence of PTSD was relatively low (8%) in the general population for a time (10), PTSD reported in combat veterans was found to be as high as 30% (11, 12), and reports are already showing increased prevalence of PTSD in numerous populations around the world due to the COVID-19 pandemic (13–15). Therefore, it is becoming increasingly critical to better understand why individuals diagnosed with PTSD have increased risk of other comorbid disorders. A better understanding of these mechanisms could provide both better treatment options and significantly improve the overall quality of life of the affected patient population.

Several reports link PTSD with increased inflammation and occurrence of inflammatory disorders (16–25). In an early report by Gola et al, researchers found that peripheral blood mononuclear cells (PBMCs) from PTSD patients exhibited a more pre-activated phenotype, having higher levels of secreting inflammatory cytokines, such as interleukin-6 (IL-6), tumor necrosis factor-alpha (TNF-α), and IL-1β when compared to control samples (26). We have since published extensively on the correlation between PTSD and inflammation, showing how epigenetic modifications (e.g. histone and DNA methylation) and modulation of microRNA (miRNA or miR), small noncoding RNA nucleotides involved in post-transcriptional regulation of genes, could potentially make PTSD patients more prone to inflammatory immune responses (27–31). Among these reports, published results revealed PBMCs from PTSD patients showed increased plasma IL-17 levels and CD4+ T helper-17 (Th17) phenotypes, which correlated with PTSD severity and global downregulation of miRNAs (22). Despite these observations, key regulators or promoters of this Th17 inflammatory phenotype in PTSD patients are yet to be fully understood.

In the current report, we noted several significantly dysregulated miRNA in PTSD PBMCs were associated with *TP53*, the human gene encoding for tumor protein 53 (TP53 or p53). Analysis of gene expression profile data in the public domain and our own evaluation of human PBMCs revealed TP53 is downregulated in PTSD subjects when compared to Controls. Whole genome methylated DNA immunoprecipitation sequencing (MeDIP-seq) data of PBMCs also showed that there was increased DNA methylation in the *TP53* promoter region of PTSD subjects compared to controls, which would suggest decreased transcription of this gene. Elsewhere in this report, we highlight that among the dysregulated miRNAs associated with TP53, let-7a was not only found to be the most significantly altered miRNA, but pathway analysis also revealed let-7a had direct and indirect links to Th17 cells. Lastly, transfection of activated CD4+ T cells purified from human PBMCs to modulate let-7a levels showed that this miRNA is directly involved in both Th17 development and function. The current report highlights an important role for the p53/miRNA(let-7a) axis in promoting a potential inflammatory Th17-skewed phenotype in the PTSD population.

MATERIALS AND METHODS

Human Patient Samples

Procedures to collect human samples presented in this report were approved and reviewed by the Institutional Review Boards (IRBs) from the University of South Carolina, the University of Michigan, and the University of North Carolina-Chapel Hill. Blood sample collection from participants was performed after obtaining proper informed and written consent. In the current report, human samples were collected from two main sources: 1) veterans from the William Jennings Bryan Dorn Veterans Medical Center (VMC) (27), or 2) study participants from the Detroit Neighborhood Health Study (DNHS) (32). PTSD samples obtained from veterans at the William Jennings Bryan Dorn (VMC) were clinically assessed by medical VMC professionals using psychometric properties of the PTSD Checklist (PCL), Clinician Administered PTSD Scale (CAPS), and formal criteria from the Diagnostic and Statistical Manual of Mental Disorder (DSM-V), as previously described (29). For DNHS samples, PTSD diagnosis was performed using structured telephone interviews and the PTSD Checklist-Civilian Version (PCL-C), which was subsequently validated with in-person clinical interviews, as previously reported (32). The source and number of PTSD and Control samples were used for the following analyses present in the current report: A.) miRNA microarray evaluation of PBMCs: Control (n=4), PTSD (n=8); source: PBMCs from William Jennings Bryan Dorn VA participants; demographics data published in previous report (29). B.) TP53 and IL-17A expression from PBMCs from public database set: Control (n=16), PTSD (n=17); source: Gene expression profiles of PBMCs from combat veterans in public database Gene Expression Omnibus (GEO) database (ID GSE860); demographics data published in previous report (33). C.) TP53/Mdm2 PCR expression and correlation data from collected PBMCs: Control (n=6), PTSD (n=19); source: PBMCs from William Jennings Bryan Dorn VA participants; demographics data available in **Table 1**. D.) DNA methylation of the TP53 promoter region: Control (n=5); PTSD (n=5); source: PBMCs from DNHS project; demographic data available in **Table 1**. For Control samples, non-PTSD volunteers were found to be comparable to PTSD samples based on age, race, and sex, as detailed in **Table 1**. In addition, exclusion criteria for both the Control and PTSD samples included non-adult participants (< 18 years of age), participants with active

infection(s) during PBMC collection, or other potentially immunocompromising conditions such as HIV, cancer, active pregnancy among female participants, or recorded history of chronic steroid use.

PBMC Isolation From Blood Samples

For PBMC isolation, researchers obtained deidentified blood samples (10-20 ml) collected in EDTA-coated tubes and began the isolation procedure within 1-2 hours of the sample collection. Blood samples were diluted in twice the volume of 1X PBS (Sigma-Aldrich, St. Louis, MO) before being layered on top of 20 ml of Ficoll-Paque (GE Healthcare, Uppsala, Sweden) and centrifuged at room temperature for 30 minutes at 1300 rpm. The upper plasma layer was carefully removed before collecting the PBMC interphase layer. PBMCs were diluted in twice the volume of 1X PBS before being centrifuged at 4°C for 5 minutes at 1300 rpm. Isolated PBMCs were washed twice in 1X PBS before further downstream processing of the cells (e.g. DNA/RNA isolation).

miRNA Microarray and Analysis of PTSD and Control Samples

PTSD (n=8) and Control (n=4) samples were processed for miRNA microarray as previously reported (27). In the current report, significantly dysregulated miRNAs associated with direct or indirect links to TP53 were the major focus, thus preventing redundant or overlapping results from the previous report using this dataset. Briefly, total RNA was isolated from PBMC samples using the miRNeasy Mini kit (Qiagen, Valencia, CA), and RNA integrity was analyzed using an Agilent 2100 BioAnalyzer (Agilent Tech, Palo Alto, CA). Microarray was performed by the Deep Sequencing and Microarray Core Facility at John Hopkins Memorial Institute in Baltimore, MD. miRNA hybridization to the Affymetrix miRNA-v1 gene chip (ThermoFisher Scientific, Waltham, MA), microarray data normalization, microarray quality control, and calculation of linear fold change of miRNA between PTSD and Control samples were performed as previously reported (27). Ingenuity Pathway Analysis (Qiagen Valencia, CA), also known as IPA, was used to analyze significantly dysregulated miRNA in PTSD samples compared to Controls (defined as ± 1.5-fold change with p value of < 0.05) in relation to known and predicted gene targets. IPA was also used to identify and visualize dysregulated miRNA, target genes, and the potential interacting networks involved in reported or highly predicted functions (e.g. Diseases and Functions, Molecular and Cellular Functions). Raw miRNA microarray data is available at ArrayExpress (Accession# E-MTAB-4880).

Evaluation of PTSD and Control Gene Expression Data From the Public Database

Initial analysis involving expression of genes of interest based on miRNA microarray data (e.g. TP53, Th17-related genes) was first evaluated in the public database, specifically from the NCBI (www.ncbi.nlm.nih.gov/) GEO database. The dataset used was ID GSE860 (33), which included normalized gene expression array data using the Affymetrix Human Genome U95A Array platform on PBMCs collected from PTSD (n=17) and Control (n=16) samples at two different time points (initial ER visit and 4 months after). Controls were defined as ER patients that experienced psychological trauma but did not develop PTSD over time. Normalized expression data was expressed as fold change relative to the average of gene expression of either Control or PTSD samples during the initial ER visit, prior to evaluation after 4 months. In the current report, results included evaluation of TP53 (31618_at) and IL-17A (1359_at) gene expression in the total of 33 PBMC samples included in the publicly available dataset, thereby reducing overlapping and repetitive results from the previous manuscript for which this data was associated with.

Evaluation of Gene Expression in PTSD and Control Samples Using Quantitative Real-Time PCR

In addition to the aforementioned publicly available dataset, we evaluated gene expression in PBMCs from William Jennings Bryan Dorn VA participants between Control (n=6) and PTSD (n=19) groups for TP53 and the TP53 regulatory protein, Mdm2, using qRT-PCR. PBMC and RNA isolation procedures were performed from collected blood samples as described above. Complementary DNA (cDNA) was synthesized using miScript II RT kit (Qiagen, Valencia, CA), followed by gene transcript detection using iQ universal SYBR Green supermix (Bio-Rad Laboratories, Hercules, CA) on a Bio-Rad CFX384 PCR platform. A total of 10ng of cDNA was used per sample for the PCR reactions, and primers for TP53 (forward: CCTCAGCA TCTTATCCGAGTGG; reverse: TGGATGGTGGTACAG TCAGAGC) and Mdm2 (forward: TGTTTGGCGTGCCAAG CTTCTC; reverse: CACAGATGTACCTGAGTCCGATG) were designed and created using Integrated DNA Technologies (IDT, Coralville, IA). Expression of genes were first normalized to 18S and then expressed as fold change using the delta-delta CT method ($2^{-\Delta\Delta Ct}$ method). PCR reactions were performed using the following 2-step cycling protocol: initial denaturing and enzyme activation (95°C, 2:00 mins,1 cycle), denaturing (95°C, 15 secs, 40 cycles), annealing and extension (55°C, 30 secs, 40 cycles), melt curve (55-95°C with 0.5°C increments, 30 secs, 1 cycle). Control and PTSD participants used in these PCR assays and subsequent correlation studies were found to be comparable in terms of age, race, and sex.

Methylated DNA Immunoprecipitation Sequencing of PTSD and Control PBMC Aamples

To investigate whole genome DNA methylation patterns, PBMCs were isolated from Control (n=5) and PTSD samples (n=5) provided from the DNHS project as described above. Genomic DNA was purified using a Zymo DNA purification kit (Zymo Research, Irvine, CA) and fragmented by Bioruptor sonicator (Diagenode, Denville, NJ). DNA fragments with sizes from 200 bp to 400 bp were purified and sequencing adaptors

were added using Illumina Chip-seq library preparation kit. dsDNA was then denatured and immunoprecipitated with anti 5-methylcytosine antibody using a MeDIP kit from Diagenode. Precipitated DNA was purified and amplified. MeDIP-seq libraries were then sequenced by Nextseq550 with single-end reads. Raw sequencing reads were mapped to human genome build hg19 using Bowtie software by allowing two mismatches in the read (34). The mapped reads were then analyzed with MEDIPS software (35). Generated WIG files were visualized in the IGB genome browser (www.bioviz.org). Control and PTSD participants used in these in the DNA methylation studies were found to be comparable in terms of age and race. However, there were uneven distributions based on sex, with males being more proportionally represented in the Control group compared to females.

MicroRNA let-7a Transfections in Activated and Purified CD4+ T Cell Cultures

PBMCs were isolated from blood of Control, non-PTSD volunteer samples as described above. PBMCs were purified for CD4 using an EasySep kit (StemCell Technologies, Cambridge, MA) and PE-conjugated monoclonal antibody (mAb) (Cat #555347, BD Biosciences, San Jose, CA). Purified CD4+ cells were assessed using FC500 flow cytometer (Beckman Coulter, Indianapolis, IN) and plated at 130,000 cell density per well in 24-well plates in complete RPMI media (Sigma-Aldrich, St. Louis, MO). Cells were left unactivated or activated with Dynabeads Human T-Activator CD3/CD28 (1:1 bead-to-cell ratio) (Cat. #111.61D, ThermoFisher Scientific, Waltham, MA) in 5% CO2 at 37 °C for 24 hours. In addition to activation, some cultures were transfected with either mock, Anti-hsa-let-7a-5p (inhibitor), or syn-has-let-7a-5 (mimic) from Qiagen (Valencia, CA). Transfections were performed using HiPerFect Transfection Reagent (Qiagen, Valencia, CA), following manufacturer's instructions, with a final concentration of inhibitors and mimics at 20 μM. Mock cultures only contained transfection reagent without addition of either the mimics or inhibitors. After 24 hours, RNA was isolated from cultured cells to test let-7a transfection by PCR as described above. PCR was performed using miScript SYBR Green PCR kit (Qiagen, Valencia, CA) and human let-7a-specific primers using Qiagen-based miScript Primer Assay as per instructions from the manufacturer. In addition, Th17 cell phenotyping by flow cytometry using fluorescently-labeled mABs for CD4 (Cat #555347, BD Biosciences, San Jose, CA) and IL-17A (Cat# 555347, Biolegend, San Diego, CA) was performed. IL-17A intracellular staining was achieved using a BD Cytofix/Cytoperm solution kit as per manufacturer's instructions (BD Biosciences, San Jose, CA). Cell culture supernatants were also assessed with human IL-17A and IL-6 ELISA kits from Biolegend (San Diego, CA).

Statistical Analysis

Statistical analysis was performed using Graphpad Prism version 9 software. For matching Control and PTSD samples to be comparable with one another, continuous variables (age, PTSD scores, anxiety score, depression score) were expressed as means with standard deviations, and p-values calculated using an unpaired, two-tailed standard t test. For categorical variables (sex and race), these were expressed as numbers with overall proportions represented within each respective group (e.g. PTSD or Control) for qualitative comparisons. For other comparison data (e.g. miRNA fold change, PCR gene expression) between two groups, an unpaired, two-tailed standard t test was performed. When comparing 3 or more groups (e.g. *in vitro* cell culture studies with flow cytometry, miRNA fold change PCR, and ELISAs), one way ANOVA and *post-hoc* multiple comparisons Tukey's test was performed. *In vitro* assays were performed at least three times and are shown as representative replicate data. For correlation studies, Pearson correlation tests were used to determine significance. Significance was defined as having a p value ≤ 0.05. For DNA methylation studies using MeDIPseq, qualitative observations with intensity of signal (peak height and width) in the focused gene promoter regions (e.g. TP53) were evaluated as previously reported (28).

RESULTS

Dysregulated miRNA in PTSD PBMCs Is Associated With TP53 and Inflammatory Th17 Response

In our previous study, we noted that compared to healthy controls, PTSD patients had significant downregulation of a number of miRNA (27). Using IPA analysis software, we noted that of the top 6 networks affected by significantly dysregulated miRNA in PTSD samples, 4 of these included TP53 (**Table 2**). Further analysis revealed that of the 184 miRNAs significantly downregulated in PTSD samples, 21 of these altered miRNAS were found to be associated with TP53 (**Figures 1A, B**). The most significantly downregulated TP53-associated miRNA with the lowest p value was let-7a (**Figure 1C**), which was followed by miR-145, miR-16, miR-221, and miR-320b (**Figures 1D–G**). To better understand what processes and functions were affected by these particular miRNAs, only the 21 TP53-associated miRNAs were input back into IPA to determine how their alteration might affect disease and function. As shown in **Figure 1H**, Inflammatory Response and Inflammatory Disease were ranked within the top 5 Disease and Functions affected by these specific miRNA. In addition to Disease and Functions, the top Molecular and Cellular processes linked to these altered TP53-associated miRNAs included Cellular Development, as well as Cellular Growth and Proliferation (**Figure 1I**). Lastly, among the 21 TP53-associated miRNA, let-7a and TP53 were found to have direct and indirect interactions linked to Th17 development and function by way of their association with IL-6 and IL-17A, respectively (**Figure 2**). Prediction analysis based on the miRNA profiles also suggested that TP53 would be inhibited in PTSD samples, while IL-6 and IL-17A were predicted to be activated. These data suggested that through a TP53/let-7a axis,

TABLE 1 | Demographics and clinical history of Control and PTSD samples for PCR gene expression and DNA methylation analysis.

TP53 and Mdm2 Gene Expression (PCR)

Parameters	Control (n = 6)	PTSD (n = 19)	P-value
Age	40.7 (7.3)	38.9 (9.4)	0.6173
Race			N/A
AA[a]	3 (0.5)	11 (0.6)	
CA[a]	3 (0.5)	6 (0.3)	
A[a]	0 (0.0)	1 (0.1)	
H[a]	0 (0.0)	1 (0.1)	
Sex			N/A
M[b]	5 (0.8)	17 (0.9)	
F[b]	1 (0.2)	2 (0.1)	
Depression score	13.3 (6.7)	31.4 (12.7)	0.0032**
Anxiety score	11.2 (11.2)	28.1 (12.7)	0.0078**
PTSD score	43.7 (3.6)	62.8 (12.1)	0.0010***

For DNA Methylation of the TP53 Promoter

Parameters	Control (n = 5)	PTSD (n = 5)	P-value
Age	55.4 (18.0)	47.8 (17.4)	0.5162
Race			N/A
AA[a]	5 (1.0)	5 (1.0)	
CA[a]	0 (0.0)	0 (0.0)	
A[a]	0 (0.0)	0 (0.0)	
H[a]	0 (0.0)	0 (0.0)	
Sex			N/A
M[b]	4 (0.8)	2 (0.4)	
F[b]	1 (0.2)	3 (0.6)	

*Values indicate the mean (standard deviation) for continuous variables (Age, Depression score, Anxiety score, PTSD score) and the number (proportion) was used for categorical variables (Race and Sex). Values were rounded to the nearest tenth. P-value was determined using unpaired two-tailed t test comparing Control and PTSD groups for continuous variable data (**P-value ≤ 0.01, ***P-value ≤ 0.001). Based on these results, Age, Race, and Sex were comparable between the two groups for the PCR data. Age and Race were comparable for the DNA methylation studies, though male proportions were skewed higher in Control samples, with higher proportions of females in the PTSD samples.*

[a]*AA, African American; CA, Caucasian; A, Asian; H, Hispanic.*

[b]*M, Male; F, Female.*

N/A, not applicable.

PTSD patients could be more prone to developing an abnormal Th17 phenotype.

TP53 Downregulation in PTSD PBMCs Correlates With Increased Inflammatory IL-17A

Since so many downregulated miRNA in PTSD samples were linked to TP53, initial evaluation of TP53 expression was undertaken in the public database. In database GSE860, normalized expression of gene data was available between PTSD and Control samples during two major time points: 1) a visit to the ER caused by trauma, and then 2) 4 months after their initial ER visits. Control subjects were deemed to not develop PTSD after the 4-month period. Control and PTSD subjects were found to have no significant differences in age, race, or sex, as detailed in the previous published report (33). As the data shows, when compared to Control samples, PBMCs collected from PTSD subjects exhibited a decrease in TP53 4 months after trauma was experienced, which trended towards significance (**Figure 3A**). In addition, it was interesting to note that in this same cohort of PTSD subjects, IL-17A expression had a noticeable trending increase after 4 months (**Figure 3B**). While both these observations trended towards significance, data showed there was in fact a significant negative correlation between TP53 and inflammatory cytokine IL-17A levels (**Figure 3C**). In addition to this publicly available data, we evaluated TP53 expression in PBMCs collected from local veterans at the William's Jennings Bryan VMC. In this study, we collected PBMCs from both PTSD (n=19) and Control volunteers (n=6), with demographic data supplied in **Table 1**. Control and PTSD participants matched comparatively in terms of age, race, and sex, with no noted significant differences among these criteria between the two groups. There was however a larger overall proportion of male to female participants in this particular study, due to limited numbers of both Control and PTSD female volunteers. However, we found that veterans diagnosed with PTSD had significantly lower expression of TP53 compared to Controls (**Figure 3D**). Interestingly, there was no significant difference in the expression of TP53-inhibiting protein Mdm2 (**Figure 3E**), suggesting that TP53 expression was being specifically altered in the PTSD group, independent of other confounding factors or regulatory mechanisms related to TP53. Indeed, based on these studies, there was a clear significant negative correlation between TP53 expression and PTSD severity (**Figure 3F**), inasmuch as when the TP53 expression decreased, PTSD scores increased among the sampled population. Additionally, even though PTSD samples in this particular

TABLE 2 | IPA-generated networks highlighting dysregulated miRNA and target genes between Control and PTSD samples.

Top Diseases and Functions Networks	Score	Focus Molecules	Molecules in Network
Cancer, Organismal Injury and Abnormalities, Reproductive System Disease	30	16	AGO2,BIRC5,DICER1,ETS1,JUN,miR-125b-5p (and other miRNAs w/seed CCCUGAG),miR-126a-3p (and other miRNAs w/seed CGUACCG),miR-128-3p (and other miRNAs w/seed CACAGUG),miR-130a-3p (and other miRNAs w/seed AGUGCAA),miR-139-5p (miRNAs w/seed CUACAGU),miR-150-5p (and other miRNAs w/seed CUCCCAA),miR-18a-5p (and other miRNAs w/seed AAGGUGC),miR-193a-5p (miRNAs w/seed GGGUCUU),miR-199a-5p (and other miRNAs w/seed CCAGUGU),miR-19b-3p (and other miRNAs w/seed GUGCAAA),miR-223-3p (miRNAs w/seed GUCAGUU),miR-23a-3p (and other miRNAs w/seed UCACAUU),miR-361-5p (miRNAs w/seed UAUCAGA),miR-487b-3p (miRNAs w/seed AUCGUAC),miR-494-3p (miRNAs w/seed GAAACAU),miR-96-5p (and other miRNAs w/seed UUGGCAC),SSB,TNRC6B,***TP53***
Cancer, Hematological Disease, Immunological Disease	29	15	AGO2,AQP4,miR-103-3p (and other miRNAs w/seed GCAGCAU),miR-151-3p (and other miRNAs w/seed UAGACUG),miR-151-5p (and other miRNAs w/seed CGAGGAG),miR-188-3p (miRNAs w/seed UCCCACA),miR-1913 (and other miRNAs w/seed CUGCCCC),miR-320b (and other miRNAs w/seed AAAGCUG),miR-342-3p (miRNAs w/seed CUCACAC),miR-342-5p (and other miRNAs w/seed GGGGUGC),miR-378a-3p (and other miRNAs w/seed CUGGACU),miR-421-3p (and other miRNAs w/seed UCAACAG),miR-423-5p (and other miRNAs w/seed GAGGGGC),miR-455-3p (miRNAs w/seed CAGUCCA),miR-501-3p (and other miRNAs w/seed AUGCACC),miR-532-3p (miRNAs w/seed CUCCCAC),miR-668-3p (and other miRNAs w/seed GUCACUC),RPS15,SSB,***TP53***
Cancer, Inflammatory Disease, Inflammatory Response	29	17	BCL6,CDC25C,CDKN2A,EIF4E,FAM3C,KLF4,LAMP2,let-7a-5p (and other miRNAs w/seed GAGGUAG),mir-9,mir-130,mir-146, miR-1246 (miRNAs w/seed AUGGAUU),miR-125b-5p (and other miRNAs w/seed CCCUGAG),miR-1275 (and other miRNAs w/seed UGGGGGA),miR-140-3p (and other miRNAs w/seed ACCACAG),miR-145-5p (and other miRNAs w/seed UCCAGUU),miR-194-5p (miRNAs w/seed GUAACAG),miR-200b-3p (and other miRNAs w/seed AAUACUG),miR-210-3p (miRNAs w/seed UGUGCGU),miR-29b-3p (and other miRNAs w/seed AGCACCA),miR-30c-5p (and other miRNAs w/seed GUAAACA),miR-324-5p (miRNAs w/seed GCAUCCC),miR-330-3p (and other miRNAs w/seed CAAAGCA),miR-339-5p (and other miRNAs w/seed CCCUGUC),miR-486-5p (and other miRNAs w/seed CCUGUAC),miR-503-5p (miRNAs w/seed AGCAGCG),miR-532-5p (and other miRNAs w/seed AUGCCUU),MYC,PPM1D,RBPJ,SSB,TOP2A,***TP53***,YBX1,ZFP36L1
Cancer, Organismal Injury and Abnormalities, Reproductive System Disease	22	14	AGO2,CCND3,CHEK1,Creb,CXCL12,CYCS,DICER1,KAT6A,KIF23,MET,mir-130,miR-132-3p (and other miRNAs w/seed AACAGUC),miR-16-5p (and other miRNAs w/seed AGCAGCA),miR-185-5p (and other miRNAs w/seed GGAGAGA),miR-191-5p (and other miRNAs w/seed AACGGAA),miR-192-5p (and other miRNAs w/seed UGACCUA),miR-194-5p (miRNAs w/seed GUAACAG),miR-210-3p (miRNAs w/seed UGUGCGU),miR-22-3p (miRNAs w/seed AGCUGCC),miR-221-3p (and other miRNAs w/seed GCUACAU),miR-24-3p (and other miRNAs w/seed GGCUCAG),miR-330-3p (and other miRNAs w/seed CAAAGCA), miR-331-3p (miRNAs w/seed CCCCUGG),miR-486-5p (and other miRNAs w/seed CCUGUAC),miR-584-5p (and other miRNAs w/seed UAUGGUU),PLK1,PRC1,PTK2,PTPN1,RHOA,SSB,***TP53***,YBX1,ZEB1,ZYX
Dermatological Diseases and Conditions, Cancer, Endocrine System Disorders	16	11	CARD11,CXCL3,CXCL8,DMBT1,estrogen receptor,FCER2,IL1RAP,IL1RL2,IL23A,IL36A,IL36B,IL36G,KRAS,LTF,mir-146,miR-143-3p (and other miRNAs w/seed GAGAUGA),miR-146a-5p (and other miRNAs w/seed GAGAACU),miR-148a-3p (and other miRNAs w/seed CAGUGCA),miR-155-5p (miRNAs w/seed UAAUGCU),miR-181a-5p (and other miRNAs w/seed ACAUUCA), miR-21-5p (and other miRNAs w/seed AGCUUAU),miR-26a-5p (and other miRNAs w/seed UCAAGUA),miR-27a-3p (and other miRNAs w/seed UCACAGU),miR-31-5p (and other miRNAs w/seed GGCAAGA),miR-491-5p (and other miRNAs w/seed GUGGGGA),miR-708-5p (and other miRNAs w/seed AGGAGCU),NFkB (complex),PELI1,PTAFR,S100A12,TIMP3,TLR1,TLR3, TLR10,VHL
Cell Cycle, Cancer, Cellular Development	7	6	AGO2,BCL2L1,BCL2L11,BIRC5,BMP2,CCND1,CDKN1B,CHUK,DICER1,EIF4E,EIF4EBP1,GSK3B,H2AFX,IGF1,KDM5B,KRAS, let-7a-5p (and other miRNAs w/seed GAGGUAG),MAP2K1/2,Mek,miR-100-5p (and other miRNAs w/seed ACCCGUA),miR-17-5p (and other miRNAs w/seed AAAGUGC),miR-193a-3p (and other miRNAs w/seed ACUGGCC),miR-199a-3p (and other miRNAs w/seed CAGUAGU),miR-92a-3p (and other miRNAs w/seed AUUGCAC),MTOR,MUC1,p70 S6k,PTEN,RPS6,RPTOR, Smad2/3,SRC,STAT3,TGFBR2,VIM

The ranking of Disease and Function Networks is based on the score and number of molecules involved in the pathways associated with significantly altered miRNA between Control (n=4) and PTSD (n=8) samples. TP53 (in 4 of the top 6 Networks) has been put in bold and italic text.

cohort had significantly higher anxiety and depression scores compared to Controls (**Table 1**), TP53 expression appeared to only be correlated with PTSD score, as there was no significant correlation between TP53 expression and the two commonly comorbid psychological conditions associated with PTSD (**Figures 3G–I**). Taken together, these data revealed that when compared to Controls, PBMCs from persons diagnosed with PTSD had lower expression of TP53.

PBMCs From PTSD Subjects Exhibited Increased Methylation in One of the Known Promoter Regions of TP53

As we already noted that DNA methylation in genes involved in inflammation were altered in PTSD subjects (29), we evaluated the methylation pattern of the *TP53* promoter regions in Control (n=5) and PTSD (n=5) PBMC samples obtained from the DHNS project using MeDIP-seq. Patient demographics showed Control and PTSD samples used were comparable to each other in terms of age, race, and sex, though there was a slight disproportionate number of males in the Control samples (**Table 1**). This more male sex bias proportion was also present when evaluating Control and PTSD TP53 expression in the current report, as noted earlier. The samples collected in the DNHS project were also all African American (AA), which correlated with a larger proportion of this ethnicity in the aforementioned studies evaluating TP53 expression among PTSD samples, at least making the DNA methylation results more comparable to the aforementioned PCR results. In assessing one of the two

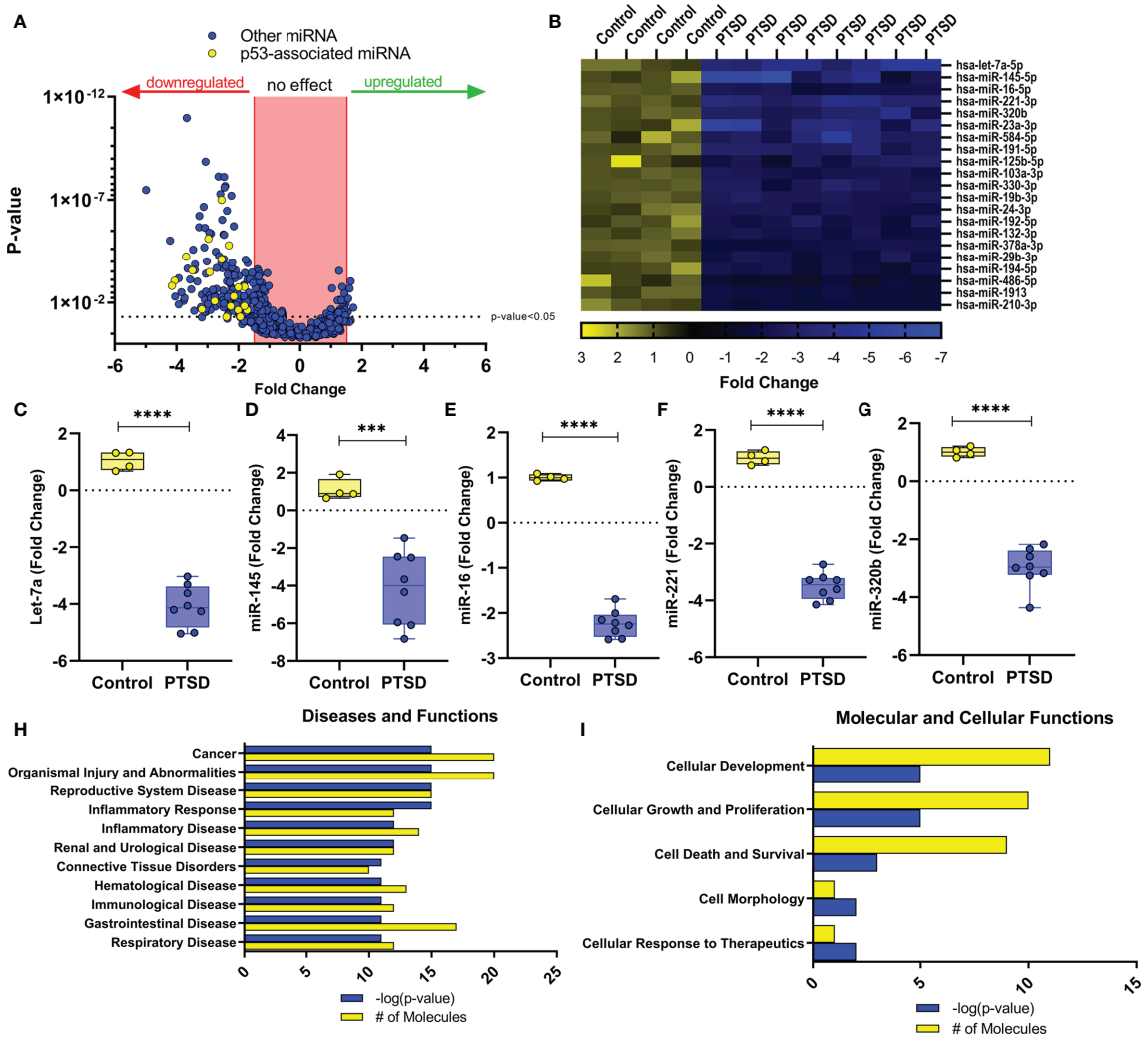

FIGURE 1 | Dysregulated miRNA in PBMCs from PTSD patients are associated with TP53. miRNA array data from PBMCs from Control (n=4) and PTSD subjects (n=8) was analyzed using IPA analysis software. **(A)** Volcano plot depicting miRNA fold change values (x-axis) of PTSD vs. Control plotted against p-values (y-axis). Yellow dots represent TP53-associated miRNAs. **(B)** Heat Map depicting 21 TP53-associated miRNA that were significantly downregulated in PTSD samples compared to control. **(C–G)** Box and whisker plots depicting top 5 downregulated TP53-associated miRNA between Control and PTSD samples to include **(C)** let-7a, **(D)** miR-145, **(E)** miR-16, **(F)** miR-122, **(G)** miR-321b. Box and whisker bars depict maximum and minimum values, with middle bar depicted at the median. **(H, I)** Top ranked networks (as determined by IPA-derived –log p-values and # of molecules) for 21 total dysregulated miRNA associated with TP53 to include **(H)** Disease and Functions, as well as I) Molecular and Cellular Functions. Significance in linear fold change was determined as any value ≥1.5 or ≤ -1.5 fold, and p-value was determined significant if this value ≤ 0.05 using an unpaired standard t test. P-values: ≤ 0.005 (***), ≤ 0.001 (****).

identified promoter regions of the human *TP53* gene on the Ensembl genome browser (ensembl.org), it was found that in general, PTSD PBMC samples had increased methylation intensity in the larger ~5kb promoter region identified in **Figure 4A**. This increased DNA methylation intensity was even more noticeable when combining the 5 samples into their respective groups (**Figure 4B**). With increased DNA methylation in the promotor region, it would stand to reason that this would lead to an impediment in the active transcription of TP53, or the gene encoding the p53 protein. This epigenetic modification could explain why PBMCs from PTSD subjects have lower expression of TP53 when compared to healthy controls.

Modulation of Let-7a in Activated CD4+ T Cells Alters Th17 Development and Function

As it has already been experimentally shown that TP53 modulation affects let-7a expression (36, 37), experiments were carried out focusing on how let-7a alterations affected CD4+ T cell phenotypes during activation. To achieve this, CD4+ cells were purified (~97% consistently) from PBMCs from a Control samples (**Figure 5A**). Next, these CD4+ cells were either left unactivated, or activated with CD3/CD28 antibodies in the presence or absence of let-7a mimic or inhibitor. Because IPA miRNA analysis pathway linked let-7a to Th17 development and

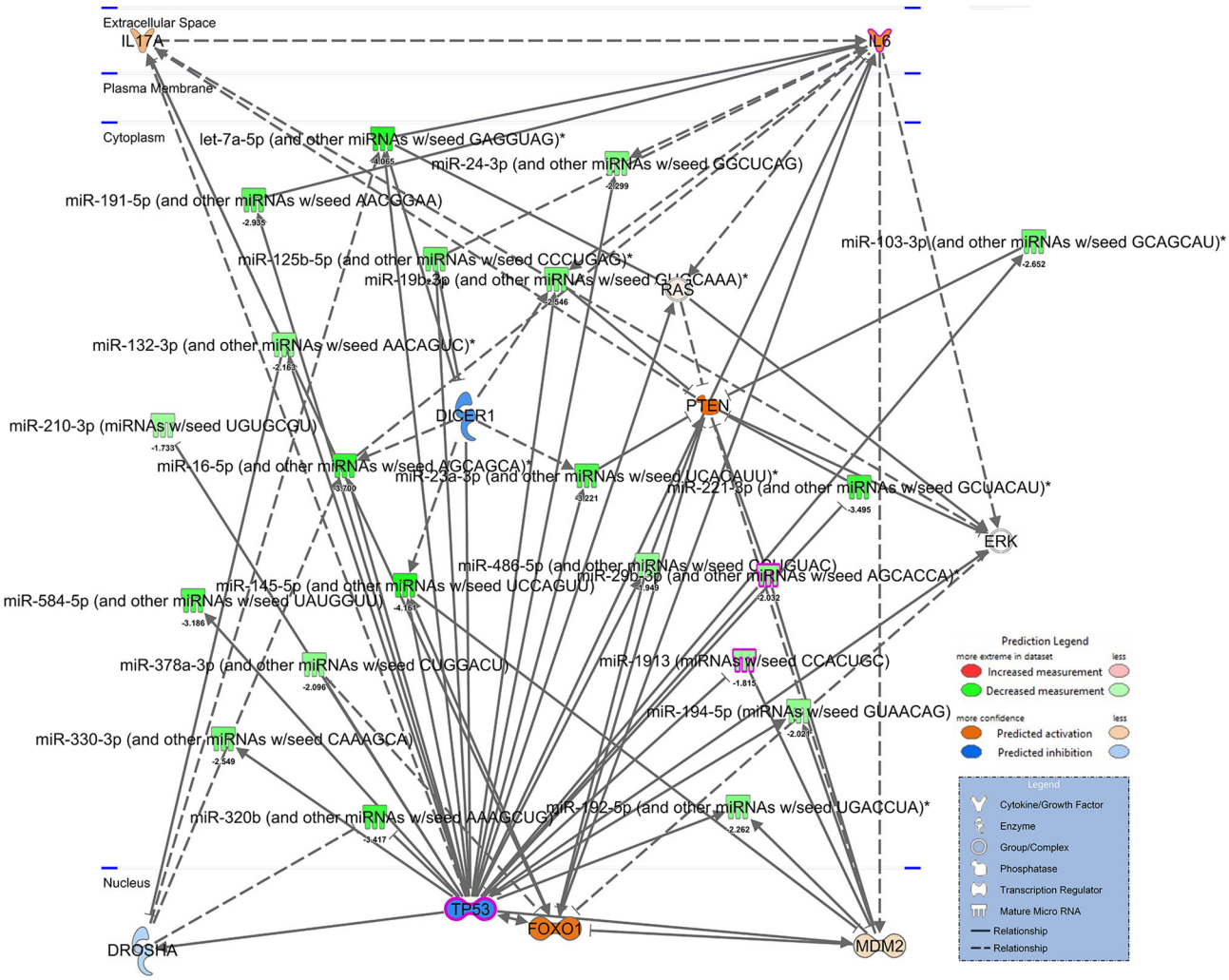

FIGURE 2 | Network of TP53 interactions with dysregulated miRNA from PTSD patients. IPA-derived network depicting dysregulated miRNA associated with TP53 from mean fold changes of Control (n=4) vs. PTSD (n=8) PMBCs. miRNA are depicted in green to denote downregulation (darker green denotes more downregulation) or red to denote decreased expression. Genes depicted in the network are predicted to be activated (orange) or inhibited (blue) based on interactions present, as noted in the Prediction Legend. A separate legend (lower right corner) is provided to identify components depicted in the network. Solid lines indicate direct interactions, and doted lines indicate either indirect or highly-predicted interactions.

function (**Figure 2**), Th17 cells (CD4+IL-17A+) were assessed under these conditions using flow cytometry (**Figure 5B**). As expected, Th17 populations expand under activating conditions when compared to cells left unactivated, but what was interesting was that the Th17 populations were altered by let-7a modulation (**Figure 5C**). Specifically, when enhancing let-7a levels with the mimic, Th17 percentages significantly decreased, while the opposite was true as inhibiting let-7a led to expansion of the Th17 population in the cultures. It is noteworthy that the activation of these CD4+ cultures resulted in significant decreased expression of let-7a in general when compared to unactivated cells. Let-7a modulation was validated by PCR to show that the mimics significantly enhanced let-7a expression, whereas inhibitors significantly decreased the expression in these cultured conditions (**Figure 5D**). Once confirmed, Th17 function and development were evaluated by way of IL-17A and Th17-inducing IL-6, respectively. It was shown that under these culturing conditions, increases in let-7a led to a significant decrease in IL-17A production (**Figure 5E**). Inhibiting let-7a however promoted significant increased secretion of IL-17A. The same trend was observed in IL-6 production levels, where inhibition of let-7a significantly enhanced IL-6 secretion, but a decrease in this miRNA resulted in significantly increased IL-6 production (**Figure 5F**). Taken altogether, these data demonstrated that let-7a negatively regulates Th17 development and function. Combined with the previous results, the data suggested that decreased TP53 correlates with decreased biogenesis of let-7a in PTSD patients, promoting an increased Th17 phenotype, which would normally be regulated by miRNA let-7a. The overall conclusions suggested that patients diagnosed with PTSD may be more prone to an inflammatory

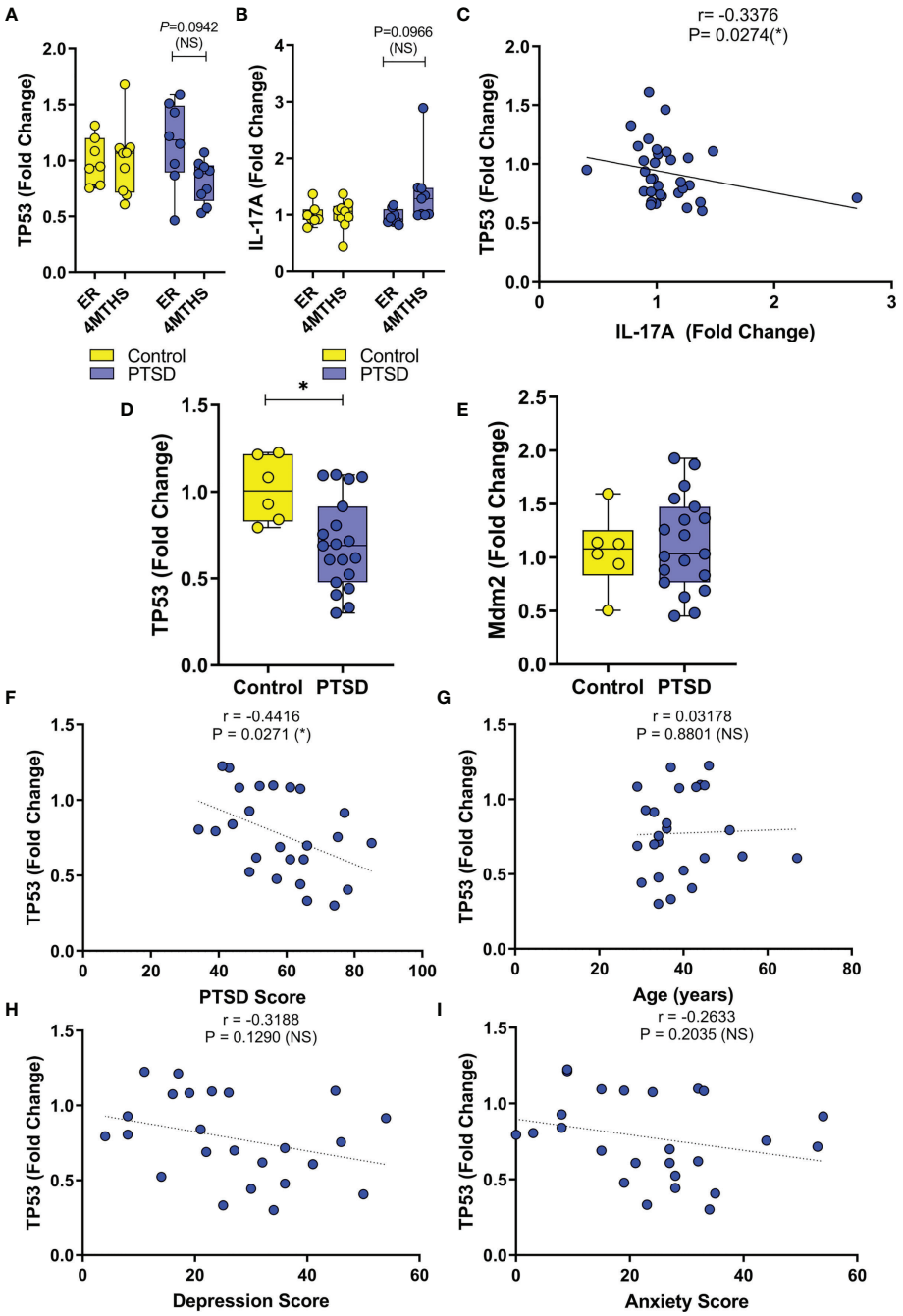

FIGURE 3 | Expression of TP53 in PBMCs is downregulated in PTSD samples compared to Control. **(A–C)** Normalized expression data was analyzed from public database (ID. GSE860) between PTSD (n=17) and Controls (n=15), with two time points during initial emergency room visit for trauma (ER) and 4 months later (4MTHS). **(A)** Box and whisker plot depicting fold change expression of TP53. **(B)** Box and whisker plot depicting fold change expression of IL-17A. **(C)** Correlation plot between TP53 and IL-17A fold change expression. **(D–I)** PBMC gene expression data was collected from VMC PTSD (n=19) and Control volunteers (n=6). **(D)** Box and whisker plot depicting TP53 expression by PCR. **(E)** Box and whisker plot depicting Mdm2 expression by PCR. Correlation plots depicting **(F)** TP53 vs. PTSD score, **(G)** TP53 vs age of cohort, **(H)** TP53 vs. Depression score, and **(I)** TP53 vs. Anxiety score. Box and whisker bars depict maximum and minimum values, with middle bar depicted at the median. For box and whisker plots, significance was determined using an unpaired standard t test. For correlation plots, Pearson correlation test was used to determine significance. Significance was defined as having p-value ≤ 0.05 (*).

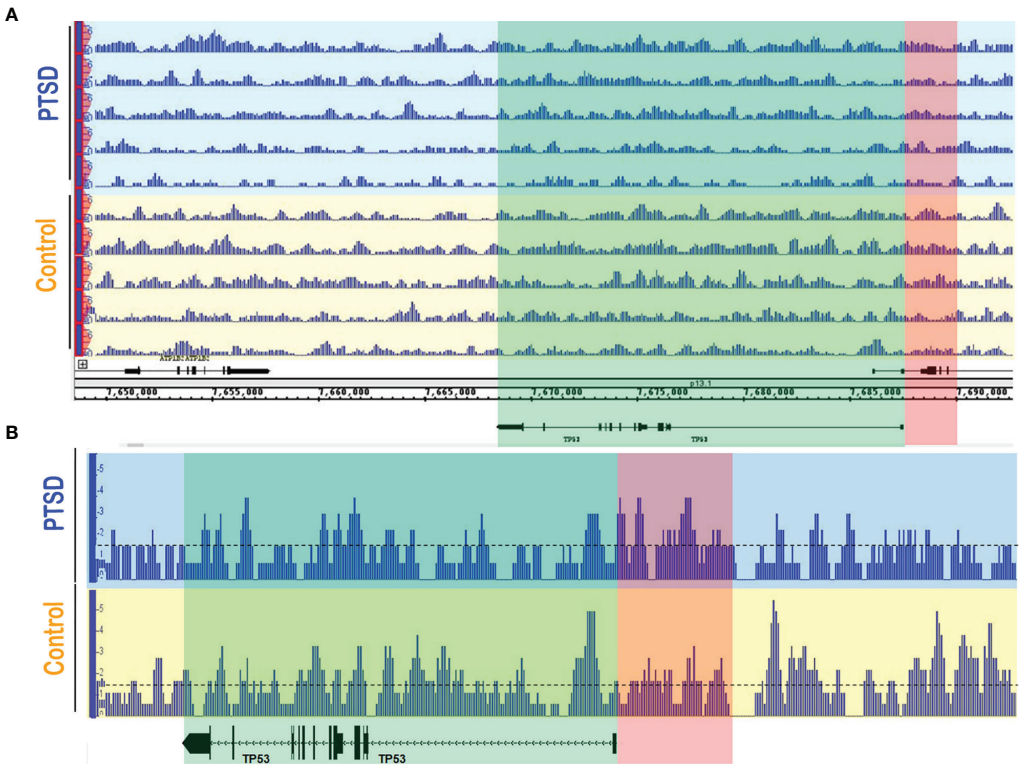

FIGURE 4 | PTSD PBMCs had increased DNA methylation in TP53 promoter region. MeDIP-seq was performed on randomly selected PTSD (n=5) and Control (n=5) PBMC samples. Visualization of the methylated genome was acquired in the IGB genome browser (www.bioviz.org) for **(A)** individual samples, and **(B)** combined samples within respective groups. Blue sections indicate PTSD samples, and yellow sections represent Controls. Green section indicates the TP53 gene, while the red section represents one of the known TP53 promoter regions (~5kb) provided in the Ensembl genome browser (www.ensembl.org). For combined data, a line at 1.5 value was drawn to better visualize methylation intensity between the two groups. Differences observed are qualitative measures in which increased signal intensity (e.g. peak height and width) signify more DNA methylation. Signal intensity in the PTSD group was greater overall in the TP53 promoter compared to Control samples.

Th17 phenotype due to dysregulation of the P53/let-7a axis, which under normal conditions would aid in regulating this T cell-mediated inflammatory response.

DISCUSSION

PTSD is a psychiatric disorder characterized by exposure to profound traumatic events that result in acute (less than 3 months), chronic (3 months or more), or delayed (occurring months or years after event) onset. Core symptoms are reminders that trigger memories of traumatic events, suppression of memories of the traumatic events, recurrence of disturbing flashbacks, avoidance or emotional numbing, and hyperarousal (4). In addition to these negative impacts on mental health, research has revealed a profound alteration of the immune system in patients with PTSD, which results in a higher risk for developing autoimmune and inflammatory disorders (16). During stressful events, the hypothalamic-pituitary-adrenal (HPA) axis is mobilized, which can activate the sympathetic nervous system to release adrenergic hormones (38). All lymphocytes express adrenergic receptors in varying degrees, including T cells (39, 40). In conjuncture with this notion that stress can have an impact on T cells, research has shown that people suffering from PTSD have increased T cell number and enhanced T cell function (6, 41–43). However, it is also important to note conflicting reports have also shown reduced T cell number and function in some cases of PTSD (44–46). Interestingly, in the cases reporting a reduction, these studies examined non-combat PTSD subjects, while cases showing an increase were from combat-associated PTSD. In this report and our previous report, we noted an increased inflammatory T cell response, but once again, this was observed more in veteran patients (27). Therefore, the type of trauma-inducing PTSD may play a significant role in T cell modulation outcome, and thus should be taken into consideration. More importantly, studies examining PTSD should also take into account certain cell types and not just general PBMCs, particularly in the case of CD4+ T cells, which have pro- and anti-inflammatory roles.

Generally, CD4+ T helper (Th) cells can be divided into pro- (Th1 and Th17) and anti- (Th2 and Treg) inflammatory subsets (47). In our previous report examining CD4+ T helper subsets in PTSD patients, we found that PTSD subjects had increased proportions of pro-inflammatory (Th1 and Th17) and reduced (Treg) or unchanged (Th2) anti-inflammatory CD4+ T cell

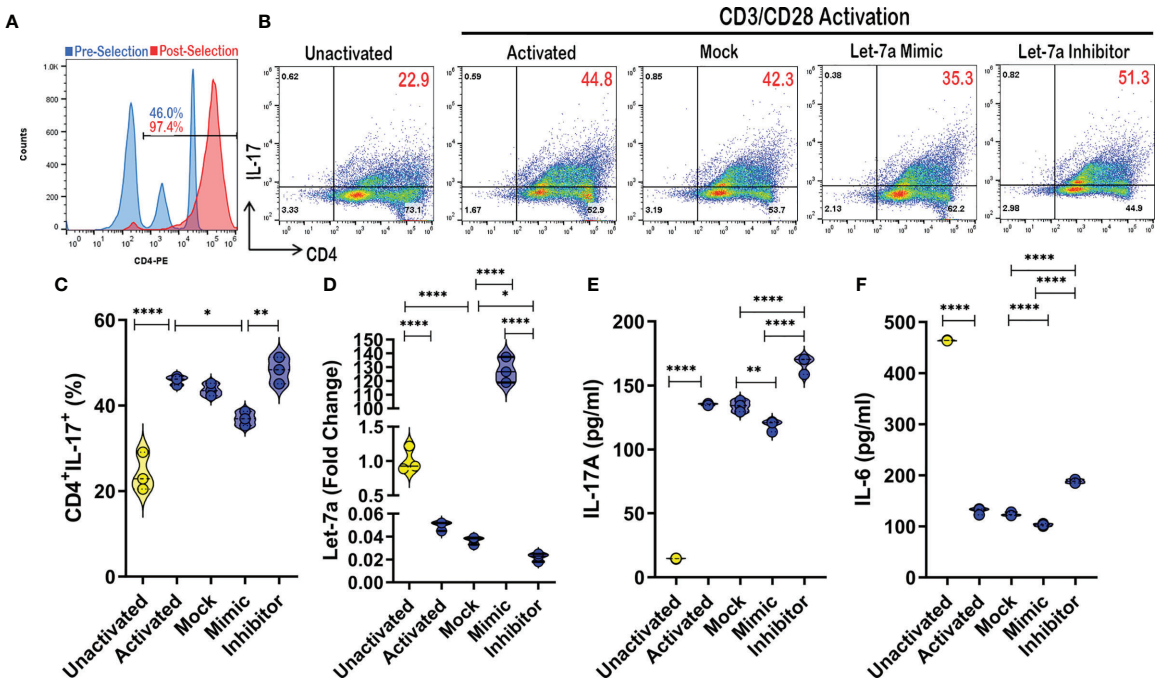

FIGURE 5 | Let-7a modulation affects Th17 development and function. **(A)** CD4+ cells were purified using magnetic bead separation from PBMCs provided by healthy control donor, which was validated using flow cytometry to ensure purity (>95%). **(B)** Representative flow cytometry plots depicting Th17 cells (CD4+IL-17A +) in unactivated or CD3/CD28 activation cultures (24 hours) in the absence or presence of mock, let-7a mimic, or let-7a inhibitor. Red numbers indicating double positive TH17 percentage. **(C)** Violin plot depicting Th17 percentages as assessed by flow cytometry. **(D)** Violin plot depicting expression of let-7a as assessed by PCR. **(E)** Violin plot depicting IL-17 concentration as assessed by ELISA from cell culture supernatants. **(F)** Violin plot depicting IL-6 concentration as assessed by ELISA from cell culture supernatants. *In vitro* data are representative of at least 3 independent experiments, with 3 samples per culture condition. One way ANOVA was used to determine significance between groups. Significance was determined as p-value ≤ 0.05(*), ≤ 0.01(**), ≤ 0.001(***).

subsets (27). In support of our findings, Gola and colleagues also showed PBMCs from PTSD patients spontaneously produced higher levels of IL-6, one of the key cytokines involved in Th17 differentiation (26). In our previous reports, we also provided possible mechanisms leading to the development of an increased inflammatory phenotype, which include miRNA modulation and epigenetic modifications to inflammatory-related genes and pathways, such as the Wnt signaling pathway (31). Building upon these results, we also noted an interesting association of PTSD with TP53 in the current study.

Our highlighted mechanism involving TP53 dysregulation in PTSD subjects is both supported and contradicted by other reports analyzing gene expression profiles of PBMCS from PTSD patients (48, 49). In the report from Dong et al., researchers noted TP53 was the most dysregulated gene in PTSD patients when compared to control samples, but interestingly the expression was elevated (48). On the other hand, in support of our current findings, Breen et al. noted that TP53 was downregulated in PTSD-positive samples (49). The discrepancy once again might be better explained with more careful analysis in the future, one that takes into account the type of trauma and cell type, admittedly a limitation even in the current report. In particular, it will be crucial in future studies to validate many of these findings (e.g. TP53 expression and DNA promoter methylation, let-7a levels) in purified CD4+ T cell populations from PTSD and control samples, as opposed to whole circulating PBMC populations, which consists of a variety of different immune cell types. However, it is interesting to take in consideration what we currently know about TP53 and how it regulates the Th17 inflammatory response. TP53 has not only been shown to negatively regulate the function and differentiation of Th17 effector cells (50), but has also been shown to play a role in the biogenesis of several miRNA (51), small non-coding RNA molecules known to regulate several cellular functions including the development of Th17 cells (52). In response to DNA damage or some abnormal oncogene activation, TP53 will act as a tumor suppressor by preventing tumor growth and development through several pathways including apoptosis, senescence, and cell cycle arrest (53). There are an abundant number of resources and research articles dedicated to the role TP53 plays in cancer and tumor development, but more studies are focusing on the role this protein plays in normal cellular processes, particularly in terms of T cell function. Watanabe and colleagues showed that TP53 plays an important role in antigen-specific CD4+ T cell responses, and proliferation of antigen-activated CD4+ T cells was dependent on the downregulation of TP53 (54). TP53 was also found to induce SLAM-associated protein (SAP), a pro-

apoptotic factor in lymphocytes, in activated primary human T cells as a means to maintain T cell homeostasis (55). More importantly, in a murine model investigating the effects of autoimmunity in p53null CD45.1 mice, these mice were shown to spontaneously develop autoimmunity, characterized by increased presence of Th17 effectors, as well as elevated serum levels of IL-17 and Th17-producing IL-6 (50). Collectively, these data suggested that TP53 is not only a major player in T cell development and function, but it may also support our current findings suggesting that the TP53/let-7a axis may also negatively regulate Th17 CD4+ subsets, warranting further investigation into the role this protein might be play in the Th17-driven immune response in the PTSD population.

It is important to note that other cell types can produce IL-17A, such as γδ T cells, innate lymphoid type cells (ILCs), mast cells, CD8 T cells, natural killer (NK) cells, and neutrophils (56, 57). However, the source of increased IL-17A observed in PTSD patient PBMCs relative to controls in our previous report (27) and highlighted in the current report is more than likely produced by Th17 cells specifically. IL-17A was co-expressed with either CD4 or a combination of CD3 and CD4. This would exclude cytotoxic CD8 T cells, neutrophils, and mast cells. While there has been reports of some mast cells expressing CD4, current literature suggests that normal mast cells do not express this particular cell surface marker (58). In addition, the source of IL-17A is most likely not attributed to γδ T cells or ILCs since even though they can express the CD4, these cell types represent a very minor population in the human PBMCs. In the case of γδ T cells, they are a minor population in circulating PBMCs (0.5-5%, compared to 50% of αβ T cells), are more often expressed in epithelial cell-rich compartments like skin, the digestive tract, and reproductive organ mucosa, and mainly exhibit a CD3+CD4-CD8- phenotype (59). ILCs (ILC1, ILC2, and ILC3) do not normally express CD4 either, and even though a subset of CD4+ILC1 cells have been identified, these cells shared more characteristics with Th1 phenotypes in their cytokine production, as opposed to Th17 (60). In addition, like γδ T cells, ILCs are mainly tissue-associated and have low frequency in circulation, such as the PBMC population (61). NK/NKT cells are also lowly expressed in PBMCs compared to T helper cell subsets (62), and in addition, NK cells do not normally express T cell-associated CD3. Collectively, these observations strongly suggest the source of increased IL-17A in PTSD patients is most likely derived from CD4+ Th17 cells, which is supported by a report from Hefele et al. which showed trauma can increase IL-17A specifically in Th17 subsets (63).

Regarding the link between TP53 and miRNA let-7a in our current report, TP53 is known to enhance the maturation of several miRNA already, such as the let-7 family, miR-200c, miR-143, miR-16, miR-145, and miR-21 (64–66). miRNA play a crucial role in the regulation of many biological cellular processes, including CD4+ T cell development, proliferation, differentiation, and function (67). Of particular interest is the fact that let-7a, a member of the let-7 family of miRNAs, was shown to decrease IL-6-dependent Th17 differentiation and production of Th17-specific cytokines in a murine model of Con A-induced hepatitis (68). Let-7 members are known to be direct negative regulators of IL-6 and small guanosine triphosphatases (GTPases) Ras proteins, which play important roles in inducing Th17 cells and IL-17, respectively (69, 70). In cancer cells, TP53 plays an important role in the induction of let-7a (37), and let-7a along with TP53 were shown to regulate Ras in a colorectal cancer cell line (36). This would suggest that let-7a-mediated effects on Th17 function involves a possible indirect relationship between this microRNA and IL-17A, since examination of publicly-available miRNA-target gene prediction websites such as miRdatabase (http://mirdb.org/) and TargetScan (http://www.targetscan.org/) revealed human let-7a did not bind directly to IL-17A transcripts. However, as noted in **Figure 2** of the current report, let-7a can inhibit Ras proteins, which have been implicated in the development of Th17 and production of IL-17 (71). In studies by Zayoud et al., Ras protein inhibitors were found to suppress *in vivo* induction of splenic Th17 cells. In the same report, *in vitro* polarization of Th17 was also perturbed using Ras inhibition. Therefore, it would stand to reason that TP53 downregulation leading to decreased let-7a would prevent directed inhibition of Ras proteins, thereby leading to increased Th17 polarization and IL-17A production in T cells.

Collectively, the current report offers support for the hypothesis that dysregulation of the TP53/let-7a axis could lead to an increased inflammatory Th17 phenotype. This provides evidence in the underreported role of TP53 in PTSD, which is becoming increasingly more prevalent as cases of PTSD are currently on the rise due to the COVID-19 pandemic (72, 73). Despite these exciting findings, the current report does have limitations that must be addressed in future studies. In addition to a relatively overall low sample size, new data generated in the current report contain samples with results more prevalent to both males (sex bias) and African Americans (race/ethnicity bias). Future studies should and must focus now on evaluating these key findings presented in larger and more diverse patient cohorts, with special emphasis on how types of trauma (e.g. combat vs non-combat) and other factors (e.g. sex or race/ethnicity) might affect the TP53/let-7a axis and the subsequent susceptibility to an inflammatory Th17 phenotype in PTSD patients. In addition, and as noted earlier in the discussion, key findings from the current report must be validated specifically in the CD4+ T cell population of patient cohorts as it relates to epigenetic modifications, such as DNA methylation in the TP53 promoter region and let-7a levels. For example, while published reports have shown that TP53 activation can induce let-7a in various human cell lines (74), these findings will need to be further corroborated in human CD4+ T cells by manipulating TP53 (activation and silencing) in this particular cell subset and evaluating how these changes effect let-7a levels. Lastly, based on the more qualitative nature of the MeDIPseq results showing hypermethylation of the TP53 promoter in PTSD patients compared to controls in the current report, ample justification is now provided to examine this observation in a more quantitative assay (e.g. methylation-specific PCR, or MSP) in a larger human subject cohort.

DATA AVAILABILITY STATEMENT

Publicly available datasets were analyzed in this study. This data can be found here: The datasets generated for this study can be found in the following online repositories: ArrayExpress (E-MTAB-4880) (https://www.ebi.ac.uk/arrayexpress/experiments/E-MTAB-4880/) or Gene Expression Omnibus (GEO; GSE860) (https://www.ncbi.nlm.nih.gov/geo/query/acc.cgi?acc=GSE860).

ETHICS STATEMENT

Procedures to collect human samples presented in this report were approved and reviewed by the Institutional Review Boards (IRBs) from the University of South Carolina, the University of Michigan, and the University of North Carolina-Chapel Hill. The patients/participants provided their written informed consent to participate in this study.

AUTHOR CONTRIBUTIONS

The following contributions in the current report acknowledge the roles of the listed authors as follows: PB, MN, and PN contributed to conception and design of the study. PB, MB, XY, JZ, OA, and JG conducted the experiments. JG, MU and AA provided samples and assisted with statistical analysis. PB wrote the first draft of the manuscript. PB, MN, PN, MB, XY, JZ, OA, JG, MU, and AA contributed to manuscript revision and read and approved the submitted version.

FUNDING

The work was supported by funding from the National Institutes of Health (NIH) [R01ES019313, R01MH094755, R01AI123947, R01AI129788, P01AT003961, P20GM103641, R01AT006888].

REFERENCES

1. Yehuda R. Post-Traumatic Stress Disorder. *N Engl J Med* (2002) 346(2):108–14. doi: 10.1056/NEJMra012941
2. Kolassa IT, Kolassa S, Ertl V, Papassotiropoulos A, De Quervain DJ. The Risk of Posttraumatic Stress Disorder After Trauma Depends on Traumatic Load and the Catechol-O-Methyltransferase Val(158)Met Polymorphism. *Biol Psychiatry* (2010) 67(4):304–8. doi: 10.1016/j.biopsych.2009.10.009
3. Gola H, Engler H, Schauer M, Adenauer H, Riether C, Kolassa S, et al. Victims of Rape Show Increased Cortisol Responses to Trauma Reminders: A Study in Individuals With War- and Torture-Related PTSD. *Psychoneuroendocrinology* (2012) 37(2):213–20. doi: 10.1016/j.psyneuen.2011.06.005
4. American Psychiatric Association and American Psychiatric Association. *DSM-5 Task Force. Diagnostic and Statistical Manual of Mental Disorders : DSM-5. 5th ed* Vol. xliv, 947. Washington, D.C: American Psychiatric Association (2013). p. ISBN: 9780890425541 (hardcover alk. paper) 9780890425558 (pbk. alk. paper).
5. Schnurr PP, Jankowski MK. Physical Health and Post-Traumatic Stress Disorder: Review and Synthesis. *Semin Clin Neuropsychiatry* (1999) 4 (4):295–304. doi: 10.153/SCNP00400295
6. Boscarino JA. Posttraumatic Stress Disorder and Physical Illness: Results From Clinical and Epidemiologic Studies. *Ann N Y Acad Sci* (2004) 1032:141–53. doi: 10.1196/annals.1314.011
7. Mikuls TR, Padala PR, Sayles HR, Yu F, Michaud K, Caplan L, et al. Prospective Study of Posttraumatic Stress Disorder and Disease Activity Outcomes in US Veterans With Rheumatoid Arthritis. *Arthritis Care Res (Hoboken)* (2013) 65(2):227–34. doi: 10.1002/acr.21778
8. Talbot LS, Maguen S, Epel ES, Metzler TJ, Neylan TC. Posttraumatic Stress Disorder Is Associated With Emotional Eating. *J Trauma Stress* (2013) 26 (4):521–5. doi: 10.1002/jts.21824
9. Ivanova JI, Birnbaum HG, Chen L, Duhig AM, Dayoub EJ, Kantor ES, et al. Cost of Post-Traumatic Stress Disorder vs Major Depressive Disorder Among Patients Covered by Medicaid or Private Insurance. *Am J Manag Care* (2011) 17(8):e314–23.
10. Keane TM, Marshall AD, Taft CT. Posttraumatic Stress Disorder: Etiology, Epidemiology, and Treatment Outcome. *Annu Rev Clin Psychol* (2006) 2:161–97. doi: 10.1146/annurev.clinpsy.2.022305.095305
11. Schlenger WE, Corry NH, Kulka RA, Williams CS, Henn-Haase C, Marmar CR. Design and Methods of the National Vietnam Veterans Longitudinal Study. *Int J Methods Psychiatr Res* (2015) 24(3):186–203. doi: 10.1002/mpr.1469
12. Cohen BE, Gima K, Bertenthal D, Kim S, Marmar CR, Seal KH. Mental Health Diagnoses and Utilization of VA non-Mental Health Medical Services Among Returning Iraq and Afghanistan Veterans. *J Gen Intern Med* (2010) 25(1):18–24. doi: 10.1007/s11606-009-1117-3
13. Holmes MR, Rentrope CR, Korsch-Williams A, King JA. Impact of COVID-19 Pandemic on Posttraumatic Stress, Grief, Burnout, and Secondary Trauma of Social Workers in the United States. *Clin Soc Work J* (2021) 2:1–10. doi: 10.1007/s10615-021-00795-y
14. Einvik G, Dammen T, Ghanima W, Heir T, Stavem K. Prevalence and Risk Factors for Post-Traumatic Stress in Hospitalized and Non-Hospitalized COVID-19 Patients. *Int J Environ Res Public Health* (2021) 18(4):2079–91. doi: 10.3390/ijerph18042079
15. Chamberlain SR, Grant JE, Trender W, Hellyer P, Hampshire A. Post-Traumatic Stress Disorder Symptoms in COVID-19 Survivors: Online Population Survey. *BJPsych Open* (2021) 7(2):e47. doi: 10.1192/bjo.2021.3
16. O'Donovan A, Chao LL, Paulson J, Samuelson KW, Shigenaga JK, Grunfeld C, et al. Altered Inflammatory Activity Associated With Reduced Hippocampal Volume and More Severe Posttraumatic Stress Symptoms in Gulf War Veterans. *Psychoneuroendocrinology* (2015) 51:557–66. doi: 10.1016/j.psyneuen.2014.11.010
17. Groer MW, Kane B, Williams SN, Duffy A. Relationship of PTSD Symptoms With Combat Exposure, Stress, and Inflammation in American Soldiers. *Biol Res Nurs* (2015) 17(3):303–10. doi: 10.1177/1099800414544949
18. Lindqvist D, Wolkowitz OM, Mellon S, Yehuda R, Flory JD, Henn-Haase C, et al. Proinflammatory Milieu in Combat-Related PTSD Is Independent of Depression and Early Life Stress. *Brain Behav Immun* (2014) 42:81–8. doi: 10.1016/j.bbi.2014.06.003
19. Wilson CB, McLaughlin LD, Nair A, Ebenezer PJ, Dange R, Francis J. Inflammation and Oxidative Stress Are Elevated in the Brain, Blood, and Adrenal Glands During the Progression of Post-Traumatic Stress Disorder in a Predator Exposure Animal Model. *PloS One* (2013) 8(10):e76146. doi: 10.1371/journal.pone.0076146
20. Heath NM, Chesney SA, Gerhart JI, Goldsmith RE, Luborsky JL, Stevens NR, et al. Interpersonal Violence, PTSD, and Inflammation: Potential Psychogenic Pathways to Higher C-Reactive Protein Levels. *Cytokine* (2013) 63(2):172–8. doi: 10.1016/j.cyto.2013.04.030
21. Pace TW, Wingenfeld K, Schmidt I, Meinlschmidt G, Hellhammer DH, Heim CM. Increased Peripheral NF-kappaB Pathway Activity in Women With Childhood Abuse-Related Posttraumatic Stress Disorder. *Brain Behav Immun* (2012) 26(1):13–7. doi: 10.1016/j.bbi.2011.07.232
22. Smith AK, Conneely KN, Kilaru V, Mercer KB, Weiss TE, Bradley B, et al. Differential Immune System DNA Methylation and Cytokine Regulation in Post-Traumatic Stress Disorder. *Am J Med Genet B Neuropsychiatr Genet* (2011) 156B(6):700–8. doi: 10.1002/ajmg.b.31212

23. Gill JM, Saligan L, Woods S, Page G. PTSD Is Associated With an Excess of Inflammatory Immune Activities. *Perspect Psychiatr Care* (2009) 45(4):262–77. doi: 10.1111/j.1744-6163.2009.00229.x
24. Fesharaki-Zadeh A, Miyauchi JT, St Laurent-Arriot K, Tsirka SE, Bergold PJ. Increased Behavioral Deficits and Inflammation in a Mouse Model of Co-Morbid Traumatic Brain Injury and Post-Traumatic Stress Disorder. *ASN Neuro* (2020) 12:1759091420979567. doi: 10.1177/1759091420979567
25. Fonkoue IT, Michopoulos V, Park J. Sex Differences in Post-Traumatic Stress Disorder Risk: Autonomic Control and Inflammation. *Clin Auton Res* (2020) 30(5):409–21. doi: 10.1007/s10286-020-00729-7
26. Gola H, Engler H, Sommershof A, Adenauer H, Kolassa S, Schedlowski M, et al. Posttraumatic Stress Disorder Is Associated With an Enhanced Spontaneous Production of Pro-Inflammatory Cytokines by Peripheral Blood Mononuclear Cells. *BMC Psychiatry* (2013) 13:40. doi: 10.1186/1471-244X-13-40
27. Zhou J, Nagarkatti P, Zhong Y, Ginsberg JP, Singh NP, Zhang J, et al. Dysregulation in microRNA Expression Is Associated With Alterations in Immune Functions in Combat Veterans With Post-Traumatic Stress Disorder. *PloS One* (2014) 9(4):e94075. doi: 10.1371/journal.pone.0094075
28. Bam M, Yang X, Zhou J, Ginsberg JP, Leyden Q, Nagarkatti PS, et al. Evidence for Epigenetic Regulation of Pro-Inflammatory Cytokines, Interleukin-12 and Interferon Gamma, in Peripheral Blood Mononuclear Cells From PTSD Patients. *J Neuroimmune Pharmacol* (2016) 11(1):168–81. doi: 10.1007/s11481-015-9643-8
29. Bam M, Yang X, Zumbrun EE, Zhong Y, Zhou J, Ginsberg JP, et al. Dysregulated Immune System Networks in War Veterans With PTSD Is an Outcome of Altered miRNA Expression and DNA Methylation. *Sci Rep* (2016) 6:31209. doi: 10.1038/srep31209
30. Bam M, Yang X, Zumbrun EE, Ginsberg JP, Leyden Q, Zhang J, et al. Decreased AGO2 and DCR1 in PBMCs From War Veterans With PTSD Leads to Diminished miRNA Resulting in Elevated Inflammation. *Transl Psychiatry* (2017) 7(8):e1222. doi: 10.1038/tp.2017.185
31. Bam M, Yang X, Busbee BP, Aiello AE, Uddin M, Ginsberg JP, et al. Increased H3K4me3 Methylation and Decreased miR-7113-5p Expression Lead to Enhanced Wnt/beta-Catenin Signaling in Immune Cells From PTSD Patients Leading to Inflammatory Phenotype. *Mol Med* (2020) 26(1):110. doi: 10.1186/s10020-020-00238-3
32. Uddin M, Aiello AE, Wildman DE, Koenen KC, Pawelec G, de Los Santos R, et al. Epigenetic and Immune Function Profiles Associated With Posttraumatic Stress Disorder. *Proc Natl Acad Sci USA* (2010) 107 (20):9470–5. doi: 10.1073/pnas.0910794107
33. Segman RH, Shefi N, Goltser-Dubner T, Friedman N, Kaminski N, Shalev AY. Peripheral Blood Mononuclear Cell Gene Expression Profiles Identify Emergent Post-Traumatic Stress Disorder Among Trauma Survivors. *Mol Psychiatry* (2005) 10(5):500–13, 425. doi: 10.1038/sj.mp.4001636
34. Langmead B, Trapnell C, Pop M, Salzberg SL. Ultrafast and Memory-Efficient Alignment of Short DNA Sequences to the Human Genome. *Genome Biol* (2009) 10(3):R25. doi: 10.1186/gb-2009-10-3-r25
35. Lienhard M, Grimm C, Morkel M, Herwig R, Chavez L. MEDIPS: Genome-Wide Differential Coverage Analysis of Sequencing Data Derived From DNA Enrichment Experiments. *Bioinf* (2014) 30(2):284–6. doi: 10.1093/bioinformatics/btt650
36. Luu C, Heinrich EL, Duldulao M, Arrington AK, Fakih M, Garcia-Aguilar J, et al. TP53 and Let-7a Micro-RNA Regulate K-Ras Activity in HCT116 Colorectal Cancer Cells. *PloS One* (2013) 8(8):e70604. doi: 10.1371/journal.pone.0070604
37. Lee JY, Kim HJ, Yoon NA, Lee WH, Min YJ, Ko BK, et al. Tumor Suppressor P53 Plays a Key Role in Induction of Both Tristetraprolin and Let-7 in Human Cancer Cells. *Nucleic Acids Res* (2013) 41(11):5614–25. doi: 10.1093/nar/gkt222
38. Griffin GD, Charron D, Al-Daccak R. Post-Traumatic Stress Disorder: Revisiting Adrenergics, Glucocorticoids, Immune System Effects and Homeostasis. *Clin Transl Immunol* (2014) 3(11):e27. doi: 10.1038/cti.2014.26
39. Anstead MI, Hunt TA, Carlson SL, Burki NK. Variability of Peripheral Blood Lymphocyte Beta-2-Adrenergic Receptor Density in Humans. *Am J Respir Crit Care Med* (1998) 157(3 Pt 1):990–2. doi: 10.1164/ajrccm.157.3.9704071
40. Landmann R. Beta-Adrenergic Receptors in Human Leukocyte Subpopulations. *Eur J Clin Invest* (1992) 22(Suppl 1):30–6.
41. Boscarino JA, Chang J. Higher Abnormal Leukocyte and Lymphocyte Counts 20 Years After Exposure to Severe Stress: Research and Clinical Implications. *Psychosom Med* (1999) 61(3):378–86. doi: 10.1097/00006842-199905000-00019
42. Sommershof A, Aichinger H, Engler H, Adenauer H, Catani C, Boneberg EM, et al. Substantial Reduction of Naive and Regulatory T Cells Following Traumatic Stress. *Brain Behav Immun* (2009) 23(8):1117–24. doi: 10.1016/j.bbi.2009.07.003
43. Altemus M, Dhabhar FS, Yang R. Immune Function in PTSD. *Ann N Y Acad Sci* (2006) 1071:167–83. doi: 10.1196/annals.1364.013
44. Kawamura N, Kim Y, Asukai N. Suppression of Cellular Immunity in Men With a Past History of Posttraumatic Stress Disorder. *Am J Psychiatry* (2001) 158(3):484–6. doi: 10.1176/appi.ajp.158.3.484
45. Ironson G, Wynings C, Schneiderman N, Baum A, Rodriguez M, Greenwood D, et al. Posttraumatic Stress Symptoms, Intrusive Thoughts, Loss, and Immune Function After Hurricane Andrew. *Psychosom Med* (1997) 59 (2):128–41. doi: 10.1097/00006842-199703000-00003
46. Sabioncello A, Kocijan-Hercigonja D, Rabatic S, Tomasic J, Jeren T, Matijevic L, et al. Immune, Endocrine, and Psychological Responses in Civilians Displaced by War. *Psychosom Med* (2000) 62(4):502–8. doi: 10.1097/00006842-200007000-00008
47. Weinmann AS. Roles for Helper T Cell Lineage-Specifying Transcription Factors in Cellular Specialization. *Adv Immunol* (2014) 124:171–206. doi: 10.1016/B978-0-12-800147-9.00006-6
48. Dong K, Zhang F, Zhu W, Wang Z. Wang G. Partial Least Squares Based Gene Expression Analysis in Posttraumatic Stress Disorder. *Eur Rev Med Pharmacol Sci* (2014) 18(16):2306–10.
49. Breen MS, Bierer LM, Daskalakis NP, Bader HN, Makotkine I, Chattopadhyay M, et al. Correction: Differential Transcriptional Response Following Glucocorticoid Activation in Cultured Blood Immune Cells: A Novel Approach to PTSD Biomarker Development. *Transl Psychiatry* (2020) 10 (1):1. doi: 10.1038/s41398-019-0665-5
50. Zhang S, Zheng M, Kibe R, Huang Y, Marrero L, Warren S, et al. Trp53 Negatively Regulates Autoimmunity *via* the STAT3-Th17 Axis. *FASEB J* (2011) 25(7):2387–98. doi: 10.1096/fj.10-175299
51. Suzuki HI, Yamagata K, Sugimoto K, Iwamoto T, Kato S, Miyazono K. Modulation of microRNA Processing by P53. *Nat* (2009) 460(7254):529–33. doi: 10.1038/nature08199
52. Wei B, Pei G. microRNAs: Critical Regulators in Th17 Cells and Players in Diseases. *Cell Mol Immunol* (2010) 7(3):175–81. doi: 10.1038/cmi.2010.19
53. Kruse JP, Gu W. Modes of P53 Regulation. *Cell* (2009) 137(4):609–22. doi: 10.1016/j.cell.2009.04.050
54. Watanabe M, Moon KD, Vacchio MS, Hathcock KS, Hodes RJ. Downmodulation of Tumor Suppressor P53 by T Cell Receptor Signaling Is Critical for Antigen-Specific CD4(+) T Cell Responses. *Immun* (2014) 40 (5):681–91. doi: 10.1016/j.immuni.2014.04.006
55. Madapura HS, Salamon D, Wiman KG, Lain S, Klein G, Klein E, et al. P53 Contributes to T Cell Homeostasis Through the Induction of Pro-Apoptotic SAP. *Cell Cycle* (2012) 11(24):4563–9. doi: 10.4161/cc.22810
56. Korn T, Bettelli E, Oukka M, Kuchroo VK. IL-17 and Th17 Cells. *Annu Rev Immunol* (2009) 27:485–517. doi: 10.1146/annurev.immunol.021908.132710
57. Geha M, Tsokos MG, Bosse RE, Sannikova T, Iwakura Y, Dalle Lucca JJ, et al. IL-17a Produced by Innate Lymphoid Cells Is Essential for Intestinal Ischemia-Reperfusion Injury. *J Immunol* (2017) 199(8):2921–9. doi: 10.4049/jimmunol.1700655
58. Soliman DS, Al-Sabbagh A, Ibrahim F, Gameil A, Yassin M, El-Omri H. Highly Aggressive CD4-Positive Mast Cell Leukaemia (Leukaemic Variant) Associated With Isolated Trisomy 19 and Hemophagocytosis by Neoplastic Mast Cells: A Case Report With Challenging Experience and Review. *Case Rep Hematol* (2019) 2019:1805270. doi: 10.1155/2019/1805270
59. Mao Y, Yin S, Zhang J, Hu Y, Huang B, Cui L, et al. A New Effect of IL-4 on Human Gammadelta T Cells: Promoting Regulatory Vdelta1 T Cells *via* IL-10 Production and Inhibiting Function of Vdelta2 T Cells. *Cell Mol Immunol* (2016) 13(2):217–28. doi: 10.1038/cmi.2015.07
60. Roan F, Stoklasek TA, Whalen E, Molitor JA, Bluestone JA, Buckner JH, et al. CD4+ Group 1 Innate Lymphoid Cells (ILC) Form a Functionally Distinct

ILC Subset That Is Increased in Systemic Sclerosis. *J Immunol* (2016) 196 (5):2051–62. doi: 10.4049/jimmunol.1501491
61. Bonne-Annee S, Bush MC, Nutman TB. Differential Modulation of Human Innate Lymphoid Cell (ILC) Subsets by IL-10 and TGF-Beta. *Sci Rep* (2019) 9 (1):14305. doi: 10.1038/s41598-019-50308-8
62. Angelo LS, Banerjee PP, Monaco-Shawver L, Rosen JB, Makedonas G, Forbes LR, et al. Practical NK Cell Phenotyping and Variability in Healthy Adults. *Immunol Res* (2015) 62(3):341–56. doi: 10.1007/s12026-015-8664-y
63. Hefele F, Ditsch A, Krysiak N, Caldwell CC, Biberthaler P, van Griensven M, et al. Trauma Induces Interleukin-17a Expression on Th17 Cells and CD4+ Regulatory T Cells as Well as Platelet Dysfunction. *Front Immunol* (2019) 10:2389. doi: 10.3389/fimmu.2019.02389
64. Boominathan L. The Tumor Suppressors P53, P63, and P73 are Regulators of microRNA Processing Complex. *PloS One* (2010) 5(5):e10615. doi: 10.1371/journal.pone.0010615
65. Garibaldi F, Falcone E, Trisciuoglio D, Colombo T, Lisek K, Walerych D, et al. Mutant P53 Inhibits miRNA Biogenesis by Interfering With the Microprocessor Complex. *Oncogene* (2016) 35(29):3760–70. doi: 10.1038/onc.2016.51
66. Gurtner A, Falcone E, Garibaldi F, Piaggio G. Dysregulation of microRNA Biogenesis in Cancer: The Impact of Mutant P53 on Drosha Complex Activity. *J Exp Clin Cancer Res* (2016) 35:45. doi: 10.1186/s13046-016-0319-x
67. Liu J, Wu CP, Lu BF, Jiang JT. Mechanism of T Cell Regulation by microRNAs. *Cancer Biol Med* (2013) 10(3):131–7. doi: 10.7497/j.issn.2095-3941.2013.03.002
68. Zhang Y, Wang X, Zhong M, Zhang M, Suo Q, Lv K. MicroRNA Let-7a Ameliorates Con A-Induced Hepatitis by Inhibiting IL-6-Dependent Th17 Cell Differentiation. *J Clin Immunol* (2013) 33(3):630–9. doi: 10.1007/s10875-012-9840-7
69. Choudhury SN, Li Y. miR-21 and Let-7 in the Ras and NF-kappaB Pathways. *Microrna* (2012) 1(1):65–9. doi: 10.2174/2211536611201010065
70. Johnson SM, Grosshans H, Shingara J, Byrom M, Jarvis R, Cheng A, et al. RAS is Regulated by the Let-7 microRNA Family. *Cell* (2005) 120(5):635–47. doi: 10.1016/j.cell.2005.01.014
71. Zayoud M, Vax E, Elad-Sfadia G, Barshack I, Pinkas-Kramarski R, Goldstein I. Inhibition of Ras GTPases Prevents Collagen-Induced Arthritis by Reducing the Generation of Pathogenic CD4(+) T Cells and the Hyposialylation of Autoantibodies. *ACR Open Rheumatol* (2020) 2(9):512–24. doi: 10.1002/acr2.11169
72. Liu N, Zhang F, Wei C, Jia Y, Shang Z, Sun L, et al. Prevalence and Predictors of PTSS During COVID-19 Outbreak in China Hardest-Hit Areas: Gender Differences Matter. *Psychiatry Res* (2020) 287:112921. doi: 10.1016/j.psychres.2020.112921
73. Dutheil F, Mondillon L, Navel V. PTSD as the Second Tsunami of the SARS-Cov-2 Pandemic. *Psychol Med* (2020) 24:1–2. doi: 10.1017/S0033291720001336
74. Tarasov V, Jung P, Verdoodt B, Lodygin D, Epanchintsev A, Menssen A, et al. Differential Regulation of microRNAs by P53 Revealed by Massively Parallel Sequencing: miR-34a is a P53 Target That Induces Apoptosis and G1-Arrest. *Cell Cycle* (2007) 6(13):1586–93. doi: 10.4161/cc.6.13.4436

Conflict of Interest: The authors declare that the research was conducted in the absence of any commercial or financial relationships that could be construed as a potential conflict of interest.

Publisher's Note: All claims expressed in this article are solely those of the authors and do not necessarily represent those of their affiliated organizations, or those of the publisher, the editors and the reviewers. Any product that may be evaluated in this article, or claim that may be made by its manufacturer, is not guaranteed or endorsed by the publisher.

frontiers in Immunology

ORIGINAL RESEARCH
published: 05 January 2022
doi: 10.3389/fimmu.2021.803633

Characteristics of Dysregulated Proinflammatory Cytokines and Cognitive Dysfunction in Late-Life Depression and Amnestic Mild Cognitive Impairment

Jing Nie[1†], Yuan Fang[1†], Ying Chen[2,3†], Aisikeer Aidina[1], Qi Qiu[1], Lu Zhao[1], Xiang Liu[1], Lin Sun[1], Yun Li[2,3], Chuwen Zhong[1], Yuan Li[1] and Xia Li[1*]*

[1] Shanghai Mental Health Center, Shanghai Jiaotong University, School of Medicine, Shanghai, China, [2] Department of Otolaryngology-Head and Neck Surgery, Shanghai Ninth People's Hospital, Shanghai Jiao Tong University School of Medicine, Shanghai, China, [3] Ear Institute, Shanghai Jiao Tong University School of Medicine, Shanghai Key Laboratory of Translational Medicine on Ear and Nose Diseases (14DZ2260300), Shanghai, China

Background: Late-life depression (LLD) and amnestic mild cognitive impairment (aMCI) are two different diseases associated with a high risk of developing Alzheimer's disease (AD). Both diseases are accompanied by dysregulation of inflammation. However, the differences and similarities of peripheral inflammatory parameters in these two diseases are not well understood.

Methods: We used Luminex assays to measure 29 cytokines simultaneously in the plasma of two large cohorts of subjects at high risk for AD (23 LLD and 23 aMCI) and 23 normal controls (NCs) in the community. Demographics and lifestyle factors were also collected. Cognitive function was evaluated with the Chinese versions of the Montreal Cognitive Assessment (C-MoCA) and neuropsychological test battery (NTB).

Results: We observed a remarkably increased level of IL-6 in the plasma and reduced levels of chemokines (CXCL11 and CCL13) in the LLD group compared with the aMCI group. The LLD group also showed lower levels of CXCL16 than the NC group. Furthermore, altered cytokine levels were associated with abnormal results in neuropsychological testing and Geriatric Depression Scale scores in both the LLD and aMCI groups. Notably, combinations of cytokines (IL-6 and CCL13) and two subitems of C-MoCA (orientation and short-term memory) generated the best area under the receiver operating characteristic curve (AUROC = 0.974).

Conclusion: A novel model based on proinflammatory cytokines and brief screening tests performs with fair accuracy in the discrimination between LLD and aMCI. These findings will give clues to provide new therapeutic targets for interventions or markers for two diseases with similar predementia syndromes.

Keywords: late-life depression, amnestic mild cognitive impairment, neuroinflammation, cytokines, chemokines

OPEN ACCESS

Edited by:
Juehua Yu,
The First Affiliated Hospital of Kunming Medical University, China

Reviewed by:
Yu Liu,
China Pharmaceutical University, China
Wei Yin,
Sun Yat-sen University, China

***Correspondence:**
Yuan Li
zmd2012spring@126.com
Xia Li
ja_1023@hotmail.com

[†]These authors have contributed equally to this work and share first authorship

Specialty section:
This article was submitted to Multiple Sclerosis and Neuroimmunology, a section of the journal Frontiers in Immunology

Received: *28 October 2021*
Accepted: *30 November 2021*
Published: *05 January 2022*

Citation:
Nie J, Fang Y, Chen Y, Aidina A, Qiu Q, Zhao L, Liu X, Sun L, Li Y, Zhong CW, Li Y and Li X (2022) Characteristics of Dysregulated Proinflammatory Cytokines and Cognitive Dysfunction in Late-Life Depression and Amnestic Mild Cognitive Impairment. Front. Immunol. 12:803633. doi: 10.3389/fimmu.2021.803633

INTRODUCTION

It is expected that by 2050, the number of people with dementia may exceed 131 million. Alzheimer's disease (AD) is the most common type of dementia and is recognized by the WHO as a global public health priority (1). There are no effective medical treatments to cure the disease. However, the prevalence of dementia would be halved if its onset was delayed by 5 years (2). Therefore, the prodromal stage of AD is a great opportunity for effective treatment and postponement of disease onset.

Peripheral inflammatory activation potentially activates the immune system within the blood–brain barrier, playing a potential role in the pathogenesis of AD. Direct and bystander damage from inflammatory mechanisms is likely to significantly exacerbate the very pathogenic processes of AD along a continuum (3). Cytokines are typically produced by cells of the immune system upon activation and play key roles in the development and control of immune responses. Chemokines represent one of the largest subfamilies of cytokines and have been divided into several subgroups based on their chemical structures. CXC and CC are two major subfamilies, depending on whether the first two N-terminal cysteines have an amino acid between them (CXC) or are adjacent to each other (CC) (4). Although chemokines have been relatively neglected in investigations of the mechanisms of psychiatric disorders, recent evidence has begun to demonstrate an association between chemokines and neurobiological processes (5, 6). Dysfunctional cytokines have been associated with both neurodegenerative and psychiatric disorders, including AD, mild cognitive impairment, schizophrenia, depression, and bipolar disorder (7, 8). Increased inflammatory markers such as soluble tumor necrosis factor receptor 2 (sTNFR2), interleukin-6 (IL-6), and monocyte chemoattractant protein-1 (MCP-1) have been reported in patients with dementia compared with controls (9, 10). Although the exact effect of proinflammatory cytokines in AD remains unknown, increasing evidence suggests that inflammation is involved in the pathological process of AD and plays a crucial role in the early stages of disease when intervention may be most beneficial (11).

Late-life depression (LLD) and amnestic mild cognitive impairment (aMCI) subtypes are strongly associated with an increased risk for AD (12). Evidence from prospective studies has supported the notion that LLD is associated with a 2- to 5-fold increased risk of developing AD (13). Older adults with aMCI show typical impairment of episodic memory, which represents the most common symptom of the prodromal stage of AD (14). Compared with 3% of the population without mild cognitive impairment at the same age, approximately 39% of patients with mild cognitive impairment develop dementia over the subsequent 3 to 10 years (15). Although LLD and aMCI are considered to be distinct clinical entities, they share multiple common clinical features (16). Elderly individuals with major depressive disorder can present with significant cognitive impairment, decreased activity, primary motivational impairment, and fewer mood symptoms (17, 18). Cognitive dysfunction in depressed older adults typically consists of memory impairment, poor attention, and impaired executive function (19). Depression is also common in individuals with MCI, with a higher prevalence in aMCI than in non-aMCI (naMCI) and may confer a higher possibility of progression to dementia (20). Identifying individuals at risk for AD or depression will be critical, as clinical trials on prevention interventions or potential treatment may become available in the clinic.

Since neuroinflammation is thought to be involved in the pathogenesis of the disease at an early stage, it is also important to study inflammatory markers in the predementia stage. However, in previous inflammatory marker studies, elderly individuals with major depressive disorder were generally neglected. Therefore, in the current study, we aimed to characterize neuroinflammation in the elderly with aMCI (aMCI) and LLD compared with sex- and age-matched normal controls. Additionally, potential correlations between clinical parameters of proinflammatory cytokines and two diseases were analyzed. This study provides new diagnostic biomarkers targeting neuroinflammation for patients in the predementia stage.

MATERIALS AND METHODS

Subjects and Study Procedure

Figure 1 describes the study design and analysis pipeline. Twenty-three participants diagnosed with aMCI and twenty-three normal controls were concurrently recruited from four different communities in Shanghai. The same number of patients with LLD was recruited according to the *Diagnostic and Statistical Manual of Mental Disorders*, Fifth Edition (DSM-V), by clinicians from an outpatient clinic (21).

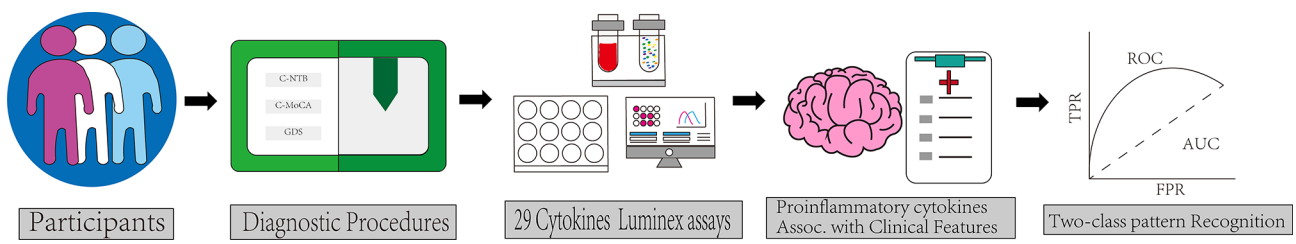

FIGURE 1 | Study design and group comparisons. Participants from Shanghai, China, underwent cytokine level measurements, and 29 cytokines were selected for group comparisons. Receiver operating characteristic (ROC) analysis was adopted to evaluate the ability of cytokines to distinguish two-class patterns.

All participants received clinical diagnoses established by three different geriatric psychiatrists using standardized assessment and review. Clinical diagnosis of aMCI was adapted from Petersen et al. (22), requiring evidence of a definite decline in memory (memory complaints corroborated by an informant and MoCA scores of >1.5 SD of age-appropriate norms or abnormal memory function for age) and without significant impact on daily living, with the severity of symptoms or consequent functional limitation not meeting the criteria for the diagnosis of dementia in DSM-V; a diagnosis of normal control was made if participants demonstrated no evidence of cognitive decline as compared with their baseline cognitive functions on clinical interview and assessment. Patients with LLD were diagnosed according to DSM-V for major depressive disorder with depression onset occurring over 60 years old. The exclusion criteria were as follows: a) dementia or suspected dementia based on clinicians' judgment, b) other psychiatric disorders (except depression) or a substance-use disorder diagnosis, c) any kind of chronic infectious or any sign of peripheral inflammation, or d) any current, clinically significant cardiovascular and cerebrovascular disease.

Clinical Data Collection

All participants were matched according to the mean age and sex. A detailed psychiatric, medical, social, and family history was obtained from each participant. All participants completed the following subtests: Chinese version of Montreal Cognitive Assessment (C-MoCA), Chinese version of neuropsychological test battery (C-NTB) including Wechsler's Memory digit span (WMDS), Category Fluency Test (CFT), Controlled Word Association Test (COWAT), and Geriatric Depression Scale (GDS). This study was approved by the Institutional Review Board of the Shanghai Mental Health Center. Written informed consent was obtained from all participants or their representatives.

Sample Collection and Preparation

Fasting blood samples of CRP were collected *via* peripheral venous access after participants fasted for more than 10 h. After centrifugation (2,500 rpm, 15 min, at 4°C), plasma was collected from EDTA tubes and then stored at −80°C until the assays were performed.

Plasma Cytokine Assays

Using Luminex microbeads, we simultaneously measured the concentrations of 29 cytokines and chemokines (**Table 1**). The plasma samples were thawed at 4°C and centrifuged at 1,500 rpm to remove any aggregate protein that could potentially obstruct the measurement. The human Magnetic Luminex Performance Assay (R&D Systems, no. LXSAHM-33, USA) was used according to the manufacturer's protocol. An X200 (Luminex, Austin, TX) was used to read the multiplex assay.

Statistical Analysis

Statistical analysis was performed using SPSS Version 22 and GraphPad Prism software (version 6.0; GraphPad, Inc.). The results are reported as mean ± SD and numbers with percentages. Student's t-test or Mann–Whitney U test for two groups and ANOVA or Kruskal–Wallis test for more than two groups were used to determine statistical significance. Pearson's chi-squared test was used to compare categorical variables in the demographic data of the three groups. To examine associations between proinflammatory cytokines and cognitive assessment scores, analysis of partial correlation was used while adjusting for the demographic variables that differed statistically among the three groups.

We then evaluated the potential diagnostic and classification performance of combinations of inflammatory biomarkers and subitems of cognition testing using a logistic regression approach. In this analysis, all biomarkers used in any particular combination were entered as predictors, and the diagnostic group was entered as the dependent variable, controlling for age, sex, and education. After model fitting, receiver operating characteristic (ROC) analysis was used to evaluate the ability of the model to discriminate population with aMCI from LLD (23). The area under the ROC curve (AUROC) with a 95% CI for the parameters was used to measure its accuracy to differentiate patients with and without depression. Statistical significance was set at $p < 0.05$ on a two-tailed test.

RESULTS

Demographic and Clinical Characteristics

Twenty-three subjects in each group (NC, aMCI, and LLD) took part in our study. There was no significant difference between any of the groups in terms of age or male-to-female ratio. Years of education was higher in the normal control group than in the other two groups. In terms of lifestyle factors, a lower proportion of patients with LLD performed regular exercise or drink tea. As expected, the control group had significantly higher mean C-MoCA scores than the other groups, and MDS, CFT, and COWAT scores were also lower in the aMCI and depression groups than in the control group. Scores of the GDS were significantly higher in the depression group than in the control and aMCI groups (**Table 2**).

TABLE 1 | The list of 29 human chemokines or cytokines tested.

CCL1/TCA-3	CCL2/MCP-1	CCL3/MIP-1α	CCL7/MCP-3	CCL8/MCP-2
CL11/Eotaxin	CCL13/MCP-4	CCL15/MIP-1δ	CCL17/TARC	CCL19/MIP-3β
CCL20/MIP-3α	CCL23/MPIF-1	CCL24/Eotaxin-2	CCL25/TECK	CCL27/CTACK
CXCL5/ENA-78	CXCL6/GCP-2	CXCL8/IL-8	CXCL9/MIG	CXCL11/I-TAC
CXCL16/SCYB16	IL-1β	MIP2	IFN-γ	VCAM-1
TNF-α	IL-2	IL-4	IL-6	

TABLE 2 | Comparison of demographic characteristics and cognitive function between patients with late-life depression (LLD), subjects with amnestic mild cognitive impairment (aMCI), and normal controls (NC).

	aMCI (n = 23)	LLD (n = 23)	NC (n = 23)	Statistics
Clinical demographic data				
Age	73.0 (4.5)	71.9 (5.7)	72.5 (0.8)	0.665
Years of education	13.0 (3.4)	11.2 (2.9)$^{\#}$	15.2 (2.2)$^{\#\&}$	<0.01
Gender (male:female)	10:13	8:15	9:14	0.833
Lifestyle (Y:N)				
Smoking	5:18	3:20	3:20	0.649
Drinking	6:17	4:19	4:19	0.097
Tea drinking habits	13:10	5:18$^{*\#}$	12:11	0.024
Regular exercise	21:2	6:17$^{*\#}$	17:6	<0.01
Global Cognitive scales				
C-MoCA score	20.8 (2.6)	18.8 (6.1)	26.3 (2.1)$^{\#\&}$	<0.01
WMDS score	12.1 (2.8)	13.4 (3.1)	16.6 (3.3)$^{\#\&}$	<0.01
CFT score	6.7 (2.5)	5.5 (3.6)	10.0 (4.2)$^{\#\&}$	<0.01
COWAT score	12.1 (3.4)	9.3 (3.5)$^{\#}$	14.8 (3.3)$^{\#\&}$	<0.01
Geriatric Depression Scale	7.0 (3.9)	22.0 (4.6)$^{*\#}$	5.1 (2.7)	<0.01

All values, except sex, anti-inflammatory medication, and lifestyle, are expressed as mean ± SD.

aMCI, amnestic mild cognitive impairment; LLD, late-life depression; NC, normal controls; C-MoCA, Chinese version of Montreal Cognitive Assessment; WMDS, Wechsler Memory Digit Span; CFT, Category Fluency Test; COWAT, Controlled Word Association Test.

*Significantly different from controls ($p < 0.05$).

$^{\#}$Significantly different from aMCI group ($p < 0.05$).

$^{\&}$Significantly different from LLD group ($p < 0.05$).

Cognitive Assessment

The comparison of the C-MoCA subitem scores among the three groups is shown in **Figure 2**.

All functional domains, with the exception of the attention, concentration, and working memory (ACW), were significantly changed between the disease and control groups. The LLD and aMCI groups scored significantly lower than the control group in language, short-term memory, and executive function. Surprisingly, LLD patients performed even worse than aMCI subjects in orientation and visual–spatial function tests [vs. function (aMCI: 3.2 ± 0.8 vs. LLD: 2.4 ± 1.3 vs. NC: 3.7 ± 0.6, $p < 0.01$), executive function (aMCI: 2.3 ± 0.9 vs. LLD: 1.8 ± 1.4 vs. NC: 3.7 ± 0.6, $p < 0.01$), ACW (aMCI: 5.4 ± 1.0 vs. LLD: 5.1 ± 1.3 vs. NC: 5.7 ± 0.5, $p > 0.05$), language (aMCI: 3.9 ± 1.3 vs. LLD: 3.8 ± 1.7 vs. NC: 4.9 ± 1.0, $p < 0.05$), orientation to time and place (aMCI: 5.7 ± 0.7 vs. LLD: 4.4 ± 1.5 vs. NC: 5.9 ± 0.5, $p < 0.01$), and short-term memory (aMCI: 0.8 ± 0.9 vs. LLD: 1.2 ± 1.6 vs. NC: 3.4 ± 1.6, $p < 0.01$)] (**Figure 2**).

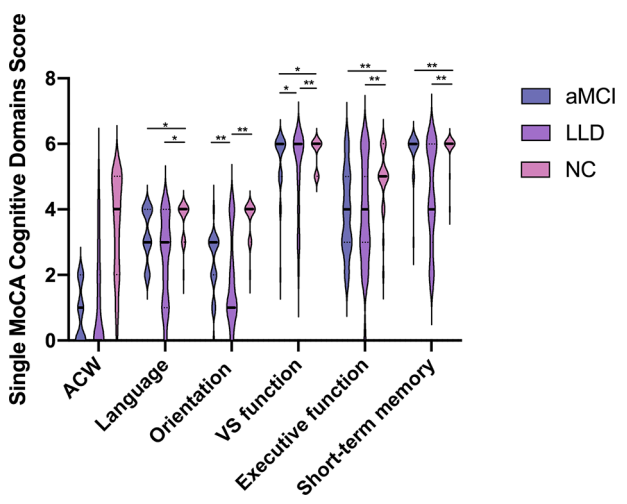

FIGURE 2 | Scores for the 6 different neurocognitive domains tested. aMCI, amnestic mild cognitive impairment; LLD, late-life depression; NC, normal controls; ACW, attention, concentration, and working memory; vs. function, visual–spatial function. Data are expressed as mean ± SD. Statistical analysis was performed by the Kruskal–Wallis test; significance levels are indicated in the top portion of the figure ($^{*}p < 0.05$, $^{**}p < 0.01$).

Inflammatory Protein Levels

Figures 3A–E show the protein concentrations of proinflammatory cytokines and chemokines. In total, patients in the LLD group had significantly higher levels of IL-6 (aMCI: 2.2 ± 0.6 vs. LLD: 2.9 ± 1.0 vs. NC: 2.3 ± 1.1, $p < 0.05$ **Figure 3A**) than the control or aMCI subjects. LLD patients showed lower levels of CXCL16 (127.8 ± 57.6 vs. 170.1 ± 122.1, $p < 0.05$ **Figure 3D**) than participants in the control group. Furthermore, the aMCI group showed a higher level of CCL15 (6,048.0 ± 3,608.5 vs. 3,713.7 ± 2,200.6, $p < 0.01$, **Figure 3E**) than subjects in the control group. Compared with depressed patients, the aMCI group had higher levels of CXCL11 (33.9 ± 8.3 vs. 28.3 ± 9.4, $p < 0.05$, **Figure 3B**) and CCL13 (60.1 ± 23.9 vs. 42.8 ± 14.2, $p < 0.01$, **Figure 3C**) in plasma. Meanwhile, no significant differences were noticed in plasma concentrations of other chemokines and cytokines among the three groups (**Table 3**).

Correlations of Peripheral Inflammatory Marker With Cognition and Depression Symptoms

Among LLD and aMCI patients, lower levels of CXCL16 ($r = 0.247$, $p = 0.041$) and CCL25 ($r = 0.255$, $p = 0.035$) were associated with worse C-MoCA summary scores, while controlling for age, sex, and education (**Figure 4A**). For further analysis, we explored the correlation between neuroinflammation and the subdomains

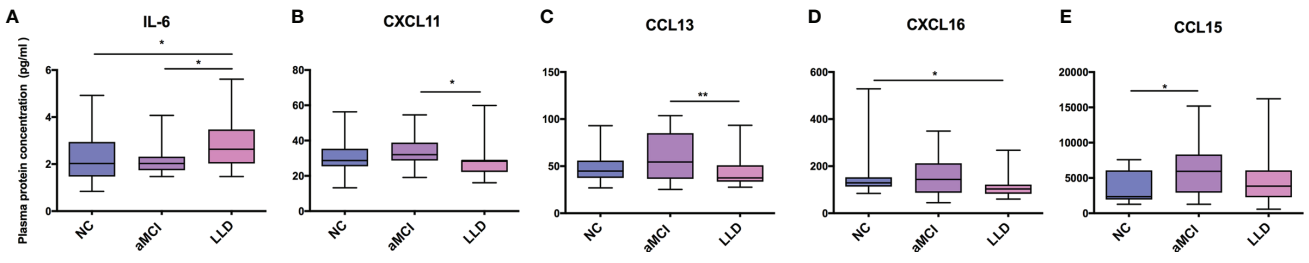

FIGURE 3 | Chemokine and proinflammatory cytokine concentrations among patients with late-life depression and amnestic mild cognitive impairment and normal controls with standard error of the mean. **(A)** IL-6 among LLD, aMCI, and control group. **(B)** CXCL11 among LLD, aMCI, and control group. **(C)** CCL13 among LLD, aMCI, and control group. **(D)** CXCL16 among LLD, aMCI, and control group. **(E)** CCL15 among LLD, aMCI, and control group. aMCI, amnestic mild cognitive impairment; LLD, late-life depression; NC, normal controls; IL-6, interleukin-6; CXCL11, C-X-C chemokine ligand 11; CXCL16, C-X-C chemokine ligand 16; CCL2, C-C chemokine ligand 2; CCL13, C-C chemokine ligand 13; CCL15, C-C chemokine ligand 15. Significance levels are indicated in the top portion of the figure (*$p < 0.05$, **$p < 0.01$).

of the MoCA. Levels of CXCL16 ($r = 0.254$, $p = 0.035$) and CCL25 ($r = 0.356$, $p < 0.01$) were also positively correlated with visual–spatial function. Levels of CXCL9 ($r = 0.051$, $p = 0.048$) and CCL23 ($r = 0.101$, $p = 0.036$) were positively associated with language function scores. The level of CCL11 was positively associated with ACW scores ($r = 0.320$, $p < 0.01$). A lower CCL27 concentration was found to be associated with higher orientation scores ($r = -0.239$, $p = 0.048$). The levels of CCL15 ($r = -0.256$, $p = 0.034$) and IL-6 ($r = -0.243$, $p = 0.044$) were found to be negatively associated with executive function scores, while the level of CXCL16 ($r = 0.261$, $p = 0.030$) was positively associated with executive function scores (**Figure 4B**).

A higher level of IL-6 was associated with lower COWAT scores ($r = -0.251$, $p = 0.037$) and increased GDS scores ($r = 0.304$, $p = 0.011$). CCL13 was also negatively associated with GDS scores ($r = -0.283$, $p = 0.018$), reflecting the severity of depression. Levels of CXCL6 ($r = 0.250$, $p = 0.038$), CXCL9 ($r = 0.261$, $p = 0.030$), and MIP2 ($r = 0.251$, $p = 0.038$) were

TABLE 3 | Level of inflammatory protein concentration in controls and patients.

	aMCI (n = 23)	LLD (n = 23)	NC (n = 23)	*P*
TNF-α (pg/ml)	5.2 (1.8)	8.7 (16.8)	5.5 (0.9)	0.280
CCL1 (pg/ml)	1.7 (0.9)	1.6 (0.8)	1.4 (0.5)	0.578
CXCL8 (pg/ml)	3.2 (2.2)	2.3 (1.7)	3.5 (2.8)	0.361
CCL7 (pg/ml)	20.3 (16.9)	13.6 (13.1)	17.7 (15.8)	0.282
MIP2 (pg/ml)	194.8 (140.4)	180.6 (260.8)	268.9 (259.4)	0.249
IL-1β (pg/ml)	3.7 (1.7)	4.5 (2.7)	3.3 (2.5)	0.175
IFN-γ (pg/ml)	26.6 (10.4)	24.9 (6.0)	24.2 (6.4)	0.741
CCL20 (pg/ml)	60.4 (29.5)	84.1 (117.1)	64.3 (54.6)	0.509
CCL24 (pg/ml)	550.5 (224.8)	446.4 (260.2)	553.1 (292.4)	0.050
CCL3 (pg/ml)	133.8 (32.5)	127.4 (41.5)	130.3 (49.4)	0.955
CCL8 (pg/ml)	279.5 (16.7)	278.4 (13.1)	275.7 (14.9)	0.557
IL-4 (pg/ml)	29.2 (6.5)	28.3 (5.0)	27.5 (5.9)	0.663
CCL19 (pg/ml)	115.9 (38.8)	158.4 (143.9)	114.4 (64.6)	0.668
IL-2 (pg/ml)	4.0 (1.9)	3.3 (2.5)	3.6 (2.2)	0.118
CXCL9 (pg/ml)	588.1 (80.7)	611.6 (81.4)	613.2 (89.3)	0.705
CCL23 (pg/ml)	421.5 (150.6)	454.6 (216.4)	458.5 (200.2)	0.784
VCAM-1 (ng/ml)	1,210.8 (452.7)	1,342.2 (594.8)	1,138.4 (599.4)	0.324
CCL27 (pg/ml)	508.8 (146.1)	488.2 (138.0)	508.5 (143.2)	0.880
CCL11 (pg/ml)	85.4 (31.5)	73.7 (17.4)	76.5 (42.2)	0.302
CXCL5 (pg/ml)	437.7 (308.0)	339.4 (223.2)	605.4 (481.5)	0.209
CXCL6 (pg/ml)	164.8 (90.2)	121.6 (62.7)	221.0 (191.4)	0.179
CCL25 (pg/ml)	172.9 (78.6)	145.2 (61.9)	205.2 (130.6)	0.258
CCL2 (pg/ml)	216.3 (117.8)	153.2 (72.5)	186.2 (98.6)	0.118
CCL17 (pg/ml)	171.0 (120.5)	115.5 (46.7)	151.1 (95.9)	0.181

All values are expressed as mean ± SD.

aMCI, amnestic mild cognitive impairment; LLD, late-life depression; NC, normal controls; TNF-α, tumor necrosis factor-alpha; IL-1β, interleukin-1-beta; (MIP)-2, macrophage inflammatory protein-2; IFN-γ, interferon-γ-inducing factor; IL-2, interleukin-2; IL-4, interleukin-4; VCAM-1, vascular cell adhesion molecule-1; CCL1, C-C chemokine ligand 1; CCL2, C-C chemokine ligand 2; CCL3, C-C chemokine ligand 3; CCL7, C-C chemokine ligand 7; CCL8, C-C chemokine ligand 8; CCL20, C-C chemokine ligand 20; CCL24, C-C chemokine ligand 24; CCL11, C-C chemokine ligand 11; CCL17, C-C chemokine ligand 17; CCL19, C-C chemokine ligand 19; CCL23, C-C chemokine ligand 23; CCL25, C-C chemokine ligand 25; CCL27, C-C chemokine ligand 27; CXCL5, C-X-C chemokine ligand 5; CXCL5, C-X-C chemokine ligand 6; CXCL8, C-X-C chemokine ligand 8; CXCL9, C-X-C chemokine ligand 9.

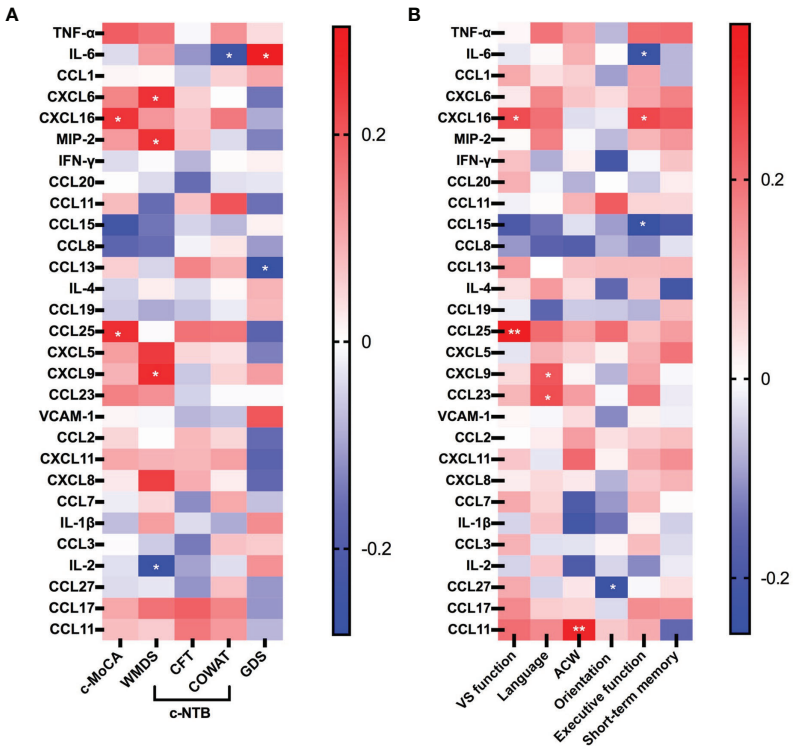

FIGURE 4 | Heatmap showing correlations between the concentrations of cytokines and chemokines with clinical characteristics of LLD and aMCI patients. **(A)** Association among proinflammatory cytokines, chemokines, and clinical scores reflecting the severity of cognition and depression. **(B)** Association among proinflammatory cytokines, chemokines, and subdomains of cognitive scores. The six neurocognitive domains shown in **Figure 3B** are the subdomains of the MoCA; red color indicates a positive correlation, and blue indicates a negative correlation; *p*-values are presented, $^{*}p < 0.05$, $^{**}p < 0.01$. C-MoCA, Chinese version of Montreal Cognitive Assessment; WMDS, Wechsler Memory digit span; CFT, Category Fluency Test; COWAT, Controlled Word Association Test; GDS, Geriatric Depression Scale; ACW, attention, concentration, and working memory; vs. function, visual–spatial function. Six CXC chemokine ligands (CXCL5, CXCL6, CXCL8, CXCL9, CXCL11, and CXCL16) and 15 CC chemokine ligands (CCL1, CCL2, CCL3, CCL7, CCL8, CCL11, CCL13, CCL15, CCL17, CCL19, CCL20, CCL23, CCL24, CCL25, and CCL27). MIP2, microphage inflammatory protein-2; IL-2ha, interleukin-2; IL-4, interleukin-4; IL-6, interleukin-6; VCAM-1, vascular cell adhesion molecule-1; TNF-α, tumor necrosis factor-alpha; IL-1β, interleukin-1-beta; IFN-γ, interferon-γ-inducing factor.

positively associated with WMDS scores. Conversely, the level of IL-2 was negatively associated with WMDS scores ($r = -0.265$, $p = 0.028$) (**Figure 4A**).

Combined Scale Items and Cytokines Across the Diagnostic Spectrum (Late-Life Depression/Amnestic Mild Cognitive Impairment)

The results of the ROC analyses, which assessed the cognitive assessment score and cytokine concentrations in discriminating between the LLD and aMCI groups, are presented in **Figure 5**.

The orientation and short-term memory testing combination distinguished LLD patients from aMCI groups with an AUROC of 0.83 (95% CI, 0.70–0.95) (**Figure 5A**). The combination [IL-6+CCL13] also showed significant value for differentiating between groups, with an AUROC of 0.81 (95% CI, 0.68–0.93) (**Figure 5B**). Subitems of the C-MoCA [orientation + short-term memory] and [IL-6+CCL13] combination discriminated LLD patients from aMCI with an AUROC of 0.97 (95% CI, 0.94–1.00) (**Figure 5C**).

DISCUSSION

To our knowledge, this is the first study scrutinizing the diagnostic contribution of a peripheral inflammatory biomarker panel—IL-6 and CCL13, both as single markers and in combination with neuropsychological testing—in the biomarker-guided differential diagnosis of LLD and aMCI. We also found that several cytokines in patients with aMCI and LLD were markedly different, and the altered chemokines were partly correlated with the clinical parameters. The results of this study will provide new leads to further understanding the etiology of the preclinical stage of dementia and improve our ability to identify high-risk individuals in the clinical setting.

Comparing Peripheral Inflammatory Markers in Late-Life Depression Versus Amnestic Mild Cognitive Impairment

Multiplex analytical technologies are crucial to the complex task of deciphering disease-specific biomarker patterns, as they provide opportunities for an all-inclusive approach, resolving

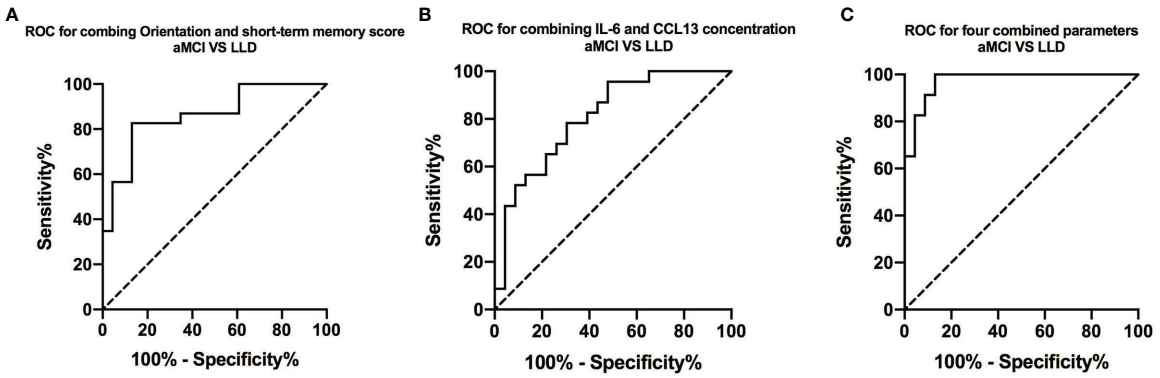

Measures	AUC	95%CI	Sensitivity (%)	Specificity (%)	PPV (%)	NPV (%)
A: orientation & short-term memory score	0.825	0.70-0.95	78.3	87.0	76.9	85.0
B: IL-6 &CCL13	0.809	0.68-0.93	78.3	69.6	70.8	72.7
C:A&B	0.974	0.94-1.00	91.3	91.3	90.9	87.5

FIGURE 5 | ROC curves for IL-6 and CCL13 concentrations between patients with late-life depression and amnestic mild cognitive impairment. **(A)** Receiver operating characteristic curve for combining orientation and short-term memory scores to discriminate between the aMCI and LLD groups. **(B)** Receiver operating characteristic curve for combining IL-6 and CCL13 to discriminate between the aMCI and LLD groups. **(C)** Receiver operating characteristic curve for combining the four parameters above to discriminate between the aMCI and LLD groups. AUROC, area under the receiver operating characteristic curve; aMCI, amnestic mild cognitive impairment; LLD, late-life depression; IL-6, interleukin-6; CCL13, C-C chemokine ligand 13. The AUROC curves result from a logistic regression model adjusted for age, sex, and education. ROC, receiver operating characteristic.

the problem that different ELISA kits do not give identical absolute values of the same analyses. In our study, using a Luminex assay, a reliable multiplex analytical technology, we were able to measure multiple different cytokines simultaneously in a single run of the assay with small sample-size requirements (24). Simultaneous measurement of multiple cytokines in peripheral blood samples reveals objective changes in multiple cytokines within one experiment, which provides a more inclusive and comprehensive depiction of the inflammatory process in the preclinical stage of dementia.

IL-6 can be produced by a variety of cells, such as immune-mediated cells, endothelial cells, and fibroblasts, which mediate immune cell expansion in response to infections and tissue injuries (25). The cytokine IL-6 has been extensively investigated in many preclinical and clinical studies as a proinflammatory cytokine that can accelerate ongoing neurodegenerative processes in AD. Previous research found that plasma circulating IL-6 may be a useful indication for future cognitive function (26), and increased IL-6 levels were reported in LLD patients in peripheral blood (27). Leung showed that elevated IL-6 in AD patients versus controls negatively correlated with Mini-Mental State Exam (MMSE) scores (28). We found similar results in our study. In our study, we found that plasma IL-6 levels were significantly increased in patients with LLD and positively associated with GDS scores. Interestingly, we did not find significant associations between IL-6 concentration and the total C-MoCA score; however, an increase in IL-6 was associated with better verbal fluency scores.

CCL13/MCP-4 is a CC family chemokine that can induce crucial immunomodulatory responses through its effects on epithelial, muscular, and endothelial cells (29). CXCL11 is a ligand of CXCR3 and has a proinflammatory effect (30). In this study, we found significantly lower levels of plasma CCL13 and CXCL11 in LLD patients than in aMCI patients. In line with our finding, people with suicidal behavior reported a similar decrease in the levels of chemokines (e.g., IL-10; CCL1, CCL8, CCL13, CCL15, CCL17, CCL19, CCL20, and CXCL11) (31). The suicide rates in the elderly are higher than those in younger adults and are more closely associated with depressive symptoms (32). We also found that the level of CCL13 was negatively associated with GDS scores, reflecting the severity of depression. Low levels of this cytokine may indicate more severe depressive symptoms and a higher risk of actually committing suicide. Longitudinal follow-up of these participants is underway to confirm this hypothesis.

The demographic characteristics in the LLD group were likely associated with a reduction in some chemokines. Personal characteristics and a series of complex factors (cultural, poor physical health, and social isolation) affect whether a person, group, or community develops a late-onset major depressive disorder. In this study, the results showed that 26.1% of the elderly led a sedentary lifestyle, while 91.3% of mild cognitive impairment subjects performed regular physical exercises. Depressive symptoms are associated with decreased physical performance in older adults in both cross-sectional and longitudinal epidemiological studies (33, 34). However, the

relationship between an increasing proportion of physical activity and depressive symptoms may be bidirectional. On the one hand, depression may lead to decreased levels of activity due to low motivation and energy. On the other hand, decreased physical activity could be a risk factor for depression. Physical activity is known to increase the secretion of multiple hormones with antidepressant properties: physical activities can temporarily change norepinephrine activity in the central system, decrease the activity of the hypothalamopituitary–adrenocortical axis, and increase the secretion of beta-endorphins (35, 36). To some extent, lower levels of chemokines may also be explained by the finding that patients with LLD tend to have a sedentary lifestyle and lack stimulation in life.

Multiple directions of regulation of cytokines and inflammation associated with proteins of AD and MCI patients have been described in different studies. CCL15 is classified as a macrophage inflammatory protein and has a proinflammatory effect (37). In this study, we found that plasma CCL15 was increased in aMCI subjects. It was negatively associated with executive function. Significant elevations in plasma CCL15 levels in AD have been reported by others; however, the data showed no changes in CCL15 in mild cognitive impairment (38). There are also conflicting data showing lower CCL15 levels in AD (39). Such results may be related to the severity of the disease and the heterogeneity of the MCI population. In previous studies, elevated peripheral vascular cell adhesion molecule-1, tumor necrosis factor (TNF)-α, IL-2, IL-6, IL-18, and interferon-γ were found in patients with mild AD, suggesting that cytokine signaling might play a role in the intermediate stages of dementia (40). The levels of CCL13, CXCL16, and CXCL11 were significantly lower in the LLD group than in the aMCI and NC groups in the present study. The results may indicate to some extent that a potential correlation between cytokine concentrations and the severity of cognitive dysfunction may not be apparent but may be more strongly correlated with mood in the early stages of the disease. These results suggest a different pattern of inflammatory dysregulation in LLD from aMCI, although they share similar clinical features. The findings herein raise the plausible possibility of LLD-induced immunosuppression and that the effects on cognition and mood are potentially mediated more significantly by IL-6 than other markers.

Montreal Cognitive Assessment as a Clinical Marker in Combination With Peripheral Inflammatory Markers

Our data show that the combination of two cytokines and subitems of the MoCA enables satisfactory differentiation between LLD patients and mild cognitive impairment subjects. Notably, neither MoCA nor biomarkers (CCL13 and IL-6) alone were sufficient. Our discriminant analysis based on orientation, short-term memory, IL-6, and CCL13 yielded a high sensitivity of 91.3% for the identification of LLD patients. Diagnostic heterogeneity remains a major obstacle to understanding and treating patients with psychiatric disorders. The lack of strictly defined physiological targets limits advances in precision medicine for determining optimal treatments or developing new interventions. Sometimes, elderly individuals with depression accompanied by cognitive impairment are diagnosed with MCI by the clinician, whereas laboratory markers have the potential to identify AD-associated alterations at a very early stage. Rigorous identification of MCI in geriatric major depression treatment trials will help to advance the effectiveness of treatments (41, 42).

The C-MoCA is one of the most widely used cognitive assessments in China, and it has shown good sensitivity and acceptable specificity in differentiating MCI from older adults with normal cognition (43, 44). In our study, attention to the performance of single cognitive items, rather than only focusing on the total score of the C-MoCA, has the potential to improve our understanding of the earliest cognitive alterations in preclinical AD.

Treating AD can be challenging because pathological changes precede the diagnosis of clinical dementia for many years. Due to the lack of pharmacological treatments to slow the progression of dementia, therapies should be developed to target people at risk of dementia. Thus, the distinguished cytokine combined with two selected cognition tests will facilitate detection of people with cognitive impairment, allowing for further investigation of the proinflammatory cytokine effects on the preclinical AD and neurodegeneration diseases and adoption of individual preventive and therapeutic measures. Further work will need to evaluate the potential role of the model in the prediction of progression from the prodromal stage of dementia to the dementia stage.

The following limitations of our study need to be discussed. It is undeniable that the cross-sectional study design and small sample size limit cause–effect conclusions regarding the relationship between inflammation and LLD. The diagnosis of MCI was made on a clinical basis according to Petersen's criteria. However, the revised NINCDS-ADRDA criteria have been reported to be reasonably accurate and are widely used in population-based studies (45). Here, recruited individuals refused to perform lumbar puncture and cerebrospinal fluid testing, which is an invasive screening method. PET imaging is expensive and difficult to accept in the elderly. All individuals were recruited from our cohort who had been diagnosed by three different geriatric psychiatrists. Given the aforementioned limitations, further studies are required to increase the statistical power by collecting larger, multisite cohorts and for detecting biomarkers of AD pathology, not only in predementia individuals but also across the AD diagnostic spectrum.

CONCLUSIONS

The results described the plasma cytokine profile in LLD patients in comparison with aMCI patients and controls, identifying neurocognitive and clinical associations with peripheral inflammatory markers. The combination of levels of cytokines and subitems of neuropsychological testing may provide a cost-effective, simple method for differentiating between LLD and

aMCI in individuals. These results suggest the involvement of different immunological mechanisms in two diseases with similar predementia syndromes, showing that further research on cytokines may inspire the development of approaches for preclinical dementia diagnosis and treatment.

DATA AVAILABILITY STATEMENT

The original contributions presented in the study are included in the article/supplementary material. Further inquiries can be directed to the corresponding authors.

ETHICS STATEMENT

The studies involving human participants were reviewed and approved by Shanghai Mental Health Center ethical standards committee on human experimentation. The patients/participants provided their written informed consent to participate in this study.

AUTHOR CONTRIBUTIONS

JN, YF, and YC performed the statistical analysis and drafted the main manuscript text. AA, QQ, LZ, XLiu, LS, YunL, and CZ performed the experiments and acquired the data. YuaL and XLi were involved in the study conception, participated in the design and coordination, and helped to draft the manuscript. All of the authors helped to draft the manuscript and gave critical comments. All of the authors are acknowledged.

FUNDING

This study was supported by grants from the National Natural Science Foundation of China National Natural Science Foundation of China (No. 81671402 & 81901170), National Key R&D Program of China (2017YFC1310500 and 2020YFC2005200), Clinical Research Plan of SHDC (SHDC2020CR1044B), and the Talent Development Program of Shanghai Mental Health Centre (2020-FX-04).

REFERENCES

1. Livingston G, Sommerlad A, Orgeta V, Costafreda SG, Huntley J, Ames D, et al. Dementia Prevention, Intervention, and Care. *Lancet* (2017) 390:2673–734. doi: 10.1016/s0140-6736(17)31363-6
2. Norton S, Matthews FE, Barnes DE, Yaffe K, Brayne C. Potential for Primary Prevention of Alzheimer's Disease: An Analysis of Population-Based Data. *Lancet Neurol* (2014) 13:788–94. doi: 10.1016/S1474-4422(14)70136-X
3. Akiyama H, Barger S, Barnum S, Bradt B, Bauer J, Cole GM, et al. Inflammation and Alzheimer's Disease. *Neurobiol Aging* (2000) 21:383–421. doi: 10.1016/s0197-4580(00)00124-x
4. Zlotnik A. Perspective: Insights on the Nomenclature of Cytokines and Chemokines. *Front Immunol* (2020) 11:908. doi: 10.3389/fimmu.2020.00908
5. Milenkovic VM, Stanton EH, Nothdurfter C, Rupprecht R, Wetzel CH. The Role of Chemokines in the Pathophysiology of Major Depressive Disorder. *Int J Mol Sci* (2019) 20:2283. doi: 10.3390/ijms20092283
6. Dowlati Y, Herrmann N, Swardfager W, Liu H, Sham L, Reim EK, et al. A Meta-Analysis of Cytokines in Major Depression. *Biol Psychiatry* (2010) 67:446–57. doi: 10.1016/j.biopsych.2009.09.033
7. Stuart MJ, Baune BT. Chemokines and Chemokine Receptors in Mood Disorders, Schizophrenia, and Cognitive Impairment: A Systematic Review of Biomarker Studies. *Neurosci Biobehav Rev* (2014) 42:93–115. doi: 10.1016/j.neubiorev.2014.02.001
8. O'Bryant SE, Lista S, Rissman RA, Edwards M, Zhang F, Hall J, et al. Comparing Biological Markers of Alzheimer's Disease Across Blood Fraction and Platforms: Comparing Apples to Oranges. *Alzheimers Dement (Amst)* (2016) 3:27–34. doi: 10.1016/j.dadm.2015.12.003
9. Kim SM, Song J, Kim S, Han C, Park MH, Koh Y, et al. Identification of Peripheral Inflammatory Markers Between Normal Control and Alzheimer's Disease. *BMC Neurol* (2011) 11:51. doi: 10.1186/1471-2377-11-51
10. Olsson B, Lautner R, Andreasson U, Ohrfelt A, Portelius E, Bjerke M, et al. CSF and Blood Biomarkers for the Diagnosis of Alzheimer's Disease: A Systematic Review and Meta-Analysis. *Lancet Neurol* (2016) 15:673–84. doi: 10.1016/S1474-4422(16)00070-3
11. Lai KSP, Liu CS, Rau A, Lanctot KL, Kohler CA, Pakosh M, et al. Peripheral Inflammatory Markers in Alzheimer's Disease: A Systematic Review and Meta-Analysis of 175 Studies. *J Neurol Neurosurg Psychiatry* (2017) 88:876–82. doi: 10.1136/jnnp-2017-316201
12. Diniz BS, Butters MA, Albert SM, Dew MA, Reynolds CF. Late-Life Depression and Risk of Vascular Dementia and Alzheimer's Disease: Systematic Review and Meta-Analysis of Community-Based Cohort Studies. *Br J Psychiatry* (2013) 202:329–35. doi: 10.1192/bjp.bp.112.118307
13. Andersen K, Lolk A, Kragh-Sorensen P, Petersen NE, Green A. Depression and the Risk of Alzheimer Disease. *Epidemiology* (2005) 16:233–8. doi: 10.1097/01.ede.0000152116.32580.24
14. Petersen RC, Stevens JC, Ganguli M, Tangalos EG, Cummings JL, DeKosky ST. Practice Parameter: Early Detection of Dementia: Mild Cognitive Impairment (an Evidence-Based Review). Report of the Quality Standards Subcommittee of the American Academy of Neurology. *Neurology* (2001) 56:1133–42. doi: 10.1212/wnl.56.9.1133
15. Davis M, Johnson OCTS, Cline S, Merikle E, Martenyi F, et al. Estimating Alzheimer's Disease Progression Rates From Normal Cognition Through Mild Cognitive Impairment and Stages of Dementia. *Curr Alzheimer Res* (2018) 15:777–88. doi: 10.2174/1567205015666180119092427
16. Richard E, Reitz C, Honig LH, Schupf N, Tang MX, Manly JJ, et al. Late-Life Depression, Mild Cognitive Impairment, and Dementia. *JAMA Neurol* (2013) 70:374–82. doi: 10.1001/jamaneurol.2013.603
17. Groeneweg-Koolhoven I, Comijs HC, Wjh Penninx B, van der Mast RC. Apathy in Early and Late-Life Depression. *J Affect Disord* (2017) 223:76–81. doi: 10.1016/j.jad.2017.07.022
18. Linnemann C, Lang UE. Pathways Connecting Late-Life Depression and Dementia. *Front Pharmacol* (2020) 11:279. doi: 10.3389/fphar.2020.00279
19. Crocco EA, Castro K, Loewenstein DA. How Late-Life Depression Affects Cognition: Neural Mechanisms. *Curr Psychiatry Rep* (2010) 12:34–8. doi: 10.1007/s11920-009-0081-2
20. Ismail Z, Elbayoumi H, Fischer CE, Hogan DB, Millikin CP, Schweizer T, et al. Prevalence of Depression in Patients With Mild Cognitive Impairment: A Systematic Review and Meta-Analysis. *JAMA Psychiatry* (2017) 74:58–67. doi: 10.1001/jamapsychiatry.2016.3162
21. Battle DE. Diagnostic and Statistical Manual of Mental Disorders (DSM). *Codas* (2013) 25:191–2. doi: 10.1590/s2317-17822013000200017
22. Petersen RC, Smith GE, Waring SC, Ivnik RJ, Tangalos EG, Kokmen E. Mild Cognitive Impairment: Clinical Characterization and Outcome. *Arch Neurol* (1999) 56:303–8. doi: 10.1001/archneur.56.3.303
23. Zhou X-H. *Statistical Methods in Diagnostic Medicine*. Hoboken: John Wiley & Sons, Inc (2011).
24. Zasada AA, Rastawicki W, Smietanska K, Rokosz N, Jagielski M. Comparison of Seven Commercial Enzyme-Linked Immunosorbent Assays for the Detection of Anti-Diphtheria Toxin Antibodies. *Eur J Clin Microbiol Infect Dis* (2013) 32:891–7. doi: 10.1007/s10096-013-1823-y
25. Tanaka T, Narazaki M, Kishimoto T. IL-6 in Inflammation, Immunity, and Disease. *Cold Spring Harb Perspect Biol* (2014) 6:a016295. doi: 10.1101/cshperspect.a016295

26. Bradburn S, Sarginson J, Murgatroyd CA. Association of Peripheral Interleukin-6 With Global Cognitive Decline in Non-Demented Adults: A Meta-Analysis of Prospective Studies. *Front Aging Neurosci* (2017) 9:438. doi: 10.3389/fnagi.2017.00438
27. Ng A, Tam MW, Zhang CS, Ho SF, Husain RS, McIntyre, et al. IL-1beta, IL-6, TNF- Alpha and CRP in Elderly Patients With Depression or Alzheimer's Disease: Systematic Review and Meta-Analysis. *Sci Rep* (2018) 8:12050. doi: 10.1038/s41598-018-30487-6
28. Leung R, Proitsi P, Simmons A, Lunnon K, Guntert A, Kronenberg D, et al. Inflammatory Proteins in Plasma Are Associated With Severity of Alzheimer's Disease. *PloS One* (2013) 8:e64971. doi: 10.1371/journal.pone.0064971
29. Mendez-Enriquez E, Garcia-Zepeda EA. The Multiple Faces of CCL13 in Immunity and Inflammation. *Inflammopharmacology* (2013) 21:397–406. doi: 10.1007/s10787-013-0177-5
30. Groom JR, Luster AD. CXCR3 in T Cell Function. *Exp Cell Res* (2011) 317:620–31. doi: 10.1016/j.yexcr.2010.12.017
31. Shinko Y, Otsuka I, Okazaki S, Horai T, Boku S, Takahashi M, et al. Chemokine Alterations in the Postmortem Brains of Suicide Completers. *J Psychiatr Res* (2020) 120:29–33. doi: 10.1016/j.jpsychires.2019.10.008
32. Fiske A, Wetherell JL, Gatz M. Depression in Older Adults. *Annu Rev Clin Psychol* (2009) 5:363–89. doi: 10.1146/annurev.clinpsy.032408.153621
33. Akturk U, Akturk S, Erci B. The Effects of Depression, Personal Characteristics, and Some Habits on Physical Activity in the Elderly. *Perspect Psychiatr Care* (2019) 55:112–8. doi: 10.1111/ppc.12322
34. Matthews MM, Hsu FC, Walkup MP, Barry LC, Patel KV, Blair SN. Depressive Symptoms and Physical Performance in the Lifestyle Interventions and Independence for Elders Pilot Study. *J Am Geriatr Soc* (2011) 59:495–500. doi: 10.1111/j.1532-5415.2011.03319.x
35. Farioli Vecchioli S, Sacchetti S, Nicolis di Robilant V, Cutuli D. The Role of Physical Exercise and Omega-3 Fatty Acids in Depressive Illness in the Elderly. *Curr Neuropharmacol* (2018) 16:308–26. doi: 10.2174/1570159X15666170912113852
36. Byeon H. Relationship Between Physical Activity Level and Depression of Elderly People Living Alone. *Int J Environ Res Public Health* (2019) 16:4051. doi: 10.3390/ijerph16204051
37. Maurer M, von Stebut E. Macrophage Inflammatory Protein-1. *Int J Biochem Cell Biol* (2004) 36:1882–6. doi: 10.1016/j.biocel.2003.10.019
38. Hochstrasser T, Marksteiner J, Defrancesco M, Deisenhammer EA, Kemmler G, Humpel C. Two Blood Monocytic Biomarkers (CCL15 and P21) Combined With the Mini-Mental State Examination Discriminate Alzheimer's Disease Patients From Healthy Subjects. *Dement Geriatr Cognit Dis Extra* (2011) 1:297–309. doi: 10.1159/000330468
39. Ray S, Britschgi M, Herbert C, Takeda-Uchimura Y, Boxer A, Blennow K, et al. Classification and Prediction of Clinical Alzheimer's Diagnosis Based on Plasma Signaling Proteins. *Nat Med* (2007) 13:1359–62. doi: 10.1038/nm1653
40. Brosseron F, Krauthausen M, Kummer M, Heneka MT. Body Fluid Cytokine Levels in Mild Cognitive Impairment and Alzheimer's Disease: A Comparative Overview. *Mol Neurobiol* (2014) 50:534–44. doi: 10.1007/s12035-014-8657-1
41. Nelson JC, Devanand DP. A Systematic Review and Meta-Analysis of Placebo-Controlled Antidepressant Studies in People With Depression and Dementia. *J Am Geriatr Soc* (2011) 59:577–85. doi: 10.1111/j.1532-5415.2011.03355.x
42. Alexopoulos GS. Mechanisms and Treatment of Late-Life Depression. *Transl Psychiatry* (2019) 9:188. doi: 10.1038/s41398-019-0514-6
43. Campbell JI, Xue Q. Cognitive Arithmetic Across Cultures. *J Exp Psychol Gen* (2001) 130:299–315. doi: 10.1037//0096-3445.130.2.299
44. Liu D, Li L, An L, Cheng G, Chen C, Zou M, et al. Urban-Rural Disparities in Mild Cognitive Impairment and Its Functional Subtypes Among Community-Dwelling Older Residents in Central China. *Gen Psychiatr* (2021) 34:e100564. doi: 10.1136/gpsych-2021-100564
45. de Jager CA, Honey TEM, Birks J, Wilcock GK. Retrospective Evaluation of Revised Criteria for the Diagnosis of Alzheimer's Disease Using a Cohort With Post-Mortem Diagnosis. *Int J Geriatr Psychiatry* (2010) 25:988–97. doi: 10.1002/gps.2448

Conflict of Interest: The authors declare that the research was conducted in the absence of any commercial or financial relationships that could be construed as a potential conflict of interest.

Publisher's Note: All claims expressed in this article are solely those of the authors and do not necessarily represent those of their affiliated organizations, or those of the publisher, the editors and the reviewers. Any product that may be evaluated in this article, or claim that may be made by its manufacturer, is not guaranteed or endorsed by the publisher.

frontiers in Immunology

ORIGINAL RESEARCH
published: 13 January 2022
doi: 10.3389/fimmu.2021.830018

Circulating Exosomal circRNAs Contribute to Potential Diagnostic Value of Large Artery Atherosclerotic Stroke

Qi Xiao[1†], Rongyao Hou[2†], Hong Li[1], Shuai Zhang[1], Fuzhi Zhang[1], Xiaoyan Zhu[3] and Xudong Pan[1*]*

[1] Department of Neurology, The Affiliated Hospital of Qingdao University, Qingdao, China, [2] Department of Neurology, The Affiliated Hiser Hospital of Qingdao University, Qingdao, China, [3] Department of Critical Care Medicine, The Affiliated Hospital of Qingdao University, Qingdao, China

OPEN ACCESS

Edited by:
Juehua Yu,
The First Affiliated Hospital of Kunming Medical University, China

Reviewed by:
Yong Jiang,
Capital Medical University, China
Fengyan Jin,
First Affiliated Hospital of Jilin University, China

***Correspondence:**
Xiaoyan Zhu
zxysdjm@163.com
Xudong Pan
drpan022@163.com

[†]These authors have contributed equally to this work

Specialty section:
This article was submitted to Multiple Sclerosis and Neuroimmunology, a section of the journal Frontiers in Immunology

Received: *06 December 2021*
Accepted: *24 December 2021*
Published: *13 January 2022*

Citation:
Xiao Q, Hou R, Li H, Zhang S, Zhang F, Zhu X and Pan X (2022) Circulating Exosomal circRNAs Contribute to Potential Diagnostic Value of Large Artery Atherosclerotic Stroke. Front. Immunol. 12:830018. doi: 10.3389/fimmu.2021.830018

Large artery atherosclerotic (LAA) stroke is closely associated with atherosclerosis, characterized by the accumulation of immune cells. Early recognition of LAA stroke is crucial. Circulating exosomal circRNAs profiling represents a promising, noninvasive approach for the detection of LAA stroke. Exosomal circRNA sequencing was used to identify differentially expressed circRNAs between LAA stroke and normal controls. From a further validation stage, the results were validated using RT-qPCR. We then built logistic regression models of exosomal circRNAs based on a large replication stage, and receiver operating characteristic (ROC) curves were constructed to assess the diagnostic efficacy. Using exosomal circRNA sequencing, large sample validation, and diagnostic model construction revealed that exosomal circ_0043837 and circ_ 0001801were independent predictive factors for LAA stroke, and had better diagnostic efficacy than plasma circRNAs. In the atherosclerotic group (AS), we developed a nomogram for clinical use that integrated the two-circRNA-based risk factors to predict which patients might have the risk of plaque rupture. Circulating exosomal circRNAs profiling identifies novel predictive biomarkers for the LAA stroke and plaque rupture, with superior diagnostic value than plasma circRNAs. It might facilitate the prevention and better management of this disease.

Keywords: large artery atherosclerotic stroke, exosome, circRNAs, atherosclerosis, biomarkers, immune cells

INTRODUCTION

Stroke is a global public health problem. According to the Global Burden of Disease Study 2019, stroke is the third leading cause of death and disability (1). Approximately 80% of strokes are ischemic, of which, the large artery atherosclerotic (LAA) stroke is an important subtype (2). LAA stroke is closely related to atherosclerosis, in which plaque rupture and thrombosis are key causes of disease onset and progression (3, 4), associated with the accumulation of immune cells in the vascular intima (5). Therefore, it is important to develop potential approaches for the diagnosis of LAA stroke and plaque rupture.

Circular RNAs (circRNAs), a type of non-coding RNAs, are candidate biomarkers and potential therapeutic targets due to their tissue specificity (6, 7). Furthermore, they play an essential role in the pathophysiology of ischemic stroke and atherosclerosis. Studies have reported that the presence of circulating circRNAs may potentially aid in the diagnosis of acute ischemic stroke (8). In atherosclerosis pathogenesis, circRNAs are involved in the apoptosis of immune cells (macrophages), migration of vascular smooth muscle cells; and formation of new intima (9, 10). However, circulating circRNAs are susceptible to degradation by biological enzymes and limitations of origin identification. Nonetheless, recent studies have shown that circRNAs are stable and present in large amounts in exosomes (11, 12).

Exosomes are endogenous vesicles (approximately 40–160 nm in diameter) and can carry circRNAs and other biomolecules (13). Thus, exosomes can play critical roles in material transport, cell communication, and targeted therapy; moreover, they protect circRNAs from biological enzymes (14). Exosomes are secreted from various cell types with membrane specificity and targeting properties (15). Furthermore, researchers have identified exosomes involved in the atherosclerotic process (16). These included the endothelium-derived exosomes carrying miRNAs, which could inhibit macrophage infiltration and regulate the atherosclerotic plaque area (17). Our previous study also found that miRNA-145 present in the umbilical cord stem cell-derived exosomes reduced atherosclerotic plaques (18). Thus, exosomes could also serve as carriers of circRNAs, which may have diagnostic value for LAA stroke.

Therefore, in this study, we aimed to identify potential diagnostic and predictive biomarkers for LAA stroke and plaque rupture through exosomal circRNA sequencing and validation, that would facilitate immediate and appropriate management and prevention of LAA stroke.

MATERIALS AND METHODS

Study Population

A total of 621 participants were enrolled in the study between June 2018 and December 2020 at the Affiliated Hospital of Qingdao University. Of the 621 participants, 366 were included in the acute ischemic stroke group (large artery atherosclerosis [LAA] group: 196 cases; small artery occlusion [SAO] group: 170 cases), 106 patients in the acute stroke (AS) group, and 149 participants in the normal control (NC) group.

The inclusion criteria for the acute ischemic stroke group were as follows (1): a diagnosis of an acute ischemic stroke using cranial CT or MRI (2); a diagnosis within 3 days of symptom onset (3); both LAA and SAO subtypes were included according to the Trial of Org 10172 in Acute Stroke Treatment (TOAST) criteria (19); and (4) those who did not undergo thrombolytic therapy. The inclusion criteria for the AS group were as follows (1): computed tomography angiography (CTA) of the head and neck assisted identification of intracranial or extracranial vascular stenosis > 50% or occlusion and (2) Exclusion of possibility of stroke by cranial CT or MRI. Healthy controls were recruited at the Medical Examination Center of the Affiliated Hospital of Qingdao University (2, 8, 20).

The exclusion criteria were as follows (1): other types of stroke such as hemorrhage, craniocerebral trauma, tumors, and neurological diseases (2); atrial fibrillation, myocardial infarction, arteritis, or any circulatory disease (3); severe pulmonary, hepatic, or renal dysfunction; and (4) malignant tumors, severe infection, autoimmune diseases, and other systemic diseases (2, 8, 20).

Specimen Collection and Exosome Extraction

Fasting venous blood samples were collected in ethylenediamine tetra acetic acid (EDTA) tubes early in the morning within 24 h of admission, stored at 4°C for 30 min, and centrifuged at 2500 × *g* for 15 min. The upper layer of plasma was collected and stored at -80°C until further use.

Plasma exosomes were extracted using the Exosome Extraction Kit (Invitrogen, Cat 4484450, Carlsbad, USA) (21). Following the manufacturer's instructions, the plasma was centrifuged at 2000 × *g* and 10,000 × *g* for 20 min at 25°C to remove impurities. Approximately 0.5 volume of phosphate buffer saline (PBS) and 0.05 volume of proteinase K were added, and the mixture was incubated at 37°C for 10 min. A total of 0.3 volume of exosome extraction reagent was added, and the mixture was incubated at 4°C for 30 min and centrifuged at 10,000 × *g* for 5 min. The creamy white precipitate of exosomes, visible at the bottom or on the wall of the tube, was resuspended in PBS.

Electron Microscopy of Exosome Identification

The morphology of the extracted exosome was evaluated using an electron microscope. Briefly, the resuspended exosome solution (10 μL) was placed on a copper grid for 2 min at room temperature. Next, 2% phosphotungstic acid was added onto exosomes after which they were washed with distilled water. Finally, they were evaluated under the electron microscope (Hitachi, Tokyo, Japan) (22, 23).

Identification of Exosome Particle Size

The diameter of the extracted exosomes was determined by measuring the particle size. Resuspended exosome solutions were analyzed using the ZetaView inspection instrument (Particle Metrix, Meerbusch, Germany) and the Network Traffic Analysis (NTA) software (ZetaView 8.04.02) to determine the size and number of exosome particles (22, 23).

Western Blot Analysis for Exosome Identification

Exosome-specific markers, including positive (CD9, CD63, and TSG101) and negative markers (GRP94), were used to identify exosomes by western blotting. Total proteins (25 μg) in the extracted resuspension of exosomes were sequentially subjected to gel electrophoresis (10% SDS-PAGE), membrane transfer,

blocking, incubation with primary antibodies specific for CD9, CD63, TSG101, and GRP94 (ab92726, ab134045, ab125011, ab238126, Abcam, Cambs, UK), incubation with the goat anti rabbit secondary antibodies, and enhanced chemiluminescence (ECL) to examine exosomal protein expression (22, 23).

Sequencing of Exosomal CircRNA

Sequencing of exosomal circRNA was performed sequentially through sample collection and preparation; RNA extraction; and qualitative and quantitative analysis of extracted RNA purity, concentration, and integrity. Library quality control were performed on the Agilent Bioanalyzer 2100 system. The library was sequenced using the Illumina HiSeq 4000 platform.

Bioinformatic analysis of circRNA sequencing was performed by quality control, and circRNAs were detected and identified using find_circ and CIRI2 (24). Raw counts were normalized using the TPM (25).

Gene Ontology and Kyoto Encyclopedia of Genes and Genomes Functional Enrichment Analysis

We performed the GO functional enrichment of the source genes of differentially expressed circRNAs using the GOseq R package, and GO terms with corrected P values < 0.05 were considered significantly enriched for differentially expressed genes. The KO-Based Annotation System (KOBAS) software was used to detect differentially expressed circRNA-derived genes enriched in the KEGG pathway (26).

Reverse Transcription for Real-Time Quantification

Total RNA was extracted from plasma and resuspended exosomes using the miRNeasy® Mini kit (Qiagen, DUS, Germany). Reverse transcription and quantitative amplification were performed sequentially using the RT6 cDNA Synthesis Kit, version 2 (TsingKe, Beijing, China) and the T5 Fast qPCR Mix (SYBR Green I) (TsingKe, Beijing, China). Amplification specificity was calibrated by generating a melting curve. *ACTB* was selected as the internal reference gene. The fold change in circRNA expression was calculated using the following formula:

$$2^{-\Delta\Delta Ct}$$

The primer sequences used in this study are listed in **Supplemental Table 1**.

Statistical Analyses

Categorical variables were expressed as percentages and analyzed using the χ^2 test. Continuous variables were expressed as mean ± SEM for those with a normal distribution or interquartile for those with a skewed distribution. Continuous variables were calculated through analysis of variance (ANOVA), *t*-test, and Kruskal-Wallis test. The Spearman test was used to calculate component correlations.

The potential factors were sequentially screened by univariate and multivariate binary logistic regression analysis. From among the set of variables, select those variables with P < 0.05 in the multivariate regression to include in the prediction model (27). The Hosmer-Lemeshow goodness-of-fit test was used to evaluate the calibration degree of the prediction model. The receiver operating characteristic (ROC) curve was used to evaluate the discrimination ability of the prediction model. Nomogram was done with the rms package of R software ver.4.1.1 (28). All analyses were performed using the Statistical Package for the Social Sciences (SPSS), ver. 26.0 (IBM Corp. in Armonk, NY) and the statistical significance was set at $P < 0.05$.

RESULTS

The Landscape of Circulating Exosomal CircRNAs

To better understand the potential role of exosomal circRNAs in the diagnosis of LAA stroke, we included 366 patients with new cerebral infarction and classified them according to TOAST (19). There were 196 patients with LAA stroke, 170 with SAO stroke, and 149 who were normal controls (**Supplemental Table 2**). As shown in **Figure 1A**, we performed circulating exosome transcriptome sequencing to determine differentially expressed circRNAs for further validation and identify possible biomarkers through diagnostic model construction.

We extracted circulating exosomes from the plasma and verified their quantity and integrity according to the standards of the International Society for Extracellular Vesicles (29). As shown in **Supplemental Figure 1**, the extracted circulating exosomes underwent morphological blood identification using electron microscopy, which showed that the exosomes appeared to be oval without a nucleus. NTA measurements showed that the diameter of exosomes ranged from 50–150 nm. Further, the markers enriched in exosomes were detected using western blotting. The positive markers were positive in the exosome group and negative in the residual supernatant. The negative markers were not detected in the exosomes. In summary, the morphology, number, and integrity of exosomes in the enriched exosome samples were assessed using the aforementioned methods.

As shown in **Figure 1B**, a workflow of the discovery, validation and replication stage of circulating exo-circRNAs. In the discovery stage, we performed exosomal circRNA sequencing of LAA stroke. We identified differentially expressed (DE) circRNAs by comparing the two groups bioinformatically. A total of 26 DE circRNAs were identified in NC and LAA subjects ($P < 0.05$, $|\text{fold change}| \geq 1.5$). There were 7 significantly upregulated and 19 significantly downregulated genes in the LAA group compared to the NC group (**Figure 1C**).

To determine the function of DE circRNAs, we performed functional enrichment of the source genes of DE circRNAs, including the GO and KEGG pathway enrichment. The KEGG pathway showed that DE circRNAs could be enriched in antigen processing and presentation, classical signaling pathways, such as ERK, NF-kappa B and mTOR (**Supplemental Figure 2A**). We found that their biological processes mainly included immune, inflammatory, and metabolic pathways circRNAs using the GO database. Other cellular components in the cell membrane such as

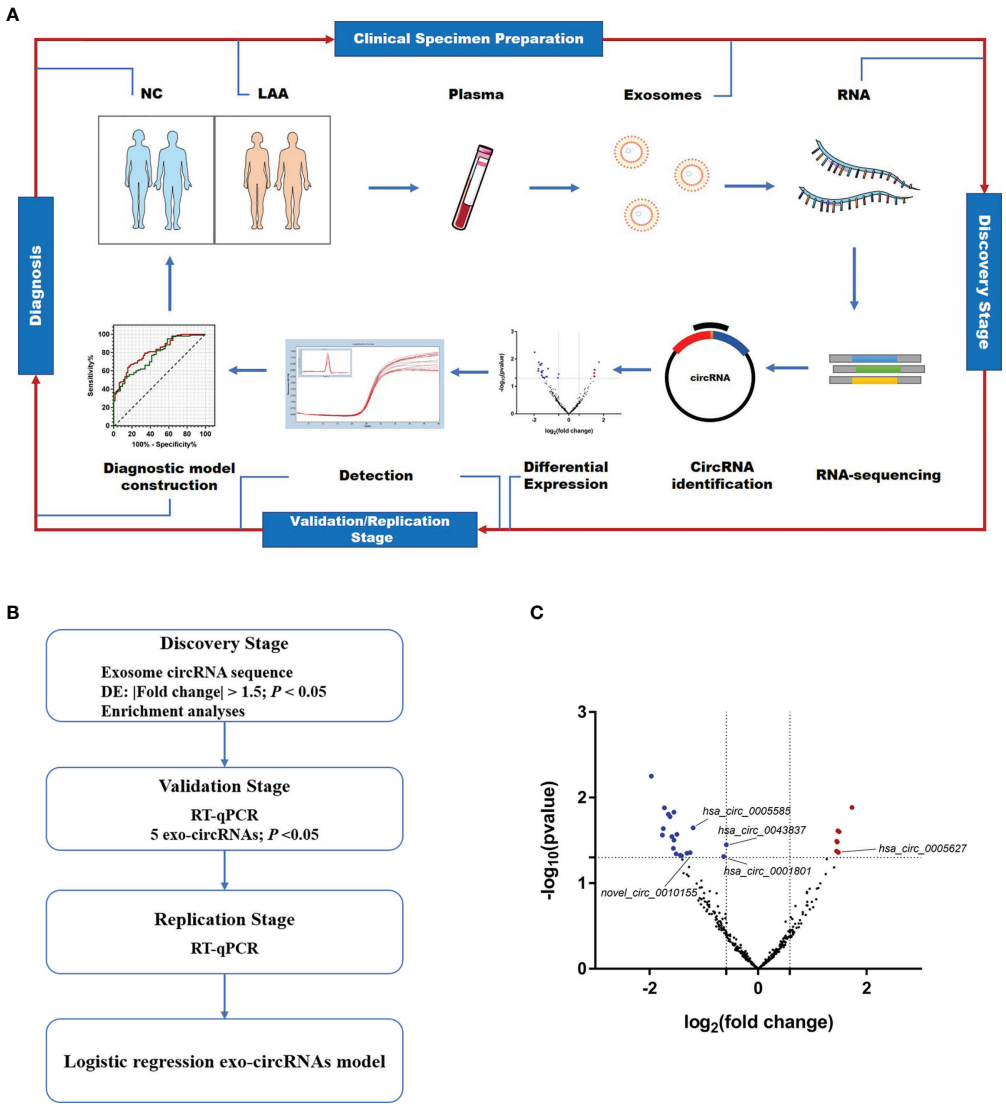

FIGURE 1 | Expression profiles of circulating exosome-circRNAs. **(A)** Workflow of the study, including clinical samples preparation, discovery stage of circRNA sequencing, detection and diagnosis. **(B)** Workflow of the discovery, validation and replication stage of circulating exo-circRNAs. **(C)** Volcano map of circRNAs in exosome RNA-seq, with red showing up-regulated expression in the LAA group and blue showing down-regulation.

vesicle membrane and other component sources were also elucidated (**Supplemental Figure 2B**).

Exosomes Derived CircRNAs as Biomarkers of LAA Stroke

Combining the differential expression and functional enrichment of immune biological process, we further selected circRNAs that might be involved in the LAA process for small sample RT-qPCR validation. We selected the following: novel_circ_0010155, circ_0043837, circ_0001801, circ_0005627, and circ_0005585. As shown in **Figure 2A**, novel_circ_0010155, circ_0043837, circ_0001801, and circ_0005585 were significantly downregulated in the LAA group and were statistically different from the SAO group. circ_0005627 was significantly upregulated in the LAA group, while the expression of the SAO and NC groups was lower than that of the LAA group.

Based on the validation of small samples, we further performed a replication stage, in which we included 150 cases of LAA, 130 cases of SAO, and 103 NCs. As shown in **Figure 2B**, there were statistically significant differences in novel_circ_0010155, circ_0043837, circ_0001801, circ_0005627, and circ_0005585 compared with NCs. Of these, the expressions of novel_circ_0010155, circ_0043837, circ_0001801, and circ_0005585 were significantly downregulated, while that of circ_0005627 was significantly upregulated in the LAA group compared with the NC group. This had the same trend as that of the results of the small sample validation. Furthermore, circ_0043837, circ_0001801 and circ_0005585 showed

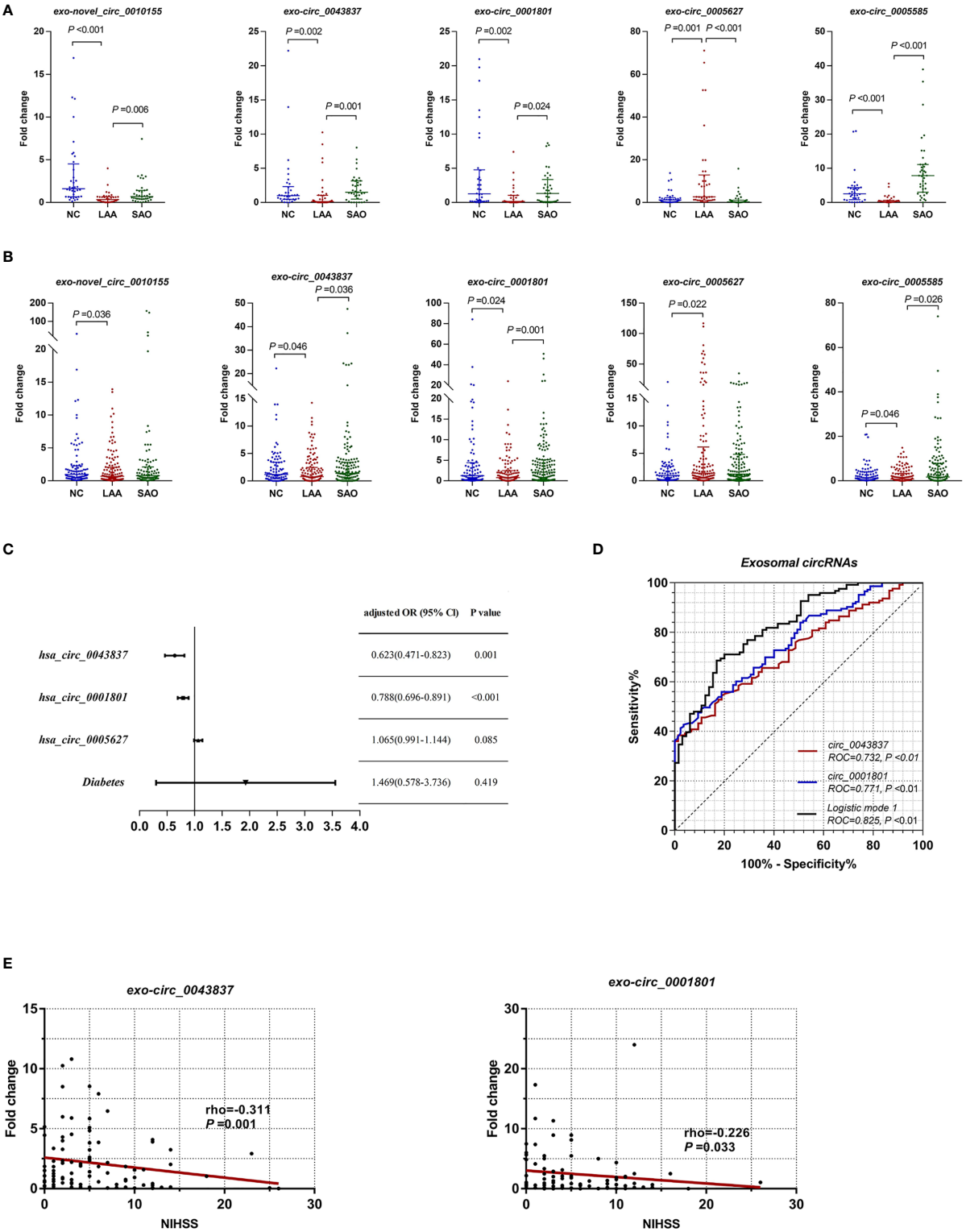

FIGURE 2 | Expression of exosomal circRNAs as novel biomarkers for LAA stroke. **(A)** Validation of exosomal novel_circ_0010155, circ_0043837, circ_0001801, circ_0005627, and circ_0005585 in NC, LAA, and SAO groups. **(B)** Replication of exosomal novel_circ_0010155, circ_0043837, circ_0001801, circ_0005627, and circ_0005585 in the NC, LAA, and SAO groups. **(C)** Multivariate logistic regression analysis for exo-circRNAs. **(D)** ROC curves of the exosomal circRNAs, logistic mode 1: Two-exo-circRNA of hsa_circ_0043837 and hsa_circ_0001801. **(E)** Comparison between exosome derived circRNA and NIHSS score.

statistically different expression levels between the LAA and SAO groups. However, novel_circ_0010155 and circ_0005627 was not statistically different among the two groups in the large sample replication.

To confirm the diagnostic value of five circRNAs for LAA stroke, we constructed the LAA diagnostic model through the logistic regression. We included five circRNAs and five clinical indicators (Smoking, drinking, hypertension, diabetes, and LDL) for binary logistic regression analysis. After multivariable adjustment by three circRNAs and diabetes, the circ_0043837 and circ_0001801 remained powerful and independent factors (**Figure 2C** and **Supplemental Table 3**). Furthermore, the LAA diagnostic model through the logistic regression, tested the regression model using the ROC. The circ_0043837 and circ_0001801 composite models showed an AUC of 0.825, its diagnostic efficacy was better than that of the single circ_0043837 (NRI=0.144) or circ_0001801 (NRI=0.097) (**Figure 2D**).

We assessed the possible severity of circRNAs with LAA. The National Institutes of Health Stroke Scale (NIHSS) is a recognized score scale corresponding to the extent and severity of the stroke (30). We performed a correlation analysis between DE circRNAs and NIHSS, in which circ_0043837 and circ_0001801 showed a negative statistically significant correlation (**Figure 2E**).

Diagnostic Efficacy Comparison Between Exosomal CircRNAs and Plasma CircRNAs

Previous studies found that plasma circRNAs could be used as diagnostic markers for ischemic stroke (8). Recent studies showed that exosomes could protect circRNAs from degradation by biological enzymes (31). Thus, we performed differential expression assays of plasma circRNAs to verify whether exosomal circRNAs had better diagnostic efficacy.

As shown in **Figure 3A**, plasma novel_circ_0010155, circ_0043837, and circ_0001801 were DE between the LAA and the NC groups. The trend was the same as that of exosomal circRNAs. In addition, plasma novel_circ_0010155, circ_0043837, and circ_0001801, and circ_0005627 were significantly different between the SAO and LAA groups. However, plasma circ_0005585 was not statistically different among the three groups in the large sample replication.

We verified whether the expressions of plasma circRNAs and circulating exosomal circRNA were correlated. Plasma novel_circ_0010155, circ_0043837, circ_0005627, and circ_0005585 were positively correlated with exosomes, while circ_0001801 was negatively correlated (**Figure 3B**).

For plasma circRNAs, we included five plasma circRNAs for multivariate binary logistic regression, of which only circ_0001801 was associated with the LAA outcome variable (**Supplemental Table 4**). We further excluded the confounding factors of clinical indicators(diabetes), suggesting that plasma circ_0001801 was an independent factor (**Figure 3C**). We then constructed the diagnostic model, tested the regression model using the ROC, and evaluated the diagnostic efficacy of exosomes and plasma. For exosomal circ_0001801, the AUC of NC/LAA was 0.771. The AUC was greater than that of plasma circ_0001801 at 0.620, NRI (exo VS plasma) =0.183 (**Figure 3D**).

Assessment Predictive Value Of Circulating Exosomal CircRNAs for LAA Plaque Rupture

Previous studies found that LAA was closely associated with unstable plaque rupture in AS (32). We further included the AS group for comparison with the LAA group to identify DE circRNAs that could predict plaque instability. First, we performed differential expression analysis of exosomal circRNAs and plasma circRNAs by RT-qPCR and assessed their diagnostic efficacy. Interestingly, there were also differences in exosomal novel_circ_0010155, circ_0043837, and circ_0001801 in AS compared with the NC and LAA groups (**Figure 4A**). Plasma circ_0043837 and circ_0001801 showed the same trend (**Figure 4B**).

Further we constructed a risk prediction model for plaque rupture. First, we included five circRNAs and the above clinical indicators for univariate logistic regression analysis, and multi-factor logistic regression analysis was performed for the meaningful risk factors ($P < 0.05$) among them (**Supplemental Table 5**). As shown in **Figure 4C**, where exosomal- circ_0043837 and circ_0001801 were independent risk factors. We analyzed the efficacy of circRNA alone and the composite model constructed by logistic regression by ROC, where the diagnostic efficacy of the composite model was superior to that of the single-factor index (**Figure 4D**). We also performed the same analysis for the five plasma circRNAs, where plasma circ_0043837 suggested an independent risk factor (**Supplemental Table 5**), where ROC analysis showed that exosomes had better diagnostic efficacy than plasma (**Figure 4D**). Subsequently, we included the above two exosomal circRNA constructs for clinical application in a nomogram, suggesting the risk of plaque rupture (**Figure 4E**).

DISCUSSION

In the present study, we evaluated exosomal circRNAs as diagnostic biomarkers for LAA stroke, which showed a superior diagnostic efficacy compared to plasma circRNAs. We also investigated its correlation with the severity of stroke. Meanwhile, our results provide evidence that exosomal circRNAs have potential predictive value of plaque rupture.

In the present study, we directly sequenced circulating exosomal circRNAs, in contrast to plasma RNA-seq reported previously. Circulating circRNAs are susceptible to degradation by biological enzymes; and the circRNAs are not specific. Recent studies found that exosomes, natural nanoparticle, being transporter-type vesicles, with a biofilm structure, protect circRNAs from biological enzymes and confer stability (12, 33, 34). Meanwhile, circRNAs are secreted by specific cells and are part of cellular targeting mediated by exosomal vesicles, which makes them reliable for the diagnosis of specific diseases (33, 35). Previous studies have shown that circulating exosomal miRNAs could be used as markers of early colon cancer with a better diagnostic efficacy than plasma (23). Therefore, in this study,

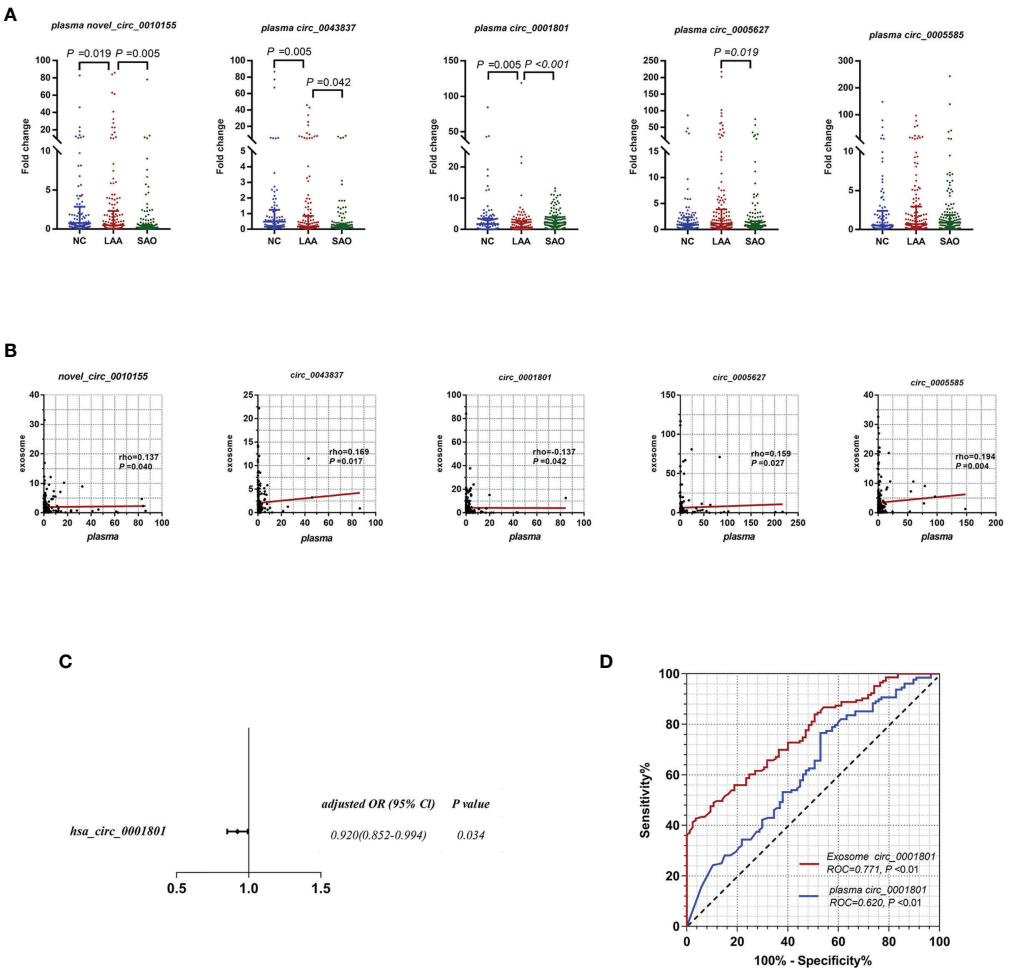

FIGURE 3 | Diagnostic efficacy of LAA stroke comparison between exosome derived circRNA and plasma circRNAs. **(A)** Replication of plasma novel_circ_0010155, circ_0043837, circ_0001801, circ_0005627, and circ_0005585 in NC, LAA, and SAO groups. **(B)** Correlation between the assessment of novel_circ_0010155, circ_0043837, circ_0001801, circ_0005627, and circ_0005585 in peripheral blood-derived exosomes and plasma. **(C)** Multivariate logistic regression analysis for plasma circRNAs. **(D)** ROC curves of the exosomal and plasma circ_0001801.

we directly sequenced exosomal circRNAs and analyzed the DE circRNAs in the LAA to better identify biomarkers and conduct mechanistic studies.

As is a chronic inflammatory disease in which a large number of immune cells are involved. Macrophage uptake of ox-LDL to form macrophage-derived foam cells, which form fatty strips with T cells (36). We further selected exosomal circRNAs associated with immune and inflammatory processes for validation according to function enrichment. Novel_circ_0010155 is derived from ZNF91, which is distributed intracellularly and intranuclearly (37). It is involved in transcriptional regulation and highly expressed in T lymphocytes (38). circ_0043837 and circ_ 0005585 are associated with mitochondrial function. Mitochondrial damage affects macrophage function and is involved in the process of AS in previous studies (39). circ_0001801 and circ_0005627 are associated with gene regulation-related processes. circ_0001801 enrichment function is involved in the cellular protein modification process. In addition, circ_0005627 function is related to RNA modification. Therefore, based on functional enrichment and prediction, circRNAs such as novel_circ_0010155, circ_0043837, circ_0001801, circ_0005627, and circ_0005585 were selected for further validation.

Furthermore, we analyzed the DE circRNAs between the LAA and NC groups using small and large sample exosomal circRNA expression assays during biomarker screening. We included the SAO group (according to TOAST typing) in the NC group to account for possible circRNA interference caused by other symptoms such as stroke and to keep the false positive rate low in the validation of the LAA screening. Exosomal novel_circ_0010155, circ_0043837, circ_0001801, circ_0005627, and circ_0005585 were statistically different among the three groups in the small sample validation. circ_0043837, circ_0001801, circ_0005585, circ_0005627, and

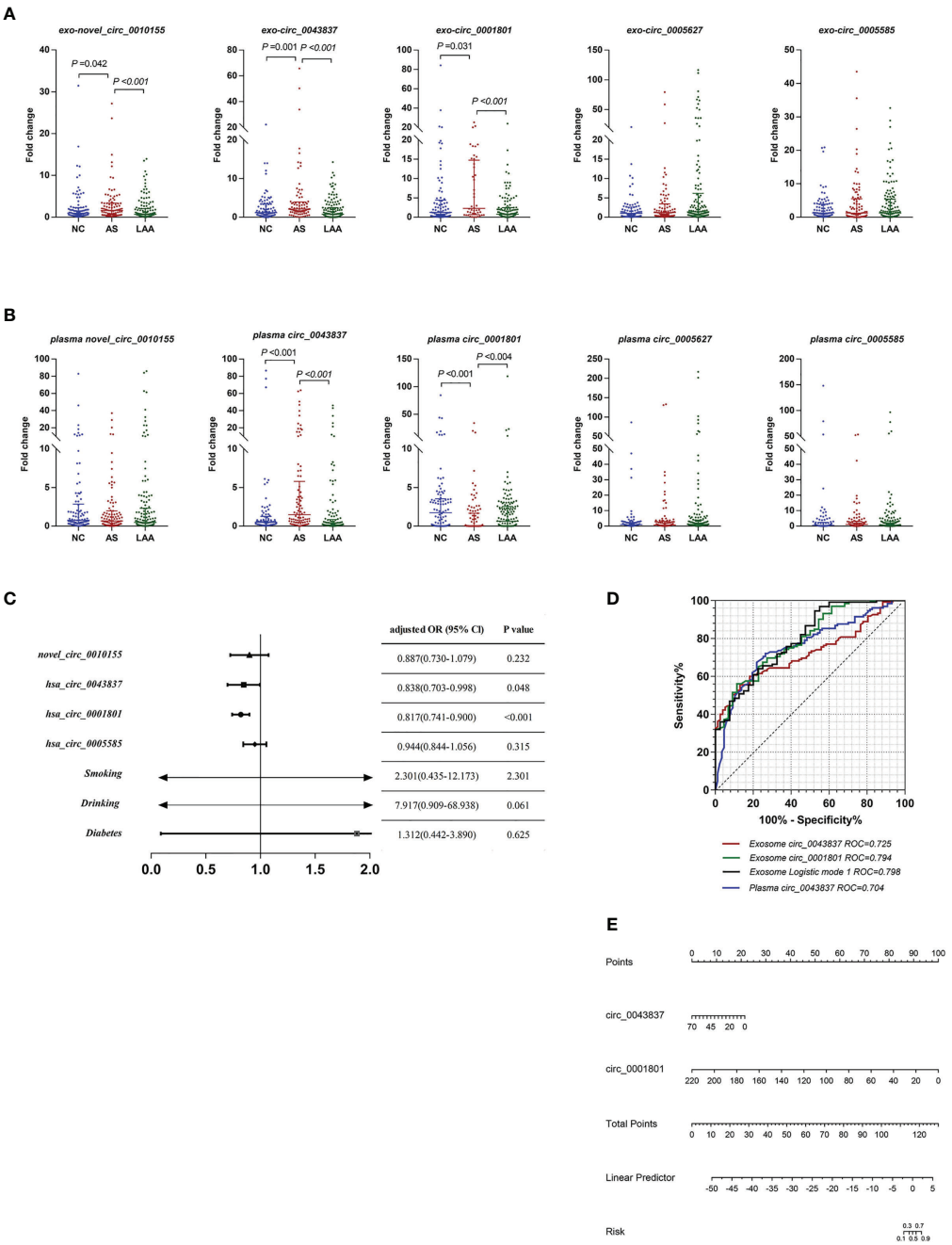

FIGURE 4 | Diagnostic efficacy of plaque rupture of exosomal and plasma circRNAs. **(A)** Replication of exosomal circRNAs between NC, AS, and LAA group. **(B)** Replication of plasma circRNAs between NC, AS, and LAA group. **(C)** Multivariate logistic regression analysis for exosomal circRNAs and clinical. **(D)** ROC curves of the exosomal circ_0043837, circ_0001801, plasma circ_0043837, and logistic mode 1: Two-exo-circRNA of circ_0043837 and circ_0001801. **(E)** Nomograms to predict risk of plaque rupture.

novel_circ_0010155 were significantly different before the LAA and NC groups in the expanded sample size assay. However, the latter two were not different between the LAA and SAO groups. This may suggest that the effect of stroke-related factors may have caused the differential expression of circ_0005627 and novel_circ_0010155 between the LAA and NC groups.

Previous studies suggested that exosomes could exert better protection against circRNAs (23, 31); therefore, in this study, we further examined plasma circRNA expression based on the study of differential expression of exosomal circRNAs and assessed the diagnostic efficacy of exosomal and plasma circRNAs. Our study found that there were statistically significant differences between the

plasma LAA group circ_0043837, circ_0001801, and novel_circ_0010155 and the healthy NC and SAO groups. The same trend was observed in the exosomal circRNAs. We further constructed a diagnostic model of logistics based on differential expression and tested the diagnostic efficacy of exosomal and plasma circRNAs by means of the ROC. The exosomal AUC was higher than the plasma AUC and the NRI between exosomal and plasma circRNAs was above zero, thus suggesting that the diagnostic efficacy of exosomal circRNAs was better than that of plasma circRNAs. By combining circ_0043837 and circ_0001801 to construct the diagnostic model, the diagnostic efficacy of combined exosomal and plasma circRNAs was higher than that of a single index. Our study further suggested that exosomal circRNAs had greater diagnostic efficacy than circulating plasma circRNAs.

To further verify that circRNAs with diagnostic efficacy play a protective or facilitative role during LAA, we included NIHSS scores that were positively correlated with LAA disease severity. circ_0043837 and circ_0001801 were negatively correlated with the NIHSS scores. It was suggested that as the circRNA expression decreased, the NIHSS score and stroke severity increased. This suggested that circ_0043837 and circ_0001801 played a protective role in stroke.

In previous studies, intracranial and extracranial arterial plaque rupture and thrombosis were the main causes of ischemic stroke (40, 41). Therefore, prediction of atherosclerotic unstable plaque may help to prevent stroke. We included the AS group with > 50% intracranial and extracranial stenosis but without morbidity in our study, compared with the LAA brain infarction group with > 50% vascular stenosis to highlight the significance of plaque instability. circ_0043837 and circ_0001801 were DE in both exosomal and plasma circRNAs in the two groups. At the same time, we suggested that the above two circRNAs were independent risk factors for LAA by including five circRNAs and five clinical indicators (Smoking, drinking, hypertension, diabetes, and LDL), in turn, by univariate and multivariate regression analysis. These findings suggested that circ_0043837 and circ_0001801 were potential biomarkers for predicting plaque rupture. Furthermore, the impact of common clinical risk factors on the circRNAs and plaque rupture needs further investigation. In addition, the current study has limitations. These include the small sample size, the single-center sample collection, and the unavoidable selective bias. In addition to this, the plaques characteristics should be further defined with the imaging.

In conclusion, our study suggests that exosomal circRNAs can be used as diagnostic markers for stroke in LAA. We also found that exosomal circRNAs have better diagnostic efficacy than plasma circRNAs. We further identified that circRNAs, as biomarkers, could indicate plaque rupture. Our study provides an important basis for the diagnosis and prevention of LAA stroke.

DATA AVAILABILITY STATEMENT

The datasets presented in this study can be found in online repositories. The names of the repository/repositories and accession number(s) can be found below: NCBI Gene Expression Omnibus—GSE190869, GSE173719.

ETHICS STATEMENT

Written informed consent was obtained from the individual(s) for the publication of any potentially identifiable images or data included in this article.

AUTHOR CONTRIBUTIONS

All authors read and approved the final version of the manuscript. XZ, XP were involved in the study design. QX, RH, HL, SZ, FZ collected the samples, performed the experiments and analyzed the data. QX, XZ completed the manuscript. All authors contributed to the article and approved the submitted version.

FUNDING

We gratefully acknowledge financial support from the National Natural Science Foundation of China (No.82171299), and Natural Science Foundation of Shandong Province (ZR2020MH138).

SUPPLEMENTARY MATERIAL

The Supplementary Material for this article can be found online at: https://www.frontiersin.org/articles/10.3389/fimmu.2021.830018/full#supplementary-material

REFERENCES

1. Vos T, Lim SS, Abbafati C, Abbas KM, Abbasi M, Abbasifard M, et al. Global Burden of 369 Diseases and Injuries in 204 Countries and Territories, 1990–2019: A Systematic Analysis for the Global Burden of Disease Study 2019. *Lancet* (2020) 396(10258):1204–22. doi: 10.1016/s0140-6736(20)30925-9
2. Shen Y, Peng C, Bai Q, Ding Y, Yi X, Du H, et al. Epigenome-Wide Association Study Indicates Hypomethylation of MTRNR2L8 in Large-Artery Atherosclerosis Stroke. *Stroke* (2019) 50(6):1330–8. doi: 10.1161/STROKEAHA.118.023436
3. Stefanadis C, Antoniou CK, Tsiachris D, Pietri P. Coronary Atherosclerotic Vulnerable Plaque: Current Perspectives. *J Am Heart Assoc* (2017) 6(3): e005543. doi: 10.1161/JAHA.117.005543
4. Libby P. The Changing Landscape of Atherosclerosis. *Nature* (2021) 592 (7855):524–33. doi: 10.1038/s41586-021-03392-8
5. Dolfi B, Gallerand A, Haschemi A, Guinamard RR, Ivanov S. Macrophage Metabolic Regulation in Atherosclerotic Plaque. *Atherosclerosis* (2021) 334:1–8. doi: 10.1016/j.atherosclerosis.2021.08.010
6. Li X, Yang L, Chen LL. The Biogenesis, Functions, and Challenges of Circular RNAs. *Mol Cell* (2018) 71(3):428–42. doi: 10.1016/j.molcel.2018.06.034

7. Chen LL. The Expanding Regulatory Mechanisms and Cellular Functions of Circular RNAs. *Nat Rev Mol Cell Biol* (2020) 21(8):475–90. doi: 10.1038/s41580-020-0243-y
8. Zuo L, Zhang L, Zu J, Wang Z, Han B, Chen B, et al. Circulating Circular RNAs as Biomarkers for the Diagnosis and Prediction of Outcomes in Acute Ischemic Stroke. *Stroke* (2020) 51(1):319–23. doi: 10.1161/strokeaha.119.027348
9. Wang Q, Liu X, Zhao J, Zhu R. Circular RNAs: Novel Diagnostic and Therapeutic Targets for Ischemic Stroke. *Expert Rev Mol Diagn* (2020) 20(10):1039–49. doi: 10.1080/14737159.2020.1826313
10. Wilusz JE. A 360° View of Circular RNAs: From Biogenesis to Functions. *Wiley Interdiscip Rev RNA* (2018) 9(4):e1478. doi: 10.1002/wrna.1478
11. Yang L, Han B, Zhang Z, Wang S, Bai Y, Zhang Y, et al. Extracellular Vesicle-Mediated Delivery of Circular RNA SCMH1 Promotes Functional Recovery in Rodent and Nonhuman Primate Ischemic Stroke Models. *Circulation* (2020) 142(6):556–74. doi: 10.1161/CIRCULATIONAHA.120.045765
12. Li Y, Zheng Q, Bao C, Li S, Guo W, Zhao J, et al. Circular RNA is Enriched and Stable in Exosomes: A Promising Biomarker for Cancer Diagnosis. *Cell Res* (2015) 25(8):981–4. doi: 10.1038/cr.2015.82
13. Kalluri R, LeBleu VS. The Biology, Function, and Biomedical Applications of Exosomes. *Science* (2020) 367(6478):eaau6977. doi: 10.1126/science.aau6977
14. Colao I, Corteling R, Bracewell D, Wall I. Manufacturing Exosomes: A Promising Therapeutic Platform. *Trends Mol Med* (2018) 24(3):242–56. doi: 10.1016/j.molmed.2018.01.006
15. van Niel G, D'Angelo G, Raposo G. Shedding Light on the Cell Biology of Extracellular Vesicles. *Nat Rev Mol Cell Biol* (2018) 19(4):213–28. doi: 10.1038/nrm.2017.125
16. Yu P, Chen W. Advances in the Diagnosis of Exosomal miRNAs in Ischemic Stroke. *Neuropsychiatr Dis Treat* (2019) 15:2339–43. doi: 10.2147/NDT.S216784
17. Wang H, Xie Y, Salvador AM, Zhang Z, Chen K, Li G, et al. Exosomes: Multifaceted Messengers in Atherosclerosis. *Curr Atheroscler Rep* (2020) 22(10):57. doi: 10.1007/s11883-020-00871-7
18. Yang W, Yin R, Zhu X, Yang S, Wang J, Zhou Z, et al. Mesenchymal Stem Cell-Derived Exosomal MiR-145 Inhibit Atherosclerosis by Targeting JAM-A. *Mol Ther - Nucleic Acids* (2020) 4(23):119–31. doi: 10.1016/j.omtn.2020.10.037
19. Adams HP Jr, Bendixen BH, Kappelle LJ, Biller J, Love BB, Gordon DL, et al. Classification of Subtype of Acute Ischemic Stroke. Definitions for Use in a Multicenter Clinical Trial. TOAST. Trial of Org 10172 in Acute Stroke Treatment. *Stroke* (1993) 24(1):35–41. doi: 10.1161/01.str.24.1.35
20. Tiedt S, Prestel M, Malik R, Schieferdecker N, Duering M, Kautzky V, et al. RNA-Seq Identifies Circulating miR-125a-5p, miR-125b-5p, and miR-143-3p as Potential Biomarkers for Acute Ischemic Stroke. *Circ Res* (2017) 121(8):970–80. doi: 10.1161/CIRCRESAHA.117.311572
21. Tian Y, Gong M, Hu Y, Liu H, Zhang W, Zhang M, et al. Quality and Efficiency Assessment of Six Extracellular Vesicle Isolation Methods by Nano-Flow Cytometry. *J Extracell Vesicles* (2020) 9(1):1697028. doi: 10.1080/20013078.2019.1697028
22. Saenz-Pipaon G, San Martin P, Planell N, Maillo A, Ravassa S, Vilas-Zornoza A, et al. Functional and Transcriptomic Analysis of Extracellular Vesicles Identifies Calprotectin as a New Prognostic Marker in Peripheral Arterial Disease (PAD). *J Extracel Vesicles* (2020) 9(1):1729646. doi: 10.1080/20013078.2020.1729646
23. Min L, Zhu S, Chen L, Liu X, Wei R, Zhao L, et al. Evaluation of Circulating Small Extracellular Vesicles Derived miRNAs as Biomarkers of Early Colon Cancer: A Comparison With Plasma Total miRNAs. *J Extracel Vesicles* (2019) 8(1):1643670. doi: 10.1080/20013078.2019.1643670
24. Memczak S, Jens M, Elefsinioti A, Torti F, Krueger J, Rybak A, et al. Circular RNAs are a Large Class of Animal RNAs With Regulatory Potency. *Nature* (2013) 495(7441):333–8. doi: 10.1038/nature11928
25. Zhou L, Chen J, Li Z, Li X, Hu X, Huang Y, et al. Integrated Profiling of microRNAs and mRNAs: microRNAs Located on Xq27.3 Associate With Clear Cell Renal Cell Carcinoma. *PloS One* (2010) 5(12):e15224. doi: 10.1371/journal.pone.0015224
26. Mao X, Cai T, Olyarchuk JG, Wei L. Automated Genome Annotation and Pathway Identification Using the KEGG Orthology (KO) as a Controlled Vocabulary. *Bioinformatics* (2005) 21(19):3787–93. doi: 10.1093/bioinformatics/bti430
27. Woodward M, Tunstall-Pedoe H, Peters SA. Graphics and Statistics for Cardiology: Clinical Prediction Rules. *Heart* (2017) 103(7):538–45. doi: 10.1136/heartjnl-2016-310210
28. Zhang J-X, Song W, Chen Z-H, Wei J-H, Liao Y-J, Lei J, et al. Prognostic and Predictive Value of a microRNA Signature in Stage II Colon Cancer: A microRNA Expression Analysis. *Lancet Oncol* (2013) 14(13):1295–306. doi: 10.1016/s1470-2045(13)70491-1
29. Lotvall J, Hill AF, Hochberg F, Buzas EI, Di Vizio D, Gardiner C, et al. Minimal Experimental Requirements for Definition of Extracellular Vesicles and Their Functions: A Position Statement From the International Society for Extracellular Vesicles. *J extracellular vesicles* (2014) 3:26913. doi: 10.3402/jev.v3.26913
30. Kvistad CE, Novotny V, Kurz MW, Ronning OM, Thommessen B, Carlsson M, et al. Safety and Outcomes of Tenecteplase in Moderate and Severe Ischemic Stroke. *Stroke* (2019) 50(5):1279–81. doi: 10.1161/STROKEAHA.119.025041
31. He AT, Liu J, Li F, Yang BB. Targeting Circular RNAs as a Therapeutic Approach: Current Strategies and Challenges. *Signal Transduct Target Ther* (2021) 6(1):185. doi: 10.1038/s41392-021-00569-5
32. Kolodgie FD, Virmani R, Burke AP, Farb A, Weber DK, Kutys R, et al. Pathologic Assessment of the Vulnerable Human Coronary Plaque. *Heart* (2004) 90(12):1385–91. doi: 10.1136/hrt.2004.041798
33. Wang Y, Liu J, Ma J, Sun T, Zhou Q, Wang W, et al. Exosomal circRNAs: Biogenesis, Effect and Application in Human Diseases. *Mol Cancer* (2019) 18(1):116. doi: 10.1186/s12943-019-1041-z
34. Witwer KW, Wolfram J. Extracellular Vesicles Versus Synthetic Nanoparticles for Drug Delivery. *Nat Rev Mater* (2021) 6(2):103–6. doi: 10.1038/s41578-020-00277-6
35. Wen G, Zhou T, Gu W. The Potential of Using Blood Circular RNA as Liquid Biopsy Biomarker for Human Diseases. *Protein Cell* (2020) 12(12):911–46. doi: 10.1007/s13238-020-00799-3
36. Soehnlein O, Libby P. Targeting Inflammation in Atherosclerosis - From Experimental Insights to the Clinic. *Nat Rev Drug Discov* (2021) 20(8):589–610. doi: 10.1038/s41573-021-00198-1
37. Guo JU, Agarwal V, Guo H, Bartel DP. Expanded Identification and Characterization of Mammalian Circular RNAs. *Genome Biol* (2014) 15(7):409. doi: 10.1186/s13059-014-0409-z
38. Bellefroid EJ, Marine JC, Ried T, Lecocq PJ, Rivière M, Amemiya C, et al. Clustered Organization of Homologous KRAB Zinc-Finger Genes With Enhanced Expression in Human T Lymphoid Cells. *EMBO J* (1993) 12(4):1363–74. doi: 10.1002/j.1460-2075.1993.tb05781.x
39. Peng W, Cai G, Xia Y, Chen J, Wu P, Wang Z, et al. Mitochondrial Dysfunction in Atherosclerosis. *DNA Cell Biol* (2019) 38(7):597–606. doi: 10.1089/dna.2018.4552
40. Capodanno D, Alberts M, Angiolillo DJ. Antithrombotic Therapy for Secondary Prevention of Atherothrombotic Events in Cerebrovascular Disease. *Nat Rev Cardiol* (2016) 13(10):609–22. doi: 10.1038/nrcardio.2016.111
41. Kowara M, Cudnoch-Jedrzejewska A. Different Approaches in Therapy Aiming to Stabilize an Unstable Atherosclerotic Plaque. *Int J Mol Sci* (2021) 22(9):4354. doi: 10.3390/ijms22094354

Conflict of Interest: The authors declare that the research was conducted in the absence of any commercial or financial relationships that could be construed as a potential conflict of interest.

Publisher's Note: All claims expressed in this article are solely those of the authors and do not necessarily represent those of their affiliated organizations, or those of the publisher, the editors and the reviewers. Any product that may be evaluated in this article, or claim that may be made by its manufacturer, is not guaranteed or endorsed by the publisher.

frontiers in Immunology

ORIGINAL RESEARCH
published: 21 January 2022
doi: 10.3389/fimmu.2021.820039

Association Between Autoimmune Diseases and Spontaneous Cervicocranial Arterial Dissection

Hao Li[1†], Pu Song[1†], Wei Yang[1†], Le Yang[2], Shanshan Diao[1], Shicun Huang[1], Yiqing Wang[1], Xingshun Xu[1,3] and Yi Yang[1*]*

[1] Departments of Neurology, The First Affiliated Hospital of Soochow University, Suzhou, China, [2] School of Public Health, Fujian Medical University, Fuzhou, China, [3] The Institute of Neuroscience, Soochow University, Suzhou, China

OPEN ACCESS

Edited by:
Juehua Yu,
The First Affiliated Hospital of Kunming Medical University, China

Reviewed by:
Quanguang Zhang,
Augusta University, United States
Hongjin Wu,
Harbin Institute of Technology, China

***Correspondence:**
Xingshun Xu
Xingshunxu@suda.edu.cn
Yi Yang
13656229395@163.com

[†]These authors have contributed equally to this work

Specialty section:
This article was submitted to Multiple Sclerosis and Neuroimmunology, a section of the journal Frontiers in Immunology

Received: *22 November 2021*
Accepted: *30 December 2021*
Published: *21 January 2022*

Citation:
Li H, Song P, Yang W, Yang L, Diao S, Huang S, Wang Y, Xu X and Yang Y (2022) Association Between Autoimmune Diseases and Spontaneous Cervicocranial Arterial Dissection. Front. Immunol. 12:820039. doi: 10.3389/fimmu.2021.820039

A series of biopsies and reports showed autoimmune diseases might be involved in the process of local inflammation related to spontaneous cervicocranial arterial dissection (SCCAD) occurrence. This retrospective case-control study examined the association between SCCADs and autoimmune diseases in patients and control subjects from 2014 to 2020. SCCAD patients and age/sex-matched control subjects were recruited, and clinical data were collected. SCCAD was confirmed by digital subtraction angiography or high-resolution magnetic resonance imaging. The study included 215 SCCAD patients and 430 control subjects. Totally, 135 (62.8%) of the 215 cases were found SCCAD in the anterior circulation, 26 (12.0%) patients involved multiple vessels. Autoimmune disease occurred in 27 (12.6%) cases with SCCAD and 4 (0.9%) control subjects ($p<0.001$). A conditional multivariable logistic regression model was used to calculate the odds ratio for SCCAD among patients with a history of autoimmune disease, adjusting for hypertension, diabetes, hyperlipidemia, and smoking. After adjustment, autoimmune diseases were associated with SCCAD ($p<0.001$). After sub-analysis by a similar modeling strategy, significant associations were still observed in different subgroups, such as female group and male group as well as intramural hematoma (IMH) group and Non-IHM group. The association of SCCAD with autoimmune disease suggested that autoimmune mechanisms may be involved in some etiologies of SCCAD.

Keywords: cervicocranial arterial dissection, autoimmune, inflammatory autoimmune disease, inflammatory, neurological disease

INTRODUCTION

With imaging technique development, spontaneous cervicocranial arterial dissection (SCCAD) is increasingly diagnosed and becomes a common cause for young adult stroke (1, 2). In a previous study, SCCAD was found to tend to affect multiple arterial segments and develop simultaneously in intracranial and extracranial vessels (2). Although etiologies and pathogenesis of SCCAD have not been fully clarified, a series of biopsies and case reports show that inflammatory alterations and autoimmune diseases might be related to the cascade events leading to SCCAD (3–5). A recent case-

control study had also shown that anti-thyroid autoimmunity might be involved in the process of local inflammation related to SCCAD occurrence (6). However, these were not consistent with other studies (7, 8). Due to the limited data, it is unclear whether autoimmune diseases are associated with SCCAD or just co-incident with SCCAD. In this study, we examined the association between SCCAD and autoimmune diseases.

MATERIALS AND METHODS

Study Population

Patients with SCCAD in the First Affiliated Hospital of Soochow University from April 2014 to October 2020 were selected. Controls were randomly selected from individuals that resided in Suzhou City and attended the annual physical examination in our hospital and matched the patients with age and gender. All patients and controls underwent cervical cerebrovascular ultrasonography to screen SCCAD. Suspected SCCAD was further confirmed by digital subtraction angiography (DSA) or high-resolution magnetic resonance imaging (HR-MRI). Key pathognomonic radiological findings of CCAD were confirmed, including intimal flap, intramural hematoma (IMH), and double lumen. Exclusion criteria were as follows: 1) patients with definite traumatic CCAD; 2) patients had a history of iatrogenic cervicocranial artery injury or craniocervical vascular surgery within 6 months; 3) patients with Stanford type A aortic dissection involving the carotid artery; 4) patients with localized subclavian artery dissection.

Autoimmune Diseases Detection

Autoimmune diseases were diagnosed according to the International Classification of Diseases-9th Revision (ICD-9) and were classified as autoinflammatory diseases and classic autoimmune diseases (9) (**Table 1** and its notes). Autoimmune disease history was defined as the definite diagnosis that should be made before or within one month after the SCCAD events. The diagnosis of autoimmune diseases was based on a clinical interview, physical examination, and a medical record system that contained medical information including medical histories, diagnostic tests, diagnosis, and treatments for individuals who resided in Suzhou city and received health care within the system.

Clinical Information Collection

For all subjects, we collected baseline data including cerebral vascular risk factors such as hypertension and diabetes; affected vessel, and vessel states (occlusion or stenosis). Antinuclear antibodies, antineutrophil cytoplasmic antibodies, anticardiolipin antibodies, anticitrullinated protein antibodies, tumor-associated antigens (including tumor specific growth factor with chemiluminescence assay), thyroid stimulating hormone, and anti-thyroid stimulating hormone receptor antibodies were detected in some patients and controls to clarify the diagnosis.

Statistical Analysis

Conditional multivariable logistic regression analysis provided the adjusted odds ratio (OR) with a 95% confidence interval (CI) for odds of SCCAD in the presence of at least 1 autoimmune

TABLE 1 | Characteristics and autoimmune diseases of all 215 cases with SCCAD and their control subjects of first SCAD event.

	SCCAD cases (n=215)	Control subjects (n=430)	*p*-value
Age in years, median (IQR)	48 (38, 58)	49 (38, 58)	0.969
Male, n (%)	134 (62.3)	268 (62.3)	1.000
Smoking, n (%)	25 (11.6)	51 (11.9)	0.931
Hypertension, n (%)	85 (39.5)	166 (38.6)	0.819
Diabetes, n (%)	28 (13.0)	53 (12.3)	0.801
Hyperlipidemia, n (%)	49 (22.8)	100 (23.3)	0.895
Anterior circulation, n (%)	135 (62.8)	N/A	N/A
Intramural hematoma, n (%)	85 (39.5)	N/A	N/A
Multiple vessels involved	26 (12.0)	N/A	N/A
Cerebral infarction	142 (66.0)	N/A	N/A
With at least 1 autoimmune disease, n (%)	27 (12.6)	4 (0.9)	<0.001
Disease*			
Systemic lupus erythematosus, n (%)	2 (0.9)	0 (0.0)	0.111
Pernicious anemia, n (%)	1 (0.5)	0 (0.0)	0.157
Takayasu arteritis, n (%)	3 (1.4)	0 (0.0)	0.014
Sjögren's syndrome, n (%)	1 (0.5)	0 (0.0)	0.157
Antiphospholipid syndrome, n (%)	4 (1.9)	0 (0.0)	0.012
Rheumatoid arthritis, n (%)	0 (0.0)	1 (0.2)	1.000
Ankylosing spondylitis, n (%)	1 (0.5)	0 (0.0)	0.157
Vasculitis, n (%)	1 (0.5)	1 (0.2)	1.000
Psoriasis or psoriatic arthritis, n (%)	0 (0.0)	2 (0.4)	0.045
Myasthenia gravis, n (%)	1 (0.5)	0 (0.0)	0.333
Autoimmune thyroid disease, n (%)	15 (7.0)	0 (0.0)	<0.001
Hepatitis, autoimmune, n (%)	1 (0.5)	0 (0.0)	0.333

**Participants could have >1 disease. None of Participants had Addison's disease, Celiac disease, Crohn's disease, Dermatomyositis/polymyositis, Guillain-Barre syndrome, Multiple sclerosis,Polymyalgia rheumatica, Primary biliary cirrhosis, Systemic sclerosis, Type 1 diabetes, Ulcerative colitis, Uveitis, or Vitiligo.*
NA, Not applicable.

disease after adjusting for other variables selected from univariate analyses. Furthermore, participants were stratified and analyzed by a similar modeling strategy as for the main model. Statistical analysis was performed in SPSS 25.0. $P<0.05$ was considered statistically significant.

RESULTS

SCCAD Cases and Characteristics

In this study, 215 patients with SCCAD and 430 control subjects were included. For patients with SCCAD, their median age was 48 (38, 58) years, 134 (62.3%) patients were male. For control subjects, their median age was 49 (38, 58) years and 268 (62.3%) patients were male. There was no difference in smoking, hypertension, diabetes, and hyperlipidemia between the two groups (**Table 1**). More importantly, 27 (12.6%) cases in SCCAD patients and 4 (0.9%) cases in control subjects had at least 1 autoimmune disease (**Table 1**). There was a significant increase in the percentage of patients with the autoimmune disease in the SCCAD group compared with controls ($p<0.001$). In addition, an increase in tumor specific growth factor (TSGF) level was observed in 72.6% SCCAD patients (45/62 patients). Five SCCAD patients had isolated anti-nuclear antibodies without clinical manifestation.

Autoimmune Disease and the Risk of SCCAD

We further analyzed the composition of autoimmune diseases in SCCAD patients and control subjects. Compared with control subjects, autoimmune thyroid disease (AITD), antiphospholipid syndrome, and Takayasu arteritis were more common in SCCAD patients ($p<0.05$, **Table 1**). Other autoimmune diseases occurred in both groups with a low frequency ($p>0.05$, **Table 1**). To demonstrate the association between autoimmune diseases and SCCAD, conditional univariate and multivariable logistic regression analyses were performed. After adjustment for hypertension, diabetes, hyperlipidemia and smoking, having autoimmune diseases was significantly associated with increased odds of SCCAD (OR: 2.873; 95% CI: 1.914-4.311; $p<0.001$, **Table 2**).

To support our hypothesis, we performed a sub-analysis including patients with or without intramural hematoma (IMH, a pathognomonic marker of SCCAD) (10–12). Interestingly, 85 (39.5%) cases with SCCAD had IMH; among them, 15 (17.6%) patients had at least one autoimmune disease; 130 (60.5%) cases of SCCAD had no IMH, and 12 (9.2%) patients had at least one autoimmune disease. There was no difference in the case ratio of autoimmune diseases between the IMH group and the Non-IMH group (**Table 3**; $p>0.05$). After the analysis with a similar modeling strategy, significant associations between were observed in both sub-groups (IMH group: OR: 3.146; 95% CI: 1.76-5.621; p<0.001; non-IMH group: OR: 2.523; 95% CI: 1.389-4.582; p=0.002; **Tables 4**, **5**), indicating that autoimmune diseases were associated with SCCAD, but not with IMH.

Previous studies showed that autoimmune diseases are more prevalent in females (13); however, this retrospective cohort study showed predominantly male with SCCAD. Therefore, we analyzed the percentage of SCCAD patients with autoimmune diseases by gender. We found that 14 (17.3%) female SCCAD patients had autoimmune diseases, but only 13 (9.7%) male SCCAD patients had autoimmune diseases, indicating that autoimmune diseases were still more prevalent in female SCCAD patients than in male SCCAD patients. To further clarify the impact of gender on the association between autoimmune diseases and SCCAD, the patients and control subjects were divided into two groups by gender. After analyzing by a similar modeling strategy as for the main model, significant associations were still observed in two sub-groups, especially in female SCCAD patients with high OR value (female: OR: 3.254; 95% CI: 1.822-5.809; $p<0.001$; male: OR: 2.677; 95% CI: 1.491-4.806; $p=0.001$).

TABLE 2 | Conditional multivariable logistic regression analysis showed having an autoimmune disease was associated with increased odds of SCCAD.

Factor	Univariate logistic regression analysis		Multivariable logistic regression analysis	
	OR (95% CI)	*p*-value	OR (95% CI)	*p*-value
With at least 1 autoimmune disease	2.845 (1.9-4.258)	<0.001	2.873 (1.914-4.311)	<0.001
Smoking	0.985 (0.649-1.495)	0.944	0.955 (0.625-1.461)	0.834
Hypertension	1.026 (0.781-1.349)	0.852	0.984 (0.736-1.316)	0.915
Diabetes	1.043 (0.701-1.551)	0.837	1.101 (0.729-1.662)	0.648
Hyperlipidemia	0.983 (0.714-1.351)	0.914	0.987 (0.715-1.364)	0.938

TABLE 3 | Characteristics in patients with and without IMH.

	IMH group (n=85)	non-IMH group (n=130)	*p*-value
Age in years, median (IQR)	47.56 ± 11.78	49.04 ± 13.83	0.419
Male, n (%)	56 (65.9)	78 (60.0)	0.384
Smoking, n (%)	12 (14.1)	13 (10.0)	0.357
Hypertension, n (%)	40 (47.1)	45 (34.6)	0.068
Diabetes, n (%)	9 (10.6)	19 (14.6)	0.391
Hyperlipidemia, n (%)	24 (28.2)	25 (19.2)	0.124
With at least 1 autoimmune disease, n (%)	15 (17.6)	12 (9.2)	0.069

TABLE 4 | Conditional multivariable logistic regression analysis in SCCAD patients with IMH.

Factor	Univariate logistic regression analysis		Multivariable logistic regression analysis	
	OR (95% CI)	p-value	OR (95% CI)	*p*-value
With at least 1 autoimmune disease	3.201 (1.833-5.591)	<0.001	3.146 (1.76-5.621)	<0.001
Smoking	1.333 (0.871-2.041)	0.186	1.243 (0.798-1.938)	0.336
Hypertension	0.96 (0.481-1.916)	0.908	1.065 (0.526-2.157)	0.86
Diabetes	0.962 (0.6-1.543)	0.873	0.987 (0.608-1.601)	0.958
Hyperlipidemia	1.068 (0.58-1.968)	0.832	0.906 (0.484-1.694)	0.756

DISCUSSION

SCCAD is an infrequent but potentially devastating cause of stroke; its pathophysiologic mechanisms remain somewhat unclear (1). Although some case studies had discussed the possible relationship between SCCAD and autoimmune diseases, available data were sparse and inconsistent (3, 6–8, 14). In our cohort study on SCCAD patients, a higher ratio of autoimmune diseases was observed. The autoimmune disease was significantly associated with SCCAD.

The pathologic and imaging evidence of inflammatory infiltrates in the wall of intracranial dissected arteries suggest that local inflammatory alterations might be a crucial step for SCCAD (6). SCCAD with mural hematoma is more frequently associated with the presence of periarterial edema compared with traumatic mural hematoma, which supported the concept of underlying arterial inflammation in SCCAD (15). Inflammatory markers were elevated in stroke patients with SCCAD and correlated with clinical prognosis (16). In addition, two reports also showed that inflammation in the arterial wall was associated with SCCAD and aspirin/steroids treatment resulted in dramatic improvement of both clinical condition and magnetic resonance imaging brain lesions (3, 17). Failure to demonstrate a specific infection agent led to a hypothesis that the activation of specific immune-mediated mechanisms rather than a specific infective agent may be responsible for a local inflammatory alteration linked to SCCAD.

Meanwhile, SCCAD biopsy specimens demonstrated the presence of a generalized arteriopathy that leads to the impairment of the stability of arterial walls (4). In a previous study on aneurysm, proinflammatory cytokines could be activated by immune mechanisms and induce the proteolytic process for the degradation of the extracellular matrix proteins (18). It is difficult to determine whether the inflammatory reaction is the cause or the consequence of histopathologic changes in SCCAD. However, immune-related inflammatory infiltration was absent in traumatic dissection (15, 19). In some case reports, these arterial anomalies disappeared rapidly after immunosuppressive therapy, which also supports the link between autoimmunity and dissection (3, 17, 20).

Most autoimmune diseases are more prevalent in females than in males (13). Symptom severity, disease course, response to therapy, and overall survival may also differ between males and females with autoimmune diseases (13). Sex hormones have a crucial role in this gender bias because estrogens are potent stimulators of autoimmunity (13). However, it appears to be a slight gender predisposition favoring males in population-based studies of SCCAD, which were similar to our results, arguing against an estrogen effect (1). This may be related to the protective influence of estrogen on the cerebral vasculature. Meanwhile, our results showed that the proportion of female SCCAD patients with autoimmune diseases was much higher than that of male patients, supporting that autoimmune diseases are more prevalent in females.

In this study, we demonstrated the close association between SCCAD and some autoimmune diseases like AITD, antiphospholipid syndrome, and Takayasu arteritis, but not other autoimmune diseases. So far, current studies have not yet elucidated why certain organs or vessels become the targets of immune injury in autoimmune diseases while others are spared. This may be explained by the presence of specific autoimmune antibodies that cross-react with proteins present in cervicocranial arteries in different autoimmune diseases, which needs more investigation.

The main strengths of our study are the inclusion of a relatively large cohort of verified SCCAD patients; however, our data should be interpreted with some caution. There may have retrospective bias inherent, and the results may not generalize outside of the studied geographic location due to the variety of autoimmune diseases by latitude.

TABLE 5 | Conditional multivariable logistic regression analysis in SCCAD patients without IMH.

Factor	Univariate logistic regression analysis		Multivariable logistic regression analysis	
	OR (95% CI)	p-value	OR (95% CI)	*p*-value
With at least 1 autoimmune disease	2.542 (1.404,4.604)	0.002	2.523 (1.389,4.582)	0.002
Smoking	0.921 (0.519,1.633)	0.777	1.003 (0.559,1.801)	0.991
Hypertension	0.837 (0.582,1.203)	0.336	0.79 (0.533,1.171)	0.241
Diabetes	1.173 (0.736,1.872)	0.502	1.264 (0.77,2.074)	0.354
Hyperlipidemia	0.967 (0.621,1.506)	0.881	0.965 (0.617,1.511)	0.878

In our study, autoimmune disease was associated with SCCAD, suggesting disorders of immunity might have a role in the mechanism of local inflammatory alterations leading to SCCAD.

DATA AVAILABILITY STATEMENT

The raw data supporting the conclusions of this article will be made available by the authors, without undue reservation.

ETHICS STATEMENT

The studies involving human participants were reviewed and approved by The Institutional Review Board of the First Affiliated Hospital of Soochow University. The patients/participants provided their written informed consent to participate in this study.

AUTHOR CONTRIBUTIONS

Conception and design of the study: XX and YY. Data acquisition and analysis of data: HL, PS, WY, LY, SD, SH, YW, and YY. Drafting the manuscript: HL, PS, XX, and YY. All authors commented on previous versions of the manuscript. All authors contributed to the article and approved the submitted version.

FUNDING

This work was supported by National Science Foundation of China (82071511), Shandong Provincial Natural Science Foundation (ZR2019ZD32), and the Priority Academic Program Development of Jiangsu Higher Education Institutions (20KJB320021).

ACKNOWLEDGMENTS

We thank all patients for their participation.

REFERENCES

1. Blum CA, Yaghi S. Cervical Artery Dissection: A Review of the Epidemiology, Pathophysiology, Treatment, and Outcome. *Arch Neurosci* (2015) 2(4): e26670. doi: 10.5812/archneurosci.26670
2. Wu Y, Wu F, Liu Y, Fan Z, Fisher M, Li D, et al. High-Resolution Magnetic Resonance Imaging of Cervicocranial Artery Dissection: Imaging Features Associated With Stroke. *Stroke* (2019) 50(11):3101–7. doi: 10.1161/STROKEAHA.119.026362
3. Herath H, Pahalagamage SP, Withana D, Senanayake S. Complete Ophthalmoplegia, Complete Ptosis and Dilated Pupil Due to Internal Carotid Artery Dissection: As the First Manifestation of Takayasu Arteritis. *BMC Cardiovasc Disord* (2017) 17(1):201. doi: 10.1186/s12872-017-0638-7
4. Volker W, Besselmann M, Dittrich R, Nabavi D, Konrad C, Dziewas R, et al. Generalized Arteriopathy in Patients With Cervical Artery Dissection. *Neurology* (2005) 64(9):1508–13. doi: 10.1212/01.WNL.0000159739.24607.98
5. Collamer AN, Battafarano D. A Pain in the Neck: Carotid Artery Dissection Presenting as Vasculitis. *Mil Med* (2013) 178(7):e851–4. doi: 10.7205/MILMED-D-12-00414
6. Pezzini A, Del Zotto E, Mazziotti G, Ruggeri G, Franco F, Giossi A, et al. Thyroid Autoimmunity and Spontaneous Cervical Artery Dissection. *Stroke* (2006) 37(9):2375–7. doi: 10.1161/01.STR.0000236500.15976.f3
7. Kronzer VL, Tarabochia AD, Lobo Romero AS, Tan NY, O'Byrne TJ, Crowson CS, et al. Lack of Association of Spontaneous Coronary Artery Dissection With Autoimmune Disease. *J Am Coll Cardiol* (2020) 76 (19):2226–34. doi: 10.1016/j.jacc.2020.09.533
8. Lichy C, Pezzini A, Becker C, Arnold ML, Brandt T, Kloss M, et al. No Evidence for a Role of Thyroid Autoimmunity in the Pathogenesis of Cervical Artery Dissection. *Cerebrovasc Dis* (2009) 28(2):203–4. doi: 10.1159/000226581
9. Cooper GS, Bynum ML, Somers EC. Recent Insights in the Epidemiology of Autoimmune Diseases: Improved Prevalence Estimates and Understanding of Clustering of Diseases. *J Autoimmun* (2009) 33(3-4):197–207. doi: 10.1016/j.jaut.2009.09.008
10. Lee SH, Jung JM, Kim KY, Kim BJ. Intramural Hematoma Shape and Acute Cerebral Infarction in Intracranial Artery Dissection: A High-Resolution Magnetic Resonance Imaging Study. *Cerebrovasc Dis* (2020) 49(3):269–76. doi: 10.1159/000508027
11. Choi YJ, Jung SC, Lee DH. Vessel Wall Imaging of the Intracranial and Cervical Carotid Arteries. *J Stroke* (2015) 17(3):238–55. doi: 10.5853/jos.2015.17.3.238
12. Gao PH, Yang L, Wang G, Guo L, Liu X, Zhao B. Symptomatic Unruptured Isolated Middle Cerebral Artery Dissection: Clinical and Magnetic Resonance Imaging Features. *Clin Neuroradiol* (2016) 26(1):81–91. doi: 10.1007/s00062-014-0337-z
13. Ortona E, Pierdominici M, Maselli A, Veroni C, Aloisi F, Shoenfeld Y. Sex-Based Differences in Autoimmune Diseases. *Ann Ist Super Sanita* (2016) 52 (2):205–12. doi: 10.4415/ANN_16_02_12
14. Tsai YD, Chien WC, Tsai SH, Chung CH, Chu SJ, Chen SJ, et al. Increased Risk of Aortic Aneurysm and Dissection in Patients With Sjogren's Syndrome: A Nationwide Population-Based Cohort Study in Taiwan. *BMJ Open* (2018) 8 (9):e022326. doi: 10.1136/bmjopen-2018-022326
15. Naggara O, Touze E, Marsico R, Leclerc X, Nguyen T, Mas JL, et al. High-Resolution MR Imaging of Periarterial Edema Associated With Biological Inflammation in Spontaneous Carotid Dissection. *Eur Radiol* (2009) 19 (9):2255–60. doi: 10.1007/s00330-009-1415-5
16. Sun G, Yang Y, Chen Z, Yang L, Diao S, Huang S, et al. Neutrophil to Lymphocyte Ratio Predicts Outcome of Stroke by Cervicocranial Arterial Dissection. *Front Med (Lausanne)* (2020) 7:598055. doi: 10.3389/fmed.2020.598055
17. Saliou V, Ben Salem D, Ognard J, Guellec D, Marcorelles P, Rouhart F, et al. A Collet-Sicard Syndrome Due to Internal Carotid Artery Dissection Associated With Cerebral Amyloid Angiopathy-Related Inflammation. *SAGE Open Med Case Rep* (2018) 6:2050313X18777176. doi: 10.1177/2050313X18777176
18. Kaneko H, Anzai T, Horiuchi K, Kohno T, Nagai T, Anzai A, et al. Tumor Necrosis Factor-Alpha Converting Enzyme Is a Key Mediator of Abdominal Aortic Aneurysm Development. *Atherosclerosis* (2011) 218(2):470–8. doi: 10.1016/j.atherosclerosis.2011.06.008
19. Forster K, Poppert H, Conrad B, Sander D. Elevated Inflammatory Laboratory Parameters in Spontaneous Cervical Artery Dissection as Compared to Traumatic Dissection: A Retrospective Case-Control Study. *J Neurol* (2006) 253(6):741–5. doi: 10.1007/s00415-006-0109-z
20. Koller PT, Cliffe CM, Ridley DJ. Immunosuppressive Therapy for Peripartum-Type Spontaneous Coronary Artery Dissection: Case Report and Review. *Clin Cardiol* (1998) 21(1):40–6. doi: 10.1002/clc.4960210108

Conflict of Interest: The authors declare that the research was conducted in the absence of any commercial or financial relationships that could be construed as a potential conflict of interest.

this article, or claim that may be made by its manufacturer, is not guaranteed or endorsed by the publisher.

frontiers in Immunology

ORIGINAL RESEARCH
published: 28 February 2022
doi: 10.3389/fimmu.2022.845011

IL-17A Mediates Demyelination by Activating A1 Astrocytes *via* SOCS3 During *Angiostrongylus cantonensis* Infection

Zongpu Zhou[1†], Tuo Lin[2†], Zhen Liu[3†], Qian Ding[2], Zhixuan Ma[1], Wanqi Li[2], Fukang Xie[4], Yue Lan[2] and Ying Feng[1*]*

[1] School of Medicine, South China University of Technology, Guangzhou, China, [2] Department of Rehabilitation Medicine, Guangzhou First People's Hospital, School of Medicine, South China University of Technology, Guangzhou, China, [3] Department of Blood Transfusion, Guangzhou First People's Hospital, Guangzhou, China, [4] Zhongshan School of Medicine, Sun Yat-Sen University, Guangzhou, China

OPEN ACCESS

Edited by:
Juehua Yu,
The First Affiliated Hospital of Kunming Medical University, China

Reviewed by:
Kittisak Sawanyawisuth,
Khon Kaen University, Thailand
Hua Yuan,
Fourth Military Medical University, China

***Correspondence:**
Yue Lan
bluemooning@163.com
Ying Feng
fengy8@scut.edu.cn

[†]These authors have contributed equally to this work

Specialty section:
This article was submitted to Multiple Sclerosis and Neuroimmunology, a section of the journal Frontiers in Immunology

Received: 29 December 2021
Accepted: 04 February 2022
Published: 28 February 2022

Citation:
Zhou Z, Lin T, Liu Z, Ding Q, Ma Z, Li W, Xie F, Lan Y and Feng Y (2022) IL-17A Mediates Demyelination by Activating A1 Astrocytes via SOCS3 During Angiostrongylus cantonensis Infection. Front. Immunol. 13:845011. doi: 10.3389/fimmu.2022.845011

Background: Demyelinating disease of the central nervous system is one of the most common neurological diseases and effective treatment is still under in-depth research. Our previous study showed that *Angiostrongylus cantonensis* infection can induce demyelination injury in mouse brains and IL-17A expression was shown to be significantly increased during this process. Moreover, we found that IL-17A inhibition attenuated the demyelination caused by *A. cantonensis* infection. However, the underlying mechanisms have not yet been fully elucidated.

Methods: IL-17A neutralizing antibodies were injected into *A. cantonensis* infected mice to decrease IL-17A levels. The activation of glial cells in the brain and the expression of cell markers were detected by a variety of methods, including real-time quantitative PCR, western blotting, and immunofluorescence staining. The relationship between IL-17A and astrocyte activation was further identified by *in vitro* experiments. The role of SOCS3 in the IL-17A stimulating process was determined using RNA-seq data collection of infected mice and the siRNA interference method.

Results: Demyelination of the corpus callosum was relieved after administration of IL-17A neutralizing antibody and this was accompanied by decreased activation of A1 type astrocytes around this region. The expression of SOCS3 was attenuated and activation of astrocytes by IL-17A was mediated by the IL-17RA/STAT3/SOCS3 pathway. IL-17A not only directly damaged oligodendrocytes but also indirectly damaged oligodendrocytes through A1 astrocyte mediation. Specific siRNA inhibition of IL-17A-inducible SOCS3 in astrocytes alleviated their damaging effects on oligodendrocytes.

Conclusion: IL-17A plays an important role in demyelination induced by *A. cantonensis* infection *via* the IL-17RA/STAT3/SOCS3 pathway in A1-type astrocytes, indicating that specific blockage of IL-17A and SOCS3 activity could be a therapeutic strategy for neuroinflammatory demyelinating diseases associated with astrocyte activation.

Keywords: *Angiostrongylus cantonensis*, IL-17A, demyelination, astrocyte, SOCS3, IL-17RA/SOCS3/STAT3 pathway

INTRODUCTION

Angiostrongyliasis is a food-borne parasitic disease caused by infection with *Angiostrongylus cantonensis*, a parasite found mostly in coastal areas. In recent years, outbreaks of this disease have been reported, such as the famous "Ampullaria gigas infection" incident in 2006 (1). Humans are mainly infected by eating raw snails infected with third-stage larvae of *A. cantonensis* or contaminated vegetables and fruits (2). The clinical manifestations of infection are headache, neck stiffness, vomiting, and fever and the pathological changes are mainly meningitis and meningoencephalitis characterized by increased eosinophils (3). After antiparasitic therapy combined with hormone therapy, patients can generally be cured; however, most patients continue to have symptoms such as skin paresthesia, limb weakness and decreased vision, which seriously affects the quality of life of these patients. If antiparasitic drugs are used alone in the late stage of infection, the disintegration products released after the death of *A. cantonensis* can induce a secondary severe inflammatory response in the brain tissue, thus aggravating the damage to the brain tissue (4). Therefore, investigating the pathological mechanism of *A. cantonensis* infection and optimizing the treatment is still a focus for researchers.

Neuronal apoptosis is related to abnormal motor behavior and a study showed a large number of apoptotic neurons were detected in the cortical and hippocampal regions of rats and mice infected with *A. cantonensis* (5). Furthermore, significant activation of microglia in the brain was observed after infection and increased levels of various microglia-associated inflammatory factors were also detected. It has been shown that microglial activation can be induced *via* stimulation by *A. cantonensis* antigens *in vitro* (6). The above evidence indicates that, in addition to typical eosinophilic meningitis, *A. cantonensis* infection can also lead to a variety of other brain parenchymal lesions. It has been reported that patients with *A. cantonensis* infection were misdiagnosed with multiple sclerosis because of several similar symptoms, including headaches, limb paresthesia, and urinary retention (7). Furthermore, the MRI results for these patients showed spot-like lesions in the subcortical frontal lobe and non-enhancement lesions in two cervical vertebrae, indicative of multiple sclerosis; however, *A. cantonensis-associated* antigens were detected in the patient's cerebrospinal fluid. Demyelinating lesions on the sagittal surface of the brain have been detected in mice infected with *A. cantonensis* and several myelin-related indicators have also been shown to increase in the brain lavage fluid (8). A previous study by our group also showed that *A. cantonensis* infection can lead to demyelination of the mouse brain and optic nerve. MRI examination of the mouse brain showed that the corpus callosum area was highlighted and electron microscopy and LFB staining showed demyelination lesions. Visual impairment and demyelination changes to the optic nerve have also been observed in mice (9). Central nerve demyelinating diseases mainly include two types: myelin formation disorder and myelin destruction (10). The former is caused by congenital dysplasia or genetic mutations, such as leukodystrophy, while the latter refers to demyelination due to inflammation caused by infection, autoimmune response, nutrition deficiency, or drug-induced injury (11). To date, the pathogenesis of the demyelinating disease is not fully understood; hence, current treatments and their efficacy are very limited.

Astrocytes are the most abundant glial cells in the brain. They are widely distributed in various regions of the brain, participate in the formation of the blood-brain barrier (BBB), maintain homeostasis in the brain, and are responsible for the immune monitoring and cell support functions of the brain (12, 13). In recent years, astrocytes have been roughly divided into A1 and A2 phenotypes according to gene expression and cell function, where A1 astrocytes promote inflammation and A2 astrocytes inhibit inflammation (14). The expression of the Interleukin-17 (IL-17) receptor can be detected on the surface of astrocytes in both human and mouse brain tissue and astrocytes can also secrete IL-17 after stimulation by inflammation (15). IL-17 inhibits the differentiation of neural stem cells into astrocytes during neural development (16). In a cerebral ischemia injury model, IL-17 and TNF-α can synergistically promote astrocyte secretion of CXCL1, an inflammatory chemokine of neutrophils, and can aggravate the severity of inflammatory response in the ischemic regions (17). In the pathogenesis of multiple sclerosis, the number of IL-17 receptors on the surface of astrocytes has been shown to increase. IL-17 stimulates astrocytes located on the BBB, causing changes to the permeability of the barrier and aggravating the progression of the disease (18).

Suppressors of cytokine signaling (SOCS) proteins are involved in the regulation of gene expression and are mainly expressed in immune cells and nerve cells (19). SOCS proteins can act on the JAK/STAT pathway by regulating the phosphorylation of STAT proteins (20). SOCS3 protein, a member of the SOCS family, inhibits the expression of many genes. In experimental autoimmune encephalomyelitis (EAE) models, miR-409-3p and miR-1896 are involved in the production of IL-17-induced inflammatory cytokines secreted by astrocytes because they target the SOCS3/STAT3 signaling pathway (21). Knockout of SOCS3 can promote the synthesis of Th17 cells because SOCS3 can regulate the synthesis of IL-23, which is also a key cytokine for Th17 formation (22). The function of SOCS3 in neurological diseases has also been studied because its expression has been detected in a variety of cells in the brain, including astrocytes, microglia, oligodendrocytes, and neurons (23), indicating that the SOCS3 gene is closely related to the development and damage of brain tissues. In a spinal cord injury model, conditional knockout of the SOCS3 gene in brain cells expressing nestin can inhibit infiltration of inflammatory cells and apoptosis of neurons and oligodendrocytes (24).

This study was based on our previous research on the role of glial cells in *A. cantonensis* induced brain damage (25). We found that IL-17A activated numerous astrocytes and this may be an important cause of IL-17A-mediated demyelination injury. To further confirm this hypothesis, we used a medium transfer and co-culture system to test the effect of IL-17A activated astrocytes on oligodendrocytes. In addition, the expression level of IL-17A was positively correlated with the SOCS3 during *A. cantonensis*

infection. SOCS3 siRNA was applied in astrocyte medium to inhibit SOCS3 expression and we verified that IL-17A stimulates astrocytes through IL-17RA, STAT3, and SOCS3. The results showed that IL-17A can activate A1 astrocytes by upregulating SOCS3 expression level, which in turn damages oligodendrocytes. We hope to shed new light on the functions of IL-17A in brain inflammatory injury, to highlight the need for further revealing the pathogenesis of the demyelinating disease, allowing for optimization of existing treatment plans and proposing new treatment methods.

METHODS

Establishment of *A. cantonensis* Infection Model and Anti-IL-17A Antibody Treatment

Male BALB/c mice were purchased from the Animal Center Laboratory of Sun Yat-Sen University (Guangzhou, China). The Institutional Animal Care and Use Committee approved all animal procedures. All mice were raised in the same room and were randomly divided into experimental and control groups. We collected larvae III (L3) of *A. cantonensis* from Biomphalaria glabrata and washed them from the snail sediment with phosphate-buffered saline (PBS). Larvae number was counted using an anatomical microscope. Gavage administration method was applied to inject 30 A. *cantonensis* L3 into experimental group mice stomach. IL-17A neutralizing antibody (0.05×10^{-3}mg/kg/day, eBioscience) or immunoglobulin G1 (IgG1) isotype control (clone MOPC-21) were separately administrated to the experimental group and control group for 3 weeks through intraperitoneal injection method. We started antibody injection from 3 days before *A. cantonensis* infection to avoid off-target effects of antibiotics.

Astrocyte Isolation, Culture and SOCS3 siRNA Interference

Neonatal mice (1-3 days) old were selected and decapitated under aseptic conditions. The brains were placed in cold HBSS solution, and the meninges and blood vessels were dissected with instruments under an anatomical microscope. Then the tissue was cut and transferred to trypsin digestion solution (containing 0.1%DNA enzyme). Tissues were digested at 37°C for 20-30min. After digestion, DMEM10S medium (DMEM/F12 supplemented with 10% FBS) was added to terminate digestion. After centrifugation, the supernatant was removed and re-added to the medium to suspend precipitation. The cells were transferred into a poly-d-Lysine (PDL) coated culture flask and cultured for 7-10 days after mixed culture. The culture flask was placed on a constant temperature rotary shaker at 37°C and 250 RPM for 1 h to wipe off microglia and was continuously placed on the rotary shaker for 17-18h to isolate oligodendrocytes by differential adhesion. Primary astrocytes were seeded in 6-well plates and transiently transfected using riboFECT^{TM} CP Reagent. Cells received serial murine SOCS3 deletion mutants and different transfected concentrations to verify the best interfering sequence and concentration. We used fluorescence labeling siRNA to infected astrocytes to ensure the transfect efficiency of siRNA. Then the transfected cells were treated with medium or IL-17A for the subsequent experiments.

Isolation, Culture, and Identification of Oligodendrocytes Lineage Cells

Fresh neonatal mice (1-3 days) brain tissues were obtained as the above method. The cortex was separated and cut into small pieces with ophthalmic scissors, and then moved into the centrifugal tube together with HBSS solution. The tissue was gently blown several times with the head of a gun until obvious tissue could not be seen by the naked eye. The tissue suspension was collected and centrifuged at 1000rpm for 5min. The supernatant was removed and the cells were washed repeatedly. Cell precipitation was blown again with neural stem cells (NSCs) growth culture medium (DMEM/F12 supplemented with 1% B27 and 20ng/ml bFGF), and the cell suspension was transferred to a culture flask for suspension culture at 37°C in an incubator of 95% air and 5% CO2. After NSCs formed the neurosphere, they were dissociated and transferred into oligodendrocyte progenitor cells (OPCs) induction medium (DMEM/F12 supplemented with 1% B27, 20ng/ml bFGF, 30ng/ml triiodothyronine, and 10 ng/ml PDGF-AA). We can use differential digestion and differential adhesion method to purify OPCs. The OPCs were cultured in the mature differentiation medium (DMEM/F12 supplemented with 1% B27, 1%N2, 20 ng/mL PDGF-AA, and 20 ng/mL IGF1, 40ng/ml T3, and 5% FBS) until the cells were fully mature and formed a "spiderweb-like" structure of oligodendrocyte and were identified by specific cell markers.

RNA Isolation and Real-Time PCR

Total RNA was extracted from the brain using a trizol reagent (TaKaRa) according to the instructions. mRNA was then reversely transcribed using the Prime Script RT reagent kit (TaKaRa) for cDNA synthesis. Then we used cDNA to perform real-time quantitative PCR using the SYBR Premix Ex Taq kit (TaKaRa). The 2-ΔΔCt method was used to assess the relative expression level of mRNA. mRNA levels were measured using the following specific primer sequences: C3d, 5'-CGTGGCCAAGC TAAGCATCA-3' and 3'-GGCCTCCATTGTCTTGGTGG -5'; S100α10, 5'-TTGCAGGCGACAAAGACCAC-3', 3'-CACTTTG CCATCTCGGCACT-5'; SOCS3, 5'-CTGGTACTGAGCCGA CCTCT -3' and 3'-GGCAGCTGGGTCACTTTCTC -5';STAT3, 5'-CATTGACCTGCCGATGTCCC -3' and 3'-GAGCGACTCA AACTGCCCTC -5'. Expression of the gene of interest was normalized to that of the housekeeping gene GAPDH (reduced glyceraldehyde-phosphate dehydrogenase).

High Throughput Sequencing and mRNA Library Construction

Our research group set RNA sequencing data library of mice brain infected with *A. cantonensis* (26). Mice were separately sacrificed at 2, 7, 14, 21 days post-infection with *A. cantonensis*, and the mice brains were immediately isolated to extract total RNAs. The same number of healthy mice samples were used as

control. Briefly, the total RNAs contained were extracted using the RNeasy® Mini Kit (Qiagen, Germany) and reversed transcription to cDNA to prepare the Illumina/Solexa sequencing library. And then we used Illumina Genome Analyzer IIx to perform the sequencing process. The expression profiles of the SOCS family were shown in a heatmap.

Histology and Immunofluorescence

Mice were anesthetized with isoflurane and perfused transcardially with ice-cold PBS followed by 4% paraformaldehyde (PFA). After fixing with PFA and 30% sucrose water, brain samples were embedded in optimal cutting temperature compound (OCT) and cut into10 μm slides at -20°C. Next, slides were permeabilized with 0.3% Triton X-100 and blocked with 2% bovine serum albumin (BSA) for 1 h at room temperature. Removing blocking buffer and incubating slides with the primary antibody in 1% BSA at 4°C overnight. Slides were washed in PBS three times and incubated with fluorescein isothiocyanate-labeled secondary antibody, which diluted 1:500 in 1% BSA at 37°C for 1 h. DAPI was then applied for 5 mins to stain the nucleus. Slides were washed again in PBS and observed under a fluorescence microscope. The antibodies used to detect the cells were as follows: anti-GFAP (CST, 3670), anti-S100β (Abcam, ab52642), anti-SOCS3 (Abcam, ab16030), anti-C3d (RD system, AF2655), anti-S100a10 (RD system, AF2377), and anti-MBP (Abcam, ab40390), anti-oligo2 (Sigma-Aldrich, AB9610). Staining samples without the primary antibody were used as negative controls.

Western Blotting

Brain tissue was lysed in extraction buffer (20 mM HEPES [pH 7.4], 2 mM EDTA, 50 mM glycerophosphate, 1 mM dithiothreitol, 1 mM Na3VO4, 1% Triton X-100, and 10% glycerol) on ice. The lysates were centrifuged at 1000 rpm for 10 mins. Supernatants were collected and their protein concentrations were determined using a bicinchoninic acid protein assay (BCA assay). Proteins were heated with sample buffer, separated in 12% sodium dodecyl sulfate-polyacrylamide gels by electrophoresis, and electroblotted onto a nitrocellulose membrane. Transferred blots were incubated with a blocking agent (5% non-fat milk in Tris-buffered saline). Anti-SOCS3, anti-STAT3(CST, 0139), anti- phosphor-STAT3(CST, 9145), and their secondary antibody blots were developed using the enhanced chemifluorescence detection kit according to the manufacturer's instructions. The same blots were subsequently stripped and reblotted with an antibody of β-tubulin to verify equal protein loading. Graphs of blots were obtained in the linear range of detection and protein levels were quantified using ImageJ software (NIH).

Quantification and Statistical Analysis

The random number generator function in Microsoft Excel was used to randomly allocate experiment mice. Positive cell counts and lesion pixel area quantification for Western Blotting were performed using ImageJ. GraphPad Prism 8.2 was used to statistically compare the data on real-time quantitative PCR, Western Blot, and immunofluorescence graphs among different groups. Data are expressed as the mean ± SEM and were analyzed using a two-tailed t-test or one-way ANOVA and Tukey's test, as appropriate. $p < 0.05$ was considered statistically significant.

RESULTS

A. cantonensis Infection Causes Activation of Type A1 and A2 Astrocytes in the Corpus Callosum

A. cantonensis infection is a typical parasitic infection that causes serious brain injury. In the late stage of infection, almost all larvae of *A. cantonensis* cross the BBB and parasitize the brain (27). As we have mentioned, demyelination is a typical pathological change in *A. cantonensis* infection and its severity is proportional to motor dysfunction in infected mice. Similar to our previous study, staining for myelin basic protein (MBP) showed apparent demyelination, especially at 21 days post-infection (dpi) (**Figure 1A**). In the present study, we attempted to identify the role of glial cells in this process. We detected different drastic astrocyte activation around the corpus callosum by staining the astrocyte markers, GFAP and S100β (**Figures 1B, C**). Importantly, astrocytes exhibited prolonged cell processes and displayed a hypertrophic cellular body, which is a typical phenotype for reactive cells.

To determine the type of activated astrocytes, we assessed the levels of the astrocyte activated marker genes, C3d and S100α10, which represent A1 astrocytes and A2 astrocytes, respectively. Both genes expression increased during infection (**Figures 1D, E**). Immunofluorescence staining results also showed that the number of astrocyte positive cells ($C3d^+$ $GFAP^+$, $S100\alpha10^+$ $GFAP^+$) increased significantly at 14 dpi (**Figures 2A, B**). These results indicated that both A1 and A2 astrocytes were highly activated after *A. cantonensis* infection and that the activation of astrocytes was mainly concentrated in the corpus callosum region.

IL-17A Mediates the Activation of A1 Astrocytes During *A. cantonensis* Infection

We previously observed that IL-17A levels increased after *A. cantonensis* infection and injection of neutralizing antibodies successfully decreased IL-17A to a low level. It has been proven that injecting IL-17A neutralizing antibodies can relieve the degree of demyelination (25). Next, we wanted to determine whether astrocytes mediated this process (**Figure 3A**). Immunofluorescence staining results showed that the expression of GFAP in brain tissues decreased after IL-17A was neutralized and C3d expression was also reduced by a statistically significant amount compared with the control group, while there was no significant difference in the expression of S100α10 (**Figures 3B**, **4A, C**). qPCR analysis of these genes showed similar results (**Figures 4B, C**). This suggested that IL-17A mainly mediated the activation of A1 astrocytes during *A. cantonensis* infection.

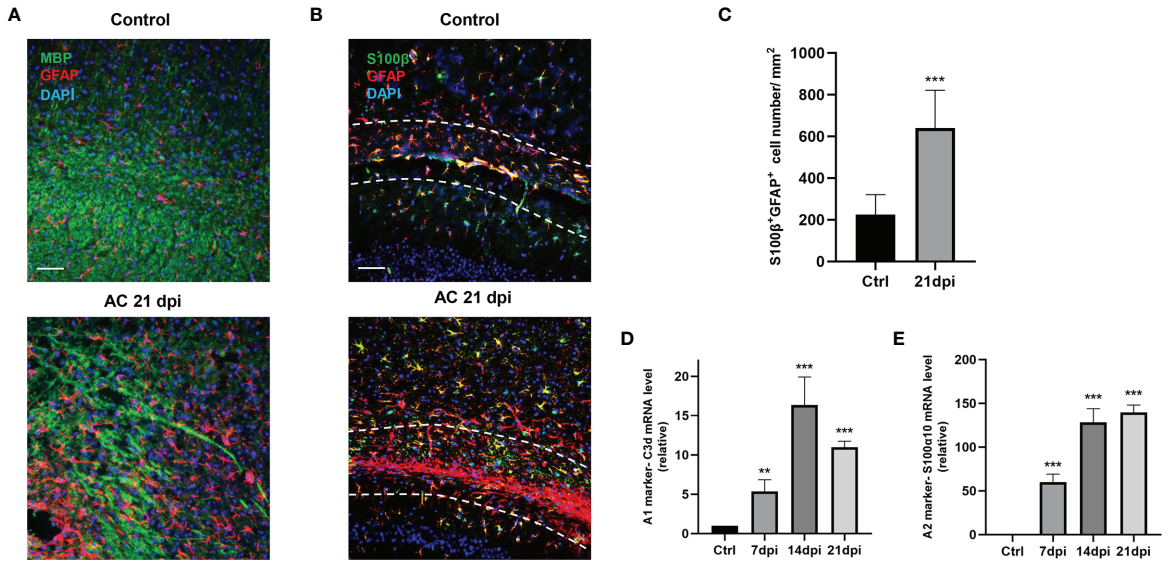

FIGURE 1 | *A. cantonensis* infection caused astrocytes activation. **(A)** Representative sections showing that immunostaining distribution MBP and GFAP in control (Ctrl) group and 21 dpi group. Scale bar = 75 μm. **(B)** Representative images of S100β and GFAP staining of control and 21 dpi groups. Scale bar = 75 μm. **(C)** Quantification of $GFAP^+$, $S100\beta^+$ cells. **(D, E)** mRNA expression of C3d and S100α10 of the brain at 7, 14, and 21 dpi. $^{**}P < 0.01$, $^{***}P < 0.001$. Data were analyzed by one-way ANOVA and followed by Tukey's *post hoc* analysis. Data in each statistical graph are presented as the mean ± SEM.

Next, we explored whether IL-17A has the capacity to influence astrocytes *in vitro* by stimulating primary astrocytes with different concentrations of IL-17A. The results showed 50 ng/mL was the optimal stimulating concentration of IL-17A. Following treatment with IL-17A, astrocytes were activated and cell expression of C3d and S100α10 increased, with a significant increase especially in $C3d^+$ $GFAP^+$ cell numbers (**Figures 5A, B**).

IL-17A Regulates SOCS3 Expression in Astrocytes Through the IL-17RA/STAT3/SOCS3 Pathway

The above results suggest that IL-17A is involved in the activation of A1 astrocytes during *A. cantonensis* infection. Through our previous gene sequencing and qPCR verification, it was proven that the mRNA level of the SOCS3 gene in astrocytes increased significantly at 14dpi and this high expression level persisted until the late stage of infection (**Figures 6A–C**). SOCS3 protein is considered to inhibit axonal regeneration, therefore we hypothesized that IL-17A induced high expression levels of SOCS3 in astrocytes, resulting in sustained myelin injury after *A. cantonensis* infection. Immunofluorescence staining was used to co-label SOCS3 and GFAP proteins and it was found that SOCS3 was highly expressed in astrocytes but not in other cells after infection (**Figures 6D, E**). Western blotting was used to detect changes in SOCS3 protein content after injection of the neutralizing antibody. The results showed that the expression level of IL-17A was positively correlated with SOCS3 and that the SOCS3 expression level in mice of the IL-17 neutralizing antibody group was lower than that of the control group, with the difference being statistically significant (**Figures 6F, G**).

The traditional pathway involving SOCS3 is the JAK/STAT pathway, therefore we further investigated the expression levels of the STAT family. We processed the IL-17A stimulation experiment in astrocytes to ascertain the expression patterns of SOCS3 and STAT3. SOCS3 and p-STAT3 expression levels were strongly increased along with the stimulation time extension (**Figures 7A–D**). To examine whether SOCS3 participates in the activation of astrocytes, a specific knockdown experiment of SOCS3 with siRNA was performed in primary astrocytes and astrocytes were then treated with an appropriate concentration of IL-17. The p-STAT3 protein was no longer inhibited by SOCS3, which indicated that IL-17A activated astrocytes through IL-17RA *via* the STAT3/SOCS3 pathway (**Figures 7E, F**). In conclusion, IL-17A promoted tyrosine phosphorylation of STAT3 and p-STAT3 induced the expression of SOCS3. In turn, phosphorylation of STAT3 was inhibited by SOCS3 in astrocytes.

High Expression of SOCS3 in A1 Astrocytes During *A. cantonensis* Infection Results in Myelin Injury

The myelin sheath is mainly formed by the myelination of oligodendrocytes in the central nervous system. Direct damage to oligodendrocytes or inhibition of the differentiation process of oligodendrocyte progenitor cells (OPCs) to oligodendrocytes is potential causes of demyelination. Some studies have indicated that A1 astrocytes act as harmful cells that inhibit OPC differentiation (28). To illustrate the relationship between IL-17A, astrocytes, and oligodendrocytes, we used indirect stimulation and cell co-culture methods. The conditioned medium from the primary astrocytes treated with IL-17A was

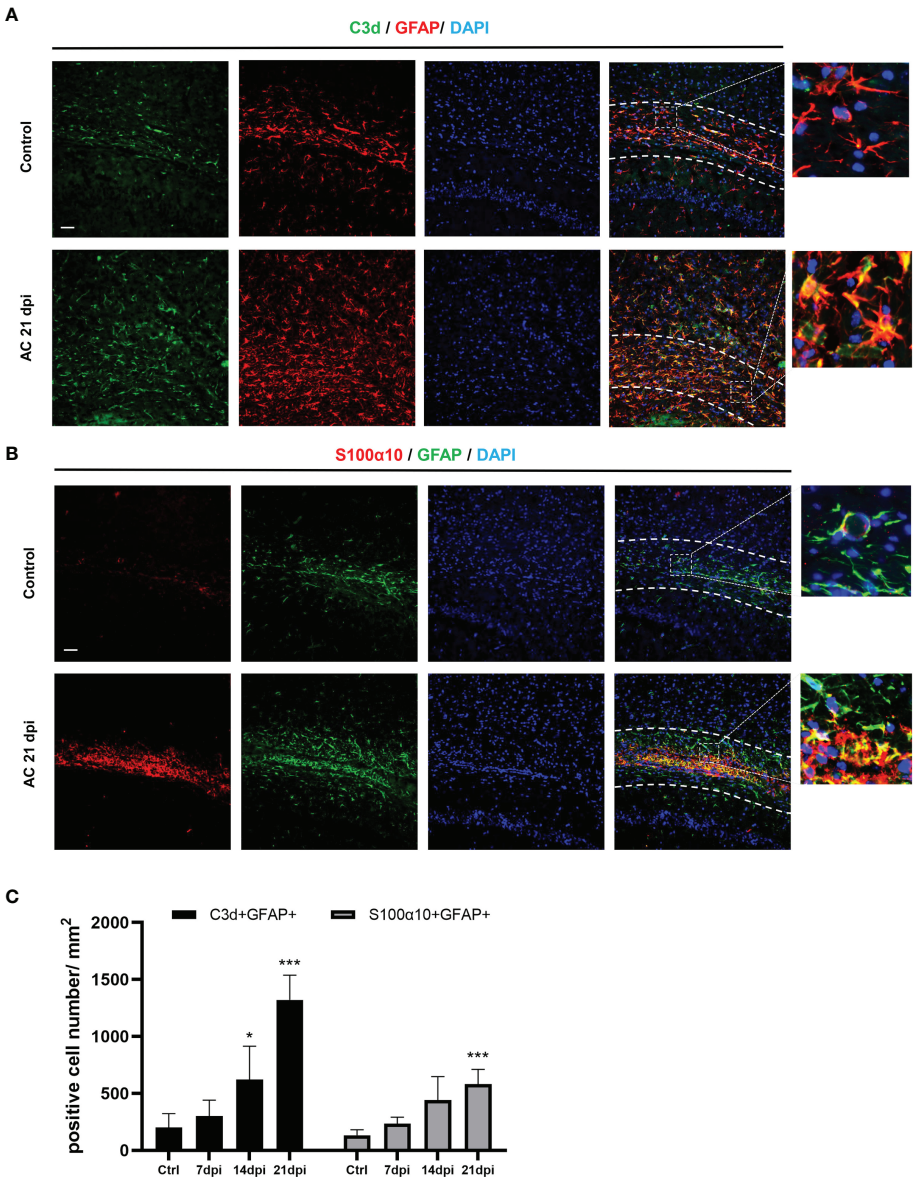

FIGURE 2 | *A. cantonensis* infection caused activation of A1 and A2 astrocytes in the corpus callosum. **(A, B)** Representative sections showing that distribution of GFAP$^+$, C3d$^+$ and GFAP$^+$, S100α10$^+$ cells in the corpus callosum. **(C)** Quantification of GFAP$^+$, C3d$^+$ and GFAP$^+$, S100α10$^+$ cells at 7, 14, and 21 dpi. Scale bar = 50 μm. n = 4-5 animals/group, *P < 0.05, ***P < 0.001. Data were analyzed by one-way ANOVA and followed by Tukey's *post hoc* analysis. Data in each statistical graph are presented as the mean ± SEM.

collected and applied to primary cells for 24, 48, 72 h to verify the effects of activated astrocytes (**Figure 8A**). Oligo2 (O2) and MBP, as two typical oligodendrocyte markers, were used to stain the mature oligodendrocytes as a previous study (29). The results suggested that the oligodendrocyte number decreased with stimulating time processing (**Figures 8B, C**). To further investigate the damaging effects of activated astrocytes induced by IL-17A on oligodendrocytes, we cultured astrocytes on top of OPCs and maintained the co-culture in the presence or absence of IL-17A for 72 h. Astrocytes were previously treated with control siRNA or SOCS3 siRNA (**Figure 9A**). We then used a similar method to assess the number of MBP$^+$ oligodendrocytes out of the total cell count. Compared with the control group, astrocytes interfered with by si-SOCS3 exhibited weakened effects on OPCs after IL-17A stimulation (**Figures 9B, C**). Hence, the damaging effect of IL-17A activated astrocytes on oligodendrocytes can be blocked through the interference of the IL-17RA/STAT3/SOCS3 pathway. Therefore, we speculated that myelin damage during *A. cantonensis* infection is partially attributed to IL-17A induced SOCS3 activation in astrocytes.

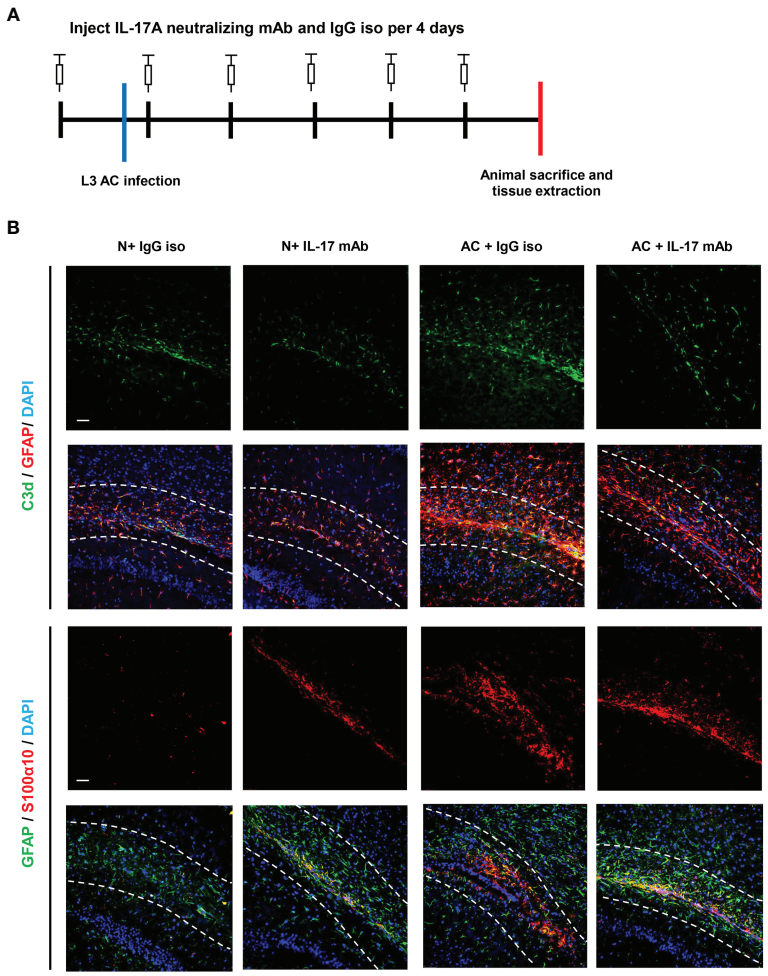

FIGURE 3 | IL-17A mediated the activation of A1 astrocytes during *A. cantonensis* infection. **(A)** Flow chart of IL-17A mAb and IgG isotype administration to mice infected with *A. cantonensis*. **(B)** Representative sections of GFAP$^+$, C3d$^+$, and S100α10$^+$ immunostaining from mice treated with IL-17A neutralizing antibody and IgG1 isotype antibody. Scale bar = 50 μm. n = 4-5 animals/group. Data in each statistical graph are presented as the mean ± SEM.

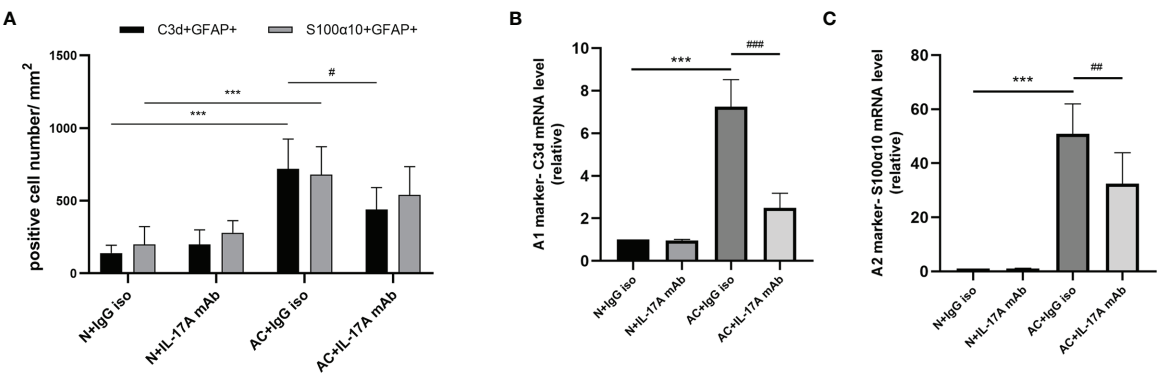

FIGURE 4 | IL-17A mediated the activation of A1 astrocytes during *A. cantonensis* infection. **(A)** Quantification of GFAP$^+$, C3d$^+$, and GFAP$^+$, and S100α10$^+$ in different groups. **(B, C)** mRNA expression of C3d and S100α10 of the brain of four groups. n = 4-5 animals/group, $^{***}P < 0.001$. Data were analyzed by one-way ANOVA and followed by Tukey's *post hoc* analysis. Data in each statistical graph are presented as the mean ± SEM. $^{\#}P < 0.05$, $^{\#\#}P < 0.01$, $^{\#\#\#}P < 0,001$.

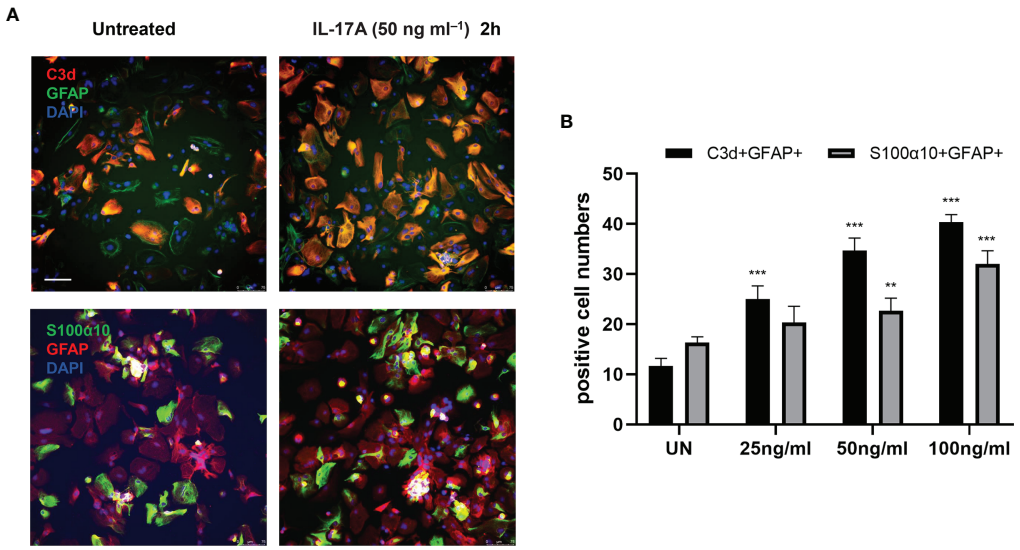

FIGURE 5 | IL-17A activated astrocytes *in vitro*. **(A)** Representative images display the expression of GFAP, C3d, and S100α10 in the presence of different concentration of IL-17A (UN=untreated). Scale bar = 75 μm. **(B)** Quantification of GFAP$^+$, C3d$^+$, and GFAP$^+$ S100α10 cells of each treated group. n = 3/group, $^{**}P < 0.01$, $^{***}P < 0.001$. Data were analyzed by one-way ANOVA and followed by Tukey's *post hoc* analysis. Data in each statistical graph are presented as the mean ± SEM.

DISCUSSION

Abnormal myelin development or damage can result in abnormal impulse transmission. Myelination is also important for cognitive function and studies have shown that myelin is involved in the development of motor learning and social interaction (30, 31). These highlight the importance of exploring the mechanism of demyelination. Our last published research showed the role of microglia in *A. cantonensis* infection, some cytokines secreted by microglia had been proved to promote the differentiation of astrocytes, such as C1q, IL-11α, and TNF (14), we subsequently found obvious astrocytes activation during this process. This indicates that the interaction between cells is important in the progression of the disease.

IL-17 is a typical pro-inflammatory factor that can induce inflammatory cell infiltration and tissue destruction, especially in autoimmune diseases such as type 1 diabetes (32, 33). At present, different studies have shown varied views on the relationship between IL-17A and demyelinating diseases. Multiple sclerosis is a representative central nervous system autoimmune disease and its animal model is EAE. It has been reported that EAE modeling in IL-17$^{-/-}$ mice lead to MOG-specific T cell sensitization, resulting in significantly reduced severity of disease damage (34). Th17 cells can interact synergistically with γδ T cells by producing IL-17 and IL-23 to accelerate disease progression in EAE models (35, 36). IL-17 is also involved in fighting off parasitic infections. Studies have shown that the secretion of IL-17 is promoted by chil3 and IL-17 and this has been shown to recruit neutrophils to fight against *Nippostrongylus brasiliensis* infection (37).

Our results showed that the increase of IL-17A induced by *A. cantonensis* infection not only caused myelin sheath injury but also activated astrocytes, with both A1 and A2 astrocytes being activated to varying degrees. In our infection model, the degree of activation of astrocytes positively correlated with the expression of IL-17A, and astrocytes were activated earlier than microglia. Therefore, we detected the activation status of astrocytes after IL-17A neutralization and the results showed that the activation of A1 astrocytes was significantly inhibited, similar to the results of *in vitro* experiments. Previous studies have shown that A1 astrocytes mainly promote inflammation, whereas A2 astrocytes inhibit inflammation (14). The changes in IL-17A, demyelination injury, and A1 astrocytes were consistent, so we inferred that the activation of A1 astrocytes induced by IL-17 might be related to demyelination injury. It has been shown that in EAE models, the activation of astrocytes is affected by IL-17 secreted by Th17 cells and this activation process is mainly mediated by the Act1 gene. Act1-specific deletion of astrocytes can interrupt the IL-17-induced cascade inflammatory response and thus affects the progression of EAE (38). In addition, astrocytes express the ubiquitin-modified enzyme A20, which inhibits the expression of the NF-κB pathway. Conditional knockdown of the A20 gene in astrocytes results in an uninhibited NF-κB pathway that exacerbates EAE progression (39). In the *in vitro* experiments, we incubated oligodendrocytes in the medium transferred from IL-17 stimulated astrocytes. The axons of oligodendrocytes were damaged and cell number decreased, which suggested IL-17A activated A1 astrocytes had an inhibiting effect on the growth of the oligodendrocytes.

Abnormal SOCS3 expression was also detected after *A. cantonensis* infection and IL-17A stimulation led to upregulation of SOCS3 expression in astrocytes *in vitro*. This process was short-lived and the highest level of SOCS3 expression

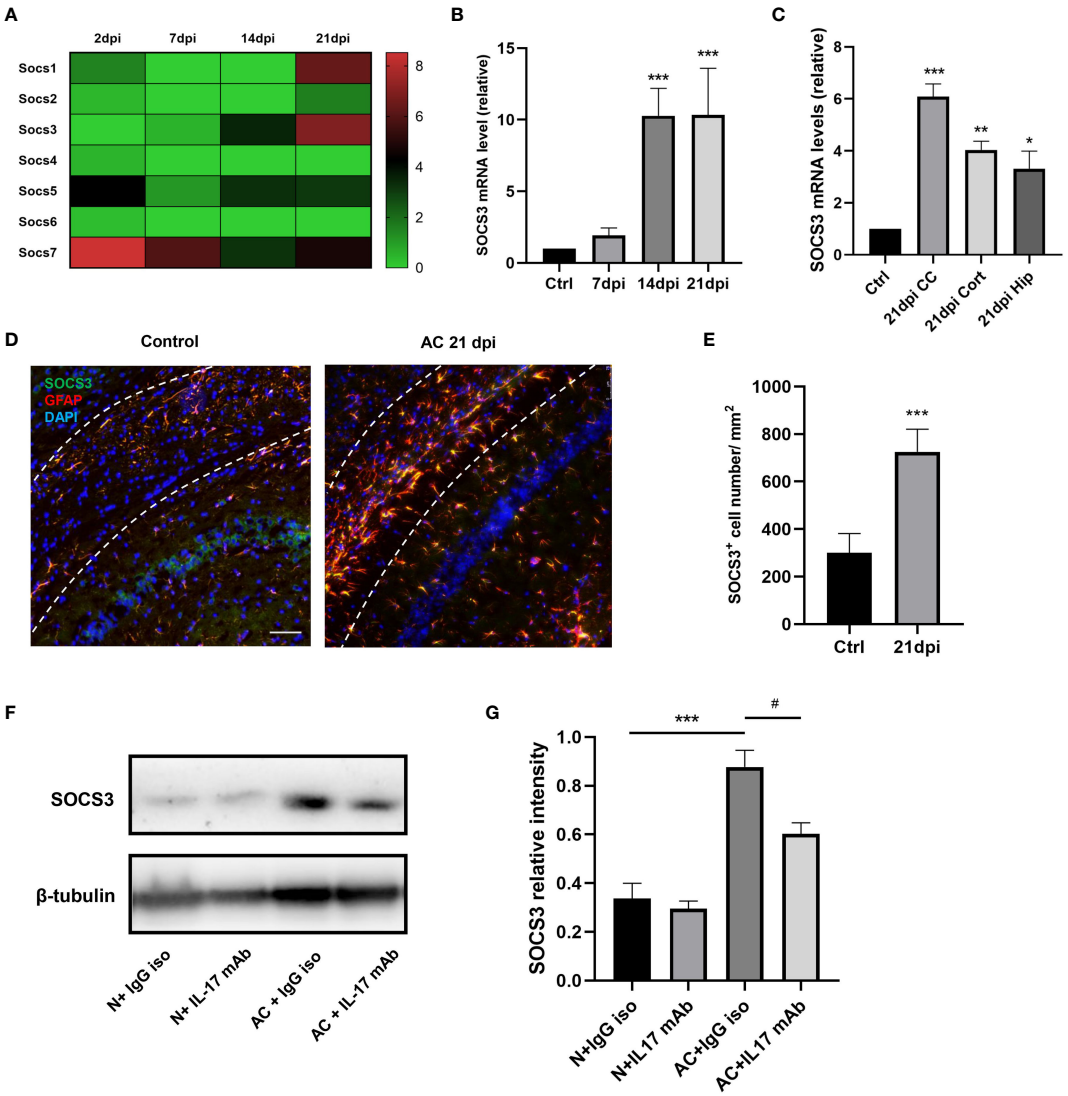

FIGURE 6 | IL-17A regulated SOCS3 expression in astrocytes during *A. cantonensis* infection. **(A, B)** Results of gene enrichment analysis was processed through comparing SOCS family mRNA levels and qPCR results of SOCS3 in infected mice brains at 2, 7, 14, and 21 dpi. **(C)** qPCR assay was performed to assess SOCS3 gene levels of different brain regions at 21 dpi (CC = corpus callosum, Cort = cortex, Hip = hippocampus). **(D)** Representative images of SOCS3 and GFAP staining of control and 21 dpi groups. Scale bar = 75 μm. **(E)** Quantification of $GFAP^+$, $SOCS3^+$ cells at 7, 14, and 21 dpi. **(F)** Western Blotting results showed SOCS3 protein levels of individual treated groups. **(G)** Relative densitometric analysis of Western Blotting is represented, as normalized to β-actin. n = 5 animals/group, *P < 0.05, **P < 0.01, ***P < 0.001, #P < 0.05. Data were analyzed by one-way ANOVA and followed by Tukey's *post hoc* analysis. Data in each statistical graph are presented as the mean ± SEM.

was approximately 2h after IL-17A was applied, thereafter SOCS3 expression declined over time. A previous study demonstrated that natural killer cell activity can be inhibited by IL-17A through SOCS3, *w*hich can interfere with tumorigenesis and viral infection (40). SOCS3 plays an important role in various nervous systems. Specific knockout of SOCS3 in neurons leads to increased leptin sensitivity in the hypothalamus region, thus inhibiting appetite and reducing body weight (41). SOCS3 is an inhibitor of STAT3 and the error of the SOCS3 regulation program on STAT3 leads to abnormal STAT3 expression in the brain tissue of glioma patients, which is due to phosphorylated STAT3 promoting the expression of many tumorigenesis genes (42). SOCS3 has been proven to be related to the axon growth process and SOCS3 knockout in mice can accelerate the recovery rate of axon-damaged nerve fibers (43). Previous studies have shown that *A. cantonensis* infection can also cause an increase in IL-6 and IFN-γ levels (44) and these two proven factors can also promote SOCS3 expression through the JAK/STAT pathway (22). Moreover, IL-17A can increase SOCS3 protein levels through upregulation of IL-6 expression, which then activates astrocytes (45). It has been shown *in vitro* that IFN-β can promote the expression of SOCS1 and SOCS3 in astrocytes, wherein STAT1α is the key protein of

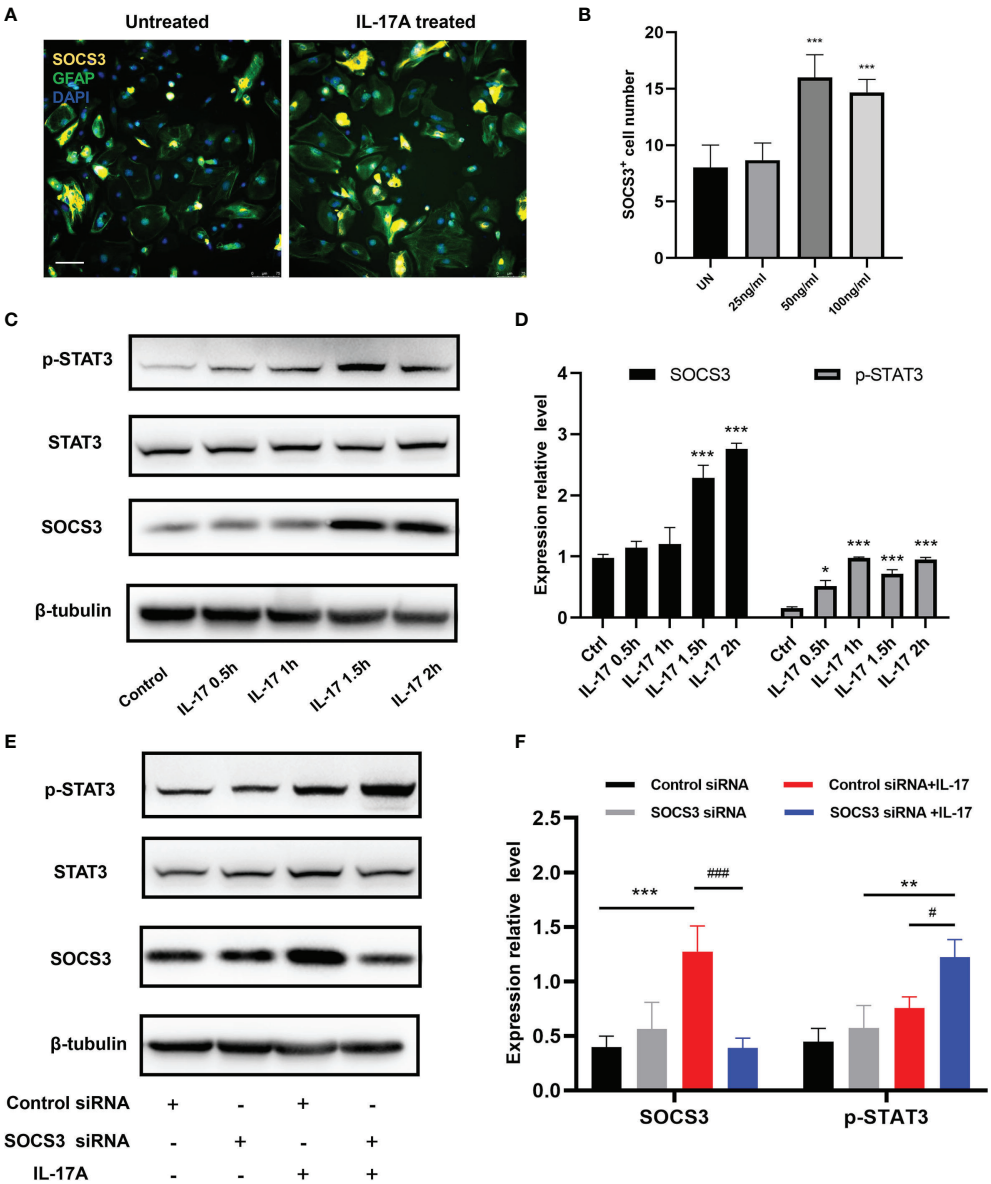

FIGURE 7 | IL-17A regulated SOCS3 expression in astrocytes through the IL-17RA/STAT3/SOCS3 pathway. **(A)** Representative images display the expression of SOCS3, GFAP in the presence of a different concentration of IL-17A. Scale bar = 75 μm. **(B)** Quantification of C3d^{+}, SOCS3^{+} cells in different treated groups. **(C)** Representative immunoblotting of SOCS3, STAT3, p-STAT3, and β-tubulin in several different stimulating time groups (0.5 h, 1 h, 1.5 h, 2 h). **(D)** Relative densitometric analysis of Western Blotting is represented, SOCS3 is normalized to β-tubulin, p-STAT3 is normalized to STAT3. **(E)** Representative Western Blotting images display the expression of SOCS3, STAT3, p-STAT3, and β-tubulin in the presence or absence of IL-17A and SOCS3 siRNA. **(F)** Relative densitometric analysis of Western Blotting in each treatment group is represented, SOCS3 is normalized to β-tubulin, p-STAT3 is normalized to STAT3. n = 3, ***P < 0.001, $^{\#}$P < 0.05, $^{\#\#\#}$P < 0,001. Data were analyzed by one-way ANOVA and followed by Tukey's *post hoc* analysis. Data in each statistical graph are presented as the mean ± SEM.

SOCS1 and STAT3 is the key protein of SOCS3, and the co-expression of SOCS1 and SOCS3 affects the secretion of chemokines in astrocytes (46).

Common demyelination disease including multiple sclerosis, optical neuromyelitis, Guillain-Barre Syndrome, etc. Many evidences indicated IL-17 play an important role in these diseases (47). Our studies first proposed that IL-17A-triggered SOCS3 mediated astrocyte activation involved *A. cantonensis* caused demyelination. However, more detailed mechanisms about how SOCS3 regulate astrocyte activation to influence myelin damage process should be studied. In the future research, we plan to specifically interfere SOCS3 gene in mice astrocyte to observe its functions in *A. cantonensis* infection induced demyelination. In addition, the effects of IL-17A and SOCS3 in typical demyelination animal model should be explored to provide more thoughts for intervening myelin damage.

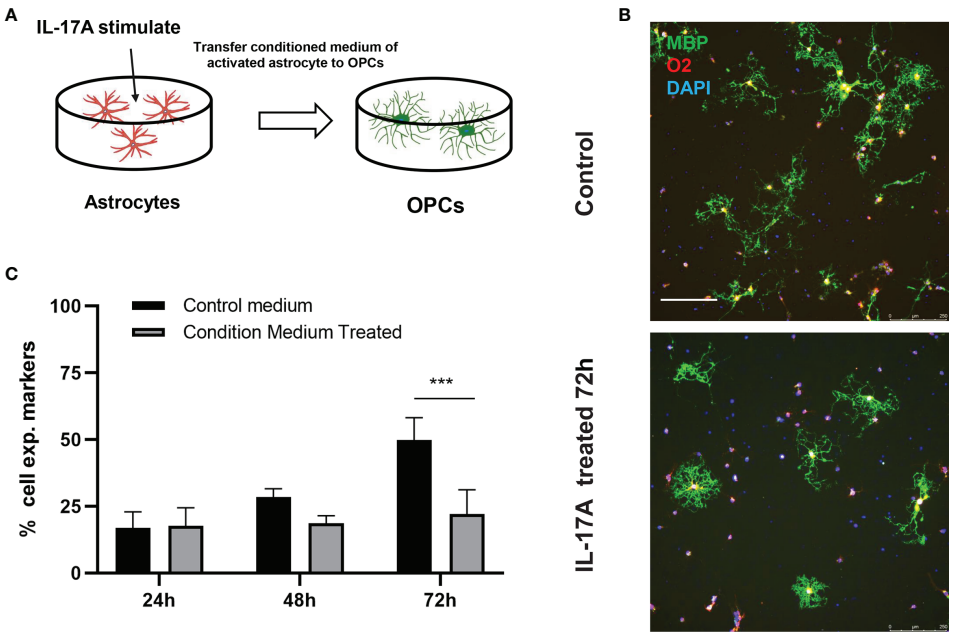

FIGURE 8 | IL-17A activation of astrocytes hindered oligodendrocytes formation. **(A)** Schematic diagram showing the collection of astrocyte medium after treatment with IL-17A which was then mixed with OPCs mature medium in 1:1 ratio to form conditioned medium and applying conditioned medium to OPCs. **(B)** Representative images of oligodendrocytes staining images of control or conditioned medium treated groups. Scale bar = 250 μm. **(C)** Percentage of MBP^+ cells to total cell numbers. n = 3, $^{\#\#}P < 0.01$, $^{***}P < 0.001$, one-way ANOVA and Tukey's test. Data in each statistical graph are presented as the mean ± SEM.

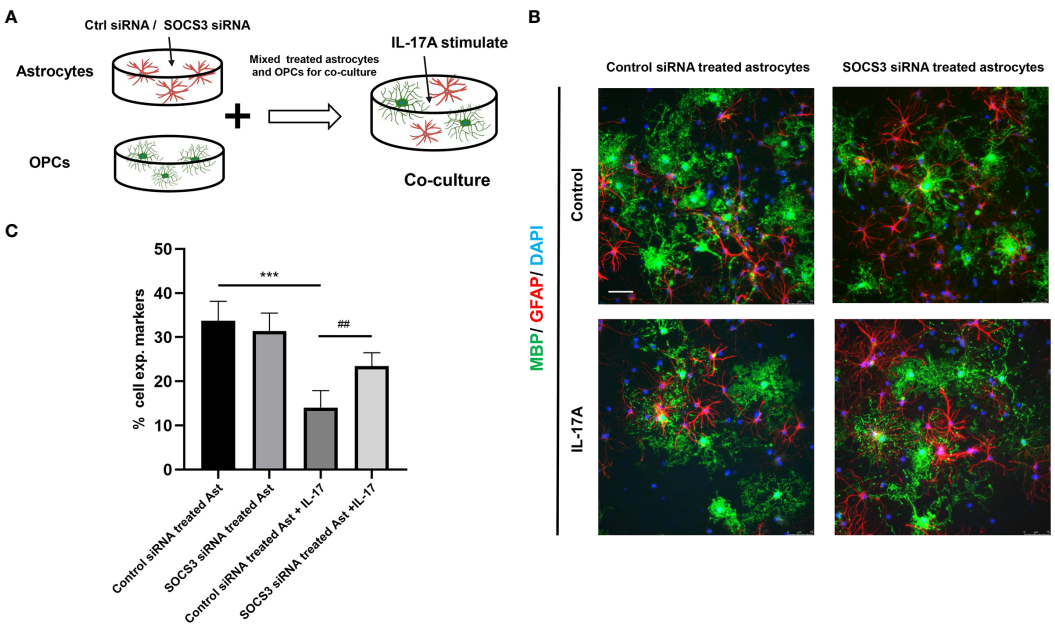

FIGURE 9 | High expression of SOCS3 in activated A1 astrocytes inhibited oligodendrocyte formation. **(A)** Schematic diagram showing the collection of astrocytes treated with control siRNA or SOCS3 siRNA, followed by culturing astrocytes with OPCs in the presence or the absence of IL-17A. **(B)** Representative images of OPCs cultured with astrocytes treated with control siRNA or SOCS3 siRNA for 72 h, which were immunostained for MBP and GFAP. Scale bar = 75 μm. **(C)** Percentage of MBP^+ cells to total cell numbers. n = 3, $^*P < 0.05$, $^{**}P < 0.01$, $^{***}P < 0.001$, one-way ANOVA and Tukey's test. Data in each statistical graph are presented as the mean ± SEM.

CONCLUSION

Our present study showed both A1 and A2 astrocytes apparent activation after *A. cantonensis* infection and promoted the demyelination of corpus callosum. Furthermore, we firstly proposed that SOCS3 not only mediated A1 astrocytes activation, but also accelerated demyelinating injury in an *A. cantonensis*-infected animal model. Therefore, the reintroduction of a specific gene SOCS3, in astrocytes could be investigated as a potential method to slow down the progression of demyelination.

DATA AVAILABILITY STATEMENT

The multiple infectious stages of the *A. cantonensis* infected mice brain tissue RNAseq reads have been deposited at NCBI in the SRA (BioProject number: PRJNA803318). The original contributions presented in the study are included in the article. Further inquiries can be directed to the corresponding authors.

ETHICS STATEMENT

The animal study was reviewed and approved by Institutional Animal Care and Use Committee of Sun Yat-Sen University.

AUTHOR CONTRIBUTIONS

ZZ, TL, and ZL carried out the experiments, ZZ, QD, ZM, and QD performed the statistical analyses. ZZ drafted the manuscript. FK, YL, and YF conceived and coordinated the study. All authors read and approved the final manuscript.

FUNDING

This work was supported by the National Natural Science Foundation of China [grant numbers 81401688, 8180051466, 81772438, 81974357]; the Guangzhou Municipal Science and Technology Program [grant number 201803010083]; Fundamental Research Funds for the Central Universities, SCUT (grant number 2018MS81); South China University of Technology Scientific Research Funding (grant number D6172910).

ACKNOWLEDGMENTS

We very appreciated Prof. Zhongdao Wu for kindly providing the infectious Biomphalaria glabrata, the raw data of mice infected with *A. cantonensis* brain tissue RNA-sequence reads, and experimental technical supports.

REFERENCES

1. Song L, Wang X, Yang Z, Lv Z, Wu Z. Angiostrongylus Cantonensis in the Vector Snails Pomacea Canaliculata and Achatina Fulica in China: A Meta-Analysis. *Parasitol Res* (2016) 115(3):913–23. doi: 10.1007/s00436-015-4849-5
2. Wang QP, Lai DH, Zhu XQ, Chen XG, Lun ZR. Human Angiostrongyliasis. *Lancet Infect Dis* (2008) 8(10):621–30. doi: 10.1016/S1473-3099(08)70229-9
3. Yii CY. Clinical Observations on Eosinophilic Meningitis and Meningoencephalitis Caused by Angiostrongylus Cantonensis on Taiwan. *Am J Trop Med Hyg* (1976) 25(2):233–49. doi: 10.4269/ajtmh.1976.25.233
4. Hidelaratchi MD, Riffsy MT, Wijesekera JC. A Case of Eosinophilic Meningitis Following Monitor Lizard Meat Consumption, Exacerbated by Anthelminthics. *Ceylon Med J* (2005) 50(2):84–6. doi: 10.4038/cmj.v50i2.1577
5. Luo S, OuYang L, Wei J, Wu F, Wu Z, Lei W, et al. Neuronal Apoptosis: Pathological Basis of Behavioral Dysfunctions Induced by Angiostrongylus Cantonensis in Rodents Model. *Korean J Parasitol* (2017) 55(3):267–78. doi: 10.3347/kjp.2017.55.3.267
6. Wei J, Wu F, He A, Zeng X, Ouyang LS, Liu MS, et al. Microglia Activation: One of the Checkpoints in the CNS Inflammation Caused by Angiostrongylus Cantonensis Infection in Rodent Model. *Parasitol Res* (2015) 114(9):3247–54. doi: 10.1007/s00436-015-4541-9
7. Long D, Green K, Derani T, Decker N, Pace RJ, Aburashed R. CNS-Disseminated Angiostrongylus Cantonensis Mimicking Atypical Demyelinating Disease. *Neurol Neuroimmunol Neuroinflamm* (2019) 6(6). doi: 10.1212/NXI.0000000000000608
8. Lin KY, Chen KM, Lan KP, Lee HH, Lai SC. Alterations of Myelin Proteins in Inflammatory Demyelination of BALB/c Mice Caused by Angiostrongylus Cantonensis. *Vet Parasitol* (2010) 171(1-2):74–80. doi: 10.1016/j.vetpar.2010.03.019
9. Ying F, Cunjing Z, Feng F, Shuo W, Xin Z, Fukang X, et al. Inhibiting Interleukin 17 Can Ameliorate the Demyelination Caused by A. Cantonensis via iNOS Inhibition. *Mediators Inflamm* (2017) p:3513651. doi: 10.1155/2017/3513651
10. Compston A, Coles A. Multiple Sclerosis. *Lancet* (2002) 359(9313):1221–31. doi: 10.1016/S0140-6736(02)08220-X
11. Feng Y, Zeng X, Li WH, Wang WC, Chen W, Ou-Yang LS, et al. The Pathogenesis of Optic Neuritis Caused by Angiostrongylus Cantonensis in BALB/c Mice. *Parasit Vectors* (2014) 7:339. doi: 10.1186/1756-3305-7-339
12. Rostene W, Kitabgi P, Parsadaniantz SM. Chemokines: A New Class of Neuromodulator? *Nat Rev Neurosci* (2007) 8(11):895–903. doi: 10.1038/nrn2255
13. Iadecola C, Nedergaard M. Glial Regulation of the Cerebral Microvasculature. *Nat Neurosci* (2007) 10(11):1369–76. doi: 10.1038/nn2003
14. Liddelow SA, Guttenplan KA, Clarke LE, Bennett FC, Bohlen CJ, Schirmer L, et al. Neurotoxic Reactive Astrocytes Are Induced by Activated Microglia. *Nature* (2017) 541(7638):481–7. doi: 10.1038/nature21029
15. Elain G, Jeanneau K, Rutkowska A, Mir AK, Dev KK. The Selective Anti-IL17A Monoclonal Antibody Secukinumab (AIN457) Attenuates IL17A-Induced Levels of IL6 in Human Astrocytes. *Glia* (2014) 62(5):725–35. doi: 10.1002/glia.22637
16. Li Z, Li K, Zhu L, Kan Q, Yan Y, Kumar P, et al. Inhibitory Effect of IL-17 on Neural Stem Cell Proliferation and Neural Cell Differentiation. *BMC Immunol* (2013) 14:20. doi: 10.1186/1471-2172-14-20
17. Gelderblom M, Weymar A, Bernreuther C, Velden J, Arunachalam P, Steinbach K, et al. Neutralization of the IL-17 Axis Diminishes Neutrophil Invasion and Protects From Ischemic Stroke. *Blood* (2012) 120(18):3793–802. doi: 10.1182/blood-2012-02-412726
18. Gaffen SL. Recent Advances in the IL-17 Cytokine Family. *Curr Opin Immunol* (2011) 23(5):613–9. doi: 10.1016/j.coi.2011.07.006
19. Croker BA, Kiu H, Nicholson SE. SOCS Regulation of the JAK/STAT Signalling Pathway. *Semin Cell Dev Biol* (2008) 19(4):414–22. doi: 10.1016/j.semcdb.2008.07.010
20. Shuai K, Liu B. Regulation of JAK-STAT Signalling in the Immune System. *Nat Rev Immunol* (2003) 3(11):900–11. doi: 10.1038/nri1226
21. Liu X, Zhou F, Yang Y, Wang W, Niu L, Zuo D, et al. MiR-409-3p and MiR-1896 Co-Operatively Participate in IL-17-Induced Inflammatory Cytokine Production in Astrocytes and Pathogenesis of EAE Mice via Targeting SOCS3/STAT3 Signaling. *Glia* (2019) 67(1):101–12. doi: 10.1002/glia.23530
22. Chen Z, Laurence A, Kanno Y, Pacher-Zavisin M, Zhu BM, Tato C, et al. Selective Regulatory Function of Socs3 in the Formation of IL-17-Secreting T Cells. *Proc Natl Acad Sci USA* (2006) 103(21):8137–42. doi: 10.1073/pnas.0600666103

23. Baker BJ, Akhtar LN, Benveniste EN. SOCS1 and SOCS3 in the Control of CNS Immunity. *Trends Immunol* (2009) 30(8):392–400. doi: 10.1016/j.it.2009.07.001
24. Herrmann JE, Imura T, Song B, Qi J, Ao Y, Nguyen TK, et al. STAT3 Is a Critical Regulator of Astrogliosis and Scar Formation After Spinal Cord Injury. *J Neurosci* (2008) 28(28):7231–43. doi: 10.1523/JNEUROSCI.1709-08.2008
25. Feng Y, Zhou Z, Liu Z, Zheng C, Feng F, Xie F, et al. Interleukin 17a Derived From Gammadelta T Cell Induces Demyelination of the Brain in Angiostrongylus Cantonensis Infection. *Mol Neurobiol* (2021) 58(8):3968–82. doi: 10.1007/s12035-021-02366-1
26. Yu L, Wu X, Wei J, Liao Q, Xu L, Luo S, et al. Preliminary Expression Profile of Cytokines in Brain Tissue of BALB/c Mice With Angiostrongylus Cantonensis Infection. *Parasit Vectors* (2015) 8:328. doi: 10.1186/s13071-015-0939-6
27. Ji L, Yiyue X, Xujin H, Minghui Z, Mengying Z, Yue H, et al. Study on the Tolerance and Adaptation of Rats to Angiostrongylus Cantonensis Infection. *Parasitol Res* (2017) 116(7):1937–45. doi: 10.1007/s00436-017-5472-4
28. Yun SP, Kam TI, Panicker N, Kim S, Oh Y, Park JS, et al. Block of A1 Astrocyte Conversion by Microglia Is Neuroprotective in Models of Parkinson's Disease. *Nat Med* (2018) 24(7):931–8. doi: 10.1038/s41591-018-0051-5
29. Dugas JC, Cuellar TL, Scholze A, Ason B, Ibrahim A, Emery B, et al. Dicer1 and miR-219 Are Required for Normal Oligodendrocyte Differentiation and Myelination. *Neuron* (2010) 65(5):597–611. doi: 10.1016/j.neuron.2010.01.027
30. Fawcett JW, Asher RA. The Glial Scar and Central Nervous System Repair. *Brain Res Bull* (1999) 49(6):377–91. doi: 10.1016/S0361-9230(99)00072-6
31. Shimizu T, Osanai Y, Ikenaka K. Oligodendrocyte-Neuron Interactions: Impact on Myelination and Brain Function. *Neurochem Res* (2018) 43(1):181–5. doi: 10.1007/s11064-017-2387-5
32. Markle JG, Mortin-Toth S, Wong AS, Geng L, Hayday A, Danska JS. Gammadelta T Cells Are Essential Effectors of Type 1 Diabetes in the Nonobese Diabetic Mouse Model. *J Immunol* (2013) 190(11):5392–401. doi: 10.4049/jimmunol.1203502
33. Park H, Li Z, Yang XO, Chang SH, Nurieva R, Wang YH, et al. A Distinct Lineage of CD4 T Cells Regulates Tissue Inflammation by Producing Interleukin 17. *Nat Immunol* (2005) 6(11):1133–41. doi: 10.1038/ni1261
34. Komiyama Y, Nakae S, Matsuki T, Nambu A, Ishigame H, Kakuta S, et al. IL-17 Plays an Important Role in the Development of Experimental Autoimmune Encephalomyelitis. *J Immunol* (2006) 177(1):566–73. doi: 10.4049/jimmunol.177.1.566
35. Sutton CE, Lalor SJ, Sweeney CM, Brereton CF, Lavelle EC, Mills KH. Interleukin-1 and IL-23 Induce Innate IL-17 Production From Gammadelta T Cells, Amplifying Th17 Responses and Autoimmunity. *Immunity* (2009) 31(2):331–41. doi: 10.1016/j.immuni.2009.08.001
36. Awasthi A, Riol-Blanco L, Jager A, Korn T, Pot C, Galileos G, et al. Cutting Edge: IL-23 Receptor Gfp Reporter Mice Reveal Distinct Populations of IL-17-Producing Cells. *J Immunol* (2009) 182(10):5904–8. doi: 10.4049/jimmunol.0900732
37. Sutherland TE, Logan N, Ruckerl D, Humbles AA, Allan SM, Papayannopoulos V, et al. Chitinase-Like Proteins Promote IL-17-Mediated Neutrophilia in a Tradeoff Between Nematode Killing and Host Damage. *Nat Immunol* (2014) 15(12):1116–25. doi: 10.1038/ni.3023
38. Kang Z, Altuntas CZ, Gulen MF, Liu C, Giltiay N, Qin H, et al. Astrocyte-Restricted Ablation of Interleukin-17-Induced Act1-Mediated Signaling Ameliorates Autoimmune Encephalomyelitis. *Immunity* (2010) 32(3):414–25. doi: 10.1016/j.immuni.2010.03.004
39. Wang X, Deckert M, Xuan NT, Nishanth G, Just S, Waisman A, et al. Astrocytic A20 Ameliorates Experimental Autoimmune Encephalomyelitis by Inhibiting NF-KappaB- and STAT1-Dependent Chemokine Production in Astrocytes. *Acta Neuropathol* (2013) 126(5):711–24. doi: 10.1007/s00401-013-1183-9
40. Wang X, Sun R, Hao X, Lian ZX, Wei H, Tian Z. IL-17 Constrains Natural Killer Cell Activity by Restraining IL-15-Driven Cell Maturation via SOCS3. *Proc Natl Acad Sci USA* (2019) 116(35):17409–18. doi: 10.1073/pnas.1904125116
41. Mori H, Hanada R, Hanada T, Aki D, Mashima R, Nishinakamura H, et al. Socs3 Deficiency in the Brain Elevates Leptin Sensitivity and Confers Resistance to Diet-Induced Obesity. *Nat Med* (2004) 10(7):739–43. doi: 10.1038/nm1071
42. Brantley EC, Nabors LB, Gillespie GY, Choi YH, Palmer CA, Harrison K, et al. Loss of Protein Inhibitors of Activated STAT-3 Expression in Glioblastoma Multiforme Tumors: Implications for STAT-3 Activation and Gene Expression. *Clin Cancer Res* (2008) 14(15):4694–704. doi: 10.1158/1078-0432.CCR-08-0618
43. Sun F, Park KK, Belin S, Wang D, Lu T, Chen G, et al. Sustained Axon Regeneration Induced by Co-Deletion of PTEN and SOCS3. *Nature* (2011) 480(7377):372–5. doi: 10.1038/nature10594
44. Chen AL, Sun X, Wang W, Liu JF, Zeng X, Qiu JF, et al. Activation of the Hypothalamic-Pituitary-Adrenal (HPA) Axis Contributes to the Immunosuppression of Mice Infected With Angiostrongylus Cantonensis. *J Neuroinflamm* (2016) 13(1):266. doi: 10.1186/s12974-016-0743-z
45. Ma X, Reynolds SL, Baker BJ, Li X, Benveniste EN, Qin H. IL-17 Enhancement of the IL-6 Signaling Cascade in Astrocytes. *J Immunol* (2010) 184(9):4898–906. doi: 10.4049/jimmunol.1000142
46. Qin H, Niyongere SA, Lee SJ, Baker BJ, Benveniste EN. Expression and Functional Significance of SOCS-1 and SOCS-3 in Astrocytes. *J Immunol* (2008) 181(5):3167–76. doi: 10.4049/jimmunol.181.5.3167
47. Waisman A, Hauptmann J, Regen T. The Role of IL-17 in CNS Diseases. *Acta Neuropathol* (2015) 129(5):625–37. doi: 10.1007/s00401-015-1402-7

Conflict of Interest: The authors declare that the research was conducted in the absence of any commercial or financial relationships that could be construed as a potential conflict of interest.

Publisher's Note: All claims expressed in this article are solely those of the authors and do not necessarily represent those of their affiliated organizations, or those of the publisher, the editors and the reviewers. Any product that may be evaluated in this article, or claim that may be made by its manufacturer, is not guaranteed or endorsed by the publisher.

frontiers in Immunology

ORIGINAL RESEARCH
published: 03 March 2022
doi: 10.3389/fimmu.2022.837336

Capturing 3D Chromatin Maps of Human Primary Monocytes: Insights From High-Resolution Hi-C

Yu Xia[1,2†], Xiaowen Liu[1,2†], Wenli Mu[1,2], Chunyan Ma[1,2], Laicheng Wang[1,2], Yulian Jiao[1,2], Bin Cui[1,2], Shengnan Hu[3], Ying Gao[3], Tao Liu[4], Huanxin Sun[1,2], Shuai Zong[1,2], Xin Liu[1,2] and Yueran Zhao[1,2]*

[1] Department of Central Laboratory, Shandong Provincial Hospital, Cheeloo College of Medicine, Shandong University, Jinan, China, [2] Department of Central Laboratory, Shandong Provincial Hospital Affiliated to Shandong First Medical University, Jinan, China, [3] Department of Clinical Laboratory, The First Affiliated Hospital of Shandong First Medical University & Shandong Provincial Qianfoshan Hospital, Jinan, China, [4] Bioinformation Center, Annoroad Gene Technology (Beijing) Co., Ltd., Beijing, China

OPEN ACCESS

Edited by:
Juehua Yu,
The First Affiliated Hospital of Kunming Medical University, China

Reviewed by:
Linshan Shang,
University of Minnesota Twin Cities, United States
Qian Li,
Joslin Diabetes Center and Harvard Medical School, United States

***Correspondence:**
Yueran Zhao
yrzhao2021@163.com

†These authors have contributed equally to this work and share first authorship

Specialty section:
This article was submitted to Multiple Sclerosis and Neuroimmunology, a section of the journal Frontiers in Immunology

Received: *16 December 2021*
Accepted: *14 February 2022*
Published: *03 March 2022*

Citation:
Xia Y, Liu X, Mu W, Ma C, Wang L, Jiao Y, Cui B, Hu S, Gao Y, Liu T, Sun H, Zong S, Liu X and Zhao Y (2022) Capturing 3D Chromatin Maps of Human Primary Monocytes: Insights From High-Resolution Hi-C. Front. Immunol. 13:837336. doi: 10.3389/fimmu.2022.837336

Although the variation in chromatin architecture during adaptive immune responses has been thoroughly investigated, the 3D landscape of innate immunity is still unknown. Herein, chromatin regulation and heterogeneity among human primary monocytes were investigated. Peripheral blood was collected from two healthy persons and two patients with systemic lupus erythematosus (SLE), and $CD14^+$ monocytes were selected to perform Hi-C, RNA-seq, ATAC-seq and ChIP-seq analyses. Raw data from the THP1 cell line Hi-C library were used for comparison. For each sample, we constructed three Hi-C libraries and obtained approximately 3 billion paired-end reads in total. Resolution analysis showed that more than 80% of bins presented depths greater than 1000 at a 5 kb resolution. The constructed high-resolution chromatin interaction maps presented similar landscapes in the four individuals, which showed significant divergence from the THP1 cell line chromatin structure. The variability in chromatin interactions around HLA-D genes in the HLA complex region was notable within individuals. We further found that the CD16-encoding gene (*FCGR3A*) is located at a variable topologically associating domain (TAD) boundary and that chromatin loop dynamics might modulate CD16 expression. Our results indicate both the stability and variability of high-resolution chromatin interaction maps among human primary monocytes. This work sheds light on the potential mechanisms by which the complex interplay of epigenetics and spatial 3D architecture regulates chromatin in innate immunity.

Keywords: 3D chromatin maps, primary monocytes, Hi-C, HLA, CD16

INTRODUCTION

Chromatin is hierarchically packaged into the nucleus of higher eukaryotes to organize the three-dimensional (3D) genome structure (1), which is responsible for precise transcriptional regulation by facilitating or restricting regulatory element interactions (2). Over the last decade, the 3D genome architecture associated with cell fate and function under both physiological and pathological

conditions has garnered much attention and has been intensively investigated through advanced techniques (3, 4). Chromosome conformation capture (3C) technologies, from 3C, 4C, 5C to chromatin interaction analysis with paired-end tag sequencing (ChIA-PET) and Hi-C, have become increasingly appreciated for their ability to facilitate the comprehensive identification of genome-wide contact frequencies (5, 6), which can reveal chromatin organization features, including A/B compartments, TADs and loops (7, 8). Evidence demonstrating the role of the 3D genome organization in governing long-range regulatory interactions is now available (9, 10), and such work provides a new blueprint for investigating the influence of spatiotemporal changes in 3D architecture during normal evolution and disease occurrence (11).

Chromatin interactions play a fundamental role in establishing and maintaining the functions of immune cells during development, differentiation and activation in autoimmune diseases (12, 13). An analysis of genome organization performed in 17 human primary hematopoietic cell samples by promoter capture Hi-C (PCHi-C) indicated that the promoter interactomes are highly cell-type specific (14). Much evidence has validated the concept that transient changes in the genomic architecture in human B cells and $CD4^+$/$CD8^+$ T cells require the recruitment of specific lineage-defining transcription factors, chromatin remodelers, and histone modifiers to modulate gene transcription and mediate B and T cell lineage commitment (15–17). While a series of studies on chromatin 3D organization have focused on adaptive immune responses, little is known about its role in innate immunity. The issue associated with 3D structure in innate immune cells that has been investigated is long-range looping interactions during differentiation from monocyte precursors (THP1 cell line) to mature macrophages (18, 19), which suggested the possibility that the spatial 3D structure might regulate innate immunologic processes. In general, almost all of the available Hi-C maps have been displayed in cultured immune cells. In addition, recent research combining associated genetic variants identified from Genome-wide Association Studies (GWASs) with 3D structures observed in different immune cell physiological states has revealed potential regulatory connections of these noncoding region variants related to the pathogenesis of autoimmune diseases (20, 21); this work has yielded pivotal insights into how autoimmunity is triggered by susceptible polymorphisms (22).

To date, chromatin architecture variation during adaptive immune response has been thoroughly investigated, although few previous research on Hi-C had been performed in primary monocytes, there still lacks a high-resolution 3D landscape in innate immunity and analysis of individual difference. SLE, as the examined autoimmune condition, is a highly heterogeneous autoimmune disease characterized by the production of numerous autoantibodies and chronic inflammation (23). SLE can systematically and severely affect multiple organs, including central nervous system and peripheral nervous system. Therefore, the present study was designed to first present high-resolution chromatin interaction maps of human primary monocytes and then to make further efforts to elucidate the immunological heterogeneity of the 3D genome structure. We hope to provide insight into the functional regulation of monocytes in innate immunity by comparing healthy controls and SLE patients to identify significant epigenetic profiles associated with chromatin accessibility as well as histone modification patterns correlated with the transcriptional profiles of human primary monocytes, as evidenced by integrated datasets from assay for transposase-accessible chromatin sequencing (ATAC-seq), chromatin immunoprecipitation with sequencing (ChIP-seq), and RNA sequencing (RNA-seq) analyses.

MATERIALS AND METHODS

Antibodies and Reagents

The antibodies and reagents used in this study were as follows: Alexa Fluor® 488 mouse anti-human CD14 was purchased from BD Pharmingen™ (561706). 7-Amino-actinomycin D (7-AAD) was purchased from BD Pharmingen™ (559925). Protease inhibitors were purchased from Sigma (P8340-5 ml). Biotin-14-dCTP and Proteinase K (Fungal) were purchased from Invitrogen (19518-018; 25530-031). DNA polymerase I, large (Klenow) fragment, was obtained from NEB (M0210S). T4 DNA ligase, T4 DNA polymerase and T4 DNA ligation buffer were all purchased from NEB (M0202L; M0203L; B0202).

Study Subjects

SLE patients (n=2, SLE-1; SLE-2) were recruited from Shandong provincial hospital affiliated to Shandong university. All patients with SLE met the revised diagnostic criteria of the American College of Rheumatology (1997), and other systematic or autoimmune diseases were excluded (24). None of the patients had been using systemic or topical medication before, and all were characterized by high ANA and dsDNA antibody levels and low-level clinical symptoms during sample collection. Disease activity was measured using the SLE Disease Activity Index scoring system. The control population (n=2, CTR-1; CTR-2) consisted of unrelated individuals matched for ethnicity, age, and sex. The four donors were all 25 years old. Valid informed consent was obtained from each participant. The study design conformed to the ethical guidelines and was approved by the ethics committee of Shandong Provincial Hospital affiliated to Shandong first medical university.

Preparation of Monocytes

From each donor, a 150 ml blood sample was collected, and 30 ml of fresh peripheral blood was collected at each sampling time to keep the cells as active as possible. Ficoll-Paque (GE 17-1440-02) density gradient centrifugation was used to separate peripheral blood mononuclear cells (PBMCs) within 2 h. The PBMCs were stained and incubated with an antibody cocktail (7-AAD and Alexa Fluor® 488 mouse anti-human CD14) in darkness at room temperature for 20 min. After incubation, the cells were washed twice with 1% heat-inactivated fetal bovine

serum diluted in PBS for fluorescence-activated cell sorting (FACS). The cells were sorted by flow cytometry using a FACS Aria III system (Becton Dickinson), and approximately 5 million cells per sample were obtained and defined as $CD14^+$ monocytes. The activity of the selected $CD14^+$ primary monocytes reached greater than 95%.

RNA-Seq and Data Analysis

The RNA-seq of monocytes was performed *via* the Smart-Seq2 method. Briefly, samples were collected in tubes with lysis components and ribonuclease inhibitors. An Oligo-dT primer was introduced to the reverse transcription reaction for first-strand cDNA synthesis, followed by PCR amplification to enrich cDNA and a MagBeads purification step to clean up the product. Then, the cDNA product was checked with a Qubit® 3.0 Fluorometer and Agilent 2100 Bioanalyzer to verify the expected product with a length of approximately 1~2 kb. Next, the cDNA was randomly sheared by ultrasonication according to the Illumina library preparation protocol, which included DNA fragmentation, end repair, 3' end A-tailing, adapter ligation, PCR amplification and library validation. After library preparation, the PerkinElmer Lab ChIP® GX Touch system and the Step OnePlus™ Real-Time PCR system were used for library quality inspection. Qualified libraries were then loaded on the Illumina HiSeq platform for PE150 sequencing. Sequencing data were mapped to the human reference genome (ucsc.hg19) using HISAT2 v2.1.0. fragments per kilobase of transcript per million mapped reads (FPKM) values for each gene were calculated. RNA-seq data were shown in **Supplementary Data Sheet 1** and the quality control of RNA-seq was in **Figure S1**.

ATAC-Seq and Data Analysis

Approximately 50,000 living cells were used for each library preparation. The cells were lysed in lysis buffer to obtain nuclei, and the TruePrep™DNA Library Prep Kit V2 for Illumina (Vazyme Biotech) was used to construct transposase-treated libraries. The mass concentration and molar concentration of the libraries were determined with a Qubit 3.0 Fluorometer and the StepOnePlus™ Real-Time PCR system, respectively, and the lengths of the inserted fragments were determined with an Agilent HS 2100 Bioanalyzer. Qualified libraries were sequenced on the Illumina HiSeq platform in paired-end 150 bp mode. The data were mapped to the human reference genome (ucsc.hg19) with Bowtie2 (version 2.2.3), and binding sites were identified by using MACS2 (version 2.1.1) with the following parameters '-q 0.05 –nomodel –extsize 150 –keep-dup all –call-summits'. ATAC-seq data were shown in **Supplementary Data Sheet 2** and the quality control of ATAC-seq was in **Figure S2**.

ChIP-Seq and Data Analysis

Nuclear extracts from approximately one million cells and chromatin were sheared to an average size of 200 bp with a sonicator (Bioruptor Pico, Diagenode). Then, the samples were immunoprecipitated with 2.5 μg of H3K27me3 (ab6002), anti-H3K4me3 (ab39915) and anti-H3K27Ac (ab39133) pAbs antibodies. After incubation at 4°C overnight, the antibodies were recovered with 25 μl of Protein A/G magnetic beads (Millipore 16-663). After reverse crosslinking, ChIP-ed DNA was extracted with a MinElute Reaction Cleanup Kit (Qiagen 28206). Purified DNA from H3K27me3, H3K27Ac and H3K4me3 ChIP assays was adapter ligated and PCR amplified for sequencing on the HiSeq2000 platform using a TruSeq DNA Library Prep Kit (Illumina). After sequencing, reads were quality-filtered according to the Illumina pipeline. The data were aligned to the human reference genome (ucsc.hg19) with Bowtie2 (version 2.2.3), and binding sites were identified with MACS2 (version 2.1.1). ChIP-seq data were shown in **Supplementary Data Sheet 3** and the quality control of ChIP-seq was in **Figure S3**.

Hi-C and Data Analyses

Hi-C Library

Approximately one million monocytes were crosslinked with 40 ml of a 1% formaldehyde solution at room temperature for 10 min, and 2.5 M glycine was added to quench the crosslinking reaction. The crosslinked cells were resuspended in 500 μl of ice-cold Hi-C lysis buffer and rotated at 4°C for 30 min. The nuclei were washed with 0.5 ml of restriction enzyme buffer, and the chromatin was solubilized with diluted SDS. After quenching the SDS with Triton X-100, overnight digestion with cutter restriction enzymes (400 units MboI) was performed at 37°C. The DNA ends were marked with biotin-14-dCTP, and blunt-end ligation of crosslinked fragments was performed. The proximal chromatin DNA was religated with a ligation enzyme, and the nuclear complexes were reverse crosslinked at 65°C. The DNA was purified, and biotin-C was removed from the nonligated fragment ends using T4 DNA polymerase. The fragments were sheared to sizes of 100-500 base pairs by sonication. The fragment ends were then repaired with a mixture of T4 DNA polymerase, T4 polynucleotide kinase and Klenow DNA polymerase. Biotin-labeled Hi-C samples were specifically enriched using streptavidin magnetic beads. The fragment ends were subjected to A-tailing with Klenow (exo-), and an Illumina paired-end sequencing adapter was then added with a ligation mixture. Finally, the Hi-C libraries were amplified *via* 8-10 cycles of PCR and sequenced on an Illumina HiSeq instrument in PE150 mode.

The raw sequence data of the THP1 cell line Hi-C library were downloaded from ENCODE (Encyclopedia of DNA Elements Project Consortium) from experiment ENCSR748LQF (https://www.encodeproject.org/experiments/ENCSR748LQF/), which included two replicates (ENCBS615XLU, assigned as THP1-1; ENCBS913QYS, assigned as THP1-2) and analyzed *via* the same pipelines.

Hi-C Data Mapping, Filtering and Generation of Contact Matrices

FASTQ files were firstly subjected to quality control with fastp (version 0.14) software before mapping stages. We used the integrated pipeline of HiC-Pro (V2.7.8) to process the data from the clean FASTQ files to obtain contact maps with default parameters (MIN_MAPQ=10; BOWTIE2_GLOBAL_OPTIONS =

very-sensitive; BOWTIE2_LOCAL_OPTIONS = very-sensitive; BIN_SIZE = 20000, 40000, 150000, 500000, 1000000), which mainly included two-step mapping using Bowtie2 and binning to generate a genome-wide interaction map. The resulting contact matrices were normalized using iterative correction and eigenvector decomposition (ICED, MAX_ITER = 100, FILTER_LOW_COUNT_PERC = 0.02; FILTER_HIGH_COUNT_PERC = 0; EPS = 0.1) (25).

The loops were called by using HiCCUPS (8) with the default parameters, which examines each pixel in a Hi-C contact matrix and identifies those with enriched contact frequencies relative to local neighborhoods.

To calculate the average contact probability (Ps), we divided the genome into 1 M bins. For each distance (1 M, 2 M, 3 M, etc.), we used the observed interaction frequency to calculate the expected value *via* LOWESS fitting at the corresponding distance (26). The relative contact probability (RCP) was computed for each chromosome, and the insulation score was used to call TADs. The above analysis was performed with GENOVA package by functions of insulation_score and callTAD.

The multiHiCcompare packages was used for comparative analysis. Briefly, the interaction matrix was firstly performed fast loess normalization (fastlo function) and performed exact test-based difference detection among groups (hic exactTest function). The composite MD plot were plotted by MD_composite function.

The visualization of chromatin interactions were preformed with the help of washU Epigenome Browser (27) and hicrep package.

Resolution Analysis

For Hi-C resolution calculation, the whole genome was divided into bins of the same size (1 M, 500 k, 200 k, 100 k, 40 k, 20 k, 10 k, 5 k, or 1 k), and valid pairs were then used to determine the coverage of every bin. We sorted the bins in descending order according to the coverage depth of the 75^{th}, 80^{th}, and 90^{th} bins. At a specific resolution, when the minimum depth of the 80^{th} bin reached 1000, we considered the sequencing depth to have reached the same resolution, which was then used as the highest resolution. The results showed that the resolution reached 5 kb and could be used for loop analysis.

Genotyping of the Human Leukocyte Antigen (HLA) Region

About 200 ng sample of genomic DNA from each individual was sheared with a Biorupter (Diagenode, Belgium) to acquire 150~200 bp fragments. The ends of the DNA fragments were repaired, and an Illumina adapter was added (Fast Library Prep Kit, iGeneTech, Beijing, China). After constructing the sequencing library, the target regions were captured with an AI-HLA-Cap Enrichment Kit (iGeneTech, Beijing, China) and sequenced on an Illumina platform (Illumina, San Diego, CA) with 150 base pair paired-end reads. Raw reads were filtered to remove low-quality reads by using FastQC, and the clean reads were then mapped to the reference sequences in the HLA dictionary and typed to generate HLA types for HLA-A, HLA-B, HLA-C, HLA-DPB1, HLA-DQB1, and HLA-DRB1 by using HLA-HD Software.

Statistics

The Mann-Whitney test (unpaired) or the Wilcoxon matched-pair signed-rank test (paired) was performed to analyze the data. For multiple comparisons, analyses were performed using the Kruskal-Wallis test followed by Tukey's test (unpaired) or Friedman's test followed by Dunn's test (paired). All analyses were performed with R 4.0. Statistical significance was reported as follows: *P < 0.05, **P < 0.01, ***P < 0.001.

RESULTS

High-resolution Chromatin Interaction Maps of Monocyte Samples

The $CD14^+$ primary monocytes from the peripheral blood of two SLE patients and two healthy donors were isolated and crosslinked to obtain high-resolution chromatin interaction maps. To determine whether the whole-genome chromatin conformation differed between the two groups, we constructed three MboI-digested Hi-C libraries for each sample. We combined the data from the replicates to obtain more than 1.2 billion valid reads in approximately 3 billion paired-end reads for the subsequent analysis. The valid rates for CTR-1, CTR-2, SLE-1 and SLE-2 were 67.02%, 63.33%, 70.39% and 68.35%, respectively (valid rate above 60%, **Table S1**).

Given the absence of high-resolution chromatin interaction maps of primary monocytes before, we used the Hi-C map of the human monocyte cell line THP1 as the reference for comparison. The data of THP1 were downloaded from the ENCODE database and processed consistently under the same pipeline as the four primary samples for the uniform standards for comparison. Due to the THP1 cell line was established from leukaemia patient, we especially checked the status of chromosomal rearrangement. In the genome wide cis and trans interactions (**Figure S4**), we could see that the normalized mean interactions within chromatin (cis) were always stronger than the interactions between chromatins, thus there was no large chromosomal rearrangement. However, the strengthened trans-interaction between the left end of 9p and right end of 11q (**Figures S4C, 4D**) suggested a proportion of chromosome rearrangement, and it might influence corresponding local chromatin structure.

The general characteristics of the high-resolution chromatin interaction maps from the four primary monocyte samples and two repeats of the THP1 cell line are summarized in **Figure 1**. The resolution analysis showed that the results for the four primary individual samples reached more than 80% of bins at a depth greater than 1000 at a 5 kb resolution, which were similar with THP1 data (**Figure 1A**). These results indicated that our data were of high quality in both breadth and depth.

High-Quality Chromatin Interaction Patterns of Monocyte Samples

We thoroughly explored the chromatin interaction patterns of the six monocyte samples at different levels. The relative contact probability (RCP) was computed to estimate the distance-

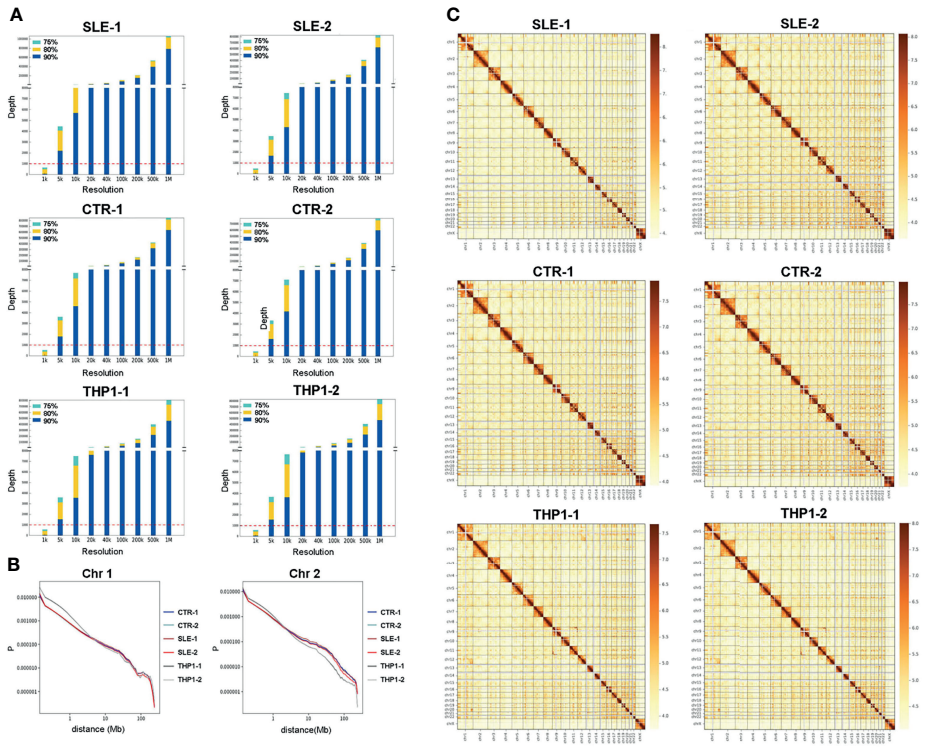

FIGURE 1 | Chromatin interaction map of monocyte. The summary of high-resolution chromatin interaction maps of monocyte, including four primary monocyte samples of SLE-1, SLE-2, CTR-1, CTR-2 and two repeats of THP1. **(A)** Resolution analysis of the Hi-C data from six samples, the horizontal axis indicates the bin size of resolution, the vertical axis indicates the depth of reads. **(B)** The relative contact probability (RCP) in chromosome 1 and chromosome 2. **(C)** The heatmap of genome-wide chromatin interaction in 1Mb bin, the colors present logarithmic transformed normalized interaction value, Both the cis- (within chromosome) and trans- (inter chromosome) interactions are presented.

dependent contact frequencies in chromosome level. The RCPs maps indicated the interaction frequency decayed with increasing distance in the six monocyte samples, while the curves for the four primary monocyte samples were largely in accord and differed slightly from those for the two THP1 repeats. Chromosome 1 and chromosome 2 are shown in **Figure 1B**, maps for other chromosomes are shown in **Figure S5**.

Subsequently, we extracted the contact matrix of the six samples for further analysis and the genome compartment classification analysis was performed to category the A/B compartments (**Figure 2**). The normalized chromatin interactions of 100 kb resolution on chromosome 1 are shown in **Figure 2A**, whose upper and lower triangles represent different samples. The delta Hi-C matrix calculated by subtracting the genome-wide Hi-C interaction were shown in **Figure S6**. The circle diagram shown in **Figure 2B** displays the genome-wide A/B compartment distribution observed in the four samples. The TADs are defined as genomic clusters of chromatin interaction that act as both structural and functional units (28). We identified TADs using the clustering-based Hi-C domain finder (CHDF) method (29). **Figure 2C** describes the TADs on chromosome 1 in the four primary monocyte samples with the Hi-C interactive heat map.

The above results roughly shown hierarchical chromatin conformations and interaction patterns revealed by Hi-C maps in the four primary monocyte samples.

Compartments and TADs Show No Significant Difference Among the Four Primary Monocyte Samples

To determine whether the chromatin conformations differed between primary cells and THP1 cell line or between the healthy and patient groups, we performed comparative analysis in different levels.

The correlation analysis of genome-wide A/B compartment exhibited high similarity among the four primary monocyte samples (**Figure S7**) with only a few regions presenting compartment switching between SLE patients and health individuals. The involved genes (353 genes) around switching regions and the KEGG enrichment analysis were presented in **Table S2**. In consist with the conservatism in genome compartmentalization, the interaction pattern shown in the heatmap of matrix also present high similarity among the four primary monocyte samples (**Figure 1C**). Subsequently, we extracted the contact matrix of the six samples for further analysis. **Figure 1C** shows the heat map of the genome-wide chromatin interactions in the 1 Mb bin, and both the cis (within-

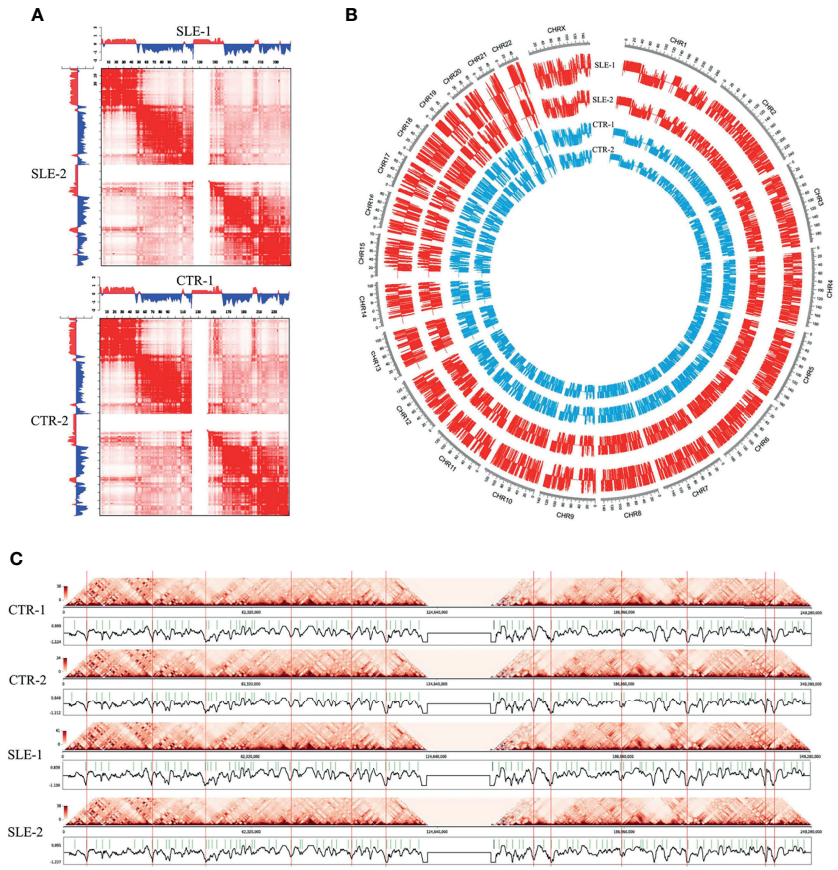

FIGURE 2 | Landscapes of primary monocytes. The different levels of Hi-C maps of four primary monocyte samples (SLE-1, SLE-2, CTR-1 and CTR-2). **(A)** Heatmaps of normalized chromatin interactions (100 kb bin) in chromosome 1. The upper and lower triangles represented different samples, and to be specific, the first heatmap represents SLE-1 (upper) and SLE-2 (lower), and the second heatmap represents CTR-1 (upper) and CTR-2 (lower). **(B)** The genome-wide A/B compartment distribution of the four samples. **(C)** The insulation scores and TAD boundaries in chromosome 1 among the four samples.

chromosome) and trans (between-chromosome) interactions are represented with logarithmic transformed normalized interaction values. The interaction pattern was distributed along the diagonal in the matrix maps, and the cis/trans ratio of our data was normal. In addition, we observed a similar organization pattern along the heatmap diagonal for the healthy and patient samples, and the contact frequency between each chromosome appeared unchanged according to the Hi-C data for the four primary monocyte samples.

Overall, the four peripheral blood monocyte samples from different individuals showed roughly similar landscapes of chromatin interaction frequencies (**Figures 1B, C**), interaction matrices (**Figure 2A**), A/B compartments (**Figure 2B**) and TAD boundaries (**Figure 2C**). The differences between two of the individuals in some genome regions were found to be relatively significant when the SLE-1 sample was compared to the CTR-2 sample (discussed later), but few consistent changes could be found between the SLE patients and healthy people. Our results indicated that the primary monocyte samples displayed a highly conserved structural pattern in terms of genome organization.

To more rigorously assess the homogeneity and divergence among individuals, we employed several comparative methods for Hi-C maps. The package of multiHiCcompare provided integrated algorithms to normalize and assess differences between Hi-C datasets, which could well remove biases across multiple datasets and detect decay of chromatin interaction frequencies. In the multiple-dataset comparative analysis, the primary samples differed significantly from the THP1 cells in the interaction matrix at a 100-kb resolution (chromosome 1 and chromosome 6 in **Figure 3A**, other chromosomes in **Figures S8** and **S9**, while the differences between SLE and control groups were mostly not significant.

The HiCRep package provided a stratum-adjusted correlation coefficient to assess the reproducibility of Hi-C data, and we used this method to do correlation analysis among the six samples (**Figure 3B** shows the correlation matrix among the six samples, and the results for chromosomes 1 to 6 are presented, other chromosome data are shown in **Figure S10**). According to the pairwise correlation coefficients, the similarly was greater than 0.97 within the THP1 repeats or within primary sample groups, but was greatly dropped between primary cells and THP1 repeats.

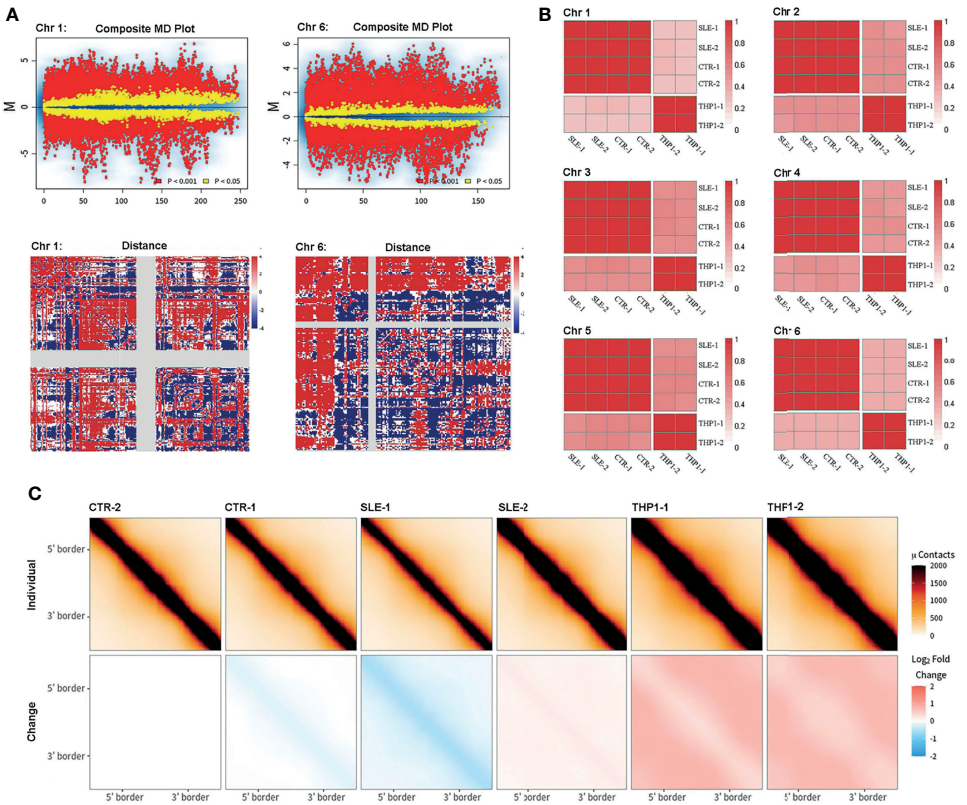

FIGURE 3 | Comparison of Hi-C. Comparison of Hi-C among primary monocytes and THP1 by different methods. **(A)** The results from multiHiCcompare. The upper part displays the MD plot of comparison between four primary samples and two repeats of THP1, the lower part displays the difference matrix between primary monocytes and THP1. Here the results of chromosome 1 and chromosome 6 are presented. **(B)** The correlation matrix between the six samples. The pair-wised stratum-adjusted correlation coefficients (SCC) are calculated using hicrep package. The results of chromosome 1-6 are presented. **(C)** The aggregate peak analysis (APA) among the six samples. Here the we set CTR-2 as reference.

The aggregate peak analysis (APA) was designed to collect loop calls from Hi-C data and detect enriched pattern of loops. To access the difference of loops in genome wide, we chose the TAD boundary of the CTR-2 (the TAD boundary of CTR-2 exhibited the strongest effect among the four primary cells) sample as a reference to calculate the interaction enrichment of each sample. The results (**Figure 3C**) were represented as the difference compared to CTR-2 (minus the value of CTR-2). We found that the loop interaction was slightly decreased in the SLE-1 sample (blue) but significantly increased in the THP1 repeats (red), while the other samples showed little difference.

Collectively, all of these analyses indicated stability of chromatin interactions within individual samples and significant divergence between the THP1 cell line and primary monocytes at chromatin higher structure.

Notable Variability of Chromatin Interactions Around the HLA Complex Region Within Individuals

Although we observed high conservation of the main structural features among the primary monocytes, the HLA complex region on chromosome 6 (6p21.3) presented notable variability in genome-wide cis-chromatin interactions (**Figure 4A**), which consists of genes belonging to MHC class I (classical genes: HLA-A, HLA-B and HLA-C; nonclassical genes: HLA-E, HLA-F and HLA-G), MHC class II (classical genes: HLA-DP, HLA-DQ and HLA-DR; nonclassical HLA genes: HLA-DM and HLA-DO) and MHC class III (complement and cytokine genes) (30). **Figure 4B** shows the insulation scores (lower) of the six samples around the HLA complex region (chr6: 29 Mb-35 Mb, hg19) and their differences between primary cells and the THP1 cell line (upper).

From the interactive matrix heat map, we deduced that in the p21.33 region, where HLA-C is located, THP1 cells presented fewer interactions than the primary samples, while THP1 presented more interactions at p21.32. Among primary monocytes, the variability was most significant around the HLA-D gene region of p21.32. Consistent with **Figure 4A**, in the p21.32 region, the SLE-1 sample showed the strongest chromatin interaction, and sample CTR-2 showed a relatively weak interaction. To show the differences between the samples, **Figure 4C** provides the heat maps of the pairwise difference matrix, where red represents enhancement, blue represents weakening, and the intensity of the color indicates the degree

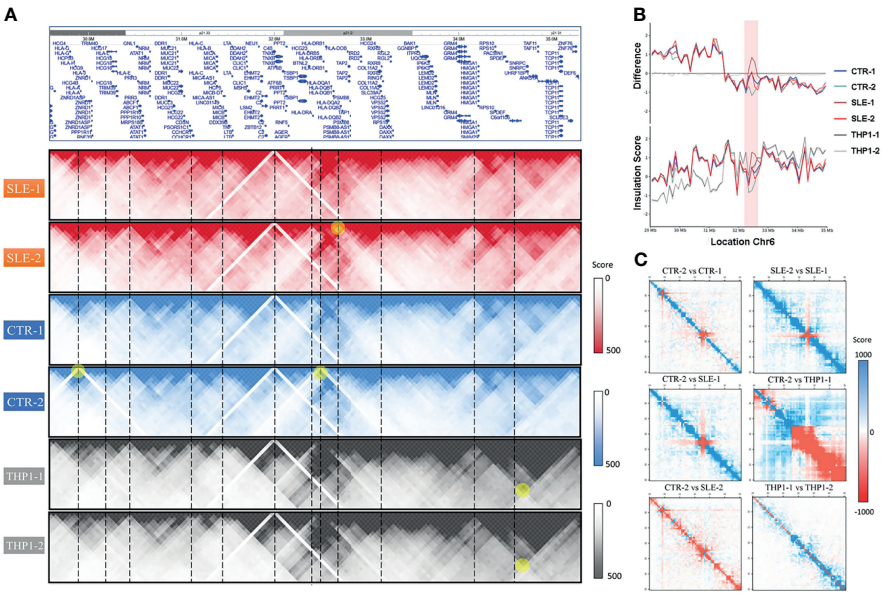

FIGURE 4 | The polymorphism around HLA complex region. **(A)** The HLA complex region in chromosome 6 (upper) and the chromatin interactions of six samples around this region. **(B)** The value of insulation score of six samples (lower) and their difference to THP1-1 around HLA complex region (chr6: 29Mb-35Mb, hg19). **(C)** The heatmaps of pair-wised difference matrix.

of the difference between samples. As shown by these comparison results, the four primary monocyte samples and the two THP1 cell line repeats showed large differences in certain regions of the polypeptides encoded by the HLA complex genes. Among the four primary cell lines, the difference between SLE-1 and CTR-2 was largest in this region, which was consistent with the results presented in **Figures 4A, B**.

Potential Effects of Chromatin Interactions in the HLA Region

To investigate how chromatin organization influences the transcription and epigenetics of primary monocytes, in addition to Hi-C library preparation, the remaining collected monocytes of the four individuals were subjected to RNA-seq and ATAC-seq. Furthermore, three of the samples (SLE-1, SLE-2, CTR-2) underwent ChIP-seq analyses of H3K4me3, H3K27ac and H3K27me3.

The RNA-seq, ATAC-seq and ChIP-seq results for HLA complex genes were presented in **Figure 5**. We found that the expression of HLA-DRB was higher in the SLE samples than in the CTR samples through RNA-seq; however, ATAC-seq and ChIP-seq did not provide consistent results, possibly because of the limited sample size and the high clinical heterogeneity and low quality of the samples. According to the RNA-seq results, HLA-DRB was strongly expressed in SLE-1 and weakly expressed in CTR-2, which was consistent with the chromatin interactions around this region, as shown in **Figure 4B**. The genotyping of the HLA regions (HLA-A, HLA-B, HLA-C, HLA-DPB1, HLA-DRB1 and HLA-DQB1) in the four primary samples was also performed (**Figure S11**), and all of these loci were heterozygous except for HLA-DRB1*15:01:01 and HLA-DQB1*06:02:01 in SLE-1. This result indicated that the high polymorphism of the DNA sequence might influence the 3D genome structure and then affect the regulation of associated gene expression patterns.

Dynamic Chromatin Loops Might Regulate CD16 Expression

We next explored the 3D genome around the *FCGR3A* (Fc gamma receptor III A, also known as CD16), which is a dominant functional regulator in primary monocytes. The CD16 positive monocytes played pivotal immune surveillance functions in central nervous system and the upregulated FCGR3A is also related to the activation of microglial phagocytic capacity in neuroinflammation. A summary of the characteristics of this region is provided in **Figure 6**, including the insulation score values (**Figure 6A**) and the presence of loops (**Figure 6B**) and chromatin interactions (**Figure 6C**) in the six samples around the CD16-encoding gene as well as the results of RNA-seq, ATAC-seq and ChIP-seq analyses of H3K27me3, H3K27ac and H3K4me4 around this region (**Figure 6D**).

There were many SLE susceptibility-related SNPs in the region, among which we used rs403016 as a landmark, which is located in the coding region of the *FCGR3A* gene and has been reported to be associated with an increased risk of developing SLE. In our primary monocyte 3D structure maps, this SNP was shown to be located near a TAD boundary on chromosome 1q23 (**Figure 6A**). The low insulation score of the rs403016 region indicated that this region contained a TAD boundary. Considering that this value varied among the primary samples, we inferred that TAD boundary sliding may have occurred. Despite the conservation of the separation of chromatin

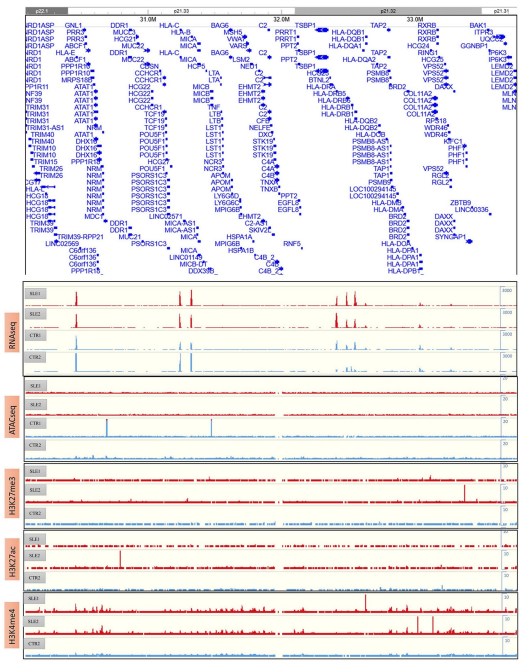

FIGURE 5 | The results of RNA-seq, ATAC-seq and ChIP-seq of H3K27me3, H3K27ac and H3K4me4 around HLA complex region.

interactions in this region on a large scale in both the cell lines and primary samples (**Figure 6A**), the contact maps varied near this region (**Figure 6C**), which was more meaningful.

In the *FCGR3A* promoter region (around rs403016), the loop distribution in the SLE-2 sample was similar to that in the THP1 cell line, while it differed considerably from those in the other three primary samples. In particular, the SLE-2 sample presented an increased interaction loop around the *FCGR3A* promoter, while the SLE-1 sample did not show this loop (**Figures 6B, C**). According to GeneHancer database, an enhancers (chr1:161,590,591-161,600,917) of *FCGR3A* had been identified by eQTLs, eRNA_co-expression assay (**Figure S12**). This enhancer overlapped the right side of varied loop (left side: 161.52M-161.53M, right side: 161.60M-161.61M), which bridged the enhancer to the promoter region of *FCGR3A*. Accordingly, the expression of *FCGR3A* was highest in the SLE-2 sample and lowest in SLE-1 (RNA-seq results in **Figure 6D**, and validated in qRT-PCR in **Figure S1E**) without significant differences according to ATAC-seq and ChIP-seq (**Figure 6D**), which could be attributed to the diverse loop to the upstream enhancer.

DISCUSSION

As yet the whole-genome 3D organization of primary human monocytes has not been thoroughly revealed. To fill this gap, herein we present 3D genomic maps of monocytes from

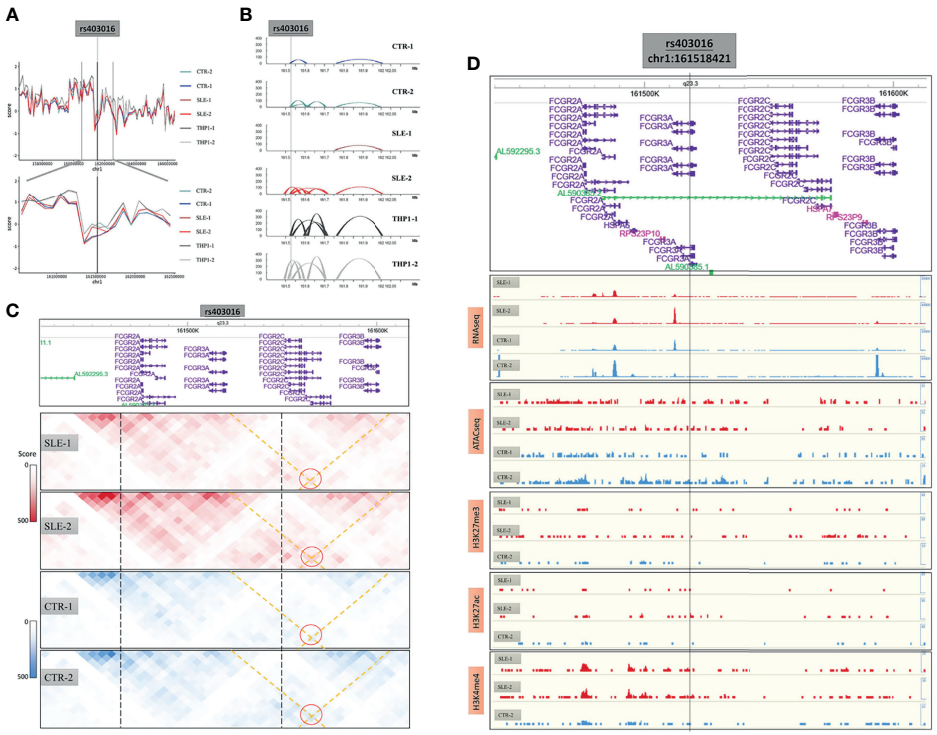

FIGURE 6 | The 3D structure around CD16 coding gene. **(A)** The insulation score value of six samples around CD16 coding genes. **(B)** The loops of six samples around this region. **(C)** The chromatin interactions around this region. **(D)** The results of RNA-seq, ATAC-seq and ChIP-seq of H3K27me3, H3K27ac and H3K4me4 around this region.

peripheral blood samples collected from four individuals. Our Hi-C maps reach 5 kb resolution with high quality, which ensures the subsequent analysis is credible.

Through careful comparative analysis, we found that the primary monocyte samples showed roughly similar chromatin landscapes in terms of chromatin interaction frequencies, interaction matrices, A/B compartments and TAD boundaries, and few consistent patterns were found between the SLE patients and healthy controls. The primary samples displayed a highly conserved structural pattern of genome organization despite the different autoimmune statuses of their donors; even though two of the samples came from SLE patients, they all consisted of normal somatic cells with no deficiency. These negative results further confirmed that chromatin undergoes significant changes in high-level structures only when major structural changes, such as balanced translocations or deletions of large regions, occur with chromosomes. The observed conservation of advanced structures was consistent with biological rules and reflects a stable structural pattern of immune cells at different stages of autoimmunity.

In the present study, Hi-C data from the human monocyte cell line THP1 were also reanalyzed as a reference. The results showed that the 3D high-resolution maps of THP1 cells significantly differed from those of our primary monocyte samples according to unbiased assessment based on APA and comparative and correlation analyses of multiple Hi-C datasets. A previous investigation involving capture Hi-C was performed to compare the commonalities and differences in promoter interactions between $CD34^+$ hematopoietic progenitor cells and the human B cell line GM12878, and the results indicated that alternate long-range interactions determined differential transcription programs in different cell types (31). The engineered THP-1 cell line, derived from the peripheral blood of an individual with acute monocytic leukemia, is usually used as a model to study the modulation of monocytes and macrophage functions (32). The divergence of the 3D chromatin structure of this cell line from that of primary monocytes is not surprising because THP1 cells are aneuploid cells; however, these differences could reduce the validity of THP1-based analysis. As shown in the correlation analysis of **Figure 3**, we found that in most of the genome region, the degree of variation between the 4 different individuals is similar to that of the two biological repeats of THP1 cells. This result also indicated that the primary monocytes are highly conserved in 3D genome.

Our 3D chromatin maps also showed significant diversity in the HLA region among individuals. The chromatin interactions around HLA-DQ and HLA-DR differed mostly among different primary monocyte samples and were associated with nearby gene expression. Genetic variation in intergenic regions of the HLA MHC-II locus is associated with multiple autoimmune diseases (33). Recent evidence has shown that significant diversity in histone modifications and super enhancer (SE) interactions within HLA-DR/DQ promoters or intergenic regions might dynamically contribute to SLE morbidity (34) or regulate the complexity of immune responses between individuals (35). Our findings indicate the underlying regulation of chromatin interactions around the HLA region, and the results were consistent with previous reports in B or T cells, while considering cell-type specificity, we firstly provide evidence of potential 3D regulation pattern in primary monocytes.

In this work, additional genotyping data showed that SLE-1 presented homozygosity of HLA-DRB1 (*15:01:01) and HLA-DQB1 (*06:02:01). Considering that SLE-1 presented the strongest chromatin interactions among the four studied individuals, we speculated that a relationship exists between the genotype and the strong chromatin interactions of these HLA regions. HLA-DRB1*15:01/DQB1*06:02 has been identified as the strongest classical SLE susceptibility-related allele in individuals of European, African, and Hispanic ancestries (36–38). Haplotypes bearing DRB1*1501/DQB1*0602 are key determinants of autoantibody production and disease susceptibility in human SLE (39). Great interest has been focused on the DRB1*1501/DQB1*0602 haplotype, which confers risk of autoimmunity resulting from changes in the epigenome (40). Therefore, it is reasonable to consider that the DRB1*1501/DQB1*0602 haplotype can potentially be therapeutically targeted by altering the 3D architecture to regulate the immune response in SLE pathogenesis.

We found that the *FCGR3A* was located at a variable TAD boundary and that the dynamics of chromatin loops might modulate CD16 expression. According to the surface expression of CD16 (*FCGR3A*), monocytes can be grouped into three subpopulations (41). The proportion of CD16-positive monocytes is tightly linked with certain autoimmune diseases (42–44), and many susceptibility-related SNPs around these regions have been validated in population studies (45, 46). Previous studies have explored the epigenetic regulatory mechanisms of CD16 in monocytes or other immune cells (47, 48). Here, we present the first evidence of chromatin loop-mediated regulation in this region based on the observed variation in the TAD boundary in the *FCGR3A* gene region, which indicated that the expression of CD16 was dominated by chromatin interactions. The identified enhancer loop regulations in *FCGR3A* suggested potential therapeutic target in autoimmune neurological diseases.

Nevertheless, taken together, our results indicate both the stability and variability of high-resolution chromatin interaction maps among human primary monocytes. The detailed 3D genomic landscape obtained in this work reveals potential regulatory functions related to monocytes. Our work highlights the complex interplay of the epigenetic and spatial 3D chromatin changes that are necessary to regulate gene expression and potentially mount an effective immune response. However, further functional experiments will be required for the validation of this work. The role of the 3D architecture in innate immunity is a topic of ongoing investigation.

DATA AVAILABILITY STATEMENT

The datasets presented in this study can be found in online repositories. The names of the repository/repositories and accession number(s) can be found in the article/**Supplementary Material**.

ETHICS STATEMENT

The studies involving human participants were reviewed and approved by the Ethics Committee of Shandong University in China. The patients/participants provided their written informed consent to participate in this study.

AUTHOR CONTRIBUTIONS

YZ designed the study and revised the manuscript. YX and XWL performed the research and wrote the manuscript. WM and CM analyzed the data. YJ and BC collected clinical samples. SH and YG sorted $CD14^+$ primary monocytes. HS and XL performed genotyping of HLA region. LW assisted in data transmission and analysis. All authors have reviewed and approved the manuscript.

FUNDING

This work was supported by grants from the National Natural Science Foundation of China (82171665, 31370897), the Natural Science Foundation of Shandong Province (ZR2020MH168) and the Key Technology Research and Development Program of Shandong Province (2018GSF118113).

ACKNOWLEDGMENTS

We would like to thank the participants who provided their peripheral blood sample to participate in this study. We appreciate Annoroad Gene Technology (beijing) Co., Ltd., for sequencing technical assistance.

SUPPLEMENTARY MATERIAL

The Supplementary Material for this article can be found online at: https://www.frontiersin.org/articles/10.3389/fimmu.2022.837336/full#supplementary-material

Supplementary Figure 1 | Quality control of RNA-seq. **(A)** The heatmap of Pearson correlation matrix of genome-wide FPKMs values within samples. **(B)** The distance and hierarchical clustering of the four samples. **(C)** The volcanos plot of difference analysis between SLE group and CTR group, under the cut off value of |log2FC|>1.5 and padj < 0.05, there were 74 genes significant upregulated and 124 genes downregulated in SLE group. **(D)** The heatmap of expression (performed z-scale by each gene) of significant genes of C (74 up and 124 down). **(E)** The validation RNA-seq by qRT-PCR in the identical samples. We selected six genes (ACTB, GAPDH, FCGR3A, STAT3, FLT3 and CXCL8) and the left heatmap indicated their expression value (FPKM) in RNA-seq. The right heatmap shown their quantitative results($2^{-deltaCt}$) by qRT-PCR compared to the inner reference of GAPDH.

Supplementary Figure 2 | Quality control of ATAC-seq. **(A)** The genome wide normalized peaks distribution of the four samples. **(B)** The heatmap of Pearson correlation matrix (upper) or Spearman correlation matrix (lower) of the four samples. **(C)** The normalized reads density distribution in gene profile of the four samples.

Supplementary Figure 3 | Quality control of ChIP-seq. **(A)** The gene body normalized reads (RPKM) density plot of the nine ChIP-seq sample. **(B)** The heatmap of correlation matrix of normalized reads within the nine samples. **(C)** The gene body normalized reads (RPKM) heatmap of the nine ChIP-seq samples.

Supplementary Figure 4 | The trans-interactions map of THP1 cell and primary monocyte. **(A)** Heatmap of all cis and trans interactions in genome wide. **(B)** The average intensity of interactions within or inter chromosomes. **(C)** The detailed interactions in chr9 to chr11 indicated rearrangement (blue box) between 9p and 11q in THP1-1 and THP1-2. **(D)** The circos plot of all significant trans interactions in genome wide.

Supplementary Figure 5 | The relative contact probability (RCP) in all chromosomes. The full landscape of.

Supplementary Figure 6 | Genome-wide all by all Hi-C interaction minus. From Delta Hi-C, it was nearly no difference in SLE group and CTR group in a comparative large scale (1M resolution).

Supplementary Figure 7 | A/B compartment correlation and switch rate stat. A/B compartment between SLE group and CTR group were similar and had low switch Rate.

Supplementary Figure 8 | The MD plot of comparison in all chromosomes. The full landscape of (upper panel).

Supplementary Figure 9 | The difference matrix between primary monocytes and THP1 in all chromosomes. The full landscape of (lower panel).

Supplementary Figure 10 | The correlation matrix between the six samples in all chromosomes. The full landscape of.

Supplementary Figure 11 | The genotyping in HLA region.

Supplementary Figure 12 | The evidence of enhancer regulation of FCGR3A. The loops of the six samples were the same as and the lower panel indicated the annotation of enhancer from GeneHancer database.

Supplementary Data Sheet 1 | Full results of RNA-seq.

Supplementary Data Sheet 2 | Full results of ATAC-seq.

Supplementary Data Sheet 3 | Full results of ChIP-seq.

REFERENCES

1. Bonev B, Cavalli G. Organization and Function of the 3D Genome. *Nat Rev Genet* (2016) 17:661–78. doi: 10.1038/nrg.2016.112
2. Ray J, Munn PR, Vihervaara A, Lewis JJ, Ozer A, Danko CG, et al. Chromatin Conformation Remains Stable Upon Extensive Transcriptional Changes Driven by Heat Shock. *Proc Natl Acad Sci* (2019) 116:19431–9. doi: 10.1073/pnas.1901244116
3. Beagrie RA, Scialdone A, Schueler M, Kraemer DCA, Chotalia M, Xie SQ, et al. Complex Multi-Enhancer Contacts Captured by Genome Architecture Mapping. *Nature* (2017) 543:519–24. doi: 10.1038/nature21411
4. Zheng H, Xie W. The Role of 3D Genome Organization in Development and Cell Differentiation. *Nat Rev Mol Cell Biol* (2019) 20:535–50. doi: 10.1038/s41580-019-0132-4
5. de Wit E, de Laat W. A Decade of 3C Technologies: Insights Into Nuclear Organization. *Genes Dev* (2012) 26:11–24. doi: 10.1101/gad.179804.111
6. Fullwood MJ, Liu MH, Pan YF, Liu J, Xu H, Mohamed YB, et al. An Oestrogen-Receptor-α-Bound Human Chromatin Interactome. *Nature* (2009) 462:58–64. doi: 10.1038/nature08497
7. Nora EP, Goloborodko A, Valton A-L, Gibcus JH, Uebersohn A, Abdennur N, et al. Targeted Degradation of CTCF Decouples Local Insulation of

Chromosome Domains From Genomic Compartmentalization. *Cell* (2017) 169:930–944.e22. doi: 10.1016/j.cell.2017.05.004
8. Rao SS, Huntley MH, Durand NC, Stamenova EK, Bochkov ID, Robinson JT, et al. A 3D Map of the Human Genome at Kilobase Resolution Reveals Principles of Chromatin Looping. *Cell* (2014) 159:1665–80. doi: 10.1016/j.cell.2014.11.021
9. Lupianez DG, Kraft K, Heinrich V, Krawitz P, Brancati F, Klopocki E, et al. Disruptions of Topological Chromatin Domains Cause Pathogenic Rewiring of Gene-Enhancer Interactions. *Cell* (2015) 161:1012–25. doi: 10.1016/j.cell.2015.04.004
10. Flavahan WA, Drier Y, Liau BB, Gillespie SM, Venteicher AS, Stemmer-Rachamimov AO, et al. Insulator Dysfunction and Oncogene Activation in IDH Mutant Gliomas. *Nature* (2015) 529:110–4. doi: 10.1038/nature16490
11. Spielmann M, Lupiáñez DG, Mundlos S. Structural Variation in the 3D Genome. *Nat Rev Genet* (2018) 19:453–67. doi: 10.1038/s41576-018-0007-0
12. Lagou V, Garcia-Perez JE, Smets I, Van Horebeek L, Vandebergh M, Chen L, et al. Genetic Architecture of Adaptive Immune System Identifies Key Immune Regulators. *Cell Rep* (2018) 25:798–810.e6. doi: 10.1016/j.celrep.2018.09.048
13. Johanson TM, Chan WF, Keenan CR, Allan RS. Genome Organization in Immune Cells: Unique Challenges. *Nat Rev Immunol* (2019) 19:448–56. doi: 10.1038/s41577-019-0155-2
14. Javierre BM, Burren OS, Wilder SP, Kreuzhuber R, Hill SM, Sewitz S, et al. Lineage-Specific Genome Architecture Links Enhancers and Non-Coding Disease Variants to Target Gene Promoters. *Cell* (2016) 167:1369–84.e19. doi: 10.1016/j.cell.2016.09.037
15. Bunting KL, Soong TD, Singh R, Jiang Y, Beguelin W, Poloway DW, et al. Multi-Tiered Reorganization of the Genome During B Cell Affinity Maturation Anchored by a Germinal Center-Specific Locus Control Region. *Immunity* (2016) 45:497–512. doi: 10.1016/j.immuni.2016.08.012
16. Robson MI, de Las Heras JI, Czapiewski R, Sivakumar A, Kerr ARW, Schirmer EC. Constrained Release of Lamina-Associated Enhancers and Genes From the Nuclear Envelope During T-Cell Activation Facilitates Their Association in Chromosome Compartments. *Genome Res* (2017) 27:1126–38. doi: 10.1101/gr.212308.116
17. Henning AN, Roychoudhuri R, Restifo NP. Epigenetic Control of CD8+ T Cell Differentiation. *Nat Rev Immunol* (2018) 18:340–56. doi: 10.1038/nri.2017.146
18. Phanstiel DH, Van Bortle K, Spacek D, Hess GT, Shamim MS, Machol I, et al. Static and Dynamic DNA Loops Form AP-1-Bound Activation Hubs During Macrophage Development. *Mol Cell* (2017) 67:1037–48.e6. doi: 10.1016/j.molcel.2017.08.006
19. Rege M, Phillips-Cremins JE. Dynamic Looping Interactions: Setting the 3D Stage for the Macrophage. *Mol Cell* (2017) 67:901–3. doi: 10.1016/j.molcel.2017.09.011
20. Simeonov DR, Gowen BG, Boontanrart M, Roth TL, Gagnon JD, Mumbach MR, et al. Discovery of Stimulation-Responsive Immune Enhancers With CRISPR Activation. *Nature* (2017) 549:111–5. doi: 10.1038/nature23875
21. Gutierrez-Arcelus M, Rich SS, Raychaudhuri S. Autoimmune Diseases — Connecting Risk Alleles With Molecular Traits of the Immune System. *Nat Rev Genet* (2016) 17:160–74. doi: 10.1038/nrg.2015.33
22. McGovern A, Schoenfelder S, Martin P, Massey J, Duffus K, Plant D, et al. Capture Hi-C Identifies a Novel Causal Gene, IL20RA, in the Pan-Autoimmune Genetic Susceptibility Region 6q23. *Genome Biol* (2016) 17:212. doi: 10.1186/s13059-016-1078-x
23. Banchereau R, Hong S, Cantarel B, Baldwin N, Baisch J, Edens M, et al. Personalized Immunomonitoring Uncovers Molecular Networks That Stratify Lupus Patients. *Cell* (2016) 165:551–65. doi: 10.1016/j.cell.2016.03.008
24. Hartman EAR, van Royen-Kerkhof A, Jacobs JWG, Welsing PMJ, Fritsch-Stork RDE. Performance of the 2012 Systemic Lupus International Collaborating Clinics Classification Criteria Versus the 1997 American College of Rheumatology Classification Criteria in Adult and Juvenile Systemic Lupus Erythematosus. A Systematic Review and Meta-Analysis. *Autoimmun Rev* (2018) 17:316–22. doi: 10.1016/j.autrev.2018.01.007
25. Schmitt AD, Hu M, Ren B. Genome-Wide Mapping and Analysis of Chromosome Architecture. *Nat Rev Mol Cell Biol* (2016) 17:743–55. doi: 10.1038/nrm.2016.104
26. Naumova N, Imakaev M, Fudenberg G, Zhan Y, Lajoie BR, Mirny LA, et al. Organization of the Mitotic Chromosome. *Science* (2013) 342:948–53. doi: 10.1126/science.1236083
27. Zhou X, Lowdon RF, Li D, Lawson HA, Madden PAF, Costello JF, et al. Exploring Long-Range Genome Interactions Using the WashU Epigenome Browser. *Nat Methods* (2013) 10:375–6. doi: 10.1038/nmeth.2440
28. Dixon JR, Selvaraj S, Yue F, Kim A, Li Y, Shen Y, et al. Topological Domains in Mammalian Genomes Identified by Analysis of Chromatin Interactions. *Nature* (2012) 485:376–80. doi: 10.1038/nature11082
29. Oluwadare O, Cheng J. ClusterTAD: An Unsupervised Machine Learning Approach to Detecting Topologically Associated Domains of Chromosomes From Hi-C Data. *BMC Bioinf* (2017) 18:480. doi: 10.1186/s12859-017-1931-2
30. Horton R, Wilming L, Rand V, Lovering RC, Bruford EA, Khodiyar VK, et al. Gene Map of the Extended Human MHC. *Nat Rev Genet* (2004) 5:889–99. doi: 10.1038/nrg1489
31. Mifsud B, Tavares-Cadete F, Young AN, Sugar R, Schoenfelder S, Ferreira L, et al. Mapping Long-Range Promoter Contacts in Human Cells With High-Resolution Capture Hi-C. *Nat Genet* (2015) 47:598–606. doi: 10.1038/ng.3286
32. Chanput W, Mes JJ, Wichers HJ. THP-1 Cell Line: An *In Vitro* Cell Model for Immune Modulation Approach. *Int Immunopharmacol* (2014) 23:37–45. doi: 10.1016/j.intimp.2014.08.002
33. Gutierrez-Arcelus M, Baglaenko Y, Arora J, Hannes S, Luo Y, Amariuta T, et al. Allele-Specific Expression Changes Dynamically During T Cell Activation in HLA and Other Autoimmune Loci. *Nat Genet* (2020) 52:247–53. doi: 10.1038/s41588-020-0579-4
34. Pelikan RC, Kelly JA, Fu Y, Lareau CA, Tessneer KL, Wiley GB, et al. Enhancer Histone-QTLs Are Enriched on Autoimmune Risk Haplotypes and Influence Gene Expression Within Chromatin Networks. *Nat Commun* (2018) 9:2905. doi: 10.1038/s41467-018-05328-9
35. Majumder P, Lee JT, Rahmberg AR, Kumar G, Mi T, Scharer CD, et al. A Super Enhancer Controls Expression and Chromatin Architecture Within the MHC Class II Locus. *J Exp Med* (2020) 217(2):e20190668. doi: 10.1084/jem.20190668
36. Langefeld CD, Ainsworth HC, Graham DSC, Kelly JA, Comeau ME, Marion MC, et al. Transancestral Mapping and Genetic Load in Systemic Lupus Erythematosus. *Nat Commun* (2017) 8:16021. doi: 10.1038/ncomms16021
37. Molineros JE, Looger LL, Kim K, Okada Y, Terao C, Sun C, et al. Amino Acid Signatures of HLA Class-I and II Molecules Are Strongly Associated With SLE Susceptibility and Autoantibody Production in Eastern Asians. *PloS Genet* (2019) 15:e1008092. doi: 10.1371/journal.pgen.1008092
38. Sun C, Molineros JE, Looger LL, X-j Z, Kim K, Okada Y, et al. High-Density Genotyping of Immune-Related Loci Identifies New SLE Risk Variants in Individuals With Asian Ancestry. *Nat Genet* (2016) 48:323–30. doi: 10.1038/ng.3496
39. Graham RR, Ortmann W, Rodine P, Espe K, Langefeld C, Lange E, et al. Specific Combinations of HLA-DR2 and DR3 Class II Haplotypes Contribute Graded Risk for Disease Susceptibility and Autoantibodies in Human SLE. *Eur J Hum Genet* (2007) 15:823–30. doi: 10.1038/sj.ejhg.5201827
40. Kim K, Bang SY, Lee HS, Okada Y, Han B, Saw WY, et al. The HLA-DRbeta1 Amino Acid Positions 11-13-26 Explain the Majority of SLE-MHC Associations. *Nat Commun* (2014) 5:5902. doi: 10.1038/ncomms6902
41. Ziegler-Heitbrock L, Ancuta P, Crowe S, Dalod M, Grau V, Hart DN, et al. Nomenclature of Monocytes and Dendritic Cells in Blood. *Blood* (2010) 116: e74–80. doi: 10.1182/blood-2010-02-258558
42. Stansfield BK, Ingram DA. Clinical Significance of Monocyte Heterogeneity. *Clin Transl Med* (2015) 4:5. doi: 10.1186/s40169-014-0040-3
43. Wong KL, Yeap WH, Tai JJ, Ong SM, Dang TM, Wong SC. The Three Human Monocyte Subsets: Implications for Health and Disease. *Immunol Res* (2012) 53:41–57. doi: 10.1007/s12026-012-8297-3
44. Wu Z, Zhang S, Zhao L, Fei Y, Wang L, Li J, et al. Upregulation of CD16-Monocyte Subsets in Systemic Lupus Erythematous Patients. *Clin Rheumatol* (2017) 36:2281–7. doi: 10.1007/s10067-017-3787-2
45. Ye D, Pan F, Zhang K, Li X, Xu J, Hao J. A Novel Single-Nucleotide Polymorphism of the Fcgamma Receptor IIIa Gene Is Associated With Genetic Susceptibility to Systemic Lupus Erythematosus in Chinese Populations: A Family-Based Association Study. *Clin Exp Dermatol* (2006) 31:553–7. doi: 10.1111/j.1365-2230.2006.02133.x
46. Zhu XW, Wang Y, Wei YH, Zhao PP, Wang XB, Rong JJ, et al. Comprehensive Assessment of the Association Between FCGRs Polymorphisms and the Risk of Systemic Lupus Erythematosus: Evidence From a Meta-Analysis. *Sci Rep* (2016) 6:31617. doi: 10.1038/srep31617
47. Victor AR, Weigel C, Scoville SD, Chan WK, Chatman K, Nemer MM, et al. Epigenetic and Posttranscriptional Regulation of CD16 Expression During Human NK Cell Development. *J Immunol* (2018) 200:565–72. doi: 10.4049/jimmunol.1701128
48. Oboshi W, Watanabe T, Yukimasa N, Ueno I, Aki K, Tada T, et al. SNPs Rs4656317 and Rs12071048 Located Within an Enhancer in FCGR3A Are in Strong Linkage Disequilibrium With Rs396991 and Influence NK Cell-

Mediated ADCC by Transcriptional Regulation. *Hum Immunol* (2016) 77:997–1003. doi: 10.1016/j.humimm.2016.06.012

Conflict of Interest: TL was employed by the company Annoroad Gene Technology.

The remaining authors declare that the research was conducted in the absence of any commercial or financial relationships that could be construed as a potential conflict of interest.

Publisher's Note: All claims expressed in this article are solely those of the authors and do not necessarily represent those of their affiliated organizations, or those of the publisher, the editors and the reviewers. Any product that may be evaluated in this article, or claim that may be made by its manufacturer, is not guaranteed or endorsed by the publisher.

frontiers | Frontiers in Immunology

ORIGINAL RESEARCH
published: 19 April 2022
doi: 10.3389/fimmu.2022.870679

Characterization of Pannexin1, Connexin32, and Connexin43 in Spotted Sea Bass (*Lateolabrax maculatus*): They Are Important Neuro-Related Immune Response Genes Involved in Inflammation-Induced ATP Release

Zhaosheng Sun[1,2,3], *Chong Xu*[1,2,3], *Yuxi Chen*[1,2,3], *Danjie Liu*[1,2,3], *Ping Wu*[4]* *and Qian Gao*[1,2,3]*

[1] *Key Laboratory of Exploration and Utilization of Aquatic Genetic Resources, Ministry of Education, Shanghai Ocean University, Shanghai, China,* [2] *International Research Center for Marine Biosciences at Shanghai Ocean University, Ministry of Science and Technology, Shanghai, China,* [3] *National Demonstration Center for Experimental Fisheries Science Education, Shanghai Ocean University, Shanghai, China,* [4] *College of Life Science and Technology, Huazhong University of Science and Technology, Wuhan, China*

OPEN ACCESS

Edited by:
Juehua Yu,
The First Affiliated Hospital of Kunming Medical University, China

Reviewed by:
Eliseo A. Eugenin,
University of Texas Medical Branch at Galveston, United States
Jia-Song Zhang,
Chinese Academy of Fishery Sciences (CAFS), United States

***Correspondence:**
Qian Gao
qgao@shou.edu.cn
Ping Wu
wu-ping@whu.edu.cn

Specialty section:
This article was submitted to Multiple Sclerosis and Neuroimmunology, a section of the journal Frontiers in Immunology

Received: *07 February 2022*
Accepted: *21 March 2022*
Published: *19 April 2022*

Citation:
Sun Z, Xu C, Chen Y, Liu D, Wu P and Gao Q (2022) Characterization of Pannexin1, Connexin32, and Connexin43 in Spotted Sea Bass (Lateolabrax maculatus): They Are Important Neuro-Related Immune Response Genes Involved in Inflammation-Induced ATP Release. Front. Immunol. 13:870679. doi: 10.3389/fimmu.2022.870679

Many immunological diseases can be treated by regulating neurobehavior, in which extracellular ATP is a vital member of endogenous danger-associated molecular pattern signaling molecule that plays a crucial part in innate neuro-related immunity. It is actively released through pannexin (Panx) and connexin (Cx) hemichannels from activated or stressed cells during inflammation, injury, or apoptosis. In addition to participating in ATP release, Panxs and Cxs also have crucial immune functions. In this study, pannexin1, three connexin32 isoforms and connexin43 were identified and characterized in spotted sea bass (*Lateolabrax maculatus*), which were named *Lm*Panx1, *Lm*Cx32.2, *Lm*Cx32.3, *Lm*Cx32.7, and *Lm*Cx43. Their similar topological structures were discovered by sequence analysis: a relatively unconserved C-terminal region and four highly conserved transmembrane (TM) domains, and so on. Each extracellular (ECL) region of Panx1 has two conserved cysteine residues. Unlike Panx1, each ECL region of Cx32 and Cx43 contains three conserved cysteine residues, forming two conserved motifs: CX_6CX_3C motif in ECL1 and CX_4CX_5C motif in ECL2. Furthermore, Panx1 and Cx43 share similar genomic organization and synteny with their counterparts in selected vertebrates. Cx32 and CX43 were located in the same locus in fish, but diverged into two loci from amphibian. Moreover, despite varying expression levels, the identified genes were constitutively expressed in all examined tissues. All genes were upregulated by PAMP [lipopolysaccharide and poly(I:C)] stimulation or bacterial infection *in vivo* and *in vitro*, but they were downregulated in the brain at 6 or 12 h after stimulation. Especially, the three *Lm*Cx32 isoforms and *Lm*Cx43 were upregulated by ATP stimulation in primary

head kidney leukocytes; however, downregulation of *Lm*Cx32.3 and *Lm*Cx43 expression were noted at 12 h. Conversely, ATP treatment inhibited the expression of *Lm*Panx1. Importantly, we showed that the spotted sea bass Panx1, Cx43, and Cx32 were localized on the cellular membrane and involved in inflammation-induced ATP release. Taken together, our results demonstrated that Panx1, Cx32, and Cx43 are important neuro-related immune response genes involved in inflammation-induced ATP release.

Keywords: pannexin1, connexin32, connexin43, innate immunity, ATP release, *Lateolabrax maculatus*

INTRODUCTION

Regulating neurobehavior shows great promise for therapeutic application in a variety of immunological diseases and clinical conditions (1). For examples, sepsis can be treated by electrical stimulation of the vagus nerve (1), and electrical stimulation can promote the flow of calcium ions into nerve cells and the synthesis and release of ATP (2, 3). As a considerable member of endogenous danger-associated molecular pattern signaling molecule, extracellular ATP plays vital roles in natural immunity (4). In mammals, extracellular ATP is actively released from activated or stressed cells during inflammation, injury or apoptosis (5, 6). What's more, extensive immune response and inflammation can also be caused by extracellular ATP (6). In particular, extracellular ATP as a primary afferent neurotransmitter participated in the process of neuro-immune interactions (7). In addition, extracellular ATP involved in the process of pro-inflammatory cytokines (IL-1β, caspases, IFN and Mx, etc.) release (8–11) and the activation of the NLRP3/NLRC3 inflammasome (12–15). Therefore, extracellular ATP was considered as an effective signaling molecule to activate the natural immune responses (16). Apparently, it is extraordinarily important to study the molecular determinants for inflammation-induced ATP release.

Connexins (Cxs) are the main members of gap junctions, which control several second messengers to diffuse between adjacent cells (17). In addition, some Cx members can form hemichannels involved in extracellular ATP release (18). Since the first Cx gene was cloned, 21 isoforms of Cxs have been identified in mammals, such as Cx26, Cx32, and Cx43 (19). They have been identified as an important component of the cell homeostasis, differentiation, inflammation and natural immune responses (20, 21). About the Cx family, Cx32 and Cx43 play a role in a variety of immune cells and participate in the release of ATP (22, 23). Consequently, Cx32 and Cx43 have been proven to play vital immune roles (24, 25).

In addition to Cxs, pannexin (Panx) hemichannels were also involved in ATP release in mammals (26). Panxs are membrane channels glycoproteins with a similar topological structure to Cxs, including four transmembrane (TM) domains, one intracellular loop, two extracellular loops, and both the N- and C- terminal regions being intracellular (27). The Panx protein family includes three members, Panx1, Panx2, and Panx3. Like Cx32 and Cx43, Panx1 is expressed in several kinds of immune cells and plays very crucial roles in physiological and pathological processes in mammals, especially in inflammasome activation (28), cytokine release (28), and T cell activation (29).

Even though the functions of Cxs and Panxs in ATP release and immune responses have been extensively studied in mammals, their effects remain not clear in fish. Several recent studies have shown that Panx1 (4), Cx32 (21), and Cx43 (30) are important immune response genes and play an essential role in inflammation-induced ATP release in Japanese flounder (*Paralichthys olivaceus*). These results first showed that the Panx1, Cx32, and Cx43 genes are involved in innate immunity in fish. Panx1 is also an important immune response gene involved in bacterial infection-induced ATP release in tilapia (*Oreochromis niloticus*) (31). Besides, Cx and Panx genes were constitutively expressed in all the tissues and have been shown to respond to the bacterial infection in turbot (*Scophthalmus maximus* L.) (32). Taken together, the evidence that Panxs and Cxs were involved in ATP release and innate immune responses in fish remains immensely limited.

As a vital commercial fishes, spotted sea bass (*Lateolabrax maculatus*) widely farmed in East Asia because of their high nutritional value and adaptation to various salinity waters (seawater, brackish water and freshwater, etc.) (33, 34). Further study on the innate immunity of *L. maculatus* will help to understand its immune mechanisms. In this study, Panx1, three Cx32 isoforms and Cx43 were identified and characterized in *L. maculatus*, which were named *Lm*Panx1, *Lm*Cx32.2, *Lm*Cx32.3, *Lm*Cx32.7, and *Lm*Cx43, and gene expression was analyzed by PAMP [lipopolysaccharide (LPS) and poly(I:C)] stimulation or bacterial infection *in vivo* and *in vitro* using real-time quantitative polymerase chain reaction (qPCR). Importantly, we determined their subcellular localization and explored their function in inflammation-induced ATP release. Our findings will contribute to further understanding of the innate immune response mediated by extracellular ATP in fish and of neuroimmunity in vertebrates.

MATERIALS AND METHODS

Experimental Fish

L. maculatus (100 ± 10 g) were farmed in a freshwater fish aquaculture system at 26°C ± 2°C for more than 2 weeks prior to experiments. Fish were sourced from a fish freshwater farm in Hangzhou city, Zhejiang province, China.

Cloning of Panx1, Cx32, and Cx43 From Spotted Sea Bass

Total RNA was extracted, and partial gene sequences were obtained as described previously (34). The full-length cDNA sequences of *Lm*Panx1, *Lm*Cx32.2, *Lm*Cx32.3, *Lm*Cx32.7, and *Lm*Cx43 were then cloned and verified by our previous methods (35). All primers are summarized in **Table 1**.

TABLE 1 | Primers used for cloning and real-time PCR.

Primers	Sequence (5′ to 3′)	Application
*Lm*Panx1-F1	CTTGGCGGGAGCAGTGGTTG	Sequence validation
*Lm*Panx1-R1	AGAGTCCGTGGCATTCGTTTT	Sequence validation
*Lm*Panx1-3F1	CTCGTCAACTTGGTCCTGTTCATT	3′-RACE
*Lm*Panx1-3F2	ACGTCAGCGAACTAAAGTCCTACAA	3′-RACE
*Lm*Panx1-5R1	TCACTGCCACCAGCAACAAAA	5′-RACE
*Lm*Panx1-5R2	CTCTGTTCGGATGTTGCGGTAT	5′-RACE
*Lm*Panx1-F2	CCGCCATGAAACTTTAACAGACA	Verify the CDS
*Lm*Panx1-R2	AAATAAATCTGCTCCTCCTTCTTCC	Verify the CDS
*Lm*Cx32.2-F1	AGTGGGGTTTTCTGTCCTCTCTC	Sequence validation
*Lm*Cx32.2-R1	GCTGTGCTGTGACTGGCATCAT	Sequence validation
*Lm*Cx32.2-3F1	CTGTACGGGTTTGTCATGGACC	3′-RACE
*Lm*Cx32.2-3F2	TTCTACCTGGCGTGTTCTCGC	3′-RACE
*Lm*Cx32.2-5R1	TCAGAGTCGGTGTTGAGACAAAGAT	5′-RACE
*Lm*Cx32.2-5R2	TGGGAAGGCATGGTCATAGCAG	5′-RACE
*Lm*Cx32.2-F2	ATTCAGCCCCACAGCAGGTGA	Verify the CDS
*Lm*Cx32.2-R2	TCAAAGAAGAGCTTGCAGCACTAAA	Verify the CDS
*Lm*Cx32.3-F1	ATGGGAGACTTTGGTTTTCTGTCA	Sequence validation
*Lm*Cx32.3-R1	ACCACTCAGCAGTTGTTTCTCCTC	Sequence validation
*Lm*Cx32.3-3F1	CCTGCTCCAAGAAGCCCTGT	3′-RACE
*Lm*Cx32.3-3F2	GATTTGTACCAGGGTCAGATGCG	3′-RACE
*Lm*Cx32.3-5R1	CCCTTGATCGTCACCTTTCCCT	5′-RACE
*Lm*Cx32.3-5R2	CCAGAAGCGAATGTGCGAGAT	5′-RACE
*Lm*Cx32.3-F2	ATCTCTCCCAGCCAGAGACAGTCC	Verify the CDS
*Lm*Cx32.3-R2	CACGCTTTCCATTATGAGATTTCC	Verify the CDS
*Lm*Cx32.7-F1	GGGCGATGAGCAATCTGACTTT	Sequence validation
*Lm*Cx32.7-R1	CCATGTTGTTGTTCTCAGGCGA	Sequence validation
*Lm*Cx32.7-3F1	TCCGTCTCCCTCGTCCTCAGT	3′-RACE
*Lm*Cx32.7-3F2	ATGGCGAGGAGGCAGGACTA	3′-RACE
*Lm*Cx32.7-5R1	GCCACCAGCATGAACCAGATG	5′-RACE
*Lm*Cx32.7-5R2	CTGGAGGGTGAAACCGTAAAGT	5′-RACE
*Lm*Cx32.7-F2	AAGCAGGACAACTGGCGACTGAA	Verify the CDS
*Lm*Cx32.7-R2	CACACCGTTTAACTTCCCCAACG	Verify the CDS
*Lm*Cx43-F1	CTGGGTCGTCTACTGGACAAGG	Sequence validation
*Lm*Cx43-R1	CTTATGCTCGTGGGTATCATCG	Sequence validation
*Lm*Cx43-3F1	TGGTGTCCCTGCTGCTCAAC	3′-RACE
*Lm*Cx43-3F2	CTGTCCGCTGCTAAGTACGCT	3′-RACE
*Lm*Cx43-5R1	CGTGCTCCTCAATGCCATACTTT	5′-RACE
*Lm*Cx43-5R2	TGGGTGTTACATTTGAAGGCAGA	5′-RACE
*Lm*Cx43-F2	CGGTCCCAAACTTGGATTTC	Verify the CDS
*Lm*Cx43-R2	GACAACAGTGATTGAGGTTAGCC	Verify the CDS
*Lm*Panx1-qF	CTGAGGAGACGAGGTCATTGC	Real-time PCR
*Lm*Panx1-qR	GCAAGGGAGTGAGCTCTTTCATC	Real-time PCR
*Lm*Cx32.2-qF	AAGGAGACCTGCTGGGAAACTAC	Real-time PCR
*Lm*Cx32.2-qR	CGAGAACACGCCAGGTAGAAG	Real-time PCR
*Lm*Cx32.3-qF	GATTTGTACCAGGGTCAGATGCG	Real-time PCR
*Lm*Cx32.3-qR	CCATCCAGGCTTCCACCAATAC	Real-time PCR
*Lm*Cx32.7-qF	CCCTCGTCCTCAGTCTGGTTG	Real-time PCR
*Lm*Cx32.7-qR	TGTTCTCAGGCGATACGTTCTTG	Real-time PCR
*Lm*Cx43-qF	ACCAATGTCCCCTCCAGGCTAC	Real-time PCR
*Lm*Cx43-qR	TTATGCTCGTGGGTATCATCGG	Real-time PCR
*Lm*EF1α-qF	ATCTCTGGATGGCACGGAGA	Real-time PCR
*Lm*EF1α-qR	CAGTGTGGTTCCGCTAGCAT	Real-time PCR

Sequence Analysis of *Lm*Panx1, *Lm*Cx32, and *Lm*Cx43

Programs on the NCBI website (https://www.ncbi.nlm.nih.gov/) and Expasy website (http://www.expasy.org) were used to analyze nucleotide and protein sequences. Phylogenetic trees and multiple sequence alignment of Panx1, Cx32, and Cx43 were analyzed using the ClustalW, GeneDoc, and MEGA 5.1 program, according to the method described previously (35). The Ensembl and NCBI genome databases were analyzed to infer the genomic organization and syntenic relationships.

Tissue Expression of *Lm*Panx1, *Lm*Cx32, and *Lm*Cx43

Eight tissue samples (head kidney, spleen, gill, intestine, brain, liver, skin, and muscle) were obtained from healthy *L. maculatus* and used for total RNA extraction by TRIzol reagent. Total RNA was then reversed to cDNA for qPCR according to the method described previously (34). All primers are summarized in **Table 1**.

Expression of *Lm*Panx1, *Lm*Cx32, and *Lm*Cx43 in Spotted Sea Bass to the PAMP or *Edwardsiella tarda* Challenge

L. maculatus were intraperitoneal (i.p.) injected with 500 μL *Edwardsiella tarda* [1×10^5 colony-forming units (CFU)/mL], LPS (1 mg/mL), poly(I:C) (1 mg/mL), or phosphate-buffered saline (PBS) (control) for the challenge experiments by our previous methods (34). Each condition was done in quadruplicate. Next, according to the method described previously, tissue samples were obtained at 6, 12, 24, and 48 h after injection, and total RNA was then reversed to cDNA for qPCR. The *E. tarda* were prepared as previously described (34, 36). LPS and poly(I:C) were purchased from Sigma–Aldrich (USA).

Expression of *Lm*Panx1, *Lm*Cx32, and *Lm*Cx43 in Primary Head Kidney Leukocytes

Primary head kidney leukocytes were isolated by using a discontinuous Percoll gradient as previously described (37). The leukocytes cultured in a six-well plate (Corning, United States) with DMEM-F12 complete medium [DMEM-F12 with 10% fetal bovine serum and 1% Pen/Strep (penicillin/streptomycin)] in a CO_2 incubator at 28°C. The leukocytes (1×10^7/well) were treated with LPS (100 μg/mL), poly(I:C) (50 μg/mL), and ATP (100 μM or 1 mM), respectively. Each condition was done in quadruplicate. Cell samples were collected at 6, 12, 24, and 48 h after stimulation, and total RNA was then reversed to cDNA for qPCR. ATP was purchased from Sigma–Aldrich, and all cell culture reagents were purchased from Gibco (USA).

Subcellular Localization

The pEGFP-N1 expression plasmid containing the coding sequence (CDS) of *Lm*Panx1, *Lm*Cx32s, or *Lm*Cx43 were

constructed, that is, pEGFP-N1-*Lm*Panx1, pEGFP-N1-*Lm*Cx32.2, pEGFP-N1-*Lm*Cx32.3, pEGFP-N1-*Lm*Cx32.7, and pEGFP-N1-*Lm*Cx43. We then transfected the recombinant pEGFP-N1 plasmids into HEK293 T cells by the same methods as before (35). The transfected cells were cultured at 24 h and treated by the method described previously (38). Next, cells were stained with DAPI (Solarbio, China) and observed using a laser confocal microscope (Leica TCS SP8, Germany). All cell culture reagents were purchased from Gibco.

Extracellular ATP Measurement

To examine the LPS-induced extracellular ATP release in primary head kidney leukocytes of *L. maculatus*, the leukocytes (1×10^5/well) were cultured in a 24-well plate (Corning, United States) and stimulated with LPS (100 μg/mL) or PBS. The supernatants were collected at 15 and 30 min after stimulation and used to measure extracellular ATP levels. Each condition was done in quadruplicate. The ATP release level was measured with Enhanced ATP Assay Kit (Beyotime, China) in LumiPro (YPHBIO, China). All cell culture reagents were purchased from Gibco.

To explore the role of *Lm*Panx1, *Lm*Cx32, and *Lm*Cx43 in LPS-induced extracellular ATP release, the pcDNA3.1 expression plasmid containing the CDS of *Lm*Panx1, *Lm*Cx32s, or *Lm*Cx43 was constructed, that is, pcDNA3.1-*Lm*Panx1, pcDNA3.1-*Lm*Cx32.2, pcDNA3.1-*Lm*Cx32.3, pcDNA3.1-*Lm*Cx32.7, and pcDNA3.1-*Lm*Cx43. The same number of HEK293 T cells transfected with expression plasmids or empty plasmid (pcDNA3.1) was cultured in a 24-well plate at 24 h, and then were stimulated with LPS (100 μg/mL). Meanwhile, the mock transfected and empty plasmid transfected cells (negative controls) were cultured in another 24-well plate at 24 h, but were not stimulated with LPS. The supernatants were collected at 15 and 30 min after stimulation and used to measure extracellular ATP levels. Each condition was done in quadruplicate. The ATP levels were then measured as described previously.

Statistical Analysis

The data were processed and statistically analyzed using the IBM SPSS package (SPSS 20.0, SPSS Inc., Chicago, IL, United States). Significant differences ($p < 0.05$ or $p < 0.01$) between experimental groups and control groups were analyzed using analysis of variance as previously described (35).

RESULTS

Sequence Identification of *Lm*Panx1, *Lm*Cx32, and *Lm*Cx43

The Panx1, Cx32, and Cx43 sequences in *L. maculatus* were submitted to the GenBank database: OM315303 (*Lm*Panx1), OM315304 (*Lm*Cx32.2), OM315305 (*Lm*Cx32.3), OM315306 (*Lm*Cx32.7), and OM315307 (*Lm*Cx43).

It can be observed from **Supplement Figure 1** that the total length cDNA of *Lm*Panx1 has been cloned, which contains 1,959 bp including a 161-bp 5′ untranslated region (UTR), an open reading frame (ORF) with 1,320 bp encoding 439 amino acids (aa), and a 478-bp 3′-UTR. Moreover, there is a polyadenylation signal (ATTAAA) at the 3′-UTR of the sequence (**Supplement Figure 1**). Multiple sequence alignment revealed that *Lm*Panx1 retains four highly conserved TM domains; meanwhile, it can be observed that TM2 has a typically innexin-specific P-X-X-X-W motif (4) (**Figure 1A**). Each of the extracellular (ECL) regions has two conserved cysteine residues distinctly, and all species except zebrafish contain a charged K or R residue relative to position 75 (**Figure 1A**), which was deemed to be involved in ATP-mediated channel regulation (39).

For the whole cDNA of *Lm*Cx32.2, it is 1,496 bp, with a 71-bp 5′-UTR, an ORF contains 786 and a 639-bp 3′-UTR containing a tail-adding signal (AATAAA) (**Supplement Figure 2A**). The total length of the cloned cDNA sequence of *Lm*Cx32.3 is 1,415 bp, including a 70-bp 5′-UTR, a 840-bp ORF, and a 505-bp 3′-UTR containing a polyadenylation signal (AATAAA) (**Supplement Figure 2B**). The cDNA of *Lm*Cx32.7 was obtained by cloning with 1,357 bp in length, including a 23-bp 5′-UTR, a 921-bp ORF, and a 413-bp 3′-UTR containing a tail-adding signal (AATAAA) (**Supplement Figure 2C**). After multiple sequence alignment, it was found that *Lm*Cx32s contain four conserved TM domains, a connexin homolog (CNX) domain, and a connexin-ccc domain (30). Unlike Panx1, three conserved cysteine residues in each of the ECL region form two conserved motifs, that is, CX_6CX_3C motif in ECL1 and CX_4CX_5C motif in ECL2 (**Figure 1B**), which play important roles in Cx channel formation (40).

As shown in **Supplement Figure 3**, the full-length cDNA of *Lm*Cx43 is 2,625 bp, with a 1,167-bp ORF encoding a protein of 388 aa. There are 129 bp of 5′-UTR and 1,329 bp of 3′-UTR on either side of the ORF area, and a polyadenylation signal (ATTAAG) at the 3′-UTR. By multiple sequence alignment, the *Lm*Cx43 protein exhibits a high degree of conservation and contains a CNX domain, a connexin-ccc domain, and a PDZ domain. Like Cx32s, three conserved cysteine residues in each of the ECL region form two conserved motifs: CX_6CX_3C motif in ECL1 and CX_4CX_5C motif in ECL2 (**Figure 1C**).

Homologous relationships between Panx1, Cx32, and Cx43 from various animal species were identified by constructing phylogenetic trees, respectively. In **Figure 2A**, *Lm*Panx1 and of *Morone saxatilis* formed one branch (88% bootstrap support) and then were clustered with homologs from other fish species. Corresponding to the clades formed by Cx32.2, Cx32.3, and Cx32.7 homologs from different fish, *Lm*Cx32s were clustered into three distinct branches (**Figure 2B**). In addition, *Lm*Cx43 and of *Larimichthys crocea* formed a clade with 46% of support rate and then were clustered together with other fish homologs into a clade (**Figure 2C**).

Genomic Organization and Synteny of *Lm*Panx1, *Lm*Cx32, and *Lm*Cx43

Our study determined the genomic structures of *Lm*Panx1, *Lm*Cx32, and *Lm*Cx43 by comparing their cDNA and genomic sequences (**Figure 3**). There are eight exons and seven introns in

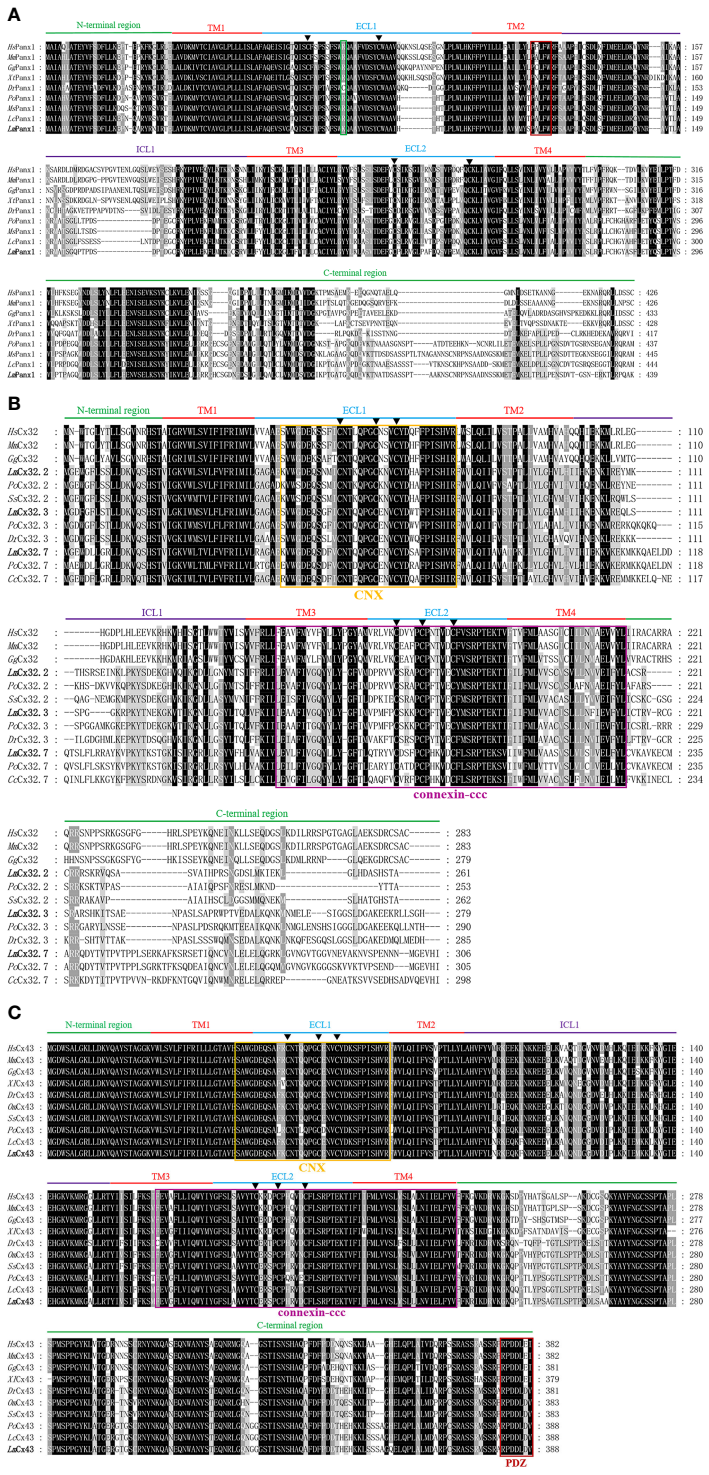

FIGURE 1 | Multiple sequence alignment analysis of Panx1 **(A)**, Cx32 **(B)**, and Cx43 **(C)**. The N-terminal region, four TM domains (TM1-4), the intracellular loop (ICL1), the extracellular loops (ECL1-2), and the C-terminal region of *Lm*Panx1, *Lm*Cx32, and *Lm*Cx43 are marked above the alignment. Symbol (▲) indicates the conserved cysteine residues. The K or R residue in position 75 and the classic innexin-specific P-X-X-X-W motif are boxed in green and red, respectively. In addition, the CNX domain, connexin-ccc domain, and PDZ domain are boxed in yellow, purple, and red, respectively. The *Lm*Panx1, *Lm*Cx32, and *Lm*Cx43 are shown in bold. The accession numbers of sequences are shown in **Figure 2**. *Hs*, *Homo sapiens*; *Mm*, *Mus musculus*; *Gg*, *Gallus gallus*; *Xt*, *Xenopus tropicalis*; *Dr*, *Danio rerio*; *Po*, *Paralichthys olivaceus*; *Ms*, *Morone saxatilis*; *Lc*, *Larimichthys crocea*; *Lm*, *Lateolabrax maculatus*; *Ss*, *Salmo salar*; *Cc*, *Cyprinus carpio*; *Om*, *Oncorhynchus mykiss*.

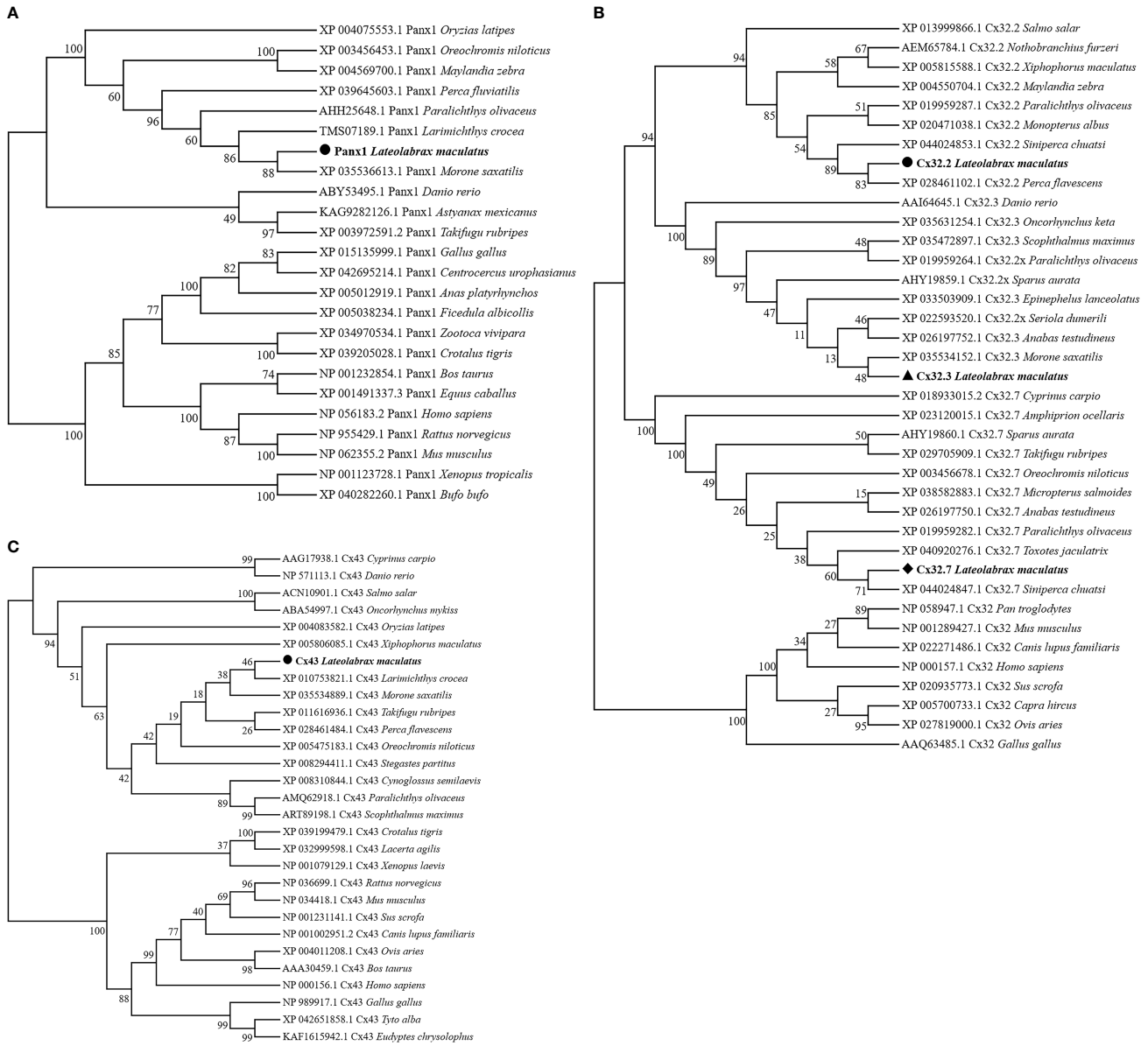

FIGURE 2 | Phylogenetic tree analysis of Panx1 **(A)**, Cx32 **(B)**, and Cx43 **(C)**. Phylogenetic tree was constructed using the NJ method and run for 10,000 replications. The *Lm*Panx1, *Lm*Cx32, and *Lm*Cx43 are shown in bold.

*Lm*Panx1 gene; the first intron is located in 5′-UTR, the same organization to that of Fugu, large yellow croaker, and spotted gar Panx1 genes (**Figure 3A**). Besides, the sizes of the first three exons and the last exon of the CDS are comparable with those of Panx1 from selected vertebrates (**Figure 3A**). Similar to Fugu and large yellow croaker, *Lm*Cx32.2, *Lm*Cx32.3, and *Lm*Cx32.7 genes consisted of three, two, and three exons, respectively (**Figure 3B**). Human, mouse, chicken, and frog Cx32 gene had two exons, and the intron is located in 5′-UTR, which is the same as the *Lm*Cx32.3 (**Figure 3B**). The *Lm*Cx43 gene also consisted of two exons, with the same organization as the Cx43 gene in other species (**Figure 3C**).

Gene synteny showing that the Panx1 loci have been well conserved during evolution, where the Panx1 linked to MRE11 and MED17, and other genes found in this locus included SMCO4, HEPHL1, IL10RA, CAPNS1, and CLIP3 (**Figure 4A**). The Cx43 and Cx32s were located in the same chromosome in different fish, forming a gene cluster, but Cx43 and Cx32 were located in different chromosomes in human, mouse, chicken, and frog (**Figure 4B**). At the same time, the Cx43 and Cx32s in different fish were located in the same gene locus as the Cx43 gene of the human, mouse, chicken, and frog, which also contains TBC1D32, MAN1A1, FAM184A, HSF2, SERINC1, and so on.

FIGURE 3 | Genomic organization of Panx1 **(A)**, Cx32 **(B)**, and Cx43 **(C)**. Blank and solid boxes indicate UTR and coding exon, respectively. The size (bp) of exons and introns is indicated. Note that the size of exons and introns is disproportionate.

Expression of *Lm*Panx1, *Lm*Cx32, and *Lm*Cx43 in Tissues

We analyzed the expression of *Lm*Panx1, *Lm*Cx32, and *Lm*Cx43 in eight tissues, including head kidney, spleen, gill, intestine, brain, liver, skin, and muscle (**Figure 5**). Despite varying expression levels, the identified genes were constitutively expressed in all examined tissues. More specifically, the highest expression levels of *Lm*Panx1, *Lm*Cx32 (*Lm*Cx32.2, *Lm*Cx32.3, and *Lm*Cx32.7), and *Lm*Cx43 were found in muscle, liver, and brain, respectively. In addition, the lowest expression levels of *Lm*Cx32 and *Lm*Cx43 were both found in head kidney. In contrast liver exhibited the lowest expression for *Lm*Panx1, and the moderate expression levels of *Lm*Cx32 and *Lm*Cx43 were found in the intestine, muscle, and skin. Differently, the moderate expression levels of *Lm*Panx1 were found in the brain, gill, and spleen.

Expression Analysis of *Lm*Panx1, *Lm*Cx32, and *Lm*Cx43 After *In Vivo* Stimulation

The expression patterns of *Lm*Panx1, *Lm*Cx32, and *Lm*Cx43 were analyzed in tissues including the head kidney, spleen, gill, intestine, brain, and liver after PAMP [LPS and poly(I:C)] and *E. tarda* challenge (**Figure 6**). *L. maculatus* were i.p. injected with 500 μL *E. tarda* (1×10^5 CFU/mL), LPS (1 mg/mL), poly(I:C) (1 mg/mL), or PBS for the challenge experiments. Tissue samples were obtained at 6, 12, 24, and 48 h after injection, and total RNA was then reversed to cDNA for qPCR. In head kidney, gill, and intestine, the expression of *Lm*Panx1 was upregulated to the different degrees after three kinds of stimulation. In spleen, the expression of *Lm*Panx1 was upregulated after poly(I:C) (at 12 h) and *E. tarda* (except 24 h) stimulation, but there was no significant change after LPS stimulation; In the brain, *Lm*Panx1 was downregulated at 6 h after LPS and *E. tarda* stimulation, but upregulated at 48 h after LPS and poly(I:C) stimulation; in the liver, *Lm*Panx1 was upregulated only at 24 h after poly(I:C) and *E. tarda* stimulation (**Figure 6A**).

As shown in **Figures 6B–D**, the *Lm*Cx32 isoforms were upregulated in the head kidney, spleen, and liver by the *E. tarda* infection, but downregulated in the brain after LPS stimulation; Furthermore, in the intestine, *Lm*Cx32.7 was upregulated after stimulation (at 24 h), whereas the expression of *Lm*Cx32.2 and *Lm*Cx32.3 remained constant. Moreover,

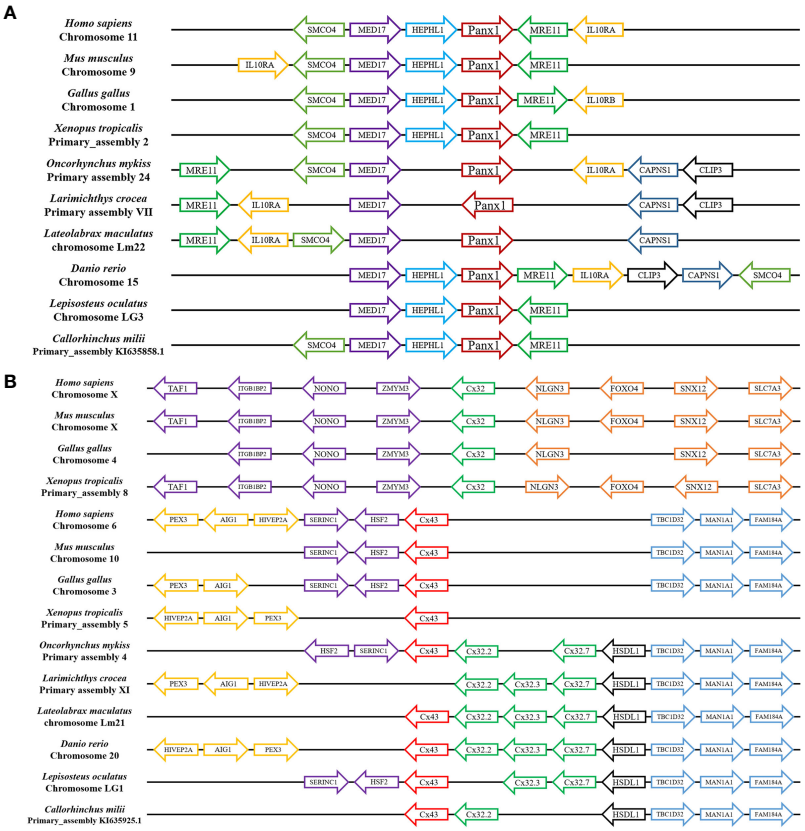

FIGURE 4 | Gene synteny of Panx1 **(A)** and Cx32 and Cx43 **(B)**. The *Lm*Panx1, *Lm*Cx32, and *Lm*Cx43 genome sequence data were obtained from the spotted sea bass genome database (https://www.ncbi.nlm.nih.gov/genome/43909). Synteny information for other vertebrates was retrieved from the Ensembl database (http://www.ensembl.org/index.html). Arrows indicate transcription orientations.

*Lm*Cx32.2 was upregulated in the spleen (at 12 h), brain (at 6 h), and liver (at 48 h), but downregulated in the gill (at 24 h) by poly (I:C) stimulation (**Figure 6B**). Similarly, *Lm*Cx32.3 was induced in the head kidney, spleen after stimulation with poly(I:C), and LPS (**Figure 6C**). For *Lm*Cx32.7, LPS stimulation inhibited its expression in the head kidney and liver, whereas it was upregulated in the gill and liver after poly(I:C) stimulation (**Figure 6D**).

Like *Lm*Panx1, the expression of *Lm*Cx43 was upregulated to the different degrees, respectively, in the head kidney, gill, intestine, and liver after poly(I:C) or *E. tarda* stimulation (**Figure 6E**). In addition, *Lm*Cx43 was upregulated in all examined tissues except the gill after LPS stimulation, but was downregulated in the brain after *E. tarda* stimulation (**Figure 6E**).

Expression Analysis of *Lm*Panx1, *Lm*Cx32, and *Lm*Cx43 after *In Vitro* Stimulation

Expression patterns of *Lm*Panx1, *Lm*Cx32, and *Lm*Cx43 were also analyzed in primary head kidney leukocytes after PAMP [LPS and poly(I:C)] and ATP stimulation (**Figure 7**). The leukocytes were treated with LPS (100 μg/mL), poly(I:C) (50 μg/mL), and ATP (100 μM or 1 mM), respectively. The cell samples were collected at 6, 12, 24, and 48 h after stimulation, and total RNA was then reversed to cDNA for qPCR. As shown in **Figure 7A**, all the genes were induced by PAMP stimulation. The *Lm*Panx1 expression was upregulated after LPS (at 6 h) and poly(I:C) (at 6 and 12 h) stimulation, whereas it remained unchanged at other stimulation conditions. Beyond that, all the genes except *Lm*Panx1 were upregulated at 48 h by PAMP stimulation. Among the three *Lm*Cx32 isoforms, *Lm*Cx32.7 responded most strongly to stimulation, and the expression of *Lm*Cx32.7 was obviously upregulated at all times except 12 h after poly(I:C) stimulation. According to the **Figure 7B**, the expression of three *Lm*Cx32 isoforms and *Lm*Cx43 was upregulated by ATP stimulation; nevertheless, when cells were stimulated with 100 μM or 1 mM ATP, the significantly downregulated expression of *Lm*Cx32.3 and *Lm*Cx43 was noted at 12 h. Conversely, treatment of 100 μM or 1 mM ATP inhibited the *Lm*Panx1 expression.

Subcellular Localization of *Lm*Panx1, *Lm*Cx32, and *Lm*Cx43

To determine the subcellular localization of *Lm*Panx1, *Lm*Cx32, and *Lm*Cx43, plasmids pEGFP-N1-*Lm*Panx1, pEGFP-N1-

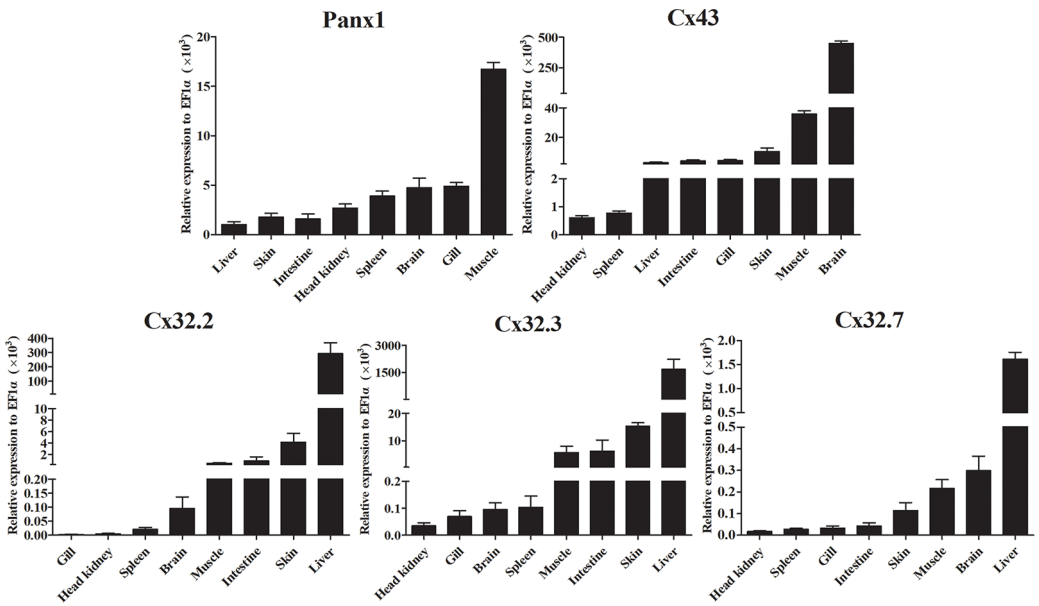

FIGURE 5 | Expression analysis of *Lm*Panx1, *Lm*Cx32, and *Lm*Cx43 in tissues by qPCR. The expression level of each gene was normalized to that of EF1α. Data are presented as mean ± SEM (N = 4).

*Lm*Cx32.2, pEGFP-N1-*Lm*Cx32.3, pEGFP-N1-*Lm*Cx32.7, and pEGFP-N1-*Lm*Cx43 were constructed to express the GFP-tagged *Lm*Panx1, *Lm*Cx32.2, *Lm*Cx32.3, *Lm*Cx32.7, and *Lm*Cx43 fusion protein in the HEK293T cells, respectively. After 24-h culture, the cells were examined under a laser confocal microscope. In HEK293 T cells transfected with expression plasmids, GFP fluorescence was mainly located on the cell membrane, whereas in HEK293 T cells transfected with empty plasmids, GFP fluorescence was mainly located in the intracellular area (**Figure 8A**). The results showed that *Lm*Panx1, *Lm*Cx32, and *Lm*Cx43 were localized on the cellular membrane and can be expressed in HEK293 T cells.

The Roles of *Lm*Panx1, *Lm*Cx32, and *Lm*Cx43 in LPS-induced Extracellular ATP Release

To investigate the function of *Lm*Panx1, *Lm*Cx32, and *Lm*Cx43 in inflammation-induced ATP release, primary head kidney leukocytes and HEK293 T cells (transfected with expression plasmids or empty plasmids) were stimulated with LPS, and the ATP levels were measured at 15 and 30 min after stimulation. In overexpression experiments, as negative controls, mock transfected and empty plasmid transfected cells were cultured in another 24-well plate at 24 h, but were not stimulated with LPS. As shown in **Figure 8B**, compared with the unstimulated, the levels of extracellular ATP have increased extremely significantly in primary head kidney leukocytes by LPS stimulation of 15 and 30 min. Furthermore, overexpression of *Lm*Panx1, *Lm*Cx32, or *Lm*Cx43 in HEK293 T cells, compared with cells transfected with empty plasmids, resulted in a significant increase in extracellular ATP levels after LPS stimulation at 15 or 30 min (**Figure 8C**).

DISCUSSION

Extracellular ATP has been shown to be an effective and conservative signaling molecule to activate natural immunity (8, 16). Therefore, it is important to study the molecular mechanisms of inflammation-induced ATP release. In mammals, substantial evidence indicates that Panx and Cx channels were participated in ATP release and had crucial immune functions (6). However, studies on the involvement of Panxs and Cxs in ATP release and natural immunity in fish remain limited. In the present article, Panx1, three Cx32 isoforms, and Cx43 were identified and characterized in *L. maculatus*, and these proteins share similar topological structure (**Figures 1** and **2**). Based on the results of our studies, Panx1 and Cx43 share similar genomic organization and synteny with their counterparts in vertebrates (**Figures 3** and **4**). In addition, there are multiple isoforms of Cx32 in selected fish, such as zebrafish (three isoforms), large yellow croaker (three isoforms), spotted gar (two isoforms), and rainbow trout (two isoforms). Accordingly, Cx32 gene containing duplicate copies may be a common characteristic in fish. It is worth noting that Cx32 and CX43 were located in the same locus in fish, but diverged into two loci from amphibian (**Figure 4B**), suggesting that during the evolution from fish to amphibians, Cx32 might have been transferred to other chromosomes.

Like their counterparts in mammals and other fish (such as Japanese flounder, zebrafish, and turbot), *Lm*Panx1, *Lm*Cx32,

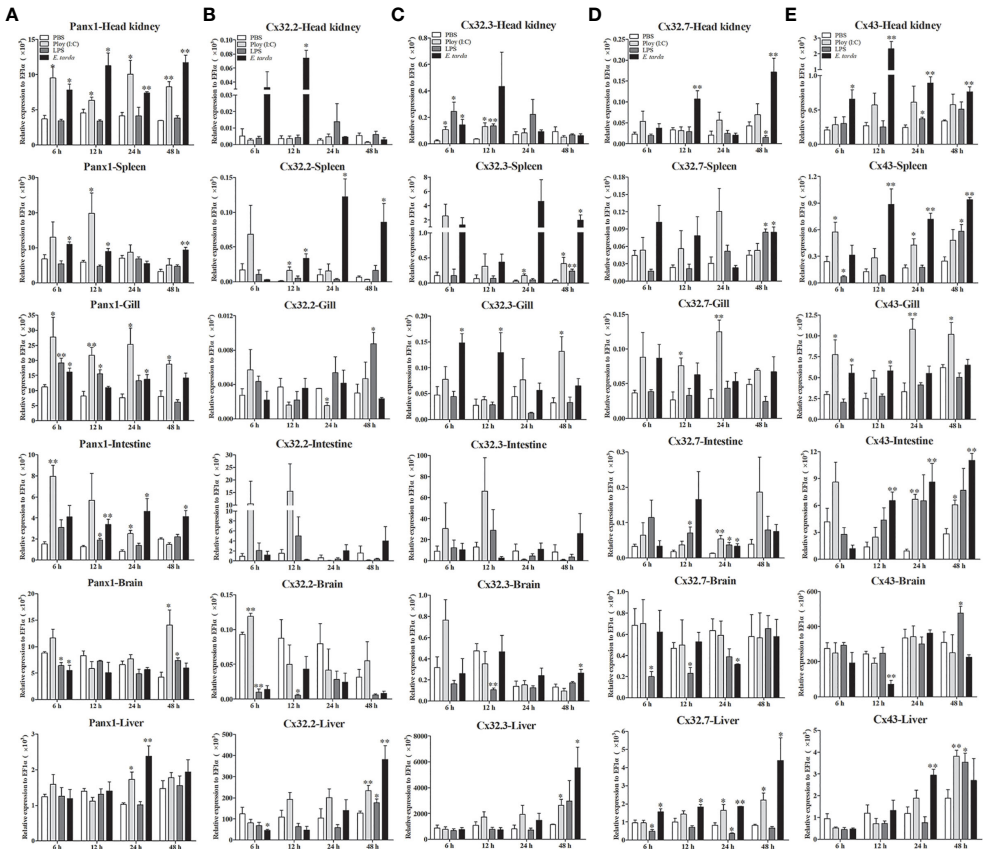

FIGURE 6 | Expression of *Lm*Panx1 **(A)**, *Lm*Cx32.2 **(B)**, *Lm*Cx32.3 **(C)**, *Lm*Cx32.7 **(D)**, and *Lm*Cx43 **(E)** after LPS, poly(I:C), or *Edwardsiella tarda* challenge. Spotted sea bass was i.p. injected with LPS (5 mg/kg body weight), poly(I:C) (5 mg/kg body weight), *E. tarda* (5×10^4 CFU/fish), or PBS (control) The relative expression levels of target genes were normalized to that of EF1α. Data are shown as mean +SEM (N = 4). $^*p < 0.05$, $^{**}p < 0.01$ are considered significant difference.

and *Lm*Cx43 were ubiquitously present in all tested tissues (**Figure 5**) (4, 21, 30, 32, 41). For instance, similar to Japanese flounder, the highest expression levels of *Lm*Cx32s (all of *Lm*Cx32.2, *Lm*Cx32.3, and *Lm*Cx32.7) and *Lm*Cx43 were found in the liver and brain, respectively. Interestingly, in mouse, Cx32 has been shown to be the major Cx protein in the liver, protecting the liver against liver injury (42), whereas Cx43 has been shown to be a "command gene" that regulates expression patterns, variability, and coordination of the brain transcriptome (43). Similar expression patterns suggest that *Lm*Cx32 and *Lm*Cx43 may play an active role in intercellular communications in tissues such as the liver and brain. Taken together, our results suggest that *Lm*Panx1, *Lm*Cx32, and *Lm*Cx43 may play distinct roles in different organs.

Studies have demonstrated that Panx1, Cx32, and Cx43 play important neural immune roles in mammals. For examples, Panx1 has been confirmed in inflammation of a variety of organs and tissues, especially the central and peripheral nervous system (44). Bacterial infection induced upregulation of Cx32 and Cx43 has also been demonstrated (45). In fish, Panx1, Cx32, and Cx43 were upregulated by PAMPs stimulation or bacterial infection (16, 31, 32). Similar to these studies, our findings showed that *Lm*Panx1, *Lm*Cx32, and *Lm*Cx43 were upregulated by PAMP [LPS and poly(I:C)] stimulation or *E. tarda* infection *in vivo* and *in vitro* (**Figures 6**, **7A**), suggesting the involvement of *Lm*Panx1, *Lm*Cx32, and *Lm*Cx43 in response to immune challenge in spotted sea bass. Interestingly, Panx1 and Cx43 are involved in mammalian neural inflammation, and multiple studies suggest that they could be targets for the treatment of neurological diseases in the future (6, 44). Therefore, we paid special attention to their expression after PAMP [LPS and poly(I:C)] and *E. tarda* infection in the brain. We found that *Lm*Panx1, *Lm*Cx32, and *Lm*Cx43 were downregulated in the brain at 6 or 12 h after stimulation, suggesting that the intercellular communication is hampered in the early stages of inflammation. Furthermore, we found that the three Cx32 isoforms and Cx43 were induced after ATP stimulation, but Panx1 was inhibited (**Figure 7B**). Interestingly, ATP may lead to hemichannel opening to release ATP by activating different purinergic receptors (46). Thus, our results suggest "ATP-induced ATP release" probably through the Cx hemichannels rather than the Panx1 hemichannel in fish.

Previous studies have demonstrated that among the Panx and Cx family proteins, Panx1, Cx32, and Cx43 are mainly expressed

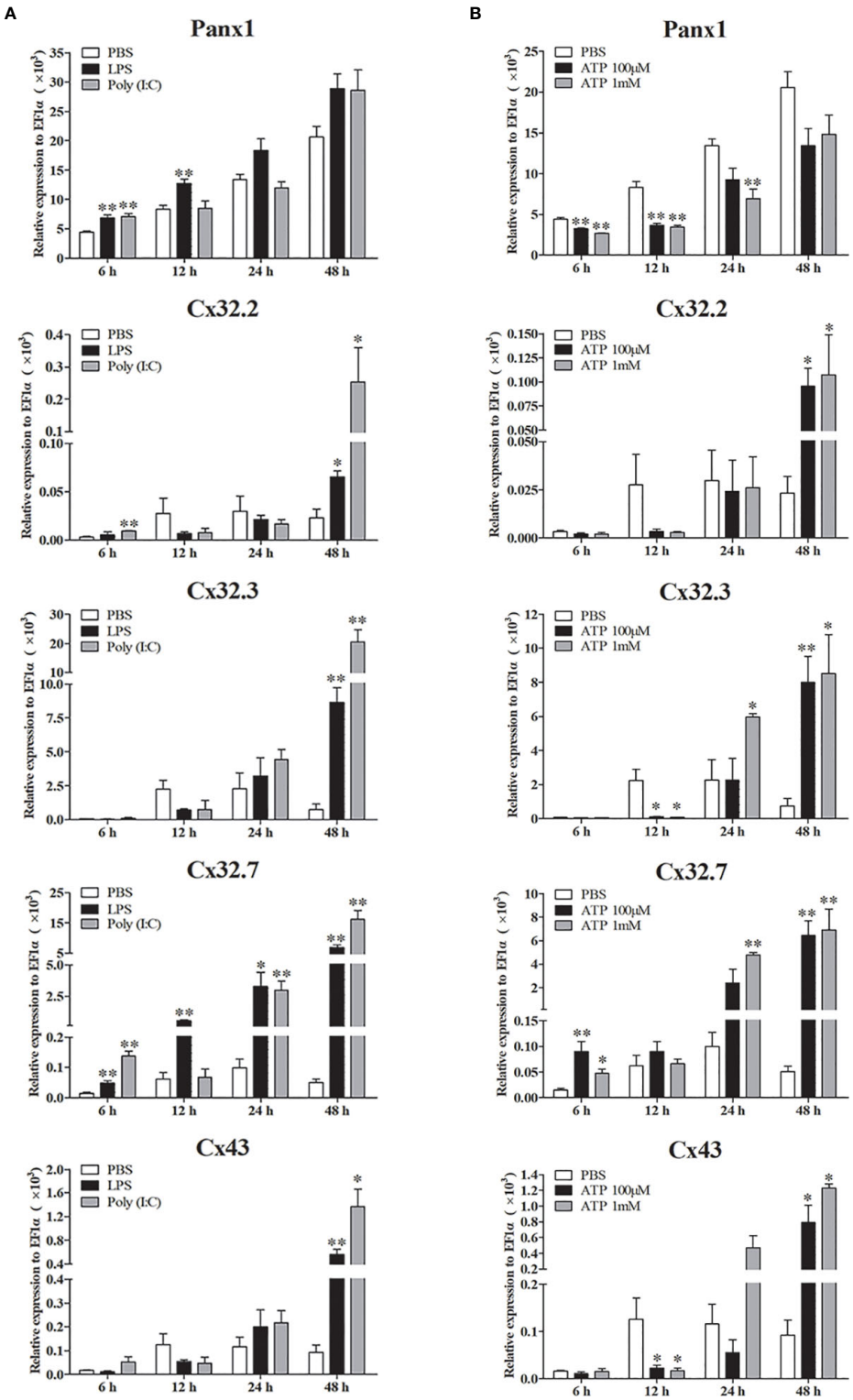

FIGURE 7 | Expression of *Lm*Panx1, *Lm*Cx32, and *Lm*Cx43 in primary head kidney leukocytes after stimulation with LPS, poly(I:C) **(A)** or ATP **(B)**. Primary head kidney leukocytes were isolated from the spotted sea bass head kidney and stimulated with LPS (100 μg/mL), poly(I:C) (50 μg/mL), 100 μM ATP, 1 mM ATP, or PBS (control). The relative expression levels of target genes were normalized to that of EF1α. The data are shown as mean +SEM (N = 4). *$p < 0.05$, **$p < 0.01$ are considered significant difference.

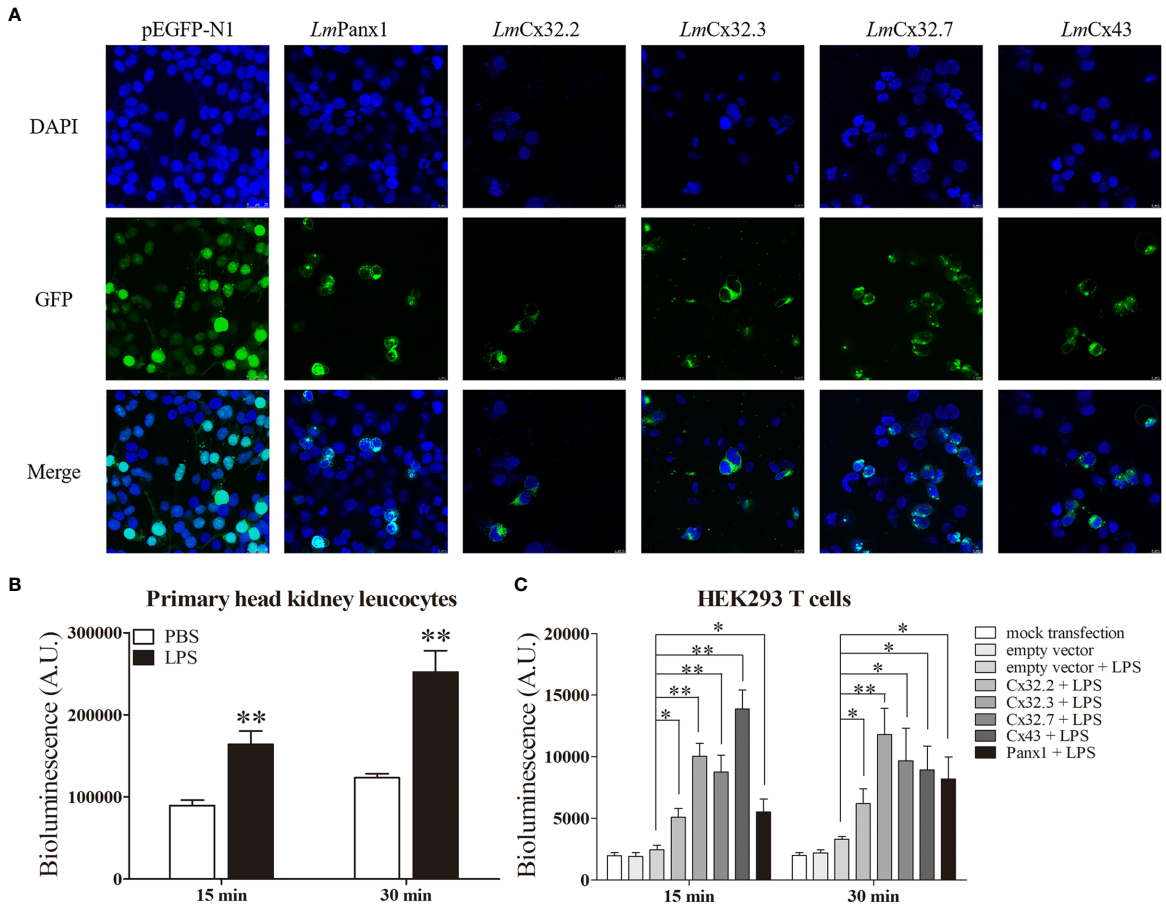

FIGURE 8 | Subcellular localization of *Lm*Panx1, *Lm*Cx32, and *Lm*Cx43 in HEK293 T cells **(A)** and LPS-induced extracellular ATP release in primary head kidney leukocytes **(B)** or HEK293 T cells **(C)**. **(A)** HEK293 T cells were transfected with pEGFP-N1-*Lm*Panx1, pEGFP-N1-*Lm*Cx32.2, pEGFP-N1-*Lm*Cx32.3, pEGFP-N1-*Lm*Cx32.7, or pEGFP-N1-*Lm*Cx43 plasmids. At 24 h posttransfection, the cells were stained with DAPI and observed under a confocal microscope. **(B, C)** The primary head kidney leukocytes were stimulated with LPS (100 μg/mL) or PBS (control). HEK293 T cells were transfected with pcDNA3.1-*Lm*Panx1, pcDNA3.1-*Lm*Cx32.2, pcDNA3.1-*Lm*Cx32.3, pcDNA3.1-*Lm*Cx32.7, or pcDNA3.1-*Lm*Cx43. After 24 h, the cells were stimulated with LPS (100 μg/mL). The supernatant was collected at 15 and 30 min after stimulation and the ATP levels were subsequently measured. The mock transfected and empty plasmid transfected cells served as controls. Data are shown as mean +SEM (N = 4). $^{*}p < 0.05$, $^{**}p < 0.01$ are considered significant difference.

in several immune cells and participated in inflammation-induced ATP release in mammals. However, in fish, the functions of Cx32 and Cx43 in ATP release were found only in Japanese flounder (4, 21, 30). Moreover, bacterial and PAMP infection resulted in the release of ATP through Panx1 in tilapia and Japanese flounder (31). Thus, the evidence that Panx1 and Cxs were inflammation-induced ATP release in fish is still limited. In this study, we demonstrated that LPS can induce extracellular ATP release from primary head kidney leukocytes in spotted sea bass (**Figure 8B**). Second, we demonstrated that *Lm*Panx1, *Lm*Cx32, and *Lm*Cx43 were localized on the cellular membrane, which are necessary for ATP release from the channel (**Figure 8A**). Finally, we found that overexpression of *Lm*Panx1, *Lm*Cx32, or *Lm*Cx43 in HEK293 T cells leads to a significant increase in extracellular ATP levels (**Figure 8C**). Taken together, our results demonstrated that Panx1, Cx32, and Cx43 are participated in inflammation-induced ATP release in spotted sea bass.

In summary, Panx1, three Cx32 isoforms, and Cx43 were identified in spotted sea bass. Sequence analysis showed that these proteins share similar topological structure. Panx1 and Cx43 share similar genomic organization and synteny with their counterparts in selected vertebrates, but Cx32 is not very conserved. All the genes were upregulated by PAMP [LPS and poly(I:C)] stimulation or *E. tarda* infection *in vivo* and *in vitro*, but were downregulated in the brain at 6 or 12 h after stimulation. Furthermore, the three Cx32 isoforms and Cx43 were induced after ATP stimulation, but Panx1 was inhibited. More importantly, Panx1, Cx32, and Cx43 are involved in inflammation-induced ATP release in spotted sea bass. The results will contribute to further understanding of the innate immune response mediated by extracellular ATP in fish.

DATA AVAILABILITY STATEMENT

The datasets presented in this study can be found in online repositories. The names of the repository/repositories and accession number(s) can be found in the article/**Supplementary Material**.

ETHICS STATEMENT

All fish experiments were conducted under the national regulations of laboratory animals of China and reviewed and approved by the ethics committee of laboratory animals of Shanghai Ocean University (SHOU-DW-2019-012).

AUTHOR CONTRIBUTIONS

ZS, YC, CX, and DL performed laboratory experiments and analyzed the data. QG and ZS designed the experiments. QG, PW, and ZS wrote the manuscript. All authors have read and approved the manuscript.

FUNDING

This work was financially supported by the National Key Research and Development Program of China (no. 2018YFD0900605).

ACKNOWLEDGMENTS

The authors would like to thank Dr. Haixia Xie, Institute of Hydrobiology, Chinese Academy of Sciences, for providing *E. tarda*.

SUPPLEMENTARY MATERIAL

The Supplementary Material for this article can be found online at: https://www.frontiersin.org/articles/10.3389/fimmu.2022.870679/full#supplementary-material

REFERENCES

1. Chen P, Wang Q, Wan X, Yang M, Liu C, Xu C, et al. Wireless Electrical Stimulation of the Vagus Nerves by Ultrasound-Responsive Programmable Hydrogel Nanogenerators for Anti-Inflammatory Therapy in Sepsis. *Nano Energy* (2021) 89:106327. doi: 10.1016/j.nanoen.2021.106327
2. Chen P, Wu P, Wan X, Wang Q, Xu C, Yang M, et al. Ultrasound-Driven Electrical Stimulation of Peripheral Nerves Based on Implantable Piezoelectric Thin Film Nanogenerators. *Nano Energy* (2021) 86:106123. doi: 10.1016/j.nanoen.2021.106123
3. Wu P, Zhao Y, Chen F, Xiao A, Du Q, Dong Q, et al. Conductive Hydroxyethyl Cellulose/Soy Protein Isolate/Polyaniline Conduits for Enhancing Peripheral Nerve Regeneration *Via* Electrical Stimulation. *Front In Bioeng And Biotechnol* (2020) 8:709. doi: 10.3389/fbioe.2020.00709
4. Li S, Li X, Chen X, Geng X, Sun J. ATP Release Channel Pannexin 1 Is a Novel Immune Response Gene in Japanese Flounder *Paralichthys olivaceus*. *Fish Shellfish Immun* (2014) 40(1):164–73. doi: 10.1016/j.fsi.2014.06.034
5. Lazarowski ER. Vesicular and Conductive Mechanisms of Nucleotide Release. *Purinerg Signal* (2012) 8(3):359–73. doi: 10.1007/s11302-012-9304-9
6. Faas MM, Saez T, de Vos P. Extracellular ATP and Adenosine: The Yin and Yang in Immune Responses? *Mol Aspects Med* (2017) 55:9–19. doi: 10.1016/j.mam.2017.01.002
7. Wood JN. Pain, Purines and Geoff. *Auton Neurosci Basic* (2022) 237:002902. doi: 10.1016/j.autneu.2021.102902
8. Li S, Chen X, Li J, Li X, Zhang T, Hao G, et al. Extracellular ATP Is a Potent Signaling Molecule in the Activation of the Japanese Flounder (*Paralichthys olivaceus*) Innate Immune Responses. *Innate Immun London* (2020) 26 (5):413–23. doi: 10.1177/1753425918804635
9. Chen H, Ding SF, Tan JC, Yang DH, Zhang YX, Liu Q. Characterization of the Japanese Flounder NLRP3 Inflammasome in Restricting *Edwardsiella piscicida* Colonization *in Vivo*. *Fish Shellfish Immun* (2020) 103:169–80. doi: 10.1016/j.fsi.2020.04.063
10. Angosto D, Lopez-Castejon G, Lopez-Munoz A, Sepulcre MP, Arizcun M, Meseguer J, et al. Evolution of Inflammasome Functions in Vertebrates: Inflammasome and Caspase-1 Trigger Fish Macrophage Cell Death But Are Dispensable for the Processing of IL-1 Beta. *Innate Immun London* (2012) 18 (6):815–24. doi: 10.1177/1753425912441956
11. Li S, Li J, Peng W, Hao G, Sun J. Characterization of the Responses of the Caspase 2, 3, 6 and 8 Genes to Immune Challenges and Extracellular ATP Stimulation in the Japanese Flounder (*Paralichthys Olivaceus*). *BMC Vet Res* (2019) 15:20. doi: 10.1186/s12917-018-1763-y
12. Li S, Chen X, Hao G, Geng X, Zhan W, Sun J. Identification and Characterization of a Novel NOD-Like Receptor Family Card Domain Containing 3 Gene in Response to Extracellular ATP Stimulation and Its Role in Regulating Lps-Induced Innate Immune Response in Japanese Flounder (*Paralichthys Olivaceus*) Head Kidney Macrophages. *Fish Shellfish Immun* (2016) 50:79–90. doi: 10.1016/j.fsi.2016.01.029
13. Xie J, Belosevic M. Characterization and Functional Assessment of the NLRC3-Like Molecule of the Goldfish (*Carassius Auratus L.*). *Dev Comp Immunol* (2018) 79:1–10. doi: 10.1016/j.dci.2017.09.021
14. Zhang X, Liu Z, Li C, Zhang Y, Wan L, Wei J, et al. Characterization of Orange-Spotted Grouper (*Epinephelus Coioides*) ASC and Caspase-1 Involved in Extracellular ATP-Mediated Immune Signaling in Fish. *Fish Shellfish Immun* (2020) 97:58–71. doi: 10.1016/j.fsi.2019.12.023
15. Li S, Peng W, Li J, Hao G, Geng X, Sun J. Characterization of Japanese Flounder (*Paralichthys Olivaceus*) Caspase1 Involved in Extracellular ATP-Mediated Immune Signaling in Fish. *Fish Shellfish Immun* (2017) 67:536–45. doi: 10.1016/j.fsi.2017.06.043
16. Li S, Zhang TT, Feng Y, Sun JS. Extracellular ATP-Mediated Purinergic Immune Signaling in Teleost Fish: A Review. *Aquaculture* (2021) 537:736511. doi: 10.1016/j.aquaculture.2021.736511
17. Maes M, Cogliati B, Yanguas SC, Willebrords J, Vinken M. Roles of Connexins and Pannexins in Digestive Homeostasis. *Cell And Mol Life Sci* (2015) 72(15):2809–21. doi: 10.1007/s00018-015-1961-8
18. Lohman AW, Isakson BE. Differentiating Connexin Hemichannels and Pannexin Channels in Cellular ATP Release. *FEBS Lett* (2014) 588(8):1379–88. doi: 10.1016/j.febslet.2014.02.004
19. Bai D, Wang AH. Extracellular Domains Play Different Roles in Gap Junction Formation and Docking Compatibility. *Biochem J* (2014) 458:1–10. doi: 10.1042/bj20131162
20. Willebrords J, Yanguas SC, Maes M, Decrock E, Wang N, Leybaert L, et al. Connexins and Their Channels in Inflammation. *Crit Rev In Biochem And Mol Biol* (2016) 51(6):413–39. doi: 10.1080/10409238.2016.1204980
21. Li S, Wang N, Zhang T, Feng Y, Wang L, Sun J. Characterization of Three Connexin32 Genes and Their Role in Inflammation-Induced ATP Release in the Japanese Flounder *Paralichthys Olivaceus*. *Fish Shellfish Immun* (2020) 106:181–9. doi: 10.1016/j.fsi.2020.07.066
22. Vinken M, Decrock E, De Vuyst E, De Bock M, Vandenbroucke RE, De Geest BG, et al. Connexin32 Hemichannels Contribute to the Apoptotic-To-Necrotic Transition During Fas-Mediated Hepatocyte Cell Death. *Cell And Mol Life Sci* (2010) 67(6):907–18. doi: 10.1007/s00018-009-0220-2

23. Kang J, Kang N, Lovatt D, Torres A, Zhao Z, Lin J, et al. Connexin 43 Hemichannels Are Permeable to ATP. *J Of Neurosci* (2008) 28(18):4702–11. doi: 10.1523/jneurosci.5048-07.2008
24. Glass AM, Snyder EG, Taffet SM. Connexins and Pannexins in the Immune System and Lymphatic Organs. *Cell And Mol Life Sci* (2015) 72(15):2899–910. doi: 10.1007/s00018-015-1966-3
25. Okamoto T, Akiyama M, Takeda M, Akita N, Yoshida K, Hayashi T, et al. Connexin 32 Protects Against Vascular Inflammation by Modulating Inflammatory Cytokine Expression by Endothelial Cells. *Exp Cell Res* (2011) 317(3):348–55. doi: 10.1016/j.yexcr.2010.10.018
26. Chekeni FB, Elliott MR, Sandilos JK, Walk SF, Kinchen JM, Lazarowski ER, et al. Pannexin 1 Channels Mediate 'Find-Me' Signal Release and Membrane Permeability During Apoptosis. *Nature* (2010) 467(7317):863–U136. doi: 10.1038/nature09413
27. Panchin Y, Kelmanson I, Matz M, Lukyanov K, Usman N, Lukyanov S. A Ubiquitous Family of Putative Gap Junction Molecules. *Curr Biol* (2000) 10 (13):R473–R4. doi: 10.1016/s0960-9822(00)00576-5
28. Silverman WR, Vaccari J, Locovei S, Qiu F, Carlsson SK, Scemes E, et al. The Pannexin 1 Channel Activates the Inflammasome in Neurons and Astrocytes. *J Of Biol Chem* (2009) 284(27):18143–51. doi: 10.1074/jbc.M109.004804
29. Woehrle T, Yip L, Elkhal A, Sumi Y, Chen Y, Yao Y, et al. Pannexin-1 Hemichannel-Mediated ATP Release Together With P2X1 and P2X4 Receptors Regulate T-Cell Activation at the Immune Synapse. *Blood* (2010) 116(18):3475–84. doi: 10.1182/blood-2010-04-277707
30. Li S, Peng W, Chen X, Geng X, Zhan W, Sun J. Expression and Role of Gap Junction Protein Connexin43 in Immune Challenge-Induced Extracellular ATP Release in Japanese Flounder *(Paralichthys Olivaceus)*. *Fish Shellfish Immun* (2016) 55:348–57. doi: 10.1016/j.fsi.2016.06.014
31. Li S, Li J, Wang N, Zhang T, Xu Y, Sun J. Expression Analysis of Pannexin 1 Channel Gene in Response to Immune Challenges and Its Role in Infection-Induced ATP Release in Tilapia (*Oreochromis Niloticus*). *Fish Shellfish Immun* (2018) 81:470–5. doi: 10.1016/j.fsi.2018.07.050
32. Cai X, Gao C, Cao M, Su B, Liu X, Wang B, et al. Genome-Wide Characterization of Gap Junction (Connexins and Pannexins) Genes in Turbot (*Scophthalmus maximus L.*): Evolution and Immune Response Following *Vibrio anguillarum* Infection. *Gene* (2022) 809:146032. doi: 10.1016/j.gene.2021.146032
33. Zhang X, Wen H, Wang H, Ren Y, Zhao J, Li Y. Rna-Seq Analysis of Salinity Stress-Responsive Transcriptome in the Liver of Spotted Sea Bass (*Lateolabrax maculatus*). *PloS One* (2017) 12(3):e0173238. doi: 10.1371/journal.pone.0173238
34. Li X, Yuan SY, Sun ZS, Lei LN, Wan S, Wang JY, et al. Gene Identification and Functional Analysis of Peptidoglycan Recognition Protein From the Spotted Sea Bass (*Lateolabrax maculatus*). *Fish Shellfish Immun* (2020) 106:1014–24. doi: 10.1016/j.fsi.2020.08.041
35. Sun Z, Qin Y, Liu D, Wang B, Jia Z, Wang J, et al. The Evolution and Functional Characterization of CXC Chemokines and Receptors in Lamprey. *Dev Comp Immunol* (2021) 116:103905. doi: 10.1016/j.dci.2020.103905
36. Yi L, Nie P, Yu HB, Xie HX. Regulation of Type Iii Secretion of Translocon and Effector Proteins by the Esab/Esal/Esam Complex in *Edwardsiella tarda*. *Infect Immun* (2017) 85(9):e00322–17. doi: 10.1128/iai.00322-17
37. Jiang XY, Gao JD, Xue YJ, Qin YT, Li X, Sun ZS, et al. Identification and Expression Analysis of IL-4/13 Receptors in Grass Carp Ctenopharyngodon Idella. *Fish Shellfish Immun* (2019) 87:254–64. doi: 10.1016/j.fsi.2019.01.009
38. Chen K, Tian J, Wang J, Jia Z, Zhang Q, Huang W, et al. Lipopolysaccharide-Induced Tnf Alpha Factor (LITAF) Promotes Inflammatory Responses and Activates Apoptosis in Zebrafish *Danio Rerio*. *Gene* (2021) 780:145487. doi: 10.1016/j.gene.2021.145487
39. Qiu F, Dahl G. A Permeant Regulating Its Permeation Pore: Inhibition of Pannexin 1 Channels by ATP. *Am J Physiol Cell Ph* (2009) 296(2):C250–C5. doi: 10.1152/ajpcell.00433.2008
40. Dahl G, Levine E, Rabadan-Diehl C, Werner R. Cell/Cell Channel Formation Involves Disulfide Exchange. *Eur J Biochem* (1991) 197(1):141–4. doi: 10.1111/j.1432-1033.1991.tb15892.x
41. Bond SR, Wang N, Leybaert L, Naus CC. Pannexin 1 Ohnologs in the Teleost Lineage. *J Of Membrane Biol* (2012) 245(8):483–93. doi: 10.1007/s00232-012-9497-4
42. Saez JC, Nairn AC, Czernik AJ, Spray DC, Hertzberg EL, Greengard P, et al. Phosphorylation of Connexin 32, a Hepatocyte Gap-Junction Protein, by Camp-Dependent Protein Kinase, Protein Kinase C and Ca2+/Calmodulin-Dependent Protein Kinase II. *Eur J Biochem* (1990) 192(2):263–73. doi: 10.1111/j.1432-1033.1990.tb19223.x
43. Iacobas DA, Iacobas S, Spray DC. Connexin43 and the Brain Transcriptome of Newborn Mice. *Genomics* (2007) 89(1):113–23. doi: 10.1016/j.ygeno.2006.09.007
44. Adamson SE, Leitinger N. The Role of Pannexin1 in the Induction and Resolution of Inflammation. *FEBS Lett* (2014) 588(8):1416–22. doi: 10.1016/j.febslet.2014.03.009
45. Ceelen L, Haesebrouck F, Vanhaecke T, Rogiers V, Vinken M. Modulation of Connexin Signaling by Bacterial Pathogens and Their Toxins. *Cell And Mol Life Sci* (2011) 68(18):3047–64. doi: 10.1007/s00018-011-0737-z
46. Svobodova I, Bhattaracharya A, Ivetic M, Bendova Z, Zemkova H. Circadian ATP Release in Organotypic Cultures of the Rat Suprachiasmatic Nucleus Is Dependent on P2x7 and P2y Receptors. *Front In Pharmacol* (2018) 9:192. doi: 10.3389/fphar.2018.00192

Conflict of Interest: The authors declare that the research was conducted in the absence of any commercial or financial relationships that could be construed as a potential conflict of interest.

Publisher's Note: All claims expressed in this article are solely those of the authors and do not necessarily represent those of their affiliated organizations, or those of the publisher, the editors and the reviewers. Any product that may be evaluated in this article, or claim that may be made by its manufacturer, is not guaranteed or endorsed by the publisher.

frontiers | Frontiers in Immunology

REVIEW
published: 26 April 2022
doi: 10.3389/fimmu.2022.856376

Microglia in the Neuroinflammatory Pathogenesis of Alzheimer's Disease and Related Therapeutic Targets

Yongle Cai[†], *Jingliu Liu*[†], *Bin Wang*, *Miao Sun*[*] *and Hao Yang*[*]

Institute for Fetology, The First Affiliated Hospital of Soochow University, Suzhou, China

Alzheimer's disease (AD) is the most prevalent neurodegenerative disease worldwide, characterized by progressive neuron degeneration or loss due to excessive accumulation of β-amyloid (Aβ) peptides, formation of neurofibrillary tangles (NFTs), and hyperphosphorylated tau. The treatment of AD has been only partially successful as the majority of the pharmacotherapies on the market may alleviate some of the symptoms. In the occurrence of AD, increasing attention has been paid to neurodegeneration, while the resident glial cells, like microglia are also observed. Microglia, a kind of crucial glial cells associated with the innate immune response, functions as double-edge sword role in CNS. They exert a beneficial or detrimental influence on the adjacent neurons through secretion of both pro-inflammatory cytokines as well as neurotrophic factors. In addition, their endocytosis of debris and toxic protein like Aβ and tau ensures homeostasis of the neuronal microenvironment. In this review, we will systematically summarize recent research regarding the roles of microglia in AD pathology and latest microglia-associated therapeutic targets mainly including pro-inflammatory genes, anti-inflammatory genes and phagocytosis at length, some of which are contradictory and controversial and warrant to further be investigated.

Keywords: alzheimer's disease, microglial cells, neuroinflammation, anti-neuroinflammation, molecular therapy

OPEN ACCESS

Edited by:
Juehua Yu,
The First Affiliated Hospital of Kunming Medical University, China

Reviewed by:
Luca Steardo,
University Magna Graecia of Catanzaro, Italy
Enquan Xu,
Duke University, United States
Xiuli Yang,
Johns Hopkins Medicine, United States

***Correspondence:**
Miao Sun
miaosunsuda@163.com
Hao Yang
yanghao.71_99@yahoo.com

[†]*These authors have contributed equally to this work*

Specialty section:
This article was submitted to Multiple Sclerosis and Neuroimmunology, a section of the journal Frontiers in Immunology

Received: *17 January 2022*
Accepted: *30 March 2022*
Published: *26 April 2022*

Citation:
Cai Y, Liu J, Wang B, Sun M and Yang H (2022) Microglia in the Neuroinflammatory Pathogenesis of Alzheimer's Disease and Related Therapeutic Targets. Front. Immunol. 13:856376. doi: 10.3389/fimmu.2022.856376

1 INTRODUCTION

Alzheimer's disease (AD) is the most common neurodegenerative disease, beginning with gradual memory and cognitive impairment, abnormal behavior, and progressive social dysfunction. Pathologically, AD is characterized by severe neuronal degeneration or loss mainly resulting from excessive production of senile plaques comprising β-amyloid (Aβ) proteins, and neurofibrillary tangles formed by hyperphosphorylated tau protein deposition. Furthermore, Lewy-related pathology and presynaptic protein α-synuclein (α-syn), which are primarily involved in dementia with Lewy bodies (DLB), Parkinson's disease (PD), and multiple system atrophy (MSA), were discovered to participate in the eliciting several parts of the pathophysiology of AD. Although compelling studies on the pathological mechanism of AD have been carried out for decades, still no effective curative treatment for AD is available. At this present, the mechanism by which drugs used in the clinical treatment of AD are mainly targeted at cholinergic neurons, eliminating or inhibiting the toxicity of Aβ or tau proteins to neurons, and reducing the oxidative stress of neurons. Unfortunately, these drugs approved by the FDA for treatment of AD are all

symptomatic treatment drugs, and are still unstable in suppression of the disease process, thus reflecting the imperious demands for effective treatments. Likewise, in molecular pathology studies, more attention has not only been paid to the neuron activities, but also the effects of microglial cells, and their abnormal changes in AD are also observed. Increasing studies have evidenced that microglial-mediated neuroinflammation also plays pivotal roles in the pathogenesis of AD. Therefore, the development of drugs that target microglia may be crucial to reverse the process of AD. This article will systematically review the latest progress of the pathogenic mechanism of AD associated with microglia cells, which is likely to discover valuable AD treatment targets so as to provide a deep insight into new therapeutic approaches for AD.

2 THE PATHOLOGICAL MECHANISM OF AD

As the leading cause of dementia in the elderly, AD is usually characterized by memory impairment, aphasia, loss of skills and personality, and behavioral changes, etc. (1, 2). The general pathology of AD is marked by hippocampal atrophy as well as the deepening and enlargement of the cerebral sulcus. The neuroinflammatory patches, basal forebrain cholinergic neuronal loss, and glial cell proliferation constitute the main histopathological features of AD. The current prevailing view is that the amyloid plaques and neurofibrillary tangles (NFTs) are the primary pathogenic mechanism contributing to the onset of AD (3). The causal relationship between neuronal apoptosis, neurite dystrophy, and AD remains to be elucidated since the progression of neurodegeneration is a chronic event and lasts a long period of time (4). With the gradual deepening of the investigation, the researchers gained a further understanding of AD. First, Amyloid precursor protein (APP) is cleaved into Aβ peptides by γ-secretase complex and its mutation is a primary cause of the accumulation of Aβ. Second, tau protein, a component of neural cytoskeleton, plays an indispensable role in the stabilization of cytoskeleton as well as neuronal transport, and it can be phosphorylated by tau kinase, particularly GSK-3β. Subsequently, the abnormally phosphorylated tau protein gathers each other into paired helical filaments (PHF) which detach from microtubules, then these dimers assemble into oligomers, and ultimately these oligomers develop into fibrils aggregating in neurons (5). Recent studies have shown that Aβ plaques can promote the propagating and seeding of tau in a mouse model and tau antibodies help block tau propagation within AD pathology (6, 7). Strikingly, amyloid plaques were not found in the brain tissue with the Arctic or Osaka familial mutation in *APP* by positron emission tomography (PET) amyloid ligand brain scans (8). Meanwhile, NFTs were found to be irrelevant to the memory loss and neurodegeneration (9). Accordingly, neither the amyloid plaques nor NFTs alone can completely elucidate the pathogenesis of AD. In the most neurodegenerative diseases, microglia and astrocyte are high proliferative with aberrant morphology. It has been proved that microglia, working as both phagocytic cells and innate immunocyte, play a central role in pathogenic and inflammatory responses in AD, and they are thought to function in the neuroprotection of damaged neurons and maintain homeostasis. Neuronal damage was also found to be negatively correlated with microgliosis rather than increasing amyloid load (10). Intriguingly, activated microglia has been found to induce a subtype of reactive astrocytes, namely, A1 subtype which is responsible for the damage of neurons and oligodendrocytes by the secretion of pro-inflammatory cytokines including TNF, C1q and IL-1 *via* nuclear factor κB(NF-κB)-dependent mechanisms, whereas reactive astrocytes induced by M2 microglia results in the elevated secretion of anti-inflammatory factors *via* STAT6 pathway conversely (11, 12). Currently, a growing number of drugs including cholinergic drugs, anti-Aβ/tau drugs and even mitochondrial-targeted drugs, have been applied for the treatment of AD and obviously ameliorated clinical symptoms. Among them, some drugs truly exert an anti-inflammatory effect as well (13). For instance, galantamine, as a common clinical cholinergic agent for improving cognitive function in elderly Alzheimer's patients, is found to effectively suppress the secretion of pro-inflammatory cytokines like TNF-α and IL-1β, indicating the indispensable role of anti-neuroinflammatory therapy in AD (14). Thus, we summarize microglia is central in the inflammatory pathogenesis of neurodegenerative diseases, especially AD (**Figure 1**). In this review, we outline the relationship between microglia and neuroinflammatory response in AD, as well as the definite or potential therapeutical strategies targeting microglia of AD.

3 THE ROLE OF MICROGLIA IN AD

3.1 Physiological and Pathological Functions of Microglia

Microglial cells, a kind of innate immune cells accounting for approximately 5-20% of the glial cells in the CNS, are presumed to derive from marrow myeloid progenitors produced by yolk sac in embryonic period (15, 16). They widely distribute throughout the CNS with morphological variability. Compelling studies have shown that microglial repopulation depends upon its self-renewal ability through multiple molecules, such as interleukin-1 (IL-1) and NF-κB, rather than the peripheral macrophages from bone marrow (17). Microglial cells not only play a crucial role in both innate and adaptive immune responses against pathogens, but also maintain the homeostasis of the CNS by constant surveillance of extracellular microenvironment to rapidly clear apoptotic cell remnants and other exogenous harmful objects, which facilitate neurons survival, and the proliferation and maturation of neuronal progenitor cells (NPCs) (18, 19). Nevertheless, some scholars also argued that macrophages should invade the brain tissue and differentiate into microglia ultimately through a multi-step process when a significant number of naturally dying neurons and axons are surveilled. Although microglial cells have been defined as a type of neuroglia of mesodermal origin, so far, the origin of microglial

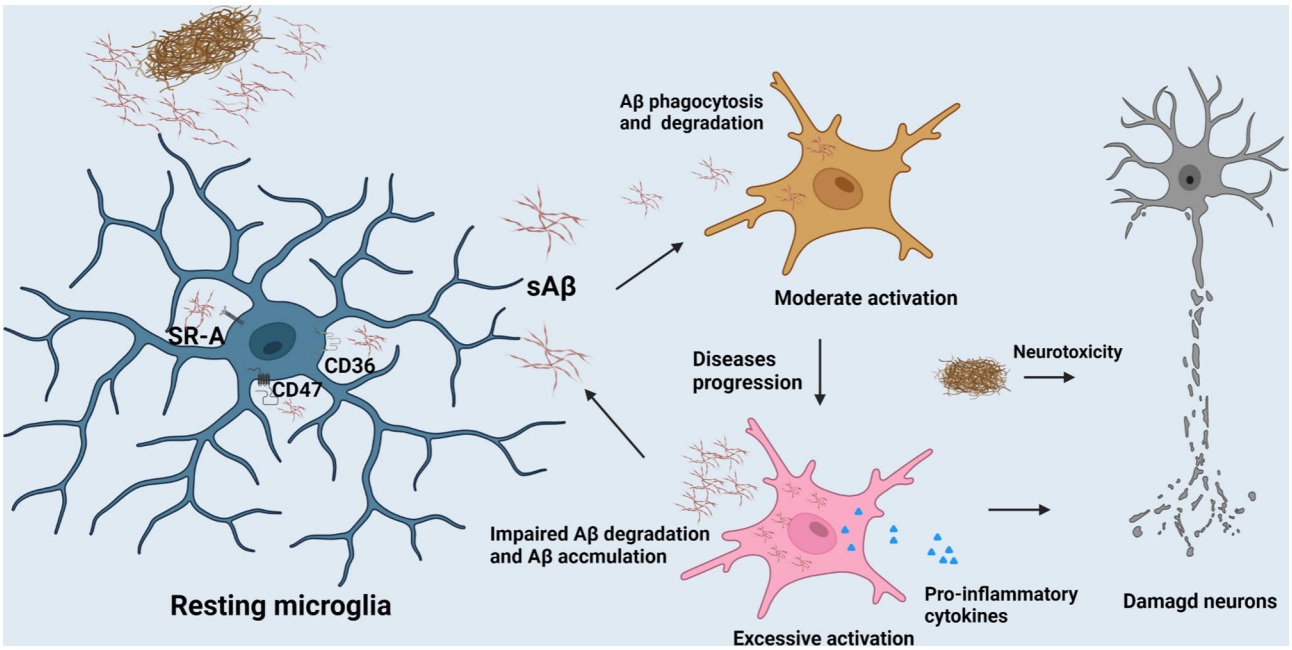

FIGURE 1 | The role of microglia in AD progression. The clearance of Aβ mediated by microglia contributes to the homeostasis maintenance of CNS. But, with the AD progression, excessive activation of microglia would release excessive pro-inflammatory factors to compromise neurons and their synapses.

cells in the CNS is still a matter of debate. In the healthy brain, the residing microglial cells usually are in the quiescent state and are easily activated with the transformation of morphology and function following by blood-brain barrier disruption, tumor, lesions, and neurodegenerative diseases. The severity of injury determines the number of reactive microglial cells (20). Synapses play a pivotal role in neuronal circuits closely associated with neuronal communication, eliciting an appropriate reaction regarding physical activities. There is evidence that microglial cells are involved in the synaptic pruning for postnatal neural circuits by complement receptor 3 (CR3), a microglia-specific phagocytic signaling pathway, and complement cascade components including C1q and C3 (18, 21). Not only that, microglia exclusively express the receptor of CX3CL1 (the chemokine fractalkine) which was positive correlation with neuronal synaptic development and plasticity by synaptic pruning like engulfment of postsynaptic and presynaptic proteins (21, 22).

3.2 Microglia and Neuroinflammation

Neuroinflammation means an inflammatory reaction in the CNS including immune cells infiltration, microglial activation and pro-inflammatory cytokine release (23). An increasing number of genes involved in neuroinflammation are up-regulated in ageing brain along with cognitive decline by genome-wide gene expression studies (24). Similarly, compelling evidence suggests that neuroinflammation plays a fundamental role in the pathogenesis of AD as well, and some inflammatory mediators have been up-regulated even a longer time prior to the onset of clinical symptoms in AD. The accumulation of activated microglia around damaged areas is one of hallmarks of the neuroinflammation in AD. The prevalent view is that microglia have various states in the CNS parenchyma such as the resting (or surveying) microglia, activated microglia and phagocytic microglia (19, 25). The resting microglia typically has oval cell bodies, as well as long and numerous ramified processes (26). The microglia could be activated by pathogens and abnormally deposited proteins such as Aβ in AD. Once activated, the microglia will adopt small round soma morphology with shorter and blunter processes than their resting state, and is accompanied by the up-regulation of specific antigens. Hereafter, guided by danger-associated molecular patterns (DAMPs) or pathogen-associated molecular patterns (PAMPs), the microglia migrate to lesion regions and exhibit amoeboid morphology (27, 28). In AD, activation of microglia is triggered after binding to soluble Aβ, which is mediated by cell surface receptors such as CD36, CD47 and α-6/β-1 integrin etc. This process is followed by the stimulation of intracellular Tyr kinase-based signaling cascades which are responsible for the secretion of inflammatory molecules and accumulation of intracellular Aβ (29). Impairment of Aβ phagocytosis of microglia has been explicated by the downregulation of Aβ scavenger receptors A (SR-A), CD36 and receptor for advanced-glycosylation endproducts (RAGE) etc. The clearance of Aβ mediated by microglia contributes to the homeostasis maintenance of CNS (As shown in **Figure 1**). However, overexpression of pro-inflammatory cytokines such as IL-1β and tumor necrosis factorα (TNF-α) released from microglia in AD progression period engender the detriment of neurons (30). It is widely acknowledged that microglia are classified into various

polarization states based on their immunophenotypic profiles: the M1 (pro-inflammatory or classically activated) and M2 (anti-inflammatory or alternatively activated phenotype) (31). However, there is mounting evidence that microglia are far more diverse than these two categories. Apart from the above, functions, morphology, ultrastructure, and gene and protein expression features, might be used to identify microglial subtypes. Another option is serendipitous identification, albeit non-systematic and erratic. Satellite microglia, which are identified by IBA1, CD11b, and CX3CR, are found on the axonal side of neurons in the cerebral cortex of non-human primates, and half of them extend a single process to interact with the axon initial segment. The subtypes of microglia are less ramified and have a lower level of monitoring (32). *KSPG*-microglia, a subset of ramified microglia defined by the expression of keratan sulfate proteoglycan (KSPG), are broadly distributed throughout the hippocampus, brainstem, and olfactory bulb (OB) and also express IBA1, CR3, and CD11b. The microglia mainly contribute to axonal development and cellular adhesion, and emerge in response to various stressors (33). *Hox8b*-microglia, which are mostly resident in the cerebral cortex and the OB, express the microglia markers IBA1 and Cd11b. Once *Hoxb8* is lost in the hematopoietic system, the neural circuits will be destroyed, leading to anxiety-like and abnormal grooming behavior (34). *CD11c*-microglia were uncovered predominantly in the cerebellar white matter and corpus callosum of neonatal mouse brains, and their number decreases with age. The type of microglia plays a pivotal role in myelination and neurogenesis. This is mainly due to an important source of insulin-like growth factor-1 which facilitates neural regeneration (35). Besides, there exists a new microglial phenotype called "dark microglia". Ultrastructural analyses revealed that that the kind of microglia appear gloomy mainly due to oxidative stress profiles including an electron-dense cytoplasm and nucleoplasm. The dark microglia mainly reside in mouse hippocampus, cerebral cortex, amygdala, and hypothalamus, and participate in maintenance of the blood–brain barrier and remodeling of neuronal circuits through extensively encircling axon terminals and dendritic spines with their highly ramified and thin processes. In general, the microglial markers IBA1, CX3CR, and P2RY12 are all downregulated in dark microglia, whilst CD11b is highly expressed (18, 36). Nevertheless, M1 and M2 microglial phenotypes are still widely applied to convey its beneficial or detrimental effects under diverse states. M1 phenotype releases pro-inflammatory cytokines including IL-1β, TNF-α, IL-6 and nitrogen oxide (NOx) etc., and neurotoxic substances, which is responsible for blocking neuronal differentiation, attenuating microglial phagocytosis, as well as extracellular matrix damage through the activation of nuclear factor κB and accumulation of Aβ (37, 38). Conversely, M2 phenotype is envisioned as a type of anti-inflammatory microglia. In M2 state, the anti-inflammatory cytokines (IL-4, IL-10, etc.) and neurotrophic factors (eg., nerve growth factor (NGF)) might be released to suppress glial accumulation, protect neuronal functions and enhance NSC differentiation (31). Along with this, the anti-inflammatory or pro-inflammatory cytokines released by other cells can also elicit microglial polarization. For instance, IL-17, a cytokine mainly produced by T cells and NK cells, can trigger microglia to produce inflammatory cytokines, whereas IL-4, an anti-inflammatory cytokine, primarily produced by mature lymphoid cells and mast cells, can polarize microglia to an anti-inflammatory phenotype (39). Baik et al. found exposure to Aβ can trigger acute microglial inflammation and display a breakdown in energy metabolisms dependent on mTOR-HIF-1α pathway. Intriguingly, the inflammation caused by defective glycolytic metabolism can be reversed by IFN-γ treatment (40). Disease-associated microglia (DAM), a new type of microglia uncovered by Amit et al. provide a new pathway for the study of the pathological mechanism of AD (41). Similarly, Rangaraju et al. have revealed that DAM can also be divided into three subgroups, namely, homeostatic, pro-inflammatory and anti-inflammatory phenotypes by flow cytometry in mouse models. Pro-inflammatory DAM express IL-1β, IL-12β and surface marker CD44 etc., while anti-inflammatory DAM is characterized by phagocytic genes such as IGF-1 and surface marker CXCR4. Although the signature of DAM in 5xFAD model is not really same as that of human microglia in AD, 67 hub genes in human brain proteome were found to predominantly be mapped to the pro-inflammatory and anti-inflammatory DAM modules in their study. The top 3 pro-inflammatory DAM genes *CD44, Cst2 and Nampt* were identified in human brain proteome which are conducive to the clinical diagnosis of AD (42). Their activation can be initiated in a Trem2-independent manner that includes downregulation of microglia checkpoints (41). While, the counterpart of DAM in humans called human AD microglia (HAM) exhibits a little resemblance with DAM profile defined in AD mice in recent research. Mancuso et al. validated the differences between the responses of human and mouse microglia to oligomeric Aβ (43). Human microglia seem to display IRF8-driven gene signature once stimulated by Aβ, which is a characteristic feature in the pathology of peripheral nerve injury rather than AD in mouse models. Surprisingly, despite species differences, TREM2 is necessary in both human and mouse AD (44). Srinivasan et al. have revealed that *APOE, ABCA7, GPR141, PTK2B, SPI1* and *ZYX* etc. seemed to be upregulated, while *MEF2C* etc. remained downregulated in HAM from AD patients when compared with the control, in which, only *APOE* upregulation and *SERPINF1* reduction achieved nominal genome-wide significance after correction for multiple testing (45). These could be explained by the differences between human and mouse innate immune responses. Another explanation is that, the activation of healthy microglia is likely more beneficial in the early stage of AD models, whereas microglial activation in human AD involves impairments (15, 41). This may be justified by the fact that human AD microglia only mirror mouse microglia responses at the very early stages of the AD (46). But the most acute controversy is that human microglia live a long time, deposition of Aβ occurs over decades, and cellular functions decrease during long-term exposure to pathogens and insults in human life span. Therefore, aging, as the largest single risk factor,

could not be simulated in any AD mouse models (47). This is consistent with the notion that accelerated aging response and disease specific response such as *APOE* overexpression, constitute microglial response in human AD. Intriguingly, the expression of resting microglia module defined from DAM increased in microglia from AD patients' tissues, and HAM from high AD pathology tissues showed an increase expression in the Aging-Up gene sets. Still, human microglia do not lose the response of DAM-like manner, and this manner such as *GPNMB* upregulation is restricted in AD human brain for certain reasons (45). Olah et al. revealed the presence of nine distinct subpopulations of microglial cells purified from human cerebral cortex samples. The microglial subsets involved in homeostasis, proliferation, interferon response, and antigen presentation are obvious examples of microglial distinct subpopulations. Among a slew of genes expressed in AD genes-enriched microglial cluster 7, antigen presentation gene *CD74* were depleted in the cortex of AD patients, and only cluster 7 gene expression is altered in pathologic and dementia diagnosed human AD cortex (48). Nevertheless, some scholars believe that pro-inflammatory cytokines like IL-1β, IL-6 and TNF-α help ameliorate Aβ burden, implying that the innate immune response in AD is extremely complex and this problem still needs to be further addressed (49). In general, we hold the view that the moderate activation of microglia binding Aβ peptide can trigger neuroinflammatory reaction in the early stage of AD, which halts the progression of AD through reducing the accumulation of Aβ, and thus this activation acts as a potential neuroprotective agent. Once the sustained and immoderate production of Aβ occurred, it will result in the excessive activation of microglia, and this can exacerbate the progress of AD instead in the process of AD.

4 MICROGLIAL CELLS-RELATED THERAPEUTIC TARGETS IN AD

4.1 AD-Associated Inflammatory Factors in Microglia

4.1.1 NOD-Like Receptor Pyrin Domain Containing 3 Inflammation

Inflammasome, a critical component of the innate immune system, is a kind of protein complexes containing three main components, the sensor/receptor proteins, the junction protein, namely, apoptosis-associated speck-like protein (ASC), and the downstream caspase family (50). Its most well-known function is capable of mediating pyroptosis, and processing pro-IL-1β and pro-IL-18 in response to microbial infection and cellular damage through caspase-1 (51, 52). In various inflammasomes, NLRP3 inflammasome seemed more closely associated with the pathogenesis of AD such as recognizing Aβ and mediating the microglial recruitment to exogenous Aβ plaques (53, 54). Notably, *Nlrp3*$^{-/-}$ or *Casp*$^{-/-}$ mice carrying mutations associated with familial AD exhibit less complications such as the loss of spatial memory and reduce the deposition of Aβ, which demonstrate the critical pathogenesis of NLRP3/caspase-1 axis in AD (54). IL-18 facilitates the deposition of Aβ through increasing APP and altering the process of APP which were initiated by β-site APP cleaving enzyme-1 (BACE-1) and N-terminal fragment (NTF) of presenilllin-1 (PS-1). Reversely, the process of APP can be inhibited by IL-18 binding protein. Likewise, IL-1β has similar but less impact on APP compared with IL-18 (55). Intriguingly, soluble Aβ and aggregated tau activate ASC speck and NLRP3 inflammasome, leading to IL-1β secretion (56, 57). In turn, IL-1β can further upregulate ROS through transient receptor potential melastatin2 (TRPM2) pathway, indicating a vicious circle in the neuron damage of AD. Notably, MCC950, a potent and selective inhibitor of the NLRP3 inflammasome, is able to block NLRP3 inflammasome activation and reverses tau pathology when delivered exogenously (58). Currently, a number of bioactive compounds have been found to suppress the expression of NLRP3 inflammasome through multiple signaling pathways. Dapansutrile (OLT1177), an orally available small molecule inhibitor for NLRP3 inflammasome which can silence caspase-1 and IL-1β and has well tolerated and free side effects in humans, could rescue synaptic plasticity, suppress inimical microglia, and reduce the number of plaques in APP/PS1 mouse model for AD (59). Besides, there are also certain drugs in clinical use, for example, Stavudine. The drug is of great benefit to patients with AD by decreasing the expression of NLRP3 inflammasome genes to hamper the assembly of NLRP3 inflammasome, and down-regulating ERK1/2 and AKT phosphorylation to enhance Aβ autophagy (60). Another NLRP3 inflammasome inhibitor, JC-124 can selectively block the NLRP3 signaling pathway in TgCRND8 mice, subsequently resulting in reduced microgliosis, Aβ deposition, β-C-terminal fragment of APP (β-CTF), oxidative stress, and increased synaptic markers (61). Furthermore, impaired autophagy may be another pathway for NLRP3 inflammasome activation. Also, the deficiency of autophagy-related 16-like 1 (ATG16L1, an autophagy protein) and BECN1/BECLIN (an indispensable part of autophagic vesicle) actively triggers inflammasome activation, resulting in the secretion of IL-1β and IL-18 in microglia (**Figure 2**) (62, 63). In addition, the overexpression of transcription factor EB (TFEB) protein to increase LAMP1 in lysosome could effectively ameliorate autophagic activity by the downregulation of caspase-1, NLRP3, and IL-1β in BV2 microglial cells (**Figure 4**) (64).

4.1.2 Apolipoprotein E

APOE, especially the *APOE 4* allele gene, was deemed as the critical genetic risk factor for late-onset AD, and accelerated the intraneuronal accumulation of Aβ in the brain. Compelling evidence reveals that APOE immunoreactivity widely overlaps with senile plaques (SPs) and neurofibrillary tangles, and more SPs were found in patients with *APOE 4* than *APOE 3* (65, 66). Conversely, APOE 2 acts as a protective factor against the development of AD by decreasing the sedimentation of Aβ, regulating the metabolism of lipid and maintenance of the plasticity of synapses (67, 68). In 2107, APOE was found to be abundantly expressed in microglia by Gosselin et al. (69). Next year, it was furthered revealed that the ability of microglia

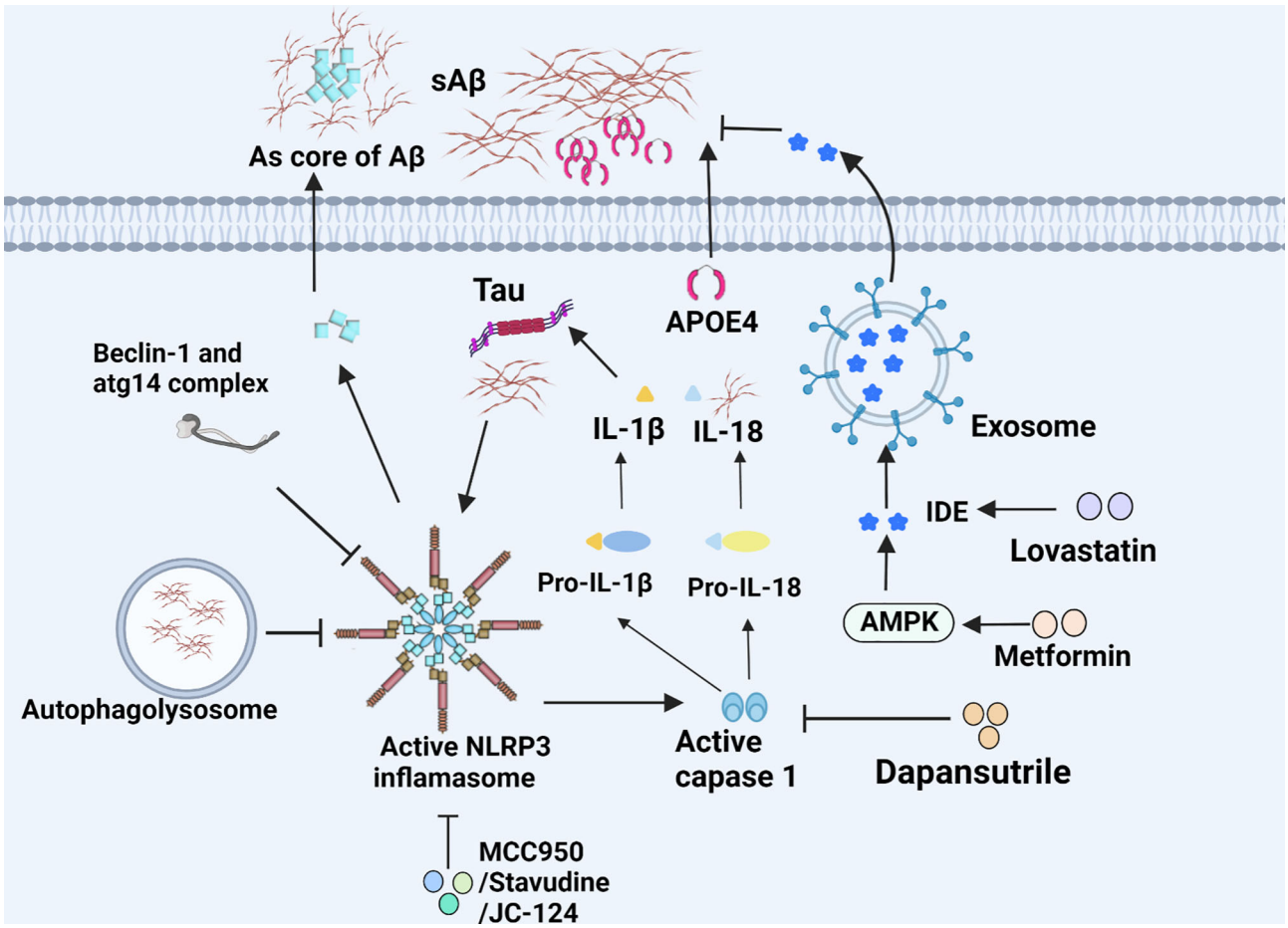

FIGURE 2 | NLRP3 inflammasome and IDE in microglia of AD. The NLRP3 inflammasome accelerates microglial inflammation and can be inhibited by various substances. The secretion of IDE helps degrade Aβ and is regulated by diverse drugs.

carrying *APOE 4* to intake Aβ was reduced, which was accompanied by the lengthening of primary processes in 3D-culture systems, implying negative correlation with its ability to phagocytose (70). In addition, APOE 4 is proved to hamper autophagy-triggered tau clearance as well. The tau-mediated neuroinflammation exacerbated by APOE 4 is identified to result in neurodegeneration independently of Aβ (71). Strikingly, Krasemann et al. also revealed that APOE signaling (not refer to APOE 4 specifically) not only suppressed the microglial homeostatic transcriptional factors, but also induced expression of inflammatory transcriptional factors such as BHLHE40, TFEC, and ATF3 etc. (4). Based on a recent study, high levels of soluble TREM2 (sTREM2) helped to ameliorate the effects of *APOE 4*-carriage on the hippocampus atrophy and cognitive decline independent of AD pathology markers in cerebrospinal fluid (72). Increasingly, JHU-083, a glutamine antagonist was found to alleviate AD pathogenesis and cognitive disorder induced by excess microglial LPS-induced glutaminase (GLS) in *APOE 4* knock-in mice (73). More interestingly, knocking down *ApoE 4* in astrocytes can rescue tau pathology and engulfment of synaptic material by microglia as well (74).

4.1.3 Prostaglandin E2

PGE2 is the most abundant eicosanoid and acts as a kind of lipid messenger and pro-inflammatory cytokine. Its activation is associated with suppression of Aβ-stimulated microglial phagocytic activity by preventing cytoskeletal reorganization. In ageing microglia, PGE2 and its receptor EP2 can mediate the transformation of glucose into glycogen, resulting in cell energy-deficient state and pro-inflammatory responses. EP2 is emerging as a novel target for development of anti-inflammatory drugs for the treatment of chronic neurodegenerative and peripheral diseases. PF-04418948, an EP2 antagonist not only can drastically reduce pro-inflammatory cytokine in hippocampus, but also ameliorate long-term memory function *via* downstream AKT signaling pathway (**Figure 3**) (75). In addition, the deficits of novel object recognition (NOR) and spatial memory are effectively ameliorated, and the level of insulin-like growth factor 1 (IGF1) is elevated in EP2 knockout

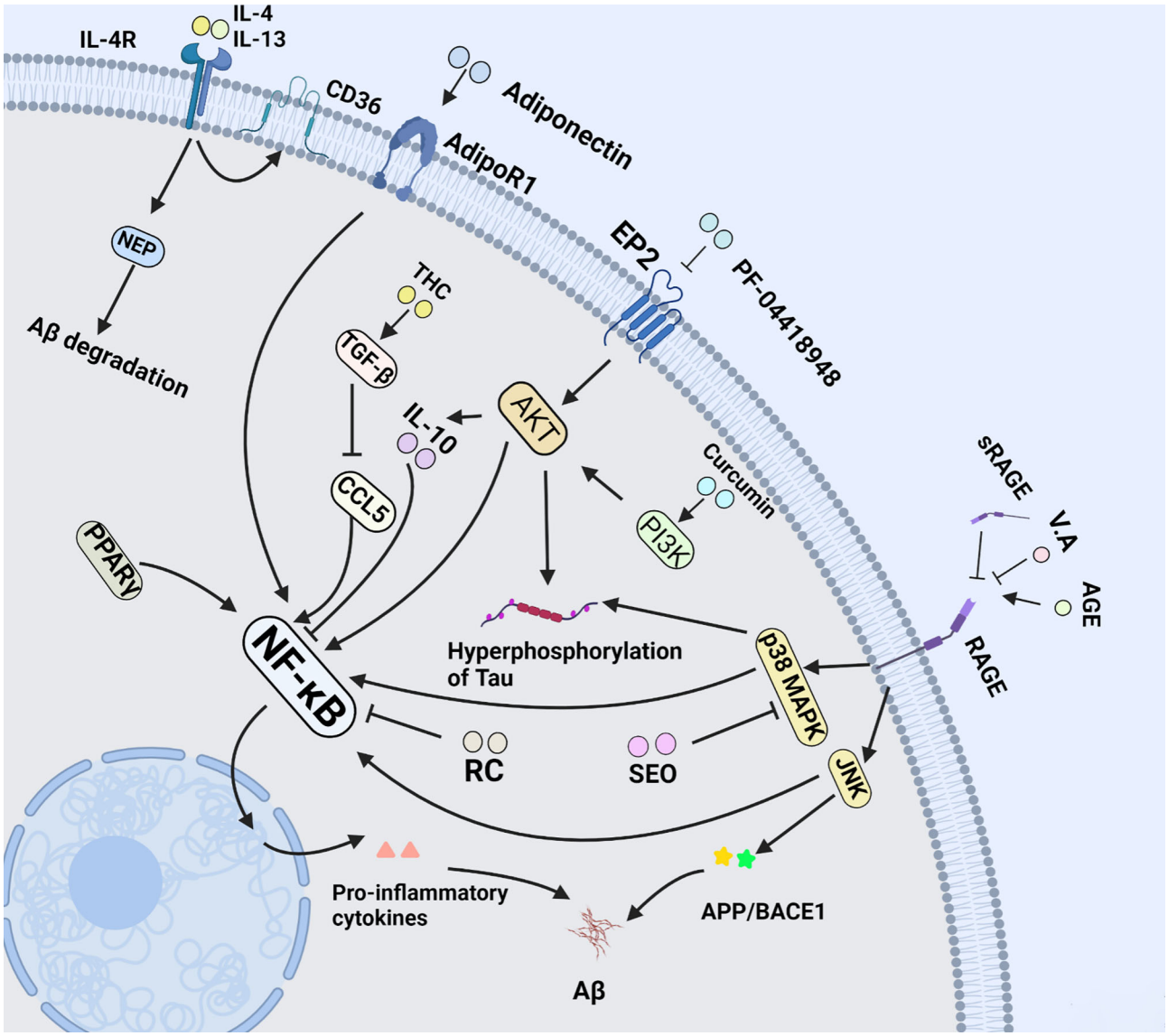

FIGURE 3 | NF-κB pathway in microglia of AD. NF-κB signal pathway plays a central role in microglia-mediated neuroinflammation. This figure introduces multiple drugs mentioned in this review above, and their effects on microglia at length *via* NF-κB signal pathway.

mouse model in parallel with down-regulation of pro-inflammatory factors (76). Likewise, Cyclooxygenase 2 (COX2) is a key enzyme in the synthesis process of prostaglandin E2. S-ibuprofen, a type of selective COX2 inhibitor, can rescue the phagocytic response triggered by Aβ in microglia after incubating with IL-1β overnight. Nevertheless, some specific nonsteroidal anti-inflammatory drugs (NSAIDs) like ibuprofen and indomethacin were identified to directly affect Aβ deposition by altering γ-secretase activity rather than COX activity (77).

4.1.4 IL-1β and IL-6

IL-1 family proteins are mainly involved in innate immunity with a broad spectrum of diseases, and normally mediate the host response to infections, injury, and immunologic challenges. Once triggered uncontrolledly, they are more likely to produce detrimental side effects. Currently, the IL-1 family is comprised of 11 members and some of which play a dual role in inflammatory response. Among them, IL-1α is constitutively present inside normal epithelial, mesenchymal and stromal cells besides microglia, whereas IL-1β, a potent pro-inflammatory cytokine, is predominantly produced under disease conditions by macrophages/microglia, monocytes and dendritic cells (78). Biologically, IL-1 (not merely IL-1β) is selectively expressed by activated, plaque-associated microglia of brain tissue in the patients with AD (79). The pathology is initiated and driven, in part, by early and sustained overexpression of IL-1 and consequent overexpression of products of IL-1-driven cascades. The secretion of mature IL-1β needs the activation of NF-κB

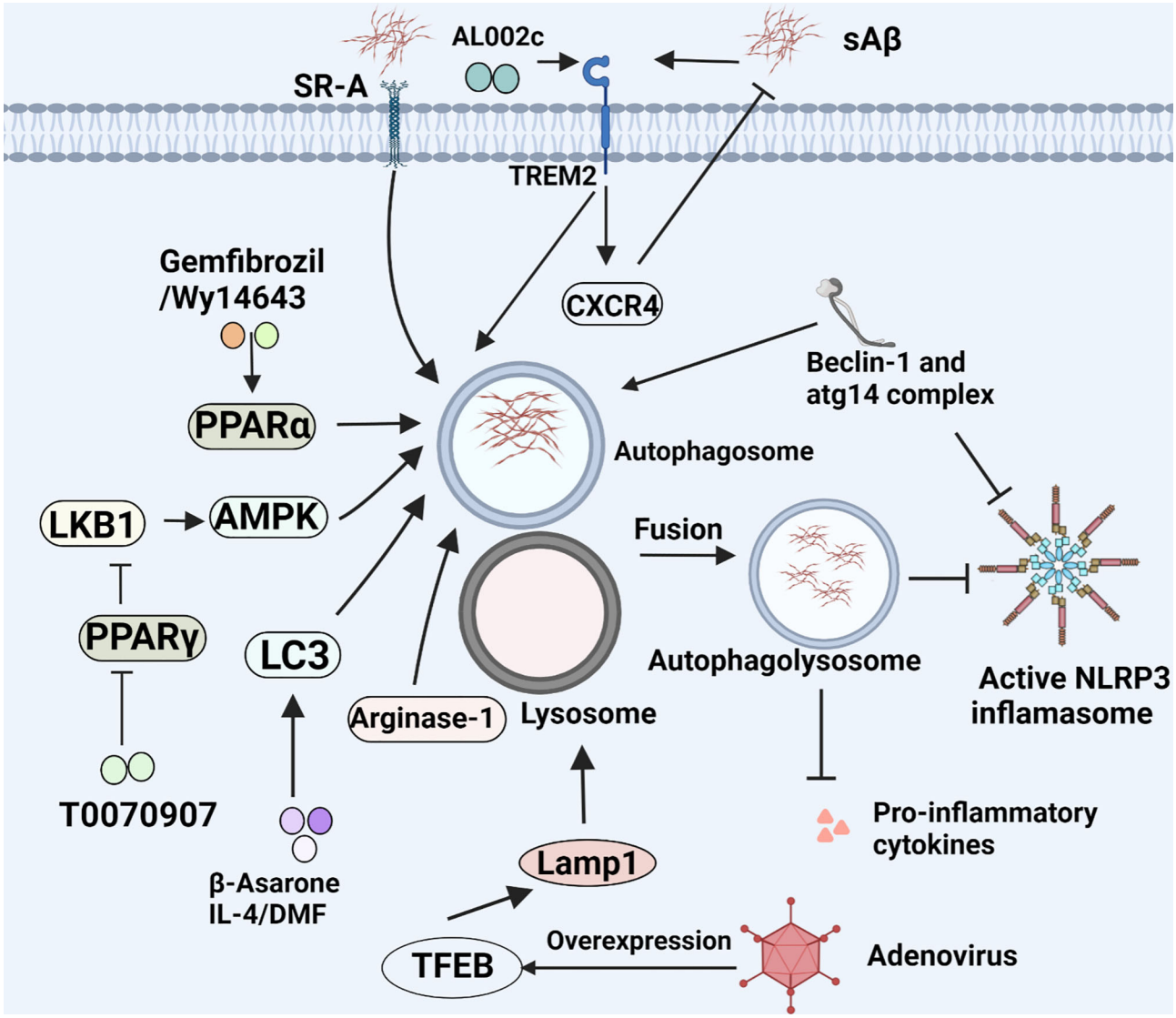

FIGURE 4 | Microglial phagocytosis and autophagy in AD. Microglia eliminate Aβ load through phagocytosis and autophagy. This figure displays the regulatory mechanism of this process.

signaling cascades, ultimately causing the upregulation of the transcription and inflammasome to process pro-IL-1β protein (80). Apart with the above-mentioned, IL-1 is also responsible for the reactive gliosis for its stimulating other pro-inflammatory cytokines, for example, TNF-α and IL-6. Similarly, Essential oil (SEO), a drug for microbial infections and inflammation could inhibit p38 activation which results in anti-AD effects by modulating neuroinflammation through the NF-κB/MAPK signaling pathway, and ultimately improve animal cognitive capacity and histopathological changes in AD model. In addition, the anti-inflammatory effects of SEO were replicated in BV-2 microglial cells (81). Of note, Aβ in serum also triggers ATP-mediated IL-1β release from microglia (82). In contrast, several studies have revealed that the successive expression of IL-1β in the hippocampus of APP/PS1 mice decreases Aβ plaque load and enhances Aβ clearance, which mainly attributes to an increase in the ability of microglia to proliferate and the up-regulation of phagocytosis-related genes caused by IL-1β (83). To date, however the mechanisms of IL-1β-induced plaque clearance remain poorly understood.

IL-6, a prototypic cytokine is not only associated with inflammation and infection responses, but also involved in the regulation of metabolic, regenerative, and neural processes. In pro-inflammation response, IL-6 can increase the amount of hyperphosphorylated tau protein, which results in the pathogenesis of all inflammatory diseases (84). Notably, due to lack of IL-6R in microglia, the involvement of both signaling modes (trans-signaling and classical) in the biology of IL-6 is responsible for pro-inflammatory or anti- inflammatory responses. Namely, IL-6 first binds to soluble IL-6R (sIL-6R)

with low affinity to form an IL-6/sIL-6R complex, and subsequently combines with gp130 on the surface of cells, which leads to a pro-inflammatory response, while IL-6 classic signaling is required for anti-inflammatory activities *via* the activation of STAT3-mediated signaling pathways (85). Regarding the IL-6-mediated activities, there is always a considerable controversy. That is to say, IL-6 has been widely regarded as a pro-inflammatory cytokine, and also has many regenerative or anti-inflammatory activities. Interestingly, a recent study showed that the repopulating microglia can stimulate the generation of neurons, modulate local microenvironment and mitigate spatial learning deficits through IL-6 trans-signaling pathway (86). Similarly, there are also some evidences that IL-6 can induce massive gliosis to suppress Aβ deposition. Although, the mechanisms underlying involvement of IL-6 are too complex and have yet to be studied, this does not abate the fact that IL-6 is still a potential target for AD.

4.1.5 Interferon-γ

IFN-γ, an inflammatory cytokine mainly released by activated natural killer (NK) cells and T helper type 1 (Th1) lymphocytes, was originally assayed as an antiviral chemokine. Its activities depend largely on the constitutive expression of membrane IL-1α (78). In general, neuroinflammation driven by IFN-γ and microglial activation has been associated with neurological disease. It was reported that IFN-γ causes reduced adult hippocampal neurogenesis, behavior despair, anhedonia, and cognitive impairment by microglial priming and polarization to M1 phenotype which leads to the release of pro-inflammatory cytokines (87). There is also evidence that IFN-γ paired with ligands of Toll-like receptors (TLRs) in microglia causes neuronal network dysfunction with NO release (88). Some drugs like glycine can reverse the pro-inflammatory markers in BV-2 microglial cells treated with IFN-γ dose-dependently (89). Of importance, another study demonstrated that rhinacanthin C (RC) could inhibit IFN-γ-mediated IL-6 and TNF-α secretion, and abrogate the activation of NF-κB and ERK signaling pathway in BV-2 microglia, which is relevant to the protection of neurons and stimulation of neurite outgrowth against Aβ toxicity (23). More interestingly, a recent study demonstrated that intraperitoneal injection of IFN-γ alleviated Aβ load both in hippocampus and cortex by initiating microglial autophagy in APP/PS1 mice, which were accompanied by the rescue of cognitive deficiency and synaptic impairments (90). Therefore, targeting microglia by modulating levels of IFN-γ in the brain may be a therapeutic strategy for neurodegenerative diseases and psychiatric disorders.

4.1.6 Tumor Necrosis Factor-α

TNF-α plays pleiotropic roles in CNS including tumor killer, cell proliferation and inflammatory response. Physiologically, TNF-α is mainly expressed in microglia. Once microglia are activated by Aβ, its expression will be increased. Of note, TNF-α has an intimate relationship with other cytokines since it can result in the up-regulation of pro-inflammatory cytokines IL-1 and IFNs. Strikingly, the up-regulation of TNF-α is reported to suppress long-term-potentiation (LTP) at hippocampal glutamatergic synapses associated with learning and memory. Intriguingly, this effect is effectively reversed by anti-TNF-α antibody in young *Trem2*$^{R47H/R47H}$ rats (91). In addition, TNF-α can directly stimulate Aβ deposition by the elevation of β-Site APP cleaving enzyme 1 (BACE1) expression (92). Adiponectin (APN), an anti-inflammatory and vasculoprotective adipokine, can halt or reverse the inflammatory morphological changes in microglia through inhibiting the secretion of TNF-α when co-cultured with Aβ (**Figure 3**). As a result, when cultured with APN, the viability of HT-22 neuronal cells is protected against the microglial cytotoxicity induced by Aβ (93). Besides, TNF-α can be suppressed by IL-10 *via* down-regulating the expression of nitric oxide synthetase (iNOS) and cyclooxygenase 2 (COX-2) (94). Apart from the aforementioned, flavonoids like Luteolin and Isoflavone also exert the neuroprotection in reducing TNF-α secretion from microglia, attenuating neuronal cell death (95). The evidence above shows that blocking TNF-α is more conductive to anti-neuroinflammation therapeutic strategy in AD.

4.2 AD-Associated Anti-Inflammatory Factors in Microglia

4.2.1 Triggering Receptor Expressed on Myeloid Cells 2

TREM2, a single pass transmembrane receptor, is specially expressed on monocyte-derived dendritic cells, osteoclasts and microglia. *In vivo*, microglia that express TREM2 can increase the phagocytosis of debris from apoptotic or damaged neurons, which influences immune functions involved in inflammation, microglial proliferation, survival and cytoskeleton remodeling in the CNS (96). When TREM2 signal is activated by its adapt protein, namely, DNAX-binding protein of 12 kDa (DAP12) through immunoreceptor tyrosine-based activation motif (ITAM) signaling pathway, it will lead to greater clearance of cell debris (97, 98). It has been proved that TREM2 mediates Aβ degradation by proteasome degradation pathways and the proteasome is interconnected with lysosome through autophagosomes (99). More notably, the TREM2-haplodeficiency microglia markedly fail to cluster and insulate around Aβ fibrils and plaques, downregulate the SDF-1α/CXCR4-mediated chemotaxis, and lose the ability of nourishing axons, thus resulting in enhanced Aβ accumulation and axonal dystrophy (100). CXCR4, a chemoattractant receptor, is vital for microglial migrating towards Aβ. Activated CXCR4 helps to rescue the ability of microglial migration. As a result, it is likely to be a potential target for AD treatment as well (100). Besides, AL002c, an anti-hTREM2 agonistic mAb, provokes TREM2-mediated beneficial roles of microglia in the mice carried with the arginine-47-histidine (R47H) mutation of *Trem2* which is associated with a substantial increase of AD risk. As a result, the systemic administration of AL002c could alleviate the load of Aβ and neurite dystrophy, impact behavior of 5xFAD mice, and temper microglial inflammatory response. Although a first-in-human phase I clinical trial of AL002 demonstrated that AL002 was generally safe and well tolerated with no serious adverse effects, and can be traced by sTREM2 and sCSF-1R. There is also evidence contrary to the view that the

master regulators SPI1, SMAD3 and SALL1 of the homeostatic microglia can be restored through deleting *TREM2*, leading to repression of TREM2-apolipoprotein E (APOE) signaling pathways (4, 97). Similar to the report, There is another evidence that TREM2 has multiple roles at diverse stages of AD. Wang et al. revealed *Trem2*$^{-/-}$ 5XFAD mice had higher Aβ burden than wild type (WT) in 8.5 month-old, but Jay et al. demonstrated that TREM2-deficient mice exhibited reduced Iba1^{+} cells, neuroinflammation and Aβ deposition at 4 months of age, indicating that TREM2 plays detrimental role at the early stages of AD and beneficial role at late stages (96, 101). Besides, Aβ is able to potentiate the interaction between TREM2 and DAP12 and bind TREM2 directly to increase the expression of pro-inflammatory cytokines including IL-6 and MIP-1α in WT microglia, while *TREM2* KO microglia show no change in response to Aβ stimulation (102). Therefore, genetic therapy targeting *TREM2* could be a potential avenue for AD therapy.

4.2.2 IL-2 and IL-4 Etc

IL-2 is a 15.5 kDa cytokine that is expressed by cells, B cells, dendritic cells, eosinophils, and macrophages/microglia. It is reported that IL-2 can nourish neurons and glia in the CNS, and further promote neurite branching such as dendrite arbors and dendritic spines (103). Unfortunately, the level of IL-2 in hippocampal of the patients with AD is remarkably reduced (104). Strikingly, the administration of IL-2 *via* an adeno-associated virus (AAV)-IL-2 vector improves memory retention, synaptic plasticity, and spine density in APP/PS1E9 mice, implying IL-2 importance in AD occurrence and therapy. In addition, IL-2 serves as an immune-modulating agent for CNS (104). In recent clinical trials, administration of low-dose IL-2 has been shown to result in the expansion of regulatory T cells (Tregs) which are inflammation-resolving mediators that regulate the microglial response to Aβ deposition and facilitate in controlling inflammation and autoimmune diseases (105). Besides, low-dose IL-2 has been shown to be safe, well tolerated, and can provide immunoregulation with few side effects (106). Therefore, it is likely that the regulatory T cells stimulated by IL-2 effectively control Aβ deposition in the brain of patients with AD.

IL-4, also known as B cell-stimulatory factor-1, is a monomeric Th2 cytokine that shows pleiotropic effects during immune responses. Currently, it has been shown that IL-4 promotes cell proliferation, survival, and immunoglobulin class switch. In the CNS, IL-4 enhances polarization of microglia/macrophages from the pro-inflammatory to the anti-inflammatory subtype, and is closely associated with tissue repair from microglia/macrophages, which suppress the pathological inflammation, and elevate expression of IL-10, TGF-β and arginase-1 (107). More importantly, it has been demonstrated that the injection of IL-4 and IL-13 decreases the density of Aβ plaque in the hippocampal of APP/PS1 mice *via* the Aβ degrading enzymes neprilysin (NEP) and CD36 (108, 109). Furthermore, in the follow-up experiment, the delivery of IL-4 was proven to improve cognitive performance and alleviate tau pathology by increasing arginase-1 positive microglia cells in the 3xTg AD mice (**Figure 3**) (110).

IL-10 was first reported as an inhibitory factor of cytokine synthesis by Fiorentino et al. in 1989 (111). In the CNS, IL-10 is mainly produced by astrocytes, microglia, and neurons, and it is capable of attenuating the expression of pro-inflammatory cytokines such as IL-1β, IL-12, TNF-α, adhesion molecules, as well as co-stimulatory molecules including CD86 and CD54 (94). IL-10 plays a critical role in the regulation of immune and inflammatory responses. In this process, IL-10 acts primarily as an inhibitor of the nuclear factor kappa B (NF-κB), and activator of transcription 1 (STAT1) signaling pathways (112, 113). Recent studies showed that once loss of IL-10, LPS could elicit higher tau hyperphosphorylation, neurotoxicity and IL-6 overexpression in mice, thereby leading to aggravation of insults to animals (114). Regarding up-regulation, compelling evidence reveals that Curcumin, an efficient pharmacological component of turmeric, has been proved to protect against neuronal loss by increasing the production of IL-10 in glial cells *via* the PI3K pathway (94) (**Figure 3**). Moreover, as a kind of anti-inflammatory leukocyte that secretes IL-10, the development of regulatory T cells (Tregs) may be aided by IL-10 (115). Therefore, IL-10 is of paramount importance in targeting therapy for neurodegenerative diseases.

IL-33, a branch of the IL-1 family and a kind of pro-inflammatory protein, is structural homology with IL-1 family cytokines. Similar to IL-1, IL-33 can be cleaved *in vitro* by caspase−1, generating an N−terminal fragment that is slightly shorter than the C−terminal fragment. IL-33 can be sequestered and blocked by soluble tumorigenicity 2 (sST2), an IL-33 decoy receptor, thereby curtailing pro-inflammatory response. However, numerous studies reveal a higher amount of serum sST2 in patients with mild cognitive impairment, suggesting that impaired IL-33/ST2 signaling may contribute to the pathogenesis of AD. Intriguingly, the exogenous administration of IL-33 has been shown to increase microglial recruitment and Aβ phagocytic activity *via* activating membrane-bound ST2 receptors and their downstream p38. This downstream cascade results in the suppression of pro-inflammatory genes and the polarization of microglia into anti-inflammatory phenotypes, which contributes to the secretion of the enzyme arginase 1 (ARG1) and the found of inflammatory zone 1 (FIZZ1) (116, 117). To sum up, anti-inflammatory cytokines are potential therapeutic agents for AD patients.

4.2.3 Transforming Growth Factor β

The transforming growth factor-β (TGF-β) belongs to an evolutionarily conserved cytokine superfamily, and acts as cellular switches that regulate processes such as immune function, proliferation and epithelial−mesenchymal transition. Alternatively, it is closely pertinent to the cell differentiation and apoptosis (118). Notably, TGF-β deficiency in mice can lead to loss of microglia and the absence of a typical ramified morphology of microglia, indicative of a milieu molecule for TGF-β required for microglia function (119). In addition, TGF-β also regulates microglial homeostatic molecular and functional signature in the brain. It antagonizes specific cytokines such as IL-1 to inhibit both Th1 and Th2 reactions, preventing these cytokines from pro-inflammation in immune responses (120).

Notably, TGF-β also functions as neurotrophic factor-promoting effects including differentiation, neuronal function maintenance, synapse plasticity, and memory formation (121). More importantly, TGF-β released primarily by microglia in response to CNS lesions protects neurons from toxins, ischemia, and Aβ aggregates, particularly *via* the phosphatidylinositol-3-kinase pathway in AD (122). Additionally, TGF-β helps to attenuate microglia clustering at neuritic plaques through SMAD2 phosphorylation and down-regulation of CCL5, ameliorating to the neuroinflammation caused by microglia in AD. As a result, the concomitant release and production of pro-inflammatory mediators and reactive oxygen species as critical contributing factors in AD pathology were further abrogated in the overactivated microglia (123). On the basis of an interesting study, 1,7-bis (4-hydroxy-3-methoxyphenyl) heptane-3,5-dione (tetrahydrocurcumin, THC) enhances the secretion of TGF-β in APP/ps1 mice. Subsequently, the study revealed that Aβ-induced reduced cell viability, cell cycle arrest and spatial memory impairment were rescued in mice by delivery of THC (124). Therefore, TGF-β may provide insights into microglial biology and the possibility of targeting microglia for the treatment of AD (**Figure 3**).

4.3 Microglial Phagocytosis, Autophagy and Aβ Degradation

As previously stated, AD is characterized as the deposition of Aβ and NFTs; thus, increasing microglial phagocytosis and autophagy to remove the overproduction of neurotoxic proteins is likely to be a promising treatment strategy.

4.3.1 Scavenger Receptors Family

The SRs family was first described as a high-affinity, trypsin-sensitive, surface binding site of acetylated low-density lipoprotein (LDL) on macrophages of patients (125). Although the SRs family was initially considered to be closely related to lipid metabolism, its role in AD has been established, particularly for scavenger receptor class A (SR-A), CD36 and receptor for advanced end glycation products (RAGE) (30). Therefore, the critical molecules will be systematically reviewed as follows.

4.3.1.1 Scavenger Receptor Class A

SR-A belongs to a large family of scavenger receptors consisting of at least 6 classes, all mediating the uptake of modified LDL. Until now, SR-A has been shown to be important in the inflammatory response in host defense, cellular activation, adhesion, and cell-cell interaction. An interesting recent study found that although SR-A and CD36 were the main receptors responsible for Aβ clearance, SR-A rather than CD36 mediated oligomeric Aβ internalization *via* adhesion to Aβ coated surfaces, and that the oligomeric Aβ was completely degraded within 30 minutes by cathepsin B, a cysteine protease in lysosomes (126). Therefore, the deficiency of SR-A causes the reduced uptake of Aβ. More than that, the decreased expression of SR-A is conducive to release of pro-inflammatory cytokines in the CNS, and reduces anti-inflammatory cytokines in plasma, which increases the inflammatory environment (127). In contrast, there is also evidence that SR-A plays a critical role in innate immune responses like inflammatory responses by combining with exotic pathogens or endogenous ligands, resulting in M1 polarization and secretion of ROS. As a result, the brain tissue may be damaged by pro-inflammatory cytokines due to overexuberant immune responses (128). Unfortunately, the drugs targeting SR-A of microglia was not hitherto discovered for AD treatment. Nevertheless, we are still optimistic about seeking an ideal target drug of molecular therapy for AD in the future.

4.3.1.2 CD36

CD36, a membrane protein also known as SR-B2, is enriched in the monocyte-macrophage system and endothelial cells. As a member of SRs family, CD36 facilitates fatty acid uptake and intracellular trafficking of cholesterol for packaging into lipoproteins, which independently regulate the secretion of Aβ and tau *via* a druggable CYP46A1 (cholesterol 24-hydroxylase) -CE (cholesteryl esters) -tau axis (129, 130). Kunjathoor et al. demonstrated that Aβ promoted the accumulation of pro-inflammatory lipid peroxides by inhibiting CD36. This state will form vicious circle in AD, implying the aggravation of AD. In addition, CD36 is involved in mediating inflammatory processes by regulating macrophage migration, phagocytosis, and the formation of foam cells (131). Along with this, CD36 can also recognize Aβ and trigger Toll-like receptor 4 (TLR4)-TLR6 signaling, which shares the same route as activator oxidized low density lipoprotein (oxLDL). Strikingly, TLR4-TLR6 signaling could promote the mRNA encoding of pro-inflammatory cytokines like pro-IL-1β, thereby priming the activation of inflammasome and the secretion of nitric oxide and ROS. Accordingly, the disruption of CD36-TLR4-TLR6 signaling in microglia can effectively protect neurons against inflammatory toxicity resulting from Aβ (132). Nevertheless, another study found that CD36 can be up-regulated by a selective PPAR agonist, DSP-8658, then leading to accumulation of microglia in and around Aβ plaques and an increase in microglial Aβ phagocytosis. This event was verified by the rescue of spatial learning in APP/PS1 transgenic mice (133). On the other side, the upregulation of CD36 can alleviate microglia phagocytosis deficiency and spatial learning impairment of AD mice by intranasal administration of a kind of lentiviral vector encoding human nuclear factor erythroid 2-related factor 2 (LV-*NRF2*) which is a transcriptional activator to up-regulate CD36 expression (134). In general, AD therapeutic strategies targeting CD36 have two main focuses: CD36 blockade with neutralizing antibodies or other small molecules to suppress the inflammatory response of microglia, and upregulating the expression of CD33 to lower the Aβ burden, respectively. The exact mechanisms involved and specific equilibrium points between the two approaches have yet to be investigated.

4.3.1.3 Receptor for Advanced End Glycation Products

RAGE is a member of the immunoglobulin superfamily of cell surface molecules. As a pattern-recognition receptor, it acts as a pro-inflammatory mediator by pairing with its ligands including advanced glycation end products (AGE), high mobility group box 1 (HMGB1) and Aβ oligomers. Critically, it also mediates plasma Aβ across blood brain barrier (BBB). Given that

HMGB1-RAGE axis triggers pro-inflammatory microglia activation through RAGE-NF-κB signaling pathway, targeting the HMGB1/RAGE/NF-κB signaling pathway may be a potential strategy for the treatment of AD (135). Likewise, the activated microglia enhance the secretion of RAGE ligands, leading to neuronal cell oxidative stress and death in rats or mice and creating a vicious cycle as well (136). Soluble RAGE (sRAGE), a decoy receptor of AGE that lacks the transmembrane domain, may participate in conservation of CNS homeostasis by dint of blocking the combination of RAGE and AGE based on its well contributions to the removal/neutralization of circulating AGE ligands (137). Subsequently, evidence for an important role of RAGE from a study demonstrated that, a flavoring agent vanillic acid (VA), could antagonize RAGE-mediated c-Jun N-terminal kinase (JNK). It exhibits a number of attractively biological activities including anti-inflammatory, antioxidant and neuroprotection. Of importance, VA treatment attenuates synapse loss and memory deficits of AD markers like APP, BACE1 and Aβ induced by LPS (138). Notably, non-specific neuroinflammation and M1 polarization could be suppressed *via* inhibiting RAGE-NF-κB signaling pathway, implying VA potential as a therapeutic agent to target AD (139). Regarding involvement of RAGE in AD target therapy, there is now evidence that Aβ dependent impairments like dependent behavior and damaged dendritic spine morphology in the entorhinal cortex (EC) are rescued in transgenic mice with silenced RAGE of microglia *via* prohibiting kinases JNK and p38 mitogen-activated protein kinase (p38MAPK). Alternatively, the EC, a brain area crucially involved in learning and memory, is one of the most susceptible to neurodegenerative disorders such as AD due to the vulnerability of superficial neurons and its number reduces significantly in the early stage of AD. Therefore, inhibiting the RAGE of microglia in EC is likely to be another sensitive therapeutical target in AD (**Figure 3**) (140).

4.3.2 Peroxisome Proliferator Activated Receptor

PPAR is a type of nuclear receptor that collaborates with PPAR response elements in the promoter region of genes to regulate glucose, lipid metabolism, as well as inflammatory processes. It has been proved that PPARα promotes the recruitment of microglia, and is closely associated with microglial Aβ phagocytosis. Nowadays, PPARα activation by its agonists Gemfibrozil and Wy14643, can improve a variety of pathological and behavioral phenotypes of AD. PPARα agonists showed an additive enhancement of the autophagy of microglia and structural neuroplasticity in APP-PSEN1ΔE9 mice (141). Therefore, PPARα activators that efficiently cross the blood–brain barrier may be considered as future therapeutics for AD. However, PPARγ appears an opposite effect. PPARγ antagonists can result in an overall reduction of Aβ levels and improved spatial memory performance. Evidence indicates that PPARγ antagonist T0070907 promotes microglia autophagy *via* Liver kinase B1 (LKB1)-adenosine 5'-monophosphate-activated protein kinase (AMPK) signaling pathway (**Figure 4**). Intriguingly, whether M1 to M2 polarization is involved in the process as well should be also concerned (142).

4.3.3 Microtubule-Associated Protein Light Chain 3

LC3 is a component of the autophagosomal membrane, characterized as an autophagy marker, and primarily participates in the formation of autophagosomes. Autophagy-related gene 4 (ATG4) is essential for autophagy by affecting full length LC3 (pro-LC3) to the soluble form LC3-I. In general, LC3 is cleaved at its C-terminus by ATG4 to form LC3-I which is distributed in the cytosol. For autophagy, LC3-I covalently binds to phosphatidylethanolamine and is converted to LC3-II on autophagosome membranes. This process is mediated by the ATG12-ATG5-ATG16L complex, followed by the formation of autophagy precursors (143). The expression of LC3 proteins could be upregulated when nuclear factor erythroid 2-related factor 2 (NRF2), a factor is dissociated from Kelch-like ECH-associated protein 1 (KEAP1), and then translocates into the nucleus and binds to antioxidant responsive element (ARE) (144). There have been evidence that LC3-associated endocytosis (LANDO) not only reduces the deposition of Aβ and tau pathology, but also inhibits the secretion of inflammatory cytokines in activated microglia induced by Aβ. Concurrently, it also rescues memory and behavioral impairment of 5xFAD mice by maintaining neuronal homeostasis (145). In addition, the β-Asarone has been shown to promote autophagy by virtue of increasing the expression of LC3-I and LC3II (**Figure 4**) (146). Consistent with the finding, IL-4 is found to rapidly increase the expression of LC3-I and LC3II in BV2 microglia and increase the uptake and degradation of Aβ. But the inhibition of IL-4-pretreated microglia M1 phenotype switching induced by Aβ is independent on this autophagy (147). Along with the above-mentioned, use of some anti-inflammatory drugs like dimethyl fumarate (DMF), a potent Nrf2 activator may be considered as a potential therapeutic strategy by up-regulating LC3 to promote autophagy of microglia (148).

4.3.4 Insulin Degrading Enzyme

Currently, pharmacological activation of the Aβ-degrading molecules represents a novel therapeutic strategy for the treatment of AD. Extracellular and intracellular degradation of Aβ depends mainly on two proteases, namely, neprilysin and insulin degrading enzyme (IDE) *in vitro* (149). IDE is a downstream region of insulin receptor signaling and mainly distributed in cytosol. The transport outside cells of IDE mainly relies on exosomes and extracellular vesicles. Compelling studies showed that decreased activity of any of these enzymes due to genetic mutation may increase the risk for AD. Farris et al. verified that mutations in *IDE* increased risk of developing AD in type 2 diabetes (T2D) (150). It is speculated that insulin resistance and overexpression compete with Aβ binding to IDE, resulting in IDE devitalization, which is responsible for impaired Aβ degradation and clearance in brain, and thereby promotes the pathogenesis of AD. Even more to the point, a slight overexpression of IDE remarkably alleviates Aβ deposition to a large extent in APP transgenic mice, implying that IDE may be an effective therapeutic target for AD (151). Statins including lovastatin and simvastatin which act as

inhibitors of 3-hydroxy-3-methylglutaryl-coenzyme A (HMG-CoA) reductase (HMGR), play an important role in lowering serum cholesterol levels and are extensively used in the treatment of hypercholesterolemia (152). Surprisingly, Walter et al. found that lovastatin can stimulate the secretion of IDE in mouse microglia cell lines (BV-2 and N9 cells) *in vitro*, and the level of IDE in serum is significantly elevated following the delivery of lovastatin to mice as well (153). There is some evidence that somatostatin stimulates microglia to express and secrete IDE too (154). Apart from lovastatin, metformin, a derivative of biguanide, has been widely used for the treatment of type 2 diabetes (T2D) for almost all country. Intriguingly, an interesting study revealed that metformin, could also be a potential therapeutic agent for AD since it accelerates the expression of IDE by the activation of the AMPK signaling pathway (155). Consistently, administrating metformin orally also improves Aβ deposition, oxidative stress, and learning and memory functions in APP/PS1 mice (156). In short, it is possible to propose a new strategy for the targeted IDE-based therapeutical target for AD (**Figure 2**).

4.4 M1 to M2 Switch

As mentioned above, the M2 phenotype of microglia plays a relatively beneficial role in the maintenance of neurological homeostasis. Thus, increasing the M2 polarization of microglial cells may be a potential strategy for treatment of AD. It is reported that when TAK-242, a specific inhibitor of toll-like receptor 4 (TLR4), is administered, the levels of M1-markers (TNF and iNOS) are markedly reduced while M2-markers (TREM-2 and Arg-1) are increased conversely. In addition, TAK-242 potentiates microglial phagocytosis *via* the MYD88/NF-κB/NLRP3 signaling pathway, and it is capable of promoting Aβ clearance and inhibiting tau hyperphosphorylation, while it effectively ameliorates the learning and memory impairments (157). Besides, resveratrol is a natural polyphenolic phytochemical with a variety of bioactivities associated with health promotion. It effectively promotes microglia polarization into the M2 phenotype *via* proliferator-activated receptor coactivator-1 (PGC-1), while inhibiting NF-κB and activating STAT3 and STAT6 to increase M2 markers (158). Moreover, some non-drug treatments, for example, low-dose ionizing radiation (LDIR), may also affect the phenotype of microglia, increase TREM2 and CD206 expression in LPS-induced BV2 microglial cells, and attenuate Aβ deposition and cognitive decline ultimately (159). In addition, the LKB1–AMPK signaling pathway is not only involved in energy homeostasis, metabolic stress, but mediates M1 to M2 switch. Similar to drug, T0070907, an agonist of the peroxisome proliferator-activated receptor γ (PPARγ), also triggers M1-to-M2 polarization and abrogates the inhibition of LPS-induced autophagy by suppressing LKB1–AMPK signaling pathway (142). Other substances with similar effects on microglia polarization have been identified including L-cysteine-derived hydrogen sulfide (H2S) and CaMKK inhibitor, STO-609 (160, 161). Apart from that, several signaling pathways including mTOR, Rho/Rho-kinase, and the NOTCH signaling pathways, also involved in microglia polarization, implying a plethora of potential therapeutic targets in microglia polarization of AD (162–164). Numerous studies have shown that M2 polarization also helps to alleviate persistent neuropathic pain (NP) and AD-related behavior impairment in a doxycycline-induced mouse AD model (165). These evidences presented above demonstrate the significance of M2 polarization for the treatment of AD.

5 CONCLUSIONS AND FUTURE EXPECTATIONS

In summary, microglia are crucial mediator and effector in the pathology of AD, but a slew of mysteries surrounding the interactions between microglia and AD remain unsolved. Neurodegeneration has been linked to microglia-associated inflammatory factors such as TNF-α, IFN-γ, and IL-1β. In this state, microglia fail to endocytose pathological Aβ and tau, and Aβ and tau deposition contributes to inflammatory activation, resulting in a vicious cycle in AD pathology. On the contrary, anti-inflammatory factors secreted by microglia such as IL-2, IL-4, IL-10 and TGF-β, and activation of certain receptors such as TREM2, aid in the restoration of learning and memory deficits in AD *via* various signaling pathways and mechanisms. Furthermore, phagocytosis and autophagy of microglia mediated by some critical receptors such as SR-A and CD36 are responsible for the degradation of deposited Aβ and tau in AD. The detailed potential interaction mechanism underlying a variety of molecular events orchestrated by microglia in AD is seen in figures mentioned above and **Table 1**. In the CNS, we believe that microglia, an obligatory member of the innate immune system, act as a protective factor against tumors, pathogens, and abnormally deposited proteins such as Aβ and tau. Notwithstanding, once Aβ and tau deposition exceeds that of clearance by microglia, the resulting excessive activation of microglia would release excessive pro-inflammatory factors to compromise neurons and their synapses associated with AD. In this review, we systemically summarized the microglia-associated factors, mechanisms of molecular activity, and relevant therapeutic strategies for AD that have been trialed in cell, animal models, or Alzheimer's patients. More research has revealed that microglia play a critical role not just in AD, but also in PD, ischemia, demyelinating disease, and even psychiatric conditions such as mood disorders. Pro-inflammatory cytokines such like TNF-α and IL-6 have been shown to be increased in patients with depression, and human volunteers were indeed induced anxiety and depression by the treatment with pro-inflammatory cytokine IFN-α. Drug-induced anti-inflammatory microglial phenotypes have been shown to alleviate depressive-like behavior in mice (166). Taking into account all the great advantages of microglial double-edged sword defenses previously described, there is no doubt that targeting expansion of the microglial various beneficial bio-functions will hold the potential to delay disease onset and further possibly preserve cognitive function of patient with AD. Once we achieve great therapeutic outcomes, the

TABLE 1 | Diverse drugs, their effects and associated signal pathways.

Drugs	Targets	Effects	Receptors	Effects	Pathways	Subjects
Galantamine	Cholinergic neuron	Activate	Cholinesterase	Inhibit	-	Cells/mice
OLT1177	NLRP3 Inflammasome	Inhibit	Caspase-1	Inhibit	-	Patients/mice
Stavudine	NLRP3 Inflammasome	Inhibit	-	-	AKT	Cells
JC-124	NLRP3 Inflammasome	Inhibit	Caspase-1	Inhibit	-	Mice
PF-04418948	Prostaglandin E2	Inhibit	EP-2	Inhibit	AKT	Cells
Indomethacin	Aβ-42	Reduce	γ-secretase	Switch	-	Cells
SEO	IL-1β	Inhibit	P38	Inhibit	NF-κB	Mice
Glycine	IFN-γ	Inhibit	-	-	-	Cells
RhinacanthinC	IFN-γ	Inhibit	-	-	NF-κB	Cells
APN	TNF-α	Inhibit	AdipoR1	Activate	AMPK-NF-κB	Cells
AL002c	TREM2	Activate	anti-hTREM2 agonistic	Activate	ITAM	Patients/mice
curcumin	IL-10	Activate	-	-	PI3K	Rats
THC	TGF-β	Activate	-	-	Ras/ERK	Cells
DSP-8658	CD36	Activate	PPARγ	Activate	-	Mice
V.A	RAGE	Inhibit	-	-	JNK	Mice
Gemfibrozil/Wy14643	PPARα	Activate	-	-	-	Mice
Metformin	IDE	Activate	-	-	AMPK	Mice
TAK-242	M1	M1 to M2 switch	TLR4	Inhibit	MyD88/NF-kappaB/NLRP3	Mice
Resveratrol	M1	M1 to M2 switch	PGC-1α	Inhibit	NF-κB/STAT	Cells

therapeutic strategy targeting microglia would represent a perspective strategy for suppression of the early stage of neuropathological change in AD, and avoid the family tragedy of end-stage AD.

AUTHOR CONTRIBUTIONS

YC and JL wrote the manuscript with support from BW, MS, and HY. All authors contributed to the article and approved the submitted version.

FUNDING

This work was supported by grants from the National Key R&D Program of China (2019YFA0802600), the National Natural Science Foundation of China (81974244, 82071551, and 81570960), and the Postgraduate Research & Practice Innovation Program of Jiangsu Province (5832013521).

ACKNOWLEDGMENTS

We try to provide readers with comprehensive and updated reviews of recent literature. However, some studies may have been omitted involuntarily. We apologize for the inconvenience caused to you, and hope our colleagues can forgive us for neglecting their work. We thank BioRender (https://app.biorender.com/) for its assistance during the preparation of these figures. We also thank the reviewers for their work.

REFERENCES

1. Ballard C, Gauthier S, Corbett A, Brayne C, Aarsland D, Jones E. Alzheimer's Disease. *Lancet* (2011) 377:9770–1019-31. doi: 10.1016/S0140-6736(10)61349-9
2. Jakob-Roetne R, Jacobsen H. Alzheimer's Disease: From Pathology to Therapeutic Approaches. *Angew Chem Int Ed Engl* (2009) 48:17–3030-59. doi: 10.1002/anie.200802808
3. Galimberti D, Scarpini E. Progress in Alzheimer's Disease. *J Neurol* (2012) 259:2–201-11. doi: 10.1007/s00415-011-6145-3
4. Krasemann S, Madore C, Cialic R, Baufeld C, Calcagno N, El Fatimy R, et al. The TREM2-APOE Pathway Drives the Transcriptional Phenotype of Dysfunctional Microglia in Neurodegenerative Diseases. *Immunity* (2017) 47:3–566-81.e9. doi: 10.1016/j.immuni.2017.08.008
5. Jouanne M, Rault S, Voisin-Chiret AS. Tau Protein Aggregation in Alzheimer's Disease: An Attractive Target for the Development of Novel Therapeutic Agents. *Eur J Med Chem* (2017) 139:153–67. doi: 10.1016/j.ejmech.2017.07.070
6. Bassil F, Brown HJ, Pattabhiraman S, Iwasyk JE, Maghames CM, Meymand ES, et al. Amyloid-Beta (Abeta) Plaques Promote Seeding and Spreading of Alpha-Synuclein and Tau in a Mouse Model of Lewy Body Disorders With Abeta Pathology. *Neuron* (2020) 105:2–260-75.e6. doi: 10.1016/j.neuron.2019.10.010
7. Dai CL, Hu W, Tung YC, Liu F, Gong CX, Iqbal K. Tau Passive Immunization Blocks Seeding and Spread of Alzheimer Hyperphosphorylated Tau-Induced Pathology in 3 X Tg-AD Mice. *Alzheimers Res Ther* (2018) 10:1–13. doi: 10.1186/s13195-018-0341-7
8. Scholl M, Wall A, Thordardottir S, Ferreira D, Bogdanovic N, Langstrom B, et al. Low PiB PET Retention in Presence of Pathologic CSF Biomarkers in Arctic APP Mutation Carriers. *Neurology* (2012) 79:3–229-36. doi: 10.1212/WNL.0b013e31825fdf18
9. Berger Z, Roder H, Hanna A, Carlson A, Rangachari V, Yue M, et al. Accumulation of Pathological Tau Species and Memory Loss in a Conditional Model of Tauopathy. *J Neurosci* (2007) 27:14–3650-62. doi: 10.1523/JNEUROSCI.0587-07.2007
10. Edison P, Archer HA, Gerhard A, Hinz R, Pavese N, Turkheimer FE, et al. Microglia, Amyloid, and Cognition in Alzheimer's Disease: An [11c](R)PK11195-PET and [11C]PIB-PET Study. *Neurobiol Dis* (2008) 32:3–412-9. doi: 10.1016/j.nbd.2008.08.001
11. Xie L, Zhang N, Zhang Q, Li C, Sandhu AF, Iii GW, et al. Inflammatory Factors and Amyloid Beta-Induced Microglial Polarization Promote

Inflammatory Crosstalk With Astrocytes. *Aging (Albany NY)* (2020) 12:22–22538-22549. doi: 10.18632/aging.103663
12. Liddelow SA, Guttenplan KA, Clarke LE, Bennett FC, Bohlen CJ, Schirmer L, et al. Neurotoxic Reactive Astrocytes Are Induced by Activated Microglia. *Nature* (2017) 541:7638–481-487. doi: 10.1038/nature21029
13. Mangialasche F, Solomon A, Winblad B, Mecocci P, Kivipelto M. Alzheimer's Disease: Clinical Trials and Drug Development. *Lancet Neurol* (2010) 9:7–702-16. doi: 10.1016/S1474-4422(10)70119-8
14. Liu Y, Zhang Y, Zheng X, Fang T, Yang X, Luo X, et al. Galantamine Improves Cognition, Hippocampal Inflammation, and Synaptic Plasticity Impairments Induced by Lipopolysaccharide in Mice. *J Neuroinflamm* (2018) 15:1–112. doi: 10.1186/s12974-018-1141-5
15. Hansen DV, Hanson JE, Sheng M. Microglia in Alzheimer's Disease. *J Cell Biol* (2018) 217:2–459-472. doi: 10.1083/jcb.201709069
16. Harry GJ. Microglia During Development and Aging. *Pharmacol Ther* (2013) 139:3–313-26. doi: 10.1016/j.pharmthera.2013.04.013
17. Bruttger J, Karram K, Wortge S, Regen T, Marini F, Hoppmann N, et al. Genetic Cell Ablation Reveals Clusters of Local Self-Renewing Microglia in the Mammalian Central Nervous System. *Immunity* (2015) 43:1–92-106. doi: 10.1016/j.immuni.2015.06.012
18. Schafer DP, Lehrman EK, Kautzman AG, Koyama R, Mardinly AR, Yamasaki R, et al. Microglia Sculpt Postnatal Neural Circuits in an Activity and Complement-Dependent Manner. *Neuron* (2012) 74:4–691-705. doi: 10.1016/j.neuron.2012.03.026
19. Hanisch UK, Kettenmann H. Microglia: Active Sensor and Versatile Effector Cells in the Normal and Pathologic Brain. *Nat Neurosci* (2007) 10:11–1387-94. doi: 10.1038/nn1997
20. Nimmerjahn A, Kirchhoff F, Helmchen F. Resting Microglial Cells Are Highly Dynamic Surveillants of Brain Parenchyma *In Vivo*. *Science* (2005) 308:5726–1314-8. doi: 10.1126/science.1110647
21. Paolicelli RC, Bolasco G, Pagani F, Maggi L, Scianni M, Panzanelli P, et al. Synaptic Pruning by Microglia Is Necessary for Normal Brain Development. *Science* (2011) 333:6048–1456-8. doi: 10.1126/science.1202529
22. Harrison JK, Jiang Y, Chen S, Xia Y, Maciejewski D, McNamara RK, et al. Role for Neuronally Derived Fractalkine in Mediating Interactions Between Neurons and CX3CR1-Expressing Microglia. *Proc Natl Acad Sci USA* (1998) 95:18–10896-901. doi: 10.1073/pnas.95.18.10896
23. Chuang KA, Li MH, Lin NH, Chang CH, Lu IH, Pan IH, et al. Rhinacanthin C Alleviates Amyloid-Beta Fibrils' Toxicity on Neurons and Attenuates Neuroinflammation Triggered by LPS, Amyloid-Beta, and Interferon-Gamma in Glial Cells. *Oxid Med Cell Longev* (2017) 2017:5414297. doi: 10.1155/2017/5414297
24. Bishop NA, Lu T, Yankner BA. Neural Mechanisms of Ageing and Cognitive Decline. *Nature* (2010) 464:7288–529-35. doi: 10.1038/nature08983
25. Streit WJ, Graeber MB, Kreutzberg GW. Functional Plasticity of Microglia: A Review. *Glia* (1988) 1:5–301-7. doi: 10.1002/glia.440010502
26. Perry VH, Gordon S. Macrophages and Microglia in the Nervous System. *Trends Neurosci* (1988) 11:6–273-7. doi: 10.1016/0166-2236(88)90110-5
27. Heneka MT, Carson MJ, El Khoury J, Landreth GE, Brosseron F, Feinstein DL, et al. Neuroinflammation in Alzheimer's Disease. *Lancet Neurol* (2015) 14:4–388-405. doi: 10.1016/S1474-4422(15)70016-5
28. Kettenmann H, Hanisch UK, Noda M, Verkhratsky A. Physiology of Microglia. *Physiol Rev* (2011) 91:2–461-553. doi: 10.1152/physrev.00011.2010
29. Bamberger ME, Harris ME, McDonald DR, Husemann J, Landreth GE. A Cell Surface Receptor Complex for Fibrillar Beta-Amyloid Mediates Microglial Activation. *J Neurosci* (2003) 23:7–2665-74. doi: 10.1523/JNEUROSCI.23-07-02665.2003
30. Hickman SE, Allison EK, El Khoury J. Microglial Dysfunction and Defective Beta-Amyloid Clearance Pathways in Aging Alzheimer's Disease Mice. *J Neurosci* (2008) 28:33–8354-60. doi: 10.1523/JNEUROSCI.0616-08.2008
31. Varnum MM, Ikezu T. The Classification of Microglial Activation Phenotypes on Neurodegeneration and Regeneration in Alzheimer's Disease Brain. *Arch Immunol Ther Exp (Warsz)* (2012) 60:4–251-66. doi: 10.1007/s00005-012-0181-2
32. Baalman K, Marin MA, Ho TS, Godoy M, Cherian L, Robertson C, et al. Axon Initial Segment-Associated Microglia. *J Neurosci* (2015) 35:5–2283-92. doi: 10.1523/JNEUROSCI.3751-14.2015
33. Bertolotto A, Agresti C, Castello A, Manzardo E, Riccio A. 5D4 Keratan Sulfate Epitope Identifies a Subset of Ramified Microglia in Normal Central Nervous System Parenchyma. *J Neuroimmunol* (1998) 85:1–69-77. doi: 10.1016/s0165-5728(97)00251-8
34. Nagarajan N, Jones BW, West PJ, Marc RE, Capecchi MR. Corticostriatal Circuit Defects in Hoxb8 Mutant Mice. *Mol Psychiatry* (2018) 23:9–1868-1877. doi: 10.1038/mp.2017.180
35. Wlodarczyk A, Holtman IR, Krueger M, Yogev N, Bruttger J, Khorooshi R, et al. A Novel Microglial Subset Plays a Key Role in Myelinogenesis in Developing Brain. *EMBO J* (2017) 36:22–3292-3308. doi: 10.15252/embj.201696056
36. Joost E, Jordao MJC, Mages B, Prinz M, Bechmann I, Krueger M. Microglia Contribute to the Glia Limitans Around Arteries, Capillaries and Veins Under Physiological Conditions, in a Model of Neuroinflammation and in Human Brain Tissue. *Brain Struct Funct* (2019) 224:3–1301-1314. doi: 10.1007/s00429-019-01834-8
37. Koenigsknecht-Talboo J, Landreth GE. Microglial Phagocytosis Induced by Fibrillar Beta-Amyloid and IgGs Are Differentially Regulated by Proinflammatory Cytokines. *J Neurosci* (2005) 25:36–8240-9. doi: 10.1523/JNEUROSCI.1808-05.2005
38. He P, Zhong Z, Lindholm K, Berning L, Lee W, Lemere C, et al. Deletion of Tumor Necrosis Factor Death Receptor Inhibits Amyloid Beta Generation and Prevents Learning and Memory Deficits in Alzheimer's Mice. *J Cell Biol* (2007) 178:5–829-41. doi: 10.1083/jcb.200705042
39. Zhu H, Wang Z, Yu J, Yang X, He F, Liu Z, et al. Role and Mechanisms of Cytokines in the Secondary Brain Injury After Intracerebral Hemorrhage. *Prog Neurobiol* (2019) 178:101610. doi: 10.1016/j.pneurobio.2019.03.003
40. Baik SH, Kang S, Lee W, Choi H, Chung S, Kim JI, et al. A Breakdown in Metabolic Reprogramming Causes Microglia Dysfunction in Alzheimer's Disease. *Cell Metab* (2019) 30:3–493-507 e6. doi: 10.1016/j.cmet.2019.06.005
41. Keren-Shaul H, Spinrad A, Weiner A, Matcovitch-Natan O, Dvir-Szternfeld R, Ulland TK, et al. A Unique Microglia Type Associated With Restricting Development of Alzheimer's Disease. *Cell* (2017) 169:7–1276-1290 e17. doi: 10.1016/j.cell.2017.05.018
42. Rangaraju S, Dammer EB, Raza SA, Rathakrishnan P, Xiao H, Gao T, et al. Identification and Therapeutic Modulation of a Pro-Inflammatory Subset of Disease-Associated-Microglia in Alzheimer's Disease. *Mol Neurodegener* (2018) 13:1–24. doi: 10.1186/s13024-018-0254-8
43. Fattorelli N, Martinez-Muriana A, Wolfs L, Geric I, De Strooper B, Mancuso R. Stem-Cell-Derived Human Microglia Transplanted Into Mouse Brain to Study Human Disease. *Nat Protoc* (2021) 16:2–1013-1033. doi: 10.1038/s41596-020-00447-4
44. Zhou Y, Song WM, Andhey PS, Swain A, Levy T, Miller KR, et al. Human and Mouse Single-Nucleus Transcriptomics Reveal TREM2-Dependent and TREM2-Independent Cellular Responses in Alzheimer's Disease. *Nat Med* (2020) 26:1–131-142. doi: 10.1038/s41591-019-0695-9
45. Srinivasan K, Friedman BA, Etxeberria A, Huntley MA, van der Brug MP, Foreman O, et al. Alzheimer's Patient Microglia Exhibit Enhanced Aging and Unique Transcriptional Activation. *Cell Rep* (2020) 31:13–107843. doi: 10.1016/j.celrep.2020.107843
46. Femminella GD, Dani M, Wood M, Fan Z, Calsolaro V, Atkinson R, et al. Microglial Activation in Early Alzheimer Trajectory Is Associated With Higher Gray Matter Volume. *Neurology* (2019) 92:12–e1331-e1343. doi: 10.1212/WNL.0000000000007133
47. Schwabe T, Srinivasan K, Rhinn H. Shifting Paradigms: The Central Role of Microglia in Alzheimer's Disease. *Neurobiol Dis* (2020) 143:104962. doi: 10.1016/j.nbd.2020.104962
48. Olah M, Menon V, Habib N, Taga MF, Ma Y, Yung CJ, et al. Single Cell RNA Sequencing of Human Microglia Uncovers a Subset Associated With Alzheimer's Disease. *Nat Commun* (2020) 11:1–6129. doi: 10.1038/s41467-020-19737-2
49. Chakrabarty P, Herring A, Ceballos-Diaz C, Das P, Golde TE. Hippocampal Expression of Murine TNFalpha Results in Attenuation of Amyloid Deposition *In Vivo*. *Mol Neurodegener* (2011) 6:16. doi: 10.1186/1750-1326-6-16
50. Petrilli V, Papin S, Tschopp J. The Inflammasome. *Curr Biol* (2005) 15:15–R581. doi: 10.1016/j.cub.2005.07.049

51. Martinon F, Burns K, Tschopp J. The Inflammasome: A Molecular Platform Triggering Activation of Inflammatory Caspases and Processing of proIL-Beta. *Mol Cell* (2002) 10:2–417-26. doi: 10.1016/s1097-2765(02)00599-3
52. Rathinam VA, Vanaja SK, Fitzgerald KA. Regulation of Inflammasome Signaling. *Nat Immunol* (2012) 13:4–333-42. doi: 10.1038/ni.2237
53. Halle A, Hornung V, Petzold GC, Stewart CR, Monks BG, Reinheckel T, et al. The NALP3 Inflammasome Is Involved in the Innate Immune Response to Amyloid-Beta. *Nat Immunol* (2008) 9:8–857-65. doi: 10.1038/ni.1636
54. Heneka MT, Kummer MP, Stutz A, Delekate A, Schwartz S, Vieira-Saecker A, et al. NLRP3 Is Activated in Alzheimer's Disease and Contributes to Pathology in APP/PS1 Mice. *Nature* (2013) 493:7434–674-8. doi: 10.1038/nature11729
55. Sutinen EM, Pirttila T, Anderson G, Salminen A, Ojala JO. Pro-Inflammatory Interleukin-18 Increases Alzheimer's Disease-Associated Amyloid-Beta Production in Human Neuron-Like Cells. *J Neuroinflamm* (2012) 9:199. doi: 10.1186/1742-2094-9-199
56. Luciunaite A, McManus RM, Jankunec M, Racz I, Dansokho C, Dalgediene I, et al. Soluble Abeta Oligomers and Protofibrils Induce NLRP3 Inflammasome Activation in Microglia. *J Neurochem* (2020) 155:6–650-661. doi: 10.1111/jnc.14945
57. Stancu IC, Cremers N, Vanrusselt H, Couturier J, Vanoosthuyse A, Kessels S, et al. Aggregated Tau Activates NLRP3-ASC Inflammasome Exacerbating Exogenously Seeded and Non-Exogenously Seeded Tau Pathology *In Vivo*. *Acta Neuropathol* (2019) 137:4–599-617. doi: 10.1007/s00401-018-01957-y
58. Aminzadeh M, Roghani M, Sarfallah A, Riazi GH. TRPM2 Dependence of ROS-Induced NLRP3 Activation in Alzheimer's Disease. *Int Immunopharmacol* (2018) 54:78–85. doi: 10.1016/j.intimp.2017.10.024
59. Lonnemann N, Hosseini S, Marchetti C, Skouras DB, Stefanoni D, D'Alessandro A, et al. The NLRP3 Inflammasome Inhibitor OLT1177 Rescues Cognitive Impairment in a Mouse Model of Alzheimer's Disease. *Proc Natl Acad Sci USA* (2020) 117:50–32145-32154. doi: 10.1073/pnas.2009680117
60. La Rosa F, Saresella M, Marventano I, Piancone F, Ripamonti E, Al-Daghri N, et al. Stavudine Reduces NLRP3 Inflammasome Activation and Modulates Amyloid-Beta Autophagy. *J Alzheimers Dis* (2019) 72:2–401-412. doi: 10.3233/JAD-181259
61. Yin J, Zhao F, Chojnacki JE, Fulp J, Klein WL, Zhang S, et al. NLRP3 Inflammasome Inhibitor Ameliorates Amyloid Pathology in a Mouse Model of Alzheimer's Disease. *Mol Neurobiol* (2018) 55:3–1977-1987. doi: 10.1007/s12035-017-0467-9
62. Saitoh T, Fujita N, Jang MH, Uematsu S, Yang BG, Satoh T, et al. Loss of the Autophagy Protein Atg16L1 Enhances Endotoxin-Induced IL-1beta Production. *Nature* (2008) 456:7219–264-8. doi: 10.1038/nature07383
63. Houtman J, Freitag K, Gimber N, Schmoranzer J, Heppner FL, Jendrach M. Beclin1-Driven Autophagy Modulates the Inflammatory Response of Microglia *via* NLRP3. *EMBO J* (2019) 38:4–. doi: 10.15252/embj.201899430
64. Zhou W, Xiao D, Zhao Y, Tan B, Long Z, Yu L, et al. Enhanced Autolysosomal Function Ameliorates the Inflammatory Response Mediated by the NLRP3 Inflammasome in Alzheimer's Disease. *Front Aging Neurosci* (2021) 13:629891:629891. doi: 10.3389/fnagi.2021.629891
65. Corder EH, Saunders AM, Strittmatter WJ, Schmechel DE, Gaskell PC, Small GW, et al. Gene Dose of Apolipoprotein E Type 4 Allele and the Risk of Alzheimer's Disease in Late Onset Families. *Science* (1993) 261:5123–921-3. doi: 10.1126/science.8346443
66. Rebeck GW, Reiter JS, Strickland DK, Hyman BT. Apolipoprotein E in Sporadic Alzheimer's Disease: Allelic Variation and Receptor Interactions. *Neuron* (1993) 11:4–575-80. doi: 10.1016/0896-6273(93)90070-8
67. Shinohara M, Kanekiyo T, Yang L, Linthicum D, Shinohara M, Fu Y, et al. APOE2 Eases Cognitive Decline During Aging: Clinical and Preclinical Evaluations. *Ann Neurol* (2016) 79:5–758-774. doi: 10.1002/ana.24628
68. Chen Y, Durakoglugil MS, Xian X, Herz J. ApoE4 Reduces Glutamate Receptor Function and Synaptic Plasticity by Selectively Impairing ApoE Receptor Recycling. *Proc Natl Acad Sci USA* (2010) 107:26–12011-6. doi: 10.1073/pnas.0914984107
69. Gosselin D, Skola D, Coufal NG, Holtman IR, Schlachetzki JCM, Sajti E, et al. An Environment-Dependent Transcriptional Network Specifies Human Microglia Identity. *Science* (2017) 356:6344–. doi: 10.1126/science.aal3222
70. Lin YT, Seo J, Gao F, Feldman HM, Wen HL, Penney J, et al. APOE4 Causes Widespread Molecular and Cellular Alterations Associated With Alzheimer's Disease Phenotypes in Human iPSC-Derived Brain Cell Types. *Neuron* (2018) 98:6–1141-1154 e7. doi: 10.1016/j.neuron.2018.05.008
71. Shi Y, Yamada K, Liddelow SA, Smith ST, Zhao L, Luo W, et al. ApoE4 Markedly Exacerbates Tau-Mediated Neurodegeneration in a Mouse Model of Tauopathy. *Nature* (2017) 549:7673–523-527. doi: 10.1038/nature24016
72. Franzmeier N, Suarez-Calvet M, Frontzkowski L, Moore A, Hohman TJ, Morenas-Rodriguez E, et al. Higher CSF Strem2 Attenuates ApoE4-Related Risk for Cognitive Decline and Neurodegeneration. *Mol Neurodegener* (2020) 15:1–57. doi: 10.1186/s13024-020-00407-2
73. Hollinger KR, Zhu X, Khoury ES, Thomas AG, Liaw K, Tallon C, et al. Glutamine Antagonist JHU-083 Normalizes Aberrant Hippocampal Glutaminase Activity and Improves Cognition in APOE4 Mice. *J Alzheimers Dis* (2020) 77:1–437-447. doi: 10.3233/JAD-190588
74. Wang C, Xiong M, Gratuze M, Bao X, Shi Y, Andhey PS, et al. Selective Removal of Astrocytic APOE4 Strongly Protects Against Tau-Mediated Neurodegeneration and Decreases Synaptic Phagocytosis by Microglia. *Neuron* (2021) 109:10–1657-1674 e7. doi: 10.1016/j.neuron.2021.03.024
75. Minhas PS, Latif-Hernandez A, McReynolds MR, Durairaj AS, Wang Q, Rubin A, et al. Restoring Metabolism of Myeloid Cells Reverses Cognitive Decline in Ageing. *Nature* (2021) 590:7844–122-128. doi: 10.1038/s41586-020-03160-0
76. Johansson JU, Woodling NS, Wang Q, Panchal M, Liang X, Trueba-Saiz A, et al. Prostaglandin Signaling Suppresses Beneficial Microglial Function in Alzheimer's Disease Models. *J Clin Invest* (2015) 125:1–350-64. doi: 10.1172/JCI77487
77. Weggen S, Eriksen JL, Das P, Sagi SA, Wang R, Pietrzik CU, et al. A Subset of NSAIDs Lower Amyloidogenic Abeta42 Independently of Cyclooxygenase Activity. *Nature* (2001) 414:6860–212-6. doi: 10.1038/35102591
78. Dinarello CA. Overview of the IL-1 Family in Innate Inflammation and Acquired Immunity. *Immunol Rev* (2018) 281:1–8-27. doi: 10.1111/imr.12621
79. Griffin WS, Stanley LC, Ling C, White L, MacLeod V, Perrot LJ, et al. Brain Interleukin 1 and S-100 Immunoreactivity are Elevated in Down Syndrome and Alzheimer Disease. *Proc Natl Acad Sci USA* (1989) 86:19–7611-5. doi: 10.1073/pnas.86.19.7611
80. Petrilli V, Dostert C, Muruve DA, Tschopp J. The Inflammasome: A Danger Sensing Complex Triggering Innate Immunity. *Curr Opin Immunol* (2007) 19:6–615-22. doi: 10.1016/j.coi.2007.09.002
81. Xu M, Zhang X, Ren F, Yan T, Wu B, Bi K, et al. Essential Oil of Schisandra Chinensis Ameliorates Cognitive Decline in Mice by Alleviating Inflammation. *Food Funct* (2019) 10:9–5827-5842. doi: 10.1039/c9fo00058e
82. Facci L, Barbierato M, Zusso M, Skaper SD, Giusti P. Serum Amyloid A Primes Microglia for ATP-Dependent Interleukin-1beta Release. *J Neuroinflamm* (2018) 15:1–164. doi: 10.1186/s12974-018-1205-6
83. Rivera-Escalera F, Pinney JJ, Owlett L, Ahmed H, Thakar J, Olschowka JA, et al. IL-1beta-Driven Amyloid Plaque Clearance Is Associated With an Expansion of Transcriptionally Reprogrammed Microglia. *J Neuroinflamm* (2019) 16:1–261. doi: 10.1186/s12974-019-1645-7
84. Quintanilla RA, Orellana DI, Gonzalez-Billault C, Maccioni RB. Interleukin-6 Induces Alzheimer-Type Phosphorylation of Tau Protein by Deregulating the Cdk5/P35 Pathway. *Exp Cell Res* (2004) 295:1–245-57. doi: 10.1016/j.yexcr.2004.01.002
85. Rose-John S. IL-6 Trans-Signaling *via* the Soluble IL-6 Receptor: Importance for the Pro-Inflammatory Activities of IL-6. *Int J Biol Sci* (2012) 8:9–1237-47. doi: 10.7150/ijbs.4989
86. Willis EF, MacDonald KPA, Nguyen QH, Garrido AL, Gillespie ER, Harley SBR, et al. Repopulating Microglia Promote Brain Repair in an IL-6-Dependent Manner. *Cell* (2020) 180:5–833-846 e16. doi: 10.1016/j.cell.2020.02.013
87. Zhang J, He H, Qiao Y, Zhou T, He H, Yi S, et al. Priming of Microglia With IFN-Gamma Impairs Adult Hippocampal Neurogenesis and Leads to Depression-Like Behaviors and Cognitive Defects. *Glia* (2020) 68:12–2674-2692. doi: 10.1002/glia.23878

88. Schilling S, Chausse B, Dikmen HO, Almouhanna F, Hollnagel JO, Lewen A, et al. TLR2- and TLR3-Activated Microglia Induce Different Levels of Neuronal Network Dysfunction in a Context-Dependent Manner. *Brain Behav Immun* (2021) 96:80–91. doi: 10.1016/j.bbi.2021.05.013
89. Egger F, Jakab M, Fuchs J, Oberascher K, Brachtl G, Ritter M, et al. Effect of Glycine on BV-2 Microglial Cells Treated With Interferon-Gamma and Lipopolysaccharide. *Int J Mol Sci* (2020) 21:3–. doi: 10.3390/ijms21030804
90. He Z, Yang Y, Xing Z, Zuo Z, Wang R, Gu H, et al. Intraperitoneal Injection of IFN-Gamma Restores Microglial Autophagy, Promotes Amyloid-Beta Clearance and Improves Cognition in APP/PS1 Mice. *Cell Death Dis* (2020) 11:6–440. doi: 10.1038/s41419-020-2644-4
91. Ren S, Yao W, Tambini MD, Yin T, Norris KA, D'Adamio L. Microglia TREM2(R47H) Alzheimer-Linked Variant Enhances Excitatory Transmission and Reduces LTP *via* Increased TNF-Alpha Levels. *Elife* (2020) 9e57513. doi: 10.7554/eLife.57513
92. Zhao J, O'Connor T, Vassar R. The Contribution of Activated Astrocytes to Abeta Production: Implications for Alzheimer's Disease Pathogenesis. *J Neuroinflamm* (2011) 8:150. doi: 10.1186/1742-2094-8-150
93. Jian M, Kwan JS, Bunting M, Ng RC, Chan KH. Adiponectin Suppresses Amyloid-Beta Oligomer (AbetaO)-Induced Inflammatory Response of Microglia *via* AdipoR1-AMPK-NF-kappaB Signaling Pathway. *J Neuroinflamm* (2019) 16:1–110. doi: 10.1186/s12974-019-1492-6
94. Mollazadeh H, Cicero AFG, Blesso CN, Pirro M, Majeed M, Sahebkar A. Immune Modulation by Curcumin: The Role of Interleukin-10. *Crit Rev Food Sci Nutr* (2019) 59:1–89-101. doi: 10.1080/10408398.2017.1358139
95. Maurya SK, Bhattacharya N, Mishra S, Bhattacharya A, Banerjee P, Senapati S, et al. Microglia Specific Drug Targeting Using Natural Products for the Regulation of Redox Imbalance in Neurodegeneration. *Front Pharmacol* (2021) 12:654489:654489. doi: 10.3389/fphar.2021.654489
96. Wang Y, Cella M, Mallinson K, Ulrich JD, Young KL, Robinette ML, et al. TREM2 Lipid Sensing Sustains the Microglial Response in an Alzheimer's Disease Model. *Cell* (2015) 160:6–1061-71. doi: 10.1016/j.cell.2015.01.049
97. Wang S, Mustafa M, Yuede CM, Salazar SV, Kong P, Long H, et al. Anti-Human TREM2 Induces Microglia Proliferation and Reduces Pathology in an Alzheimer's Disease Model. *J Exp Med* (2020) 217:9–. doi: 10.1084/jem.20200785
98. Kleinberger G, Yamanishi Y, Suarez-Calvet M, Czirr E, Lohmann E, Cuyvers E, et al. TREM2 Mutations Implicated in Neurodegeneration Impair Cell Surface Transport and Phagocytosis. *Sci Transl Med* (2014) 6:243–243ra86. doi: 10.1126/scitranslmed.3009093
99. Kwon YT, Ciechanover A. The Ubiquitin Code in the Ubiquitin-Proteasome System and Autophagy. *Trends Biochem Sci* (2017) 42:11–873-886. doi: 10.1016/j.tibs.2017.09.002
100. McQuade A, Kang YJ, Hasselmann J, Jairaman A, Sotelo A, Coburn M, et al. Gene Expression and Functional Deficits Underlie TREM2-Knockout Microglia Responses in Human Models of Alzheimer's Disease. *Nat Commun* (2020) 11:1–5370. doi: 10.1038/s41467-020-19227-5
101. Jay TR, Miller CM, Cheng PJ, Graham LC, Bemiller S, Broihier ML, et al. TREM2 Deficiency Eliminates TREM2+ Inflammatory Macrophages and Ameliorates Pathology in Alzheimer's Disease Mouse Models. *J Exp Med* (2015) 212:3–287-95. doi: 10.1084/jem.20142322
102. Zhao Y, Wu X, Li X, Jiang LL, Gui X, Liu Y, et al. TREM2 Is a Receptor for Beta-Amyloid That Mediates Microglial Function. *Neuron* (2018) 97:5–1023-1031 e7. doi: 10.1016/j.neuron.2018.01.031
103. Awatsuji H, Furukawa Y, Nakajima M, Furukawa S, Hayashi K. Interleukin-2 as a Neurotrophic Factor for Supporting the Survival of Neurons Cultured From Various Regions of Fetal Rat Brain. *J Neurosci Res* (1993) 35:3–305-11. doi: 10.1002/jnr.490350310
104. Alves S, Churlaud G, Audrain M, Michaelsen-Preusse K, Fol R, Souchet B, et al. Interleukin-2 Improves Amyloid Pathology, Synaptic Failure and Memory in Alzheimer's Disease Mice. *Brain* (2017) 140:3–826-842. doi: 10.1093/brain/aww330
105. Dansokho C, Ait Ahmed D, Aid S, Toly-Ndour C, Chaigneau T, Calle V, et al. Regulatory T Cells Delay Disease Progression in Alzheimer-Like Pathology. *Brain* (2016) 139:Pt 4–1237-51. doi: 10.1093/brain/awv408
106. Klatzmann D, Abbas AK. The Promise of Low-Dose Interleukin-2 Therapy for Autoimmune and Inflammatory Diseases. *Nat Rev Immunol* (2015) 15:5–283-94. doi: 10.1038/nri3823
107. Murray PJ, Allen JE, Biswas SK, Fisher EA, Gilroy DW, Goerdt S, et al. Macrophage Activation and Polarization: Nomenclature and Experimental Guidelines. *Immunity* (2014) 41:1–14-20. doi: 10.1016/j.immuni.2014.06.008
108. Boccardi V, Westman E, Pelini L, Lindberg O, Muehlboeck JS, Simmons A, et al. Differential Associations of IL-4 With Hippocampal Subfields in Mild Cognitive Impairment and Alzheimer's Disease. *Front Aging Neurosci* (2018) 10:439. doi: 10.3389/fnagi.2018.00439
109. Cherry JD, Olschowka JA, O'Banion MK. Arginase 1+ Microglia Reduce Abeta Plaque Deposition During IL-1beta-Dependent Neuroinflammation. *J Neuroinflamm* (2015) 12:203. doi: 10.1186/s12974-015-0411-8
110. Dionisio-Santos DA, Behrouzi A, Olschowka JA, O'Banion MK. Evaluating the Effect of Interleukin-4 in the 3xtg Mouse Model of Alzheimer's Disease. *Front Neurosci* (2020) 14:441. doi: 10.3389/fnins.2020.00441
111. Fiorentino DF, Bond MW, Mosmann TR. Two Types of Mouse T Helper Cell. IV. Th2 Clones Secrete a Factor That Inhibits Cytokine Production by Th1 Clones. *J Exp Med* (1989) 170:6–2081-95. doi: 10.1084/jem.170.6.2081
112. Hovsepian E, Penas F, Siffo S, Mirkin GA, Goren NB. IL-10 Inhibits the NF-kappaB and ERK/MAPK-Mediated Production of Pro-Inflammatory Mediators by Up-Regulation of SOCS-3 in Trypanosoma Cruzi-Infected Cardiomyocytes. *PloS One* (2013) 8:11–e79445. doi: 10.1371/journal.pone.0079445
113. Stewart CA, Metheny H, Iida N, Smith L, Hanson M, Steinhagen F, et al. Interferon-Dependent IL-10 Production by Tregs Limits Tumor Th17 Inflammation. *J Clin Invest* (2013) 123:11–4859-74. doi: 10.1172/JCI65180
114. Weston LL, Jiang S, Chisholm D, Jantzie LL, Bhaskar K. Interleukin-10 Deficiency Exacerbates Inflammation-Induced Tau Pathology. *J Neuroinflamm* (2021) 18:1–161. doi: 10.1186/s12974-021-02211-1
115. Proto JD, Doran AC, Gusarova G, Yurdagul AJr., Sozen E, Subramanian M, et al. Regulatory T Cells Promote Macrophage Efferocytosis During Inflammation Resolution. *Immunity* (2018) 49:4–666-677 e6. doi: 10.1016/j.immuni.2018.07.015
116. Fu AK, Hung KW, Yuen MY, Zhou X, Mak DS, Chan IC, et al. IL-33 Ameliorates Alzheimer's Disease-Like Pathology and Cognitive Decline. *Proc Natl Acad Sci USA* (2016) 113:19–E2705-13. doi: 10.1073/pnas.1604032113
117. Liew FY, Pitman NI, McInnes IB. Disease-Associated Functions of IL-33: The New Kid in the IL-1 Family. *Nat Rev Immunol* (2010) 10:2–103-10. doi: 10.1038/nri2692
118. Miyazono K, Katsuno Y, Koinuma D, Ehata S, Morikawa M. Intracellular and Extracellular TGF-Beta Signaling in Cancer: Some Recent Topics. *Front Med* (2018) 12:4–387-411. doi: 10.1007/s11684-018-0646-8
119. Butovsky O, Jedrychowski MP, Moore CS, Cialic R, Lanser AJ, Gabriely G, et al. Identification of a Unique TGF-Beta-Dependent Molecular and Functional Signature in Microglia. *Nat Neurosci* (2014) 17:1–131-43. doi: 10.1038/nn.3599
120. Musil R, Schwarz MJ, Riedel M, Dehning S, Cerovecki A, Spellmann I, et al. Elevated Macrophage Migration Inhibitory Factor and Decreased Transforming Growth Factor-Beta Levels in Major Depression–No Influence of Celecoxib Treatment. *J Affect Disord* (2011) 134:1–3-217-25. doi: 10.1016/j.jad.2011.05.047
121. Caraci F, Spampinato S, Sortino MA, Bosco P, Battaglia G, Bruno V, et al. Dysfunction of TGF-Beta1 Signaling in Alzheimer's Disease: Perspectives for Neuroprotection. *Cell Tissue Res* (2012) 347:1–291-301. doi: 10.1007/s00441-011-1230-6
122. Caraci F, Battaglia G, Busceti C, Biagioni F, Mastroiacovo F, Bosco P, et al. TGF-Beta 1 Protects Against Abeta-Neurotoxicity *via* the Phosphatidylinositol-3-Kinase Pathway. *Neurobiol Dis* (2008) 30:2–234-42. doi: 10.1016/j.nbd.2008.01.007
123. Huang WC, Yen FC, Shie FS, Pan CM, Shiao YJ, Yang CN, et al. TGF-Beta1 Blockade of Microglial Chemotaxis Toward Abeta Aggregates Involves SMAD Signaling and Down-Regulation of CCL5. *J Neuroinflamm* (2010) 7:28. doi: 10.1186/1742-2094-7-28
124. Xiao Y, Dai Y, Li L, Geng F, Xu Y, Wang J, et al. Tetrahydrocurcumin Ameliorates Alzheimer's Pathological Phenotypes by Inhibition of Microglial Cell Cycle Arrest and Apoptosis *via* Ras/ERK Signaling. *BioMed Pharmacother* (2021) 139:111651. doi: 10.1016/j.biopha.2021.111651
125. Goldstein JL, Ho YK, Basu SK, Brown MS. Binding Site on Macrophages That Mediates Uptake and Degradation of Acetylated Low Density

Lipoprotein, Producing Massive Cholesterol Deposition. *Proc Natl Acad Sci USA* (1979) 76:1–333-7. doi: 10.1073/pnas.76.1.333
126. Yang CN, Shiao YJ, Shie FS, Guo BS, Chen PH, Cho CY, et al. Mechanism Mediating Oligomeric Abeta Clearance by Naive Primary Microglia. *Neurobiol Dis* (2011) 42:3–221-30. doi: 10.1016/j.nbd.2011.01.005
127. Cornejo F, Vruwink M, Metz C, Munoz P, Salgado N, Poblete J, et al. Scavenger Receptor-A Deficiency Impairs Immune Response of Microglia and Astrocytes Potentiating Alzheimer's Disease Pathophysiology. *Brain Behav Immun* (2018) 69:336–50. doi: 10.1016/j.bbi.2017.12.007
128. Lu C, Hua F, Liu L, Ha T, Kalbfleisch J, Schweitzer J, et al. Scavenger Receptor Class-A has a Central Role in Cerebral Ischemia-Reperfusion Injury. *J Cereb Blood Flow Metab* (2010) 30:12–1972-81. doi: 10.1038/jcbfm.2010.59
129. Glatz JFC, Luiken J. Dynamic Role of the Transmembrane Glycoprotein CD36 (SR-B2) in Cellular Fatty Acid Uptake and Utilization. *J Lipid Res* (2018) 59:7–1084-1093. doi: 10.1194/jlr.R082933
130. van der Kant R, Langness VF, Herrera CM, Williams DA, Fong LK, Leestemaker Y, et al. Cholesterol Metabolism Is a Druggable Axis That Independently Regulates Tau and Amyloid-Beta in iPSC-Derived Alzheimer's Disease Neurons. *Cell Stem Cell* (2019) 24:3–363-375 e9. doi: 10.1016/j.stem.2018.12.013
131. PrabhuDas MR, Baldwin CL, Bollyky PL, Bowdish DME, Drickamer K, Febbraio M, et al. A Consensus Definitive Classification of Scavenger Receptors and Their Roles in Health and Disease. *J Immunol* (2017) 198:10–3775-3789. doi: 10.4049/jimmunol.1700373
132. Stewart CR, Stuart LM, Wilkinson K, van Gils JM, Deng J, Halle A, et al. CD36 Ligands Promote Sterile Inflammation Through Assembly of a Toll-Like Receptor 4 and 6 Heterodimer. *Nat Immunol* (2010) 11:2–155-61. doi: 10.1038/ni.1836
133. Yamanaka M, Ishikawa T, Griep A, Axt D, Kummer MP, Heneka MT. PPARgamma/RXRalpha-Induced and CD36-Mediated Microglial Amyloid-Beta Phagocytosis Results in Cognitive Improvement in Amyloid Precursor Protein/Presenilin 1 Mice. *J Neurosci* (2012) 32:48–17321-31. doi: 10.1523/JNEUROSCI.1569-12.2012
134. Wang CY, Wang ZY, Xie JW, Cai JH, Wang T, Xu Y, et al. CD36 Upregulation Mediated by Intranasal LV-NRF2 Treatment Mitigates Hypoxia-Induced Progression of Alzheimer's-Like Pathogenesis. *Antioxid Redox Signal* (2014) 21:16–2208-30. doi: 10.1089/ars.2014.5845
135. Fan H, Tang HB, Chen Z, Wang HQ, Zhang L, Jiang Y, et al. Inhibiting HMGB1-RAGE Axis Prevents Pro-Inflammatory Macrophages/Microglia Polarization and Affords Neuroprotection After Spinal Cord Injury. *J Neuroinflamm* (2020) 17:1–295. doi: 10.1186/s12974-020-01973-4
136. Son M, Oh S, Park H, Ahn H, Choi J, Kim H, et al. Protection Against RAGE-Mediated Neuronal Cell Death by sRAGE-Secreting Human Mesenchymal Stem Cells in 5xfad Transgenic Mouse Model. *Brain Behav Immun* (2017) 66:347–58. doi: 10.1016/j.bbi.2017.07.158
137. Paudel YN, Angelopoulou E, Piperi C, Othman I, Aamir K, Shaikh MF. Impact of HMGB1, RAGE, and TLR4 in Alzheimer's Disease (AD): From Risk Factors to Therapeutic Targeting. *Cells* (2020) 9:2–. doi: 10.3390/cells9020383
138. Ullah R, Ikram M, Park TJ, Ahmad R, Saeed K, Alam SI, et al. Vanillic Acid, a Bioactive Phenolic Compound, Counteracts LPS-Induced Neurotoxicity by Regulating C-Jun N-Terminal Kinase in Mouse Brain. *Int J Mol Sci* (2020) 22:1–. doi: 10.3390/ijms22010361
139. Chen J, Sun Z, Jin M, Tu Y, Wang S, Yang X, et al. Inhibition of AGEs/RAGE/Rho/ROCK Pathway Suppresses Non-Specific Neuroinflammation by Regulating BV2 Microglial M1/M2 Polarization Through the NF-kappaB Pathway. *J Neuroimmunol* (2017) 305:108–14. doi: 10.1016/j.jneuroim.2017.02.010
140. Criscuolo C, Fontebasso V, Middei S, Stazi M, Ammassari-Teule M, Yan SS, et al. Entorhinal Cortex Dysfunction Can Be Rescued by Inhibition of Microglial RAGE in an Alzheimer's Disease Mouse Model. *Sci Rep* (2017) 7:42370. doi: 10.1038/srep42370
141. Luo R, Su LY, Li G, Yang J, Liu Q, Yang LX, et al. Activation of PPARA-Mediated Autophagy Reduces Alzheimer Disease-Like Pathology and Cognitive Decline in a Murine Model. *Autophagy* (2020) 16:1–52-69. doi: 10.1080/15548627.2019.1596488
142. Ji J, Xue TF, Guo XD, Yang J, Guo RB, Wang J, et al. Antagonizing Peroxisome Proliferator-Activated Receptor Gamma Facilitates M1-To-M2 Shift of Microglia by Enhancing Autophagy *via* the LKB1-AMPK Signaling Pathway. *Aging Cell* (2018) 17:4–e12774. doi: 10.1111/acel.12774
143. Zhang W, Feng C, Jiang H. Novel Target for Treating Alzheimer's Diseases: Crosstalk Between the Nrf2 Pathway and Autophagy. *Ageing Res Rev* (2021) 65:101207. doi: 10.1016/j.arr.2020.101207
144. Frias DP, Gomes RLN, Yoshizaki K, Carvalho-Oliveira R, Matsuda M, Junqueira MS, et al. Nrf2 Positively Regulates Autophagy Antioxidant Response in Human Bronchial Epithelial Cells Exposed to Diesel Exhaust Particles. *Sci Rep* (2020) 10:1–3704. doi: 10.1038/s41598-020-59930-3
145. Heckmann BL, Teubner BJW, Tummers B, Boada-Romero E, Harris L, Yang M, et al. LC3-Associated Endocytosis Facilitates Beta-Amyloid Clearance and Mitigates Neurodegeneration in Murine Alzheimer's Disease. *Cell* (2019) 178:3–536-551 e14. doi: 10.1016/j.cell.2019.05.056
146. Wang N, Wang H, Li L, Li Y, Zhang R. Beta-Asarone Inhibits Amyloid-Beta by Promoting Autophagy in a Cell Model of Alzheimer's Disease. *Front Pharmacol* (2019) 10:1529:1529. doi: 10.3389/fphar.2019.01529
147. Tang RH, Qi RQ, Liu HY. Interleukin-4 Affects Microglial Autophagic Flux. *Neural Regener Res* (2019) 14:9–1594-1602. doi: 10.4103/1673-5374.255975
148. Lee YS, Gupta DP, Park SH, Yang HJ, Song GJ. Anti-Inflammatory Effects of Dimethyl Fumarate in Microglia *via* an Autophagy Dependent Pathway. *Front Pharmacol* (2021) 12:612981:612981. doi: 10.3389/fphar.2021.612981
149. Kurochkin IV, Guarnera E, Berezovsky IN. Insulin-Degrading Enzyme in the Fight Against Alzheimer's Disease. *Trends Pharmacol Sci* (2018) 39:1–49-58. doi: 10.1016/j.tips.2017.10.008
150. Farris W, Mansourian S, Leissring MA, Eckman EA, Bertram L, Eckman CB, et al. Partial Loss-of-Function Mutations in Insulin-Degrading Enzyme That Induce Diabetes Also Impair Degradation of Amyloid Beta-Protein. *Am J Pathol* (2004) 164:4–1425-34. doi: 10.1016/s0002-9440(10)63229-4
151. Leissring MA, Farris W, Chang AY, Walsh DM, Wu X, Sun X, et al. Enhanced Proteolysis of Beta-Amyloid in APP Transgenic Mice Prevents Plaque Formation, Secondary Pathology, and Premature Death. *Neuron* (2003) 40:6–1087-93. doi: 10.1016/s0896-6273(03)00787-6
152. Istvan ES, Deisenhofer J. Structural Mechanism for Statin Inhibition of HMG-CoA Reductase. *Science* (2001) 292:5519–1160-4. doi: 10.1126/science.1059344
153. Tamboli IY, Barth E, Christian L, Siepmann M, Kumar S, Singh S, et al. Statins Promote the Degradation of Extracellular Amyloid {Beta}-Peptide by Microglia *via* Stimulation of Exosome-Associated Insulin-Degrading Enzyme (IDE) Secretion. *J Biol Chem* (2010) 285:48–37405-14. doi: 10.1074/jbc.M110.149468
154. Tundo GR, Di Muzio E, Ciaccio C, Sbardella D, Di Pierro D, Polticelli F, et al. Multiple Allosteric Sites Are Involved in the Modulation of Insulin-Degrading-Enzyme Activity by Somatostatin. *FEBS J* (2016) 283:20–3755-3770. doi: 10.1111/febs.13841
155. Lv Z, Guo Y. Metformin and Its Benefits for Various Diseases. *Front Endocrinol (Lausanne)* (2020) 11:191:191. doi: 10.3389/fendo.2020.00191
156. Lu XY, Huang S, Chen QB, Zhang D, Li W, Ao R, et al. Metformin Ameliorates Abeta Pathology by Insulin-Degrading Enzyme in a Transgenic Mouse Model of Alzheimer's Disease. *Oxid Med Cell Longev* (2020) 2020:2315106. doi: 10.1155/2020/2315106
157. Cui W, Sun C, Ma Y, Wang S, Wang X, Zhang Y. Inhibition of TLR4 Induces M2 Microglial Polarization and Provides Neuroprotection *via* the NLRP3 Inflammasome in Alzheimer's Disease. *Front Neurosci* (2020) 14:444:444. doi: 10.3389/fnins.2020.00444
158. Yang X, Xu S, Qian Y, Xiao Q. Resveratrol Regulates Microglia M1/M2 Polarization *via* PGC-1alpha in Conditions of Neuroinflammatory Injury. *Brain Behav Immun* (2017) 64:162–72. doi: 10.1016/j.bbi.2017.03.003
159. Kim S, Chung H, Ngoc Mai H, Nam Y, Shin SJ, Park YH, et al. Low-Dose Ionizing Radiation Modulates Microglia Phenotypes in the Models of Alzheimer's Disease. *Int J Mol Sci* (2020) 21:12–. doi: 10.3390/ijms21124532
160. Zhou X, Chu X, Xin D, Li T, Bai X, Qiu J, et al. L-Cysteine-Derived H2S Promotes Microglia M2 Polarization *via* Activation of the AMPK Pathway in Hypoxia-Ischemic Neonatal Mice. *Front Mol Neurosci* (2019) 12:58. doi: 10.3389/fnmol.2019.00058

161. Li C, Zhang C, Zhou H, Feng Y, Tang F, Hoi MPM, et al. Inhibitory Effects of Betulinic Acid on LPS-Induced Neuroinflammation Involve M2 Microglial Polarization *via* CaMKKbeta-Dependent AMPK Activation. *Front Mol Neurosci* (2018) 11:98:98. doi: 10.3389/fnmol.2018.00098
162. He T, Li W, Song Y, Li Z, Tang Y, Zhang Z, et al. Sestrin2 Regulates Microglia Polarization Through mTOR-Mediated Autophagic Flux to Attenuate Inflammation During Experimental Brain Ischemia. *J Neuroinflamm* (2020) 17:1–329. doi: 10.1186/s12974-020-01987-y
163. Xu Y, Cui K, Li J, Tang X, Lin J, Lu X, et al. Melatonin Attenuates Choroidal Neovascularization by Regulating Macrophage/Microglia Polarization *via* Inhibition of RhoA/ROCK Signaling Pathway. *J Pineal Res* (2020), 69(1): e12660.doi: 10.1111/jpi.12660
164. Li QQ, Ding DH, Wang XY, Sun YY, Wu J. Lipoxin A4 Regulates Microglial M1/M2 Polarization After Cerebral Ischemia-Reperfusion Injury *via* the Notch Signaling Pathway. *Exp Neurol* (2021) 339:113645. doi: 10.1016/j.expneurol.2021.113645
165. Jin J, Guo J, Cai H, Zhao C, Wang H, Liu Z, et al. M2-Like Microglia Polarization Attenuates Neuropathic Pain Associated With Alzheimer's Disease. *J Alzheimers Dis* (2020) 76:4–1255-1265. doi: 10.3233/JAD-200099
166. Duan CM, Zhang JR, Wan TF, Wang Y, Chen HS, Liu L. SRT2104 Attenuates Chronic Unpredictable Mild Stress-Induced Depressive-Like Behaviors and Imbalance Between Microglial M1 and M2 Phenotypes in the Mice. *Behav Brain Res* (2020) 378:112296. doi: 10.1016/j.bbr.2019.112296

Conflict of Interest: The authors declare that the research was conducted in the absence of any commercial or financial relationships that could be construed as a potential conflict of interest.

Publisher's Note: All claims expressed in this article are solely those of the authors and do not necessarily represent those of their affiliated organizations, or those of the publisher, the editors and the reviewers. Any product that may be evaluated in this article, or claim that may be made by its manufacturer, is not guaranteed or endorsed by the publisher.

frontiers | Frontiers in Immunology

ORIGINAL RESEARCH
published: 03 May 2022
doi: 10.3389/fimmu.2022.870029

Acutely Inhibiting AQP4 With TGN-020 Improves Functional Outcome by Attenuating Edema and Peri-Infarct Astrogliosis After Cerebral Ischemia

Chengfeng Sun[1†], Luyi Lin[1†], Lekang Yin[2], Xiaozhu Hao[1], Jiaqi Tian[3], Xiaoxue Zhang[4], Yan Ren[1], Chanchan Li[1*] and Yanmei Yang[1*]*

[1] Department of Radiology, Huashan Hospital, Fudan University, Shanghai, China, [2] Department of Radiology, Zhongshan Hospital, Fudan University, Shanghai, China, [3] Department of Radiology, Renji Hospital, Shanghai Jiao Tong University, Shanghai, China, [4] Department of Radiotherapy, Shanghai Eastern Hepatobiliary Surgery Hospital, Shanghai, China

OPEN ACCESS

Edited by:
Juehua Yu,
The First Affiliated Hospital of Kunming Medical University, China

Reviewed by:
Enquan Xu,
Duke University, United States
Kundlik Gadhave,
Johns Hopkins University, United States
Xiuli Yang,
Johns Hopkins Medicine, United States

***Correspondence:**
Yan Ren
renyan_richard@aliyun.com
Chanchan Li
11111220032@fudan.edu.cn
Yanmei Yang
yym9876@sohu.com

[†]These authors have contributed equally to this work

Specialty section:
This article was submitted to Multiple Sclerosis and Neuroimmunology, a section of the journal Frontiers in Immunology

Received: 05 February 2022
Accepted: 11 April 2022
Published: 03 May 2022

Citation:
Sun C, Lin L, Yin L, Hao X, Tian J, Zhang X, Ren Y, Li C and Yang Y (2022) Acutely Inhibiting AQP4 With TGN-020 Improves Functional Outcome by Attenuating Edema and Peri-Infarct Astrogliosis After Cerebral Ischemia. Front. Immunol. 13:870029. doi: 10.3389/fimmu.2022.870029

Background: Ischemic stroke is one of the leading causes of human death and disability. Brain edema and peri-infarct astrocyte reactivity are crucial pathological changes, both involving aquaporin-4 (AQP4). Studies revealed that acute inhibition of AQP4 after stroke diminishes brain edema, however, its effect on peri-infarct astrocyte reactivity and the subacute outcome is unclear. And if diffusion-weighted imaging (DWI) could reflect the AQP4 expression patterns is uncertain.

Methods: Rats were subjected to middle cerebral artery occlusion (MCAO) and allocated randomly to TGN 020-treated and control groups. One day after stroke, brain swelling and lesion volumes of the rats were checked using T2-weighted imaging (T2-WI). Fourteen days after stroke, the rats successively underwent neurological examination, T2-WI and DWI with standard b-values and ultra-high b-values, apparent diffusion coefficient (ADC) was calculated correspondingly. Finally, the rats' brains were acquired and used for glial fibrillary acidic protein (GFAP) and AQP4 immunoreactive analysis.

Results: At 1 day after stroke, the TGN-020-treated animals exhibited reduced brain swelling and lesion volumes compared with those in the control group. At 14 days after stroke, the TGN-020-treated animals showed fewer neurological function deficits and smaller lesion volumes. In the peri-infarct region, the control group showed evident astrogliosis and AQP4 depolarization, which were reduced significantly in the TGN-020 group. In addition, the ultra-high b-values of ADC (ADCuh) in the peri-infarct region of the TGN-020 group was higher than that of the control group. Furthermore, correlation analysis revealed that peri-infarct AQP4 polarization correlated negatively with astrogliosis extent, and ADCuh correlated positively with AQP4 polarization.

Conclusion: We found that acutely inhibiting AQP4 using TGN-020 promoted neurological recovery by diminishing brain edema at the early stage and attenuating peri-infarct astrogliosis and AQP4 depolarization at the subacute stage after stroke. Moreover, ADCuh could reflect the AQP4 polarization.

Keywords: ischemic stroke, astrogliosis, AQP4 polarization, glymphatic system, ultra-high b-values diffusion weighted imaging

INTRODUCTION

Ischemic stroke is a leading cause of death and disability in humans, with few pathophysiological therapies other than recanalizing occluded blood vessels (1, 2). Acutely inhibiting aquaporin-4 (AQP4) was proposed recently as a promising new pathophysiological therapy targeting central nervous system (CNS) edema post-injury (3, 4). Because water transportation through AQP4 is a passive process, depending on osmotic gradients. AQP4 contributes to the formation of cellular toxic edema at first, but it is also essential for the resolution of vasogenic edema in CNS injury. And studies revealed that AQP4 deficient animals displayed higher levels of CNS water content than control animals at a later phase of CNS injury (5). AQP4 is the most abundant aquaporins in the brain, it has a polarized distribution tendency on the astrocyte endfeet facing vessels under physiological conditions, this distribution tendency is critical for the formation and resolution of edema, and clearance of interstitial solutes in the brain (6). Commonly, methods of inhibiting AQP4 mainly include gene knockout, small interfering RNA, heavy metal ions, and small molecule inhibitors (7). Small molecule inhibitors have the potential to be applied in clinical for their security. N-(1,3,4-thiadiazol-2-yl) pyridine-3-carboxamide dihydrochloride (TGN-020) is one of them and has been proven to inhibit AQP4 *in vitro* and *in vivo via* the intracellular ubiquitin-proteasome system (8, 9).

AQP4 is implicated not only in edema formation and resolution, but also in astrocyte migration and astrogliosis (10, 11). However, the changes in peri-infarct astrocyte reactivity related to acute inhibition of AQP4 have not been clarified, which are crucial for peri-infarct tissue repair and neurological function recovery. After stroke, reactive astrogliosis and loss of perivascular AQP4 polarization occur and persist for long time in the peri-infarct area (12–14). Reactive astrogliosis is beneficial for limiting the infarct territory initially; however, its increasing dysregulation at the recovery stage accentuates inflammation and inhibits axon regeneration, thus interfering with long-term sensorimotor functional recovery (15, 16). Besides, loss of AQP4 polarization impairs the glymphatic system, a newly-discovered waste clearance system in the brain (17), causing toxic protein deposition and cognitive deficits (18, 19). Modulating reactive astrogliosis and the loss of AQP4 polarization in the peri-infarct area might be beneficial therapeutic strategies during later stages to promote neurological function recovery.

In this study, we acutely inhibited AQP4 using TGN-020 in transient middle cerebral artery occlusion (MCAO) rats, evaluated the brain edema and infarct volume at 1 and 14 days, and the peri-infarct astrogliosis extent, AQP4 expression patterns, and neurological function at 14 days after MCAO. In addition, we analyzed correlations of the AQP4 expression patterns and the ultra-high b-values apparent diffusion coefficient (ADCuh). We aimed to investigate the effect of acutely inhibiting AQP4 on peri-infarct astrocyte reactivity and subacute outcome and the feasibility of ADC to reflect the expression patterns of AQP4.

MATERIAL AND METHODS

Animals

This experiment was approved by the Fudan University Institutional Animal Care and Use Committee. A total of 16 adult (260–280 g) Sprague–Dawley rats (Charles River Laboratories, Beijing, China) were used in this experiment. They were maintained under an automatically controlled 12 h light–dark cycle, with freely accessible food and water. After fasting for 1 day, the rats were subjected to 90 min of MCAO and then allocated randomly to the TGN-020 treated group or the control group (n = 8 per group). The ischemic lesion and edema volume were checked by MRI 1 d post-stroke. At 14 days post-stroke, neurological function, MRI, and histology features were evaluated in turn. One rat in the TGN-020-treated group and three rats in the control group died from severe ischemic stroke. Finally, six rats of each group were included in the data analysis.

Surgical Procedure and Treatment

For all rats, the left middle cerebral artery was occluded by the same researcher as in our previous study (20). Specifically, the anesthetized rats were immobilized in a supine position using a tooth holder and all limbs were tied up. A skin incision was made in the midline of the neck, and the muscle and fascia were separated to expose the left internal carotid artery (ICA), external carotid artery, and common carotid artery. Then, a poly L-lysine coated nylon filament (2634A4, Cinontech Co. Ltd., Beijing, China) was inserted into the left ICA to block blood flow to the MCA. The TGN-020 treated group was administrated intraperitoneally with TGN-020 (200 mg/kg) at 10 minutes after successful occlusion. The control group was given the same volume of 0.9% normal saline at the same timepoint. After occlusion for 90 minutes, the filament was withdrawn gently to allow reperfusion under anesthesia.

MRI and Quantitative Analysis

The MRI images were captured using a 3.0T horizontal magnet (Discovery MR750, GE Medical Systems, Milwaukee, WI, USA) with a 60-mm-diameter gradient coil (Magtron Inc., Jiangyin, China). Anesthetized rats were scanned in the prone position, with continuous monitoring of their temperature, heart rate, and respiration. The main scan parameters were as follows: For fast spin echo T2-weighted imaging, repetition time (TR)/echo time (TE) = 4000 ms/96 ms, field of view (FOV) = 6 cm × 6 cm, matrix = 256 × 256, slice thickness = 1.8 mm, interslice distance = 2 mm, number of slices = 15. For ultra-high diffusion-weighted imaging (DWIuh), TR/TE = 3000/minimum, FOV = 6 cm × 6 cm, slice thickness = 1.8 mm, interslice distance = 2 mm, number of slices = 15, b values = 2000, 2500, 3000, 3500, 4000, and 4500 s/mm^2. Standard DWI (DWIst) was performed with the same parameters as DWIuh, except that the b values = 0, 800 s/mm^2. T2-WI was scanned at 1 day and 14 days post-stroke, while DWIst and DWIuh were scanned at 14 days post-stroke.

All MRI data were processed and measured on the GE ADW4.6 workstation using Functool software, and DWI images were processed to generate ADC maps. The ischemic lesion volume was calculated as percentage of hemispheric lesion

volume (%HLV) after correction of hemispheric space-occupying effects, according to methods proposed by Gerriets et al. (21). The percentage of brain swelling volume (%BSV) was used to quantitatively evaluate the extent of brain swelling. The specific equations used are as follows:

$$\%\,\mathrm{HLV} = \left\{ \begin{array}{r} [\text{contralateral hemisphere volume} - \\ (\text{ipsilateral hemisphere volume} - \text{infarct volume})] \\ /\text{contralateral hemisphere volume} \end{array} \right\} \times 100$$

$$\%\,\mathrm{BSV} = \left(\begin{array}{l} \text{ipsilateral hemisphere volume}/ \\ \text{contralateral hemisphere volume} \end{array} \right) \times 100.$$

Imaging artifacts increase when the b-values rise, especially in the cortical region, thus the estimation of ADCuh was only carried out in the peri-infarct striatum. Equivalent regions of interest (ROIs) were drawn in the peri-infarct striatum and corresponding contralateral area on ADCuh maps. The ratio of ipsilateral ADCuh to contralateral ADCuh was used for comparisons between groups.

Sensorimotor and Cognitive Function Examination

A neurological behavior scale of 0 to 20 scores was used to assess the sensorimotor function of the rats, as in our previous study (22). Higher scores represent more neurological deficits. The Y-maze was used to test the spatial working memory of the rats, based on the inherent characterization of rats to explore a novel environment without the need to learn skills. The maze is consisted of three identical arms (50 cm × 16 cm × 32 cm), and the angle between each arm was 120°. Rats were placed at the end of the initial arm and were allowed to explore freely for 5 minutes. The sequence and total number of arm entries were recorded using a video camera. Entrance into different arms for three consecutive times was recorded as a correct alternating response. Rodents with impaired working memory could not memorize which arm was just visited and thus had lower spontaneous alternation rates. Correct alternating response times were counted, and the spontaneous alternation rate was calculated using the following equation:

$$\text{Spontaneous alternation rate} = [\text{correct alternating response times}/(\mathrm{N}-2)] \times 100\,\%,\ \text{where N is the total number of arm entries}.$$

Immunofluorescence Staining and Quantitative Analysis

Rats were perfused with phosphate buffer, followed by 4% paraformaldehyde, and then their brains were removed and postfixed overnight at 4°C. After dehydration, wax leaching, embedding, and slicing, three serial coronary brain sections (thickness: 5 μm) for each animal were obtained at approximately 0.24 mm relative to the bregma, according to the atlas reported by Paxinos and Watson (2005). Well preserved sections were picked and immunostained using anti-glial fibrillary acidic protein (GFAP, 1:1000, Abcam, Cambridge, MA, USA) and anti-AQP4 (1:1000, Abcam) antibodies. Alexa Fluor 488- and 568-conjugated donkey anti-rabbit and anti-mouse antibodies (1:1000, Abcam) were used as secondary antibodies. Finally, the sections were incubated with 4′,6-diamidino-2-phenylindole, dihydrochloride (DAPI, 1: 1000; Sigma-Aldrich, St. Louis, MO, USA).

Immunofluorescence sections were scanned using a Vslide scanning microscope (Nikon, Chiyoda, Tokyo, Japan) with a ×20 primary objective. All images were acquired using constant scanning settings, and further semi-quantitatively analyzed to characterize the expression patterns of AQP4 and GFAP using Image J (National Institutes of Health, Bethesda, MD, USA).

To evaluate AQP4 expression and polarization in the peri-infarct area, the mean fluorescence intensity of AQP4 emission channels was measured, and AQP4 polarization was calculated as the ratio of the low-threshold AQP4-positive area to the high-threshold AQP4 positive area (23). The percentage of GFAP immunostained area of the ROIs (GFAP area%) was used to analyze reactive astrogliosis. ROIs (600 μm × 300 μm) were placed in the peri-infarct cortex and striatum separately for analysis. Immunostained sections that had similar lesion morphologies and anatomical structures to those in the ADCuh images were picked for analysis, and ROIs in the peri-infarct striatum were placed according to those ROIs placed in the ADCuh images. All histological data were normalized by contralateral values and were calculated twice to minimize measurement error.

Statistical Analysis

All data were presented as the mean ± the standard deviation (SD), $P < 0.05$ was considered to be statistically significant. One-way analysis of variance (ANOVA) and *post hoc* least significant difference (LSD) tests were used to compare differences among groups. Pearson Product correlation analysis was performed to analyze correlations. The above data analyses were carried out using GraphPad Prism, version 8.0 (GraphPad Software Inc., La Jolla, CA, USA).

RESULTS

T2-WI Revealed That Acute Inhibition of AQP4 Decreased Edema and the Infarct Volume

Ischemic lesion volume and brain swelling extent of the rats were derived from T2-WI at 1 day and 14 days post stroke (**Figure 1**). One day post stroke, the TGN-020-treated group presented significantly decreased infarct and swelling volumes (%HLV: 39.05 ± 6.43, %BSV: 111.98 ± 7.18), compared with those of the control group (%HLV: 57.94 ± 6.68, %BSV: 129.32 ± 4.69). Fourteen days later, the ischemic lesion volume and brain

swelling extent of both groups had decreased. The TGN-020-treated group had a smaller infarct volume (%HLV: 24.30 ± 1.88) than that of control group (%HLV: 45.25 ± 3.11). Regarding the extent of brain swelling, no significant difference was found between two groups. Our results showed a 67% smaller lesion volume with 86% less swelling in TGN-020-treated rats compared with those of the control rats at 1 day-post stroke (both $P < 0.01$), and a 53% smaller lesion volume at 14 days ($P < 0.001$).

Acute Inhibition of AQP4 Ameliorated Neurological Deficits

At fourteen days post stroke, the sensorimotor function of the rats was evaluated using the behavior scale. Significantly fewer sensorimotor deficits were observed in the TGN-020-treated group ($P < 0.001$ *vs*. the control group). Spatial working memory was assessed using Y maze spontaneous alternation, in which the TGN-020-treated group showed a superior cognition performance compared with that of the control group ($P < 0.001$) (**Figure 2**).

Acutely Inhibiting AQP4 Ameliorated Peri-Infarct Astrogliosis and Loss of AQP4 Polarization

In the peri-infarct cortex and striatum, the TGN-020-treated group showed fewer and smaller astrocytes than those in the control group. AQP4 in the control group was located diffusely on the neuropil, while AQP4 in the TGN-020-treated group was distributed mainly in the perivascular district, which is close to the polarized distribution under normal conditions. Corresponding immunofluorescence images of each group are shown in **Figure 3**. Quantitively, in the peri-infarct area, the TGN-020-treated group exhibited smaller cortical and striatal GFAP area (7.57 ± 2.18 and 10.72 ± 2.32, respectively) than those of the control group (both $P < 0.001$). The AQP4 expression intensity (the AQP4 mean fluorescence intensity) of the two groups were similar ($P > 0.05$). The cortical and striatal AQP4 polarizations of the TGN-020-treated group were higher than those of the control group (cortex: 0.78 ± 0.06 in TGN-020-treated group *vs*. 0.48 ± 0.09 in the control group, $P < 0.01$; striatum: AQP4 polarization: 0.75 ± 0.07 in TGN-020-treated group *vs*. 0.43 ± 0.15

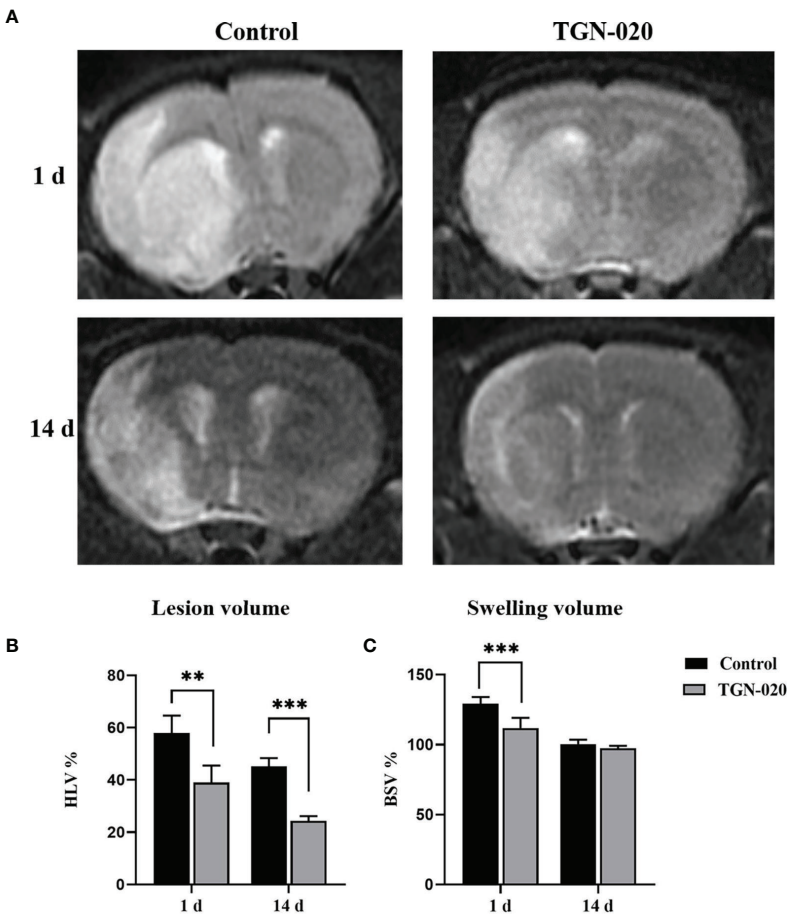

FIGURE 1 | Comparison of ischemic lesion volumes and brain swelling volumes between groups. **(A)** Representative T2-WI images of rats in the TGN-020-treated and control groups at 1 day and 14 days post-stroke. **(B)** The ischemic Lesion volumes of each group at 1 day and 14 days post-stroke. **(C)** The brain swelling volumes of each group at 1 day and 14 days post-stroke. $^{**}P < 0.01$, $^{***}P < 0.001$.

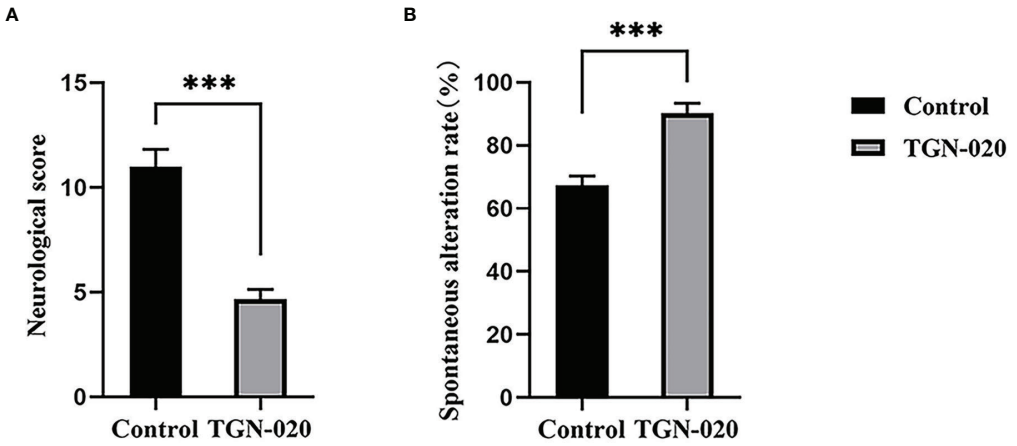

FIGURE 2 | TGN-020-treated rats showed improved neurological function. **(A)** Comparison of neurological scores between groups revealed fewer sensorimotor deficits in the TGN-020 treated rats compared with those in the control rats. **(B)** Comparison of spatial working memory by spontaneous alternation in the Y maze showed that the TGN-020 treated rats had better cognitive function than the control rats. ***$P < 0.001$.

in the control group, $P < 0.001$). Further correlation analysis showed that peri-infarct AQP4 polarization correlated negatively with the astrogliosis area ($r = -0.72$, $P < 0.01$).

Relationship of the ADCuh With AQP4 Expression Patterns

On the standard ADC (ADCst) maps, there were no evident signal differences between the peri-infarct area and contralateral hemisphere in all rats, while on the ADCuh maps, the peri-infarct area appeared as dark rings surrounding the ischemic core in the two groups of rats (**Figure 4**). The ratio of the ipsilateral to contralateral ADC was used for group comparison, and was only analyzed in the striatum for restriction of ADCuh map's artifacts. No significant difference in ADCst was found between the TGN-020-treated group and the control group ($P > 0.05$), while the TGN-020-treated group had a slightly but significantly increased ADCuh (0.78 ± 0.04) compared with that of the control group (0.73 ± 0.03, $P < 0.05$).

Both groups of rats showed reactive astrogliosis and loss of AQP4 polarization in the peri-infarct area, in which the ADCuh decreased concurrently (**Figure 4**). Further correlation analysis showed that the peri-infarct ADCuh correlated positively with AQP4 polarization ($r = 0.64$, $P < 0.05$), but had no statistical correlation with the AQP4 mean fluorescence intensity ($r = 0.03$, $P = 0.92$).

DISCUSSION

In the present study, acute inhibition of AQP4 using TGN-020 decreased the edema and infarct lesion volume 1day post-stroke, attenuated peri-infarct astrogliosis, AQP4 depolarization, and infarct lesion volume, promoting neurological recovery at 14 days post-stroke. Additionally, we found that AQP4 polarization correlated negatively with astrogliosis, and ADCuh could reflect the AQP4 polarization.

Our results showed that acute inhibition of AQP4 by TGN-020 reduced brain edema 1day post-stroke, which is consistent with previous research (24, 25). Traditionally, it is thought that post-stroke edema comprises cytotoxic edema and vasogenic edema, in which AQP4 plays inductive and counteractive roles, respectively, with edematous fluid mainly coming from blood plasma (26, 27). However, recently, researchers found that cerebrospinal fluid immediately flowed towards the brain parenchyma through the influx pathway of the glymphatic system after ischemic stroke, and an absence of AQP4 reduced the cerebrospinal fluid influx significantly (4, 28). Regardless, the traditional or newly-found mechanism of edema both suggest that acute inhibition of AQP4 could reduce post-stroke edema at the early stage (29, 30). However, perivascular AQP4 is essential for the dissipation of vasogenic edema and the glymphatic clearance of Aβ and tau (8, 9). The deficiency of AQP4 would cause the accumulation of water and neurotoxic protein in the recovery stage of CNS injury (3, 31). In this study, we further investigated the peri-infarct expression patterns of AQP4 14 days after acute inhibition of AQP4. No differences in AQP4 expression intensity were found between the TGN-020 group and the control group, but AQP4 polarization of the TGN-020 group was higher than that of the control group, in other words, the perivascular AQP4 was increased in the TGN-020 group when compared with the control group. As is shown in our study, swelling extent of the ipsilateral hemisphere has turned to normal in both groups 14 days post stroke. These AQP4 might not contribute to water transmembrane diffusivity, but play roles in neurotoxic waste elimination. Researchers found that toxic molecules present in the area of liquefactive necrosis can leak across the glial scar and were removed by the glymphatic system in peri-infarct tissue (32). So, it can be inferred that the higher AQP4 polarization of the TGN-020 group is beneficial for glymphatic clearance and neurological recovery.

For ischemic stroke and other multiple CNS diseases, peri-infarct reactive astrogliosis is usually accompanied by loss of

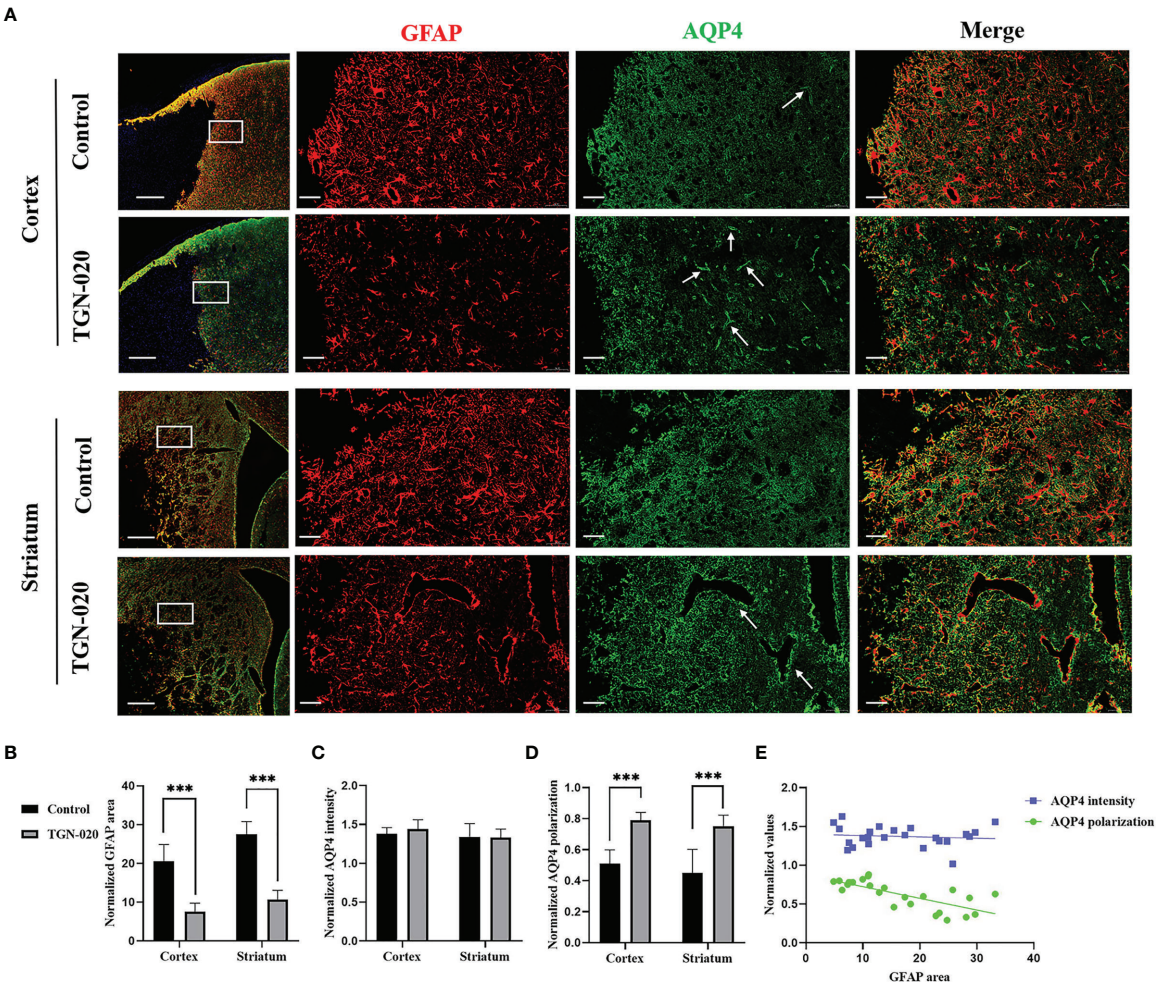

FIGURE 3 | Peri-infarct astrogliosis and AQP4 expression patterns in the two groups of rats. **(A)** Immunostaining of GFAP (red) and AQP4 (green) in the peri-infarct cortex and striatum in TGN-020- treated rats and control rats. White boxes in the first column indicate the ROIs used for GFAP and AQP4 analysis. The arrows show AQP4 located in the perivascular region. Scale bars = 500 and 50 μm. **(B–D)** Comparisons of GFAP-positive area and AQP4 expression patterns in the peri-infarct cortex and striatum between the two groups. **(E)** Correlations between peri-infarct AQP4 expression patterns and the extent of astrogliosis. ***$P < 0.001$.

AQP4 polarization in the same area (23, 33–35). Our experiment showed that the polarization of AQP4 correlated negatively with the astrogliosis area, indicating that the astrogliosis extent might affect the polarization of AQP4. The close relationship between astrogliosis and AQP4 polarization was also discovered in rodent models of traumatic brain injury and multiple microinfarcts, though needing further investigations to determine the underlying mechanisms. Some researchers regard the loss of AQP4 polarization as an important feature of reactive astrocytes rather than a pathological consequence of endfeet damage (34, 36). We consider that the decreased astrogliosis after acute inhibition of AQP4 might contribute to the preservation of AQP4 polarization.

The reactive astrogliosis that occurs after ischemic stroke is extremely complex and incompletely understood, playing both detrimental and beneficial roles on neurological recovery (37–39). Some studies found that reactive astrocyte was beneficial for vascular repair and axonal regrowth after CNS injury (40, 41), while other studies revealed that reactive astrocyte could restrict neural repair by expressing growth inhibitory factors and forming glial scars (42). These contradictory roles of reactive astrocytes may be due to different reactive phenotypes induced by injury (43, 44). The reactive astrocytes in neuroinflammation of ischemia could be classified into A1s and A2s, which exert different functions (45, 46). The A1s exert the neurotoxic role with classical complement cascade gene upregulation, while the A2s upregulate many neurotrophic factors to promote neuronal recovery (47, 48). Therapies aimed at enhancing pro-reparative functions and reducing harmful functions in reactive astrocytes may benefit the outcome of ischemic stroke (49).

In this study, acute inhibition of AQP4 reduced peri-infarct astrogliosis and preserved AQP4 polarization, accompanied by a decreased lesion volume and improved neurological function. AQP4 is implicated in astrocyte migration and astrogliosis after

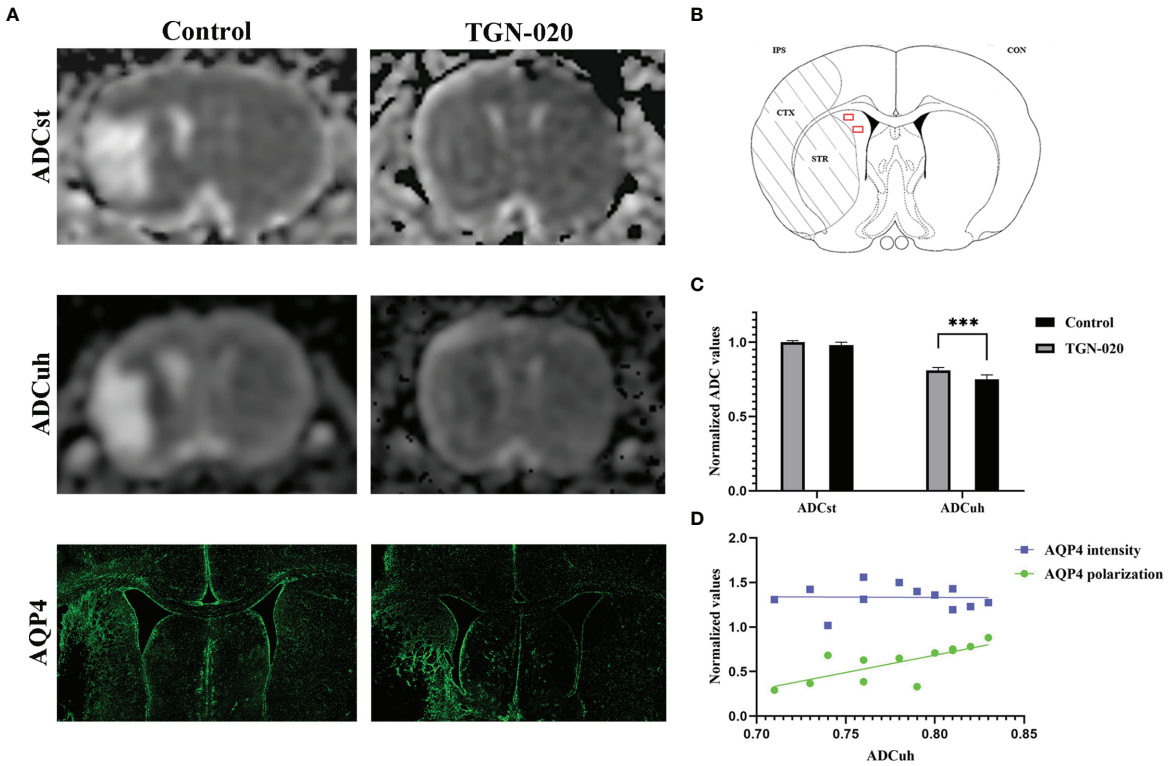

FIGURE 4 | Correspondence between ADC and AQP4 expression patterns. **(A)** Representative ADCst and ADCuh maps, and AQP4 staining patterns in TGN-020-treated and control rats. **(B)** Anatomical reference showing the ROIs (red boxes) used to estimate the ADCuh in the peri-infarct striatum. **(C)** Comparison of ADCuh in the peri-infarct striatum between the two groups. **(D)** Correlations between the peri-infarct AQP4 expression patterns and ADCuh. ***P < 0.001. Con, contralateral; CTX, cortex; IPS, ipsilateral; STR, striatum.

brain insult (50, 51), which was supported by the reduced peri-infarct astrogliosis after inhibition of AQP4 observed in our study. Moreover, we inferred that the reduced astrogliosis might attenuate inflammation and promote neural rejuvenation by reducing the number of neurotoxic A1s astrocytes, contributing to peri-infarct tissue repair and functional outcomes. Reactive astrocytes of different phenotypes exhibit double-edged effects on pathological progression (49, 52, 53), our experiments and substantive studies that demonstrated inhibiting reactive astrogliosis facilitated neural rejuvenation and the long-term functional outcome might be attributed to a decrease of the neurotoxic A1s astrocytes (54–56). Besides, we speculated that the preserved AQP4 polarization benefits the cognitive recovery of TGN-020-treated rats by increasing the drainage of toxic extracellular fluid in the core of the infarct. Perivascular AQP4 is a critical component of the brain glymphatic system (57, 58). The loss of AQP4 polarization would impair the clearance efficiency of the glymphatic system, resulting in toxic protein deposition and the induction of cognitive deficits after stroke (59, 60). Therapeutic strategies that improved the AQP4 polarization might be effective to enhance the glymphatic function and contribute to the neurological recovery (61).

Deciphering changes in AQP4 are helpful to understand its roles in the pathology of ischemic stroke; however, most analytical methods remain highly invasive or destructive. According to the literature, aquaporin overexpression produces contrast in DWI by increasing tissue water diffusivity (62). ADCuh (b values > 2000 s/mm^2) could reflect the expression level of aquaporin by estimating water transmembrane diffusivity (63). However, the relationship between ADCuh and aquaporin expression patterns in different studies are controversial. Some studies found that ADCuh correlated positively with the aquaporins expression intensity in tumors (64, 65), however, studies on ischemic stroke showed that ADCuh correlated negatively with aquaporin expression intensity (66–68). In our study, ADCuh correlated positively with the polarization of AQP4 rather than its expression intensity. This was probably the result of no adequate deviations among the AQP4 expression intensity of rats in this study, which did not allow us to infer a statistically significant correlation with ADCuh. Besides, the polarization of AQP4 might be more consequential for the functions of the protein than its expression intensity, as implied by other studies (69, 70).

The present study had certain limitations. Firstly, the inconsistency of lesion volumes before intervention between groups was avoided to the greatest extent, however, it could still not be excluded from the analysis. Longitudinal studies including data before inhibiting AQP4 might be more

conclusive. Secondly, because higher b-value images lead to more imaging artifacts, the correlations between ADCuh and AQP4 expression patterns were only analyzed in the peri-infarct striatum, thus further studies should be carried out using MRI machines with a higher performance. Thirdly, we didn't use the gene transcriptome analysis or key molecular markers immunostaining to differentiate the specific changes of two groups of reactive astrocytes after acute inhibition of AQP4, which will be carried out in our further studies. Besides, we only evaluate the role of AQP4 inhibition after ischemia onset, without investigating the effect of AQP4 inhibition on astrocyte and venules after recirculation, giving the TGN-020 along with the removal of filament in establishing the artery occlusion stroke animal model may be helpful to answer that.

In conclusion, we found acutely inhibiting AQP4 with TGN-020 not only decreased the edema at the early stage of ischemic stroke but also reduced peri-infarct astrogliosis and AQP4 depolarization, promoting sensorimotor and cognitive recovery at the subacute stage. This study extends the evaluation timepoint of previous studies investigating the effect of TGN-020 on ischemic stroke, providing further supportive evidence that acute inhibition of AQP4 after stroke is a viable therapeutic strategy. Furthermore, we revealed that AQP4 polarization correlated negatively with astrogliosis in the peri-infarct area, indicating therapies targeting astrogliosis might be effective to preserve AQP4 polarization and promote neurological recovery in ischemic stroke. And our results showed that ADCuh could reflect the AQP4 expression patterns, it might be a useful tool to decipher the AQP4 expression noninvasively.

DATA AVAILABILITY STATEMENT

The raw data supporting the conclusions of this article will be made available by the authors, without undue reservation.

ETHICS STATEMENT

The animal study was reviewed and approved by Fudan University Institutional Animal Care and Use Committee.

AUTHOR CONTRIBUTIONS

Study conception and design: YY and CS; experiment implementation, statistical analysis and figure preparation: CS, LL, XH, JT, and XZ; manuscript writing: CS and LY; paper reviewing: CL and YY. All authors read and approved the final manuscript.

FUNDING

This research was supported by the National Natural Science Foundation of China, Nos. 81771788. The funding sources had no role in study conception and design, data analysis or interpretation, paper writing or deciding to submit this paper for publication.

ACKNOWLEDGMENTS

We would like to thank the support by the Fudan University and its affiliated Huashan Hospital.

REFERENCES

1. Benjamin EJ, Virani SS, Callaway CW, Chamberlain AM, Chang AR, Cheng S, et al. Heart Disease and Stroke Statistics-2018 Update: A Report From the American Heart Association. *Circulation* (2018) 137(12):E67–492. doi: 10.1161/cir.0000000000000558
2. Ornello R, Degan D, Tiseo C, Di Carmine C, Perciballi L, Pistoia F, et al. Distribution and Temporal Trends From 1993 to 2015 of Ischemic Stroke Subtypes a Systematic Review and Meta-Analysis. *Stroke* (2018) 49(4):814–+. doi: 10.1161/strokeaha.117.020031
3. Kitchen P, Salman MM, Halsey AM, Clarke-Bland C, MacDonald JA, Ishida H, et al. Targeting Aquaporin-4 Subcellular Localization to Treat Central Nervous System Edema. *Cell* (2020) 181(4):784–99.e19. doi: 10.1016/j.cell.2020.03.037
4. Mestre H, Du T, Sweeney AM, Liu G, Samson AJ, Peng W, et al. Cerebrospinal Fluid Influx Drives Acute Ischemic Tissue Swelling. *Science* (2020) 367(6483):eaax7171. doi: 10.1126/science.aax7171
5. Yates D. Targeting Transport in Cns Oedema. *Nat Rev Neurosci* (2020) 21(7):350–1. doi: 10.1038/s41583-020-0324-0
6. Klostranec JM, Vucevic D, Bhatia KD, Kortman HGJ, Krings T, Murphy KP, et al. Current Concepts in Intracranial Interstitial Fluid Transport and the Glymphatic System: Part I-Anatomy and Physiology. *Radiology* (2021) 301(3):502–14. doi: 10.1148/radiol.2021202043
7. Vandebroek A, Yasui M. Regulation of Aqp4 in the Central Nervous System. *Int J Mol Sci* (2020) 21(5):1603. doi: 10.3390/ijms21051603
8. Rosu GC, Catalin B, Balseanu TA, Laurentiu M, Claudiu M, Kumar-Singh S, et al. Inhibition of Aquaporin 4 Decreases Amyloid Abeta40 Drainage Around Cerebral Vessels. *Mol Neurobiol* (2020) 57(11):4720–34. doi: 10.1007/s12035-020-02044-8
9. Harrison IF, Ismail O, Machhada A, Colgan N, Ohene Y, Nahavandi P, et al. Impaired Glymphatic Function and Clearance of Tau in an Alzheimer's Disease Model. *Brain* (2020) 143(8):2576–93. doi: 10.1093/brain/awaa179
10. Steliga A, Kowianski P, Czuba E, Waskow M, Morys J, Lietzau G. Neurovascular Unit as a Source of Ischemic Stroke Biomarkers-Limitations of Experimental Studies and Perspectives for Clinical Application. *Transl Stroke Res* (2020) 11(4):553–79. doi: 10.1007/s12975-019-00744-5
11. De Ieso ML, Yool AJ. Mechanisms of Aquaporin-Facilitated Cancer Invasion and Metastasis. *Front Chem* (2018) 6:135. doi: 10.3389/fchem.2018.00135
12. Mogoanta L, Ciurea M, Pirici I, Margaritescu C, Simionescu C, Ion DA, et al. Different Dynamics of Aquaporin 4 and Glutamate Transporter-1 Distribution in the Perineuronal and Perivascular Compartments During Ischemic Stroke. *Brain Pathol* (2014) 24(5):475–93. doi: 10.1111/bpa.12134
13. Filchenko I, Blochet C, Buscemi L, Price M, Badaut J, Hirt L. Caveolin-1 Regulates Perivascular Aquaporin-4 Expression After Cerebral Ischemia. *Front Cell Dev Biol* (2020) 8:371. doi: 10.3389/fcell.2020.00371
14. Ji C, Yu X, Xu W, Lenahan C, Tu S, Shao A. The Role of Glymphatic System in the Cerebral Edema Formation After Ischemic Stroke. *Exp Neurol* (2021) 340:113685. doi: 10.1016/j.expneurol.2021.113685
15. Moeendarbary E, Weber IP, Sheridan GK, Koser DE, Soleman S, Haenzi B, et al. The Soft Mechanical Signature of Glial Scars in the Central Nervous System. *Nat Commun* (2017) 8(1):14787. doi: 10.1038/ncomms14787
16. Abeysinghe HC, Phillips EL, Chin-Cheng H, Beart PM, Roulston CL. Modulating Astrocyte Transition After Stroke to Promote Brain Rescue and Functional Recovery: Emerging Targets Include Rho Kinase. *Int J Mol Sci* (2016) 17(3):288. doi: 10.3390/ijms17030288
17. Iliff JJ, Wang M, Liao Y, Plogg BA, Peng W, Gundersen GA, et al. A Paravascular Pathway Facilitates Csf Flow Through the Brain Parenchyma and the Clearance of Interstitial Solutes, Including Amyloid Beta. *Sci Transl Med* (2012) 4(147):147ra11. doi: 10.1126/scitranslmed.3003748
18. Arbel-Ornath M, Hudry E, Eikermann-Haerter K, Hou S, Gregory JL, Zhao L, et al. Interstitial Fluid Drainage Is Impaired in Ischemic Stroke and Alzheimer's Disease Mouse Models. *Acta Neuropathol* (2013) 126(3):353–64. doi: 10.1007/s00401-013-1145-2

19. Nedergaard M, Goldman SA. Glymphatic Failure as a Final Common Pathway to Dementia. *Science* (2020) 370(6512):50–6. doi: 10.1126/science.abb8739
20. Lin L, Hao X, Li C, Sun C, Wang X, Yin L, et al. Impaired Glymphatic System in Secondary Degeneration Areas After Ischemic Stroke in Rats. *J Stroke Cerebrovasc Dis* (2020) 29(7):104828. doi: 10.1016/j.jstrokecerebrovasdis.2020.104828
21. Gerriets T, Stolz E, Walberer M, Müller C, Kluge A, Bachmann A, et al. Noninvasive Quantification of Brain Edema and the Space-Occupying Effect in Rat Stroke Models Using Magnetic Resonance Imaging. *Stroke* (2004) 35 (2):566–71. doi: 10.1161/01.Str.0000113692.38574.57
22. Hao XZ, Yin LK, Zhang XX, Tian JQ, Li CC, Feng XY, et al. Combining Systemic and Stereotactic Memri to Detect the Correlation Between Gliosis and Neuronal Connective Pathway at the Chronic Stage After Stroke. *J Neuroinflamm* (2016) 13(1):156. doi: 10.1186/s12974-016-0622-7
23. Wang M, Iliff JJ, Liao Y, Chen MJ, Shinseki MS, Venkataraman A, et al. Cognitive Deficits and Delayed Neuronal Loss in a Mouse Model of Multiple Microinfarcts. *J Neurosci* (2012) 32(50):17948–60. doi: 10.1523/JNEUROSCI.1860-12.2012
24. Igarashi H, Huber VJ, Tsujita M, Nakada T. Pretreatment With a Novel Aquaporin 4 Inhibitor, Tgn-020, Significantly Reduces Ischemic Cerebral Edema. *Neurol Sci* (2011) 32(1):113–6. doi: 10.1007/s10072-010-0431-1
25. Abir-Awan M, Kitchen P, Salman MM, Conner MT, Conner AC, Bill RM. Inhibitors of Mammalian Aquaporin Water Channels. *Int J Mol Sci* (2019) 20 (7):1589. doi: 10.3390/ijms20071589
26. Verkman AS, Smith AJ, Phuan PW, Tradtrantip L, Anderson MO. The Aquaporin-4 Water Channel as a Potential Drug Target in Neurological Disorders. *Expert Opin Ther Targets* (2017) 21(12):1161–70. doi: 10.1080/14728222.2017.1398236
27. He ZP, Lu H. Aquaporin-4 Gene Silencing Protects Injured Neurons After Early Cerebral Infarction. *Neural Regener Res* (2015) 10(7):1082–7. doi: 10.4103/1673-5374.160099
28. Fang Y, Shi H, Ren R, Huang L, Okada T, Lenahan C, et al. Pituitary Adenylate Cyclase-Activating Polypeptide Attenuates Brain Edema by Protecting Blood-Brain Barrier and Glymphatic System After Subarachnoid Hemorrhage in Rats. *Neurotherapeutics* (2020) 17(4):1954–72. doi: 10.1007/s13311-020-00925-3
29. Sylvain NJ, Salman MM, Pushie MJ, Hou H, Meher V, Herlo R, et al. The Effects of Trifluoperazine on Brain Edema, Aquaporin-4 Expression and Metabolic Markers During the Acute Phase of Stroke Using Photothrombotic Mouse Model. *Biochim Biophys Acta Biomembr* (2021) 1863(5):183573. doi: 10.1016/j.bbamem.2021.183573
30. Shi ZF, Fang Q, Chen Y, Xu LX, Wu M, Jia M, et al. Methylene Blue Ameliorates Brain Edema in Rats With Experimental Ischemic Stroke *Via* Inhibiting Aquaporin 4 Expression. *Acta Pharmacol Sin* (2021) 42(3):382–92. doi: 10.1038/s41401-020-0468-5
31. Howe MD, Atadja LA, Furr JW, Maniskas ME, Zhu L, McCullough LD, et al. Fibronectin Induces the Perivascular Deposition of Cerebrospinal Fluid-Derived Amyloid-Beta in Aging and After Stroke. *Neurobiol Aging* (2018) 72:1–13. doi: 10.1016/j.neurobiolaging.2018.07.019
32. Zbesko JC, Nguyen TV, Yang T, Frye JB, Hussain O, Hayes M, et al. Glial Scars Are Permeable to the Neurotoxic Environment of Chronic Stroke Infarcts. *Neurobiol Dis* (2018) 112:63–78. doi: 10.1016/j.nbd.2018.01.007
33. Ren Z, Iliff JJ, Yang L, Yang J, Chen X, Chen MJ, et al. 'Hit & Run' Model of Closed-Skull Traumatic Brain Injury (Tbi) Reveals Complex Patterns of Post-Traumatic Aqp4 Dysregulation. *J Cereb Blood Flow Metab* (2013) 33(6):834–45. doi: 10.1038/jcbfm.2013.30
34. Smith AJ, Duan T, Verkman AS. Aquaporin-4 Reduces Neuropathology in a Mouse Model of Alzheimer's Disease by Remodeling Peri-Plaque Astrocyte Structure. *Acta Neuropathol Commun* (2019) 7(1):74. doi: 10.1186/s40478-019-0728-0
35. Eide PK, Hansson HA. Astrogliosis and Impaired Aquaporin-4 and Dystrophin Systems in Idiopathic Normal Pressure Hydrocephalus. *Neuropathol Appl Neurobiol* (2018) 44(5):474–90. doi: 10.1111/nan.12420
36. Liddelow SA, Barres BA. Reactive Astrocytes: Production, Function, and Therapeutic Potential. *Immunity* (2017) 46(6):957–67. doi: 10.1016/j.immuni.2017.06.006
37. Liu Z, Chopp M. Astrocytes, Therapeutic Targets for Neuroprotection and Neurorestoration in Ischemic Stroke. *Prog Neurobiol* (2016) 144:103–20. doi: 10.1016/j.pneurobio.2015.09.008
38. Patabendige A, Singh A, Jenkins S, Sen J, Chen R. Astrocyte Activation in Neurovascular Damage and Repair Following Ischaemic Stroke. *Int J Mol Sci* (2021) 22(8):4280. doi: 10.3390/ijms22084280
39. Liddelow SA, Guttenplan KA, Clarke LE, Bennett FC, Bohlen CJ, Schirmer L, et al. Neurotoxic Reactive Astrocytes Are Induced by Activated Microglia. *Nature* (2017) 541(7638):481–7. doi: 10.1038/nature21029
40. Williamson MR, Fuertes CJA, Dunn AK, Drew MR, Jones TA. Reactive Astrocytes Facilitate Vascular Repair and Remodeling After Stroke. *Cell Rep* (2021) 35(4):109048. doi: 10.1016/j.celrep.2021.109048
41. Anderson MA, Burda JE, Ren Y, Ao Y, O'Shea TM, Kawaguchi R, et al. Astrocyte Scar Formation Aids Central Nervous System Axon Regeneration. *Nature* (2016) 532(7598):195–200. doi: 10.1038/nature17623
42. Burda JE, Sofroniew MV. Reactive Gliosis and the Multicellular Response to Cns Damage and Disease. *Neuron* (2014) 81(2):229–48. doi: 10.1016/j.neuron.2013.12.034
43. Hatakeyama M, Ninomiya I, Otsu Y, Omae K, Kimura Y, Onodera O, et al. Cell Therapies Under Clinical Trials and Polarized Cell Therapies in Pre-Clinical Studies to Treat Ischemic Stroke and Neurological Diseases: A Literature Review. *Int J Mol Sci* (2020) 21(17):6194. doi: 10.3390/ijms21176194
44. Sofroniew MV. Astrocyte Reactivity: Subtypes, States, and Functions in Cns Innate Immunity. *Trends Immunol* (2020) 41(9):758–70. doi: 10.1016/j.it.2020.07.004
45. Zamanian JL, Xu L, Foo LC, Nouri N, Zhou L, Giffard RG, et al. Genomic Analysis of Reactive Astrogliosis. *J Neurosci* (2012) 32(18):6391–410. doi: 10.1523/jneurosci.6221-11.2012
46. Xu S, Lu J, Shao A, Zhang JH, Zhang J. Glial Cells: Role of the Immune Response in Ischemic Stroke. *Front Immunol* (2020) 11:294. doi: 10.3389/fimmu.2020.00294
47. Zhao N, Xu X, Jiang Y, Gao J, Wang F, Xu X, et al. Lipocalin-2 May Produce Damaging Effect After Cerebral Ischemia by Inducing Astrocytes Classical Activation. *J Neuroinflamm* (2019) 16(1):168. doi: 10.1186/s12974-019-1556-7
48. Rakers C, Schleif M, Blank N, Matuskova H, Ulas T, Handler K, et al. Stroke Target Identification Guided by Astrocyte Transcriptome Analysis. *Glia* (2019) 67(4):619–33. doi: 10.1002/glia.23544
49. Ito M, Komai K, Mise-Omata S, Iizuka-Koga M, Noguchi Y, Kondo T, et al. Brain Regulatory T Cells Suppress Astrogliosis and Potentiate Neurological Recovery. *Nature* (2019) 565(7738):246–50. doi: 10.1038/s41586-018-0824-5
50. Saadoun S, Papadopoulos MC, Watanabe H, Yan D, Manley GT, Verkman AS. Involvement of Aquaporin-4 in Astroglial Cell Migration and Glial Scar Formation. *J Cell Sci* (2005) 118(Pt 24):5691–8. doi: 10.1242/jcs.02680
51. Auguste KI, Jin S, Uchida K, Yan D, Manley GT, Papadopoulos MC, et al. Greatly Impaired Migration of Implanted Aquaporin-4-Deficient Astroglial Cells in Mouse Brain Toward a Site of Injury. *FASEB J* (2007) 21(1):108–16. doi: 10.1096/fj.06-6848com
52. Yiu G, He Z. Glial Inhibition of Cns Axon Regeneration. *Nat Rev Neurosci* (2006) 7(8):617–27. doi: 10.1038/nrn1956
53. Li X, Li M, Tian L, Chen J, Liu R, Ning B. Reactive Astrogliosis: Implications in Spinal Cord Injury Progression and Therapy. *Oxid Med Cell Longev* (2020) 2020:9494352. doi: 10.1155/2020/9494352
54. Pirici I, Balsanu TA, Bogdan C, Margaritescu C, Divan T, Vitalie V, et al. Inhibition of Aquaporin-4 Improves the Outcome of Ischaemic Stroke and Modulates Brain Paravascular Drainage Pathways. *Int J Mol Sci* (2017) 19 (1):46. doi: 10.3390/ijms19010046
55. Li J, Jia Z, Xu W, Guo W, Zhang M, Bi J, et al. Tgn-020 Alleviates Edema and Inhibits Astrocyte Activation and Glial Scar Formation After Spinal Cord Compression Injury in Rats. *Life Sci* (2019) 222:148–57. doi: 10.1016/j.lfs.2019.03.007
56. Lee JS, Hsu YH, Chiu YS, Jou IM, Chang MS. Anti-Il-20 Antibody Improved Motor Function and Reduced Glial Scar Formation After Traumatic Spinal Cord Injury in Rats. *J Neuroinflamm* (2020) 17(1):156. doi: 10.1186/s12974-020-01814-4
57. Kress BT, Iliff JJ, Xia M, Wang M, Wei HS, Zeppenfeld D, et al. Impairment of Paravascular Clearance Pathways in the Aging Brain. *Ann Neurol* (2014) 76 (6):845–61. doi: 10.1002/ana.24271
58. Zeppenfeld DM, Simon M, Haswell JD, D'Abreo D, Murchison C, Quinn JF, et al. Association of Perivascular Localization of Aquaporin-4 With Cognition and Alzheimer Disease in Aging Brains. *JAMA Neurol* (2017) 74(1):91–9. doi: 10.1001/jamaneurol.2016.4370
59. Lv T, Zhao B, Hu Q, Zhang X. The Glymphatic System: A Novel Therapeutic Target for Stroke Treatment. *Front Aging Neurosci* (2021) 13:689098. doi: 10.3389/fnagi.2021.689098

60. Gaberel T, Gakuba C, Goulay R, Martinez De Lizarrondo S, Hanouz JL, Emery E, et al. Impaired Glymphatic Perfusion After Strokes Revealed by Contrast-Enhanced Mri a New Target for Fibrinolysis? *stroke* (2014) 45(10):3092–6. doi: 10.1161/STROKEAHA.114.006617
61. He XF, Li G, Li LL, Li MY, Liang FY, Chen X, et al. Overexpression of Slit2 Decreases Neuronal Excitotoxicity, Accelerates Glymphatic Clearance, and Improves Cognition in a Multiple Microinfarcts Model. *Mol Brain* (2020) 13 (1):135. doi: 10.1186/s13041-020-00659-5
62. Mukherjee A, Wu D, Davis HC, Shapiro MG. Non-Invasive Imaging Using Reporter Genes Altering Cellular Water Permeability. *Nat Commun* (2016) 7:13891. doi: 10.1038/ncomms13891
63. Xueying L, Zhongping Z, Zhoushe Z, Li G, Yongjin T, Changzheng S, et al. Investigation of Apparent Diffusion Coefficient From Ultra-High B-Values in Parkinson's Disease. *Eur Radiol* (2015) 25(9):2593–600. doi: 10.1007/s00330-015-3678-3
64. Tan Y, Zhang H, Wang XC, Qin JB, Wang L. The Value of Multi Ultra High-B-Value Dwi in Grading Cerebral Astrocytomas and Its Association With Aquaporin-4. *Br J Radiol* (2018) 91(1086):20170696. doi: 10.1259/bjr.20170696
65. Zhang G, Ma W, Dong H, Shu J, Hou W, Guo Y, et al. Based on Histogram Analysis: Adcaqp Derived From Ultra-High B-Value Dwi Could Be a Non-Invasive Specific Biomarker for Rectal Cancer Prognosis. *Sci Rep* (2020) 10 (1):10158. doi: 10.1038/s41598-020-67263-4
66. Chen Q, Wu F, Peng X, Li C, Jiang M, Chen T, et al. Resarch on Correlation Between Aquaporin Magnetic Resonance Molecular Imaging and AQP4 Expression. *J Chin Clin Med Imaging* (2016) 27(12):837–41. doi: 10.3969/j.issn.1008-1062.2016.12.001
67. Peng X, Yu B, Chen Q, Chen T, Wu F, Wei D. Assessment of Ischemic Penumbra Using Aquaporin Magnetic Resonance Imaging. *Chin J Med Imaging* (2020) 28(1):6–11. doi: 10.3969/j.issn.1005-5185.2020.01.002
68. Xing P, Chen Q, Wu F, Peng X, Jiang M, Chen T, et al. Study of Aquaporin Magnetic Resonance Molecular Imaging in Transient Cerebral Ischemia Rat Model. *Chin J Magn Reson Imaging* (2017) 8(1):51–6. doi: 10.12015/issn.1674-8034.2017.01.012
69. Amiry-Moghaddam M, Otsuka T, Hurn PD, Traystman RJ, Haug FM, Froehner SC, et al. An Alpha-Syntrophin-Dependent Pool of Aqp4 in Astroglial End-Feet Confers Bidirectional Water Flow Between Blood and Brain. *Proc Natl Acad Sci USA* (2003) 100(4):2106–11. doi: 10.1073/pnas.0437946100
70. Neely JD, Amiry-Moghaddam M, Ottersen OP, Froehner SC, Agre P, Adams ME. Syntrophin-Dependent Expression and Localization of Aquaporin-4 Water Channel Protein. *Proc Natl Acad Sci USA* (2001) 98(24):14108–13. doi: 10.1073/pnas.241508198

Conflict of Interest: The authors declare that the research was conducted in the absence of any commercial or financial relationships that could be construed as a potential conflict of interest.

Publisher's Note: All claims expressed in this article are solely those of the authors and do not necessarily represent those of their affiliated organizations, or those of the publisher, the editors and the reviewers. Any product that may be evaluated in this article, or claim that may be made by its manufacturer, is not guaranteed or endorsed by the publisher.

frontiers | Frontiers in Immunology

ORIGINAL RESEARCH
published: 23 May 2022
doi: 10.3389/fimmu.2022.870577

Nanoformulated Bumetanide Ameliorates Social Deficiency in BTBR Mice Model of Autism Spectrum Disorder

Hui Lv[1†], Xiao Gu[2†], Xingyue Shan[3], Tailin Zhu[1], Bingke Ma[3], Hao-Tian Zhang[4], Victorio Bambini-Junior[5], Tiantian Zhang[3], Wei-Guang Li[6], Xiaoling Gao[2] and Fei Li[1*]*

[1] Department of Developmental and Behavioral Pediatric & Child Primary Care, Brain and Behavioural Research Unit of Shanghai Institute for Pediatric Research and Ministry of Education-Shanghai Key Laboratory for Children's Environmental Health, Xinhua Hospital, Shanghai Jiao Tong University School of Medicine, Shanghai, China, [2] Department of Pharmacology and Chemical Biology, Shanghai Universities Collaborative Innovation Center for Translational Medicine, Shanghai Jiao Tong University School of Medicine, Shanghai, China, [3] Shanghai Key Laboratory of Brain Functional Genomics (Ministry of Education), School of Life Sciences, East China Normal University, Shanghai, China, [4] Brain and Behavioral Research Unit of Shanghai Institute for Pediatric Research and Ministry of Education (MOE)-Shanghai Key Laboratory for Children's Environmental Health, Xinhua Hospital, Shanghai Jiao Tong University School of Medicine, Shanghai, China, [5] Division of Biomedical and Life Sciences, Faculty of Health and Medicine, Lancaster University, Lancaster, United Kingdom, [6] Department of Rehabilitation Medicine, Huashan Hospital, Institute for Translational Brain Research, State Key Laboratory of Medical Neurobiology and Ministry of Education Frontiers Center for Brain Science, Fudan University, Shanghai, China*

Autism spectrum disorder (ASD) is a prevalent neurodevelopmental disorder with few medication options. Bumetanide, an FDA-approved diuretic, has been proposed as a viable candidate to treat core symptoms of ASD, however, neither the brain region related to its effect nor the cell-specific mechanism(s) is clear. The availability of nanoparticles provides a viable way to identify pharmacological mechanisms for use in ASD. Here, we found that treatment with bumetanide, in a systemic and medial prefrontal cortex (mPFC) region-specific way, attenuated social deficits in BTBR mice. Furthermore, using poly (ethylene glycol)-poly(l-lactide) (PEG-PLA) nanoparticles [NP(bumetanide)], we showed that the administration of NP(bumetanide) in a mPFC region-specific way also alleviated the social deficits of BTBR mice. Mechanistically, the behavioral effect of NP(bumetanide) was dependent on selective microglia-specific targeting in the mPFC. Pharmacological depletion of microglia significantly reduced the effect of nanoencapsulation and depletion of microglia alone did not improve the social deficits in BTBR mice. These findings suggest the potential therapeutic capabilities of nanotechnology for ASD, as well as the relevant link between bumetanide and immune cells.

Keywords: autism spectrum disorder, bumetanide, nanoparticle, social behavior, microglia

OPEN ACCESS

Edited by:
Mingyao Ying,
Johns Hopkins Medicine,
United States

Reviewed by:
Ji Hu,
ShanghaiTech University, China
Zikai Zhou,
Chinese Academy of Sciences (CAS), China
Xiaobo Mao,
Johns Hopkins Medicine,
United States

***Correspondence:**
Fei Li
feili@shsmu.edu.cn
Xiaoling Gao
shellygao1@sjtu.edu.cn

[†]These authors have contributed equally to this work

Specialty section:
This article was submitted to Multiple Sclerosis and Neuroimmunology, a section of the journal Frontiers in Immunology

Received: *07 February 2022*
Accepted: *21 April 2022*
Published: *23 May 2022*

Citation:
Lv H, Gu X, Shan X, Zhu T, Ma B, Zhang H-T, Bambini-Junior V, Zhang T, Li W-G, Gao X and Li F (2022) Nanoformulated Bumetanide Ameliorates Social Deficiency in BTBR Mice Model of Autism Spectrum Disorder. Front. Immunol. 13:870577. doi: 10.3389/fimmu.2022.870577

HIGHLIGHTS

1. Systemic or mPFC-specific delivery of bumetanide improves social deficit in BTBR mice
2. Nanoformulated bumetanide with microglia-specific targeting capability in mPFC improves social deficit in BTBR mice
3. Microglia depletion in the mPFC fails to affect social deficiency in BTBR mice
4. The therapeutic effects of nanoformulated bumetanide depend on the presence of mPFC microglia

INTRODUCTION

Autism spectrum disorder (ASD) is a highly prevalent neurodevelopmental disorder characterized by social interaction and communication deficits and repetitive patterns of interests, with no efficient, FDA-approved pharmacological options available for its core symptoms (1, 2). Bumetanide, an FDA-approved loop diuretic, has been proposed as a viable candidate to treat core symptoms of ASD. To elucidate the efficacy and molecular mechanisms of bumetanide, rodent models with phenotypes relevant to the core feature of ASD have been widely used (3). BTBR T+tf/J (BTBR) mice were derived from the inbred strain carrying the at (nonagouti; black and tan), T (brachury), and the Itpr3tf (tufted) mutations with marked ASD-like behavior phenotypes such as social deficits and repetitive behaviors (4, 5). Indeed, the ranges of ASD-like phenotypes in BTBR mice highlight this model as a useful preclinical tool for evaluating therapeutic strategies.

One of the mechanisms involved in the manifestation of ASD phenotype is an imbalance of excitatory and inhibitory neurotransmission, which suggests a potential therapeutic target for drug discovery (6). Recent evidence from both preclinical and clinical studies has implicated bumetanide as a promising candidate for ASD therapy (7–10), yet the efficacy of bumetanide remains unclear (11, 12). The classical mechanism explains the action of bumetanide in the regulation of neuronal intracellular chloride flux by inhibition of the sodium (Na^+)-potassium(K^+)-Cl^-transporter isoform1 (NKCC1, *SLC12A2*) and the restoration of GABA polarity in the brain (7). Maternal bumetanide treatment could shift GABA from excitation to inhibition state while rescuing autistic-like behaviors in the offspring of animal models of ASD (7, 8). Clinical evidence has shown that bumetanide could improve the symptoms including social communication and restricted interest of ASD patients (13). This action of bumetanide is mediated by GABA since the decreased insular GABA was observed in ASD patients with bumetanide (10, 14). Despite the effects of bumetanide that have been demonstrated in animal models and patients with ASD, the effects of bumetanide have remained controversial, mainly because the brain region and cell-type specific mechanisms(s) underlying bumetanide in ASD are unclear.

The medial prefrontal cortex (mPFC) is a brain region mechanistically linked to multiple cognitive functions, including social behaviors (15–17). In mice, excitation of excitatory neurons *via* optogenetic manipulation in the mPFC leads to social deficits (15), whilst lesion of the mPFC reduces social behaviors (16). In addition, functional magnetic resonance imaging (fMRI) (18) and functional near-infrared spectroscopy (fNIRS) (19) have revealed the involvement of mPFC in social-associated tasks in humans, and dysfunctional mPFC activity in patients with ASD (20). Considering the critical involvement of mPFC in social behaviors, we thus tried to investigate whether the mPFC acts as a critical brain region underlying the therapeutic actions of bumetanide in ASD.

Despite the majority of studies have examined the neuronal mechanism that underlies bumetanide's action, the involvement of other non-neuronal mechanisms cannot be completely excluded. Bumetanide is a non-selective NKCC1 inhibitor. Notably, NKCC1 expression is found in several non-neuronal cell types of the brain, including microglia (21). Furthermore, a growing body of evidence suggests that microglia, the resident immune cells in the brain, have a central role in the pathophysiology of ASD (22–26). Microglia dysfunction in ASD has been identified by autopsy and positron emission tomography studies, which showed increased numbers and altered morphology of microglia cells (22, 23), and genomic transcriptional analysis revealed an altered expression of microglia-specific genes in cortical regions of patients with ASD (24, 25). In addition, analysis with positron-emission tomography (PET) has revealed increased microglial activation in young adult patients with ASD (26). As the cell-specific effects of bumetanide have not been extensively characterized (due to its non-selective action), and taking into consideration that none of the previous studies have selectively targeted microglia (despite the evidence demonstrating its important role in ASD) using bumetanide in ASD, we hypothesized that microglia can be one of the primary targets of bumetanide. In previous studies, nanoparticles were used to induce a microglia-specific accumulation of molecules in the brain; this approach can help overcome the constraint of targeting microglial cells specifically (27). The development of a nano-delivery system has provided a new framework for targeted delivery and release for different diseases. For instance, a nano-delivery system established a promising therapeutic approach in Alzheimer's disease (AD) (28).

In this study, we developed a strategy to evaluate the effects of bumetanide encapsulated in a core of polyethylene glycol-polylactic acid (PEG-PLA) nanoparticles [NP (bumetanide)], using the BTBR mice model of ASD. BTBR mice displayed autistic-like behavioral including social impairments and excess of repetitive behaviors and characterized by aberrant inflammatory phenotypes in both peripheral and central nervous immune system which provided a unique model of ASD to investigate the possible link between bumetanide and immunity. Initially, to characterize the efficiency of the nanoparticles and the specific brain region underlying bumetanide's mechanism, we tested behavior changes in BTBR mice induced by systemic and mPFC region-specific delivery of bumetanide. Furthermore, we sought to identify the microglia-

specific mechanisms involved in the therapeutic effects of bumetanide. For this purpose, we used NP(bumetanide) to target microglia in mPFC. We examined the therapeutic effect of NP(bumetanide) in BTBR mice, as well as how pharmacologically depletion of microglia affects social deficit and the therapeutic effect of NP(bumetanide).

MATERIALS AND METHODS

Male C57BL/6 mice were obtained from Shanghai Jihui Laboratory Animal Co., Ltd (Shanghai, China). BTBR mice were obtained from Shanghai model organisms center, Inc. (Shanghai, China). Mice were housed in a standardized environment with a 12 h light/dark cycle and free access to food and water. Behavioral experiments were performed during the light phase of the cycle and mice were randomly grouped. All experimental protocols were approved by the Animal Ethics Committee of East China Normal University (Shanghai, China) and all efforts were made to minimize animal suffering and reduce the number of mice used. All mice used in this experiment were males.

Drug and Drug Administration

The bumetanide was purchased from Sigma (catalog no. 28395-03-01, USA). For intraperitoneal administration, bumetanide was first dissolved in DMSO and then diluted in 3% Tween80-NS solution to final concentration. Intraperitoneal administration of bumetanide (i.p., 10 mg/kg) was performed daily for 7 days in BTBR mice (6 weeks). For mPFC region-specific administration, bumetanide (100 μM) was dissolved in DMSO and then diluted in NS solution to final concentration. mPFC administration was performed daily for 3 days in BTBR mice (6 weeks). The dose of bumetanide was selected based on previous laboratory results and paper (29, 30).

Compounds

PLX3397 was purchased from SelleckChem (S7818, China) and formulated in AIN-76A standard chow by Shanghai biopikeChem at 290 mg/kg doses.

Nanoparticles Preparation

Briefly, NP(bumetanide) was prepared as described previously (27, 31). To address the low solubility of bumetanide during fabrication, we added methyl bonds to bumetanide to promote dissolution and facilitate fabrication into nanoparticles. The previous finding has defined that the bumetanide ester could release bumetanide *in vivo* upon hydrolysis. Firstly, 10 mg of MePEG-PLA and 0.5 mg of bumetanide prodrugs were dissolved in 1 ml of dichloromethane. Afterward, 2 ml of aqueous sodium cholate (1%, w/v) was added to the solution and then sonicated on ice (220 w, 2 min) using a probe sonicator (Ningbo Scientific Instruments Co., Ltd., China) to form O/W emulsions. The emulsion was diluted into an 18 ml of sodium cholate solution (0.5%, w/v) with magnetic stirring for 5 min and evaporation of dichloromethane with a ZX-98 rotary evaporator (Shanghai Institute of Organic Chemistry, China). The nanoparticles were collected by centrifugation at 14,000 × g for 45 min and separated by a 1.5 × 20 cm sepharose CL-4B column. The fluorescently labeled nanoparticles were prepared by a process similar to that of NP(bumetanide), using rhodamine as the fluorescent probe. Rhodamine (0.2mg) was dissolved by dichloromethane in 1 ml of dichloromethane, and then the procedure for the preparation of NP (bumetanide) was followed.

Surgical Procedures and Micro-Infusion of Bumetanide Administration

For cannula implantation, 5 weeks BTBR mice were anesthetized with 5% chloral hydrate (5 mg/kg) and gently placed in a stereotaxic frame (RWD Life Science, China). Cannulae (62203, RWD Life Science, China) were bilaterally impanated at 1.0 mm above. Stereotaxic coordinates according to the Paxinos and Watson mouse brain atlas (32). The target area to the mPFC at the following coordinates: +1.70 mm; posterior to bregma, ± 1.65 mm; lateral to the midline, and -1.05 mm; dorsoventral. The cannula was angled at 30°, positioned with acrylic dental cement, and secured with cranial screws. A stylet was placed in the introducer cannula to prevent occlusion. Mice were allowed to recover from surgery for several days prior to experimental manipulation. For drug administration, the infusion tube was connected to a microinjector driven by a microinfusion pump (KDS 310, KD Scientific, USA) through PE20 tubing. 0.5 ul per side of bumetanide was infused into the mPFC at a rate of 0.5 ul/min. The infusion tube was left in place for an additional 3 min to allow the diffusion of medicine.

Behavior Protocol

BTBR mice were examined after 7 days (i.p.) or three times (mPFC infusion) of treatment with bumetanide or vehicle. On the testing day, mice were transferred into the testing room for accommodation for 1 h. During the day of behavioral testing, mice were treated with bumetanide, and tests began 30 min after injection. The devices were cleaned with 70% ethanol after trails to avoid odor cue.

Three-Chamber test. The three-chamber test consisted of three stages in one session to assess different social aspects of the mice. The test used a Plexiglas apparatus (60 × 40 × 25 cm) containing three chambers with an empty wire cage (8 × 12 cm) in the side chambers. ANY-maze tracking system software (Stoelting Co, USA) with a camera was used to track the position of the mice during each tracking session. Briefly, in the habituation stage, test mice were placed in the central chamber only for 5 min and then were allowed to explore the whole apparatus with its empty wire cage for 10 minutes. In the sociability stage, a stimulus mouse (stranger 1, S1, same age and sex) was randomly placed in one of the empty wire cages and the test mice were brought back to explore the apparatus for 10 min. After the social ability stage, a new stimulus mouse (stranger 2, S2, same age and sex) was inserted into the previous empty wire cage and the subject mice were allowed to explore the chambers for another 10 min. The time spent by the animals in each chamber was analyzed by ANY-maze tracking system software. Mice with a preference for one side of the chamber were excluded from the data analysis.

Open field test. The open field test was used to assess the effects of locomotor responses to novel environments in mice. We conducted the open field test in a square Plexiglas apparatus (40 × 40 × 35 cm) under diffuse light. During the experiment, mice were gently placed in the center square of the apparatus and allowed to explore freely for 30 min. At the end of each trial, the apparatus was cleaned and the animals were returned to cages. Tru scan (Coulbourn Instruments, USA) activity software was used to detect the activity of the mice and record data. The total distance traveled during the 30 min was analyzed.

Elevated plus maze. The elevated plus maze could be used to assess anxiety-like behaviors in rodents. This apparatus consists of two walled elevated arms and two open arms that branch off a central platform forming a plus shape. The apparatus was raised to a height of 50 cm above the ground. For testing, subject mice were placed in the center area facing the close arm and allowed to explore for 5 min. ANY-maze tracking system software was used to track the position of the mice during the session and the time spent in the open arms of the maze was analyzed.

Elevated zero maze. The elevated zero maze was used to assess anxiety-like behaviors in rodents. The apparatus consists of two open (stressful) and two enclosed (protecting) elevated arms that form a zero or circle elevating it 50 cm above the ground. Quadrant lanes of the apparatus were 5 cm wide. The subject mice were placed randomly in the boundary between a close and an open arm, facing the close arm and allowed for exploring 5 min. ANY-maze tracking system software was used to track the position of the mice during the session and the time spent in the open arm of the maze was analyzed by ANY-maze tracking system software.

Grooming test. The grooming test was used to examine the repetitive behaviors of the mice. The test cage was lined with bedding (<1cm) in order to reduce neophobia but prevent digging. For the self-grooming test, mice were placed individually in a new clean cage for 15 min habituation and recorded for 10 min using Mouse Home Cage Behavior Analyzing System (Clever Sys. Inc, USA). The time spent self-grooming was analyzed by Mouse Home Cage Behavior Analyzing System.

Immunohistochemistry

Briefly, mice were deeply anesthetized with 5% chloral hydrate and transcranial perfused with 40-60 ml of 1 × PBS followed by 20 ml 4% paraformaldehyde. The brain was removed from the skull and immersed into 0.1M PBS containing 4% paraformaldehyde and incubated at 4°C overnight. Coronal brain sections of 45-μm thickness (Leica VT1200S, Germany) were made with oscillating slices. The section was pasted on the poly Lys-coated glass slide and baked at 60°C for 50 minutes. Sections were washed 5 minutes with 1 × PBS for one time. The section was incubated in a blocking buffer composed of PBS containing 0.3% Triton X-100 and 5% normal goat serum for 90 min at room temperature. The sections were then incubated with the primary antibody in the blocking buffer at 4°C for 24 h. The primary antibodies used in this study were rabbit polyclonal anti-Iba1 antibody (1:1000 dilution, 019-19741, wako, Japan), anti-NeuN antibody (1:500, ab104224, Abcam) and anti-GFAP antibody (1:500, 60190-1, proteintech, USA). After incubation, the sections were washed for 5 min with 1 × PBS containing 0.1% Tween-20 for 3 times. For immunofluorescent staining, the sections were incubated with Alexa Fluor 488-labeled secondary antibodies (1:1000 dilution; Life Technologies, USA) for 2h at RT. The sections were washed 5 minutes for three times with PBS containing 0.1% Tween-20. Slides were mounted in the dark with glass coverslips using mounting media containing 4',6-Diamidina-2-phenylindole (P0131, Beyotime, China). The signal of slices was captured by immunofluorescence microscopy (Leica DM4000 B, Germany).

Statistical Analyses

Data were shown by means ± standard error of the mean (S.E.M). The p values were calculated using two-tailed Student's t-test or one-way analyses of variance (ANOVA) with Bonferroni *post hoc*. The GraphPad Prism Software was used for all analyses. Significance is reported as $^{*}p < 0.05$, $^{**}p < 0.01$, $^{***}p < 0.001$, and not significant values are not denoted except for emphasis.

RESULTS

Systemic Treatment With Bumetanide Alleviated Autistic-Like Behaviors in BTBR Mice

BTBR mice were injected with bumetanide (10mg/kg, intraperitoneally, once daily) or vehicle followed by a series of behavioral tests (**Figure 1A**). To assess their social behavior, we used a three-chamber test to examine social approach (sociability stage) and social recognition (social novelty stage), as is shown in **Figures 1B, C**. In the sociability stage, compared to WT mice, BTBR mice spent less time both in the social stimulus chamber (stranger 1, S1) and direct interaction with the stimulus. Bumetanide administration failed to rescue the social ability of BTBR mice, which we assessed by counting the time in the social stimulus chamber and direct interaction time with the stimulus (**Figure 1B**). However, when presented with both familiar stimuli (S1) and novel stimulus (stranger 2, S2), BTBR mice spent more time exploring familiar stimulus than novel stimulus, while bumetanide-treated BTBR mice spent more time in the novel stimulus chamber (**Figure 1C**) and interacted more time with novel stimulus (**Figure 1C**) to the level of WT controls. Together, the increased social investigate time indicated that systemic treatment of bumetanide partially alleviated the impaired social phenotype in BTBR mice. Next, we examined repetitive behavior after systemic treatment with bumetanide in BTBR mice. The grooming test revealed that bumetanide-treated BTBR mice, compared to the untreated group, spent less time self-grooming (**Figure 1D**) which indicated that bumetanide improved the repetitive behaviors. Lastly, we tested basal locomotor activity and anxiety using open field and elevated plus maze, respectively. In the open field test, vehicle- or bumetanide-treated BTBR mice displayed similar total distance traveled, which was higher than WT mice as previously reported (**Figure 1E**) (33), implying a

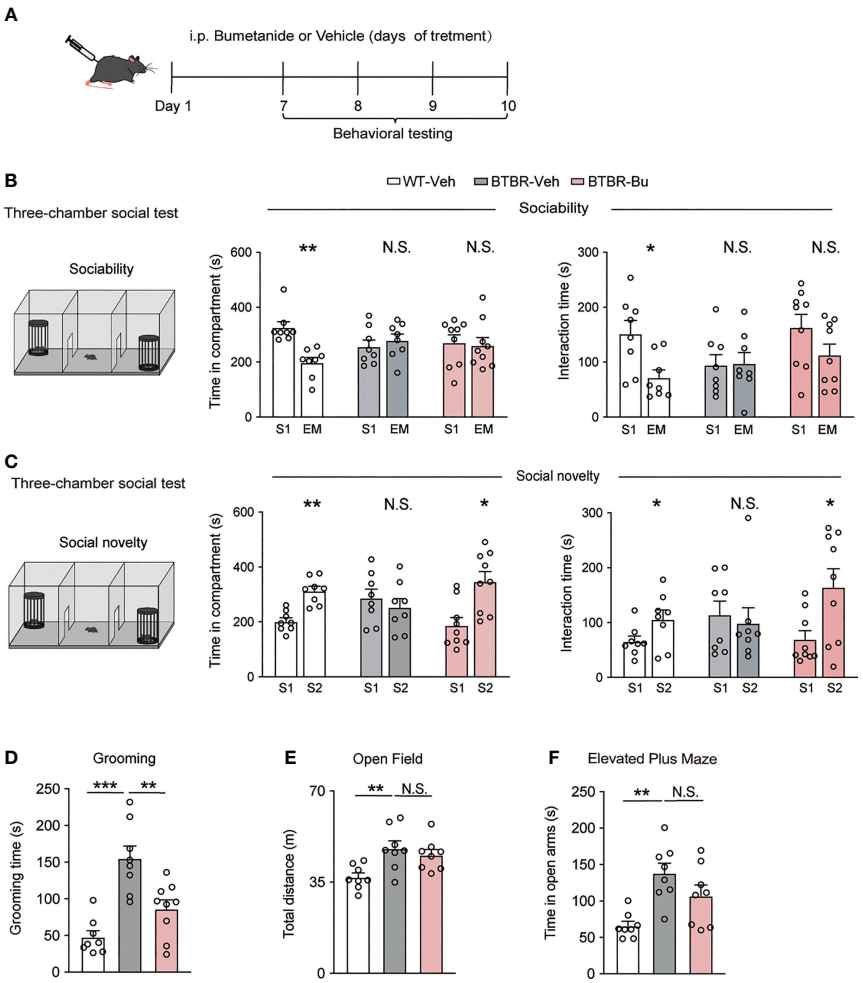

FIGURE 1 | Systemic treatment with bumetanide alleviated autistic-like behavioral in BTBR mice. **(A)** Schematic representation of the experimental procedure. Male BTBR mice were injected intraperitoneally (i.p.) with bumetanide (10 mg/kg) or vehicle. **(B)** Time spent in the social stimulus or empty chamber and total interaction time with stimulus mouse or empty wire during sociability stage (WT-vehicle, n = 8; BTBR-vehicle, n = 8; BTBR-bumetanide, n = 9, paired Student's *t*-test. Time in compartments, $^{**}p < 0.01$, WT-vehicle S1 vs. EM; N.S., not significant, BTBR-vehicle S1 vs. EM; N.S., not significant, BTBR-bumetanide S1 vs. EM; interaction time, $^{*}p < 0.05$, WT-vehicle S1 vs. EM; N.S., not significant, BTBR-vehicle S1 vs. EM; N.S., not significant, BTBR-bumetanide S1 vs. EM; S1 represent stranger stimuli mouse 1, EM represent empty cage). **(C)** Time spent in familiar or novel stimulus chamber and total interaction time with familiar or novel stimulus mouse during social novelty stage (WT-vehicle, n = 8; BTBR-vehicle, n = 8; BTBR-bumetanide, n = 9, paired Student's *t*-test. Time in compartments, $^{**}p < 0.01$, WT-vehicle S1 vs. S2; N.S., not significant, BTBR-vehicle S1 vs. S2; $^{*}p < 0.05$, BTBR-bumetanide S1 vs. S2; interaction time, $^{*}p < 0.05$ WT-vehicle S1 vs. S2; N.S., not significant, BTBR-vehicle S1 vs. S2; $^{*}p < 0.05$, BTBR-bumetanide S1 vs. S2; S1 represent familiar stimuli mouse 1, S2 represent a novel stranger stimuli mouse 2). **(D)** Time spent self-grooming in grooming test (WT-vehicle, n = 8; BTBR-vehicle, n = 8; BTBR-bumetanide, n = 9. one-way ANOVA, $F_{(2,22)} = 16.77$, $p < 0.0001$, Bonferroni *post hoc*: $^{***}p<0.001$, WT-vehicle vs. BTBR-vehicle; N.S., not significant, WT-vehicle vs. BTBR- bumetanide; $^{**}p<0.01$; BTBR-vehicle vs. BTBR-bumetanide). **(E)** Total distance traveled in the open-field test (n = 8 each group; one-way ANOVA, $F_{(2,21)} = 6.453$, $p = 0.0065$, Bonferroni *post hoc*: $^{*}p < 0.05$, WT-vehicle vs. BTBR-vehicle; N.S., not significant; BTBR-vehicle vs. BTBR-bumetanide). **(F)** Time spent in the open arms elevated plus maze test (n = 8, each group. One-way ANOVA, $F_{(2,21)} = 8.918$, $p = 0.0016$, Bonferroni *post hoc*: $^{**}p < 0.01$, WT-vehicle vs. BTBR-vehicle; N.S., not significant; BTBR-vehicle vs. BTBR- bumetanide). All Data were presented as mean ± s.e.m.

negligible impact of bumetanide on locomotor activity of BTBR mice. In the elevated plus maze, bumetanide-treated BTBR mice showed a non-significant change toward vehicle-BTBR levels (**Figure 1F**), suggesting that bumetanide did not alter anxiogenic effects (**Figure 1F**). Overall, treatment of bumetanide is efficacious to treat autistic-like behaviors and did not significantly affect the locomotor activity or anxiety behavior in BTBR mice.

mPFC Region-Specific Infusion of Bumetanide Alleviated Social Deficits in BTBR Mice

The mPFC has been recognized as a critical region in the regulation of social behavior. To examine whether mPFC region-specific delivery of bumetanide could affect social behaviors in BTBR mice, we employed region infusion with bumetanide (100 μM,

0.5 ul each side) to the mPFC in BTBR mice (**Figure 2A**). In the sociability stage of three-chamber test, similarly to systemic treatment, intra-mPFC bumetanide treatment had no significant effect in improving sociability of BTBR mice (**Figure 2B**, Top), as measured by both time spent in the chamber and direct interaction time with social stimulus. In social novelty stage, intra mPFC bumetanide ameliorates the social novelty preference of BTBR mice, reflected both by time investigated in the novel social stimulus (S2) chamber and direct interaction time with the novel stimulus as compared to the familiar stimulus (S1)

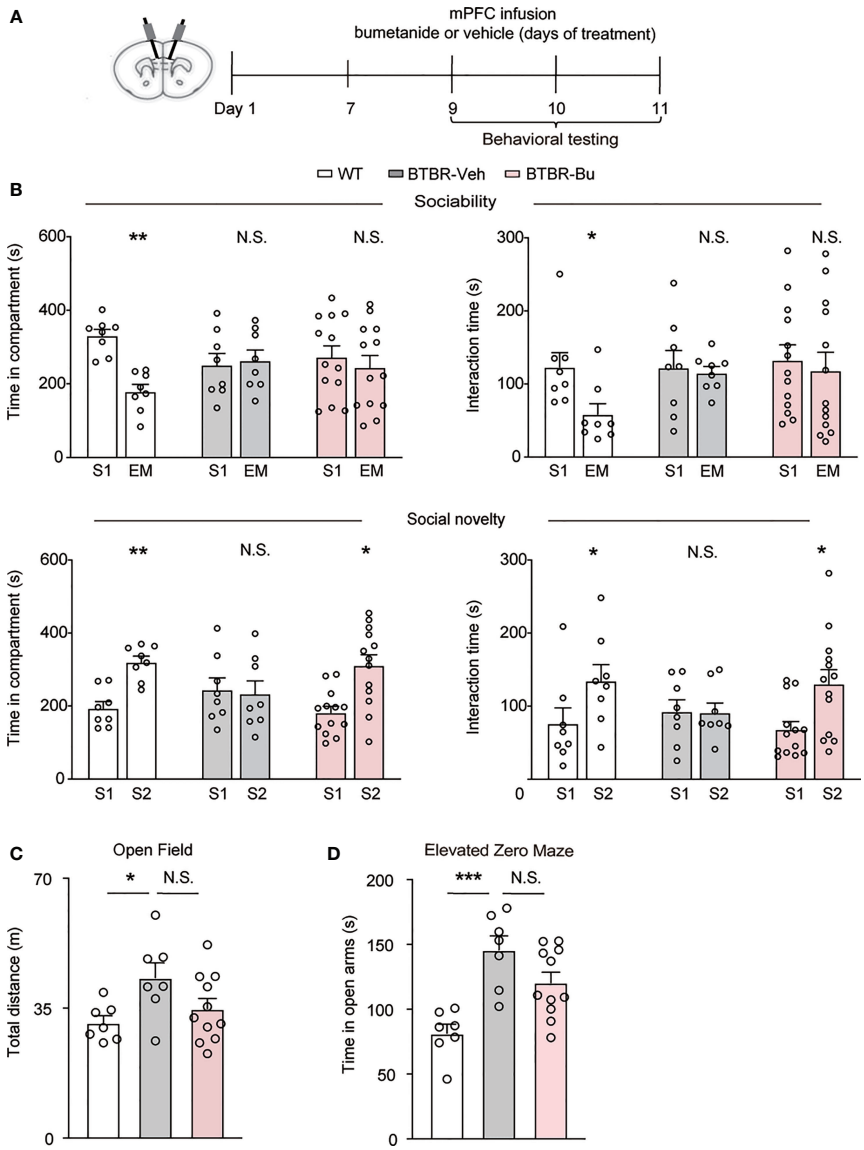

FIGURE 2 | mPFC region-specific infusion with bumetanide alleviated social deficit in BTBR mice. **(A)** Schematic representation of the experimental procedure. Male BTBR mice were administrated with bumetanide (100 μM) or vehicle into mPFC. **(B)** Top: time spent in the social stimulus or empty chamber and total interaction time with stimulus mouse or empty wire during sociability stage (WT, n = 8; BTBR-vehicle, n = 8; BTBR-bumetanide, n = 13. paired Student's *t*-test. Time in compartments, $^{**}p < 0.01$, WT S1 vs. EM; N.S., not significant, BTBR-vehicle S1 vs. EM; N.S., not significant, BTBR-bumetanide S1 vs. EM; interaction time, $^{*}p < 0.05$, WT S1 vs. EM; N.S., not significant, BTBR-vehicle S1 vs. EM; N.S., not significant, BTBR-bumetanide S1 vs. EM). Bottom: time spent in familiar or novel stimulus chamber and total interaction time with familiar or novel stimulus mouse during social novelty stage (paired Student's *t*-test. Time in compartments, $^{**}p < 0.01$, WT S1 vs. S2; N.S., not significant, BTBR-vehicle S1 vs. S2; $^{*}p < 0.05$, BTBR-bumetanide S1 vs. S2; interaction time, $^{*}p < 0.05$, WT S1 vs. S2; N.S., not significant, BTBR-vehicle S1 vs. S2; $^{*}p < 0.05$, BTBR-bumetanide S1 vs. S2). **(C)** Total distance traveled in the open field test (WT, n = 7; BTBR-vehicle, n = 7; BT BR-bumetanide, n = 11, one-way ANOVA, $F_{(2,22)} = 3.651$, $p = 0.0427$, Bonferroni *post hoc*: $^{*}p < 0.05$, WT vs. BTBR-vehicle; N.S., not significant, BTBR-vehicle vs. BTBR-bumetanide). **(D)** Time spent in the open arm during 5 min in elevated zero maze test (WT, n = 7; BTBR-vehicle, n = 7; BTBR-bumetanide, n = 11, one-way ANOVA, $F_{(2,22)} = 11.74$, p=0.0003, Bonferroni *post hoc*: $^{***}p$<0.001, WT vs. BTBR-vehicle; N.S., not significant, BTBR-vehicle vs. BTBR-bumetanide). Data were presented as mean ± s.e.m.

(**Figure 2B**, Bottom). This suggested that bumetanide alleviated social deficit in a mPFC region-specific way. Furthermore, in the open field test, no significant differences were observed with infusion of bumetanide to mPFC in total distance of locomotion behavior compared to vehicle-treated BTBR mice (**Figure 2C**). In the elevated zero maze test, vehicle-BTBR mice spent more time in the open arm than WT mice, and bumetanide-treated BTBR mice spent similar amounts of time in the open arm as vehicle group suggesting that bumetanide did not alter anxiogenic effects (**Figure 2D**). These data suggest that the effectiveness of bumetanide in alleviating social deficit is a mPFC region-specific way without causing nonspecific behavioral effects.

Formation and Brain Distribution of the Nanoparticles Following Intra-mPFC Administration

We wrapped bumetanide in a core of PEG-PLA as illustrated in **Figure 3A**. To explore the cell distribution of the NP (bumetanide) in BTBR mice, we performed rhodamine-labeled nanoparticles to directly visualize NP(bumetanide). We then administered rhodamine-labeled NP(bumetanide) (100 μM) into mPFC and sacrificed the mice. Immunostaining of several markers for different types of cells to determine the co-localization of NP(bumetanide). As shown in **Figure 3B**, we examined Iba1, which is a typical microglia marker, and found that NP(bumetanide) accumulated in microglia. We further examined NeuN and GFAP, which represent neurons and astrocytes, respectively, and found no overlap of NeuN-positive cells and astrocytic cells with NP(bumetanide). These findings suggest that NP(bumetanide) targets microglia *in vivo*.

NP (bumetanide) Infusion in the mPFC Alleviated Social Deficits in BTBR Mice

Next, we further examined the therapeutic effect of NP (bumetanide) in BTBR mice. Behavior tests were performed in BTBR mice after intra-mPFC NP(bumetanide) (100 μM)

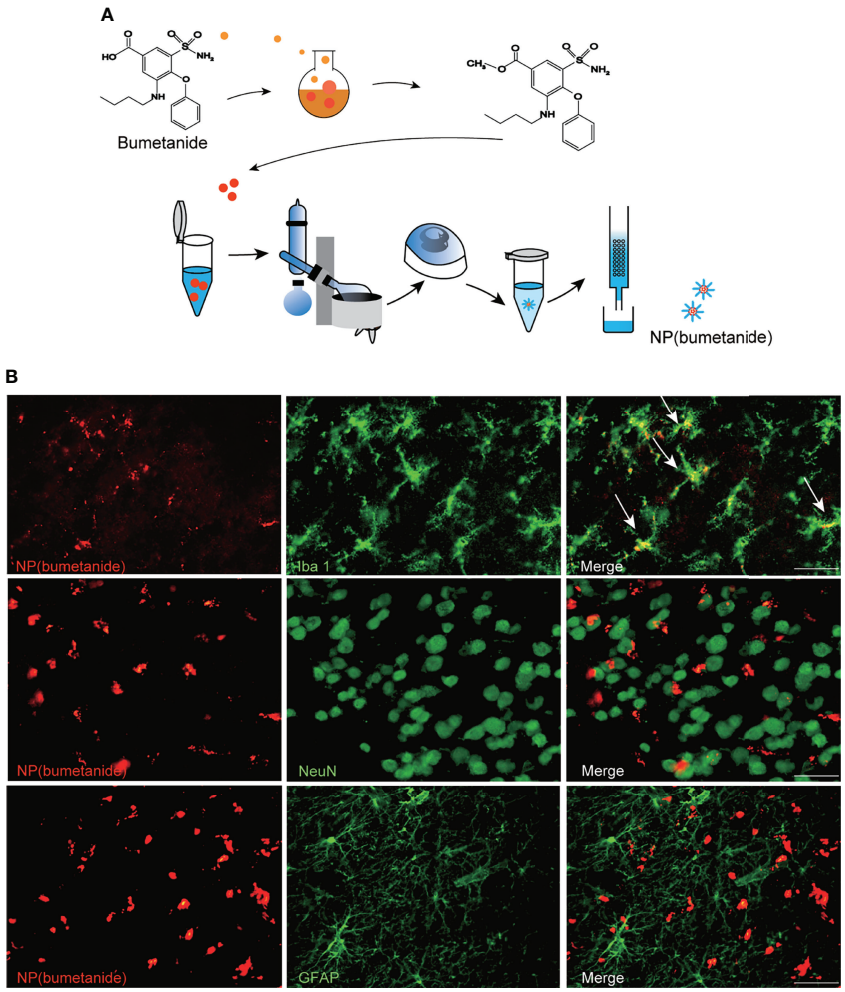

FIGURE 3 | NP(bumetanide) selectively targeting microglia of mPFC *in vivo*. **(A)** Schematic representation of the nanoformulated bumetanide experimental procedure. **(B)** Representative images of the fluorescence staining. NP(bumetanide) (Rhodamine-label, Red), microglia (Iba1, Green), Neuron (NeuN, Green), and astrocyte (GFAP, Green) and merged image in mPFC slices of BTBR mice, and co-localization of NP (bumetanide) and Iba1 are shown as arrow. Scale bar 100 μm.

infusion (**Figure 4A**). Like NP-blank-treated BTBR mice, sociability stage analysis revealed no significant change in the amount of time spent in the S1 chamber or direct with S1 (**Figure 4B**, Top) in NP(bumetanide)-treated BTBR mice. We detected a statistically significant difference for the social novelty stage, showing that NP(bumetanide)-treated BTBR mice have increased social approach in this social novelty stage, while measured by time spent in the novel chamber and interaction time with the novel stimulus (**Figure 4B**, bottom). In addition, no changes were observed in total distance traveled between groups in the open field test (**Figure 4C**). NP(bumetanide)- and NP-blank-treated-BTBR mice spent nearly equal time in the open arm in the elevated zero-maze test, suggesting that NP(bumetanide) treated mice did not have increased anxiety levels (**Figure 4D**). Taken together, these data suggest that NP(bumetanide) is effective

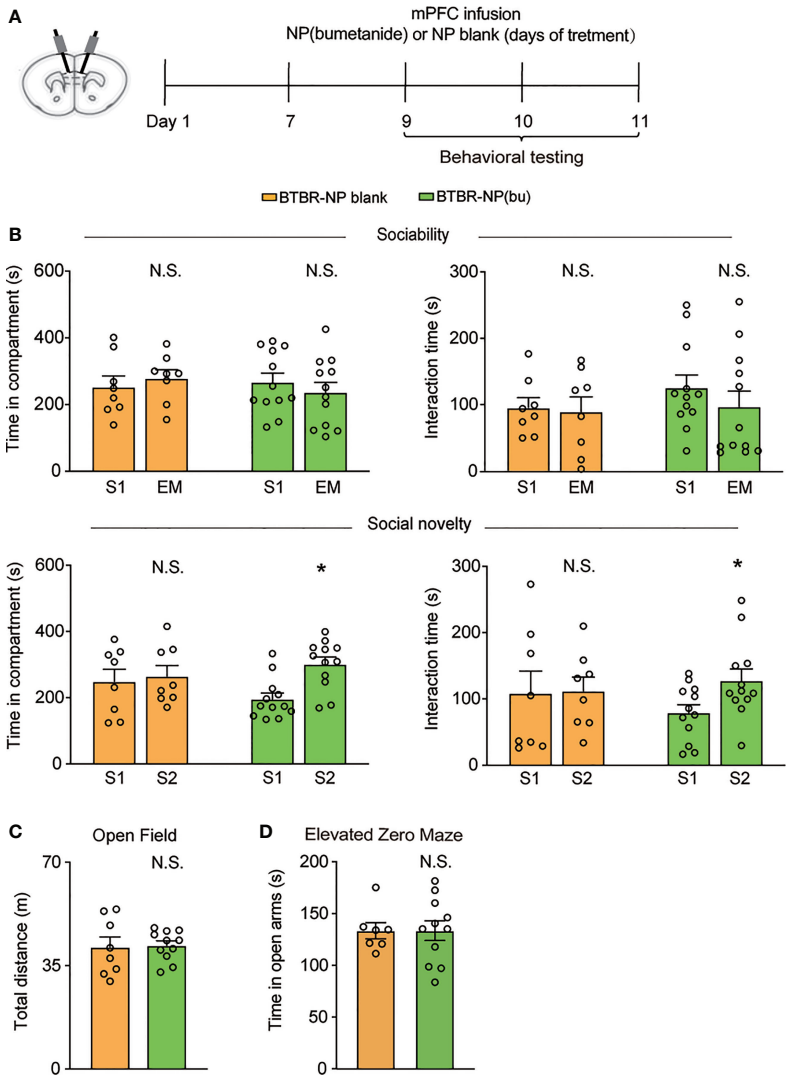

FIGURE 4 | mPFC region specific administration of NP(bumetanide) alleviated social deficits in BTBR mice. **(A)** Schematic representation of the experimental procedure. Male BTBR mice were intra-mPFC infusion of NP(bumetanide) (100 μM) or NP blank. **(B)** Top: time spent in the social stimulus or empty chamber and total interaction time with stimulus mouse or empty wire during sociability stage (BTBR-NP blank, n = 8; BTBR-NP(bumetanide), n = 12, paired Student's *t*-test. Time in compartments, N.S., not significant, BTBR-NP blank S1 vs. EM; N.S., not significant, BTBR-NP(bumetanide) S1 vs. EM; interaction time, N.S., not significant, BTBR-NP blank S1 vs. EM; N.S., not significant, BTBR-NP(bumetanide) S1 vs. EM). Bottom: time spent in familiar or novel stimulus chamber and total interaction time with familiar or novel stimulus mouse during social novelty stage (paired Student's *t*-test. Time in compartments, N.S., not significant, BTBR-NP blank S1 vs. S2; $^*p<0.05$, BTBR-NP(bumetanide) S1 vs. S2; interaction time, N.S., not significant, BTBR-NP blank S1 vs. S2; $^*p<0.05$, BTBR-NP(bumetanide) S1 vs. S2). **(C)** Total distance traveled in the open-field test (BTBR-NP blank, n = 8; BTBR-NP(bumetanide), n = 11, unpaired student *t*-test, N.S., not significant). **(D)** Time spent in the open arm in elevated zero maze test (BTBR-NP blank, n = 7; BTBR-NP(bumetanide), n = 11; unpaired student *t*-test, N.S., not significant). All data were presented as mean ± s.e.m.

in alleviating social deficits in a non-neuronal manner without causing non-specific behavioral effects.

NP (bumetanide) Alleviated Social Deficits in BTBR Mice Necessitate Microglia in mPFC

To explore whether the therapeutic efficacy of NP(bumetanide) was due to the cell-specific mechanism, we pretreated BTBR mice with PLX3397 to deplete microglia. PLX3397 is an orally selective CSF1R kinase inhibitor that has been reported to pharmacologically deplete more than 99% of microglia in the brain (34). Five-week-old BTBR mice were pre-treated with PLX3397 (290 mg/kg, standard chow) for 25 days with age-matched controls on standard chow, and infusion with NP (bumetanide) or vehicle in the mPFC for three times from day 21. Mice were tested on behavior tests (**Figure 5A**). Immunostaining for Iba1 showed a reduction in microglia in the mPFC of BTBR mice (**Figure 5B**). In the sociability stage, microglia-depleted BTBR mice spent less time on exploration of social stimulation chamber and social stimulus similar to the BTBR mice, indicating that microglia-depleted BTBR mice had no improvement in social approach in this stage (**Figure 5C** Top). In contrast, NP(bumetanide)-treated microglia depletion BTBR mice also spent less time in the social stimulation chamber compared to WT control. Next, we found that microglia depletion BTBR mice spent less time on exploration of S2 than on S1 in the social novelty stage, showing that microglial depletion throughout the brain had no improvement on social deficits in BTBR mice. In particular, NP(bumetanide)-treated microglia depletion BTBR mice showed no significant improvement in investigating of S2 over S1 (**Figure 5C** Bottom), showing that microglia depletion blocked the therapeutic effect of NP (bumetanide) in BTBR mice. In addition, no changes were observed in total distance traveled between BTBR groups in the open field test (**Figure 5D**). Neither depletion of microglia group nor NP(bumetanide)-treated microglia depletion BTBR group have increased anxiety levels in BTBR mice compared to BTBR control group (**Figure 5E**). Together, these behavioral results demonstrate that microglia depletion alone has no effects on social behaviors, and NP (bumetanide) improved social behaviors necessitates the presence of mPFC microglia in BTBR mice.

DISCUSSION

In this study, we reported that bumetanide alleviated social deficits in BTBR mice in a region- and cell type-specific manner **(Figure 6)**. Specifically, both systemic and mPFC region-specific delivery of bumetanide treated social deficits without influencing basic locomotor activity and anxiety-like behaviors in BTBR mice. Moreover, using a nanoparticulate drug delivery system, we showed that NP(bumetanide) also has a therapeutic effect in BTBR mice, in a microglia-dependent fashion. Mechanistically, NP(bumetanide) selectively targets microglia but not neurons or astrocytes and it was enough to alleviate social novelty impairments in BTBR mice in a mPFC region-specific way. These findings demonstrated a novel therapeutic strategy for ASD and a new insight into the function of bumetanide on immune cells.

Although preclinical and clinical studies have reported bumetanide attenuates symptoms of ASD (7, 9, 14, 35), two phase III clinical trials of bumetanide in ASD patients were terminated because of ineffective outcomes. These failure outcomes may be due to the difference in methodology including the dosage of bumetanide, multi-center trials, the possible high dropout rate, and the variability population with ASD (36). The precise effectiveness and action of bumetanide should be clarified. The effects of bumetanide were identified previously in maternal treatment of ASD mice (FRX and VPA) offspring (7). In our study, the results are consistent with previous findings in the systemic treatment of adolescent mice. The partial alleviation in social deficit alterations (improvement in social novelty exploration) that we observed in BTBR mice is implicated with the efficiency of bumetanide in treating social deficits, which is directly relevant to a core symptom of ASD. Despite the differences in the experimental methods, including model differences, inconsistent age of treatment starting, and treatment duration, our present study demonstrated reproducibility of bumetanide treatment in multiple models of ASD.

Furthermore, our results showed that bumetanide reduced repetitive behavior in BTBR mice. Indeed, BTBR mice are not the only ones that responded to bumetanide in several ASD mice models, including FRX and VPA, which also have improved repetitive behavior outcomes after treatment with bumetanide (7, 8, 37). Our results not only confirm previous findings as they provide evidence for the therapeutic effect of bumetanide, and complement in immune alterations found in rodent models of ASD.

Based on the wide tissue and cellular expression of NKCC1, combined with the low brain penetration and non-selective effects of bumetanide, it is proper to question if the effects of bumetanide in ASD are peripherally or centrally mediated. Recent investigations validated the role of NKCC1 as a pharmacological effector in rodent models of neurological diseases (38). Indeed, bumetanide modulated neuronal electrical parameters *in vitro* brain slice (7, 39), suggesting a central actions of bumetanide in ASD models. Enhancement of inhibitory neurotransmission by treatment with low doses of benzodiazepines improved deficits in autistic behavior in BTBR mice (40). To elucidate the roles of bumetanide at central nervous system level in ASD models, we investigated the effect of region-specific delivery of bumetanide in BTBR. The mPFC processes information related to social behavior especially in exploration of novelty social target (17), and the dysfunction of E/I ration in the mPFC contribute to ASD-like behavior in mice (15). We demonstrate the effects of mPFC-specific delivery of bumetanide and found this pattern was sufficient to improve social novelty exploration, similar to the therapeutic effects of the systemic way, suggesting a centrally-mediated mechanism by which bumetanide exerts its therapeutic effect on mice model of ASD. This finding is also consistent with

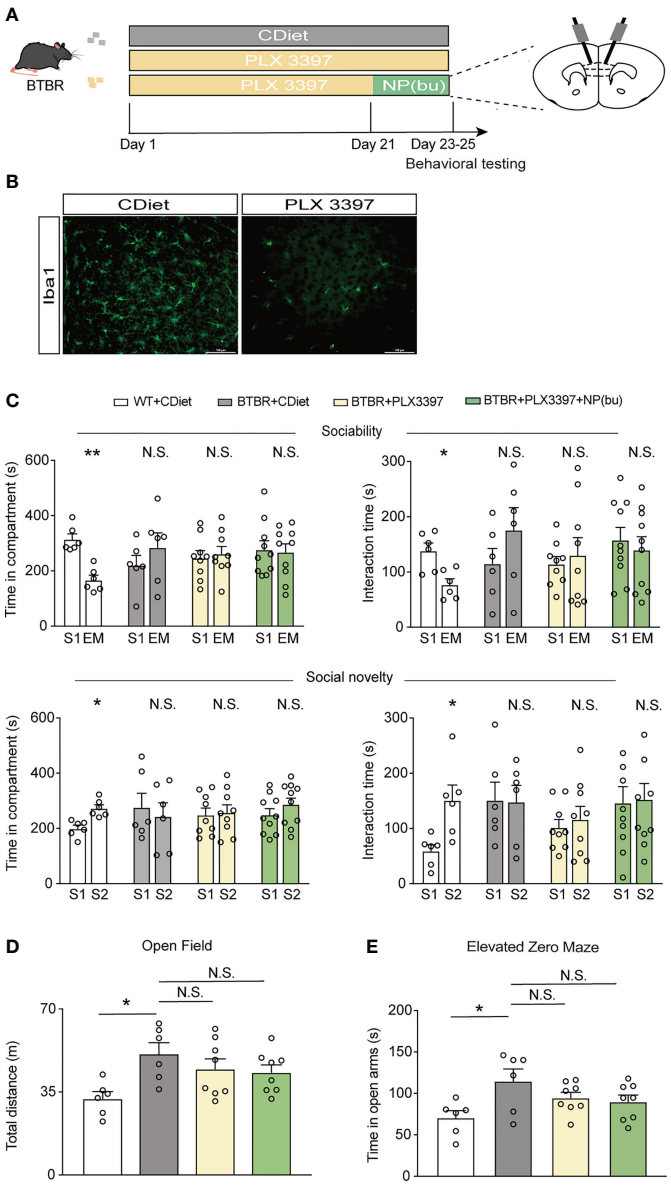

FIGURE 5 | NP(bumetanide) improved social behaviors in BTBR mice necessitate microglia in mPFC. **(A)** Schematic representation of the experimental procedure. Male BTBR mice were pretreated diets formulated with PLX3397 (CSF1R antagonist) or control diets for 25 days. NP(bumetanide) was provided for 3 times from day 21 and behavior tests were tested. **(B)** Representative Iba1 immunofluorescent staining from the mPFC region of CDiet (Left) and PLX3397 (Right)- treated BTBR mice. Scale bar 100 μm. **(C)** Top: time spent in social stimulus or empty chamber and total interaction time with stimulus mouse or empty wire during sociability stage (WT + CDiet, n = 6; BTBR + CDiet, n = 6; BTBR + PLX3397, n = 9, BTBR + PLX3397 + NP(bumetanide), n = 10, paired Student's *t*-test. Time in compartments, $^{**}p<0.01$, WT + CDiet S1 vs. EM; N.S., not significant, BTBR + CDiet S1 vs. S2; N.S., not significant, BTBR+PLX3397 S1 vs. S2; N.S., not significant, BTBR+PLX3397+NP(bumetanide) S1 vs. EM; interaction time, $^{*}p<0.05$, WT + CDiet S1 vs. EM; N.S., not significant, BTBR + CDiet S1 vs. EM; N.S., not significant, BTBR+PLX3397 S1 vs. EM; N.S., not significant, BTBR+PLX3397+NP(bumetanide). Bottom: time spent in familiar or novel stimulus chamber and total interaction time with familiar or novel stimulus mouse during social novelty stage (paired Student's *t*-test. Time in compartments, $^{*}p<0.05$, WT + CDiet S1 vs. S2; N.S., not significant, BTBR + CDiet S1 vs. S2; N.S., not significant, BTBR + PLX3397 S1 vs. S2; N.S., not significant, BTBR + PLX3397 + NP(bumetanide) S1 vs. S2; interaction time, $^{*}p<0.05$, WT + CDiet S1 vs. S2; N.S., not significant, BTBR + CDiet S1 vs. S2; N.S., not significant, BTBR + PLX3397 S1 vs. S2; N.S., not significant, BTBR + PLX3397 + NP(bumetanide) S1 vs. S2). **(D)** Total distance traveled in the open-field test (WT + CDiet, n = 6; BTBR + CDiet, n= 6; BTBR + PLX3397, n =8; BTBR + PLX3397 + NP(bumetanide), n = 8, one-way ANOVA, $F(3,24) = 3.704$, $p=0.0254$, Bonferroni *post hoc*: $^{*}p < 0.05$, WT + CDiet vs. BTBR + CDiet; N.S., not significant, BTBR + CDiet vs. BTBR + PLX3397; N.S., not significant, BTBR + CDiet vs. BTBR + PLX3397 + NP(bumetanide). **(E)** Time spent in the open arm in elevated zero maze test (WT + CDiet, n = 6; BTBR + CDiet, n= 6; BTBR + PLX3397, n =8; BTBR + PLX3397 + NP(bumetanide), n = 8, one-way ANOVA, $F(3,24) = 3.326$, $p=0.0366$, Bonferroni *post hoc*: $^{*}p < 0.05$, WT + CDiet vs. BTBR + CDiet; N.S., not significant, BTBR + CDiet vs. BTBR + PLX3397; N.S., not significant, BTBR + CDiet vs. BTBR + PLX3397 + NP(bumetanide). Data were presented as mean ± s.e.m.

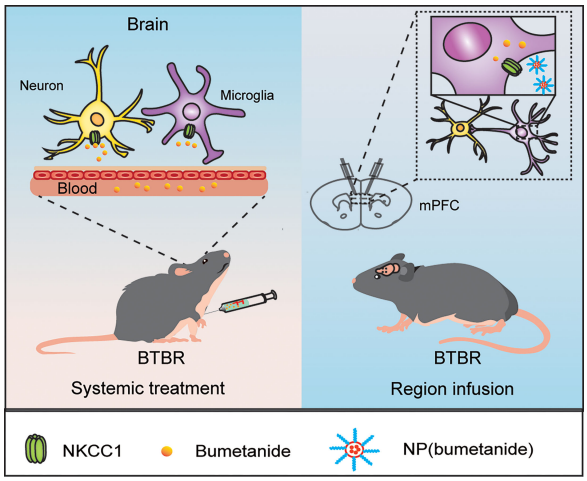

FIGURE 6 | A proposed work model by bumetanide and NP(bumetanide) in the BTBR mice.

the evidence that restoring the E/I balance is sufficient to ameliorate social approach in the VPA rodent models of ASD, as reported in previous findings (41), which could be due to manipulated E/I balance in the mPFC. Therefore, these findings emphasize the importance of the mPFC for the effect of bumetanide, and that the effects of systemic bumetanide treatment may be dependent on central targets, namely the mPFC region in the BTBR.

Besides the neuronal actions of bumetanide and its precise cellular targets of bumetanide in ASD, the effects of bumetanide on diverse cell types should also be investigated. Importantly, the pathophysiological factors of ASD include immune mechanism, and treatment targeting immune factors may be considered a novel therapeutic strategy for ASD. Microglia are the resident immune cells of the brain, and previous studies have shown microglia dysfunction in both patients with ASD and in preclinical models (26, 42, 43). We observed that NP (bumetanide) accumulated in microglia, and the infusion of NP(bumetanide) in the mPFC improved social novelty in BTBR strain. In order to provide mechanistic evidence that microglia-specific targeting can improve social deficit in BTBR mice, we established a pharmacological depletion of microglia in BTBR mice using a CSF1R inhibitor. Microglia are the only resident immune cells of the brain that express CSF1R, and it has been identified that short-term administration (3 weeks) of PLX3397 can eliminate virtually all microglia in the brain (34). Interestingly, in this study, no improvement was observed in microglia depletion BTBR mice as determined by social tests. It seems that microglia function is subtle in the brain and plays a complex role of microglia in ASD brain, as elimination of microglia alone is not sufficient to rescue social behavior. Microglia could secrete soluble factors and directly interact with neurons, participating in brain function. Indeed, depletion of microglia at an early development stage has led to autistic-like behavior in mice, which was associated with the deficit of synaptic pruning (44). Modulation of microglial function, rather than eliminating it, seems to be a more efficient strategy in ASD, and future research could use genetic manipulation tools to target microglia to further answer this question.

Crucially, the depletion of microglia significantly blocked the beneficial effects of NP(bumetanide) treatment in BTBR mice. Further understanding of the underlying molecular mechanisms of how bumetanide regulates microglia function remains to be elucidated. NKCC1 is expressed in glial cells, and a single-cell transcriptomic study (BRAIN-SAT database) has supported NKCC1 expression in microglia (21), which consisted of a recent study showing microglial NKCC1 expression in the brain (45), but its role in neurodevelopment conditions like ASD remains unknown. Researchers found that bumetanide attenuated LPS-induced acute lung injury by inhibiting NKCC1-mediated macrophage volume alteration and inflammatory function in a mouse model of LPS-induced lung injury (30). This indicates that the beneficial actions of NP(bumetanide) may be based on the anti-inflammatory action caused by the inhibition of NKCC1 in the microglia. However, there is an intriguing finding that the direct administration of bumetanide into the brain *in vivo* displayed the opposite effect of a systemic administration and can be explained by changes in K^+ efflux mechanism in microglia (45). Therefore, the precise mechanism through the NKCC1 inhibitor bumetanide modulates the function of microglia in BTBR mice needs to be further investigated. We reasoned about several underlying mechanisms as follows: firstly, systemic treatment of bumetanide recently was reported to reduce inflammatory response in the brain of LPS-induced mice (45), and in the lung of LPS-induced lung injury mice (30), suggesting the therapeutic effects of systemic treatment of bumetanide in BTBR mice could be partially due to anti-inflammatory action. However, due to the non-selective action of bumetanide, neuronal and non-neuronal (both periphery and central) cells may be involved in this action; secondly, In this study, we used a nanoparticle system to deliver bumetanide, and the NP(bumetanide) would be easier to induce the phagocytosis function of microglia given the microglia are detector cells in the brain. Microglia phagocytosis is often reported to be suppressed in ASD models due to the lack of elimination of synapses by microglia. For instance, *Fmr1* KO mice (Fragile X syndrome) showed impaired microglia-mediated synaptic elimination during the developmental period in CA region of the brain (46). TREM2 (a risk gene of Alzheimer's disease related to microglial phagocytosis) KO mice displayed autistic-like behaviors and reduced microglial synaptic elimination (47). More recently reported that enhanced protein synthesis in microglia increased the number of excitatory synapses in the mPFC and caused autistic-like behavior in mice which may be related to a decrease in microglia motility and phagocytosis of synapses (48). In a maternal immune activation (MIA) mice model of ASD, minocycline treatment suppressed the inflammatory activation of microglia and restored the phagocytic of microglia whilst alleviating the autistic-like behaviors (49). Restoration of the motility and phagocytosis of

microglia may be involved in NP(bumetanide)'s action in BTBR mice; thirdly, although bumetanide is a well-known inhibitor of NKCC1, it is possible to find out that the effects of bumetanide are due to other pharmacological effects independent of the NKCC1 inhibition.

Finding the specific cellular mechanism of bumetanide's modulation of behavioral and cellular features related to ASD can provide instrumental information to better understand the pathophysiology of ASD. Using the nanoparticle drug system as a tool, we also demonstrated that NP(bumetanide) alleviates social behavior in an mPFC-microglia-dependent way in BTBR mice. The proposed link between bumetanide and microglia, which is involved in the recovery of social deficit in BTBR mice, provides an important set of evidence relating to neuroimmunology and ASD, as well as generating scope for future therapeutic targets.

DATA AVAILABILITY STATEMENT

The raw data supporting the conclusions of this article will be made available by the authors, without undue reservation.

ETHICS STATEMENT

The animal study was reviewed and approved by Animal Ethics Committee of East China Normal University.

AUTHOR CONTRIBUTIONS

FL and XLG conceptualized the study; HL, XG, XS, TLZ, BM, TTZ, and H-TZ performed animal research and data analysis; HL, VB-J, W-GL, and FL wrote the manuscript with contributions from all authors. All authors read and approved the final manuscript.

FUNDING

This study was supported by grants from the National Natural Science Foundation of China (82125032, 81930095 and 81761128035), the Science and Technology Commission of Shanghai Municipality (19410713500 and 2018SHZDZX01), the Shanghai Municipal Commission of Health and Family Planning (GWV-10.1-XK07, 2020CXJQ01, 2018YJRC03), the Shanghai Clinical Key Subject Construction Project (shslczdzk02902), the Guangdong Key Project (2018B030335001), and innovative research team of high-level local universities in Shanghai.

ACKNOWLEDGMENTS

We thank East China Normal University (Shanghai, China) for providing us with experimental facilities in completing this work.

REFERENCES

1. Lord C, Brugha TS, Charman T, Cusack J, Dumas G, Frazier T, et al. Autism Spectrum Disorder. *Nat Rev Dis Primers* (2020) 6:5. doi: 10.1038/s41572-019-0138-4
2. Accordino RE, Kidd C, Politte LC, Henry CA, McDougle CJ. Psychopharmacological Interventions in Autism Spectrum Disorder. *Expert Opin Pharmacother* (2016) 17:937–52. doi: 10.1517/14656566.2016.1154536
3. Kim KC, Gonzales EL, Lázaro MT, Choi CS, Bahn GH, Yoo HJ, et al. Clinical and Neurobiological Relevance of Current Animal Models of Autism Spectrum Disorders. *Biomol Ther* (2016) 24:207–43. doi: 10.4062/biomolther.2016.061
4. Bolivar V, Walters S, Phoenix J. Assessing Autism-Like Behavior in Mice: Variations in Social Interactions Among Inbred Strains. *Behav Brain Res* (2007) 176:21–6. doi: 10.1016/j.bbr.2006.09.007
5. Amodeo DA, Jones JH, Sweeney JA, Ragozzino ME. Differences in BTBR T+ Tf/J and C57BL/6J Mice on Probabilistic Reversal Learning and Stereotyped Behaviors. *Behav Brain Res* (2012) 227:64–72. doi: 10.1016/j.bbr.2011.10.032
6. Rubenstein JLR, Merzenich MM. Model of Autism: Increased Ratio of Excitation/Inhibition in Key Neural Systems: Model of Autism. *Genes Brain Behav* (2003) 2:255–67. doi: 10.1034/j.1601-183X.2003.00037.x
7. Tyzio R, Nardou R, Ferrari DC, Tsintsadze T, Shahrokhi A, Eftekhari S, et al. Oxytocin-Mediated GABA Inhibition During Delivery Attenuates Autism Pathogenesis in Rodent Offspring. *Science* (2014) 343:675–9. doi: 10.1126/science.1247190
8. Eftekhari S, Shahrokhi A, Tsintsadze V, Nardou R, Brouchoud C, Conesa M, et al. Response to Comment on "Oxytocin-Mediated GABA Inhibition During Delivery Attenuates Autism Pathogenesis in Rodent Offspring". *Science* (2014) 346:176–6. doi: 10.1126/science.1256009
9. Lemonnier E, Degrez C, Phelep M, Tyzio R, Josse F, Grandgeorge M, et al. A Randomised Controlled Trial of Bumetanide in the Treatment of Autism in Children. *Transl Psychiatry* (2012) 2:e202–2. doi: 10.1038/tp.2012.124
10. Dai Y, Zhang L, Yu J, Zhou X, He H, Ji Y, et al. Improved Symptoms Following Bumetanide Treatment in Children Aged 3–6 Years With Autism Spectrum Disorder: A Randomized, Double-Blind, Placebo-Controlled Trial. *Sci Bull* (2021) 66:1591–8. doi: 10.1016/j.scib.2021.01.008
11. Sprengers JJ, van Andel DM, Zuithoff NPA, Keijzer-Veen MG, Schulp AJA, Scheepers FE, et al. Bumetanide for Core Symptoms of Autism Spectrum Disorder (Bambi): A Single Center, Double-Blinded, Participant-Randomized, Placebo-Controlled, Phase-2 Superiority Trial. *J Am Acad Child Adolesc Psychiatry* (2021) 60:865–76. doi: 10.1016/j.jaac.2020.07.888
12. Crutel V, Lambert E, Penelaud P-F, Albarrán Severo C, Fuentes J, Rosier A, et al. Bumetanide Oral Liquid Formulation for the Treatment of Children and Adolescents With Autism Spectrum Disorder: Design of Two Phase III Studies (Sign Trials). *J Autism Dev Disord* (2021) 51:2959–72. doi: 10.1007/s10803-020-04709-8
13. James BJ, Gales MA, Gales BJ. Bumetanide for Autism Spectrum Disorder in Children: A Review of Randomized Controlled Trials. *Ann Pharmacother* (2019) 53:537–44. doi: 10.1177/1060028018817304
14. Zhang L, Huang C-C, Dai Y, Luo Q, Ji Y, Wang K, et al. Symptom Improvement in Children With Autism Spectrum Disorder Following Bumetanide Administration Is Associated With Decreased GABA/glutamate Ratios. *Transl Psychiatry* (2020) 10:9. doi: 10.1038/s41398-020-0692-2
15. Yizhar O, Fenno LE, Prigge M, Schneider F, Davidson TJ, O'Shea DJ, et al. Neocortical Excitation/Inhibition Balance in Information Processing and Social Dysfunction. *Nature* (2011) 477:171–8. doi: 10.1038/nature10360
16. Murray AJ, Woloszynowska-Fraser MU, Ansel-Bollepalli L, Cole KLH, Foggetti A, Crouch B, et al. Parvalbumin-Positive Interneurons of the Prefrontal Cortex Support Working Memory and Cognitive Flexibility. *Sci Rep* (2015) 5:16778. doi: 10.1038/srep16778
17. Liang B, Zhang L, Barbera G, Fang W, Zhang J, Chen X, et al. Distinct and Dynamic on and OFF Neural Ensembles in the Prefrontal Cortex Code Social Exploration. *Neuron* (2018) 100:700–14.e9. doi: 10.1016/j.neuron.2018.08.043
18. Kana RK, Maximo JO, Williams DL, Keller TA, Schipul SE, Cherkassky VL, et al. Aberrant Functioning of the Theory-of-Mind Network in Children and Adolescents With Autism. *Mol Autism* (2015) 6:59. doi: 10.1186/s13229-015-0052-x

19. Urakawa S, Takamoto K, Ishikawa A, Ono T, Nishijo H. Selective Medial Prefrontal Cortex Responses During Live Mutual Gaze Interactions in Human Infants: An fNIRS Study. *Brain Topogr* (2015) 28:691–701. doi: 10.1007/s10548-014-0414-2
20. Pierce K. The Brain Response to Personally Familiar Faces in Autism: Findings of Fusiform Activity and Beyond. *Brain* (2004) 127:2703–16. doi: 10.1093/brain/awh289
21. Loo L, Simon JM, Xing L, McCoy ES, Niehaus JK, Guo J, et al. Single-Cell Transcriptomic Analysis of Mouse Neocortical Development. *Nat Commun* (2019) 10:134. doi: 10.1038/s41467-018-08079-9
22. Morgan JT, Chana G, Pardo CA, Achim C, Semendeferi K, Buckwalter J, et al. Microglial Activation and Increased Microglial Density Observed in the Dorsolateral Prefrontal Cortex in Autism. *Biol Psychiatry* (2010) 68:368–76. doi: 10.1016/j.biopsych.2010.05.024
23. Tetreault NA, Hakeem AY, Jiang S, Williams BA, Allman E, Wold BJ, et al. Microglia in the Cerebral Cortex in Autism. *J Autism Dev Disord* (2012) 42:2569–84. doi: 10.1007/s10803-012-1513-0
24. Voineagu I, Wang X, Johnston P, Lowe JK, Tian Y, Horvath S, et al. Transcriptomic Analysis of Autistic Brain Reveals Convergent Molecular Pathology. *Nature* (2011) 474:380–4. doi: 10.1038/nature10110
25. Gandal MJ, Haney JR, Parikshak NN, Leppa V, Ramaswami G, Hartl C, et al. Shared Molecular Neuropathology Across Major Psychiatric Disorders Parallels Polygenic Overlap. *Science* (2018) 359:693–7. doi: 10.1126/science.aad6469
26. Suzuki K, Sugihara G, Ouchi Y, Nakamura K, Futatsubashi M, Takebayashi K, et al. Microglial Activation in Young Adults With Autism Spectrum Disorder. *JAMA Psychiatry* (2013) 70:49. doi: 10.1001/jamapsychiatry.2013.272
27. Yao L, Gu X, Song Q, Wang X, Huang M, Hu M, et al. Nanoformulated Alpha-Mangostin Ameliorates Alzheimer's Disease Neuropathology by Elevating LDLR Expression and Accelerating Amyloid-Beta Clearance. *J Controlled Release* (2016) 226:1–14. doi: 10.1016/j.jconrel.2016.01.055
28. Song Q, Huang M, Yao L, Wang X, Gu X, Chen J, et al. Lipoprotein-Based Nanoparticles Rescue the Memory Loss of Mice With Alzheimer's Disease by Accelerating the Clearance of Amyloid-Beta. *ACS Nano* (2014) 8:2345–59. doi: 10.1021/nn4058215
29. Silvestre de Ferron B, Vilpoux C, Kervern M, Robert A, Antol J, Naassila M, et al. Increase of KCC2 in Hippocampal Synaptic Plasticity Disturbances After Perinatal Ethanol Exposure: Prenatal Ethanol and KCC2. *Addict Biol* (2017) 22:1870–82. doi: 10.1111/adb.12465
30. Hung C-M, Peng C-K, Wu C-P, Huang K-L. Bumetanide Attenuates Acute Lung Injury by Suppressing Macrophage Activation. *Biochem Pharmacol* (2018) 156:60–7. doi: 10.1016/j.bcp.2018.08.013
31. Gao X, Tao W, Lu W, Zhang Q, Zhang Y, Jiang X, et al. Lectin-Conjugated PEG–PLA Nanoparticles: Preparation and Brain Delivery After Intranasal Administration. *Biomaterials* (2006) 27:3482–90. doi: 10.1016/j.biomaterials.2006.01.038
32. Konsman J-P. The Mouse Brain in Stereotaxic Coordinates. *Psychoneuroendocrinology* (2003) 28:827–8. doi: 10.1016/S0306-4530(03)00088-X
33. McFarlane HG, Kusek GK, Yang M, Phoenix JL, Bolivar VJ, Crawley JN. Autism-Like Behavioral Phenotypes in BTBR T+Tf/J Mice. *Genes Brain Behav* (2008) 7:152–63. doi: 10.1111/j.1601-183X.2007.00330.x
34. Elmore MRP, Najafi AR, Koike MA, Dagher NN, Spangenberg EE, Rice RA, et al. Colony-Stimulating Factor 1 Receptor Signaling Is Necessary for Microglia Viability, Unmasking a Microglia Progenitor Cell in the Adult Brain. *Neuron* (2014) 82:380–97. doi: 10.1016/j.neuron.2014.02.040
35. Bambini-Junior V, Nunes GDF, Schneider T, Gottfried C. Comment on "Oxytocin-Mediated GABA Inhibition During Delivery Attenuates Autism Pathogenesis in Rodent Offspring". *Science* (2014) 346:176–6. doi: 10.1126/science.1255679
36. Savardi A, Borgogno M, De Vivo M, Cancedda L. Pharmacological Tools to Target NKCC1 in Brain Disorders. *Trends Pharmacol Sci* (2021) 42:1009–34. doi: 10.1016/j.tips.2021.09.005
37. Savardi A, Borgogno M, Narducci R, La Sala G, Ortega JA, Summa M, et al. Discovery of a Small Molecule Drug Candidate for Selective Nkcc1 Inhibition in Brain Disorders. *Chem* (2020) 6:2073–96. doi: 10.1016/j.chempr.2020.06.017
38. Kim HR, Rajagopal L, Meltzer HY, Martina M. Depolarizing GABA A Current in the Prefrontal Cortex is Linked With Cognitive Impairment in a Mouse Model Relevant for Schizophrenia. *Sci Adv* (2021) 7:eaba5032. doi: 10.1126/sciadv.aba5032
39. Lozovaya N, Nardou R, Tyzio R, Chiesa M, Pons-Bennaceur A, Eftekhari S, et al. Early Alterations in a Mouse Model of Rett Syndrome: The GABA Developmental Shift is Abolished at Birth. *Sci Rep* (2019) 9:9276. doi: 10.1038/s41598-019-45635-9
40. Han S, Tai C, Jones CJ, Scheuer T, Catterall WA. Enhancement of Inhibitory Neurotransmission by GABA A Receptors Having α 2,3 -Subunits Ameliorates Behavioral Deficits in a Mouse Model of Autism. *Neuron* (2014) 81:1282–9. doi: 10.1016/j.neuron.2014.01.016
41. Brumback AC, Ellwood IT, Kjaerby C, Iafrati J, Robinson S, Lee AT, et al. Identifying Specific Prefrontal Neurons That Contribute to Autism-Associated Abnormalities in Physiology and Social Behavior. *Mol Psychiatry* (2018) 23:2078–89. doi: 10.1038/mp.2017.213
42. Heo Y, Zhang Y, Gao D, Miller VM, Lawrence DA. Aberrant Immune Responses in a Mouse With Behavioral Disorders. *PloS One* (2011) 6:e20912. doi: 10.1371/journal.pone.0020912
43. Eissa N, Jayaprakash P, Stark H, Łażewska D, Kieć-Kononowicz K, Sadek B. Simultaneous Blockade of Histamine H3 Receptors and Inhibition of Acetylcholine Esterase Alleviate Autistic-Like Behaviors in BTBR T+ Tf/J Mouse Model of Autism. *Biomolecules* (2020) 10:1251. doi: 10.3390/biom10091251
44. Zhan Y, Paolicelli RC, Sforazzini F, Weinhard L, Bolasco G, Pagani F, et al. Deficient Neuron-Microglia Signaling Results in Impaired Functional Brain Connectivity and Social Behavior. *Nat Neurosci* (2014) 17:400–6. doi: 10.1038/nn.3641
45. Tóth K, Lénárt N, Berki P, Fekete R, Szabadits E, Pósfai B, et al. The NKCC1 Ion Transporter Modulates Microglial Phenotype and Inflammatory Response to Brain Injury in a Cell-Autonomous Manner. *PloS Biol* (2022) 20:e3001526. doi: 10.1371/journal.pbio.3001526
46. Jawaid S, Kidd GJ, Wang J, Swetlik C, Dutta R, Trapp BD. Alterations in CA1 Hippocampal Synapses in a Mouse Model of Fragile X Syndrome. *Glia* (2018) 66:789–800. doi: 10.1002/glia.23284
47. Filipello F, Morini R, Corradini I, Zerbi V, Canzi A, Michalski B, et al. The Microglial Innate Immune Receptor TREM2 Is Required for Synapse Elimination and Normal Brain Connectivity. *Immunity* (2018) 48:979–991.e8. doi: 10.1016/j.immuni.2018.04.016
48. Xu Z-X, Kim GH, Tan J-W, Riso AE, Sun Y, Xu EY, et al. Elevated Protein Synthesis in Microglia Causes Autism-Like Synaptic and Behavioral Aberrations. *Nat Commun* (2020) 11:1797. doi: 10.1038/s41467-020-15530-3
49. Mattei D, Ivanov A, Ferrai C, Jordan P, Guneykaya D, Buonfiglioli A, et al. Maternal Immune Activation Results in Complex Microglial Transcriptome Signature in the Adult Offspring That is Reversed by Minocycline Treatment. *Transl Psychiatry* (2017) 7:e1120–0. doi: 10.1038/tp.2017.80

Conflict of Interest: The authors declare that the research was conducted in the absence of any commercial or financial relationships that could be construed as a potential conflict of interest.

frontiers | Frontiers in Neurology

ORIGINAL RESEARCH
published: 30 May 2022
doi: 10.3389/fneur.2022.812439

The Detection of Invisible Abnormal Metabolism in the FDG-PET Images of Patients With Anti-LGI1 Encephalitis by Machine Learning

Jian Pan[1], Ruijuan Lv[2], Guifei Zhou[1], Run Si[1], Qun Wang[2], Xiaobin Zhao[3], Jiangang Liu[1,4,5] and Lin Ai[3]**

[1] School of Computer and Information Technology, Beijing Jiaotong University, Beijing, China, [2] Department of Neurology, Beijing Tiantan Hospital, Capital Medical University; China National Clinical Research Center for Neurological Diseases, Beijing, China, [3] Department of Nuclear Medicine, Beijing Tiantan Hospital, Capital Medical University, Beijing, China, [4] Beijing Advanced Innovation Center for Big Data-Based Precision Medicine, School of Engineering Medicine, Beihang University, Beijing, China, [5] Key Laboratory of Big Data-Based Precision Medicine (Beihang University), Ministry of Industry and Information Technology of the People's Republic of China, Beijing, China

OPEN ACCESS

Edited by:
Joseph Scafidi,
Kennedy Krieger Institute,
United States

Reviewed by:
Bastien Joubert,
Hospices Civils de Lyon, France
Gabriel Gonzalez-Escamilla,
Johannes Gutenberg University
Mainz, Germany

***Correspondence:**
Jiangang Liu
jgliu@buaa.edu.cn
Lin Ai
ailin@bjtth.org

Specialty section:
This article was submitted to Multiple Sclerosis and Neuroimmunology, a section of the journal Frontiers in Neurology

Received: 10 November 2021
Accepted: 27 April 2022
Published: 30 May 2022

Citation:
Pan J, Lv R, Zhou G, Si R, Wang Q, Zhao X, Liu J and Ai L (2022) The Detection of Invisible Abnormal Metabolism in the FDG-PET Images of Patients With Anti-LGI1 Encephalitis by Machine Learning. Front. Neurol. 13:812439. doi: 10.3389/fneur.2022.812439

Objective: This study aims to detect the invisible metabolic abnormality in PET images of patients with anti-leucine-rich glioma-inactivated 1 (LGI1) encephalitis using a multivariate cross-classification method.

Methods: Participants were divided into two groups, namely, the training cohort and the testing cohort. The training cohort included 17 healthy participants and 17 patients with anti-LGI1 encephalitis whose metabolic abnormality was able to be visibly detected in both the medial temporal lobe and the basal ganglia in their PET images [completely detectable (CD) patients]. The testing cohort included another 16 healthy participants and 16 patients with anti-LGI1 encephalitis whose metabolic abnormality was not able to be visibly detected in the medial temporal lobe and the basal ganglia in their PET images [non-completely detectable (non-CD) patients]. Independent component analysis (ICA) was used to extract features and reduce dimensions. A logistic regression model was constructed to identify the non-CD patients.

Results: For the testing cohort, the accuracy of classification was 90.63% with 13 out of 16 non-CD patients identified and all healthy participants distinguished from non-CD patients. The patterns of PET signal changes resulting from metabolic abnormalities related to anti-LGI1 encephalitis were similar for CD patients and non-CD patients.

Conclusion: This study demonstrated that multivariate cross-classification combined with ICA could improve, to some degree, the detection of invisible abnormal metabolism in the PET images of patients with anti-LGI1 encephalitis. More importantly, the invisible metabolic abnormality in the PET images of non-CD patients showed patterns that were similar to those seen in CD patients.

Keywords: FDG-PET, anti-LGI1 encephalitis, independent component analysis, machine learning, multivariate cross-classification

INTRODUCTION

Leucine-rich glioma-inactivated 1 (LGI1) antibody encephalitis is one of the subtypes of autoimmune limbic encephalitis (ALE) that is characterized by a rapid progression of neurological and psychiatric deficits (1). It has been clinically demonstrated that the outcomes of ALE can be improved by early diagnosis and treatment (2–4). In the existing criteria, antibody testing is necessary and effective in the diagnosis of autoimmune encephalitis (1, 2). However, antibody testing is time-consuming and not easily accessible and therefore, a diagnosis based on antibody testing is likely to delay the treatment (2). In fact, as suggested by a position paper (2), a preliminary treatment can be initiated by an early assessment based on some traditional clinical characteristics and commonly used methods of diagnosis, such as magnetic resonance imaging (MRI), electroencephalography (EEG), or cerebrospinal fluid (CSF), before obtaining the results of antibody testing, which, in turn, will refine the initial diagnosis and treatment. However, the MRI results in some patients with anti-LGI1 encephalitis were normal (5–7) and positron emission tomography (PET) can increase the sensitivity to LGI1 encephalitis compared to MRI (6, 8, 9). Therefore, PET may be a prospective imaging tool for the early diagnosis of LGI1 encephalitis. Nevertheless, for a proportion of patients with anti-LGI1 encephalitis, the metabolic disorders were not yet perceptible (6). A recent study found the abnormal intensity of the PET signal in some areas within the medial temporal lobe and/or the basal ganglia for patients with autoimmune encephalitis (including many patients with anti-LGI1 encephalitis) who could not be identified by visual inspection (10). This finding implied that quantitative analysis may improve the identification of non-completely detectable (non-CD) patients.

Machine learning (ML), a multivariate analysis method, presents higher sensitivity than traditional univariate analysis (11, 12) and it is increasingly applied to medical imaging analysis, such as MRI, PET, and computed tomography (CT) (13–15). However, for the analysis of medical images based on ML, the number of samples is usually less than that of features, resulting in "overfitting" (16). To address this problem, feature selection or dimension reduction is conducted before training a classifier (17, 18). Independent component analysis (ICA) has been proved to be an effective method for dimension reduction (18), particularly for the multivariate analysis with a limited number of data samples (e.g., PET images).

The aim of this study was to use the combination of ICA and a method of multivariate cross-classification (MVCC) (19) to discriminate between patients with anti-LGI1 encephalitis whose metabolic disorders within the medial temporal lobe and the basal ganglia were not able to be visually detected from their PET images (referred to as non-CD patients) and healthy participants. We further aimed to explore the consistency in PET image features between the non-CD patients and the patients with anti-LGI1 encephalitis whose metabolic disorders within both the medial temporal lobe and the basal ganglia could be visually detected from their PET images [referred to as completely detectable (CD) patients].

TABLE 1 | Demographics of participants.

	Age (years)		Gender	
	Range	Mean ± *SD*	Male	Female
Patients with anti-LGI1 encephalitis ($n = 33$)	31–78	57.91 ± 11.91	22	11
Healthy participants ($n = 33$)	40–69	54.64 ± 7.44	23	10
p value	0.19[a]		1.00[b]	

LGI1, leucine-rich glioma-inactivated 1; SD, standard deviation.
[a] *Two-sample Student's t-test.*
[b] *Fisher's exact test.*

MATERIALS AND METHODS

Participants

This study recruited 33 patients with anti-LGI1 encephalitis (57.91 ± 11.91 years; 22 males), and part of them had been recruited in the study by Lv et al. (10). These 33 patients were in acute or subacute disease courses for in-patient care and were confirmed by the neurology physicians based on clinical symptoms and modified Rankin Scale score (all ≥3). The inclusion criteria (10) for patients are as follows: (1) the LGI1 antibodies were positive in serum and/or CSF; (2) patients presented clinical symptoms of the medial temporal lobe damage (such as drug-resistant epilepsy, cognitive impairment, and behavioral abnormalities), sleep, and autonomic dysfunctions (20); (3) PET/CT images were available; and (4) new-onset seizures showing response to immunomodulatory therapies. The exclusion criteria (10) for cases are as follows: (1) patients with acute infectious encephalitis; (2) patients with seizures caused by severe metabolic abnormalities, such as renal or hepatic failure, malignant hypertension, or severe hypo/hyperglycemia; (3) patients with seizures caused by brain structural lesions, such as stroke and tumor. We also recruited 33 healthy participants (54.64 ± 7.44 years; 23 men) without any neurologic diseases or psychiatric illnesses, who had been recruited in the study by Lv et al. (10). **Table 1** summarizes the demographics of the participants. There was no significant difference in age or gender between patients with anti-LGI1 encephalitis and healthy participants ($p > 0.05$). All participants underwent ^{18}Fluorodeoxyglucose (^{18}F-FDG) PET/CT scan in our tertiary epilepsy center (May 2014 to November 2018). The Medical Ethics Committee of Beijing Tiantan Hospital of Capital Medical University approved this study in accordance with the Declaration of Helsinki. All participants provided written informed consent before participating in the study.

Image Acquisition

For each participant, a brain ^{18}F-FDG PET/CT scan was performed in order to evaluate the metabolism. Blood glucose level was confirmed to be normal after a fast of at least 6 h. Then, 0.10–0.15 mCi of ^{18}F-FDG per kg of body weight was injected. PET/CT images were acquired using a multidetector helical PET/CT scanner (Discovery 690, GE Medical Systems) after 30 min of rest in a dark room with eyes opened. To avoid the effect of seizures, video EEG was used to monitor brain activity to

ensure the absence of seizures 1–2 h before the PET/CT scanning. In addition, before and after the PET/CT scanning, the physician observed the participant's status and confirmed the absence of seizures. Thus, during the PET/CT image acquisition, none of the patients presented seizures.

Visual Assessment

Anti-LGI1 encephalitis is reported to be related to abnormal metabolism of the medial temporal lobe (left and/or right) (2, 21, 22). Additionally, many previous studies found that the metabolism of the basal ganglia was also abnormal for patients with anti-LGI1 encephalitis (21–24). Therefore, in the PET image of the patient with anti-LGI1 encephalitis, the medial temporal lobe and the basal ganglia of the brain were reviewed blindly and independently by an attending doctor of nuclear medicine and two experienced neurology specialists to inspect whether or not the glucose metabolism of these brain areas was abnormal. Inconsistent diagnoses were reconciled by discussion among the reviewers. Regardless of hemispheres, the patients with visible metabolic abnormality in both the medial temporal lobe and the basal ganglia in PET images were referred to as "CD patients" and those without were referred to as "non-CD patients."

Image Preprocessing

All image preprocessing was performed using Statistical Parametric Mapping software (SPM12, Wellcome Trust Center for Neuroimaging, London, United Kingdom; http://www.fil.ion.ucl.ac.uk/spm/software/spm12/). First, the CT images were co-registered to the corresponding PET images, and then the co-registered CT images were normalized into the Montreal Neurological Institute (MNI) template. The CT normalization was performed using an open-source Clinical Toolbox (https://www.nitrc.org/projects/clinicaltbx/), which is used as a plug-in in SPM12 (25). Second, using the transformation of CT image spatial normalization, the PET images were normalized into the MNI template. The PET images were then resampled to 2 ×

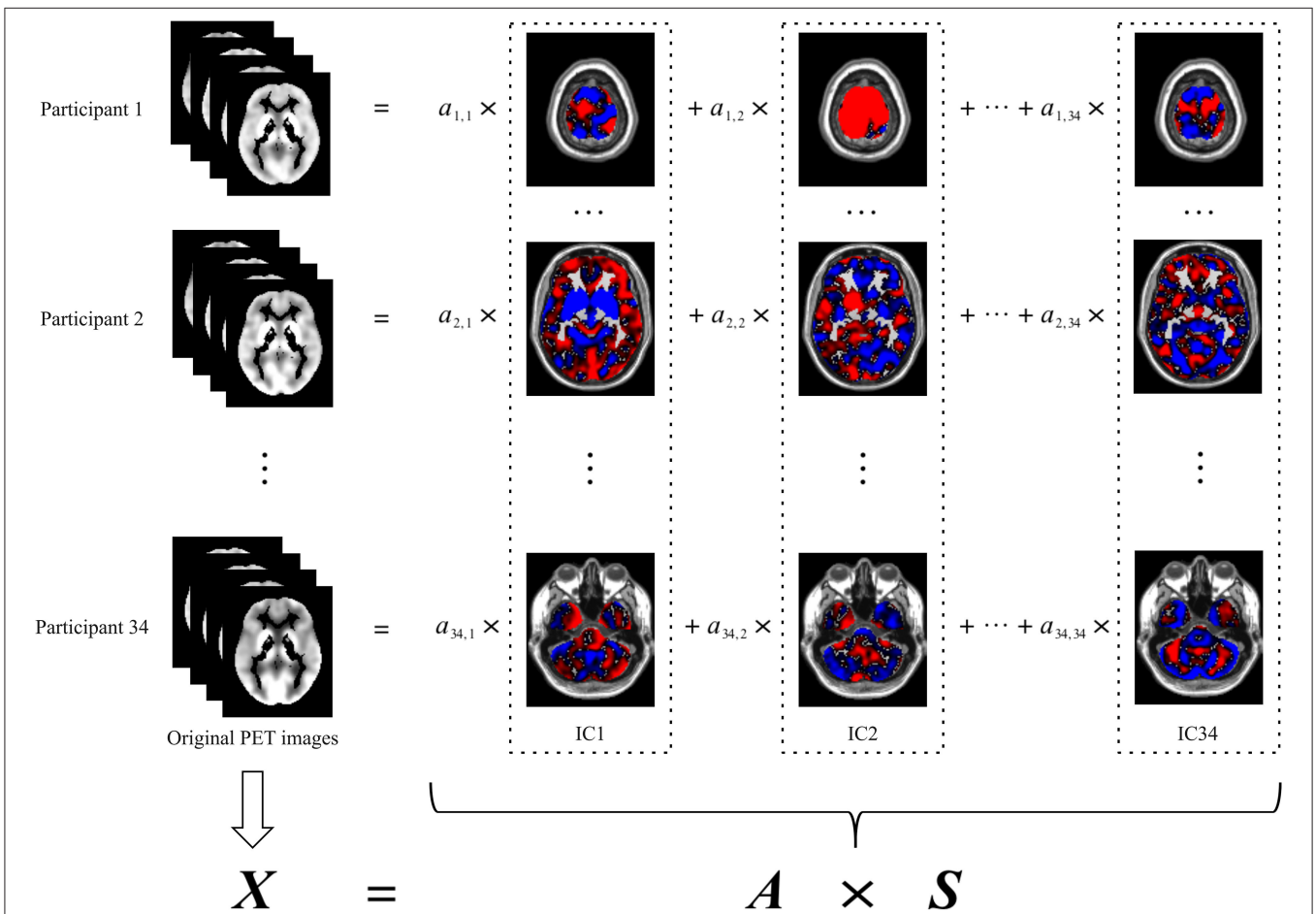

FIGURE 1 | Spatial ICA decomposition of original PET images. The left column indicates the original PET image for each participant. The images in each dash rectangles indicate the corresponding independent component, which is invariant to all participants. The coefficients of each row are specific to the participant of the same row, which is used in the subsequent construction of the classification model in place of the original PET image of the corresponding participant. The coefficients of all participants, namely, $a_{i,j}$ ($i = 1,2,\ldots,34$; $j = 1,2,\ldots,34$), constitute the coefficient matrix (i.e., ***A***). ***X*** denotes the original PET images, each row of which corresponds to an original PET image reshaped into a vector. ***S*** denotes the independent components, each row of which corresponds to an independent component reshaped into a vector. ICA, independent component analysis; IC, independent component.

2×2 mm^3. Third, the normalized PET images were spatially smoothed using an 8-mm isotropic full width at half maximum (FWHM). Fourth, each smoothed PET image was normalized by dividing the intensity of each voxel by the average of the intensities across the highest 20% of the voxels whose intensities were greater than one-eighth of the mean of the PET image (26, 27). Finally, the gray matter voxels in PET images were reserved using a gray matter binary mask that was produced based on a mask of gray matter included in SPM12.

Independent Component Analysis

In this study, the preprocessed PET image of each participant was the original PET image. Spatial ICA decomposed the original PET images of all participants into spatially independent components with the same resolution and size as the original PET images. As shown in **Figure 1**, each original PET image was the summation of the products of the independent components and their respective coefficients. The independent components were invariant to all participants, whereas the coefficients were specific to each of the participants. Thus, the original PET image could be represented by the corresponding coefficients. Because the number of these coefficients was less than the dimension of the original PET image, these coefficients were used in the subsequent construction of the classification model in place of the original PET image. The coefficients corresponding to all participants constituted the coefficient matrix (i.e., the matrix $\boldsymbol{A}$ in **Figure 1**).

In this study, spatial ICA was performed using the ICASSO toolbox included in GIFT (http://trendscenter.org/software/). Specifically, in the training cohort, the original PET images

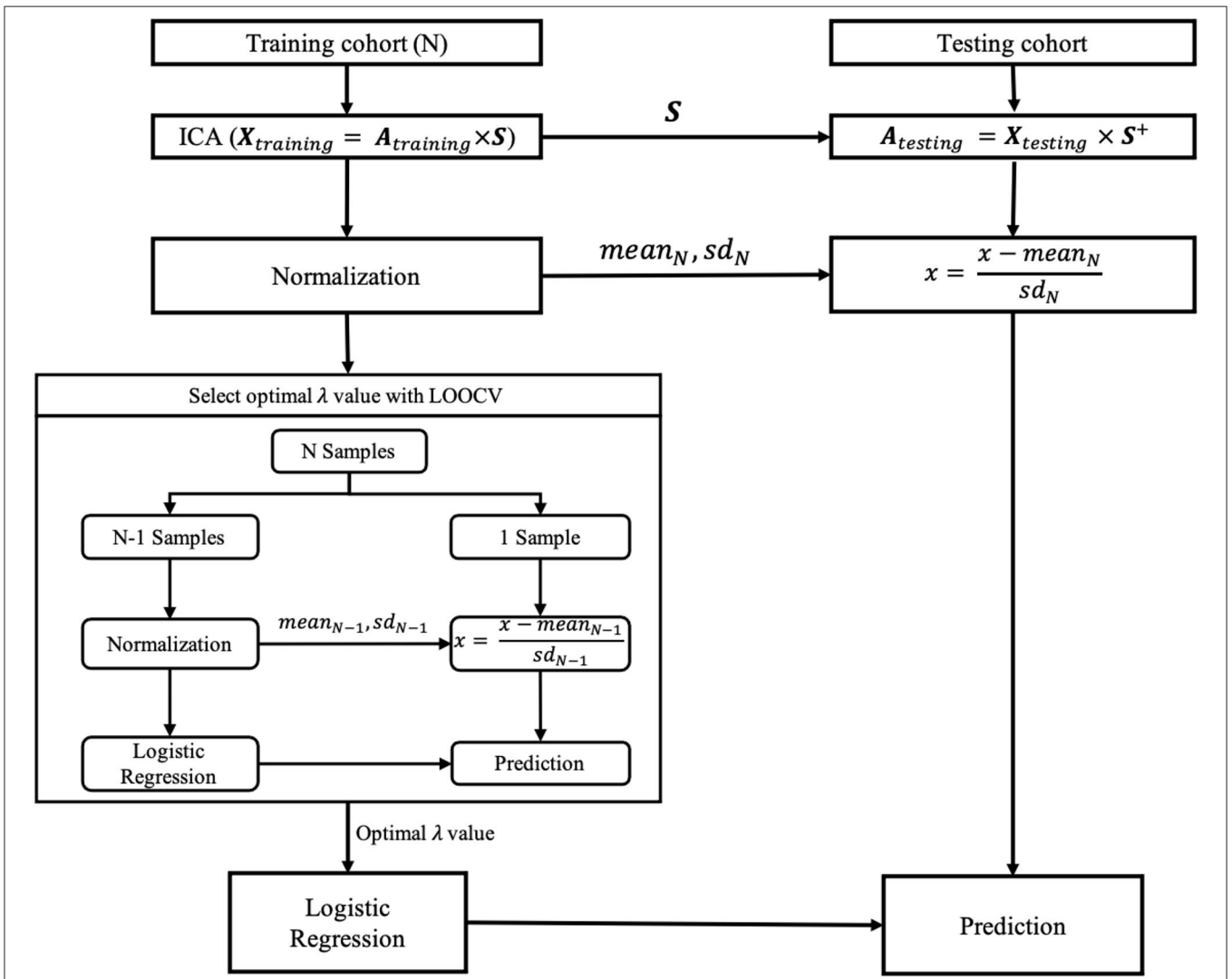

FIGURE 2 | The training and testing of the classification model. $\boldsymbol{X}_{\text{training}}$ and $\boldsymbol{X}_{\text{testing}}$ denote the original PET images of training and testing cohorts, respectively, each row of which corresponds to an original PET image reshaped into a vector. $\boldsymbol{A}_{\text{training}}$ and $\boldsymbol{A}_{\text{testing}}$ are the coefficient matrixes for training and testing cohorts, respectively. $\boldsymbol{S}$ denotes the independent components in the training cohort, each row of which corresponds to an independent component reshaped into a vector. $\boldsymbol{S}^{+}$, the pseudo inverse of the $\boldsymbol{S}$; SD, standard deviation; LOOCV, leave-one-out cross-validation; λ, the hyper-parameter of the logistic regression model.

were decomposed into the coefficient matrix ($\boldsymbol{A}_{\text{training}}$) and 34 spatially independent components ($\boldsymbol{S}$) by ICA (**Figure 2**). To ensure the reliability of the spatially independent components, the decomposition based on ICA was repeated 200 times. Then, all independent components were clustered according to their mutual similarities. For each cluster, the independent component that showed the maximum similarity to the other independent components in the same cluster was considered a more reliable independent component. Thus, 34 reliable independent components from 34 clusters were selected, respectively. Then, the coefficient matrix of the testing cohort ($\boldsymbol{A}_{\text{testing}}$) was calculated by the production of the original PET images of the testing cohort and the pseudo inverse of the $\boldsymbol{S}$ obtained in the training cohort (**Figure 2**). The rows of $\boldsymbol{A}_{\text{training}}$ and $\boldsymbol{A}_{\text{testing}}$ were used as the feature vectors to train and test the classification model, respectively.

The coefficients of each column of $\boldsymbol{A}_{\text{training}}$ were normalized by first removing their mean value and then dividing them by their *SD*. In contrast, the coefficients of each column of $\boldsymbol{A}_{\text{testing}}$ were normalized by first removing the mean value and then dividing by the *SD* across the coefficients of the corresponding column of $\boldsymbol{A}_{\text{training}}$.

For the normalized $\boldsymbol{A}_{\text{training}}$ and $\boldsymbol{A}_{\text{testing}}$, the coefficients of each row were specific to the corresponding original PET images in the training and testing cohorts and, therefore, were used in the subsequent training and testing of classification models in place of those corresponding original PET images, respectively.

TABLE 2 | Comparison of clinical characteristics between CD patients of the training cohort and non-CD patients of the testing cohort.

	CD patients	Non-CD patients	*p* value
Age (years)	57.53 ± 11.76	58.31 ± 12.45	0.85[a]
Gender (male)	12 (70.59%)	10 (62.50%)	0.72[b]
Interval time (weeks)	16.00 ± 15.45	17.56 ± 16.50	0.78[a]
Treatment, *n* (%)	7 (41.18%)	6 (37.50%)	1.00[b]
MRI abnormalities, *n* (%)			
Total	12 (70.59%)	6 (37.50%)	0.08[b]
Only MTL	12 (70.59%)	5 (31.25%)	0.04[b]
Only BG	0	1 (6.25%)	0.48[b]
Both MTL and BG	0	0	1.00[b]
Clinical symptoms, *n* (%)			
Seizures	17 (100%)	16 (100%)	1.00[b]
FBDS	7 (41.18%)	7 (43.75%)	1.00[b]
Temporal lobe seizures	9 (52.94%)	7 (43.75%)	0.73[b]
Other types	5 (29.41%)	6 (37.50%)	0.72[b]
Memory loss	3 (17.65%)	5 (31.25%)	0.44[b]
Sleep disorder	0	1 (6.25%)	0.48[b]
Headache	1 (5.88%)	0	1.00[b]
Psychiatric symptoms	1 (5.88%)	3 (18.75%)	0.34[b]
Hallucinations	0	1 (6.25%)	0.48[b]

MTL, the medial temporal lobe; BG, the basal ganglia; FBDS, faciobrachial dystonic seizures; CD, completely detectable; non-CD, non-completely detectable.
[a] *Two-sample Student's t-test.*
[b] *Fisher's exact test.*

Multivariate Cross-Classification

In this study, the logistic regression model was used to discriminate between non-CD patients and healthy participants. In total, 33 healthy participants were randomly divided into two groups. There was no significant difference in age between the two groups [$t_{(31)} = 1.59$; $p > 0.05$]. The training cohort included all CD patients ($n = 17$; 57.53 ± 11.76 years; 12 men) and one group of healthy participants ($n = 17$; 56.59 ± 9.80 years; 13 men) as controls. The testing cohort included all non-CD patients ($n = 16$; 58.31 ± 12.45 years; 10 men) and another group of healthy participants ($n = 16$; 52.56 ± 2.61 years; 10 men) as controls. There was no significant difference in age between patients and healthy participants for the training cohort [$t_{(32)} = 0.25$; $p > 0.05$] or for the testing cohort [$t_{(30)} = 1.81$; $p > 0.05$]. **Table 2** lists the clinical characteristics of the CD patients in the training cohort and those of the non-CD patients in the testing cohort. As summarized in **Table 2**, when comparing CD patients of the training cohort with the non-CD patients of the testing cohort, a significant difference was observed only in the number of MRI abnormalities of the medial temporal lobe ($p < 0.05$). In contrast, there was no significant difference in each of the other clinical characteristics between the CD patients of the training cohort and the non-CD patients of the testing cohort ($p > 0.05$). Such differences in clinical characteristics were assessed using the two-sample Student's *t*-test for continuous data and Fisher's exact test for categorical data. The two-sample Student's *t*-test was performed using the SPSS Statistics software (SPSS for macOS, version 26.0, Chicago, IL, United States), and Fisher's exact test was performed using Python, version 3.6.

As mentioned earlier, each row of the $\boldsymbol{A}_{\text{training}}$ and the $\boldsymbol{A}_{\text{testing}}$ was specific to the corresponding original PET image in the training and testing cohorts, respectively. Thus, the rows of $\boldsymbol{A}_{\text{training}}$ and $\boldsymbol{A}_{\text{testing}}$ were used as the feature vectors to train and test the logistic regression model, respectively. To determine the optimal value of the hyperparameter (λ) of the logistic regression model, leave-one-out cross-validation (LOOCV) was performed for each of 21 potential values [i.e., $\lambda = (2^{-10}, 2^{-9}, ..., 2^{9}, 2^{10})$]. The optimal λ value with the highest area under the curve (AUC) value was selected, with which a final logistic regression model was constructed using all samples from the training cohort, and then was tested by the testing cohort. The logistic regression model was implemented using scikit-learn version 0.23.2 (https://scikit-learn.org/stable/index.html).

Given the labels one and zero for patients and healthy participants in the classification model, respectively, 0.5 was set as a classification threshold. Thus, a sample with the prediction probability > 0.5 was classified as a patient, and that with the prediction probability ≤ 0.5 was classified as a healthy participant. In the testing cohort, the accuracy was calculated by dividing the number of correct predictions of the testing cohort by the number of all samples of the testing cohort. The sensitivity was calculated by dividing the number of correct predictions of the non-CD patients by the number of all non-CD patients. The specificity was calculated by dividing the number of correct predictions of controls by the total number of

controls. A receiver operating characteristic (ROC) curve, which is independent of the classification threshold, was also used to evaluate the performance of the classification model. The ROC curve was plotted with the true-positive rate (i.e., sensitivity) and false-positive rate (i.e., 1-specificity) as vertical and horizontal coordinates, respectively, both of which varied as the functions of the classification threshold. The AUC was defined by the area under the ROC curve.

Significant Independent Components Selection

In the logistic regression model, the weights corresponded to the independent components one by one, respectively. The absolute value of each weight indicated the contribution of the corresponding independent component to discriminate between patients and healthy participants. Thus, we first ranked all weights according to their absolute values and then selected the top two weights (i.e., about the top 5% or $p < 0.05$). Two independent components corresponding to these top two weights were selected as significant independent components, which presented the difference in PET images between patients and healthy participants. The significant regions of these two independent components can be identified by converting them to z-score maps.

However, in this study, the interpretation of the z-score maps should be done by considering the signs of the weights in the classification model to which these z-score maps corresponded, respectively. This is because the sign of the weight in the classification model indicated the association between the z-score map and the signal of the PET image. For example, if the weight was positive, then the positively significant regions in the z-score map indicated increased PET signals and therefore hypermetabolism, and the negatively significant regions indicated hypometabolism for patients. However, if the weight was negative, then the positively significant regions in the z-score map indicated hypometabolism, and the negatively significant regions indicated hypermetabolism for patients.

Thus, for ease of understanding, two significant independent components were first multiplied by the signs of their respective weights in the classification model. Then, these two sign-corrected independent components were converted to z-score maps, and the clusters with $|z| > 2.58$ ($p < 0.01$) and cluster extent $\geq$50 voxels were identified as significant clusters. Thus, for the patients with anti-LGI1 encephalitis, the positively significant and negatively significant regions in the z-score map indicated hypermetabolism and hypometabolism, respectively.

RESULTS

Visual Assessment Results

For all 17 CD patients, abnormal metabolism was found in both the medial temporal lobe and the basal ganglia in their PET images. **Table 3** summarizes the results of visual assessment for non-CD patients. Among the 16 non-CD patients, the abnormal metabolism was not able to be identified in the medial temporal lobe or the basal ganglia for seven patients and was able to be identified only in the medial temporal lobe for four patients and only in the basal ganglia for five patients.

TABLE 3 | The patients with anti-LGI1 encephalitis who were non-completely detectable by visual assessment (non-CD patients).

Patient no.	Visual assessment	
	Medial temporal lobe	Basal ganglia
Patient 1	Yes	No
Patient 2	No	Yes
Patient 3	No	No
Patient 4	No	Yes
Patient 5	No	Yes
Patient 6	Yes	No
Patient 7	Yes	No
Patient 8	No	No
Patient 9	No	No
Patient 10	No	No
Patient 11	Yes	No
Patient 12	No	No
Patient 13	No	No
Patient 14	No	Yes
Patient 15	No	No
Patient 16	No	Yes

Yes: the abnormal metabolism was able to be detected by visual assessment.
No: the abnormal metabolism couldn't be identified by visual assessment.

Multivariate Cross-Classification

In the training cohort, 2^{-10} was selected as the optimal λ value by using LOOCV. The accuracy was 100% in the training cohort. In the testing cohort, the constructed classifier had good generalization ability, with a sensitivity of 81.25%, a specificity of 100%, an overall accuracy of 90.63%, and an AUC value of 0.95. Thus, four non-CD patients, whose abnormal metabolism was able to be visually identified only in the medial temporal lobe, and five non-CD patients, whose abnormal metabolism was able to be visually identified only in the basal ganglia, were fully detected by our model. In contrast, only four out of seven non-CD patients, whose abnormal metabolism was not able to be visually identified in the medial temporal lobe or the basal ganglia, were detected by our model. The ROC curve of the testing cohort is shown in **Figure 3**.

Significant Independent Components for Classifier

There were a total of 34 weights in the logistic regression model, which corresponded to the independent components one by one, respectively (**Supplementary Table 1**). We ranked all weights according to their absolute values. As shown in **Supplementary Figure 1**, the absolute values of the first weight and the seventh weight were evidently larger than those of the other weights. Thus, IC1 and IC7 were selected as significant independent components. Then, IC1 and IC7 were multiplied by the signs of their respective weights in the classification model. The z-score maps of the sign-corrected

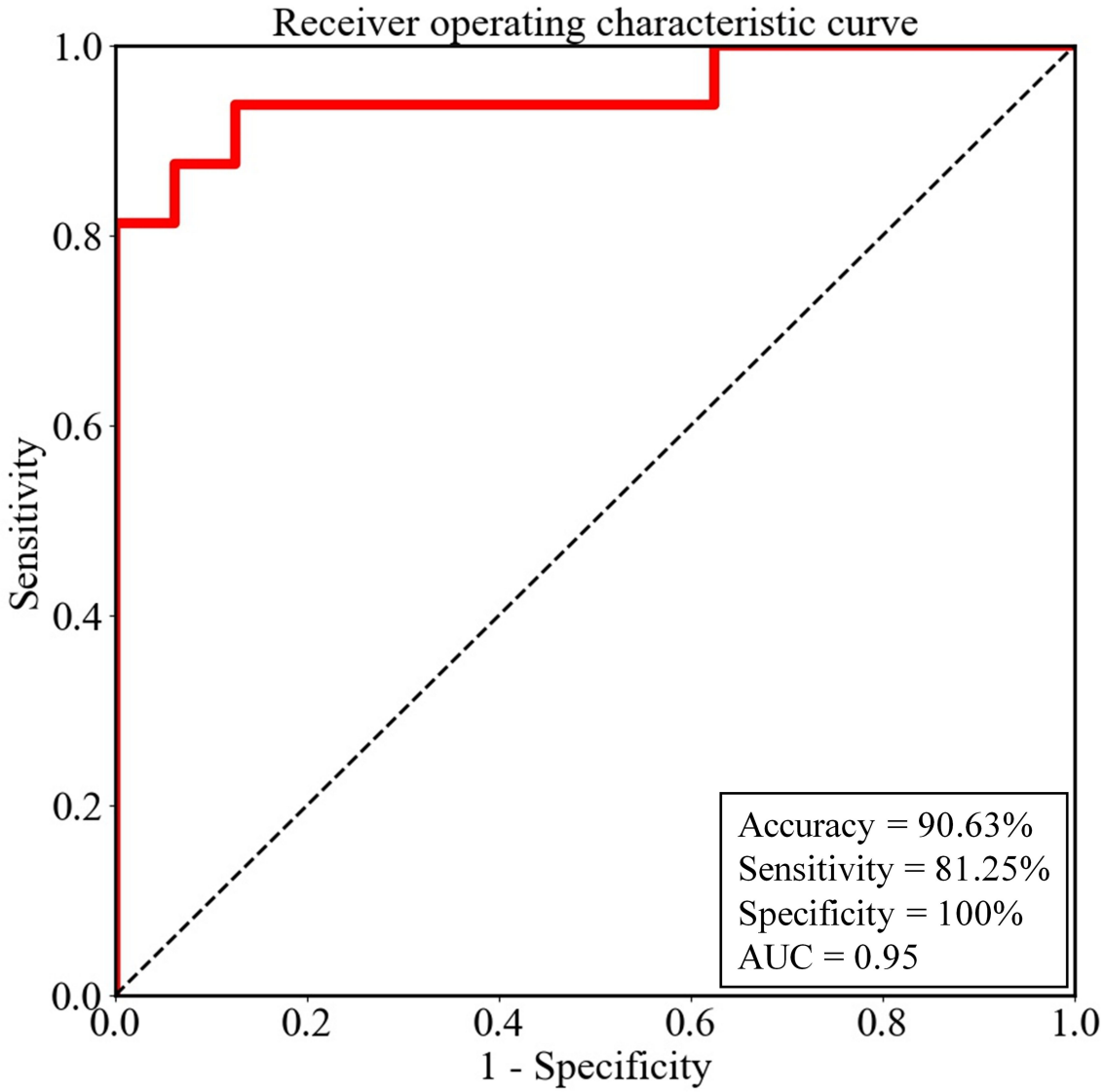

FIGURE 3 | The performance of the logistic regression model for the testing cohort was evaluated by the receiver operating characteristic (ROC) curve. AUC, the area under the ROC curve.

IC1 and the sign-corrected IC7 were shown in **Figure 4**. For each of these two z-score maps, all local peaks within each significant cluster and their respective corresponding brain regions are listed in **Table 4**. As shown in **Figure 4** and summarized in **Table 4**, significantly increased PET signals were observed in the bilateral medial temporal lobe, the bilateral basal ganglia, the left precuneus, the left medial part of the superior frontal gyrus, the right postcentral gyrus, and the left calcarine fissure and surrounding cortex, indicating that the patients with anti-LGI1 encephalitis presented hypermetabolism in these brain regions. In contrast, significantly decreased PET signals were observed in the right supplementary motor area, the bilateral calcarine fissure and surrounding cortex, and the lobule III of the vermis, indicating that the patients with anti-LGI1 encephalitis presented hypometabolism in these brain regions. These findings suggest that abnormal metabolism of these brain regions played an important role in discriminating between the patients with anti-LGI1 encephalitis and healthy participants.

Additionally, there was also an obvious cutoff of the absolute value of weight between the top seven weights and the other ones. The z-score maps of the sign-corrected independent components corresponding to these weights (except the top two weights) are shown in **Supplementary Figure 2**, and the significant regions of these sign-corrected independent components are summarized in **Supplementary Table 2**.

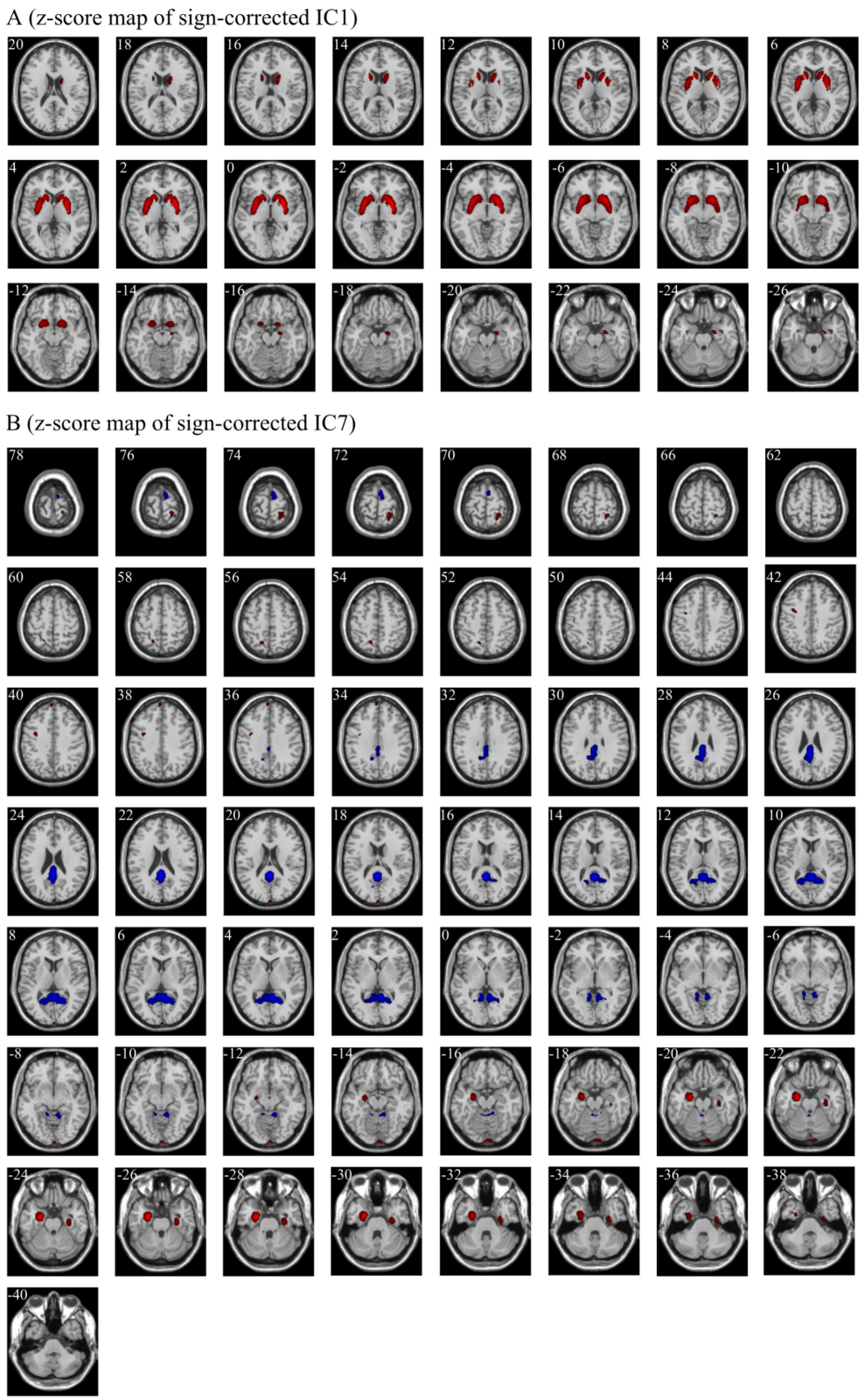

FIGURE 4 | The significant regions in the z-score maps of sign-corrected IC1 **(A)** and sign-corrected IC7 **(B)** ($|z| > 2.58$, $p < 0.01$, cluster extent $\geq$ 50 voxels). Red indicates the regions with a z value > 2.58 and a cluster extent $\geq$50 voxels, and blue indicates the regions with a z value < -2.58 and a cluster extent $\geq$50 voxels. The positively significant regions (red) and the negatively significant regions (blue) indicate hypermetabolism and hypometabolism in patients with anti-LGI1 encephalitis, respectively. The white number in the upper left of each sub-figure indicates the Montreal Neurological Institute coordinates of transversal slices. R/L, right/left.

TABLE 4 | The significant brain regions ($|z| > 2.58$, $p < 0.01$, cluster extent $\geq$ 50 voxels) included in the two sign-corrected independent components corresponding to the first two weights in the rank of the absolute values of all weights of the logistic regression model.

IC	Cluster	Peak level				Brain regions	
		z value	x (mm)	y (mm)	z (mm)	L/R	Name
IC1	101	3.73	20	−10	−18	R	Medial temporal lobe (Hippocampus)
(−17.90*)	1,796	6.98	−16	16	4	L	Basal ganglia (Caudate nucleus)
		7.74	−32	−6	0	L	Basal ganglia (Putamen)
		7.94	−30	0	0	L	Basal ganglia (Putamen)
		8.18	−26	8	−4	L	Basal ganglia (Putamen)
	1,860	9.35	26	6	0	R	Basal ganglia (Putamen)
IC7	51	3.21	−14	−58	54	L	Precuneus
(14.93*)	59	3.41	−2	58	38	L	Superior frontal gyrus (medial part)
	62	3.65	−34	−2	38	–	–
	146	−4.15	8	−2	74	R	Supplementary motor area
	151	3.89	26	−44	72	R	Postcentral gyrus
	244	3.57	2	−102	10	L	Calcarine fissure and surrounding cortex
		3.64	2	−100	18	–	–
		4.03	4	−102	−8	–	–
		4.33	8	−98	−18	–	–
		4.44	4	−100	−14	–	-
	308	5.37	32	−18	−26	R	Medial temporal lobe (Parahippocampal gyrus)
	750	10.07	−24	−6	−26	L	Medial temporal lobe (Hippocampus)
	2,816	−6.34	0	−48	18	–	–
		−5.01	20	−56	8	R	Calcarine fissure and surrounding cortex
		−4.25	−18	−58	8	L	Calcarine fissure and surrounding cortex
		−2.74	−2	−46	−20	–	Lobule III of vermis

IC, independent component; -, there were no relevant results; R/L, right/left.
**The weight corresponding to the independent component.*

DISCUSSION

In this study, an MVCC method combined with ICA was used to analyze the PET data to detect non-CD patients and explore the consistency in PET image features between non-CD patients and CD patients. To the best of our knowledge, this is the first study in which the MVCC method combined with ICA was used to analyze PET images of patients with anti-LGI1 encephalitis. In the MVCC, a logistic regression model was first trained using the PET images of CD patients and then tested using the PET images of non-CD patients. By transferring the learning from the former to the latter, the MVCC can detect the relatively weak PET signal changes related to anti-LGI1 encephalitis of non-CD patients and therefore discriminate between non-CD patients and healthy participants with higher accuracy. Compared to visual assessment, the MVCC increased the sensitivity of the detection of non-CD patients and, at the same time, preserved the highest specificity. However, it should be noted that for the non-CD patients whose abnormal metabolism was not able to be visually identified in the medial temporal lobe or the basal ganglia, only four out of seven (about 57.14%) were detected by our ML method. One probable reason for this relatively low detection rate of this type of patient may be that there was no such type of patient in the training cohort. Thus, in future studies, more patients without visible metabolic abnormalities in the medial temporal lobe or the basal ganglia should be included in the training cohort to improve the performance of the classification model.

In this study, the important roles of ICA were feature extraction and dimension reduction. The PET image of the patient with anti-LGI1 encephalitis is actually the compound of multiple different patterns of PET signals resulting from different sources, such as metabolic abnormality related to anti-LGI1 encephalitis, other brain activities, noise, and background. Among these patterns of PET signals, if the one related to anti-LGI1 encephalitis metabolic abnormality is relatively strong, it will be visible in PET images (i.e., CD patient). However, if this pattern of PET signal is relatively weak, it will be covered by the superposition of the other patterns of PET signals and therefore is not able to be detected by visual assessment (i.e., non-CD patient). In this study, these overlapping patterns of PET signals related to different sources were separated by ICA into different spatially independent components. As revealed by the results of MVCC, the independent components with PET signal changes in the medial temporal lobe and the basal ganglia provided the most contribution to the discrimination between non-CD patients and healthy participants. Thus, the important findings of the present study were that non-CD patients presented similar patterns of metabolic abnormality as those of CD patients, though the PET signals related to anti-LGI1 encephalitis metabolic abnormality

were unable to be detected in them. These findings are consistent with previous studies about patients with anti-LGI1 encephalitis (6, 28, 29), suggesting that anti-LGI1 encephalitis is closely related to the metabolic abnormality in the medial temporal lobe and the basal ganglia. A recent study (7) also found that patients with anti-LGI1 encephalitis presented hypermetabolism in the medial temporal lobe and the basal ganglia (i.e., including the putamen and the caudate), consistent with the findings of the present study. However, some other brain regions showing metabolic abnormalities in the study (7) (e.g., angular gyrus, olfactory, and pons) were observed as normal regions in the present study. It should be noted that, in the study (7), the mean of standardized uptake values across the regions of interest was used to measure the metabolic abnormalities. In contrast, in this study, the independent images related to anti-LGI1 encephalitis were separated by ICA. This difference in the methods of feature extraction may be one of the potential reasons for the discrepancies in the findings between these studies.

In addition to the medial temporal lobe and the basal ganglia, other brain regions of patients with anti-LGI1 encephalitis were also revealed to present different PET signals from those of the healthy participants (**Table 4**). A previous study found that patients with anti-LGI1 encephalitis presented abnormal metabolism in the precuneus (23). A recent study reported that the supplementary motor area of two patients with anti-LGI1 encephalitis presented hypometabolism in their PET images (30). This existing evidence along with our findings suggests that the metabolic abnormality of the left precuneus and the right supplementary motor area may also play important roles in anti-LGI1 encephalitis.

As for the left medial part of the superior frontal gyrus, the right postcentral gyrus, the bilateral calcarine fissure and surrounding cortex, and the lobule III of the vermis, they are rarely specifically reported by previous studies about anti-LGI1 encephalitis. These brain regions are a part of the frontal lobe, the parietal lobe, the occipital lobe, and the cerebellum, respectively. The existing studies using PET have reported that metabolic abnormalities were observed in these lobes of the patients with anti-LGI1 encephalitis, for example, the bilateral frontal lobe (8), the bilateral (8) and right (31) parietal lobe, the occipital lobe (8, 29) and the cerebellum (29). Thus, these brain regions with abnormal PET signals in the present study may also be related to the anti-LGI1 encephalitis. In the present study, the mixed PET signals were separated by ICA and then analyzed as a whole by the classifier. Additionally, as confirmed in the present study, the multivariate analysis is more sensitive to the changes in PET signals than visual assessment. Thus, compared to conventional visual assessment, the MVCC method combined with ICA can reveal more potential brain regions with metabolic abnormalities related to anti-LGI1 encephalitis. However, the roles of these brain regions in anti-LGI1 encephalitis need to be further explored.

The present study still had some limitations. First, the number of samples was small. This is because the prevalence and incidence of anti-LGI1 encephalitis are relatively low (32, 33). Further work will include as many as possible patients with anti-LGI1 encephalitis, particularly the data from multiple institutes to improve the performance of the classifier. Second, the good performance may be partly due to the involvement of the patients with visible abnormal metabolism either only in the medial temporal lobe or only in the basal ganglia in the testing cohort. Thus, more patients whose abnormal metabolism was not able to be visually identified in either the medial temporal lobe or the basal ganglia should be included in future studies to improve the ability of the classification model to identify this type of patient.

In general, as a relatively new imaging methodology, ^{18}F-FDG-PET has presented a wide application prospect in the diagnosis of autoimmune encephalitis (34). This study used an MVCC method of PET imaging based on ICA and logistic regression, which was able to take the best advantage of the information of PET images to reveal the difference in PET signals between the patients with anti-LGI1 encephalitis and healthy participants, even in cases where this difference is not accessible with visual assessment. Our method is helpful to promote the application of PET imaging in the early diagnosis of autoimmune encephalitis, whose clinical effectiveness needs to be further validated by many prospective studies.

CONCLUSION

This study used an MVCC method combined with ICA to detect non-CD patients and explore the consistency in PET image features between non-CD patients and CD patients. This method can improve, to some degree, the detection of invisible abnormal metabolism in the PET images of patients with anti-LGI1 encephalitis. More importantly, this study suggested that the patterns of PET signal changes caused by metabolic abnormalities associated with anti-LGI1 encephalitis were similar in CD patients and non-CD patients.

DATA AVAILABILITY STATEMENT

The original contributions presented in the study are included in the article/**Supplementary Material**, further inquiries can be directed to the corresponding authors.

ETHICS STATEMENT

The studies involving human participants were reviewed and approved by the Medical Ethics Committee of Beijing Tiantan Hospital of Capital Medical University. The patients/participants provided their written informed consent to participate in this study.

AUTHOR CONTRIBUTIONS

JP and JL contributed to the conception and design of the study and drafted the manuscript. JP, GZ, and RS contributed to the analysis of data. RL, QW, and XZ contributed to the acquisition of data. JL, RL, XZ, and LA revised the manuscript. JL and LA supervised the study. All authors contributed to the study conception and design. All authors contributed to the article and approved the submitted version.

FUNDING

This study was supported by grants from the Beijing Natural Science Foundation (Grant Nos. Z200027 and 7192054), the Application Research of Capital Clinical Characteristics (Grant No. Z181100001718082), the Beijing Dongcheng District Outstanding Talent Funding Project (Grant No. 2019DCT-M-18), the National Natural Science Foundation of China (Grant No. 81771143), and the National Key Research and Development Program of China (Grant No. 2018YFC1315201).

SUPPLEMENTARY MATERIAL

The Supplementary Material for this article can be found online at: https://www.frontiersin.org/articles/10.3389/fneur.2022.812439/full#supplementary-material

REFERENCES

1. Budhram A, Leung A, Nicolle MW, Burneo JG. Diagnosing autoimmune limbic encephalitis. *CMAJ.* (2019) 191:E529–34. doi: 10.1503/cmaj.181548
2. Graus F, Titulaer MJ, Balu R, Benseler S, Bien CG, Cellucci T, et al. A clinical approach to diagnosis of autoimmune encephalitis. *Lancet Neurol.* (2016) 15:391–404. doi: 10.1016/S1474-4422(15)00401-9
3. Vincent A, Buckley C, Schott JM, Baker I, Dewar BK, Detert N, et al. Potassium channel antibody-associated encephalopathy: a potentially immunotherapy-responsive form of *Limbic encephalitis*. *Brain.* (2004) 127(Pt. 3):701–12. doi: 10.1093/brain/awh077
4. Ances BM, Vitaliani R, Taylor RA, Liebeskind DS, Voloschin A, Houghton DJ, et al. Treatment-responsive limbic encephalitis identified by neuropil antibodies: mri and pet correlates. *Brain.* (2005) 128(Pt. 8):1764–77. doi: 10.1093/brain/awh526
5. Nobrega PR, Pitombeira MS, Mendes LS, Krueger MB, Santos CF, Morais NMM, et al. Clinical features and inflammatory markers in autoimmune encephalitis associated with antibodies against neuronal surface in brazilian patients. *Front Neurol.* (2019) 10:472. doi: 10.3389/fneur.2019.00472
6. Shin YW, Lee ST, Shin JW, Moon J, Lim JA, Byun JI, et al. Vgkc-complex/Lgi1-antibody encephalitis: clinical manifestations and response to immunotherapy. *J Neuroimmunol.* (2013) 265:75–81. doi: 10.1016/j.jneuroim.2013.10.005
7. Rissanen E, Carter K, Cicero S, Ficke J, Kijewski M, Park MA, et al. Cortical and subcortical dysmetabolism are dynamic markers of clinical disability and course in anti-lgi1 encephalitis. *Neurol Neuroimmunol Neuroinflamm.* (2022) 9:e1136. doi: 10.1212/NXI.0000000000001136
8. Solnes LB, Jones KM, Rowe SP, Pattanayak P, Nalluri A, Venkatesan A, et al. Diagnostic value of (18)F-FDG PET/Ct *vs*. MRI in the setting of antibody-specific autoimmune encephalitis. *J Nucl Med.* (2017) 58:1307–13. doi: 10.2967/jnumed.116.184333
9. Liu X, Shan W, Zhao X, Ren J, Ren G, Chen C, et al. The clinical value of (18) F-FDG-PET in autoimmune encephalitis associated with LGI1 antibody. *Front Neurol.* (2020) 11:418. doi: 10.3389/fneur.2020.00418
10. Lv RJ, Pan J, Zhou G, Wang Q, Shao XQ, Zhao XB, et al. Semi-quantitative FDG-PET analysis increases the sensitivity compared with visual analysis in the diagnosis of autoimmune encephalitis. *Front Neurol.* (2019) 10:e576. doi: 10.3389/fneur.2019.00576
11. Hebart MN, Baker CI. Deconstructing multivariate decoding for the study of brain function. *Neuroimage.* (2018) 180(Pt. A):4–18. doi: 10.1016/j.neuroimage.2017.08.005
12. Norman KA, Polyn SM, Detre GJ, Haxby JV. Beyond mind-reading: multi-voxel pattern analysis of FMRI data. *Trends Cogn Sci.* (2006) 10:424–30. doi: 10.1016/j.tics.2006.07.005
13. Li Y, Qian Z, Xu K, Wang K, Fan X, Li S, et al. MRI features predict P53 status in lower-grade gliomas via a machine-learning approach. *Neuroimage Clin.* (2018) 17:306–11. doi: 10.1016/j.nicl.2017.10.030
14. Li L, Mu W, Wang Y, Liu Z, Liu Z, Wang Y, et al. A non-invasive radiomic method using (18)F-FDG PET predicts isocitrate dehydrogenase genotype and prognosis in patients with glioma. *Front Oncol.* (2019) 9:e1183. doi: 10.3389/fonc.2019.01183
15. Parmar C, Grossmann P, Rietveld D, Rietbergen MM, Lambin P, Aerts HJ. Radiomic machine-learning classifiers for prognostic biomarkers of head and neck cancer. *Front Oncol.* (2015) 5:e272. doi: 10.3389/fonc.2015.00272
16. Arbabshirani MR, Plis S, Sui J, Calhoun VD. Single subject prediction of brain disorders in neuroimaging: promises and pitfalls. *Neuroimage.* (2017) 145(Pt. B):137–65. doi: 10.1016/j.neuroimage.2016.02.079
17. Wang S, Summers RM. Machine learning and radiology. *Med Image Anal.* (2012) 16:933–51. doi: 10.1016/j.media.2012.02.005
18. Mwangi B, Tian TS, Soares JC. A review of feature reduction techniques in neuroimaging. *Neuroinformatics.* (2014) 12:229–44. doi: 10.1007/s12021-013-9204-3
19. Kaplan JT, Man K, Greening SG. Multivariate cross-classification: applying machine learning techniques to characterize abstraction in neural representations. *Front Human Neurosci.* (2015) 9:e151. doi: 10.3389/fnhum.2015.00151
20. Bastiaansen AEM, van Sonderen A, Titulaer MJ. Autoimmune encephalitis with anti-leucine-rich glioma-inactivated 1 or anti-contactin-associated protein-like 2 antibodies (formerly called voltage-gated potassium channel-complex antibodies). *Curr Opin Neurol.* (2017) 30:302–9. doi: 10.1097/WCO.0000000000000444
21. Kunze A, Drescher R, Kaiser K, Freesmeyer M, Witte OW, Axer H. Serial FDG PET/CT in autoimmune encephalitis with faciobrachial dystonic seizures. *Clin Nucl Med.* (2014) 39:e436–8. doi: 10.1097/RLU.0000000000000372
22. Lopez Chiriboga AS, Siegel JL, Tatum WO, Shih JJ, Flanagan EP. Striking basal ganglia imaging abnormalities in LGI1 Ab faciobrachial dystonic seizures. *Neurol Neuroimmunol Neuroinflamm.* (2017) 4:e336. doi: 10.1212/NXI.0000000000000336
23. Navarro V, Kas A, Apartis E, Chami L, Rogemond V, Levy P, et al. Motor cortex and hippocampus are the two main cortical targets in lgi1-antibody encephalitis. *Brain.* (2016) 139(Pt. 4):1079–93. doi: 10.1093/brain/aww012
24. Jang Y, Lee ST, Bae JY, Kim TJ, Jun JS, Moon J, et al. LGI1 expression and human brain asymmetry: insights from patients with lgi1-antibody encephalitis. *J Neuroinflammation.* (2018) 15:279. doi: 10.1186/s12974-018-1314-2
25. Rorden C, Bonilha L, Fridriksson J, Bender B, Karnath HO. Age-specific CT and MRI templates for spatial normalization. *Neuroimage.* (2012) 61:957–65. doi: 10.1016/j.neuroimage.2012.03.020
26. Pagani M, Oberg J, De Carli F, Calvo A, Moglia C, Canosa A, et al. Metabolic spatial connectivity in amyotrophic lateral sclerosis as revealed by independent component analysis. *Hum Brain Mapp.* (2016) 37:942–53. doi: 10.1002/hbm.23078
27. Dukart J, Mueller K, Horstmann A, Vogt B, Frisch S, Barthel H, et al. Differential effects of global and cerebellar normalization on detection and differentiation of dementia in FDG-PET studies. *Neuroimage.* (2010) 49:1490–5. doi: 10.1016/j.neuroimage.2009.09.017
28. Shan W, Liu X, Wang Q. Teaching neuroimages: (18)F-FDG-PET/SPM analysis in 3 different stages from a patient with LGI-1 autoimmune encephalitis. *Neurology.* (2019) 93:e1917–e8. doi: 10.1212/WNL.0000000000008473
29. Wegner F, Wilke F, Raab P, Tayeb SB, Boeck AL, Haense C, et al. Anti-leucine rich glioma inactivated 1 protein and anti-n-methyl-D-aspartate receptor encephalitis show distinct patterns of brain glucose metabolism in 18F-fluoro-2-deoxy-D-glucose positron emission tomography. *BMC Neurol.* (2014) 14:e136. doi: 10.1186/1471-2377-14-136

30. Liu X, Han Y, Yang L, Wang B, Shao S, Feng Y, et al. The exploration of the spectrum of motor manifestations of anti-LGI1 encephalitis beyond FBDS. *Seizure.* (2020) 76:22–7. doi: 10.1016/j.seizure.2019.12.023
31. Tripathi M, Tripathi M, Roy SG, Parida GK, Ihtisham K, Dash D, et al. Metabolic topography of autoimmune non-paraneoplastic encephalitis. *Neuroradiology.* (2018) 60:189–98. doi: 10.1007/s00234-017-1956-2
32. Dubey D, Pittock SJ, Kelly CR, McKeon A, Lopez-Chiriboga AS, Lennon VA, et al. Autoimmune encephalitis epidemiology and a comparison to infectious encephalitis. *Ann Neurol.* (2018) 83:166–77. doi: 10.1002/ana.25131
33. van Sonderen A, Thijs RD, Coenders EC, Jiskoot LC, Sanchez E, de Bruijn MA, et al. Anti-LGI1 encephalitis: clinical syndrome and long-term follow-up. *Neurology.* (2016) 87:1449–56. doi: 10.1212/WNL.0000000000003173
34. Morbelli S, Djekidel M, Hesse S, Pagani M, Barthel H, Neuroimaging Committee of the European Association of Nuclear Medicine, et al. Role of (18)F-FDG-PET imaging in the diagnosis of autoimmune encephalitis. *Lancet Neurol.* (2016) 15:1009–10. doi: 10.1016/S1474-4422(16)30140-5

Conflict of Interest: The authors declare that the research was conducted in the absence of any commercial or financial relationships that could be construed as a potential conflict of interest.

Publisher's Note: All claims expressed in this article are solely those of the authors and do not necessarily represent those of their affiliated organizations, or those of the publisher, the editors and the reviewers. Any product that may be evaluated in this article, or claim that may be made by its manufacturer, is not guaranteed or endorsed by the publisher.

frontiers | Frontiers in Immunology

ORIGINAL RESEARCH
published: 09 June 2022
doi: 10.3389/fimmu.2022.907851

Schizophrenia and Inflammation Research: A Bibliometric Analysis

He-Li Sun[1,2,3†], Wei Bai[1,2,3†], Xiao-Hong Li[4†], Huanhuan Huang[5†], Xi-Ling Cui[6], Teris Cheung[7], Zhao-Hui Su[8], Zhen Yuan[1], Chee H. Ng[9] and Yu-Tao Xiang[1,2,3*]*

[1] Unit of Psychiatry, Department of Public Health and Medicinal Administration, & Institute of Translational Medicine, Faculty of Health Sciences, University of Macau, Macao, Macao SAR, China, [2] Centre for Cognitive and Brain Sciences, University of Macau, Macao, Macao SAR, China, [3] Institute of Advanced Studies in Humanities and Social Sciences, University of Macau, Macao, Macao SAR, China, [4] The National Clinical Research Center for Mental Disorders & Beijing Key Laboratory of Mental Disorders, Beijing Anding Hospital & the Advanced Innovation Center for Human Brain Protection, Capital Medical University, Beijing, China, [5] Department of Nursing, The First Affiliated Hospital of Chongqing Medical University, Chongqing, China, [6] Department of Business Administration, Hong Kong Shue Yan University, Hong Kong, Hong Kong SAR, China, [7] School of Nursing, Hong Kong Polytechnic University, Hong Kong, Hong Kong SAR, China, [8] School of Public Health, Southeast University, Nanjing, China, [9] Department of Psychiatry, The Melbourne Clinic and St Vincent's Hospital, University of Melbourne, Richmond, VIC, Australia

Background: Schizophrenia (SCZ) is a severe psychiatric disorder that involves inflammatory processes. The aim of this study was to explore the field of inflammation-related research in SCZ from a bibliometric perspective.

Methods: Regular and review articles on SCZ- and inflammation-related research were obtained from the Web of Science Core Collection (WOSCC) database from its inception to February 19, 2022. R package "bibliometrix" was used to summarize the main findings, count the occurrences of the top keywords, visualize the collaboration network between countries, and generate a three-field plot. VOSviewer software was applied to conduct both co-authorship and co-occurrence analyses. CiteSpace was used to identify the top references and keywords with the strongest citation burst.

Results: A total of 3,596 publications on SCZ and inflammation were included. Publications were mainly from the USA, China, and Germany. The highest number of publications was found in a list of relevant journals. Apart from "schizophrenia" and "inflammatory", the terms "bipolar disorder," "brain," and "meta-analysis" were also the most frequently used keywords.

Conclusions: This bibliometric study mapped out a fundamental knowledge structure consisting of countries, institutions, authors, journals, and articles in the research field of SCZ and inflammation over the past 30 years. The results provide a comprehensive perspective about the wider landscape of this research area.

Keywords: schizophrenia, inflammation, bibliometrics, VOSviewer, hotspots

OPEN ACCESS

Edited by:
Juehua Yu,
The First Affiliated Hospital of Kunming Medical University, China

Reviewed by:
Andy Wai Kan Yeung,
University of Hong Kong, Hongkong SAR, China
Peter Kokol,
University of Maribor, Slovenia
Hassan Hussein Musa,
University of Khartoum, Sudan

***Correspondence:**
Yu-Tao Xiang
ytxiang@um.edu.mo
Chee H. Ng
cng@unimelb.edu.au

†These authors have contributed equally to this work and share first authorship

Specialty section:
This article was submitted to Multiple Sclerosis and Neuroimmunology, a section of the journal Frontiers in Immunology

Received: *30 March 2022*
Accepted: *02 May 2022*
Published: *09 June 2022*

Citation:
Sun H-L, Bai W, Li X-H, Huang H, Cui X-L, Cheung T, Su Z-H, Yuan Z, Ng CH and Xiang Y-T (2022) Schizophrenia and Inflammation Research: A Bibliometric Analysis. Front. Immunol. 13:907851. doi: 10.3389/fimmu.2022.907851

1 INTRODUCTION

Schizophrenia (SCZ), a severe psychiatric disorder with strong heritability, is characterized by persistent delusions and hallucinations (1). Approximately 24 million people worldwide suffer from SCZ, which has an onset from late adolescence to early adulthood (2). Patients with SCZ often have a significantly reduced life expectancy than the general population (3).

In recent years, the role of inflammation in the pathogenesis of SCZ has gained wide attention. Inflammation is an adaptive biological response activated by a poisonous stimulus (4). For instance, one study found increased concentrations of inflammatory cytokines in SCZ patients compared with healthy controls (5). A meta-analysis revealed that patients with SCZ had increased levels of pro-inflammatory cytokine compared to healthy control subjects (6). A longitudinal study also found that a higher serum C-reactive protein level at the age of 15 or 16 years was associated with a greater risk of SCZ in adulthood (7). As such, certain inflammatory biomarkers could serve as possible treatment targets in SCZ. A meta-analysis of 26 randomized controlled trials revealed that anti-inflammatory agents such as estrogens and aspirin may have therapeutic potential for SCZ (8). Despite the rapid growth of published literature on the topic of inflammation and SCZ, accurate and useful information such as the number of relevant publications, countries, institutions, journals, authors, and the frequently used keywords in inflammation-related research in SCZ remains lacking.

Bibliometrics is a widely used approach for examining academic publications (9). With the emergence of scientific databases such as Web of Science (WOS), research data is currently easily accessible, which facilitates the development of bibliometric research (10). Bibliometrics is a comprehensive method comprising quantitative and qualitative analyses that can reveal various features of publications, such as identifying countries, journals, authors, and institutions contributing to a research area, showing commonly cited studies and frequently used keywords, and establishing the cooperation between countries, institutions, and authors in a specific scientific research field (11). Moreover, the bibliometric method can conveniently provide new researchers with an overview of the evolution and developmental frontiers of a certain research field (12). Several bibliometric analyses have investigated the publication trend on either the field of SCZ or inflammation alone (13–16). For instance, a bibliometric study of 51,117 articles on SCZ published from 1975 to 2020 found that "inflammation" has been a trending keyword in recent years (16). Another bibliometric analysis provided a comprehensive overview of the development of motivation in SCZ (17). To date, however, no bibliometric analysis on the topic of SCZ and inflammation together has been published. To fill this gap, this bibliometric analysis constructed a global map of the scientific publications on SCZ and inflammation related research.

2 METHODS

2.1 Data Acquisition and Search Strategy

Web of Science (WOS) is one of the most commonly used academic database sources which contains more than 12,000 influential journals (18). Compared with other databases such as Scopus and PubMed, it is widely recognized as the most comprehensive and reliable database for bibliometric analysis (18, 19). In this study, the relevant literature was searched and exported in the Web of Science Core Collection database (WOSCC) on February 19, 2022. WOSCC with all editions (i.e., Science Citation Index Expanded (SCI-expanded), Social Sciences Citation Index (SSCI), Conference Proceedings Citation Index-Science (CPCI-S), Emerging Sources Citation Index (ESCI), Conference Proceedings Citation Index – Social Science & Humanities (CPCI-SSH), Arts & Humanities Citation Index (A&HCI), Book Citation Index – Science (BKCI-S), Book Citation Index – Social Sciences & Humanities (BKCI-SSH), Index Chemicus (IC), and Current Chemical Reactions (CCR-EXPANDED)) was used. Following previous studies, the search strategy was set as the following (16): (TS = (inflammatory OR inflammation OR inflammations)) AND TS = (schizophren*)—literature types including regular and review articles, with no limitation in publication language. Relevant articles were exported and stored in the form of plain.txt (including full record and cited references) for further analyses.

2.2 Data Analysis

Bibliometric analyses were performed using three tools, namely, R version 3.5.6 (20), VOSviewer (21), and CiteSpace (22).

Bibliometrix is an R package containing a series of functions for scientometric quantitative research. In this study, it was used to 1) summarize the number of publications and citations of bibliometric analysis; 2) identify annual cumulative occurrences of the top keywords/terms; 3) calculate the cooperation frequency among countries; and 4) visualize a three-field plot of the Keywords Plus analysis.

VOSviewer is a distance-based bibliometric tool that focuses on the visualization of bibliometric networks (23). It can assign a set of closely related nodes into several clusters, where the same color indicates higher correlations of nodes (24). Additionally, VOSviewer supports the overlay visualization map, in which the color and distance of nodes represent how nodes are distributed in two-dimensional spaces (i.e., the time and associations) (25). VOSviewer was used in this study to perform 1) a co-authorship network that explored the authors' and their institutions' collaboration networks and 2) co-occurrence network that reflected the associations between authors' keyworks.

CiteSpace is a free Java application, with a focus on dynamic visualizations that reflect the evolution of the bibliometric network over time (26). In this study, it was used to identify highly cited references and keywords with the strongest citation burst during a certain period.

Moreover, the generalized additive model was used to estimate the trend and number of publications through R with

the *mgcv* package (27). An online bibliometric website (https://bibliometric.com/) was used to visualize the international collaboration between countries.

3 RESULTS

3.1 Publication Summary

A total of 3,596 publications on SCZ and inflammation were included, with 2,757 regular and 839 review articles. Of these articles, 3,518 (97.8%) were published in English, while 20 were published in French, 20 in German, 12 in Spanish, 12 in Polish, 6 in Japanese, 3 in Turkish, 2 in Russian and 1 each published in Chinese, Hungarian, and Italian languages.

Figure 1 illustrates the number and trend of the annual publications on SCZ and inflammation. The annual growth rate was 10.72%. The first article was published in 1991, with the growth of the number of articles increasing steadily from 2 in 1991 to 72 in 2010. In the following 10 years, the number of articles has exponentially increased, growing from 115 articles in 2011 to 449 in 2021; there was a substantial growth from 286 in 2017 to 371 in 2018 (growth rate: 38.4%). Additionally, a generalized additive model was used to assess the relationship between the number of articles and the publication year (excluding 2022), which showed that the model fitted perfectly with the publications' annual trend (R^2 = 0.999). According to the prediction curve, during the next 10 years till 2032, the trend of the literature on SCZ and inflammation will continue to increase, with an expected number of 811 in 2032.

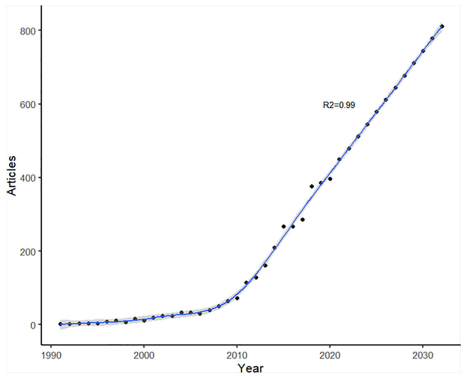

FIGURE 1 | Number of annual articles on schizophrenia and inflammation by years.

3.2 Analysis of the Most Productive Countries

Figure 2 shows the number of articles in each country/territory. The USA had the greatest number of publications (N = 785), followed by China (N = 324), Germany (N = 213), and UK (N = 211). Each of the remaining countries published less than 200 articles.

Supplement Figure 1 shows the international cooperation between countries/territories. Most of the research collaborations occurred between North American, European, Oceania, and East Asian countries, with the most frequent cooperation between the USA and China (frequency = 106), followed by the cooperation between the USA and UK (frequency = 101) and between Australia and Thailand (frequency = 74).

3.3 Analysis of the Most Productive Institutions

Approximately 3,800 institutions contributed to the research on SCZ and inflammation. **Figure 3** shows the 10 most productive institutions, with the UK, USA, Australia, and Norway each had two most productive institutions in the list. The co-authorship analysis of affiliations could estimate relationships among different institutions by the number of coauthored publications. In the overlay network of co-authorship analysis, the size of the circle indicates the number of publications and the color represents the average commencement year of publications in the specific research field in each institution. As shown in **Supplement Figure 2**, 60 institutions, with the minimum of 20 publications, were identified. Researchers at University of Cambridge in the UK and Johns Hopkins University in the USA started early in the research field of SCZ and inflammation. In contrast, those at Deakin University in Australia and at Chulalongkorn University in Thailand conducted more recent research in this area.

3.4 Analysis of the Higher-Impact Journals

The articles on SCZ and inflammation research were published across 918 journals. **Table 1** displays the top 10 journals with the greatest number of publications and their recent impact factor (IF). In terms of Journal Citation Reports (JCR), most of the

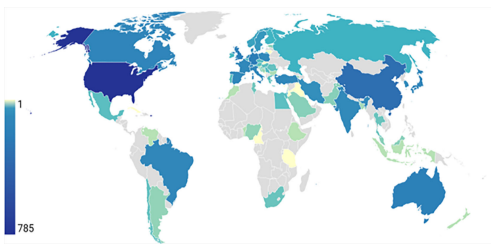

Country	Articles
USA	785
CHINA	324
GERMANY	213
UNITED KINGDOM	211
AUSTRALIA	179
JAPAN	134
CANADA	129
TURKEY	114
ITALY	113
BRAZIL	112

FIGURE 2 | A world map depicting the contribution of each country based on publication counts.

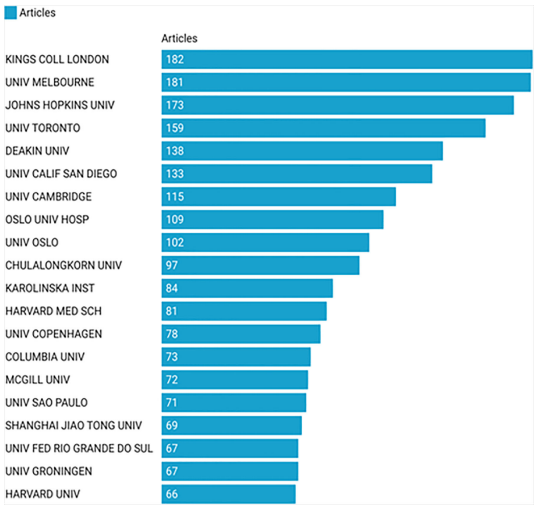

FIGURE 3 | Top 10 institutions with most publications in the field of schizophrenia and inflammation research.

journals were classified into Q1 (90%), with 70% of the journal classified as psychiatry. As for the publisher location, of the top 10 journals, five out of the top 10 journals were in the USA, 3 in the UK, and 2 in Netherlands.

3.5 Analysis of the Most Influential Authors

As presented in **Table 2**, 15,692 authors contributed to SCZ- and inflammation-related publications. Michael Maes' team/lab was the most productive which published 98 articles (h_index = 32), followed by Michael Berk (60 articles with h_index = 27), Marion Leboyer (55 articles with h_index = 21), and Norbert Muller (47 articles with h_index = 28). **Supplement Figure 3** shows the maps of cooperation between researchers; the minimum number of papers per author was set as 10. Of the remaining 94 authors, there were several communities, with each community clustering near one or two frequently published authors. The links between different communities were relatively sparse, which indicates that cooperation between research teams/labs conducting SCZ- and inflammation-related studies was not well established.

3.6 Analysis of Research Hotspots

3.6.1 Most Cited Articles

Citation analysis is a valuable method to assess the most highly cited articles; the frequency of citations could reflect the influence of articles in a specific research field (28). **Supplement Table 1** shows the 10 most cited articles, all of which were published between 1997 and 2019, and 80% of them have reached more than 500 citations. Of these articles, the top three were meta-analyses, with two published in Biological Psychiatry. Specifically, the article entitled "Meta-analysis of cytokine alterations in schizophrenia: clinical status and antipsychotic effects" published in 2011 is the top-cited article in this field with 1,031 citations (6). This meta-analysis included 40 studies and revealed that certain cytokines (e.g., IL-1β, IL-6, and TGF-β) were state markers of acute exacerbations, while others (e.g., IL-12, IFN-γ, TNF-α, and sIL-2R) were trait markers. It also suggested that the association between cytokine and acute exacerbations of SCZ was independent of any antipsychotics.

3.6.2 Analysis of References With Citation Burst

Figure S4 illustrates the top 20 references with the highest citation burst. The minimum duration of the burst was 5 years, while the blue line represents the observed time interval from 1992 to 1991 and the red line represents the burst duration. Of these articles, the article entitled "Inflammatory Cytokine Alterations in Schizophrenia: A Systematic Quantitative Review" published in Biological Psychiatry has the strongest citation burst value during 2008–2013. Moreover, the citation burst for several articles is still ongoing, such as "Postmortem evidence of cerebral inflammation in schizophrenia: a systematic review," which suggests that such research topics are likely to remain popular in the future and may become potential frontiers in the SCZ and inflammation research field.

3.6.3 Analysis of the Most Frequently Used Keywords

Of the 5,906 keywords, with a minimum number of occurrences as 30, 60 keywords met the criteria and were included for analyses. Following a previous study (29), keywords with similar meanings were merged. **Figure 4A** shows the network visualization of these keywords. The size of nodes reflects the

TABLE 1 | Top 10 journals with most publications in the field of schizophrenia and inflammation research.

Ranking	Sources	Articles	Country	IF	JCR-c
1	Schizophrenia Research	165	Netherlands	4.939	Q1
2	Brain Behavior and Immunity	143	USA	7.217	Q1
3	Psychiatry Research	103	Netherlands	3.222	Q1
4	Progress in Neuro-psychopharmacology & Biological Psychiatry	85	UK	5.067	Q1
5	Frontiers in Psychiatry	76	USA	4.157	Q2
6	Translational Psychiatry	73	USA	6.222	Q1
7	Journal of Psychiatric Research	66	UK	4.791	Q1
8	PLOS One	62	USA	3.240	Q1
9	Molecular Psychiatry	54	UK	15.992	Q1
10	Schizophrenia Bulletin	53	USA	9.306	Q1

IF, impact factor (2020–2021); JCR-c, Journal Citation Reports category (2021).

TABLE 2 | Top 10 authors with the most publications in the field of schizophrenia and inflammation research.

Ranking	Authors	Articles	h_index
1	MAES M Maes, Michael	98	32
2	BERK M Berk, Michael	60	27
3	LEBOYER M Leboyer, Marion	55	21
4	MULLER N Muller, Norbert	47	28
5	YOLKEN RH Yolken, Robert	40	23
6	LEZA JC Leza, Juan C	39	17
7	MEYER U Meyer, Urs A	34	25
8	TEIXEIRA AL Teixeira, Antonio L	34	20
9	WEICKERT CS Weickert, Cynthia Shannon	34	17
10	ANDREASSEN OA Andreassen, Ole A	33	16

occurrence frequency of keywords, while the distance between two nodes reflects the strength of their association. Keywords with a closer distance were classified into the same cluster, which roughly reflects the main topics in the SCZ and inflammation research area. Cluster 1 is colored in red, with the main keywords focusing on psychiatric disorder- and inflammation-related terms such as "bipolar disorder," "depression," "immune," and "immunology," cluster 2 in green focused on antipsychotics, with the main keywords "clozapine," "minocycline," and "olanzapine." In addition, several terms, such as "c-reactive protein" and "interleukin-6," were also included in cluster 2. Cluster 3 in blue color focused on the pathways related to SCZ and inflammation, with the main keywords "biomarkers," "gene system," and "brain." Cluster 4 in yellow color focused on the central nervous system (CNS), mainly involving "neuroinflammation," "microglia," "Parkinson's disease," "Alzheimer's disease," and "Multiple sclerosis." Cluster 5 in purple color focused on "cytokines," "dopamine," "glutamate," and "animal model." **Figure 4B** presents the overlay visualization of author keywords. The keywords that appeared earlier are colored in blue, while the orange color represents the keywords that have appeared recently. Keywords, such as "cytokines," "antipsychotic," "neurodevelopment," "infection," and "animal model," were the major topics in the early period. In contrast, keywords "biomarker," "immune activation," "microbiome," and "neuroinflammation" have been popular topics in recent years.

Figure 4C shows the 10 most frequent keywords, with "schizophrenia" being the most used keyword with 1,187 frequencies, followed by "inflammation" (N = 632) and "bipolar disorder" (N = 440). Of the commonly used keywords, "Meta-analysis" (N = 328) was a statistical-related term. **Figure 5** shows the relationships between affiliations, authors, and keywords in the field of SCZ and inflammation research.

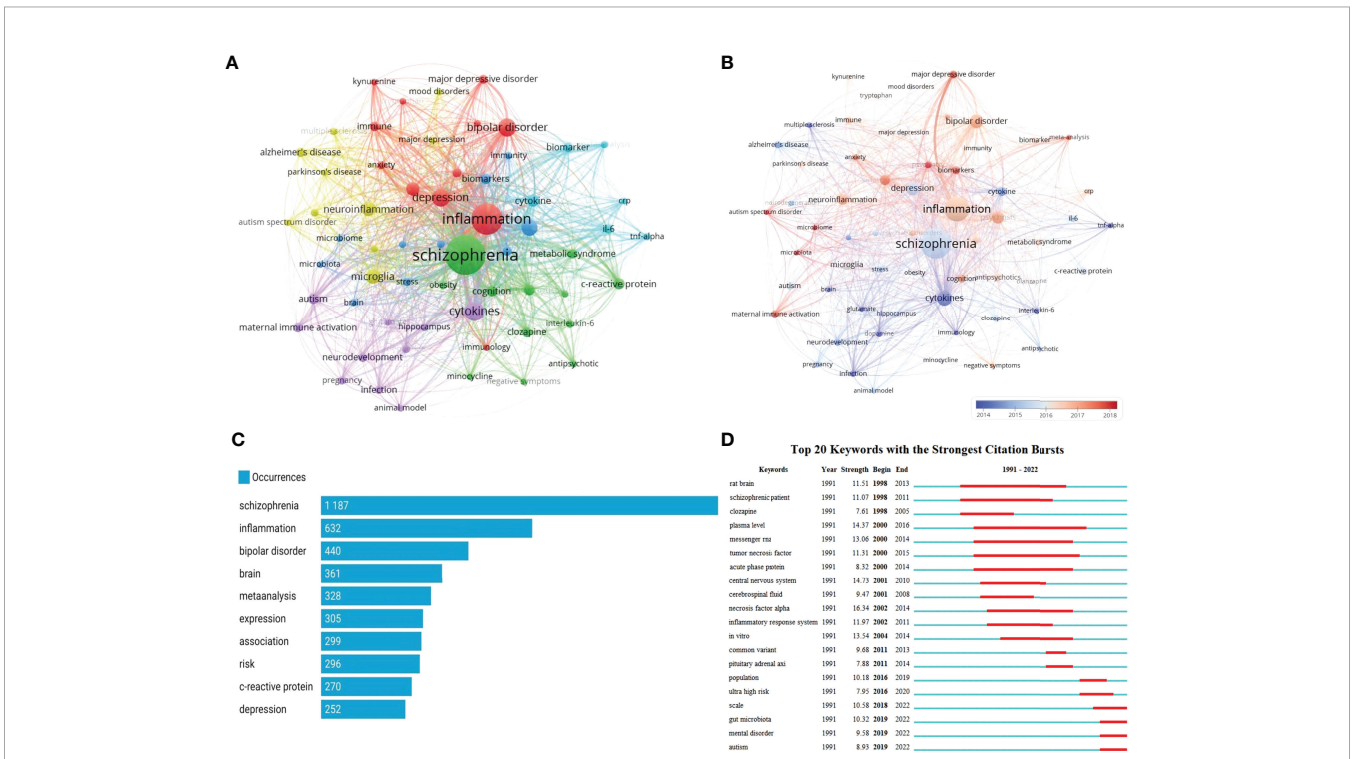

FIGURE 4 | Analysis of the research hotspots on schizophrenia and inflammation (**A**, network visualization of author keywords; **B**, overlay visualization of author keywords; **C**, top 10 most frequent keywords; **D**, visualization map of top 20 keywords with the strongest citations bursts).

3.6.4 Analysis of Keywords With Citation Burst

Figure 4D shows the top 20 keywords with the strongest citations bursts, with the minimum duration of the burst being 3 years. The keywords "rat brain" (1998–2013), "plasma level" (2000–2016), "tumor necrosis factor" (2000–2015), and "schizophrenic patients" (1991–2011) have received the longest attention during the past period. The keywords "gut microbiota" (2019–2022), "mental disorder" (2019–2022), and "autism" (2019–2022) have been used more recently, which indicates that these keywords have attracted sufficient attention lately and potentially may be a hot research topic in the future.

4 DISCUSSION

This bibliometric analysis study analyzed the development of SCZ- and inflammation-related research in the past 30 years. Articles on SCZ and inflammation showed a growing trend over the past decades, particularly since 2011. A similar trend was observed in a previous bibliometric study on SCZ alone, which found that the publication number has also grown substantially since 2011 (15). The potential reason for the expansion of research might be due to the increasing recognition of the role of inflammation (30) in the development of SCZ (31) and, therefore, increased research funding in this field. More than 90% of the articles were published in English, which is not surprising because the WOSCC database mainly included English journal articles, and English is the most widely used academic language globally (32).

In this bibliometric analysis, most of the relevant articles were published by corresponding authors from several countries such as the USA, China, Germany, and the UK. Similar patterns have been found in bibliometric studies in other fields such as depression (33), bipolar disorders (34), and general neuropharmacology (35). Academic capability is largely determined by the economic status of a country (36). Additionally, governmental expenditure on healthcare may be another important indicator of medical research outputs (37). The USA outspends all other countries in health expenditure with USD10,202 per resident (38), which may partly explain the largest number of publications in the USA. Most of the collaborations on SCZ and inflammation research are also centered on the USA, which is consistent with the prominent contribution of USA in this academic field, which indicates that collaborations between other countries/territories need to be enhanced.

Similar to the findings on the contribution of individual countries on relevant publications, a number of institutions in the UK, USA, and Australia published widely on SCZ and inflammation. In contrast, only one Chinese institution was among the top 15 institutions in the ranking list, even though China is the second most productive country in terms of publications, while one university in Thailand alone published almost 100 articles on SCZ and inflammation research, which is not consistent with the volume of country contribution. Most of these articles were based on collaboration, suggesting that interinstitutional collaboration is an important approach to improving the quantity and quality of publications.

Analyzing the characteristic of international peer-reviewed journals is helpful to understanding the current trends (39, 40). Among the top 10 most active journals in the field of SCZ and inflammation research, most of the publishers are in the USA and Western Europe. Schizophrenia Research was the most productive journal in the SCZ and inflammation research field; not surprisingly, this journal was also the most active journal with the maximum number of articles in other schizophrenia-related academic fields such as motivation in SCZ (17), cognitive behavioral therapy for SCZ (41), and magnetic resonance imaging studies of SCZ (42). In contrast, no publishers are based in East Asia although China and Japan were also two key countries contributing to SCZ and inflammation research. This highlights the importance of developing influential international journals in Asia. The IF of journals is a crucial evaluation indicator. JCR is also a commonly used index for

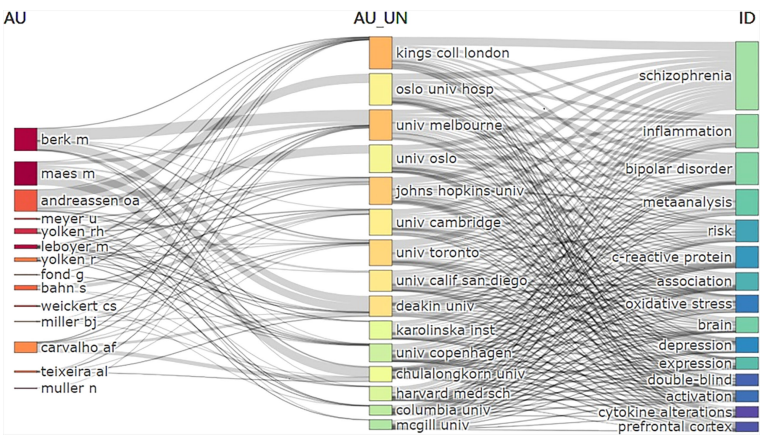

FIGURE 5 | Three-field plot of the Keywords Plus analysis on schizophrenia and inflammation Notes: three-field plot of the keywords plus analysis: (middle field: affiliations; left field: authors; right field: keywords plus).

evaluating the quality of journals based on the ranking of IF with four classifications, ranging from the top quartile (Q1) to the fourth quartile (Q4). However, no significant associations were found between number of articles, IF value, and JCR quartile in this study, which indicates that journals may use different approaches to establish research impact. Some journals prefer to publish a large number of articles, while others may prefer high-quality articles that may have more frequent citations with higher IF values or JCR quartile.

The number of articles published by a research team could reflect its activity and contribution in a certain scientific area. In 1995, a team in Thailand published an article on the association of immune-inflammatory variables in SCZ and mania, which has been highly cited (number of citations = 480) (43). The coauthorship between researchers is helpful to exploring existing collaborations and finding potential collaborators. Co-authorship analysis is a useful method to identifying existing partnerships and facilitating developing potential partners. Two teams in Thailand and Australia have collaborated closely, with one of their publications on the pathway between inflammation and bipolar disorder having more than 1,000 citations (44).

Hotspots refers to a scientific topic in a specific research area during a certain period of time, which is one of the key methodologies in bibliometric analysis (29). Citation analysis could reflect the academic influence of publications. Among the 10 most cited articles identified in this study, the key focus was inflammatory cytokine alterations in SCZ patients (45–48). Previous studies found that the imbalance of Th1/Th2 cytokines plays a vital role in SCZ, with a slant toward the Th2 system (45, 49, 50). In addition, IL-6 levels significantly decreased, while sIL-2R, IL-1RA, and IL-6 levels increased in SCZ patients (47). Among the 10 most cited articles, two articles were reviews on the pathology under SCZ and inflammation (51, 52), and another two articles focused on the treatment of psychiatric disorders (53, 54). In contrast, recent research focused more on SCZ- and inflammation-related genetic variants (55, 56). A genome-wide association study found that six immune candidates, namely, DPP*4*, *HSPD1*, *EGR1*, *CLU*, *ESAM*, and *NFATC3*, were associated with schizophrenia (57). Hence, this research field has been focusing on biomarker discovery and the development of precision treatments for SCZ patients. Keyword is an important indicator in scientific research as it reflects the core content of the relevant paper. The co-occurrence analysis of keywords could show the closeness and prevalence of the research topics in scientific areas (58). For the most frequently used keywords, apart from terms "schizophrenia" and "inflammation," other commonly used keywords focused on the potential mechanisms of SCZ that involve inflammation. Additionally, biomarkers of inflammation c-reactive protein (CRP) appeared frequently. Researchers have found that the association between elevated CRP and SCZ was independent of confounding factors, such as BMI and smoking, which may lead to the development of immune treatments of SCZ (59). Bipolar disorder is another high-frequency keyword; SCZ and bipolar disorder often shared the same clinical attributes (60) and genetic factors (61); thus, they are usually investigated together.

The co-occurrence clustering function roughly divided the whole network into five clusters, with each cluster as a main topic. Cluster 2 in green color included keywords on antipsychotic medications. Some studies found that certain antipsychotic drugs may have immunomodulatory effects through targeting cytokines (62, 63). In addition, other studies found that certain anti-inflammatory drugs (e.g., aspirin) could be used as adjuncts to antipsychotic drugs, and their efficacy and safety in treating schizophrenia might be better than antipsychotics alone (54, 64). Cluster 4 in yellow color contained several CNS-related terms. Neuroinflammation, an innate activation response to an inflammatory stimulus, was often used in connection with microglia (65). Microglia, as the CNS-resident macrophages, has been shown to be involved in the initiation or progression of several CNS disorders, such as Parkinson's disease, Alzheimer's disease, multiple sclerosis, and SCZ (66, 67). One explanation is that microglia can facilitate the maturation of neuronal progenitors by secreting insulin-like growth factors; thus, it may play a crucial role in CNS immune responses (68).

The burst detection analysis is an important approach to explore the evolution of research hotspots in an academic interest area. Articles or keywords with high citation bursts imply that they are actively discussed or used during a specific period. Gut microbiota has been an ongoing burst keyword since 2019, which is consistent with the development of microbiota–microglia axis hypothesis in the SCZ and inflammation field. Specifically, gut microbiota work as a regulator of microglial function, and microglia are involved in mediating inflammation and neurodegenerative disorders such as SCZ (69). Compared to healthy controls, immunomodulatory bacterial genera, such as Lactobacilli and Bifidobacteria, are relatively more prevalent in SCZ patients (70). Therefore, targeting a specific gut microbiome may be a future direction in SCZ treatment.

This study has several limitations. First, the data were retrieved from WOSCC alone. Although WOS has been recommended as the most reliable database for bibliometric studies (71–74), some articles may be still missed. Second, the majority of articles were published in English, which may lead to selection bias in terms of publication language. Third, certain inconsistencies may exist in various aspects; for example, one institution may use different names across different periods.

5 CONCLUSION

In conclusion, research on the role of inflammation in SCZ has received growing attention. The substantial growth in the number of annual publications suggests that this research field has gained importance globally, with the USA having the largest number of publications. This study has identified the key researchers and institutions involved in SCZ- and inflammation-related research globally. Schizophrenia Research was the most productive journal in this research field, while Molecular Psychiatry has the highest IF in this field. Inflammatory cytokine and genetic variants have

been regarded as the hot topics, while gut microbiota may be a key direction of future research. These findings provide a comprehensive perspective for new researchers and policymakers about the wider landscape of this research field.

DATA AVAILABILITY STATEMENT

All the data used in the study have been included in the article/**Supplementary Material**.

AUTHOR CONTRIBUTIONS

Study design: H-LS, WB, X-HL, CN, Y-TX; data collection, analysis, and interpretation: H-LS, WB, X-HL, HH, X-LC. TC, ZS, ZY; drafting of the manuscript: H-LS, WB, Y-TX; critical revision of the manuscript: CN. All authors contributed to the article and approved the submitted version.

FUNDING

The study was supported by the Beijing Municipal Science & Technology Commission (Grant No.: Z181100001718124), Beijing Talents Foundation (Grant No.: 2017000021469G222), and the University of Macau (MYRG2019-00066-FHS).

SUPPLEMENTARY MATERIAL

The Supplementary Material for this article can be found online at: https://www.frontiersin.org/articles/10.3389/fimmu.2022.907851/full#supplementary-material

REFERENCES

1. Bloomfield MA, Buck SC, Howes ODJTLP. Schizophrenia: Inorganic No More. *Lancet Psychiatr* (2016) 3(7):600–2. Macao Sar. doi: 10.1016/S2215-0366(16)30096-7
2. Charlson FJ, Ferrari AJ, Santomauro DF, Diminic S, Stockings E, Scott JG, et al. Global Epidemiology and Burden of Schizophrenia: Findings From the Global Burden of Disease Study 2016. *Schizophr Bull* (2018) 44(6):1195–203. Macao Sar. doi: 10.1093/schbul/sby058
3. Hjorthøj C, Stürup AE, McGrath JJ, Nordentoft M. Years of Potential Life Lost and Life Expectancy in Schizophrenia: A Systematic Review and Meta-Analysis. *Lancet Psychiatry* (2017) 4(4):295–301. Macao Sar. doi: 10.1016/S2215-0366(17)30078-0
4. Medzhitov R. Origin and Physiological Roles of Inflammation. *Nature* (2008) 454(7203):428–35. doi: 10.1038/nature07201
5. Hughes HK, Mills-Ko E, Yang H, Lesh TA, Carter CS, Ashwood P. Differential Macrophage Responses in Affective Versus Non-Affective First-Episode Psychosis Patients. *Front Cell Neurosci* (2021) 15:583351. doi: 10.3389/fncel.2021.583351
6. Miller BJ, Buckley P, Seabolt W, Mellor A, Kirkpatrick B. Meta-Analysis of Cytokine Alterations in Schizophrenia: Clinical Status and Antipsychotic Effects. *Biol Psychiatry* (2011) 70(7):663–71. Macao Sar. doi: 10.1016/j.biopsych.2011.04.013
7. Metcalf SA, Jones PB, Nordstrom T, Timonen M, Mäki P, Miettunen J, et al. Serum C-Reactive Protein in Adolescence and Risk of Schizophrenia in Adulthood: A Prospective Birth Cohort Study. *Brain Behav Immun* (2017) 59:253–9. Macao Sar. doi: 10.1016/j.bbi.2016.09.008
8. Sommer IE, van Westrhenen R, Begemann MJH, de Witte LD, Leucht S, Kahn RS. Efficacy of Anti-Inflammatory Agents to Improve Symptoms in Patients With Schizophrenia: An Update. *Schizophr Bull* (2013) 40(1):181–91. doi: 10.1093/schbul/sbt139
9. Gauthier É. *Bibliometric Analysis of Scientific and Technological Research: A User's Guide to the Methodology*. Science and Technology Redesign Project: Citeseer (1998).
10. Donthu N, Kumar S, Mukherjee D, Pandey N, Lim WM. How to Conduct a Bibliometric Analysis: An Overview and Guidelines. *J Business Res* (2021) 133:285–96. doi: 10.1016/j.jbusres.2021.04.070
11. Song Y, Chen X, Hao T, Liu Z, Lan Z. Exploring Two Decades of Research on Classroom Dialogue by Using Bibliometric Analysis. *Comput Education* (2019) 137:12–31. doi: 10.1016/j.compedu.2019.04.002
12. Hao T, Chen X, Li G, Yan J. A Bibliometric Analysis of Text Mining in Medical Research. *Soft Comput* (2018) 22(23):7875–92. doi: 10.1007/s00500-018-3511-4
13. Fei X, Wang S, Zheng X, Liu K, Liang XJGP. Global Research on Cognitive Behavioural Therapy for Schizophrenia From 2000 to 2019: A Bibliometric Analysis *via* CiteSpace. *Gen Psychiatry* (2021) 34(1):e100327. doi: 10.1136/gpsych-2020-100327
14. Najas-Garcia A, Carmona VR, Gómez-Benito J. Trends in the Study of Motivation in Schizophrenia: A Bibliometric Analysis of Six Decades of Research (1956–2017). *Front Psychol* (2018) 9:63. doi: 10.3389/fpsyg.2018.00063
15. Kiraz S, Demir EJPQ. Global Scientific Outputs of Schizophrenia Publications From 1975 to 2020: A Bibliometric Analysis. *Psychiatric Quart* (2021) 92(4):1725–44. doi: 10.1007/s11126-021-09937-4
16. Kiraz S, Demir E. Global Scientific Outputs of Schizophrenia Publications From 1975 to 2020: A Bibliometric Analysis. *Psychiatr Quarterly* (2021) 92(4):1725–44. doi: 10.1007/s11126-021-09937-4
17. Najas-Garcia A, Carmona VR, Gómez-Benito J. Trends in the Study of Motivation in Schizophrenia: A Bibliometric Analysis of Six Decades of Research (1956–2017). *Front Psychol* (2018) 9. doi: 10.3389/fpsyg.2018.00063
18. Wu H, Li Y, Tong L, Wang Y, Sun Z. Worldwide Research Tendency and Hotspots on Hip Fracture: A 20-Year Bibliometric Analysis. *Arch Osteoporosis* (2021) 16(1):1–14. doi: 10.1007/s11657-021-00929-2
19. Marzi G, Caputo A, Garces E, Dabić M. A Three Decade Mixed-Method Bibliometric Investigation of the IEEE Transactions on Engineering Management. *IEEE Trans Eng Management* (2018) 67(1):4–. doi: 10.1109/TEM.2018.2870648
20. Derviş H. Bibliometric Analysis Using Bibliometrix an R Package. *J Scientomet Res* (2019) 8(3):156–60. doi: 10.5530/JSCIRES.8.3.32
21. Van Eck N, Waltman L. Software Survey: VOSviewer, a Computer Program for Bibliometric Mapping. *Scientometrics* (2010) 84(2):523–38. doi: 10.1007/s11192-009-0146-3
22. Chen C. *CiteSpace: A Practical Guide for Mapping Scientific Literature*. New York: Nova Science Publishers (2016).
23. Eck NJV, Waltman L. Visualizing Bibliometric Networks. In: *Measuring Scholarly Impact*. Springer: Cham Press (2014). p. 285–320.
24. Van Eck N, Waltman L. Software Survey: VOSviewer, a Computer Program for Bibliometric Mapping. *scientometrics* (2010) 84(2):523–38. doi: 10.48550/arXiv.1109.2058
25. Van Eck NJ, Waltman L, van Raan AF, Klautz RJ, Peul WC. Citation Analysis may Severely Underestimate the Impact of Clinical Research as Compared to Basic Research. *PloS One* (2013) 8(4):e62395. doi: 10.1371/journal.pone.0062395
26. Chen C. CiteSpace II: Detecting and Visualizing Emerging Trends and Transient Patterns in Scientific Literature. *J Am Soc Inf Sci Technol* (2006) 57(3):359–77. doi: 10.1002/asi.20317
27. Wood S. *Mixed GAM Computation Vehicle With Automatic Smoothness Estimation*, Vol. 1. (2018). pp. 8–12.
28. Gao Q, Zhang C, Wang J, Wei Q, Wei Q, Miyamoto A, et al. The Top 100 Highly Cited Articles on Osteoporosis From 1990 to 2019: A Bibliometric and

Visualized Analysis. *Arch Osteoporos* (2020) 15(1):144. doi: 10.1007/s11657-020-0705-z
29. Wu H, Zhou Y, Wang Y, Tong L, Wang F, Song S, et al. Current State and Future Directions of Intranasal Delivery Route for Central Nervous System Disorders: A Scientometric and Visualization Analysis. *Front Pharmacol* (2021) 12. doi: 10.3389/fphar.2021.717192
30. Müller N. Inflammation in Schizophrenia: Pathogenetic Aspects and Therapeutic Considerations. *Schizophr Bull* (2018) 44(5):973–82. doi: 10.1093/schbul/sby024
31. Hartwig FP, Borges MC, Horta BL, Bowden J, Davey Smith G. Inflammatory Biomarkers and Risk of Schizophrenia: A 2-Sample Mendelian Randomization Study. *JAMA Psychiatry* (2017) 74(12):1226–33. doi: 10.1001/jamapsychiatry.2017.3191
32. Crystal D. *English as a Global Language*. Cambridge university press (2003).
33. Wang H, Tian X, Wang X, Wang Y. Evolution and Emerging Trends in Depression Research From 2004 to 2019: A Literature Visualization Analysis. *Front Psychiatry* (2021) 12:705749. doi: 10.3389/fpsyt.2021.705749
34. López-Muñoz F, Vieta E, Rubio G, García-García P, Alamo C. Bipolar Disorder as an Emerging Pathology in the Scientific Literature: A Bibliometric Approach. *J Affect Disord* (2006) 92(2):161–70. doi: 10.1016/j.jad.2006.02.006
35. Yeung AWK, Tzvetkov NT, Atanasov AG. When Neuroscience Meets Pharmacology: A Neuropharmacology Literature Analysis. *Front Neurosci* (2018) 852. doi: 10.3389/fnins.2018.00852
36. Kiraz MJEJMI. A Holistic Investigation of Global Outputs of Covid-19 Publications in Neurology and Neurosurgery. *Eur J Med Invest* (2020) 4 (4):506–12. doi: 10.14744/ejmi.2020.36601
37. Wu H, Cheng K, Guo Q, Yang W, Tong L, Wang Y, et al. Mapping Knowledge Structure and Themes Trends of Osteoporosis in Rheumatoid Arthritis: A Bibliometric Analysis. *Front Med* (2021) 8:787228. doi: 10.3389/fmed.2021.787228
38. Statista Research Department. *Health Expenditures in the U.S. – Statistics & Facts: Statista Research Department* (2022). Available at: https://www.statista.com/topics/6701/health-expenditures-in-the-us/#topicHeader:wrapper.
39. Wu H, Li Y, Tong L, Wang Y, Sun Z. Worldwide Research Tendency and Hotspots on Hip Fracture: A 20-Year Bibliometric Analysis. *Arch Osteop* (2021) 16(1):1–14. doi: 10.1007/s11657-021-00929-2
40. Zhao Y, Zhang X, Song Z, Wei D, Wang H, Chen W, et al. Bibliometric Analysis of ATAC-Seq and Its Use in Cancer Biology via Nucleic Acid Detection. *Front Med* (2020) 715:584728. doi: 10.3389/fmed.2020.584728
41. Fei X, Wang S, Zheng X, Liu K, Liang X. Global Research on Cognitive Behavioural Therapy for Schizophrenia From 2000 to 2019: A Bibliometric Analysis *via* CiteSpace. *Gen Psychiatr* (2021) 34(1):e100327–e. doi: 10.1136/gpsych-2020-100327
42. Duan L, Zhu G. Mapping Theme Trends and Knowledge Structure of Magnetic Resonance Imaging Studies of Schizophrenia: A Bibliometric Analysis From 2004 to 2018. *Front Psychiatry* (2020) 11. doi: 10.3389/fpsyt.2020.00027
43. Maes M, Bosmans E, Calabrese J, Smith R, Meltzer H. Interleukin-2 and Interleukin-6 in Schizophrenia and Mania: Effects of Neuroleptics and Mood Stabilizers. *J Psychiatr Res* (1995) 29(2):141–52. doi: 10.1016/0022-3956(94)00049-W
44. Berk M, Kapczinski F, Andreazza AC, Dean OM, Giorlando F, Maes M, et al. Pathways Underlying Neuroprogression in Bipolar Disorder: Focus on Inflammation, Oxidative Stress and Neurotrophic Factors. *Neurosci Biobehav Rev* (2011) 35(3):804–17. doi: 10.1016/j.neubiorev.2010.10.001
45. Miller BJ, Buckley P, Seabolt W, Mellor A, Kirkpatrick B. Meta-Analysis of Cytokine Alterations in Schizophrenia: Clinical Status and Antipsychotic Effects. *Biol Psychiatry* (2011) 70(7):663–71. doi: 10.1016/j.biopsych.2011.04.013
46. Potvin S, Stip E, Sepehry AA, Gendron A, Bah R, Kouassi E. Inflammatory Cytokine Alterations in Schizophrenia: A Systematic Quantitative Review. *Biol Psychiatry* (2008) 63(8):801–8. doi: 10.1016/j.biopsych.2007.09.024
47. Goldsmith D, Rapaport M, Miller B. A Meta-Analysis of Blood Cytokine Network Alterations in Psychiatric Patients: Comparisons Between Schizophrenia, Bipolar Disorder and Depression. *Mol Psychiatry* (2016) 21 (12):1696–709. doi: 10.1038/mp.2016.3
48. Maes M, Bosmans E, De Jongh R, Kenis G, Vandoolaeghe E, Neels H. Increased Serum IL-6 and IL-1 Receptor Antagonist Concentrations in Major Depression and Treatment Resistant Depression. *Cytokine* (1997) 9 (11):853–8. doi: 10.1006/cyto.1997.0238
49. Müller N, Riedel M, Gruber R, Ackenheil M, Schwarz MJ. The Immune System and Schizophrenia: An Integrative View. *Ann New Y Acad Sci* (2000) 917(1):456–67. doi: 10.1111/j.1749-6632.2000.tb05410.x.
50. Schwarz M, Müller N, Riedel M, Ackenheil M. The Th2-Hypothesis of Schizophrenia: A Strategy to Identify a Subgroup of Schizophrenia Caused by Immune Mechanisms. *Med Hypotheses* (2001) 56(4):483–6. doi: 10.1054/mehy.2000.1203
51. Patterson PH. Immune Involvement in Schizophrenia and Autism: Etiology, Pathology and Animal Models. *Behav Brain Res* (2009) 204(2):313–21. doi: 10.1016/j.bbr.2008.12.016
52. Meyer U, Nyffeler M, Engler A, Urwyler A, Schedlowski M, Knuesel I, et al. The Time of Prenatal Immune Challenge Determines the Specificity of Inflammation-Mediated Brain and Behavioral Pathology. *J Neurosci* (2006) 26(18):4752–62. doi: 10.1523/JNEUROSCI.0099-06.2006
53. Müller N, Schwarz M, Dehning S, Douhe A, Cerovecki A, Goldstein-Müller B, et al. The Cyclooxygenase-2 Inhibitor Celecoxib has Therapeutic Effects in Major Depression: Results of a Double-Blind, Randomized, Placebo Controlled, Add-on Pilot Study to Reboxetine. *Mol Psychiatry* (2006) 11 (7):680–4. doi: 10.1038/sj.mp.4001805
54. Berk M, Dean O, Drexhage H, McNeil JJ, Moylan S, O'Neil A, et al. Aspirin: A Review of its Neurobiological Properties and Therapeutic Potential for Mental Illness. *BMC Med* (2013) 11(1):1–17. doi: 10.1186/1741-7015-11-74
55. Pickrell JK, Berisa T, Liu JZ, Ségurel L, Tung JY, Hinds DA. Detection and Interpretation of Shared Genetic Influences on 42 Human Traits. *Nat Genet* (2016) 48(7):709–17. doi: 10.1038/ng.3570
56. Martin AR, Kanai M, Kamatani Y, Okada Y, Neale BM, Daly MJ. Clinical Use of Current Polygenic Risk Scores may Exacerbate Health Disparities. *Nat Genet* (2019) 51(4):584–91. doi: 10.1038/s41588-019-0379-x
57. Pouget JG, Gonçalves VF, Spain SL, Finucane HK, Raychaudhuri S, Kennedy JL, et al. Genome-Wide Association Studies Suggest Limited Immune Gene Enrichment in Schizophrenia Compared to 5 Autoimmune Diseases. *Schizophr Bull* (2016) 42(5):1176–84. doi: 10.1093/schbul/sbw059
58. Deng Z, Wang H, Chen Z, Wang T. Bibliometric Analysis of Dendritic Epidermal T Cell (DETC) Research From 1983 to 2019. *Front Immunol* (2020) 11:259. doi: 10.3389/fimmu.2020.00259
59. Dickerson F, Stallings C, Origoni A, Vaughan C, Khushalani S, Yang S, et al. C-Reactive Protein is Elevated in Schizophrenia. *Schizophr Res* (2013) 143 (1):198–202. doi: 10.1016/j.schres.2012.10.041
60. Grande I, Berk M, Birmaher B, Vieta EJTL. Bipolar Disorder. *Lancet* (2016) 387(10027):1561–72. doi: 10.1016/S0140-6736(15)00241-X
61. Smeland OB, Bahrami S, Frei O, Shadrin A, O'Connell K, Savage J, et al. Genome-Wide Analysis Reveals Extensive Genetic Overlap Between Schizophrenia, Bipolar Disorder, and Intelligence. *Mol Psychiatry* (2020) 25 (4):844–53. doi: 10.1038/s41380-018-0332-x
62. Kato TA, Monji A, Mizoguchi Y, Hashioka S, Horikawa H, Seki Y, et al. Anti-Inflammatory Properties of Antipsychotics *via* Microglia Modulations: Are Antipsychotics a 'Fire Extinguisher' in the Brain of Schizophrenia? *Mini Rev Med Chem* (2011) 11(7):565–74. doi: 10.2174/138955711795906941
63. Zajkowska Z, Mondelli V. First-Episode Psychosis: An Inflammatory State? *Neuroimmunomodulation* (2014) 21(2-3):102–8. doi: 10.1159/000356536
64. Cho M, Lee TY, Kwak YB, Yoon YB, Kim M, Kwon JS. Adjunctive Use of Anti-Inflammatory Drugs for Schizophrenia: A Meta-Analytic Investigation of Randomized Controlled Trials. *Aust New Z J Psychiatry* (2019) 53(8):742–59. doi: 10.1177/0004867419835028
65. Graeber MB, Li W, Rodriguez ML. Role of Microglia in CNS Inflammation. *FEBS Lett* (2011) 585(23):3798–805. doi: 10.1016/j.febslet.2011.08.033
66. Prinz M, Jung S, Priller J. Microglia Biology: One Century of Evolving Concepts. *Cell* (2019) 179(2):292–311. doi: 10.1016/j.cell.2019.08.053
67. Derecki NC, Katzmarski N, Kipnis J, Meyer-Luehmann M. Microglia as a Critical Player in Both Developmental and Late-Life CNS Pathologies. *Acta Neuropathol* (2014) 128(3):333–45. doi: 10.1007/s00401-014-1321-z
68. Kierdorf K, Prinz M. Microglia in Steady State. *J Clin Invest* (2017) 127 (9):3201–9. doi: 10.1172/JCI90602

69. Mossad O, Erny D. The Microbiota-Microglia Axis in Central Nervous System Disorders. *Brain Pathol* (2020) 30(6):1159–77. doi: 10.1111/bpa.12908
70. Castro-Nallar E, Bendall ML, Pérez-Losada M, Sabuncyan S, Severance EG, Dickerson FB, et al. Composition, Taxonomy and Functional Diversity of the Oropharynx Microbiome in Individuals With Schizophrenia and Controls. *PeerJ* (2015) 3:e1140. doi: 10.7717/peerj.1140
71. Falagas ME, Pitsouni EI, Malietzis GA, Pappas G. Comparison of PubMed, Scopus, Web of Science, and Google Scholar: Strengths and Weaknesses. *FASEB J* (2008) 22(2):338–42. doi: 10.1096/fj.07-9492LSF
72. Caputo A, Marzi G, Maley J, Silic M. Ten Years of Conflict Management Research 2007-2017: An Update on Themes, Concepts and Relationships. *Int J Conf Manag* (2019) 30(1):87–110. doi: 10.1108/IJCMA-06-2018-0078
73. Gu YJS. Global Knowledge Management Research: A Bibliometric Analysis A Bibliometric Analysis. *Scientometrics* (2004) 61(2):171–90. doi: 10.1023/B:SCIE.0000041647.01086.f4
74. Ding Y, Rousseau R, Wolfram D. *Measuring Scholarly Impact*. Springer: Cham Press (2016).

Conflict of Interest: The authors declare that the research was conducted in the absence of any commercial or financial relationships that could be construed as a potential conflict of interest.

frontiers | Frontiers in Immunology

SYSTEMATIC REVIEW
published: 10 June 2022
doi: 10.3389/fimmu.2022.874064

Aberrant IL-17 Levels in Rodent Models of Autism Spectrum Disorder: A Systematic Review

Alexandra Jade Thawley[1], *Luciana Peixoto Veneziani*[1,2,3,4], *Francisco Diego Rabelo-da-Ponte*[1,5], *Ingo Riederer*[1,2,3,4], *Daniella Areas Mendes-da-Cruz*[1,2,3,4*] *and Victorio Bambini-Junior*[1,3,6*]

[1] School of Pharmacy and Biomedical Sciences, University of Central Lancashire, Preston, United Kingdom, [2] Laboratory on Thymus Research, Oswaldo Cruz Foundation, Oswaldo Cruz Institute, Rio de Janeiro, Brazil, [3] National Institute of Science and Technology on Neuroimmunomodulation (INCT-NIM), Oswaldo Cruz Institute, Oswaldo Cruz Foundation, Rio de Janeiro, Brazil, [4] Rio de Janeiro Research Network on Neuroinflammation (RENEURIN), Oswaldo Cruz Institute, Oswaldo Cruz Foundation, Rio de Janeiro, Brazil, [5] Laboratory of Molecular Psychiatry, Centro de Pesquisa Experimental (CPE) and Centro de Pesquisa Clínica (CPC), Hospital de Clínicas de Porto Alegre (HCPA), Porto Alegre (RS), Brazil, [6] Division of Biomedical and Life Sciences, Faculty of Health and Medicine, Lancaster University, Lancaster, United Kingdom

OPEN ACCESS

Edited by:
Juehua Yu,
The First Affiliated Hospital of Kunming Medical University, China

Reviewed by:
Hongjin Wu,
Harbin Institute of Technology, China
Marcela Davoli-Ferreira,
University of Calgary, Canada

***Correspondence:**
Daniella Areas Mendes-da-Cruz
daniella@ioc.fiocruz.br
Victorio Bambini-Junior
v.bambini@lancaster.ac.uk

Specialty section:
This article was submitted to Multiple Sclerosis and Neuroimmunology, a section of the journal Frontiers in Immunology

Received: *11 February 2022*
Accepted: *04 May 2022*
Published: *10 June 2022*

Citation:
Thawley AJ, Veneziani LP, Rabelo-da-Ponte FD, Riederer I, Mendes-da-Cruz DA and Bambini-Junior V (2022) Aberrant IL-17 Levels in Rodent Models of Autism Spectrum Disorder: A Systematic Review. Front. Immunol. 13:874064. doi: 10.3389/fimmu.2022.874064

Autism spectrum disorder (ASD) is a heterogeneous neurodevelopmental disorder characterised by stereotyped behaviours, specific interests, and impaired communication skills. Elevated levels of pro-inflammatory cytokines, such as interleukin-17A (IL-17A or IL-17), have been implicated as part of immune alterations that may contribute to this outcome. In this context, rodent models have helped elucidate the role of T-cell activation and IL-17 secretion in the pathogenesis of ASD. Regarding the preclinical findings, the data available is contradictory in offspring but not in the pregnant dams, pointing to IL-17 as one of the main drivers of altered behaviour in some models ASD, whilst there are no alterations described in IL-17 levels in others. To address this gap in the literature, a systematic review of altered IL-17 levels in rodent models of ASD was conducted. In total, 28 studies that explored IL-17 levels were included and observed that this cytokine was generally increased among the different models of ASD. The data compiled in this review can help the choice of animal models to study the role of cytokines in the development of ASD, seeking a parallel with immune alterations observed in individuals with this condition.

Systematic Review Registration: PROSPERO, identifier CRD42022306558.

Keywords: IL-17, autism spectrum disorder, animal model, systematic review, inflammation

INTRODUCTION

Autism spectrum disorder (ASD) is a complex, heterogeneous neurodevelopmental disorder characterised by restricted patterns of repetitive behaviour, activities, interests and impairments in social skills and communication (1). In Europe, the prevalence was 0.38% in children aged 4 years and 1.55% in children aged 8 years, while in the USA, the prevalence ranged between 1.70% and 1.85%, respectively (2). ASD is also etiologically heterogeneous, and its precise mechanism remains

undefined. However, studies have suggested that it results from a combination of immunological, environmental, and genetic factors which can affect brain development and synaptic plasticity (3).

There are currently no biomarkers identified for ASD as its diagnosis is mainly based on clinical assessments (4). However, increasing evidence suggests that an aberrant immune phenotype may be linked to the development of ASD (5). Elevated levels of inflammatory cytokines, such as IL-6, TNF-α, IFN-γ, IL-1β, and IL-12, have been detected in several tissues of individuals with ASD, such as serum, plasma, and brain (6, 7). Elevations in these cytokine levels have been associated with increased stereotypical behaviours, increased aberrant behavioural scores, increased impaired neurodevelopment, and a regressive form of ASD (8, 9). Further studies have also observed increased concentrations of pro-inflammatory cytokines in the amniotic fluid of mothers whose children developed ASD, supporting the role of increased immune activity in ASD development (10, 11).

Another pro-inflammatory cytokine implicated in ASD is IL-17 (12). IL-17 comprises a family of six structurally related cytokines that includes IL-17A (commonly referred to as IL-17), IL-17B, IL-17C, IL-17D, IL-17E, and IL-17F (12). Although IL-17 is well known for its role in pathogenic responses, physiological effects of IL-17 include maintenance of mucosal integrity (13).

Elevated levels of IL-17 have been described in the serum of children with ASD (14), and enrichment in IL-17 genes was reported in individuals with ASD, indicating a possible role for this cytokine in the pathophysiology of this condition (15). Data suggesting the involvement of IL-17 in the development of ASD is also supported by findings in preclinical models of maternal immune activation (MIA) that linked the upregulation of IL-17 during pregnancy to the development of ASD-like behaviours (16).

Animal models have provided ground-breaking data in investigating the relationship between features related to ASD and altered IL-17 levels. It has been demonstrated that inducible models such as MIA by injection of polyinosinic:polycytidylic acid (poly(I:C)) or lipopolysaccharide (LPS), displayed elevated levels of IL-17 in maternal serum followed by upregulation of IL17Ra in foetal brains (16, 17). However, IL-17 levels in foetal, postnatal, and adult offspring of inducible or genetic models of ASD display conflicting data (18–20).

Therefore, a systematic review of data reporting altered IL-17 levels in rodent models of ASD was conducted. We aimed to answer the following questions (1): Are there IL-17 aberrations across rodent models of ASD? (2); If there are IL-17 aberrations across models, what is the magnitude of the difference? (3); Do these IL-17 aberrations differ across the age of rodent models?

METHODS

Study Selection

Seven electronic databases were utilised for this systematic review: Web of Science, PubMed, BMC, Scopus, SciELO, Proquest Dissertations and Theses — Global, and British Library EthOS. SciELO (South America) was included to address English language bias. The search terms used and the number of records found in each electronic database can be seen in the Supplementary Material (see **Supplementary Table 1**).

We included records containing mouse or rat models of ASD that fitted our inclusion criteria, presenting ASD-like phenotypes and IL-17 analysis. We included all records regardless of the sex or age of the animals. Furthermore, we added all records published between January 1st, 2000, and January 1st, 2022.

We excluded studies that did not analyse IL-17 levels and were not original research studies. Additionally, review articles, posters, and abstracts from conferences, case studies, and retracted articles were excluded.

Data Extraction, Synthesis, and Quality Assessment

Three reviewers (AJT, LPV, and FDRP) independently screened abstracts, assessed full-text articles, extracted data, and evaluated the risk of bias. Disagreements and inconsistencies were resolved by the consensus of all review group members. The study search strategy is outlined by the Preferred Reporting Items for Systematic Reviews and Meta-Analyses (PRISMA) guidelines. The study is registered on PROSPERO (CRD42022306558).

Data extracted included the type of mouse or rat model, IL-17 alterations, intervention characteristics (i.e. dosing regimen for MIA models), the age, and sex of the animals. Studies were assessed using the CAMARADES' study quality checklist criteria adapted as follows (21): peer-reviewed publication; random allocation to treatment or control; appropriate animal model (MIA, chemically induced, inbred strain); sex-matched animals; age-matched animals; sample size calculation; compliance with animal welfare regulations; and statement of potential conflict of interests. Each study was given a quality score out of eight points. These criteria were chosen to identify the overall methodological quality of those records.

Furthermore, by amending the quality checklist to include age and sex match animals, this review seeks to ensure that appropriate comparisons between control and treatment groups were made. It is possible that cytokine aberrations in ASD models significantly differ across age and sex and ensuring that animals were age and sex-matched may reduce this bias (**Table 1**).

One reviewer (AJT) assessed the risk of bias and included records using the Systematic Review Centre for Laboratory Animal Experimentation (SYRCLE) (46). This risk of bias tool assessed methodological quality using animal study-specific criteria and was adapted (46) from the Cochrane Risk of Bias tool. For each included study, the parameters for each type of bias were marked as Yes (Y), No (N), or Unclear (U). A final score out of 10 was given to each study (**Table 2**).

RESULTS

Study Selection

A total of 643 records were obtained from the database search (see **Supplementary Table 1**). Following duplicate removal, we

TABLE 1 | Bias assessment and study quality using animal data from experimental studies (CAMARADES) checklist items.

Author	Peer-reviewed publication	Random allocation	Animal model	Sex-matched animals	Age-matched animals	Sample size calculation	Compliance with animal welfare regulations	Statement of conflict of interests	Total
Ozaki et al, 2020 (22)	X		X		X		X	X	5
Arrode-Brusés and Brusés, 2012 (23)	X		X	X	X		X	X	6
Schwartzer et al, 2013 (24)	X		X	X	X		X	X	6
Pendyala et al, 2017 (25)	X		X		X		X	X	5
Xu et al., 2017 (26)	X	X	X		X		X	X	6
Reed et al., 2020 (19)	X	X	X	X			X	X	6
Choi et al., 2016 (16)	X		X				X	X	4
Ahmad et al, 2018 (27)	X		X	X	X		X	X	6
Nadeem et al, 2019 (28)	X		X	X	X		X	X	6
Lammert et al, 2018 (29)	X	X	X	X	X		X	X	7
Yasumatsu et al, 2020 (17)	X		X		X		X		4
Bakheet et al, 2017 (30)	X		X				X	X	4
Ansari et al, 2017 (31)	X		X	X	X		X	X	6
Hsiao et al, 2012 (32)	X		X		X		X	X	5
Zhang et al, 2013 (20)	X		X	X			X	X	5
Luan et al, 2015 (33)	X	X	X	X	X		X		6
Chen et al, 2019 (34)	X		X	X			X	X	5
Gumusoglu et al., 2020 (35)	X			X	X		X	X	5
Afroz et al., 2021 (36)	X	X	X	X	X		X	X	6
Alhosani et al., 2021 (37)	X		X		X		X	X	5
Heo et al., 2011 (38)	X		X	X	X		X	X	5
Jaini et al., 2021 (39)	X		X		X		X	X	5
Kalish et al., 2021 (40)	X		X	X	X		X	X	6
Schwartzer et al., 2017 (41)	X	X			X		X	X	5
Senkal et al., 2021 (42)	X	X		X	X		X	X	6
Shin et al., 2021 (43)	X		X		X		X	X	5
Shimizu et al., 2021 (44)	X		X		X		X	X	5
Kim et al., 2022 (45)	X	X	X	X	X		X	X	7

screened 630 records, and 28 studies met inclusion criteria (**Figure 1**). All these articles were considered appropriate and were included in this review. Among them, two articles - Chen et al., 2019 and Ozaki et al. (22, 34) - were added using a snowballing technique as they fitted the inclusion criteria but did not show up in the total searches and one article - Kim et al. (45) - was included as it met the inclusion criteria and was published in January, 11 2022. A total of 28 papers were analysed in this review.

Only two studies using rat models matched the criteria for this review (26, 42). Many of the studies generated by the database searches focused on mouse models of ASD. This indicates a data gap and raises the question of if mouse models have better mechanical viability when modelling immune aberrations of ASD compared to rat models; however, this may also be due to the broader availability of mouse cytokine evaluation kits and the prevalence of mouse models in immunology.

Quality Assessment

According to CAMARADES' quality scale, the 28 records included articles had a mean score of 5.42 ± 0.77 (mean ± standard deviation) out of a possible 8 (**Table 1**). All papers were published in peer-reviewed journals, and most used models of ASD. Most records used age and sex-matched animals. However, some articles were unclear on whether female rodents were included. This may affect the results obtained since sex-biased alterations of IL-17 in rodent models of ASD is unknown. Furthermore, none of the articles showed the sample size calculations, further affecting the results. Also, the allotment of treatment groups, the use of different litters, and the number of pups per litter were not mentioned. Nevertheless, all articles complied with animal welfare regulations, and many articles included disclosure of potential conflicts of interest.

The assessment of the risk of bias can be seen in **Table 2**. The mean SYRCLE score among all included records was 3.82 ± 1.41. Of the 28 studies included, no papers randomly housed the animals within the animal unit. Most of the records did not blind investigators, and similarly, only 9 papers utilised blinded outcome assessors. In addition, many of the studies did not appropriately generate and apply a sequence generation to the animals used. One study completed a random outcome assessment (26). Similarly, only 8 studies addressed incomplete data.

Furthermore, only 1 of the studies included in this review, Reed et al. (19), concealed the allocation of control and treatment groups (19). All papers had no other apparent sources of bias when reviewed with the SYRCLE guidelines. All studies also established the baseline characteristic of control IL-17 levels compared with ASD rodent models.

Qualitative Synthesis

Altered IL-17 in MIA Models

A total of 16 studies identified from the database search utilised MIA models of ASD, and all of them described alterations in

TABLE 2 | Systematic Review Centre for Laboratory animal Experimentation (SYRCLE) scale for risk of bias.

Author	Sequence generation	Baseline characteristics	Allocation concealment	Random Housing	Blinding (Investigators)	Random (outcome assessment)	Blinding (outcome assessors)	Incomplete outcome data addressed	No selective outcome reporting	No other source of bias	Total Score
Ozaki et al, 2020 (22)	N	Y	U	N	N	U	N	U	Y	Y	3
Arrode-Brusés and Brusés, 2012 (23)	N	Y	N	N	N	N	U	Y	Y	Y	4
Schwartzer et al, 2013 (24)	N	Y	N	N	U	U	U	Y	Y	Y	4
Pendyala et al, 2017 (25)	N	Y	N	N	U	N	U	Y	Y	Y	4
Xu et al., 2017 (26)	Y	Y	N	N	U	Y	Y	Y	Y	Y	7
Reed et al., 2020 (19)	Y	Y	Y	U	Y	U	Y	Y	Y	Y	8
Choi et al., 2016 (16)	N	Y	N	N	U	U	N	U	Y	Y	3
Ahmad et al, 2018 (27)	N	Y	N	N	N	U	N	N	U	Y	2
Lammert et al, 2018 (29)	Y	Y	U	U	Y	U	U	U	Y	Y	5
Yasumatsu et al, 2020 (17)	N	Y	N	N	N	N	N	U	Y	Y	3
Bakheet et al, 2017 (30)	N	Y	N	N	N	U	N	N	U	Y	2
Ansari et al, 2017 (31)	N	Y	N	N	N	N	N	Y	U	Y	3
Hsiao et al, 2012 (32)	N	Y	N	N	N	N	Y	U	Y	Y	4
Zhang et al, 2013 (20)	N	Y	N	N	N	N	N	U	U	Y	2
Luan et al, 2015 (33)	Y	Y	N	U	N	N	N	U	Y	Y	4
Chen et al, 2019 (34)	N	Y	N	N	N	N	N	Y	Y	Y	4
Nadeem et al., 2019 (28)	N	Y	N	N	U	U	Y	U	U	Y	3
Gumusoglu et al., 2020 (35)	N	Y	N	N	Y	U	U	Y	Y	Y	5
Afroz et al., 2021 (36)	N	Y	N	N	N	N	Y	U	Y	Y	4
Alhosani et al., 2021 (37)	N	Y	N	N	N	N	N	U	U	Y	2
Heo et al., 2011 (38)	N	Y	N	N	N	N	N	U	N	Y	3
Jaini et al., 2021 (39)	N	Y	N	N	Y	U	Y	U	Y	Y	5
Kalish et al., 2021 (40)	N	Y	N	N	N	U	N	U	Y	Y	3
Schwartzer et al., 2017 (41)	N	Y	N	N	Y	N	N	N	Y	Y	4
Senkal et al., 2021 (42)	N	Y	N	N	Y	U	Y	U	Y	Y	5
Shin et al., 2021 (43)	N	Y	N	N	N	N	N	U	U	Y	2
Shimizu et al., 2021 (44)	N	Y	N	N	Y	N	Y	U	Y	Y	5
Kim et al., 2022 (45)	N	Y	N	N	Y	N	N	U	Y	Y	4

Y (Yes) = 1 score; N (No) = 0 score; U (Unclear) = 0.

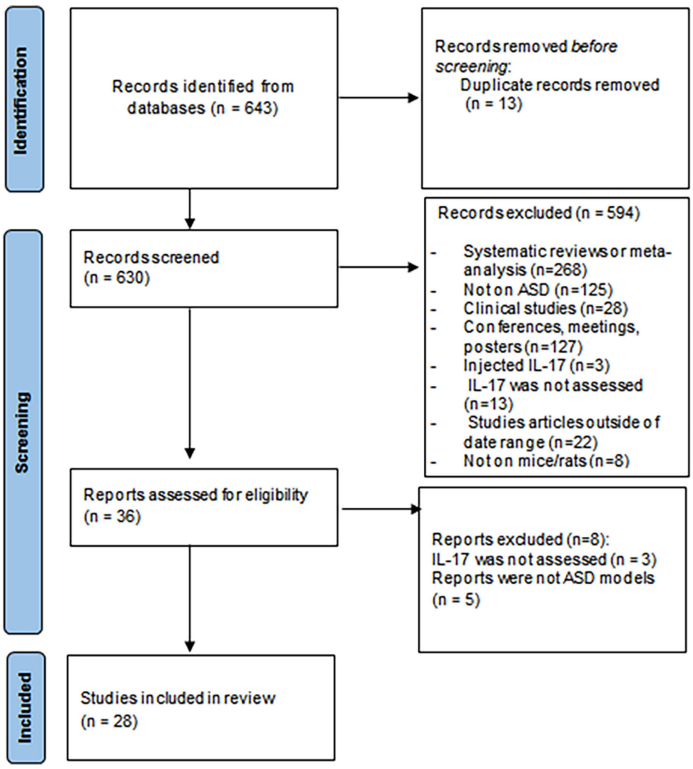

FIGURE 1 | Preferred Reporting Items for Systematic Reviews and Meta-Analyses (PRISMA) flowchart.

IL-17 levels (16, 17, 19, 22–26, 29, 32, 33, 35, 41, 42, 44) (**Table 3**). Most of the papers used one of two different protocols of inducing MIA, either utilising an intraperitoneal (i.p.) injection of 20 mg/kg of poly(I:C), or an injection of 0.05 mg/kg of LPS, at embryonic day (E) 12.5. One study used a subcutaneous osmotic pump releasing IL-17 at a rate of 0.025 mg/kg per hour to simulate chronic inflammation (35). A further study induced the MIA model through sensitisation with 10μg of ovalbumin to mimic chronic maternal allergic asthma in C57BL/6 and FVB mice, which develop mild and a more severe asthma respectively (41). Out of the 15 studies, 13 reported increases in IL-17 levels, with one article reporting no alteration in IL-17 production compared to BTBR mice (a well-established model of ASD) (24) and a second report noting a significant decrease in IL-17 at postnatal day 30 (25). A further study found that IL-17 levels decreased at 48 hours post injection (44). IL-17 was assessed at different ages throughout the studies, from foetal to adult (15 weeks old) and in both offspring and dams. When comparing results for each age point, much of the data obtained for each age was similar. There was also a variety of tissues used, the most frequent being offspring serum, brain, kidney, spleen, maternal serum, placenta, and uterus. One study examined IL-17 secretion in lymphocytes from the lamina propria derived from colon tissue (45). Many of the papers that used the same tissue types for the analysis reported similar IL-17 alterations. The studies utilised a variety of techniques, including ELISA, flow cytometry, cytometric bead array, and real-time PCR to assess and infer IL-17 levels.

Altered IL-17 in Chemically Induced Models

One study investigated if exposure to teratogens during pregnancy could induce similar alterations to the well-established model of maternal activation poly(I:C) (34). In this case, pregnant C57BL/6 mice were exposed to the polybrominated diphenyl ether (PBDE) 209 and lead (Pb), common pollutants that co-exist in the environment. The study suggested that the perinatal exposure to the mixture of PBDE209 and Pb elicited restricted, repetitive patterns of behaviour and affected learning in male offspring, and IL-17 levels were increased in the serum of mice at postnatal day 30 (34). However, social behaviour was not impaired after chemical exposure, differently from the observed in the poly(I:C) model (34). This suggests that although not all behavioural alterations typically associated with animal models of ASD were induced by these teratogens, neurobehavioral alterations were still present and therefore presenting relevant validities as a model. A further study found that neonatal and P1 pups from dams treated with valproic acid to induce chronic immune response had significantly higher IL-17A in both the skin and brain. These IL-17A increases were also correlated to ASD-like features, as examined through the Morris Water Maze (43).

TABLE 3 | Qualitative synthesis of studies included.

Author	Species	Strain	Sex	Sample size	Rodent ASD model	Dose (mg/kg)	Inducement	Route	Treatment age	Testing age	Tissue used	Technique used	IL-17 alteration	Statistically significant
Ozaki, 2020 (22)	mice	C57BL/6N	male	4	MIA	10	Poly(I:C)	i.p	E12, E15	foetal, E12, E15, P10	microglia, liver, placenta, brain, serum	RT-PCR,	increase	No
Arrode-Brusés, 2012 (23)	mice	C57BL/6N	both	NS	MIA	20	Poly(I:C)	i.p	GD16, PND4	P4, foetal	maternal serum, offspring brains	Milliplex Map	increase	Yes
Schwartzer, 2013 (24)	mice	C57BL/6N /BTBR	both	12 to 18	MIA/BTBR	20	Poly(I:C)	i.p	E12.5	11 weeks	spleen	murine multiplexing bead immunoassays	increase	Yes
Pendyala, 2017 (25)	mice	(Pcp2-EGFP) BT153Gsat/ Mmmh	both	P1,P7= 4; P14, P30 =6	MIA	20	Poly(I:C)	i.p	E12.5	P1, P7, P14, P30	cerebellar lysates	multiplex ELISA, QAM-CYT-5	decrease at P30	Yes
Xu, 2017 (26)	rats	Wistar	both	10	MIA	0,05	LPS	i.p	E12.5	1 month	serum	ELISA	increase	No
Reed, 2020 (19)	mice	C57BL/6N	male	4 to 8	MIA	20	Poly(I:C)	i.p	E12.5	E12.5	serum	ELISA	Increase after immune stimuli	Yes
Choi, 2016 (16)	mice	C57BL/6N	male	NS	MIA	20	Poly(I:C)	i.p	E12.5	E14.5	placenta, decidua, maternal serum	ELISA, RT-PCR, Flow cytometry	increase	Yes
Ahmad, 2018 (27)	mice	n/a	male	NS	BTBR	n/a	n/a	n/a	n/a	7-9 weeks	spleen, brain	Flow cytometry, western blotting, RT-PCR	increase	Yes
Nadeem, 2019 (28)	mice	n/a	male	NS	BTBR	n/a	n/a	n/a	n/a	8-10 weeks	Splenocytes, CD4+ cells, cerebellum	Flow cytometry, RT-PCR	increase	Yes
Lammert, 2018 (29)	mice	C57BL/6N	both	NS	MIA	20	Poly(I:C)	i.p.	E11.5, E12.5	E14.5	maternal serum	ELISA, Cytokine blockade	increase	Yes
Yasumatsu, 2020 (17)	mice	C57BL/6N	male	NS	MIA	0.05	LPS	i.p	E14	foetal, mother	maternal uterus, brain	ELISA, qRT-PCR, Flow cytometry	increase	Yes
Bakheet, 2017 (30)	mice	n/a	male	NS	BTBR	n/a	n/a	n/a	n/a	6-8 week	spleen, brain, CD4 t cells	Flow cytometry, RT-PCR, intracellular staining	increase	Yes
Ansari, 2017 (31)	mice	n/a	male	6	BTBR	n/a	n/a	n/a	n/a	6-8 week	spleen, brain	Flow cytometry, western blotting, RT-PCR	increase	Yes
Hsiao, 2012 (32)	mice	C57BL/6N	both	NS	MIA	20	Poly(I:C)	ip	E12.5	15 weeks	CD4+ T cells	ELISA	increase	Yes
Zhang, 2013 (20)	mice	BTBR/ C57BL/6	both	NS	BTBR	n/a	n/a	n/a	n/a	2-3 months	Splenic TCD4	Flow cytometry	increase	Unclear
Luan, 2015 (33)	mice	B6	both	NS	MIA	0,05	LPS	i.p	E12.5	dam, 8-12-week offspring	CD4 T cells from liver and, spleen	Intracellular cytokine staining	increase	Yes
Chen, 2019 (34)	mice	C57BL/6N	male	5	Chemical and MIA	0.25 µl/hr 20	BDE209, Pb, BDE209/Pb poly (I:C)	subcutaneous osmotic pump i.p	E9.5 E12.5	P 30	serum	Cytometric bead array	increase	Yes
Gumusoglu, 2020 (35)	mice	C57BL/6N	both	8	MIA	25	IL-17	subcutaneous osmotic pump	chronic (hourly)	E18	kidney, placenta, brains	ELISA	increase	No
Afroz, 2021 (36)	mice	C57Bl6	Female	8 -9 per group	Parental High salt diet (HSD)	chow supplemented with 0.1% NaCl	8 weeks HSD	Oral	3-4 weeks		Maternal serum	Flow Cytometry	No	No
Alhosaini, 2021 (37)	mice	C57 /BTBR	Male	6 per group	BTBR	n/a	n/a	n/a	n/a	10-12 week	Splenocytes, Brain Tissue	Flow Cytometry, RT-qPCR, Western Blotting	Increase in BTBR	Yes
Heo, 2011 (38)	mice	C57BL/6 / BTBR/ BCF1/CBF1	both	3 - 5 per group	BTBR/ BCF1/CBF1	N/A	N/A	N/A	N/A	PND 21 and 70	Liver	ND	Increase	Yes ** data not shown
Jaini, 2021 (39)	mice	PtenWT/ m3m4 and PtenWT/WT	Female	5 per group	PtenWT/m3m4 and PtenWT/ WT	N/A	N/A	N/A	N/A	Pregnant dams at E17.5	Maternal Spleen/Serum	qRT-PCR, ELISA	No	n/a
Kim, 2022 (45)	mice	C57Bl6	both	12 - 18 (Variable)	MIA	20 mg/kg	poly(I:C)	i.p.	E12.5	8-10 weeks	Offspring Serum, colonic lymphocytes	Flow cytometry	Increase after immune challenge	yes
Sekal, 2021 (42)	Rat	Sprague Dawley	both	10 per group	Neurodevelopment disorder induced by hyperosmotic consumption by mothers	5 mL/kg	21 days	Oral Gavage	n/a	PND 50	offspring brain homogenates	Elisa	Increase	yes
Schwartzer 2017 (41)	mice	C57 and FVB/Ant	Female	12-17	OVA-induced MIA	1% (wt/vl)	aerosolised solution of 1% (wt/vl) OVA in PBS	aerosolised	Gestational days 9.5, 12.5, and 17.5	On gestational day 17.5	Maternal serum	Flow cytometry	Increase in C57 pregnant dams exposed to OVA	yes

(Continued)

TABLE 3 | Continued

Author	Species	Strain	Sex	Sample size	Rodent ASD model	Dose (mg/kg)	Inducement	Route	Treatment age	Testing age	Tissue used	Technique used	IL-17 alteration	Statistically significant
Shimizu, 2021 (44)	mice	C57BL/6J	both	8-9 per group	MIA	20 mg/kg during pregnancy and 20 mg/kg or 4 mg/kg postnatally	poly(I:C)	i.p.	E12.5, 15.5 and 16.5. Pups also received poly(I:C) injections at 3-4 weeks old	3-4 weeks	Offspring serum	ELISA	Increase in MIA-offspring and MIA-offspring that received postnatal injections of poly(I:C)	yes
Shin, 2021 (43)	mice	BALB/c hairless mice	both	9 - 13	VPA	600 mg/kg	VPA	i.p.	E12.5	PND 1, 4, 12 and 21	Offspring blood, skin and brain	ELISA	Increase on the skin on PND1, 4 and 21 and brain in PND1	yes
Kalish, 2021 (40)	mice	C57BL/6	both	8	MIA	20 mg/kg	Poly(I:C)	i.p.	E12.5	E14.5 and 18.5	Foetal cortex	No measurement of IL-17	IL-17 blockage led to the suppression of integrated stress responses in males	yes** alterations are dependent on IL-17

***Observation.*

Altered IL-17 in Inbred Models

A total of 8 studies utilised inbred rodent models of ASD, and 6 of them found alterations in IL-17 concentrations (20, 24, 27, 28, 30, 31). All papers used the BTBR mice, with five of the eight papers only using males. However, some studies used a smaller age range of mice than the papers that used the MIA models, with a range of 6-13 weeks. Out of the eight studies that observed IL-17 aberrations, all found a significant increase in IL-17 intracellular levels and mRNA expression (**Table 3**). One paper found a significant increase in IL-17A intracellular staining in T CD4+ cells from the spleen, as well as increase in IL-17A mRNA expression and protein expression in brain tissue when compared to C57BL/6 mice (37).

A 2011 study by Heo et al. found that 3 days following infection with Keyhole limpet haemocyanin (KLH) and *Listeria monocytogenes*, BTBR mice had significantly increased levels of IL-17 in the liver when compared to C57BL/6 mice. However, the data regarding IL-17 alterations found in this study is not shown, making it difficult to fully understand and evaluate the immune alterations related to IL-17 (38).

Interestingly, BTBR mice, which present higher basal levels of IL-17 when compared to controls, were described to increase these levels even further when exposed to perinatal poly(I:C), suggesting that BTBR mice may have a dysregulated cytokine response that could impact the ASD-like behavioural alterations (24).

All 8 studies utilised similar tissues including the spleen and brain, mostly focusing on investigating intracellular levels of IL-17 in splenocytes from BTBR mice, as well as IL-17 expression in brain tissue. Techniques varied from ELISA assays, flow cytometry, Western blotting, and real-time PCR to assess IL-17 concentrations.

Altered IL-17 in Genetic Models

A total of 2 studies utilised genetically modified rodent model of ASD (19, 39). Reed et al. (19) utilised mice models in which the animals harbour mutations in genes related to an increased chance of ASD, including contactin-associated protein-like 2 (Cntnap2), fragile X mental retardation-1 (Fmr1), and multiple ankyrin repeat domains 3 (Shank3) genes, for comparison with environmental ASD model such as MIA. This paper showed that inflammatory response caused by LPS injection on offspring born to mothers injected with poly(I:C) at embryonic day (E)12.5 (MIA-offspring) rescued social behaviour deficits, and that this LPS-induced rescue is dependent on IL-17A. However, this same result was not observed in the monogenic models of ASD, suggesting that differences in cytokine production across models are instrumental to the behavioural rescue observed. This hypothesis was further supported since after LPS injection both (a) the monogenic mice did not display an increase in plasmatic IL-17A and (b) IL-17A blockage in the MIA-offspring mice prevented the sociability rescue (19).

Jaini et al. (39) utilised $Pten^{WT/m3m4}$ mouse dams to breed 2 offspring genotypes, $Pten^{WT/m3m4}$ and $Pten^{WT/WT}$, which were then bred to produce offspring. PTEN mutations are associated with ASD, accounting for 2% of all ASD and 17% of macrocephalic-ASD cases (39). Inflammatory markers, cellular

phenotypes and gene expression were examined in the dams and offspring *via* multiplex ELISA, multiplex bead-based cytokine assays and gene expression panel analysis on E17.5. This paper found no IL-17A transcripts in the spleen from either mouse genotype used in this study and no differences in IL-17A in the serum were found (39).

Altered IL-17 in High Salt Diet Model

A total of 2 papers used a model in which animals were fed diets that included parental high salt consumption in an attempt to induce the development of ASD-like characteristics in the offspring. Afroz et al. (2021) used 8% NaCl in chow and an additional 1% NaCl in drinking water for male and female C57BL/6 mice for 8 weeks, after this period of time animals were used for breeding (36). IL-17A was detected on maternal serum without any alterations as compared to controls using flow cytometry-based assay (36). Another study exposed pregnant Sprague-Dawley rats to three different hypertonic solutions, including 3% NaCl, mineral water (3% NaHCO3 +magnesium+calcium content) and Ayran (0.8% NaCl content) (42). Pregnant rats were exposed to hypertonic solutions throughout the pregnancy (21 days) *via* oral gavage at a dose of 5 mL/kg with dosing repeated up to 3 times within 24 h period (42). IL-17A increase was detected in the brain homogenate from male offspring of hypertonic solution fed-rats *via* ELISA kit (42).

DISCUSSION

To our knowledge, this is the first systematic review assessing IL-17 levels in rodent models of ASD. Our findings show that IL-17 levels are increased in different tissues and in the serum of ASD rodent models, as reported by 23 out of 28 studies included in this review. Also, increased IL-17 levels could be observed in pregnant mice, embryos, and offspring, highlighting the possible role of this cytokine during neurodevelopment, pathogenesis and pathophysiology of ASD, as well as in behavioural alterations.

This review has also highlighted the potential role of IL-17 in the establishment of ASD-like behaviours across rodent models with a specific focus on offspring and maternal IL-17 levels. The studies examined in this review have demonstrated the role of the maternal immune state and the increase in IL-17 production in the development of ASD-like features. Several papers stressed the importance of the maternal immune state and how it relates to microbiota (29, 45), genetics (39), and nutrition (36).

Several papers have suggested the important role of homeostatic maternal immune state is and the development of ASD (11, 16, 22). Whereas other studies found increased pro-inflammatory cytokine levels in the amniotic fluid of mothers whose children develop ASD, including IL-6, a cytokine necessary for the differentiation of Th17 cells (10, 47).

As previously discussed in this review, much of the increased IL-17 production appeared to be derived from Th17 cells (27, 28, 30, 31). However, another possible producer of IL-17 in ASD models seems to be γδ T cells. Increased concentrations of IL-17 producing γδ T cells were observed in the uterus of pregnant mice after MIA (17). Previous data have shown that residential IL-17 producing γδ T cells in the meninges of the brain can control anxiety-like behaviour in mice *via* IL-17 receptor A signalling (18, 48). Other studies found that increased meningeal γδ T cells reduce synaptic density *via* IL-17 pathways (48). Taken together, these findings suggest that whilst the increase of uterine γδ T cells may induce a systemic increase of IL-17 in pregnant mice, the increase may cause a localised inflammatory response in the brain of their offspring, which may affect synaptic density (48). However, uterine γδ T cells may not be the only source of upregulated IL-17. Kim et al. (49) have demonstrated that T cells isolated from gut connective tissue of poly(I:C) treated mice expressed increased levels of IL-17A when compared to tissue from PBS treated mice (49). This study offers insightful data relating to the role of the gut in ASD mouse models. This study, however, did not match the inclusion criteria and was not included in the present systematic review.

In the gut, another factor potentially playing a role in the development of ASD-like features is maternal microbiota. Lammert et al. (29) found that C57BL/6 mice from Taconic Biosciences (Tac) displayed higher levels of IL-17A after poly (I:C) injections when compared to C57BL/6 Jackson Laboratory's (JAX) mice. They also presented a high relative abundance of segmented filamentous bacteria (SFB), known to promote IL-17A inflammatory response (29). Offspring from poly(I:C) treated Tac mice displayed ASD-like behavioural alterations. However, those alterations were not observed in saline controls or in the offspring of JAX mice. Additionally, experiments of co-housing were able to induce behavioural alterations in JAX mice offspring and led to an increase in IL-17A in maternal serum after poly(I:C) injection, further relating the role of the gut microbiota in the production and regulation of IL-17 and Th17 cells (49). Those findings are also supported by Choi et al. (16), who demonstrated that upregulation of IL-17A after poly(I:C) led to abnormal cortical development in the offspring as well as ASD-like altered behaviour (16). Those alterations were reversed after pre-treatment with IL-17A blocking antibodies, reinforcing the hypothesis that altered maternal IL-17A response plays an important role in the development of ASD in the offspring (16). Furthermore, data from Kim et al. (2022) (45) have demonstrated that MIA immune alterations observed in the offspring may happen postnatally, as crossfostering pups from PBS-treated mothers with MIA mothers led to an increase in the percentage of colonic IL-17A and IFN- γ -producing Th17 cells in the pups after infection (37). This immune priming seems to be related to the maternal microbiota as experiments with stool transfer have demonstrated that offspring from animals that received stool transfer from MIA-mothers displayed pro-inflammatory immune phenotype after immune challenge (45).

Clinical evidence also supports that microbiota plays a role in the pathogenesis and development of ASD. It has been demonstrated that children with ASD displayed a decrease in anti-inflammatory *Faecalibacterium* bacteria and an increase in the pathogenic inflammatory *Enterobacteriaceae* and *Sutterellaceae* bacteria in the faecal microbiome (50). A further

study found that an oral administration of the endogenous human micro-organism, *B. fragilis*, improved the behavioural ASD-like features in mouse models as well as metabolite modulation in the gut (51).

In line with alterations induced by maternal microbiota, data resulting from altered diet and the development of ASD-like features in the offspring has also been debated (36, 42). Previous reports have demonstrated that excess dietary salt leads to cognitive impairment, increased Th17 differentiation in the intestine and IL-17 plasmatic levels in mice (52). This impairment is dependent on lymphocytes, as it was not observed in mice lacking IL-17 or Rag1$^{-/-}$ mice (52). However, Afroz et al. (2021) have demonstrated that a high salt diet (HSD) did not induce any behavioural or immune alteration in HSD-fed mice. Furthermore, behaviour alterations were present in the offspring of HSD-fed mice, including altered social behaviour and increased repetitive behaviours (36, 52). In another paper analysed in this review, Senkal et al. (2021) (42) have demonstrated that male offspring rats from animals exposed to hypertonic solutions during pregnancy displayed a pro-inflammatory immune profile in brain tissue with increased IL-17 as well as ASD-like behaviours, reinforcing the hypothesis that maternal state in regards to diet and microbiota may play a role in the development of ASD-like characteristics in the offspring (42).

The kinetics of induction of MIA may play a pivotal role in the development and severity of ASD-like features in rodent models, with alteration of IL-17 levels being associated with specific points of synaptogenesis (25). Synaptic genes were also enriched in the brains of the offspring (35), suggesting a link between the MIA induction time point, maternal and foetal IL-17 levels, and synaptic development, which may induce autistic-like behaviour and affect the immune phenotype (53, 54). However, further studies are necessary to confirm the association between the aberrant IL-17 levels and unregulated synapses seen in ASD.

ASD has a strong genetic component, as demonstrated by high heritability amongst siblings (55). Another evidence for the genetic impact of ASD comes from single gene alterations linked with developmental disorders such as mutations in FMR1 (fragile X syndrome), MECP2 (Rett syndrome), TSC1/TSC2 (tuberous sclerosis complex), and CACNA1C (Timothy syndrome), as well as mutations in CNTNAP2 (cortical dysplasia–focal epilepsy syndrome) (55, 56). Animal models with single gene alterations allow for the understatement of how those mutations play a role in the development of the core characteristics of ASD, such as behavioural alterations (56). However, as it was described by Reed et al. (19), animal models for Cntnap2, Fmr1, and Shank3 did not display any IL-17 alteration after immune challenge with LPS as compared to the MIA-offspring model, indicating that immune alterations may be related to environmental factors or alteration in several genes (19). In this regard, Jaini et al. 2021 (39) hypothesised that maternal genetics may be an important modulator of neuro-immune alterations in the offspring and using the mice model for mutation in PTEN (Pten$^{WT/m3m4}$), which has also been associated with ASD, set to investigate the influence of maternal genetics on ASD development in offspring (39). However, no IL-17A transcription was detected on the spleen of pregnant mice, nor any difference in the cytokine was detected in serum (39). Nevertheless, the authors demonstrated that low IL-10 during pregnancy was directly correlated with decreased complement expression in the foetal liver and offspring from mutant mice also displayed altered social and repetitive behaviours without external immune insult (39).

Several limitations should be highlighted when describing our analyses. We were not able to perform a meta-analysis due to the high methodological heterogeneity among studies, including diverse outcomes, distinct species, experimental designs, and types of animal models. Most of the studies analysed in this systematic review used male mice or did not explicitly examine the differences between the sexes. Although this is understandable due to the increased prevalence of ASD in male individuals, excluding one sex can hinder the translational validity of the results (57, 58). The exclusion of female-specific results could potentially lead to a data gap regarding immune aberrations in females, which could affect research and potential future treatments.

Another aspect that could affect IL-17 levels is receptor desensitisation due to persistent stimulation (59). Further studies are necessary to examine how IL-17 receptors could be altered in rodent models of ASD and how their altered signalling can affect pathways dependent on IL-17, such as mRNA stabilisation *via* the ACT1 dependent pathway (60).

IL-17 production and the effects of IL-17 have been noted to change with age within the papers examined in this review. The study by Pendyala et al. showed that although IL-17 was altered at all stages of development, the aberration was only significant at postnatal day 30 when IL-17 was decreased (25). Equivalent results were found with IL-17 concentrations significantly up-regulated by MIA after poly(I:C) exposure at gestational day 17 followed by lower levels at postnatal day 5 in the study by Arrode-Brusés and Brusés (2012) (23). These results suggest that MIA primes offspring's immune system for a pro-inflammatory response following secondary exposure to poly(I:C), and IL-17 levels may be altered with age. However, this requires further exploration in both clinical and preclinical settings.

Additionally, the technique used to measure cytokine levels, which can changed between the studies, may play a role in the observed outcome. While some methods used in the papers, i.e. ELISA and flow cytometry, measure IL-17 protein levels, qRT-PCR measures IL-17 mRNA levels. Many of the studies that utilised qRT-PCR also included a technique to measure the IL-17 protein concentration, such as in a study where ELISA assays and flow cytometry were used to measure protein IL-17 and IL-17 producing cells alongside RT-PCR (16). One study confirmed the presence of elevated levels of IL-17 in BTBR mice by intracellular staining. However, they did not provide the data demonstrating such increase, mainly pointing out that even though there were elevated levels of IL-17, there was no differentiation into a Th17 profile (20). It is difficult to understand the full scope of IL-17 alterations in the model used in this work, as some data was not shown in the article; this absence of data also makes it difficult to incorporate the findings of this article in a meta-analyses.

In despite of that, the study was included in this systematic review as it met all inclusion criteria.

In summary, this systematic review identified common alterations in IL-17 across different models of ASD and almost the totality of the paper reported increases in the level of IL-17 or in IL-17 producing cells, across different detection techniques. The selection of the papers and parameters analysed may help the choice of animal models to study the role of IL-17 and other cytokines in the development of ASD and/or behavioural alterations. It is important to notice that, although the results were consistent, there is a need for further characterisation of the meaning of IL-17 increase, and its importance to the pathophysiology of ASD.

DATA AVAILABILITY STATEMENT

The original contributions presented in the study are included in the article/**Supplementary Material**. Further inquiries can be directed to the corresponding authors.

AUTHOR CONTRIBUTIONS

Conception and design of the work: AT, DM-d-C, VB-J, IR. Acquisition, analysis, and interpretation of data for the work: AT, LV, and FR-d-P. Drafting of the work: AT, LV, and FR-d-P. Revision: FR-d-P, DM-d-C, IR, VB-J. Final approval of the version to be published: DM-d-C, IR, VB-J. All authors contributed to the article and approved the submitted version.

FUNDING

This study was supported by the University of Central Lancashire, UK; the Oswaldo Cruz Foundation, the National Institute of Science and Technology on Neuroimmunomodulation (INCT-NIM, CNPq), the Rio de Janeiro Research Network on Neuroinflammation (RENEURIN - Faperj), Brazil; the MercoSur Fund for Structural Convergence (FOCEM); and the ERASMUS+ programme.

ACKNOWLEDGMENTS

The authors thank their institutions and funding agencies/programs, for providing the support needed for this work.

SUPPLEMENTARY MATERIAL

The Supplementary Material for this article can be found online at: https://www.frontiersin.org/articles/10.3389/fimmu.2022.874064/full#supplementary-material

REFERENCES

1. American Psychiatric Association. *Diagnostic and Statistical Manual of Mental Disorders (DSM-5®)*. 5th ed. Arlington, VA, American Psychiatric Pub (2013). 991 p.
2. Bougeard C, Picarel-Blanchot F, Schmid R, Campbell R, Buitelaar J. Prevalence of Autism Spectrum Disorder and Co-Morbidities in Children and Adolescents: A Systematic Literature Review. *Front Psychiatry* (2021) 12:744709. doi: 10.3389/fpsyt.2021.744709
3. Lyall K, Croen L, Daniels J, Fallin MD, Ladd-Acosta C, Lee BK, et al. The Changing Epidemiology of Autism Spectrum Disorders. *Annu Rev Public Health* (2017) 38:81–102. doi: 10.1146/annurev-publhealth-031816-044318
4. Masi A, Glozier N, Dale R, Guastella AJ. The Immune System, Cytokines, and Biomarkers in Autism Spectrum Disorder. *Neurosci Bull* (2017) 33:194–204. doi: 10.1007/s12264-017-0103-8
5. Wei H, Alberts I, Li X. Brain IL-6 and Autism. *Neuroscience* (2013) 252:320–5. doi: 10.1016/j.neuroscience.2013.08.025
6. Siniscalco D, Schultz S, Brigida AL, Antonucci N. Inflammation and Neuro-Immune Dysregulations in Autism Spectrum Disorders. *Pharmaceuticals (Basel)* (2018) 11(2):56. doi: 10.3390/ph11020056
7. Depino AM. Peripheral and Central Inflammation in Autism Spectrum Disorders. *Mol Cell Neurosci* (2013) 53:69–76. doi: 10.1016/j.mcn.2012.10.003
8. Ashwood P, Nguyen DV, Hessl D, Hagerman RJ, Tassone F. Plasma Cytokine Profiles in Fragile X Subjects: Is There a Role for Cytokines in the Pathogenesis? *Brain Behav Immun* (2010) 24:898–902. doi: 10.1016/j.bbi.2010.01.008
9. Estes ML, McAllister AK. Immune Mediators in the Brain and Peripheral Tissues in Autism Spectrum Disorder. *Nat Rev Neurosci* (2015) 16:469–86. doi: 10.1038/nrn3978
10. Goines PE, Croen LA, Braunschweig D, Yoshida CK, Grether J, Hansen R, et al. Increased Midgestational IFN-γ, IL-4 and IL-5 in Women Bearing a Child With Autism: A Case-Control Study. *Mol Autism* (2011) 2:13. doi: 10.1186/2040-2392-2-13
11. Abdallah MW, Larsen N, Mortensen EL, Atladóttir HÓ, Nørgaard-Pedersen B, Bonefeld-Jørgensen EC, et al. Neonatal Levels of Cytokines and Risk of Autism Spectrum Disorders: An Exploratory Register-Based Historic Birth Cohort Study Utilising the Danish Newborn Screening Biobank. *J Neuroimmunol* (2012) 252:75–82. doi: 10.1016/j.jneuroim.2012.07.013
12. Amatya N, Garg AV, Gaffen SL. IL-17 Signaling: The Yin and the Yang. *Trends Immunol* (2017) 38:310–22. doi: 10.1016/j.it.2017.01.006
13. Li X, Bechara R, Zhao J, McGeachy MJ, Gaffen SL. IL-17 Receptor–Based Signaling and Implications for Disease. *Nat Immunol* (2019) 20:1594–602. doi: 10.1038/s41590-019-0514-y
14. Suzuki K, Matsuzaki H, Iwata K, Kameno Y, Shimmura C, Kawai S, et al. Plasma Cytokine Profiles in Subjects With High-Functioning Autism Spectrum Disorders. *PloS One* (2011) 6:e20470. doi: 10.1371/journal.pone.0020470
15. van der Zwaag B, Franke L, Poot M, Hochstenbach R, Spierenburg HA, Vorstman JAS, et al. Gene-Network Analysis Identifies Susceptibility Genes Related to Glycobiology in Autism. *PloS One* (2009) 4:e5324. doi: 10.1371/journal.pone.0005324
16. Choi GB, Yim YS, Wong H, Kim S, Kim H, Kim SV, et al. The Maternal Interleukin-17a Pathway in Mice Promotes Autism-Like Phenotypes in Offspring. *Science* (2016) 351:933–9. doi: 10.1126/science.aad0314
17. Yasumatsu K, Nagao J-I, Arita-Morioka K-I, Narita Y, Tasaki S, Toyoda K, et al. Bacterial-Induced Maternal Interleukin-17A Pathway Promotes Autistic-Like Behaviors in Mouse Offspring. *Exp Anim* (2020) 69:250–60. doi: 10.1538/expanim.19-0156
18. Ribeiro M, Brigas HC, Temido-Ferreira M, Pousinha PA, Regen T, Santa C, et al. Meningeal γδ T Cell–Derived IL-17 Controls Synaptic Plasticity and Short-Term Memory. *Sci Immunol* (2019) 4(40):eaay5199. doi: 10.1126/sciimmunol.aay5199
19. Reed MD, Yim YS, Wimmer RD, Kim H, Ryu C, Welch GM, et al. IL-17a Promotes Sociability in Mouse Models of Neurodevelopmental Disorders. *Nature* (2020) 577:249–53. doi: 10.1038/s41586-019-1843-6
20. Zhang Y, Gao D, Kluetzman K, Mendoza A, Bolivar VJ, Reilly A, et al. The Maternal Autoimmune Environment Affects the Social Behavior of Offspring. *J Neuroimmunol* (2013) 258:51–60. doi: 10.1016/j.jneuroim.2013.02.019

21. Macleod MR, O'Collins T, Howells DW, Donnan GA. Pooling of Animal Experimental Data Reveals Influence of Study Design and Publication Bias. *Stroke* (2004) 35:1203–8. doi: 10.1161/01.STR.0000125719.25853.20
22. Ozaki K, Kato D, Ikegami A, Hashimoto A, Sugio S, Guo Z, et al. Maternal Immune Activation Induces Sustained Changes in Fetal Microglia Motility. *Sci Rep* (2020) 10:21378. doi: 10.1038/s41598-020-78294-2
23. Arrode-Brusés G, Brusés JL. Maternal Immune Activation by Poly(I:C) Induces Expression of Cytokines IL-1β and IL-13, Chemokine MCP-1 and Colony Stimulating Factor VEGF in Fetal Mouse Brain. *J Neuroinflamm* (2012) 9:83. doi: 10.1186/1742-2094-9-83
24. Schwartzer JJ, Careaga M, Onore CE, Rushakoff JA, Berman RF, Ashwood P. Maternal Immune Activation and Strain Specific Interactions in the Development of Autism-Like Behaviors in Mice. *Transl Psychiatry* (2013) 3: e240. doi: 10.1038/tp.2013.16
25. Pendyala G, Chou S, Jung Y, Coiro P, Spartz E, Padmashri R, et al. Maternal Immune Activation Causes Behavioral Impairments and Altered Cerebellar Cytokine and Synaptic Protein Expression. *Neuropsychopharmacology* (2017) 42:1435–46. doi: 10.1038/npp.2017.7
26. Xu X, Wu D, Hou S, Zhu J, Li J, Tang J. Prenatal Exposure to TAK242 Affects the Childhood Autism in Offspring in Animal Models of Autism Spectrum Disorder. *Iran J Basic Med Sci* (2017) 20:1016–20. doi: 10.22038/IJBMS.2017.9270
27. Ahmad SF, Ansari MA, Nadeem A, Bakheet SA, Alshammari MA, Attia SM. Protection by Tyrosine Kinase Inhibitor, Tyrphostin AG126, Through the Suppression of IL-17a, Rorγt, and T-Bet Signaling, in the BTBR Mouse Model of Autism. *Brain Res Bull* (2018) 142:328–37. doi: 10.1016/j.brainresbull.2018.08.020
28. Nadeem A, Ahmad SF, Al-Harbi NO, Attia SM, Bakheet SA, Ibrahim KE, et al. Nrf2 Activator, Sulforaphane Ameliorates Autism-Like Symptoms Through Suppression of Th17 Related Signaling and Rectification of Oxidant-Antioxidant Imbalance in Periphery and Brain of BTBR T+tf/J Mice. *Behav Brain Res* (2019) 364:213–24. doi: 10.1016/j.bbr.2019.02.031
29. Lammert CR, Frost EL, Bolte AC, Paysour MJ, Shaw ME, Bellinger CE, et al. Cutting Edge: Critical Roles for Microbiota-Mediated Regulation of the Immune System in a Prenatal Immune Activation Model of Autism. *J Immunol* (2018) 201:845–50. doi: 10.4049/jimmunol.1701755
30. Bakheet SA, Alzahrani MZ, Ansari MA, Nadeem A, Zoheir KMA, Attia SM, et al. Resveratrol Ameliorates Dysregulation of Th1, Th2, Th17, and T Regulatory Cell-Related Transcription Factor Signaling in a BTBR T + Tf/J Mouse Model of Autism. *Mol Neurobiol* (2017) 54:5201–12. doi: 10.1007/s12035-016-0066-1
31. Ansari MA, Nadeem A, Attia SM, Bakheet SA, Raish M, Ahmad SF. Adenosine A2A Receptor Modulates Neuroimmune Function Through Th17/retinoid-Related Orphan Receptor Gamma T (Rorγt) Signaling in a BTBR T Itpr3/J Mouse Model of Autism. *Cell Signal* (2017) 36:14–24. doi: 10.1016/j.cellsig.2017.04.014
32. Hsiao EY, McBride SW, Chow J, Mazmanian SK, Patterson PH. Modeling an Autism Risk Factor in Mice Leads to Permanent Immune Dysregulation. *Proc Natl Acad Sci U S A* (2012) 109:12776–81. doi: 10.1073/pnas.1202556109
33. Luan R, Cheng H, Li L, Zhao Q, Liu H, Wu Z, et al. Maternal Lipopolysaccharide Exposure Promotes Immunological Functional Changes in Adult Offspring CD4+ T Cells. *Am J Reprod Immunol* (2015) 73:522–35. doi: 10.1111/aji.12364
34. Chen Y, Liu S, Xu H, Zheng H, Bai C, Pan W, et al. Maternal Exposure to Low Dose BDE209 and Pb Mixture Induced Neurobehavioral Anomalies in C57BL/6 Male Offspring. *Toxicology* (2019) 418:70–80. doi: 10.1016/j.tox.2019.02.016
35. Gumusoglu SB, Hing BWQ, Chilukuri ASS, Dewitt JJ, Scroggins SM, Stevens HE. Chronic Maternal Interleukin-17 and Autism-Related Cortical Gene Expression, Neurobiology, and Behavior. *Neuropsychopharmacology* (2020) 45:1008–17. doi: 10.1038/s41386-020-0640-0
36. Afroz KF, Reyes N, Young K, Parikh K, Misra V, Alviña K. Altered Gut Microbiome and Autism Like Behavior are Associated With Parental High Salt Diet in Male Mice. *Sci Rep* (2021) 11(1):8364. doi: 10.1038/s41598-021-87678-x. Erratum in: *Sci Rep* (2022) 12(1):5686.
37. Alhosaini K, Ansari MA, Nadeem A, Bakheet SA, Attia SM, Alhazzani K, et al. 5-Aminoisoquinolinone, a PARP-1 Inhibitor, Ameliorates Immune Abnormalities Through Upregulation of Anti-Inflammatory and Downregulation of Inflammatory Parameters in T Cells of BTBR Mouse Model of Autism. *Brain Sci* (2021) 11:249. doi: 10.3390/brainsci11020249
38. Heo Y, Zhang Y, Gao D, Miller VM, Lawrence DA. Aberrant Immune Responses in a Mouse With Behavioral Disorders. *PloS One* (2011) 6: e20912. doi: 10.1371/journal.pone.0020912
39. Jaini R, Wolf MR, Yu Q, King AT, Frazier TWJr, Eng C. Maternal Genetics Influences Fetal Neurodevelopment and Postnatal Autism Spectrum Disorder-Like Phenotype by Modulating *in-Utero* Immunosuppression. *Transl Psychiatry* (2021) 11:348. doi: 10.1038/s41398-021-01472-x
40. Kalish BT, Kim E, Finander B, Duffy EE, Kim H, Gilman CK, Yim YS, et al. Maternal Immune Activation in Mice Disrupts Proteostasis in the Fetal Brain. *Nat Neurosci* (2021) 24(2):204–13. doi: 10.1038/s41593-020-00762-9
41. Schwartzer JJ, Careaga M, Coburn MA, Rose DR, Hughes HK, Ashwood P. Behavioral Impact of Maternal Allergic-Asthma in Two Genetically Distinct Mouse Strains. *Brain Behav Immun* (2017) 63:99–107. doi: 10.1016/j.bbi.2016.09.007
42. Senkal E, Bagcioglu E, Eryigit U, Erbas O, Solmaz V. Exposure to Hypertonic Solutions During Pregnancy Induces Autism-Like Behaviors *via* the NFAT-5 Pathway in Offspring in a Rat Model. *Physiol Behav* (2021) 240:113545. doi: 10.1016/j.physbeh.2021.113545
43. Shin K-O, Crumrine DA, Kim S, Lee Y, Kim B, Abuabara K, et al. Phenotypic Overlap Between Atopic Dermatitis and Autism. *BMC Neurosci* (2021) 22:43. doi: 10.1186/s12868-021-00645-0
44. Shimizu Y, Tsukada T, Sakata-Haga H, Sakai D, Shoji H, Saikawa Y, et al. Exposure to Maternal Immune Activation Causes Congenital Unfolded Protein Response Defects and Increases the Susceptibility to Postnatal Inflammatory Stimulation in Offspring. *J Inflamm Res* (2021) 14:355–65. doi: 10.2147/JIR.S294238
45. Kim E, Paik D, Ramirez RN, Biggs DG, Park Y, Kwon H-K, et al. Maternal Gut Bacteria Drive Intestinal Inflammation in Offspring With Neurodevelopmental Disorders by Altering the Chromatin Landscape of CD4 T Cells. *Immunity* (2022) 55:145–158.e7. doi: 10.1016/j.immuni.2021.11.005
46. Hooijmans CR, Rovers MM, de Vries RBM, Leenaars M, Ritskes-Hoitinga M, Langendam MW. Syrcle's Risk of Bias Tool for Animal Studies. *BMC Med Res Method* (2014) 14:43. doi: 10.1186/1471-2288-14-43
47. Abdallah MW, Larsen N, Grove J, Nørgaard-Pedersen B, Thorsen P, Mortensen EL, et al. Amniotic Fluid Inflammatory Cytokines: Potential Markers of Immunologic Dysfunction in Autism Spectrum Disorders. *World J Biol Psychiatry* (2013) 14:528–38. doi: 10.3109/15622975.2011.639803
48. Alves de Lima K, Rustenhoven J, Da Mesquita S, Wall M, Salvador AF, Smirnov I, et al. Meningeal γδ T Cells Regulate Anxiety-Like Behavior *via* IL-17a Signaling in Neurons. *Nat Immunol* (2020) 21:1421–9. doi: 10.1038/s41590-020-0776-4
49. Kim S, Kim H, Yim YS, Ha S, Atarashi K, Tan TG, et al. Maternal Gut Bacteria Promote Neurodevelopmental Abnormalities in Mouse Offspring. *Nature* (2017) 549:528–32. doi: 10.1038/nature23910
50. De Angelis M, Piccolo M, Vannini L, Siragusa S, De Giacomo A, Serrazzanetti DI, et al. Fecal Microbiota and Metabolome of Children With Autism and Pervasive Developmental Disorder Not Otherwise Specified. *PloS One* (2013) 8:e76993. doi: 10.1371/journal.pone.0076993
51. Hsiao EY, McBride SW, Hsien S, Sharon G, Hyde ER, McCue T, et al. Microbiota Modulate Behavioral and Physiological Abnormalities Associated With Neurodevelopmental Disorders. *Cell* (2013) 155:1451–63. doi: 10.1016/j.cell.2013.11.024
52. Faraco G, Brea D, Garcia-Bonilla L, Wang G, Racchumi G, Chang H, et al. Dietary Salt Promotes Neurovascular and Cognitive Dysfunction Through a Gut-Initiated TH17 Response. *Nat Neurosci* (2018) 21:240–9. doi: 10.1038/s41593-017-0059-z
53. Thomas MSC, Davis R, Karmiloff-Smith A, Knowland VCP, Charman T. The Over-Pruning Hypothesis of Autism. *Dev Sci* (2016) 19:284–305. doi: 10.1111/desc.12303
54. Sacai H, Sakoori K, Konno K, Nagahama K, Suzuki H, Watanabe T, et al. Autism Spectrum Disorder-Like Behavior Caused by Reduced Excitatory Synaptic Transmission in Pyramidal Neurons of Mouse Prefrontal Cortex. *Nat Commun* (2020) 11:5140. doi: 10.1038/s41467-020-18861-3

55. Gaugler T, Klei L, Sanders SJ, Bodea CA, Goldberg AP, Lee AB, et al. Most Genetic Risk for Autism Resides With Common Variation. *Nat Genet* (2014) 46:881–5. doi: 10.1038/ng.3039
56. Chen JA, Peñagarikano O, Belgard TG, Swarup V, Geschwind DH. The Emerging Picture of Autism Spectrum Disorder: Genetics and Pathology. *Annu Rev Pathol* (2015) 10:111–44. doi: 10.1146/annurev-pathol-012414-040405
57. Werling DM, Geschwind DH. Sex Differences in Autism Spectrum Disorders. *Curr Opin Neurol* (2013) 26:146–53. doi: 10.1097/WCO.0b013e32835ee548
58. Karp NA, Reavey N. Sex Bias in Preclinical Research and an Exploration of How to Change the Status Quo. *Br J Pharmacol* (2019) 176:4107–18. doi: 10.1111/bph.14539
59. Shi P, Zhu S, Lin Y, Liu Y, Liu Y, Chen Z, et al. Persistent Stimulation With Interleukin-17 Desensitises Cells Through Scfβ-TrCP-Mediated Degradation of Act1. *Sci Signal* (2011) 4:ra73. doi: 10.1126/scisignal.2001653
60. Xu S, Cao X. Interleukin-17 and its Expanding Biological Functions. *Cell Mol Immunol* (2010) 7:164–74. doi: 10.1038/cmi.2010.21

Conflict of Interest: The authors declare that the research was conducted in the absence of any commercial or financial relationships that could be construed as a potential conflict of interest.

Frontiers in Immunology

Explores novel approaches and diagnoses to treat immune disorders.

The official journal of the International Union of Immunological Societies (IUIS) and the most cited in its field, leading the way for research across basic, translational and clinical immunology.

Discover the latest Research Topics

See more →

Frontiers

Avenue du Tribunal-Fédéral 34
1005 Lausanne, Switzerland
frontiersin.org

Contact us

+41 (0)21 510 17 00
frontiersin.org/about/contact